Group VIII Transition Metal Complexes for Nonlinear Optical Switching

Patrick J. West

B.Sc. (Hons)

A thesis submitted for the degree of

Doctor of Philosophy

of The Australian National University

September 2011

Errata for the thesis entitled

Group VIII Transition Metal Complexes for Nonlinear Optical Switching

Patrick J. West

B.Sc. (Hons)

A thesis submitted for the degree of

Doctor of Philosophy

of The Australian National University

September 2011

I would like to thank the reviewers for providing advice and feedback on the submitted thesis. Below is a list of changes in response to the reviewers suggestions

Page and line reference	Previous text	New text
p. iv, l. 4 p. 109, l. 5	then	than
p. 7, l. 9-10,17	μ	μ_0
p. 16, l. 4	d8	d^8
p. 30, l. 3	of the terpy.	of the terpy at 1.34μm.
p. 30, l. 10	phenathroline	1,10-phenanthroline
p. 34, chart	**123**:M = Os	**123**: M = Os
p. 42, l. 1	1,10-phenthroline	1,10-phenanthroline
p. 43, chart 1	WLC	TPEF
p. 45, chart	reference 321	reference 328
p. 46, chart	GM esu	GM
p. 47, 49, 51, 52, chart		[Ru] = *trans*-[Ru(dppe)$_2$]
p. 53, chart		o = open DTE, c = closed DTE, a = alkynyl, v = vinylidene, II/III = (formal) metal-centered oxidation states
p. 62, l. 15	Chemphyschem	ChemPhysChem
p. 67, l. 39	Ledoux-Rack	Ledoux-Rak
p. 76, l. 10	Previously, chloro-alkynyl	Previously, in the group chloro-alkynyl
p. 80, l. 8,11,15 p. 81, l. 9,11	ca	ca.
p. 88, l. 6	suggests an IVCT	suggests that an IVCT
p. 88, l. 8	alternate	alternative
p. 91, Table 2.2	(NBu$^n_4$)PF$_6$	NBu$^n_4$PF$_6$

p. 93, l. 15,21 p. 141, legend p. 146, legend p. 188, legend p. 222, legend p. 224, l. 14		
p. 93,150,197, l. 16	solvent	THF or CH_2Cl_2
p. 99, l. 7	$([RuCl(NCMe)(dppe)_2]^+$	$([RuCl(CH_3CN)(dppe)_2]^+$
p. 99, l. 20	$([M - Cl + CNCH_3]^+$	$([M - Cl + CH_3CN]^+$
p. 110, l. 7	solent	solvent
p. 126, l. 14	at: 3302 cm^{-1}	at 3302 cm^{-1}
p. 129, legend	Os-Cl , Os-C(1) 2.5202(8),	Os-Cl 2.5202(8), Os-C(1) 2.005(3)
p. 136, legend	0.46 V [1] (CH_2Cl_2) and 0.56 V [1] THF	0.46 V (CH_2Cl_2) and 0.56 V (THF)
p. 138, legend p. 185, legend	0.56 V [1].	0.56 V.
p. 141, table heading	[e]	[ε]
p. 141	**Table 3.3**	**Table 3.4**
p. 146	**Table 3.4**	**Table 3.5**
p. 148	**Table 3.5**	**Table 3.6**
p. 153, l. 9	1299 ($[M - Cl + CH_3OH]^+$, 90), 1308 ($[M - Cl + CH_3CN]^+$, 80). Anal. Calcd	1299 ($[M - Cl + CH_3OH]^+$, 90). Anal. Calcd
p. 153, l. 5 p. 157, l. 5	ml	mL
p. 155, l. 1	1267 ($[M - NH3-PF6]^+$	1267 ($[M - NH_4PF_6]^+$
p. 156, l. 20	6.40 – 7.43 (m, 52H, Ph)	6.40 – 7.43 (m, 48H, Ph)
p. 157, l. 18	$SiPr^i_3)(dppe)_2$	$SiPr^i_3)(dppe)_2$

p. 158, l. 11 p. 159, l. 1,12 p. 204, l. 17		
p. 163, l. 12	7.90 – 6.33 (m, 132H, Ar)	6.33 – 7.90 (m, 136H, Ar)
p. 177, l. 5 p. 180, l. 3	**35,**	**35,**
p. 177, l. 7	pendent	pendant
p. 183, l. 11	ν(C≡C-Si). As shown previously	ν(C≡C-Si). No other bands assigned as ν(C≡C) were observed. As shown previously
p. 194, l. 3	to ≤ the maximum	to the maximum
p. 201, l. 19	7.55 – 6.69 (m, 295H, Ar)	6.69 – 7.55 (m, 303H, Ar)
p. 202, l. 23	0.99 (s, br, 3H, NH_3)	0.99 (s, br, 6H, NH_3)
p. 219, legend	0.46 V [1]	0.46 V
p. 222, legend	**Table 4.3**	**Table 5.4**
p. 225, l. 3	(C_6D_6, 200 MHz)	(C_6D_6)
p. 225, l. 4	(C_6D_6, 50 MHz)	(C_6D_6)
p. 225, l. 21	9.6 (C_5Me_5)	9.6 (C_5Me_5),
p. 226, l. 26	7.47 (d, 1H, ^3J = 7.5 Hz, Ar), 7.29 (d, 1H, ^3J = 7.7 Hz, Ar), 6.85 (dd, 1H, ^3J = 7.8 Hz, Ar)	7.47 (d, 1H, ^3J = 8.0 Hz, Ar), 7.29 (d, 1H, ^3J = 7.7 Hz, Ar), 6.85 (dd, 1H, ^3J = 8.0 Hz, Ar)
p. 228, l. 16	7.49 (d, 1H, ^3J = 7.5, Ar), 7.24 (d, 1H, ^3J = 7.6, Ar), 6.85 (dd, 1H, ^3J = 7.7, Ar)	7.49 (d, 1H, ^3J = 8.0, Ar), 7.24 (d, 1H, ^3J = 7.6, Ar), 6.85 (dd, 1H, ^3J = 8.0, Ar)
p. 229, l. 7 p. 229, l. 19	J_{CP}	$^1J_{CP}$

The following abbreviations are added to the list on page vii

DBU	1,8-Diazabicyclo[5.4.0]undec-7-ene
DTE	5,5′-dithienylperfluorocyclopentene
ITO	indium tin oxide
ILCT	intraligand charge transfer
TPEF	two-photon excited fluorescence

For the Instrumentation sections on pages 93, 150 and 197 the following text

Electrospray ionisation mass spectra (ESIMS) were obtained using a Waters-micromass LCT-ZMD single quadrupole liquid chromatograph instrument; peaks are reported as *m/z* (assignment, relative intensity).

is replaced by:

Electrospray ionization mass spectra (ESIMS) were obtained from MeCN or MeOH solutions (a small amount of CH_2Cl_2 was used to increase solubility) using a VG Quattro II triple quadrupole MS instrument; peaks are reported as *m/z* (assignment, relative intensity (%)).

The Chart on page 119 is to be replaced with the following Chart which includes the numbering for C_{42}

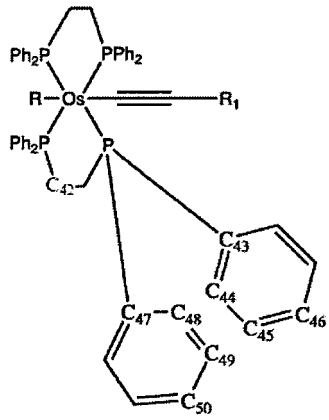

The paragraph on page 146 describing the quantum mechanical calculations carried out on complexes **17** and $\mathbf{17}^+$ is to be replaced with the following paragraph which contains the orbital bases used.

3.2.2.7 Quantum mechanical calculations

DFT calculations at the SAOP/TZP//PBE/TZP level of theory were carried out on **17** and $\mathbf{17}^+$ in order to assign the UV-Vis absorption bands for the osmium bis-alkynyl complexes. In all calculations and for all atoms, the all-electron Slater type orbital basis sets used were of triple-ζ-plus-polarization quality (TZP). Orbital diagrams are shown in Figure 3.21 and results tabulated and compared to experimental data in Table 3.5.

The Chart on page 40 is to be replaced with the following chart, excluding complexes **163** – **165**.

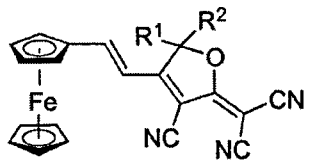

159: $R^1 = R^2 = CH_3$,
$\beta/\beta_{Chloroform}$ (HRS) = 279 (MeCN)[146]

160: $R^1 = CF_3$, R^2 = Ph,
$\beta/\beta_{Chloroform}$ (HRS) = 450 (MeCN)[146]

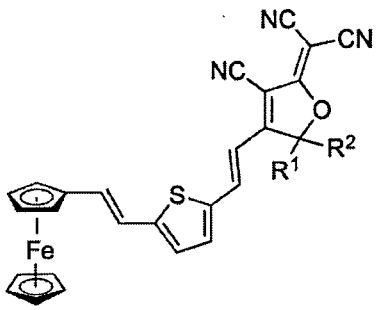

161: $R^1 = R^2 = CH_3$,
$\beta/\beta_{Chloroform}$ (HRS) = 2633 (MeCN)[146]

162: $R^1 = CF_3$, R^2 = Ph,
$\beta/\beta_{Chloroform}$ (HRS) = 3333 (MeCN)[146]

The experimentally obtained $\mu\beta$ for complexes **163** – **165** were erroneously attributed to reference 146 and were instead obtained via the EFISH method in the following reference:

Alain, V.; Blanchard-Desce, M.; Chen, C.; Marder, S. R.; Fort, A.; Barzoukas, M. *Synth. Met.* **1996**, *81*, 133.

The following references are provided for further information on virtual coupling as discussed on page 122:

Verstuyft, A. W.; Cary, L. W.; Nelson, J. H. *Inorg. Chem.* **1975**, *14*, 1495.
King, R. B. *Inorg. Chem.* **1963**, *2*, 936.

The following reviewers comments have not resulted in changes to this thesis

Reviewers comment: Title: Modern nomenclature would expect the use of Group 8 (specifically the iron group) rather than the archaic Group VIII which also encompassed metals from Groups 9 and 10

Response: Whilst it is acknowledged that Group VIII doesn't exclusively refer to iron, ruthenium and osmium (the transition metals used in this work) but also includes Group 9 and 10 transition metals, the title of the thesis is still appropriate as the Group 8 transition metals are included in Group VIII.

Reviewers comment: Summary. This is very general and while it covers the work reported it gives much less detail than would normally be presented in an abstract.

Response: The summary was intended to provide a brief overview of the content in each of the chapters without the level of detail of an abstract. Each of the chapters contains an introduction which provides details about past work in the area and the rational for the work presented in each chapter.

Reviewers comment: (page 25 chart) In the legend of cpnds 55 and 56, "$\beta_{1.91}$" should be written as "β_{1910}" to be consistent with the following text.

Reviewers comment: In the legend of cpnds 59 and 60, "$\beta_{1.34}$" should be written as "β_{1340}" to be consistent with the rest.

Response: Both μm and nm are used throughout the nonlinear optical literature. The wavelength unit used in each example are those used in the reference cited. The unit of wavelength used (nm or μm) is given in the text.

Reviewers comment: Note that in contrast to other chapters, Schemes and Figures were not numbered in Chapter 1

Response: Due to the large number of Schemes and Figures in Chapter 1 it was decided not to number the Schemes and Figures and instead have each of the compounds numbered.

Contents

Statement

I certify that the content of this thesis has never been submitted for any degree and is not currently being submitted for any other degree or qualification, that all the work and results are original unless due reference is made, and that any help has been acknowledged.

Patrick J. West

Summary

Metal alkynyl complexes have been shown to be potentially useful third-order nonlinear optical switches, with large two-photon absorption cross-sections and strong changes in photon absorption properties on oxidation. By forming multinuclear complexes, switches with more then two states can be made.

Chapter 1 presents an introduction to nonlinear optics and reviews some inorganic materials which have had their nonlinear optical properties measured.

Chapter 2 details new synthetic routes into binuclear complexes incorporating an osmium chloro-alkynyl metal centre. Structural, electrochemical and spectroelectrochemical studies on selected examples have been carried out.

Chapter 3 details new facile synthetic routes into osmium ammine-alkynyl and osmium bis-alkynyl complexes. Synthesis of osmium and ruthenium binuclear and trinuclear complexes with both diethynyl and triethynyl bridges between the metal atoms has been explored. Structural, electrochemical, spectroelectrochemical and theoretical studies have been carried out on selected complexes.

Chapter 4 reports the synthesis of a number of branched multinuclear complexes incorporating both osmium and ruthenium metal atoms. Electrochemical and spectroelectrochemical studies have been carried out on selected examples. The Z-scan technique has been used to investigate the third-order nonlinear optical properties of a number of linear and branched bimetallic complexes, showing large effects but some photo-induced instability.

Chapter 5 details the formation of a number of new mononuclear and unsymmetrical binuclear iron alkynyl complexes. The electrochemical and spectroelectrochemical behaviour of the complexes exhibiting a reversible redox process has been explored.

Acknowledgements

I am very grateful for the guidance, support and encouragement of my supervisors, Prof. Mark Humphrey and Dr Marie Cifuentes.

Chapter 1 has been adapted from a review co-written with Torsten Schwich, Prof. Marek Samoc, Dr Marie Cifuentes and Prof. Mark Humphrey.

Torsten Schwich and Dr Mike Randles are thanked and acknowledged for the crystal structure determinations and analysis within this project.

Dr Marie Cifuentes is thanked and acknowledged for assistance with electrochemistry and spectroelectrochemistry and for carrying out the associated studies of complexes **13** and **17**.

Prof. Marek Samoc and Malgorzata Wielgus are thanked for the Z-scan measurements and analysis presented in this work and for patiently answering queries and teaching me to fit the theoretical curves. Dr Chris Corkery, Paul Gugger and Dr Marie Cifuentes are thanked for additional Z-scan assistance.

Erandi Kulasekera, Dr Simon Petrie and Prof. Rob Stranger are thanked for the theoretical calculations.

Torsten Schwich is thanked for providing many synthetic precursors and assistance in carrying out the reactions in Chapter 4.

Dr Frederic Paul is thanked for hosting me in his lab in Rennes, France, and assisting me with the iron chemistry in Chapter 5. Dr Gilles Argouarch and Dr Katy Green are thanked for providing many synthetic precursors and assistance with the iron chemistry in Chapter 5.

Paul Gugger is thanked for technical assistance and insightful discussions.

An ANU PhD Scholarship is gratefully acknowledged.

I would like to thank all members of the group for their friendship and support, in particular, Torsten, Mike, Rachel, Katy, Bandar, Chris, Mark, Adam, Pete, Mahbod, Guillaume, Vivek, Fazira, Aisyah, Erandi, Najib, Jennifer and Alan.

Special thanks must go to my family for their support and encouragement during my studies, in particular, Trista, Pauline, Arthur, Margaret, James, Stuart, Alex and Nathan.

Abbreviations

Ar	aryl
Bu	butyl
Cp	η^5-cyclopentadienyl
Cp*	η^5-pentamethylcyclopentadienyl
CT	charge transfer
d	doublet
dd	doublet-of-doublets
DFWM	degenerate four-wave mixing
dmso	dimethyl sulfoxide
dppe	1,2-bis(diphenylphosphino)ethane
dppm	bis(diphenylphosphino)methane
EFISH	electric field-induced second harmonic generation
ESI	electro-spray ionisation
Et	ethyl
FT	fourier transform
GOF	goodness of fit
HOMO	highest-occupied molecular orbital
HRS	hyper-Rayleigh scattering
i	*iso*
i_{pa}	anodic current
i_{pc}	cathodic current
IR	infrared
LMCT	ligand to metal charge transfer
LUMO	lowest-unoccupied molecular orbital
m	multiplet
Me	methyl
MLCT	metal to ligand charge transfer

MS	mass spectrometry
n	*normal*
NLO	nonlinear optical
NMR	nuclear magnetic resonance
OTTLE	optically transparent thin-layer electrochemical
Ph	phenyl
Pr	propyl
s	singlet
SHG	second-harmonic generation
SOMO	singly occupied molecular orbital
t	*tertiary*
t	triplet
thf	tetrahydrofuran
THG	third-harmonic generation
TPA	two-photon absorption
TPL	two-photon luminescence
UV	ultraviolet
vis	visible
vtt	virtual triplet-of-triplets
WLD	wavelength dependence
2PA	two-photon absorption

Chapter 1

Inorganic materials for nonlinear optics: a review

Chapter 1

Inorganic materials for nonlinear optics: a review

Contents

1.1 Theory

Light is an electromagnetic wave and the propagation of light and its interaction with matter involve both the electrical and magnetic field components of that wave, both of which oscillate at the same frequency ω. In most cases, however, it is sufficient to consider only the electrical component $F(t,\mathbf{r})$, which for a monochromatic wave may be written as:

$$F(t,\mathbf{r}) = F_\omega \exp\left[i(\omega t - \mathbf{kr})\right] + c.c. \qquad (1)$$

where $\mathbf{k}$ is the wavevector. As light propagates in a medium, the electric field interacts with matter, forcing the electrons in matter to oscillate at the light frequency. This interaction may lead to various effects including refraction, scattering, and absorption of light beams. At low light intensities, the oscillating electrical polarization induced in matter by a light beam is proportional to the amplitude of the electrical field F_ω. However, intense laser beams, and especially pulses of light from pulsed lasers, may involve electrical field strengths that approach in magnitude the internal electrical fields corresponding to the interactions of electrons with atomic nuclei. Under such circumstances, the proportionality of the electrical response to F_ω is no longer assured, and nonlinear optical effects may arise.

For optical media composed of molecules, it is useful to consider the response of a molecule to the electrical field as an expansion of the Cartesian components of its electrical dipole moment in a power series:

$$\mu_i(F) = \mu_{0,i} + \alpha_{ij}F_j + \beta_{ijk}F_jF_k + \gamma_{ijkl}F_jF_kF_l + \ldots \quad (2)$$

where α, β and γ are the linear polarizability and the first and second hyperpolarizabilities, also termed the second-order and third-order polarizabilities, respectively. The field components F_i refer to the local field inside the medium. To appreciate the meaning of the polarizabilities, we note first that they are tensors of consecutively increasing rank (the above equation is written using Einstein's

convention of summing over repeated indices), and thus the effects depend on the direction of the electric field vector in relation to the directions of the molecular axes. In addition to that, however, one needs to account for the fact that the electric field is given by Eq. (1), or, more generally, by a combination of such terms with various values of ω, $\mathbf{k}$ and F_ω. By substituting the sums of such terms into Eq. (2), one can verify that the presence of the quadratic term (the "β term") leads to the appearance of dipole oscillations at new frequencies that are sums and differences of the input frequencies (sum and difference frequency generation, SFG and DFG). When there is only a single frequency in the input, the nonlinear response includes a term oscillating at 2ω (second harmonic generation, SHG) as well as a time-independent term. In a similar way, the cubic "γ term" is capable of mixing three different components of the input field, or generating the third harmonic of a single input frequency (THG). An important term in the oscillation of the molecular dipole is that having the same frequency as the input field, but arising from the combination of three same-frequency input components.

The introduction of time-varying fields into Eq. (2) necessitates that one accounts for the possible lag between the field oscillation and the response of the electrons in the molecule. Such a lag, or a phase shift between the two oscillations, is treated by considering Fourier components of the input field and of the response, and defining all polarizabilities as complex quantities exhibiting frequency dispersion. This is relatively simple in the case of α, which should be treated as a complex quantity $\alpha(\omega)$, but becomes more complicated for β, which may depend on two different input frequencies, and γ, which may depend on three frequencies. The traditional notation for these two quantities is $\beta(-\omega_3;\omega_1,\omega_2)$ and $\gamma(-\omega_4;\omega_1,\omega_2,\omega_3)$, respectively, where the first of the arguments is the output frequency which is equal to the sum of the input frequencies. For example, the quadratic polarizability responsible for SHG is denoted as $\beta(-2\omega;\omega,\omega)$, while the cubic polarizability responsible for a degenerate cubic response is $\gamma(-\omega;\omega,-\omega,\omega)$. The latter quantity is of considerable interest because its real part contributes to the technologically important effect of nonlinear refraction, the dependence of the refractive index of a medium on the light intensity, while its

imaginary part contributes to the very useful effect of nonlinear absorption.[1] The nonlinear absorption of molecules is usually quantified by presenting it in the form of the nonlinear absorption cross-section. When nonlinear absorption corresponds to the simultaneous absorption of two photons of the same energy, this quantity is called the two-photon absorption cross-section, σ_2, and is most often given in Goeppert-Mayer units where 1 GM = 10^{-50} cm^4 s.

From a practical point of view, the microscopic properties of molecules forming a photonic material must be summed together to provide the macroscopic NLO properties, while accounting for the differences between the microscopic (local) electric field and the macroscopic (external) field. By analogy to Eq. (2), the macroscopic effects are described by the power series:

$$P_i(F) = P_{0,i} + C\left[\chi_{ij}^{(1)}F_j + \chi_{ijk}^{(2)}F_jF_k + \chi_{ijkl}^{(3)}F_jF_kF_l + \ldots\right] \qquad (3)$$

where the constant C depends on the choice of the system of units (1 for cgs units, ε_0 for SI units), P is the macroscopic polarization vector, the field F is the external field and $\chi^{(n)}$ are susceptibilities of consecutive orders. As with polarizabilities, the macroscopic susceptibilities are complex quantities with complicated frequency dependences; the calculation of a susceptibility of crystalline media from molecular properties of the constituent molecules requires the knowledge of the orientations of the molecules as well as the local field factors, and is a particularly tedious task. This is simplified considerably in the case of isotropic media such as solutions or glasses.

1.2 Measurement techniques

1.2.1 Quadratic NLO properties of molecules

The quadratic polarizability β is a third-rank tensor, i.e. it can be presented as a 3 x 3 x 3 matrix. As is true for all molecular property tensors, it has to fulfill the Neumann principle (at a minimum, a physical property has to possess the same symmetry as

that of the molecule). From this it follows that the existence of a center of symmetry in a molecule causes all the elements of the β tensor to vanish. In a similar way, all elements of the 3 x 3 x 3 $\chi^{(2)}$ tensor are equal to zero for isotropic media, so a perfectly random liquid or a solid solution of second-order NLO-active molecules should not exhibit second-order NLO effects such as coherent second-harmonic generation.

Measurements carried out on crystals belonging to noncentrosymmetric symmetry classes afford second-order nonlinear optical properties; however, such measurements are cumbersome because of the necessity to grow large (typically a few millimetres in size) optical quality single crystals of the compound to be studied, coupled to the need to take measurements with different orientations of the crystallographic axes of the sample while varying the polarization of the laser beam, etc. Usually, the SHG signals are collected as so-called Maker fringes, the amplitude and periodicity of the fringes being analyzed. Such measurements are rarely attempted for new materials unless there is the prospect of practical applications in the crystal form. Measurements of the second-harmonic signals from solutions or solid samples in which the NLO chromophores have net noncentrosymmetric alignment are considerably simpler. Various procedures to effect alignment have been employed, the most common being application of a dc electric field. The SHG effect arising under such circumstances is electric field-induced second-harmonic generation (EFISHG or EFISH). In a typical experiment (see, for example, ref. 2), a series of solutions of the compound of interest in an organic solvent are prepared, and are then examined in a special cell that permits application of intense electric fields (typically of the order of 10^5 V m^{-1}). To minimize problems with electron and ionic conduction in the samples, the field is usually applied in the form of a relatively short voltage pulse that is timed to start just before the laser pulse (which is shorter than the voltage pulse). The molecules of the solute and the solvent can contribute to the generation of the second harmonic of the laser frequency in two ways. All molecules, independent of their symmetry, will contribute through their cubic

hyperpolarizabilities. This arises from a polarization term at the second harmonic that involves the product of the orientationally-averaged cubic hyperpolarizability and the dc field amplitude $<\gamma(-2\omega;\omega,\omega,0)>F_{dc}$. The molecules possessing a static dipole moment μ_0 provide another (usually larger) contribution: they tend to align with the dc field direction along their dipole moment direction. Since thermal motions counteract such alignment, the net alignment can be found from consideration of the balance between these two tendencies, which leads to the Langevin formula. In effect, the contribution of dipolar orientation to the nonlinear polarization at 2ω is found to be proportional to $\frac{\boldsymbol{\mu\beta}}{kT}F_{dc}$. The tensor product $\boldsymbol{\mu\beta}$ appearing here needs a comment: it can be considered a scalar product of the $\boldsymbol{\mu}$ vector and the so-called vectorial part of the β tensor. Since many molecules of importance for second-order nonlinear optics are elongated in one direction and possess a dipole moment in that direction, it is often the case that the value of this product (the quantity that is determined experimentally in EFISH experiments) can be treated as the product of the length of the dipole moment of the molecules and the magnitude of the diagonal component of β along the molecular axis (often denoted β_{333}, 3 being the molecular axis). It should be noted that the product $\boldsymbol{\mu\beta}$ may have different signs for different molecules; this explains the need for measurements on several concentrations of the chromophore in the solvent, so as to correctly account for the same-sign or opposite-sign contribution of the solvent.

This principle of determining the second-order nonlinearity through electric field alignment of dipolar molecules can also be applied when the molecules are not in a liquid, but in a solid solution, e.g. in a polymer or sol-gel glass matrix. The main difference is that the dipoles must be aligned by electric-field poling when the system is in a state allowing for reorientation of the dipoles, i.e. above the glass transition temperature in a polymer, or before crosslinking of a matrix. SHG measurements in poled matrices are often used for NLO polymers, but are not common for organometallics.

The EFISH method cannot be applied for determining the NLO properties of second-order NLO molecules possessing trigonal symmetry, which have no net electric dipole but may have an electric octupole moment. The β tensor of such molecules is dominated by the octupolar components (see, for example, ref. 3 for a discussion of the dipolar and octupolar components of β). Another deficiency of EFISH is that it is difficult to apply to conducting solutions (i.e. those containing ions). Octupolar and conducting systems can be studied with an alternative technique, namely hyper-Rayleigh scattering (HRS).[4] As mentioned above, solutions of second-order NLO chromophores cannot generate coherent SHG beams because the contributions of individual molecules cancel out through the randomness of their orientations in space. However, such solutions can generate SHG in a non-coherent way: as a signal scattered in all directions. The principle of the effect is similar to that of ordinary Rayleigh scattering, in which light is scattered without the change of its frequency. The experiment to measure this is rather simple. A beam from a pulsed laser (nanosecond, picosecond or femtosecond) is tightly focused inside a cell containing the solution of interest. Light scattered from the vicinity of the focal point is collected with low f-number optics and the component at 2ω is separated with narrow band filters or a monochromator, before being passed to a sensitive detector. The intensity of the HRS signal is proportional to the square of the fundamental light intensity and to the square of a product of a certain combination of the components of the β tensor and the concentration of the chromophore. The experiment can be conveniently calibrated by performing measurements on a solution of a well-known NLO chromophore (e.g. *p*-nitroaniline). This technique is currently the most popular way of examining the second-order NLO effects in organometallic molecules. Its main drawback is the fact that the light intensities employed in the experiments are quite high, and can therefore induce effects additional to HRS. The main problem is upconverted emission from multiphoton absorption-induced fluorescence of the solution. Although the fluorescence component can, in principle, be rejected[5] based on the fact that it has a finite lifetime, unlike HRS which is instantaneous, and also

because its bandwidth is much broader than the SHG emission,[6] the results obtained for fluorescent molecules should be treated with care.

In both cases (EFISH and HRS), the important factor is the choice of the fundamental wavelength of the experiment. This is significant because of the dispersion of β and because of the possibility of artifacts such as multiphoton-excited emission, which can take place if the energies of two photons (or three in the case of three-photon absorption) are sufficient to reach an excited state of the chromophore.

An important second-order NLO effect is the linear (Pockels) electro-optic effect. Measurements of this effect can be relatively easily accomplished by several techniques including the ATR technique[7] and the Teng-Man technique.[8] The measured quantity is then the electro-optic coefficient r, which involves the $\beta(-\omega;\omega,0)$ hyperpolarizability.

1.2.2 Cubic NLO properties of molecules

The cubic hyperpolarizability γ is a fourth rank tensor (3 x 3 x 3 x 3 matrix). Unlike second-order NLO effects, orientational averaging for a random collection of third-order NLO chromophore molecules always leads to non-zero effects. In most cases, the average hyperpolarizability is given by:

$$\langle\gamma\rangle = \frac{1}{15}\left(\gamma_{iijj} + \gamma_{ijij}\right)$$

which reduces to $<\gamma> = 1/5\gamma_{1111}$ when one element of the tensor, γ_{1111}, is dominant. The macroscopic cubic susceptibility $\chi^{(3)}_{ijkl}$ for an isotropic system, such as a solution, has twenty-one non-zero elements, three of which are independent.[9] One usually determines $\chi^{(3)}_{1111}$, which can then be used to calculate $<\gamma>$.

While polarizabilities of all orders and corresponding to various frequency mixing schemes should be treated as complex, the real and imaginary parts of some have more immediate practical significance than others. There is little interest in the imaginary part of the second-order hyperpolarizability $\beta(-2\omega;\omega,\omega)$, because the second-harmonic generation process is usually carried out at frequencies well removed from the resonance frequencies of the material. On the other hand, both the real and imaginary parts of the above-mentioned degenerate cubic hyperpolarizability are of considerable practical interest.

The common techniques for the determination of the cubic NLO properties of molecules address different frequency combinations possible for $\gamma(-\omega_4;\omega_1,\omega_2,\omega_3)$. Currently, the most popular techniques are third-harmonic generation (THG), Z-scan, and degenerate four-wave mixing (DFWM). In all cases, solutions in liquid solvents or in solid matrices can be examined.

The third-harmonic generation experiments are performed with a pulsed laser beam impinging on a sample, the intensity of the beam generated at the third harmonic usually being monitored as a function of the angle of inclination of the sample with respect to that of the fundamental beam, which leads to the formation of Maker fringes similar to those from SHG measurements.[10] There is no need to electrically pole the sample; on the contrary, one needs to account for the contributions of THG generated in all components of the system (e.g. glass walls or glass substrate, in addition to the liquid or solid sample). The interference between the signals from components of the system may be helpful in resolving the real and imaginary contributions to the cubic susceptibility $\chi^{(3)}(-3\omega;\omega,\omega,\omega)$ or the corresponding hyperpolarizabilities. A major limitation for organometallics is that ω needs to be chosen to avoid material resonances at ω, 2ω, and 3ω, which is difficult for molecules absorbing in the visible region.

Z-scan[11] is currently the most widely applied technique for determining the real and imaginary parts of $\gamma(-\omega;\omega,-\omega,\omega)$. This technique measures two technologically relevant NLO parameters of a sample: its nonlinear refractive index and its nonlinear absorption coefficient. The former parameter can be defined by the relation $\Delta n = n_2 I$, while the latter parameter is defined by the analogous expression $\Delta\alpha_a = \alpha^{(2)} I$, where n is the refractive index, n_2 is the nonlinear refractive index, $\alpha^{(2)}$ is the nonlinear absorption coefficient, and $\Delta\alpha_a$ represents the change in the linear absorption coefficient induced by the intensity I (the index a is used here to distinguish this absorption coefficient from the linear polarizability).

The principle of Z-scan is as follows: a laser beam is focused by a lens, and the sample travels on a stage from a point before the beam focus ($-z$) through the focus ($z = 0$) to a point beyond the focus ($+z$). As the sample travels, it starts from a location where the light intensity is moderate, crosses the point of the highest intensity at $z = 0$ (because of the smallest beam diameter at that point) to a location where the intensity becomes much smaller again at $+z$. The changes of the intensity cause two effects. The change in the absorbance of the sample will influence the total power transmitted through the sample. The change in the refractive index, on the other hand, causes the sample to act as an induced lens, which contributes to the distortion of the beam in the far field (well after the sample). Both effects can be studied simultaneously: the nonlinear absorption, through monitoring the total power in the transmitted beam as a function of z (so called open-aperture Z-scan), and the nonlinear refraction, through monitoring the power transmitted through a small pinhole located at the centre of the beam in the far-field (closed-aperture Z-scan). The nonlinear refraction and nonlinear absorption coefficients obtained from the Z-scan data can then be used to compute the real and imaginary parts of the hyperpolarizability of the solute, taking into account the contribution to the signal coming from the solvent and the cell walls measured in a separate experiment.

The major difficulty with Z-scan measurements is that contributions to absorption and refraction at high light intensities may arise from a number of disparate processes. For example, a common problem is that linear and nonlinear absorption may lead to local heating of the solution, causing thermo-optic phenomena (changes in the refractive index and absorption coefficient due to a change of temperature). To avoid such contributions, it is necessary to use low repetition rate (usually 1 kHz or slower) short (typically 100 fs) laser pulses for Z-scan measurements. Nevertheless, distinguishing between various possible contributions to the Z-scan signals is only possible with additional, time-resolved experiments.

Historically, the most frequently employed time-resolved technique for determining cubic nonlinearities is degenerate four-wave mixing (DFWM). In the so-called BOXCARS geometry of the experiment, suitable for use with short-pulse lasers, a sample is subjected to the simultaneous action of three light beams, which are all derived from a single source by splitting the beam and adjusting the beam paths to ensure all beams arrive at the sample simultaneously. The beams are usually positioned in space in such a way that they arrive at a screen after the sample defining three corners of a rectangle. The interaction of the beams in the sample leads to the formation of volume gratings: periodic structures formed by changes in the refractive index and absorption coefficient of the material. The gratings contribute to the formation of new light beams: in the BOXCARS geometry, there is the possibility of forming a phase-matched beam pointing into the fourth corner of the above-mentioned rectangle, as well as several (usually weaker) non-phase matched beams.[12] The intensities of the beams created in the DFWM process are proportional to $|\chi^{(3)}|^2$, and so resolving the contributions into those from nonlinear refraction and those from nonlinear absorption requires additional study. This can be accomplished by a separate measurement of nonlinear absorption, or by determination of the phase of the DFWM signal through other means (for example,

using concentration dependences for a series of solutions of a chromophore in a solvent,[13] or through coherent detection[14]). The advantage of DFWM when performed with short laser pulses is the possibility of studying the temporal behavior of the induced changes in the refractive index and the absorption coefficient.

A simpler way of performing time-resolved experiments is by using the pump-probe technique, in which two pulsed laser beams of the same or different wavelengths arrive at the sample with a varied delay. The first beam, the pump, induces a change in the sample and the second, the probe, can sense these changes through the change of transmittance of the sample. This simplest manifestation (using the same wavelength for the pump and probe) affords the nonlinear absorption coefficient related to $\mathrm{Im}[\gamma(-\omega;\omega,-\omega,\omega)]$, while the use of two different wavelengths provides $\mathrm{Im}[\gamma(-\omega_1;\omega_1,-\omega_2,\omega_2)]$. A useful way of implementing the experiment is with white light supercontinuum as the probe, because this can provide a complete spectrum of the non-degenerate nonlinear absorption coefficient in a single experiment.

The use of the pump-probe principle for the determination of nonlinear refraction requires some modification to the experiment. The Kerr gate experiment uses a pump-probe setup in which the transmission of the probe beam, polarized at 45 degrees to the pump beam, is monitored through a crossed analyzer. The intensity of the probe transmitted through the analyzer can then be related to a combination of off-diagonal components of $\chi^{(3)}$. Resolution of the effect into that due to refractive and absorptive NLO properties requires a modification of the technique called heterodyne Kerr gate.

Nonlinear absorption is often investigated in an indirect way by two-photon excited fluorescence.[15] In this technique, a spectrum of the nonlinear absorption coefficient can be obtained by simply recording the dependence of the fluorescence induced by

two-photon absorption on the wavelength of the excitation, and then comparing the wavelength dependence of the fluorescence with that of a standard well-known fluorescent dye. The spectrum obtained is of the product of the two-photon absorption cross-section of a molecule and its fluorescence quantum yield; the quantum yield is usually assumed to be equal to that measured under ordinary one-photon excitation.

The cubic NLO properties can also be observed when one of the exciting fields is not derived from a light beam but from a dc source. The refractive behavior observed under these conditions is the quadratic electro-optic effect or Kerr effect, while the absorptive behavior is electroabsorption or the Stark effect. The nonlinear susceptibilities derived from these measurements are the real and imaginary parts of $\chi^{(3)}(-\omega;\omega,0,0)$, respectively.

1.3 Units (conversions, definitions, difficulties)

Much confusion may arise when attempts are made to compare results of different authors using various conventions of defining the NLO parameters, different units systems and employing various experimental techniques. These issues have been discussed at length in the literature.[9,16] In short, the difficulties arise from three sources.

- The first source of difficulties lies in the definitions of the NLO parameters. Eq. (2) and (3) are power series that can be written with or without explicitly including the 1/n! factors in the power expansion terms. This in itself may lead to quantities differing by a factor of 2! = 2 and 3! = 6 in the cases of second-order and third-order NLO effects, respectively. It should also be noted that the transition from Eqs (2) and (3) to frequency-dependent NLO parameters involves substituting in Eq. (1) which is often written with an additional factor of ½ in front of the field amplitude. This leads to another

factor which will be 4 and 8 in the cases of second-order and third-order processes, respectively. An uncertainty is also the question of including so-called degeneracy factors in the definition of the NLO parameters. Since NLO susceptibilities and hyperpolarizabilities are defined for a given combination of the input frequencies, degeneracy factors arise as an effect of summing over the field amplitudes of fields with the same frequency. For example, the γ used to describe the process of third-harmonic generation and that used to describe nonlinear refraction may differ by a factor of 3 depending on whether the degeneracy factor is included in the definition of γ or not. It is usually considered prudent to define the hyperpolarizabilities in such a way that they collapse to the same value as the frequencies ω_i all go to zero.

- The second important consideration is that of using the proper units system. Traditionally, the cgs system was used for molecular parameters while the SI system and mixed units systems (e.g. cm^2/W for the values of the nonlinear refractive index n_2) are more common for macroscopic nonlinear parameters. In addition to that, quantum chemists use the atomic units system for the quantities calculated theoretically and care needs to be taken when converting from those units to the experimental ones.

- The third difficulty is in comparing results of different experiments. Even if the degeneracy factors and other contentious issues are dealt with, the remaining problem is always the specificity of the experiment carried out, the frequency dependence of the parameters and the possible dependences of the parameters on factors such as the laser pulse duration See, e.g., ref. 17.

1.4 Second-Order Nonlinearities

Selected second-order nonlinearities of pyridyl, polypyridyl, and porphyrin complexes through 2004 have been summarized,[18] and a review of quadratic NLO properties of square planar d8-metal dithiolene complexes through 2008 has appeared.[19]

1.4.1 Complexes of Pyridyl or Polypyridyl Ligands

Pyridyl complexes were amongst the first inorganic complexes to be assessed for optical nonlinearity[20] and they continue to attract attention with a large number of complexes assayed for second-order properties.[21-59] The N-heterocycle is typically 4-functionalized with donor or acceptor substituents. The quadratic NLO response in N-ligated pyridyl complexes is dominated by a low-energy transition that is MLCT in nature for acceptor substituents and ILCT in character for donor groups, the metal functioning as an inductive electron acceptor for the latter.[60] Coe's group has explored the effect on quadratic nonlinearity of a variety of structural modifications in this system, and has reviewed his group's studies through 2005 of pyridyl complexes with pyridinium groups as quadratic NLO switches.[21]

Ruthenium complexes bearing a variety of co-ligand sets, namely chlorobis(diarsine),[37,38] tetra(ammine)pyridine/N-methylpyrazole,[35,38,47,48] penta(ammine),[35,42,47,48] and penta(cyano) co-ligands,[45] have been examined. Varying the quaternizing substituent in chlorobis(diarsine) complexes of 4-functionalized pyridines results in an increase in Stark spectroscopy-derived quadratic nonlinearities on proceeding from Me to Ph or pyrimidyl group (**1** to **2** or **3**).[37] Oligo(ethynyl)-connected N-methylpyridinium-functionalized pyridine complexes **6-13** afford Stark- and HRS-derived β_0 values that increase on proceeding from n = 0 to 1 and then 2, with lower absolute values than those of the analogous ethenyl-linked complexes.[38]

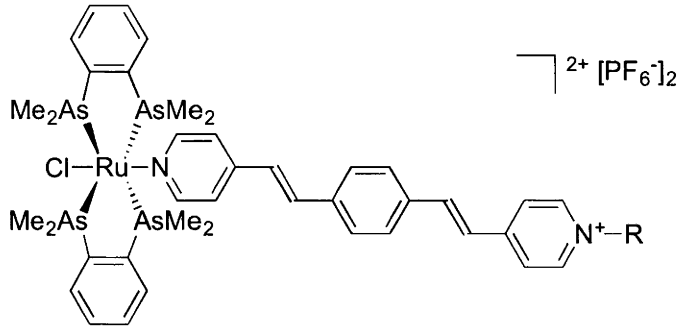

1: R = Me, β_0 (Stark) = 131 x 10^{-30} esu (PrCN)[37]

2: R = Ph, β_0 (Stark) = 203 x 10^{-30} esu (PrCN)[37]

3: R = 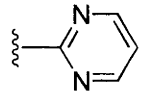 β_0 (Stark) = 200 x 10^{-30} esu (PrCN)[37]

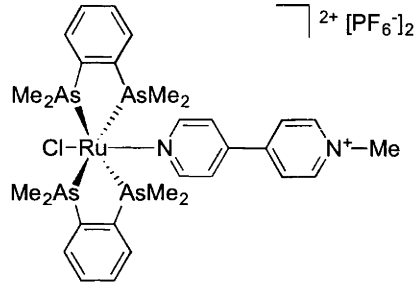

4: λ_{max} = 491 nm (PrCN), β_0 (Stark) = 113 x 10^{-30} esu (PrCN), β_0 (HRS) = 45 x 10^{-30} esu (MeCN)[38]

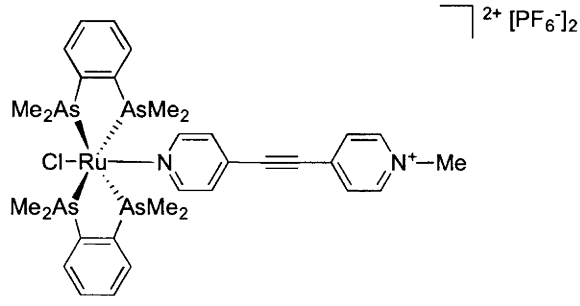

5: λ_{max} = 509 nm (PrCN), β_0 (Stark) = 146 x 10^{-30} esu (PrCN), β_0 (HRS) = 45 x 10^{-30} esu (MeCN)[38]

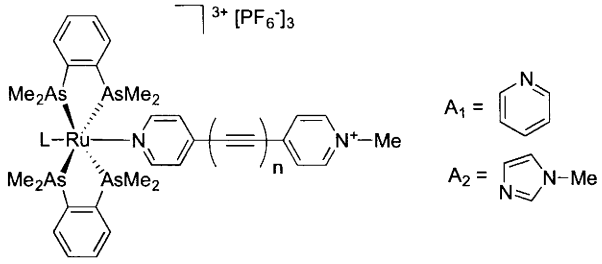

6: L = NH_3, n = 1, λ_{max} = 648 nm (PrCN), β_0 (Stark) = 216 x 10^{-30} esu (PrCN), β_0 (HRS) = 169 x 10^{-30} esu (MeCN)[38]
7: L = NH_3, n = 2, λ_{max} = 664 nm (PrCN), β_0 (Stark) = 308 x 10^{-30} esu (PrCN), β_0 (HRS) = 117 x 10^{-30} esu (MeCN)[38]
8: L = A_1, n= 1, λ_{max} = 618 nm (PrCN), β_0 (Stark) = 178 x 10^{-30} esu (PrCN), β_0 (HRS) = 78 x 10^{-30} esu (MeCN)[38]
9; L = A_1, n = 2, λ_{max} = 627 nm (PrCN), β_0 (Stark) = 331 x 10^{-30} esu (PrCN), β_0 (HRS) = 50 x 10^{-30} esu (MeCN)[38]
10: L = A_2, n= 1, λ_{max} = 661 nm (PrCN), β_0 (Stark) = 241 x 10^{-30} esu (PrCN), β_0 (HRS) = 200 x 10^{-30} esu (MeCN)[38]
11: L = A_2, n = 2, λ_{max} = 667 nm (PrCN), β_0 (Stark) = 457 x 10^{-30} esu (PrCN), β_0 (HRS) = 193 x 10^{-30} esu (MeCN)[38]

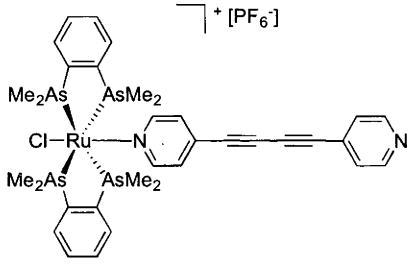

12: λ_{max} = 506 nm (PrCN)
β_0 (Stark) = 106 x 10^{-30} esu (PrCN)
β_0 (HRS) = 70 x 10^{-30} esu (MeCN)[38]

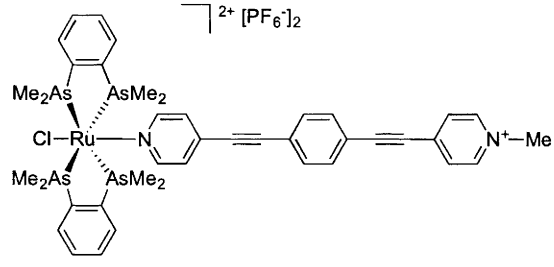

13: λ_{max} = 472 nm (PrCN)
β_0 (Stark) = 114 x 10^{-30} esu (PrCN)
β_0 (HRS) = 76 x 10^{-30} esu (MeCN)[38]

Coe and co-workers have also examined oligo(ethenyl)-connected N-methylpyridinium-functionalized pyridine complexes **14-27** in which the *trans*-disposed ligand is ammine, *N*-methylimidazole, or pyridine.[47,48] The CT bands in the visible region of these complexes are d → π* metal-to-ligand in character; these CT bands are unusual in that they blue-shift on increasing the number of ethenyl linkages. HRS- and Stark-derived frequency-independent nonlinearities β_0 are maximized at two ethenyl linkages, unlike related organic compounds for which the nonlinearity increases on *E*-ethenyl chain lengthening.

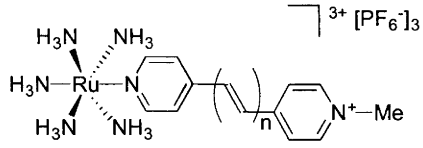

14: n = 0, λ_{max} = 646 nm (PrCN), β_0 (Stark) = 120 x 10^{-30} esu (PrCN), β_0 (HRS) = 123 x 10^{-30} esu (MeCN)[47]
15: n = 1, λ_{max} = 682 nm (PrCN), β_0 (Stark) = 175 x 10^{-30} esu (PrCN), β_0 (HRS) = 142 x 10^{-30} esu (MeCN)[47]
16: n = 2, λ_{max} = 675 nm (PrCN), β_0 (Stark) = 482 x 10^{-30} esu (PrCN), β_0 (HRS) = 372 x 10^{-30} esu (MeCN)[47]
17: n = 3, λ_{max} = 671 nm (PrCN), β_0 (Stark) = 475 x 10^{-30} esu (PrCN), β_0 (HRS) = 131 x 10^{-30} esu (MeCN)[47]

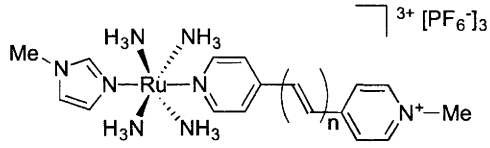

18: n = 0, λ_{max} = 660 nm (PrCN), β_0 (Stark) = 170 x 10^{-30} esu (PrCN), β_0 (HRS) = 100 x 10^{-30} esu (MeCN)[47]
19: n = 1, λ_{max} = 690 nm (PrCN), β_0 (Stark) = 256 x 10^{-30} esu (PrCN), β_0 (HRS) = 168 x 10^{-30} esu (MeCN)[47]
20: n = 2, λ_{max} = 686 nm (PrCN), β_0 (Stark) = 586 x 10^{-30} esu (PrCN), β_0 (HRS) = 237 x 10^{-30} esu (MeCN)[47]
21: n = 3, λ_{max} = 678 nm (PrCN), β_0 (Stark) = 563 x 10^{-30} esu (PrCN), β_0 (HRS) = 175 x 10^{-30} esu (MeCN)[47]

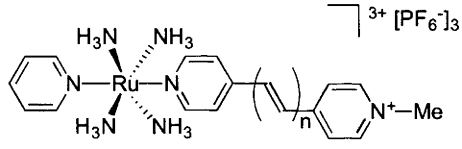

22: n = 0, λ_{max} = 611 nm (PrCN), β_0 (Stark) = 171 x 10^{-30} esu (PrCN), β_0 (HRS) = 85 x 10^{-30} esu (MeCN)[48]
23: n = 2, λ_{max} = 631 nm (PrCN), β_0 (Stark) = 514 x 10^{-30} esu (PrCN), β_0 (HRS) = 75 x 10^{-30} esu (MeCN)[48]
24: n = 3, λ_{max} = 625 nm (PrCN), β_0 (Stark) = 412 x 10^{-30} esu (PrCN), β_0 (HRS) = 43 x 10^{-30} esu (MeCN)[48]

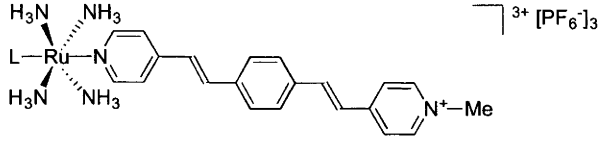

25: L = NH_3, λ_{max} = 610 nm (PrCN), β_0 (Stark) = 373 x 10^{-30} esu (PrCN), β_0 (HRS) = 19 x 10^{-30} esu (MeCN)[48]

26: L =  λ_{max} = 573 nm (PrCN), β_0 (Stark) = 343 x 10^{-30} esu (PrCN), β_0 (HRS) = 88 x 10^{-30} esu (MeCN)[48]

27: L =  λ_{max} = 610 nm (PrCN), β_0 (Stark) = 397 x 10^{-30} esu (PrCN), β_0 (HRS) = 46 x 10^{-30} esu (MeCN)[48]

Coe and co-workers have used similar complexes to demonstrate quadratic NLO "switching", the earlier solution studies[61] having been extended to the solid-state.[42] The penta(ammine)ruthenium complex **14A**, featuring an aryl-quaternized 4,4'-bipyridinium ligand, was assembled into a non-centrosymmetric multi-layer Langmuir-Blodgett film by alternately depositing the complex and arachidic acid, and the resultant film deposited onto ITO-coated glass. Oxidation reduced the SHG intensity by ca 50%, but continued redox cycling degraded the signal (Figure below).

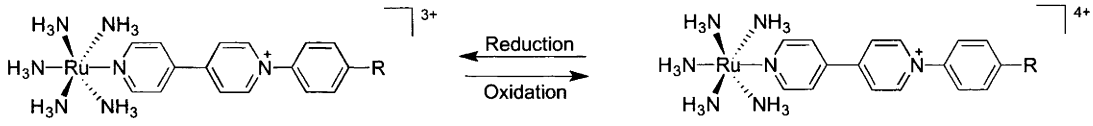

14A: R = $C_{16}H_{33}$[42]

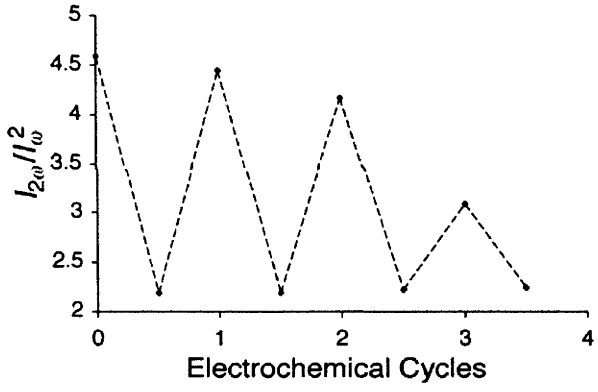

Electrochemical switching of the 532 nm SHG from an alternating LB of **14A** on ITO coated glass.[42]

The $[Fe(CN)_5]^{3-}$ center is very electron-rich, functioning as a very strong donor when coupled to N-methyl/aryl-pyridinium acceptors in donor-bridge-acceptor arrays, and affording complexes with intense and very broad MLCT transitions that are strongly solvatochromic. Stark spectroscopy suggests substantial NLO responses that increase with chromophore length.[36] Not surprisingly, comparison to analogous $[Ru(NH_3)_5]^{2+}$

complexes reveal an increase in HRS-derived nonlinearity in moving to the iron examples. Protic switching of nonlinearity was demonstrated in these complexes using both HRS and Stark spectroscopy, with a ca four-fold decrease in the magnitude of β being observed on protonation.[45]

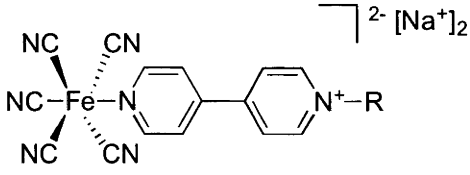

28: R = Me, λ_{max} = 534 nm (H_2O), β_0 (Stark) = 61 x 10^{-30} esu (Glycerol/H_2O, 50/50), β_0 (HRS) = 2 x 10^{-30} esu (H_2O)[45]

29: R = Ph, λ_{max} = 566 nm (H_2O), β_0 (Stark) = 88 x 10^{-30} esu (Glycerol/H_2O, 50/50), β_0 (HRS) = 22 x 10^{-30} esu (H_2O)[45]

30: R = 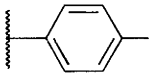 λ_{max} = 584 nm (H_2O), β_0 (Stark) = 114 x 10^{-30} esu (Glycerol/H_2O, 50/50), β_0 (HRS) = 31 x 10^{-30} esu (H_2O)[45]

31: R = 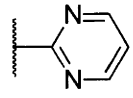 λ_{max} = 618 nm (H_2O), β_0 (Stark) = 166 x 10^{-30} esu (Glycerol/H_2O, 50/50), β_0 (HRS) = 50 x 10^{-30} esu (H_2O)[45]

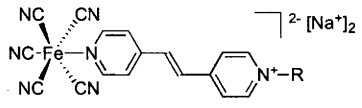

32: R = Me, λ_{max} = 538 nm (H_2O), β_0 (Stark) = 119 x 10^{-30} esu (Glycerol/H_2O, 50/50), β_0 (HRS) = 4 x 10^{-30} esu (H_2O)[45]

33: R = Ph, λ_{max} = 562 nm (H_2O), β_0 (Stark) = 174 x 10^{-30} esu (Glycerol/H_2O, 50/50), β_0 (HRS) = 22 x 10^{-30} esu (H_2O)[45]

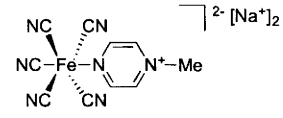

34: λ_{max} = 660 nm (H_2O), β_0 (Stark) = 45 x 10^{-30} esu (Glycerol/H_2O, 50/50), β_0 (HRS) = 165 x 10^{-30} esu (H_2O)[36]

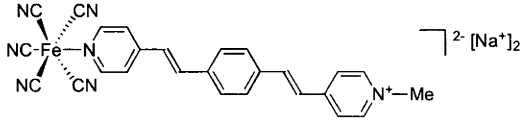

37: λ_{max} = 465 nm (H_2O), β_0 (Stark) = 56 x 10^{-30} esu (Glycerol/H_2O, 50/50), β_0 (HRS) = 228 x 10^{-30} esu (H_2O)[36]

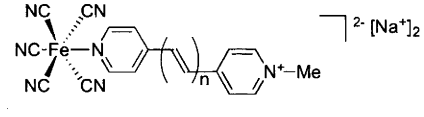

35: n = 2, λ_{max} = 520 nm (H_2O), β_0 (Stark) = 54 x 10^{-30} esu (Glycerol/H_2O, 50/50), β_0 (HRS) = 73 x 10^{-30} esu (H_2O)[36]

36: n = 3, λ_{max} = 502 nm (H_2O), β_0 (Stark) = 59 x 10^{-30} esu (Glycerol/H_2O, 50/50), β_0 (HRS) = 56 x 10^{-30} esu (H_2O)[36]

The crucial CT interaction in these complexes is along the molecular dipole. Coe's group has also extended these studies to embrace V-shaped complexes with *cis*-disposed *N*-pyridyl ligands,[30,44] the resultant complexes possessing large NLO responses with 2D character. While HRS studies suggest that β_{zzz} is the dominant tensor component, Stark measurements and FF calculations are consistent with similar or even greater contribution to the global β value from the β_{zyy} tensor component.[44]

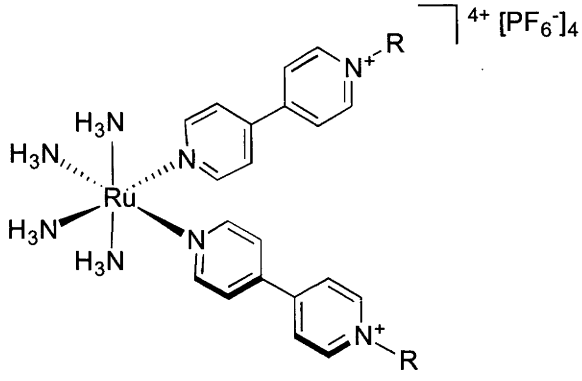

38: R = Me, λ_{max} = 628 nm (PrCN), β_0 (Stark) = 137 x 10^{-30} esu (PrCN), β_0 (HRS) = 58 x 10^{-30} esu (MeCN)[30,44]

39: R = 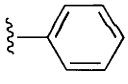 λ_{max} = 632 nm (PrCN), β_0 (Stark) = 231 x 10^{-30} esu (PrCN), β_0 (HRS) = 53 x 10^{-30} esu (MeCN)[30,44]

40:R = 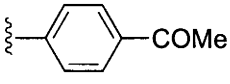

λ_{max} = 684 nm (PrCN), β_0 (Stark) = 248 x 10^{-30} esu (PrCN), β_0 (HRS) = 59 x 10^{-30} esu (MeCN)[30,44]

41: R = 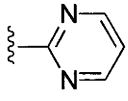

λ_{max} = 731 nm (PrCN), β_0 (Stark) = 298 x 10^{-30} esu (PrCN), β_0 (HRS) = 59 x 10^{-30} esu (MeCN)[30,44]

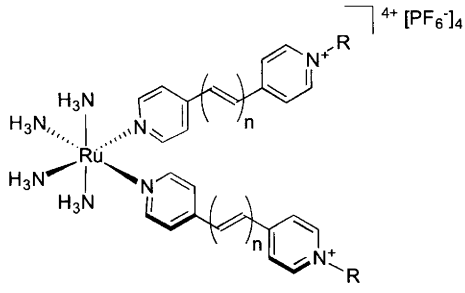

42: n = 1, R = Me, λ_{max} = 719 nm (PrCN), β_0 (Stark) = 155 x 10^{-30} esu (PrCN), β_0 (HRS) = 121 x 10^{-30} esu (MeCN)[44]
43: n = 1, R = Ph, λ_{max} = 763 nm (PrCN), β_0 (Stark) = 213 x 10^{-30} esu (PrCN), β_0 (HRS) = 92 x 10^{-30} esu (MeCN)[44]
44: n = 1, R =  λ_{max} = 822 nm (PrCN), β_0 (Stark) = 302 x 10^{-30} esu (PrCN), β_0 (HRS) = 160 x 10^{-30} esu (MeCN)[44]
45: n = 2, R = Me, λ_{max} = 718 nm (PrCN), β_0 (Stark) = 202 x 10^{-30} esu (PrCN), β_0 (HRS) = 184 x 10^{-30} esu (MeCN)[44]
46: n = 2, R = Ph, λ_{max} = 755 nm (PrCN), β_0 (Stark) = 233 x 10^{-30} esu (PrCN), β_0 (HRS) = 374 x 10^{-30} esu (MeCN)[44]
47: n = 3, R = Me, λ_{max} = 717 nm (PrCN), β_0 (Stark) = 583 x 10^{-30} esu (PrCN), β_0 (HRS) = 164 x 10^{-30} esu (MeCN)[44]

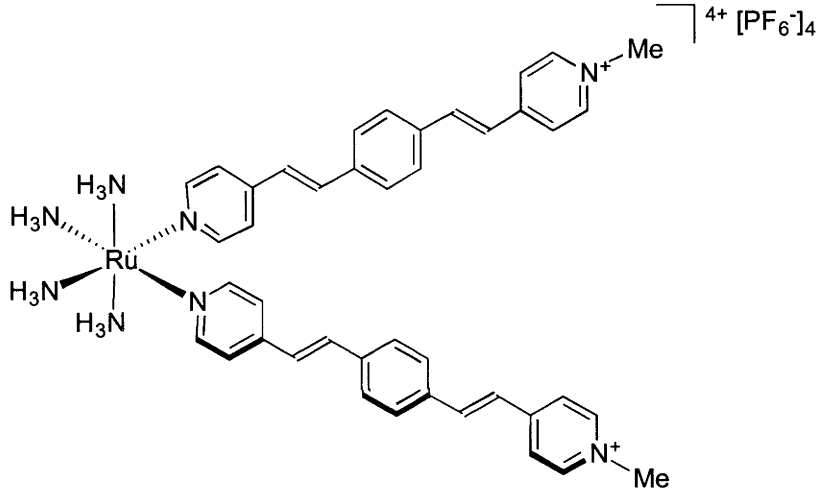

48: λ_{max} = 652 nm (PrCN), β_0 (Stark) = 545 x 10^{-30} esu (PrCN),
β_0 (HRS) = 440 x 10^{-30} esu (MeCN)[44]

Coe has also explored an alternative 2D approach, employing pyrazinyl-4,4'-bipyridinium bridges to link multiple ruthenium centers.[35] Depolarization ratios from HRS studies at 1064 nm are consistent with dominant off-diagonal β_{zyy} components contributing strongly to 2D NLO responses in these complexes.

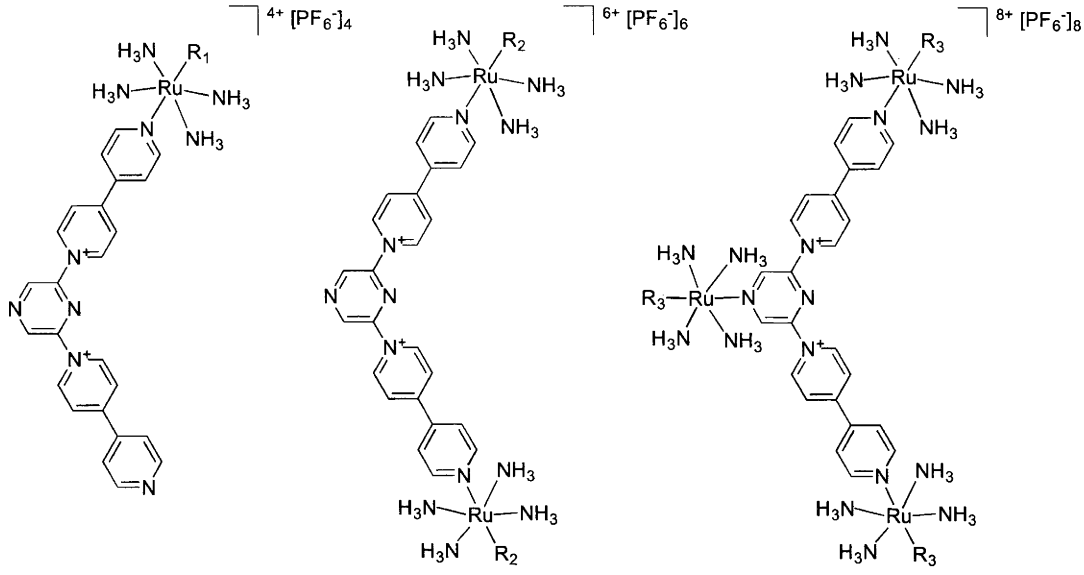

49: $R_1 = NH_3$, λ_{max} = 707nm (MeCN), β_0 (Stark) = 252 x 10^{-30} esu (PrCN), β_0 (HRS) = 257 x 10^{-30} esu (MeCN)[35]

50: R_1 = λ_{max} = 675 nm (MeCN), β_0 (Stark) = 259 x 10^{-30} esu (PrCN), β_0 (HRS) = 200 x 10^{-30} esu (MeCN)[35]

51: $R_2 = NH_3$, λ_{max} = 713 nm (MeCN), β_0 (Stark) = 662 x 10^{-30} esu (PrCN), β_0 (HRS) = 336 x 10^{-30} esu (MeCN)[35]

52: R_2 = λ_{max} = 674 nm (MeCN), β_0 (Stark) = 816 x 10^{-30} esu (PrCN), β_0 (HRS) = 326 x 10^{-30} esu (MeCN)[35]

53: $R_3 = NH_3$, λ_{max} = 711 nm (MeCN), β_0 (HRS) = 261 x 10^{-30} esu (MeCN)[35]

54: R_3 = λ_{max} = 665 nm (MeCN), β_0 (HRS) = 309 x 10^{-30} esu (MeCN)[35]

Co-ligand variation in zinc complexes has been examined,[23] the EFISH-derived quadratic nonlinearity at 1.91 μm increasing on replacing acetate by triflate (proceeding from **55** to **56**); this is accompanied by an increase in dipole moment and a red-shift of the ILCT transition for this structural modification. Dilution of solutions of the triflate complexes results in significant increases in nonlinearity, an effect explained by solvolysis of the triflate anion and concomitant strong ion-pairing.

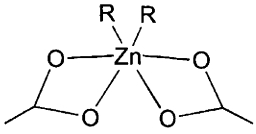

55: λ_{max} = 406 nm ($CHCl_3$), $\beta_{1.91}$(EFISH) = 101 x 10^{-30} cm^5 esu ($CHCl_3$)[23]

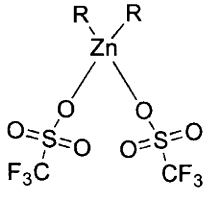

56: λ_{max} = 519 nm ($CHCl_3$), $\beta_{1.91}$ (EFISH) = 261 x 10^{-30} cm^5 esu ($CHCl_3$)[23]

R = 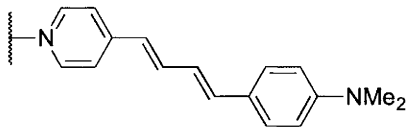

Ruthenium polypyridyl complexes have attracted attention for their NLO properties; their quadratic nonlinearities are associated with ILCT bands that are red-shifted on complexation of the free ligand,[60] and directionally opposed to MLCT transitions. Earlier studies had functionalized the bipy ligands with electron donating groups, so in order for MLCT effects to dominate nonlinearity, Coe *et al.* employed 4,4'-disubstituted bipy ligands with electron-withdrawing pyridinium groups, the Ru^{II} examples revealing larger β coefficients that their Fe^{II} analogues.[43,46]

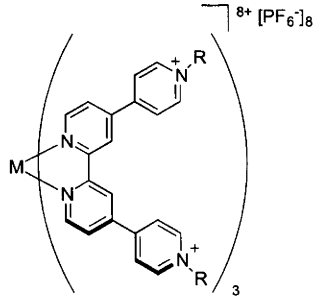

57: M= Ru, R= Me, λ_{max} = 576nm (PrCN), β_0 (Stark) = 41 x 10^{-30} esu (PrCN), β_{800}(HRS) = 170 x 10^{-30} esu (MeCN)[46]

58: M= Ru, R= Ph, λ_{max} = 589 nm (PrCN), β_0 (Stark) = 76 x 10^{-30} esu (PrCN), β_{800} (HRS) = 270 x 10^{-30} esu (MeCN)[46]

59: M= Ru, R= 4-AcC_6H_4, λ_{max} = 594nm (PrCN), β_0 (Stark) = 44 x 10^{-30} esu (PrCN), β_{800} (HRS) = 281 x 10^{-30} esu (MeCN)[46]

]

60: M= Fe, R= Me, λ_{max} = 581 nm (PrCN), β_0 (Stark) = 56 x 10^{-30} esu (PrCN), β_{800} (HRS) = 78 x 10^{-30} esu (MeCN)[46]

61: M= Fe, R= Ph, λ_{max} = 590 nm (PrCN), β_0 (Stark) = 82 x 10^{-30} esu (PrCN), β_{800} (HRS) = 80 x 10^{-30} esu (MeCN)[46]

62: M= Fe, R= 4-AcC_6H_4, λ_{max} = 596 nm (PrCN), β_0 (Stark) = 112 x 10^{-30} esu (PrCN), β_{800} (HRS) = 110 x 10^{-30} esu (MeCN)[46]

63: M = Ru, R = 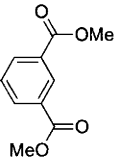

λ_{max} = 593 nm (PrCN), β_0 (Stark) = 56 x 10^{-30} esu (PrCN), β_{800} (HRS) = 290 x 10^{-30} esu (MeCN)[46]

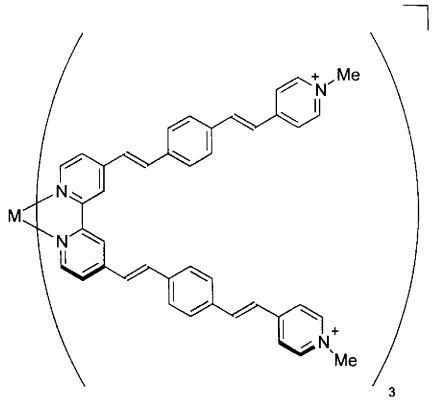

64: M = Ru, λ_{max} = 573 nm (PrCN), β_0 (Stark) = 393 x 10^{-30} esu (PrCN), β_{1064} (HRS) = 5600 x 10^{-30} esu (MeCN)[43]

65: M = Fe, λ_{max} = 604 nm (PrCN), β_0 (Stark) = 259 x 10^{-30} esu (PrCN), β_{1064} (HRS) = 700 x 10^{-30} esu (MeCN)[43]

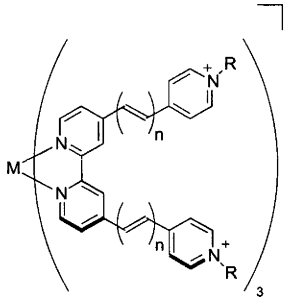

66: n = 1, M = Ru, R = Me, λ_{max} = 574 nm (PrCN), β_0 (Stark) = 98 x 10^{-30} esu (PrCN), β_{1064} (HRS) = 850 x 10^{-30} esu (MeCN)[43]

67: n = 1, M = Ru, R = Ph, λ_{max} = 566 nm (PrCN), β_0 (Stark) = 181 x 10^{-30} esu (PrCN), β_{1064} (HRS) = 1200 x 10^{-30} esu (MeCN)[43]

68: n = 2, M = Ru, R = Me, λ_{max} = 582 nm (PrCN), β_0 (Stark) = 217 x 10^{-30} esu (PrCN), β_{1064} (HRS) = 3100 x 10^{-30} esu (MeCN)[43]

69: n = 1, M = Fe, R = Me, λ_{max} = 614 nm (PrCN), β_0 (Stark) = 91 x 10^{-30} esu (PrCN), β_{1064} (HRS) = 275 x 10^{-30} esu (MeCN)[43]

70: n = 1, M = Fe, R = Ph, λ_{max} = 623 nm (PrCN), β_0 (Stark) = 201 x 10^{-30} esu (PrCN), β_{1064} (HRS) = 480 x 10^{-30} esu (MeCN)[43]

71: n = 2, M = Fe, R = Me, λ_{max} = 620 nm (PrCN), β_0 (Stark) = 217 x 10^{-30} esu (PrCN), β_{1064} (HRS) = 340 x 10^{-30} esu (MeCN)[43]

72: n = 1, M = Fe, R = 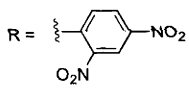

λ_{max} = 633 nm (PrCN), β_0 (Stark) = 180 x 10^{-30} esu (PrCN), β_{1064} (HRS) = 400 x 10^{-30} esu (MeCN)[43]

A similar strategy was employed by Mayer and co-workers[39] – elaboration of bipy and terpy ligands with 4-(4-*N*,*N*-dimethylaminostyryl)-1-methylpyridinium (DASP) moieties was explored because of the significant bulk susceptibility of this organic cation as its tosylate salt.[62] The quadratic nonlinearities for the Ru-containing complexes were discussed as a superposition of β_{DASP}, β_{ICT}, and $\beta_{d-\pi^*}$, where the latter two may be either positive or negative compared to β_{DASP}, while the Zn(II) complex performance was explained by competing contributions of β_{DASP} and β_{ICT}.

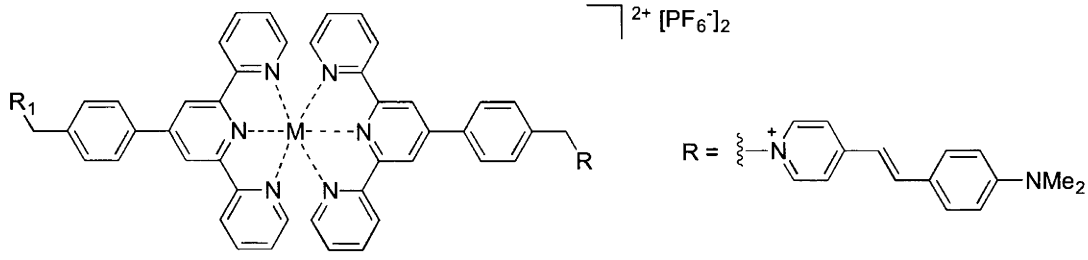

73: M = Ru, R_1 = R, λ_{max} = 493 nm (MeCN), β_{1640} (HRS) = 630 x 10^{-30} esu (MeCN)[39]
74: M = Zn, R_1 = R, λ_{max} = 487 nm (MeCN), β_{1640} (HRS) = 370 x 10^{-30} esu (MeCN)[39]
75: M = Ru, R_1 = NMe, λ_{max} = 500 nm (MeCN), β_{1640} (HRS) = 340 x 10^{-30} esu (MeCN)[39]

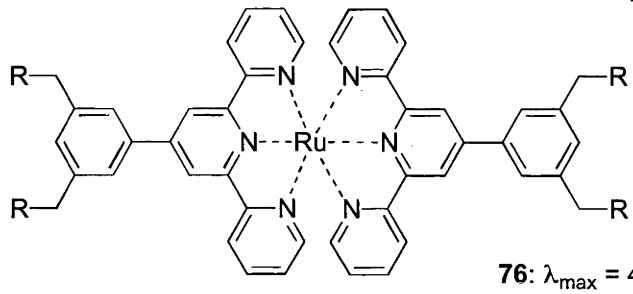

76: λ_{max} = 494 nm (MeCN),
β_{1640} (HRS) = 610 x 10^{-30} esu (MeCN)[39]

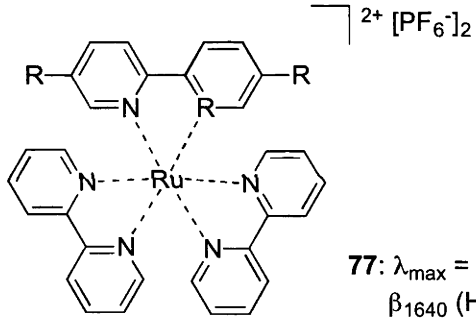

77: λ_{max} = 495 nm (MeCN),
β_{1640} (HRS) = 750 x 10^{-30} esu (MeCN)[39]

Le Bozec and co-workers have functionalized 4,4'-bis(dialkylaminostyryl)-[2,2']-bipyridines and incorporated them into the main chain of a polyimide, and used the resultant assembly to construct octupolar tris(bipyridine)ruthenium-containing macromolecules that exhibit intense linear absorption in the visible region, long-lived luminescence, and quadratic nonlinearities at 1.91 μm consistent with octupolar ordering in the metallodendrimer.[49,51,52]

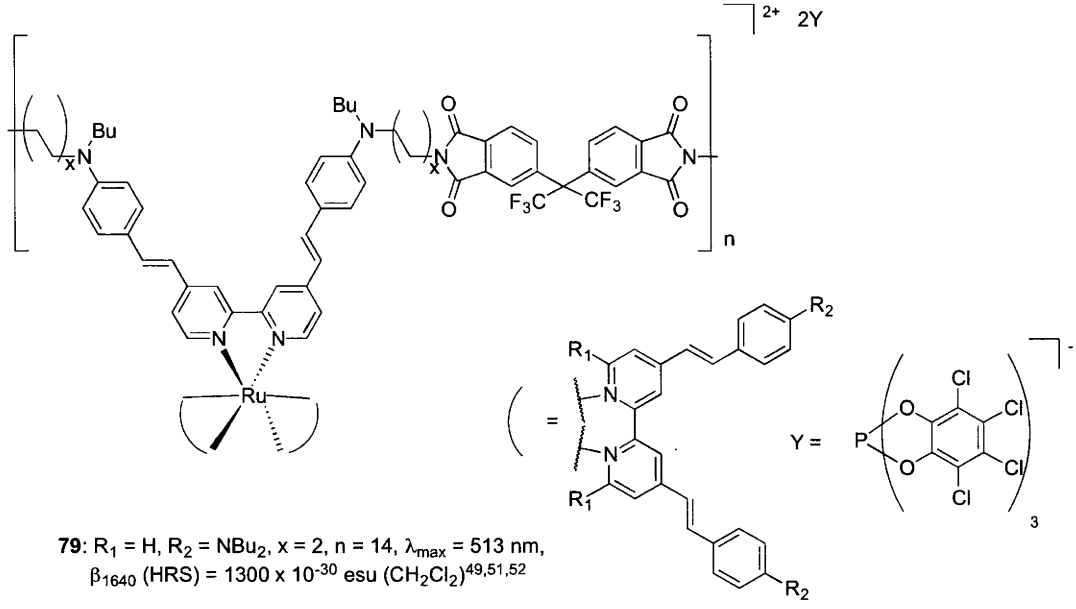

79: R_1 = H, R_2 = NBu_2, x = 2, n = 14, λ_{max} = 513 nm, β_{1640} (HRS) = 1300 x 10^{-30} esu (CH_2Cl_2)[49,51,52]

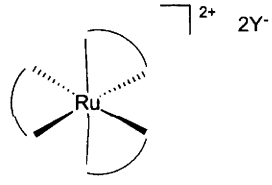

78: R^1 = H, R^2 = NEt_2, λ_{max} = 520 nm (CH_2Cl_2), β_{1640} (HRS) = 320 x 10^{-30} esu (CH_2Cl_2)[49,51,52]

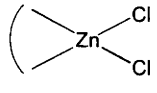

80: R_1 = H, R_2 = NBu_2, λ_{max} = 459 nm ($CHCl_3$), β_0 (EFISH) = 62 x 10^{-30} esu ($CHCl_3$)[50]

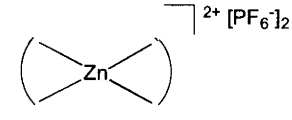

81: R_1 = Me, R_2 = NBu_2, λ_{max} = 529 nm (CH_2Cl_2), β_0 (HRS) = 157 x 10^{-30} esu (CH_2Cl_2)[50]

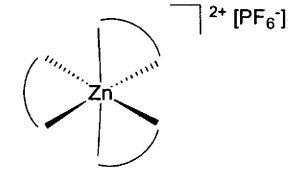

82: R_1 = H, R_2 = NBu_2, λ_{max} = 466 nm (CH_2Cl_2), β_0 (HRS) = 241 x 10^{-30} esu (CH_2Cl_2)[50]

Le Bozec and co-workers have used the Zn(II) center as a template to assemble functionalized bipy ligands in dipolar and octupolar arrangements (the latter both D_{2d} and D_3).[50] The UV-vis spectra are dominated by ILCT bands that are red-shifted

from that of the free ligand. Both octupolar complexes are more quadratic NLO-efficient than the dipolar example, even after scaling for the number of bipy ligands.

Similar Zn(II) complexation of functionalized bipy ligands has been employed to demonstrate photoswitching of quadratic NLO properties.[22] The continuous π-conjugation of the bridge connecting the donor dialkylamino group to the metal-bound pyridyl acceptor exhibited when the dithienylperfluorocyclopentene unit is in the "closed" state is broken on photoisomerization to the "open" form. This structural change is accompanied by dramatic changes in both the linear optical properties (loss of an absorption band centered at 690 nm) and an order of magnitude decrease in the $\mu\beta_0$ product evaluated by EFISH at 1.907 μm.

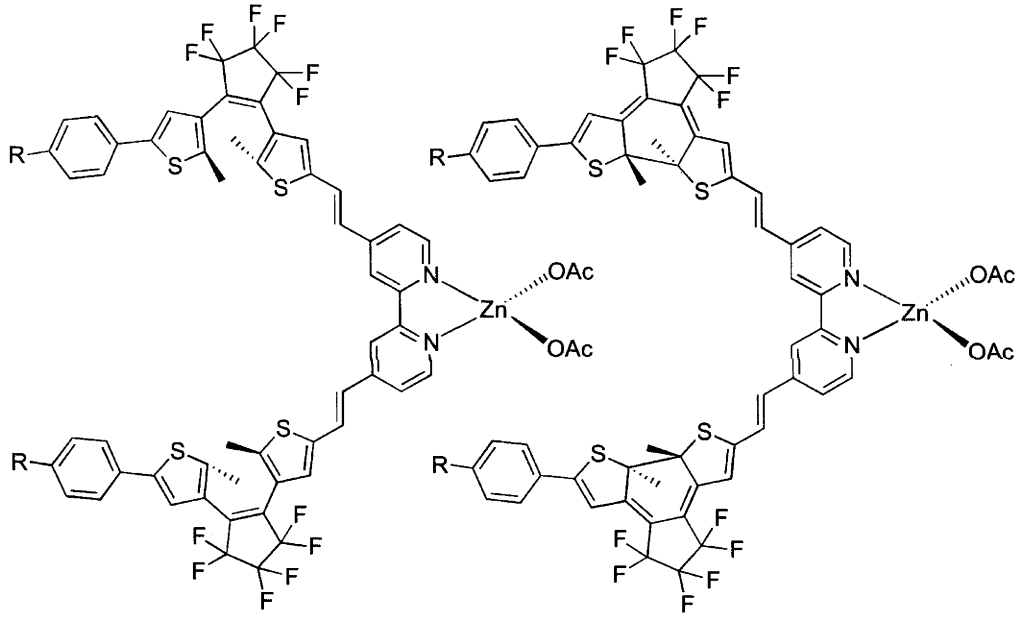

83: R = H, λ_{max} = 357 nm (CH_2Cl_2),
$\mu\beta_0$ (EFISH) = 75 x 10^{-48} esu (CH_2Cl_2)[22]

84: R = NMe_2, λ_{max} = 360 nm (CH_2Cl_2),
$\mu\beta_0$ (EFISH) = 160 x 10^{-48} esu (CH_2Cl_2)[22]

85: R = H, λ_{max} = 357 nm (CH_2Cl_2),
$\mu\beta_0$ (EFISH) = 1020 x 10^{-48} esu (CH_2Cl_2)[22]

86: R = NMe_2, λ_{max} = 360 nm (CH_2Cl_2),
$\mu\beta_0$ (EFISH) = 1800 x 10^{-48} esu (CH_2Cl_2)[22]

Coordination of 4'-donor or –acceptor functionalized 2,2':6',2"-terpy ligands to Ru(III), Ir(III) and Zn(II) centers significantly increases the absolute value of the quadratic nonlinearity of the terpy.[26,40] In addition to ILCT bands, which for all complexes are red-shifted from those of the free ligands, crucial charge-transfer transitions are seen that are LMCT (Ru(III)) and MLCT (Ir(III)) in character. Quadratic nonlinearities of these complexes are strongly dependent on the nature of these CT transitions, and can be modified significantly by π-ligand and co-ligand variation.

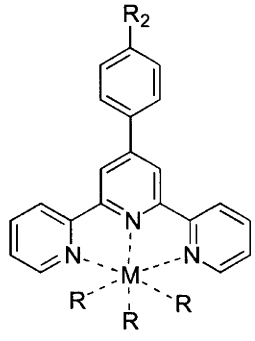

87: M = Ir, R = Cl, R_2 = NBu_2, λ_{max} = 465 nm ($CHCl_3$), $\beta_{1.34}$ (EFISH) = -109 x 10^{-30} esu ($CHCl_3$)[26,40]

88: M = Ru, R = CF_3CO_2, R_2 = NBu_2, λ_{max} = 416 nm ($CHCl_3$), $\beta_{1.34}$ (EFISH) = -70 x 10^{-30} esu ($CHCl_3$)[26,40]

89: M = Ir, R = 4-$EtC_6H_4CO_2$, R_2 = NBu_2 λ_{max} = 463 nm ($CHCl_3$), $\beta_{1.34}$ (EFISH) = -64 x 10^{-30} esu ($CHCl_3$)[26,40]

90: M = Ir, R = Cl, R_2 = A_1 λ_{max} = 476 nm ($CHCl_3$), $\beta_{1.34}$ (EFISH) = -30 x 10^{-30} esu ($CHCl_3$)[26,40]

91: M = Ir, R = 4-$EtC_6H_4CO_2$, R_2 = NO_2 λ_{max} = 413 nm ($CHCl_3$), $\beta_{1.34}$ (EFISH) = -230 x 10^{-30} esu ($CHCl_3$)[26,40]

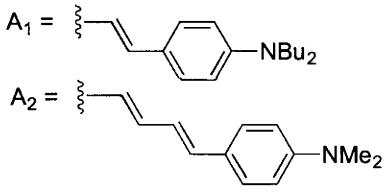

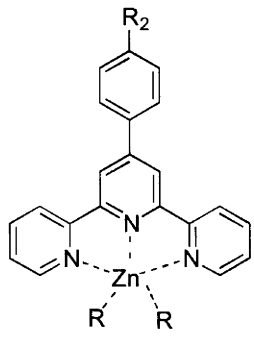

92: R = Cl, R_2 = NBu_2, λ_{max} = 425 nm ($CHCl_3$), $\beta_{1.34}$ (EFISH) = 67 x 10^{-30} esu ($CHCl_3$)[26,40]

93: R = CF_3CO_2,R_2 = NBu_2, λ_{max} = 427 nm ($CHCl_3$), $\beta_{1.34}$ (EFISH) = 88 x 10^{-30} esu ($CHCl_3$)[26,40]

94: R = CF_3CO_2, R_2 = A_1, λ_{max} = 454 nm ($CHCl_3$), $\beta_{1.34}$ (EFISH) = 181 x 10^{-30} esu ($CHCl_3$)[26,40]

95: R = CF_3CO_2, R_2 = A_2, λ_{max} = 444 nm ($CHCl_3$), $\beta_{1.34}$ (EFISH) = 137 x 10^{-30} esu ($CHCl_3$)[26,40]

Iridium complexes of substituted phenanthrolines show significant second-order nonlinearity that is a function of the acceptor strength of the phenathroline

substituent, rather than the nature of the cyclometalated co-ligands.[24,28,41] The important CT process that controls the magnitude of the nonlinearity is MLCT in character. Nonlinearities for salts of weakly interacting counter-ions (e.g. PF_6^-) are dependent on concentration, whereas those for salts of ions that ion-pair (e.g. $C_{12}H_{25}SO_3^-$, I^-) are lower and independent of concentration, an outcome likely to result from perturbation of the LUMO π^* levels of the phenanthroline in the former case.

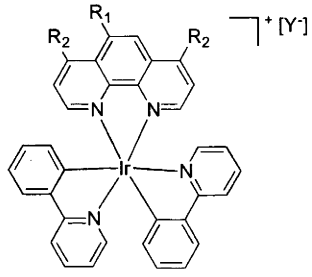

96: R_1 = Me, R_2 = H, Y = PF_6, λ_{max} = 377 nm (CH_2Cl_2), $\mu\beta_{1.907}$ (EFISH) = -1565 x 10^{-30} D cm^5 esu^{-1} (CH_2Cl_2)[24,28,41]
97: R_1 = Me, R_2 = H, Y = $C_{12}H_{25}SO_3$, λ_{max} = 376 nm (CH_2Cl_2), $\mu\beta_{1.907}$ (EFISH) = -1350 x 10^{-30} D cm^5 esu^{-1} (CH_2Cl_2)[24,28,41]
98: R_1 = NO_2, R_2 = H, Y = PF_6, λ_{max} = 378 nm (CH_2Cl_2), $\mu\beta_{1.907}$ (EFISH) = -2230 x 10^{-30} D cm^5 esu^{-1} (CH_2Cl_2)[24,28,41]
99: R_1 = NO_2, R_2 = H, Y = $C_{12}H_{25}SO_3$, λ_{max} = 378 nm (CH_2Cl_2), $\mu\beta_{1.907}$ (EFISH) = -1430 x 10^{-30} D cm^5 esu^{-1} (CH_2Cl_2)[24,28,41]
100: R_1 = H, R_2 = H, Y = PF_6, λ_{max} = 377 nm (CH_2Cl_2), $\mu\beta_{1.907}$ (EFISH) = -1270 x 10^{-30} D cm^5 esu^{-1} (CH_2Cl_2)[24,28,41]
101: R_1 = NMe_2, R_2 = H, Y = PF_6, λ_{max} = 334 nm (CH_2Cl_2), $\mu\beta_{1.907}$ (EFISH) = -1330 x 10^{-30} D cm^5 esu^{-1} (CH_2Cl_2)[24,28,41]
102: R_1 = H, R_2 = Me, Y = PF_6, λ_{max} = 375 nm (CH_2Cl_2), $\mu\beta_{1.907}$ (EFISH) = -1454 x 10^{-30} D cm^5 esu^{-1} (CH_2Cl_2)[24,28,41]
103: R_1 = H, R_2 = Ph, Y = PF_6, λ_{max} = 385 nm (CH_2Cl_2), $\mu\beta_{1.907}$ (EFISH) = -1997 x 10^{-30} D cm^5 esu^{-1} (CH_2Cl_2)[24,28,41]

A major problem in converting significant molecular quadratic nonlinearity into appreciable bulk susceptibility is the proclivity of dipoles to align in an antiparallel fashion. Réau and co-workers exploited the trans-effect at palladium to assemble pyridylphosphole ligands and construct a bis(dipole). The resultant complexes exhibit nonlinearities greater than twice those of the constituent pyridylphospholes.[25]

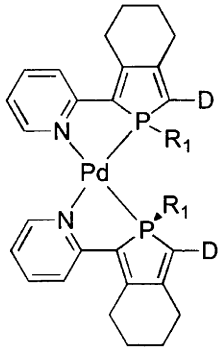

R_1 = C_6H_5, D = 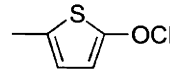 **104**: λ_{max} = 420 nm (CH_2Cl_2), $\beta_{1.91}$ (HRS) = 170 x 10^{-30} esu (CH_2Cl_2)[25]

R_1 = C_6H_5, D = 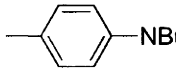 **105**: λ_{max} = 452 nm (CH_2Cl_2), $\beta_{1.91}$ (HRS) = 180 x 10^{-30} esu (CH_2Cl_2)[25]

1.4.2 Complexes of Porphyrins and Related Ligands

The quadratic nonlinearities of complexes with phthalocyanines and porphyrins has been an active area of research[63-96], with phthalocyanines (through 2002)[97] and porphyrins and related ligands (through 2005)[98] summarized. Therien and co-workers have explored 5-donor-15-acceptor-functionalized porphyrins incorporating solubilizing substituents at the 10- and 20-positions.[67,80,83] Varying the chain length of two series of nitro-functionalized oligo(thienyl) groups afforded complexes with essentially identical linear optical properties for each bridge type, but with very different NLO behavior. Nonlinearities of these complexes at the telecommunications wavelength of 1300 nm are exceptionally large.[83] These studies were extended to include carbazolylthiophenyl-containing donor groups and thiazolyl- or dicyanovinyl-containing acceptor groups. The energies and oscillator strengths of the low-energy Q-bands are very similar across these complexes, but the nonlinearities are not, a result ascribed to transfer of oscillator strength between overlapping π-π^* and CT transitions in the low-energy transition manifold. One expected outcome is the increase in nonlinearity observed on decreasing the aromatic stabilization energy of these substituents (proceeding from **106** to **116-119**).[80] Similar donor-porphyrin-acceptor complexes **111** and **112** have been used by Clays and Anderson and their co-workers as dyes for SHG imaging.[67]

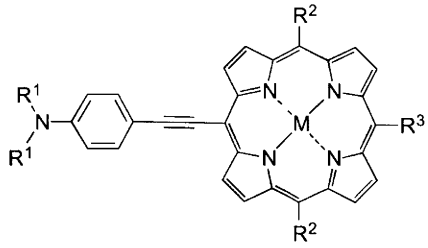

A =

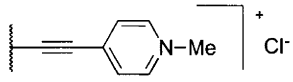

D =

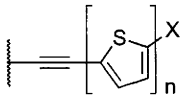

E =

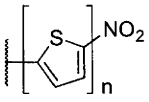

G =

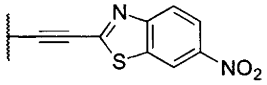

J =

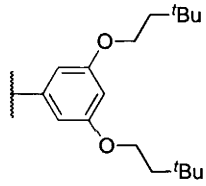

L =

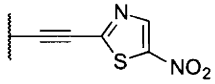

Q =

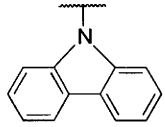

106: M = Zn, R^1 = Me, R^2 = J, R^3 = D (X = NO_2, n = 1)
λ_{max} = 685 nm (THF), $\beta_{1.3}$ (HRS) = 690 x 10^{-30} esu (THF)[83]

107: M = Zn, R^1 = Me, R^2 = J, R^3 = D (X = NO_2, n = 2)
λ_{max} = 683 nm (THF), $\beta_{1.3}$ (HRS) = 674 x 10^{-30} esu (THF)[83]

108: M = Zn, R^1 = Me, R^2 = J, R^3 = D (X = NO_2, n = 3)
λ_{max} = 683 nm (THF), $\beta_{1.3}$ (HRS) = 1170 x 10^{-30} esu (THF)[83]

109: M = Zn, R^1 = Me, R^2 = J, R^3 = D (X = CHO, n = 1)
λ_{max} = 676 nm (THF), $\beta_{1.3}$ (HRS) = 1020 x 10^{-30} esu (THF)[80]

110: M = Zn, R^1 = Me, R^2 = J, R^3 = D (X = $CH=C(CN)_2$, n = 1)
λ_{max} = 698 nm (THF), $\beta_{1.3}$ (HRS) = 785 x 10^{-30} esu (THF)[80]

111: M = Cu, R^1 = $-CH_2(CH_2)_6$-Me, R^2 = Ph, R^3 = A
λ_{max} = n.a., $\beta_{0.84}$ (HRS) = 4000 x 10^{-30} esu (CH_2Cl_2)[67]

112: M = Ni, R^1 = $-CH_2(CH_2)_6$-Me , R^2 = Ph, R^3 = A
λ_{max} = n.a., $\beta_{0.84}$ (HRS) = 612 x 10^{-30} esu (CH_2Cl_2)[67]

113: M = Zn, R^1 = Me, R^2 = J, R^3 = E (n = 1)
λ_{max} = 640 nm (THF), $\beta_{1.3}$ (HRS) = 2400 x 10^{-30} esu (THF)[83]

114: M = Zn, R^1 = Me, R^2 = J, R^3 = E (n = 2)
λ_{max} = 641 nm (THF), $\beta_{1.3}$ (HRS) = 2200 x 10^{-30} esu (THF)[83]

115: M = Zn, R^1 = Me, R^2 = J, R^3 = E (n = 3)
λ_{max} = 641 nm (THF), $\beta_{1.3}$ (HRS) =4350 x 10^{-30} esu (THF)[83]

116: M = Zn, R^1 = Me, R^2 = J, R^3 = G
λ_{max} = 686 nm (THF), $\beta_{1.3}$ (HRS) = 1140 x 10^{-30} esu (THF)[80]

117: M = Zn, R^1 = Me, R^2 = J, R^3 = L
λ_{max} = 694 nm (THF), $\beta_{1.3}$ (HRS) = 1000 x 10^{-30} esu (THF)[80]

118: M = Zn, R^1 = O, R^2 = J, R^3 = D (X = NPh_2, n = 1)
λ_{max} = 674 nm (THF), $\beta_{1.3}$ (HRS) = 810 x 10^{-30} esu (THF)[80]

119: M = Zn, R^1 = O, R^2 = J, R^3 = D (X = Q, n = 1)
λ_{max} = 665 nm (THF), $\beta_{1.3}$ (HRS) = 1400 x 10^{-30} esu (THF)[80]

Coupling (terpyridyl)metal centers as donor groups to zinc(porphyrin) bridges affords complexes **120/121** with exceptionally large nonlinearities at 1064 nm, with a further doubling of response on introduction of nitrophenylethynyl acceptor units at the *meso* site (proceeding to **122/123**).[94] Replacing the classical organic acceptor with a bis(terpyridyl)metal group (proceeding to **124**) results in retention of the large quadratic nonlinearity. The (terpyridyl)metal center is a potent donor group, and

significantly more stable than the extensively exploited dialkylamino or diarylamino groups in conventional organic chromophores.

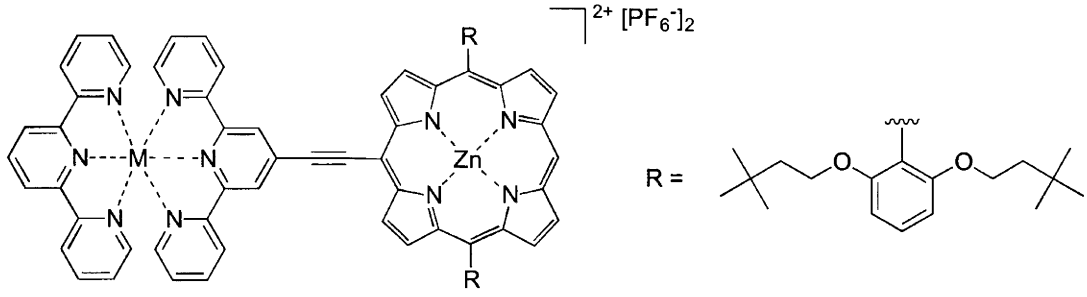

120: M = Ru, λ_{max} = 639 nm (CH_2Cl_2), $\beta_{1.064}$ (HRS) = 2100 x 10^{-30} esu (CH_2Cl_2)[94]
121: M = Os, λ_{max} = 675 nm (CH_2Cl_2), $\beta_{1.064}$ (HRS) = 2600 x 10^{-30} esu (CH_2Cl_2)[94]

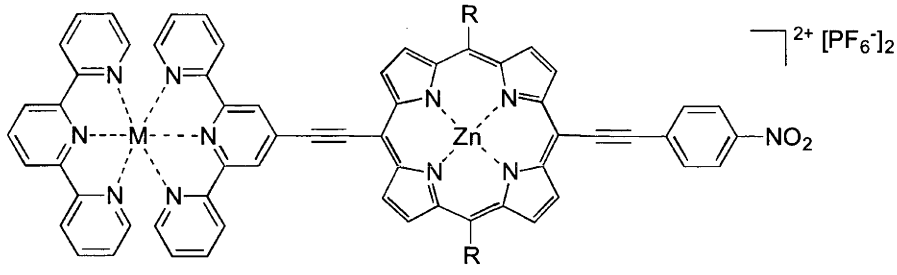

122: M = Ru, λ_{max} = 625 nm (CH_2Cl_2), $\beta_{1.064}$ (HRS) = 4000 x 10^{-30} esu (CH_2Cl_2)[94]
123:M = Os, λ_{max} = 702 nm (CH_2Cl_2), $\beta_{1.064}$ (HRS) = 5000 x 10^{-30} esu (CH_2Cl_2)[94]

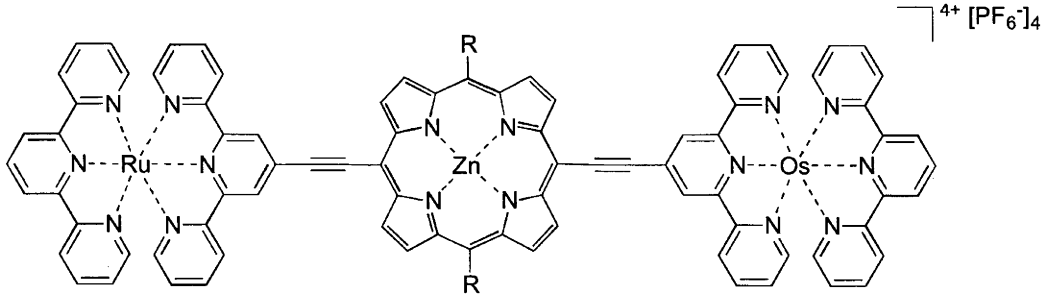

124: λ_{max} = 715 nm (CH_2Cl_2), $\beta_{1.064}$ (HRS) = 4500 x 10^{-30} esu (CH_2Cl_2)[94]

Linked porphyrin dimers have been the subject of earlier studies,[98] and it is therefore not surprising that *meso,meso*-linked corrole dimers have also attracted interest.[76] While the HRS-derived quadratic nonlinearities at 1064 nm for the dimers **127** and **128** are larger than those of the corresponding monomers **125** and **126**, reflecting the increased size of the π-system, the values are low, consistent with the lack of

strongly polarizing donor or acceptor substituents and orthogonality of the rings. Chandrashekar and co-workers have conjugated an expanded form of the corrole unit with the ferrocenyl group, the nonlinearities of the resultant adducts being dependent on the nature of the spacer group; the absolute values are again modest, and again consistent with the orthogonality of the appended group.[85]

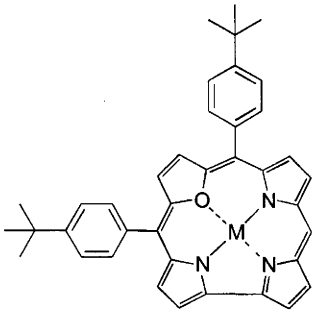

125: M = Cu, λ_{max} = 750 nm (CH_2Cl_2), $\beta_{1.064}$ (HRS) = 18 x 10^{-30} esu (CH_2Cl_2)[76]

126: M = Ni, λ_{max} = 750 nm (CH_2Cl_2), $\beta_{1.064}$ (HRS) = 13 x 10^{-30} esu (CH_2Cl_2)[76]

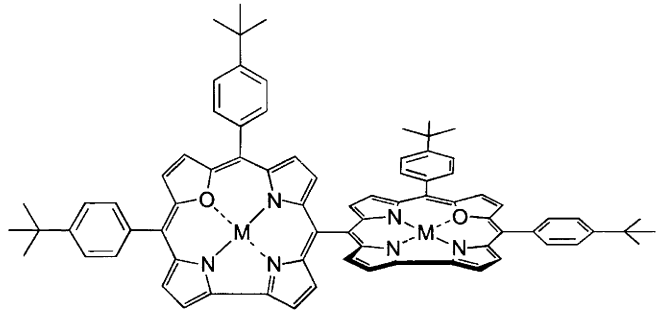

127: M = Cu, λ_{max} = 750 nm (CH_2Cl_2), $\beta_{1.064}$ (HRS) = 32 x 10^{-30} esu (CH_2Cl_2)[76]

128: M = Ni, λ_{max} = 750 nm (CH_2Cl_2), $\beta_{1.064}$ (HRS) = 43 x 10^{-30} esu (CH_2Cl_2)[76]

1.4.3 Schiff Base Complexes

The quadratic nonlinearities of bis(salicylaldiminato)metal Schiff base complexes have been an active area of research[99-118], and have been reviewed through 1999,[119] with interest stemming from the flexibility of their composition (and in particular the facile incorporation of open shell as well as closed shell metals), ease of derivatization, their enforced planarity with square planar-coordinating metals, and their comparative robustness. Coordination of *N*-diethylaminosalicylidene-*N'*-4-nitrobenzoylhydrazine (to form, for example, **129** or **130**) tautomerizes this ligand from the free keto form to the complexed enol form, and thereby completes the conjugation from the dialkylamino donor to the nitro acceptor, the resultant complexes showing appreciable EFISH-derived $\mu\beta_{vec}$ products at 1.907 μm; it is

therefore an example of complexation "switching on" nonlinearity. The complexes are prepared as dimeric aggregates, but on heating **131** in refluxing pyridine, the monomer **133** is formed, with a concomitant doubling of the $\mu\beta_{vec}$ product.[118]

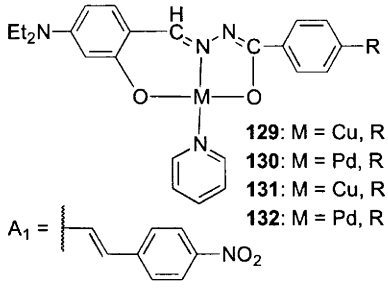

129: M = Cu, R = NO_2, λ_{max} = 460 nm (DMSO), $\mu\beta_{1.907}$ (EFISH) = 460 x 10^{-48} esu (DMSO)[118]
130: M = Pd, R = NO_2, λ_{max} = 459 nm ($CHCl_3$), $\mu\beta_{1.907}$ (EFISH) = 380 x 10^{-48} esu ($CHCl_3$)[118]
131: M = Cu, R = A_1, λ_{max} = 455 nm (DMSO), $\mu\beta_{1.907}$ (EFISH) = 650 x 10^{-48} esu (DMSO)[118]
132: M = Pd, R = A_1, λ_{max} = 450 nm (DMSO), $\mu\beta_{1.907}$ (EFISH) = 1500 x 10^{-48} esu (DMSO)[118]

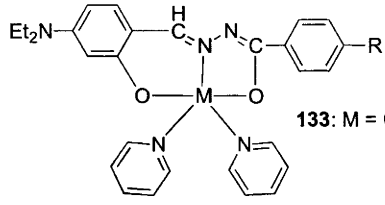

133: M = Cu, R = A_1, λ_{max} = n.a., $\mu\beta_{1.907}$ (EFISH) = 1390 x 10^{-48} esu ($CHCl_3$)[118]

Ferrocenyl-functionalized Schiff base complexes such as **134/135** potentially combine the advantages of both key inorganic NLO-phores. Related complexes in which the phenoxy aryl is π-complexed to a RuCp* unit (**136-138**) were also prepared, the arene metallation having no appreciable effect on the HRS-derived nonlinearity at 1.91 μm.[99]

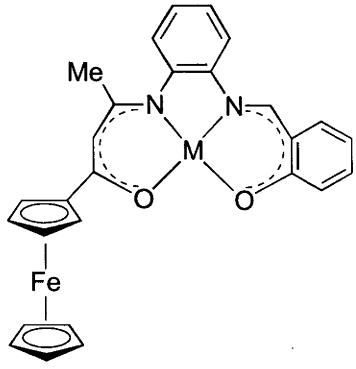

134: M = Ni, λ_{max} = 587 nm (CH_2Cl_2),
$\beta_{1.91}$ (HRS) = 250 x 10^{-30} esu ($CHCl_3$)[99]

135: M = Cu, λ_{max} = 445 nm (CH_2Cl_2),
$\beta_{1.91}$ (HRS) = 212 x 10^{-30} esu ($CHCl_3$)[99]

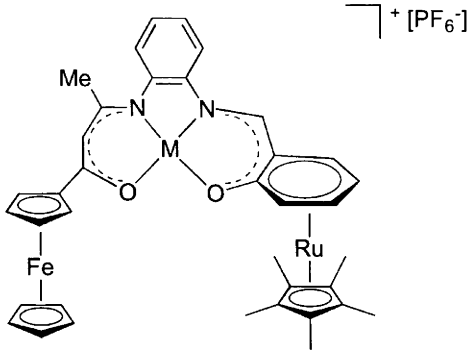

136: M = Ni, λ_{max} = 229 nm (CH_2Cl_2), $\beta_{1.91}$ (HRS) = 235 x 10^{-30} esu (DMF)[99]

137: M = Cu, λ_{max} = 474 nm (CH_2Cl_2), $\beta_{1.91}$ (HRS) = 237 x 10^{-30} esu (DMF)[99]

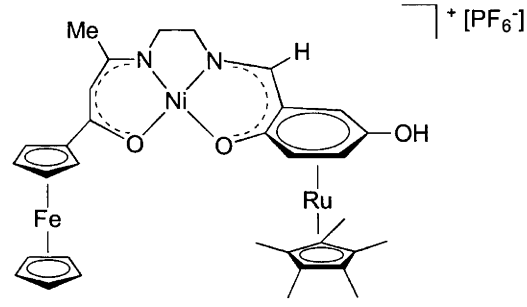

138: λ_{max} = 455 nm (CH_2Cl_2), $\beta_{1.91}$ (HRS) = 247 x 10^{-30} esu (DMF)[99]

1.4.4 Metal Alkynyl Complexes

The quadratic and cubic NLO properties of metal alkynyl complexes through 2002 have been surveyed.[120] Since 2002 there have been a number of reports on the quadratic NLO properties of metal alkynyl complexes.[121-134] Earlier studies by Humphrey and co-workers had defined the impact on quadratic nonlinearity of varying the ligated metal center, co-ligands, π-bridge, and acceptor group, in donor-bridge-acceptor complexes with short π-bridge alkynyl ligands. The bis(bidentate diphosphine)chlororuthenium center proved amongst the most efficient donor groups, so has been used to explore the effect of π-bridge lengthening with phenylenevinylene and/or phenyleneethynylene units.[122,124] Studies with the series of complexes **139-152** revealed several trends. The (formally) $Ru^{II/III}$ redox potentials can be tuned in a systematic fashion, as they increase on replacing yne-linkage by ene-linkage at the phenylene adjacent to the metal, and on replacing dppe by dppm co-ligands, and decrease on π-bridge lengthening. The low-energy UV-vis-NIR bands are MLCT in nature, blue-shifting on π-bridge lengthening by addition of phenyleneethynylene units, and replacing *E*-ene by yne linkages. The β_0 values

increase on π-bridge lengthening, replacing yne linkage by *E*-ene linkage at the phenylene adjacent to the metal center, and replacing dppm by dppe co-ligands, until the tri(phenyleneethynylene) is reached, further lengthening (from **154** to **155** or **157** to **158**) resulting in a reduction of nonlinearity.

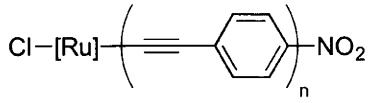

139: [Ru] = $Ru(dppm)_2$, n = 1, λ_{max} = 473 nm (THF), β_0 (HRS) = 130 x 10^{-30} esu (THF)[122]
140: [Ru] = $Ru(dppe)_2$, n =1, λ_{max} = 477 nm (THF), β_0 (HRS) = 88 x 10^{-30} esu (THF)[122]
141: [Ru] = $Ru(dppm)_2$, n = 2, λ_{max} = 466 nm (THF), β_0 (HRS) = 33 x 10^{-30} esu (THF)[122]
142: [Ru] = $Ru(dppe)_2$, n = 2, λ_{max} = 468 nm (THF), β_0 (HRS) = 225 x 10^{-30} esu (THF)[122]
143: [Ru] = $Ru(dppm)_2$, n = 3, λ_{max} = 439 nm (THF), $\beta_{1.907}$ (EFISH) = 77 x 10^{-30} esu ($CHCl_3$)[122]
144: [Ru] = $Ru(dppe)_2$, n = 3, λ_{max} = 429 nm (THF), β_0 (HRS) = 388 x 10^{-30} esu (THF)[122]

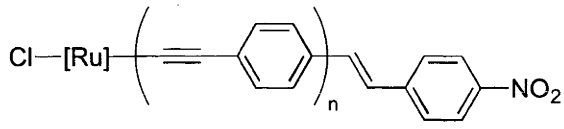

145: [Ru] = $Ru(dppe)_2$, n = 1, λ_{max} = 489 nm (THF), β_0 (HRS) = 52 x 10^{-30} esu (THF)[122]
146: [Ru] = $Ru(dppm)_2$, n = 1, λ_{max} = 491 nm (THF), β_0 (HRS) = 250 x 10^{-30} esu (THF)[122]
147: [Ru] = $Ru(dppe)_2$, n = 2, λ_{max} = 448 nm (THF), β_0 (HRS) = 430 x 10^{-30} esu (THF)[122]
148: [Ru] = $Ru(dppm)_2$, n = 2, λ_{max} = 446 nm (THF), β_0 (HRS) = 441 x 10^{-30} esu (THF)[122]

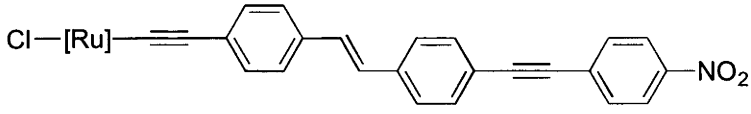

149: [Ru] = $Ru(dppe)_2$, λ_{max} = 459 nm (THF), β_0 (HRS) = 580 x 10^{-30} esu (THF)[122]
150: [Ru] = $Ru(dppm)_2$, λ_{max} = 452 nm (THF), β_0 (HRS) = 495 x 10^{-30} esu (THF)[122]

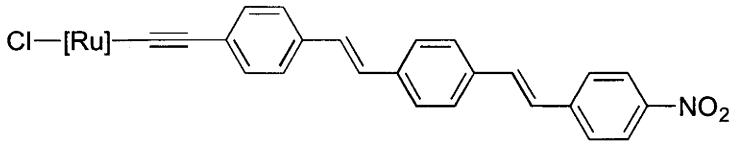

151: [Ru] = $Ru(dppe)_2$, λ_{max} = 468 nm (THF), β_0 (HRS) = 460 x 10^{-30} esu (THF)[122]
152: [Ru] = $Ru(dppm)_2$, λ_{max} = 466 nm (THF), β_0 (HRS) = 395 x 10^{-30} esu (THF)[122]

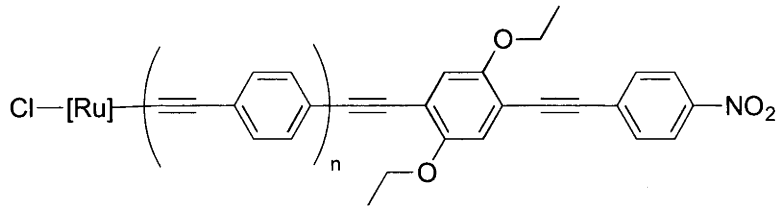

153: [Ru] = $Ru(dppm)_2$, n = 0, λ_{max} = 510 nm (THF), β_0 (HRS) = 40 x 10^{-30} esu (THF)[124]
154: [Ru] = $Ru(dppm)_2$, n = 1, λ_{max} = 459 nm (THF), β_0 (HRS) = 400 x 10^{-30} esu (THF)[124]
155: [Ru] = $Ru(dppm)_2$, n = 2, λ_{max} = 411 nm (THF), β_0 (HRS) = 217 x 10^{-30} esu (THF)[124]

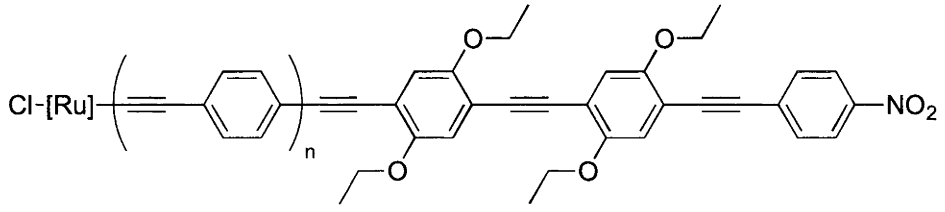

156: [Ru] = $Ru(dppe)_2$, n = 0, λ_{max} = 426 nm (THF), β_0 (HRS) = 160 x 10^{-30} esu (THF)[124]
157: [Ru] = $Ru(dppm)_2$, n = 0, λ_{max} = 424 nm (THF), β_0 (HRS) = 208 x 10^{-30} esu (THF)[124]
158: [Ru] = $Ru(dppm)_2$, n = 2, λ_{max} = 423 nm (THF), β_0 (HRS) = 185 x 10^{-30} esu (THF)[124]

1.4.5 Metallocenyl Complexes

An article in *Nature* by Green and co-workers describing the SHG merit of a substituted ferrocene[135] alerted researchers to the potential of organometallics in nonlinear optics, and metallocenyl complexes have continued to attract attention.[136-148] Earlier reports utilized aryl bridges and nitro and other simple organic acceptor groups in conventional donor-bridge-acceptor compositions. Since then, studies in the purely organic sphere by Dalton and co-workers have revealed improvements to this design.[149,150] Coupling analogues of the Dalton 2-dicyanomethylene-3-cyano-4-methyl-2,5-dihydrofuran acceptor to ferrocene afforded **159-162**, the quadratic nonlinearities of which increase on replacement of methyl by trifluoromethyl and phenyl groups at the acceptor, and on incorporation of a thienylvinylene unit into the bridge. The bond-length alternation along the chromophore charge-transfer axis in these molecules fall in the range 0.05-0.10 Å, and correlate closely with the

magnitude of the hyperpolarizabilities. Complex **162** was doped into amorphous polycarbonate at a loading of 20% w/w, and a solution in cyclopentanone of the resulting composite was spin-coated onto an ITO slide. After poling, the film exhibited an electrooptic r_{33} coefficient of 25 pm V^{-1} at 1300 nm, similar in magnitude to efficient organic chromophore-doped films, despite the absence of sterically encumbering groups designed to disfavor aggregation that are usually found with the latter.[146]

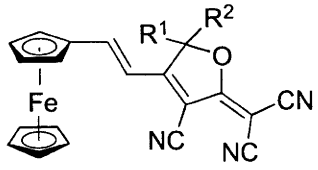

159: $R^1 = R^2 = CH_3$,
$\beta/\beta_{Chloroform}$ (HRS) = 279 (MeCN)[146]

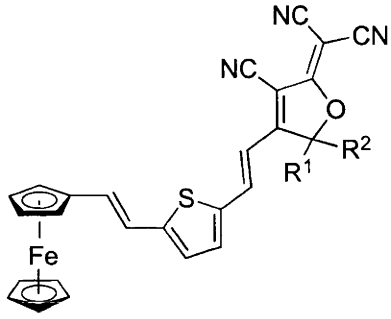

161: $R^1 = R^2 = CH_3$,
$\beta/\beta_{Chloroform}$ (HRS) = 2633 (MeCN)[146]

160: $R^1 = CF_3$, R^2 = Ph,
$\beta/\beta_{Chloroform}$ (HRS) = 450 (MeCN)[146]

162: $R^1 = CF_3$, R^2 = Ph,
$\beta/\beta_{Chloroform}$ (HRS) = 3333 (MeCN)[146]

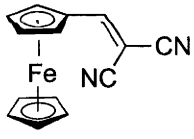

163: $\mu\beta$ (HRS) = 92 x 10^{-48} esu (MeCN)[146]

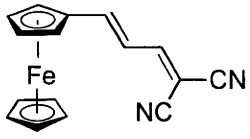

164: $\mu\beta$ (HRS) = 420 x 10^{-48} esu (MeCN)[146]

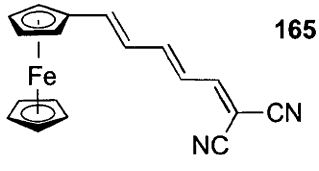

165: $\mu\beta$ (HRS) = 1120 x 10^{-48} esu (MeCN)[146]

1.5 Third-Order Nonlinearities

1.5.1 Complexes of Pyridyl or Polypyridyl Ligands

The cubic NLO properties of complexes incorporating pyridyl and polypyridyl have been reported for a number of complexes.[43,151-180] The 2PA properties of polypyridine and alkynyl complexes through 2007 have been summarized.[181] Single-wavelength fs Z-scan studies on pyridinium-functionalized tris(bipy) complexes **64** to **74** by Coe *et al.* have revealed a consistent increase in 2PA merit for π-system lengthening, while metal variation affords unclear outcomes.[43]

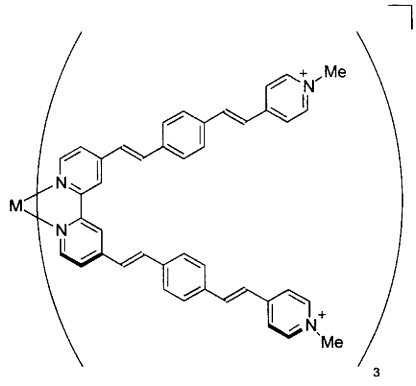

64: M = Ru, λ_{max} = 573 nm (PrCN), σ_2 (z-scan, fs, 750 nm) = 2500 GM (DMF)[43]

65: M = Fe, λ_{max} = 604 nm (PrCN), σ_2 (z-scan, fs, 750 nm) = 1400 GM (DMF)[43]

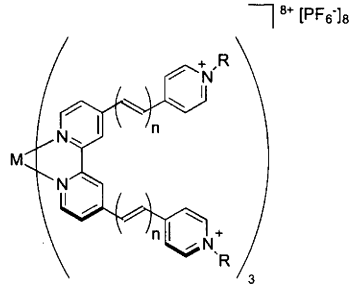

66: n = 1, M = Ru, R = Me, λ_{max} = 574 nm (PrCN), σ_2 (z-scan, fs, 750 nm) = 720 GM (DMF)[43]

67: n = 1, M = Ru, R = Ph, λ_{max} = 566 nm (PrCN), σ_2 (z-scan, fs, 750 nm) = 1200 GM (DMF)[43]

68: n = 2, M = Ru, R = Me, λ_{max} = 582 nm (PrCN), σ_2 (z-scan, fs, 750 nm) = 1500 GM (DMF)[43]

69: n = 1, M = Fe, R = Me, λ_{max} = 614 nm (PrCN), σ_2 (z-scan, fs, 750 nm) = 350 GM (DMF)[43]

70: n = 1, M = Fe, R = Ph, λ_{max} = 623 nm (PrCN), σ_2 (z-scan, fs, 750 nm) = 600 GM (DMF)[43]

71: n = 2, M = Fe, R = Me, λ_{max} = 620 nm (PrCN), σ_2 (z-scan, fs, 750 nm) = 1500 GM (DMF)[43]

72: n = 1, M = Fe, λ_{max} = 633 nm (PrCN), σ_2 (z-scan, fs, 750 nm) = 265 GM (DMF)[43]

R = 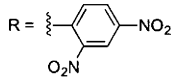

Whereas the functionalized 1,10-phenthroline ligands in complexes **166 - 168** fluoresce strongly in the free state, complexation to Ni(II) quenches the fluorescence.[169] A fs white-light continuum was used to assess the 2PA cross-sections, the maxima red-shifting on complexation and increasing the donor strength of the substituents. The maximal values increase on complexation, but are invariant across the three nickel(II) complexes. Related ruthenium(II) complexes (for photosensitizing) that incorporate fluorenyl substituents (to enhance fluorescence) and triethyleneglycol groups (to ensure lipophilicity) have been explored for use in spatially-confined photodynamic therapy.[157] While the maximal value at 740 nm is low (ca 40 GM), it is much greater than those of common commercial dyes.

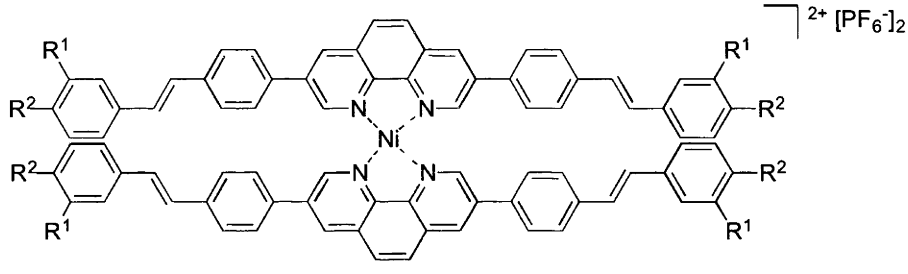

166, R^1 = H, R^2 = S(^{t}Bu), λ_{max} = 392 nm ($CHCl_3$), $\sigma_{2,max}$ (WLC, fs, 760 nm) = 578 GM ($CHCl_3$)[169]
167, R^1 = R^2 = OC_6H_{13}, λ_{max} = 411 nm ($CHCl_3$), $\sigma_{2,max}$ (WLC, fs, 789 nm) = 569 GM ($CHCl_3$)[169]
168, R^1 = H, R^2 = $N(C_6H_{13})_2$, λ_{max} = 369 nm ($CHCl_3$), $\sigma_{2,max}$ (WLC, fs, 839 nm) = 592 GM ($CHCl_3$)[169]

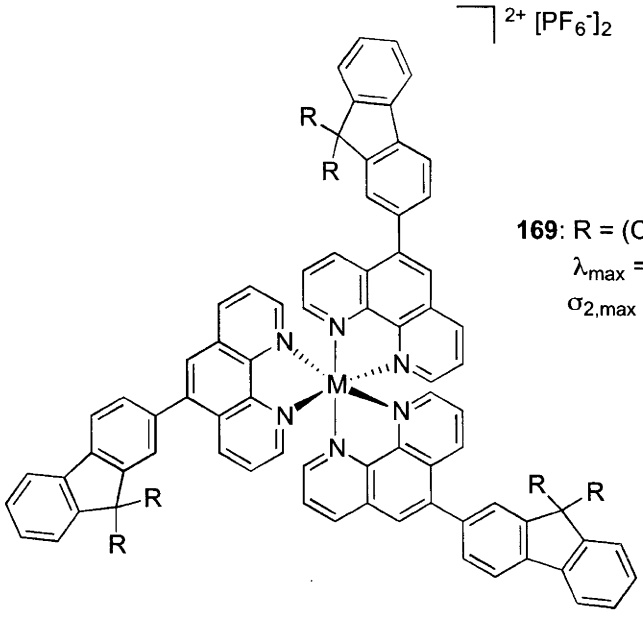

169: R = $(CH_2)_3(O(CH_2)_2)_3OMe$,
λ_{max} = 450 nm ($CHCl_3$),
$\sigma_{2,max}$ (WLC, fs, 740 nm) = 40 GM ($CHCl_3$)[157]

The 2PA efficiency of zinc(II) terpyridine complexes functionalized by aminostilbene units has been examined by fs 2PA-induced photoluminescence.[168] Cross-sections are lower than those of the free terpy ligands. This has been rationalized by (a) the orthogonal terpy ligands acting independently, and (b) coordination to zinc(II) increasing the acceptor properties of the terpy end of the ligand which as a consequence has an increasingly cyanine-like behavior, although a significant cyanine-like contribution from a polyaromatic chromophore is unlikely.

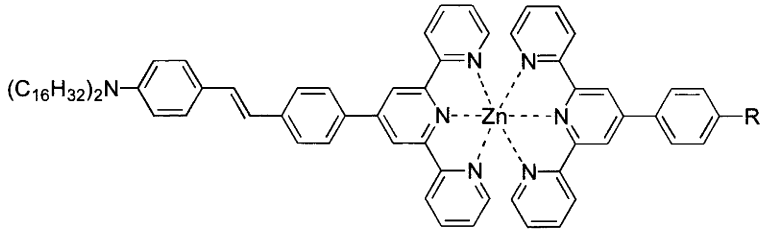

170: R = 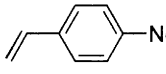 λ_{max} = 459 nm (Acetone), $\sigma_{2,max}$ (WLC, fs, 815 nm) = 95 GM (Acetone)[168]

171: R = Me, λ_{max} = 453 nm (Acetone), $\sigma_{2,max}$ (WLC, fs, 815 nm) = 77 GM (Acetone)[168]
172: R = NO_2, λ_{max} = 426 nm (DMF), $\sigma_{2,max}$ (WLC, fs, 830 nm) = 30 GM (Acetone)[168]

1.5.2 Complexes of Porphyrins and Related Ligands

The cubic nonlinearities of complexes with phthalocyanines (through 2002)[97] and porphyrins and related ligands (through 2005) have been summarized,[98] and a selected summary of 2PA properties of porphyrins through 2007 has appeared,[182] the robust nature of the core, established functionalization strategies, biocompatible nature of these molecules, and their strong nonlinear absorption properties serving to maintain strong interest in this area.[66,75,183-320]

1.5.3 Schiff Base Complexes

A number of reports have investigated the cubic NLO properties of Schiff base complexes.[321-337] The zinc(II) complexes **175** and **176** have been shown by Goswami, Bharadwaj and co-workers to possess very large 2PA cross-sections at 890 nm (fs Z-scan), in contrast to the free ligand which is inactive at this wavelength; complexation enhances the weak acceptor character of the central diimine unit in these ligands with a formally D-π-A-π-D composition. Proceeding to the zinc(II) and copper(I) complexes **173** and **174** results in a further six-fold increase, concomitant with the progression to an octupolar structure. The zinc complex is the more efficient, consistent with the greater acceptor character of zinc(II) compared to copper(I).[328]

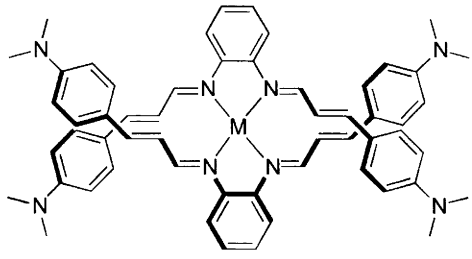

173: M = $Zn(ClO_4)_2$, λ_{max} = 459 nm (CH_2Cl_2), σ_2 (z-scan, fs, 890 nm) = 10736 GM (CH_2Cl_2)[321]

174: M = $Cu(BF_4)$, M = $Zn(ClO_4)_2$, λ_{max} = 461 nm (CH_2Cl_2), σ_2 (z-scan, fs, 890 nm) = 10918 GM (CH_2Cl_2)[321]

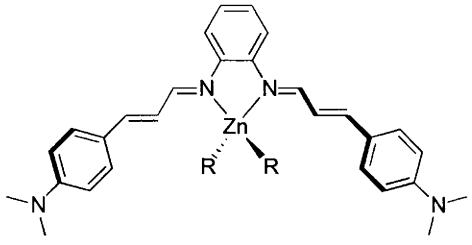

175: R = Cl, M = $Zn(ClO_4)_2$, λ_{max} = 448 nm (CH_2Cl_2), σ_2 (z-scan, fs, 890 nm) = 1769 GM (CH_2Cl_2)[321]

176: R = CN,M = $Zn(ClO_4)_2$, λ_{max} = 446 nm (CH_2Cl_2), σ_2 (z-scan, fs, 890 nm) = 1700 GM (CH_2Cl_2)[321]

1.5.4 Metal Alkynyl Complexes

Metal alkynyl complexes continue to attract considerable interest for their cubic NLO properties.[124,131,132,134,338-365] Humphrey and Samoc and their co-workers have examined the third-order NLO behavior of dipolar, quadrupolar, and octupolar ruthenium alkynyl complexes. Z-scan spectral dependence studies of **139**, **141**, **154**, **155** and **158** revealed an approximate correspondence between twice the energy of the one-photon absorption bands and the energy of the major two-photon absorption bands, with evidence of the long wavelength features having a three-photon absorption behavior.[124] As with quadratic nonlinearity, the two-photon absorption cross-section for these complexes is maximized at the tri(phenyleneethynylene) complex **154**; further π-system lengthening results in decreasing importance of the LUMO ← HOMO transition and on-axis rotation-mediated change in the relative intensities of two or more crucial low-lying transitions, both of which serve to reduce the nonlinearity from the continuing increase that may otherwise have been anticipated.

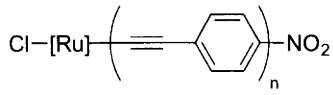

139: [Ru] = $Ru(dppm)_2$, n = 1, λ_{max} = 473 nm (THF), $\sigma_{2,max}$ (z-scan, fs, 940 nm) = 135 GM esu (CH_2Cl_2)[124]
141: [Ru] = $Ru(dppm)_2$, n = 2, λ_{max} = 466 nm (THF), $\sigma_{2,max}$ (z-scan, fs, 890 nm) = 567 GM esu (CH_2Cl_2)[124]

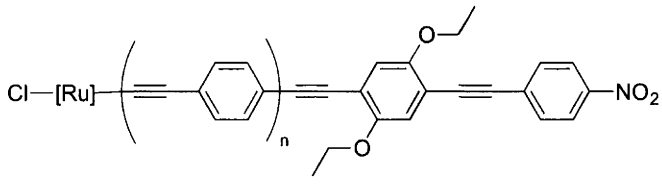

154: [Ru] = $Ru(dppm)_2$, n = 1, λ_{max} = 459 nm (THF), $\sigma_{2,max}$ (z-scan, fs, 900 nm) = 1160 GM esu (CH_2Cl_2)[124]
155: [Ru] = $Ru(dppm)_2$, n = 2, λ_{max} = 411 nm (THF), $\sigma_{2,max}$ (z-scan, fs, 840 nm) = 780 GM esu (CH_2Cl_2)[124]

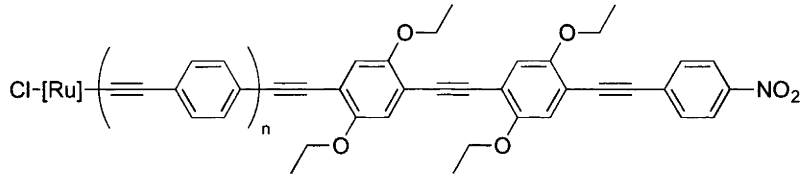

158: [Ru] = $Ru(dppm)_2$, n = 2, λ_{max} = 423 nm (THF), $\sigma_{2,max}$ (z-scan, fs, 840 nm) = 853 GM esu (CH_2Cl_2)[124]

Wavelength dependence studies of the cubic NLO properties of the octupolar complexes **177 - 181** revealed that refractive nonlinearities are maximized at a longer wavelength for the stilbene-linked dendrimers than for the tolane-linked examples, with the maximal values experiencing a nonlinear increase upon increasing dendrimer generation.[340,351] The absorptive nonlinearities are positive through the spectral range for these complexes (i.e. they are two- or three-photon absorbers through this range); the stilbene examples exhibit appreciable nonlinear absorption at the "telecommunications wavelength" of 1300 nm, while **181** possesses a record 3PA coefficient under fs conditions (note: large branched complexes are displayed in a contracted form, where the arm shown is repeated at the wavy lines).

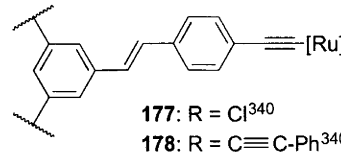

177: R = Cl[340]
178: R = C≡C-Ph[340]

179[340]

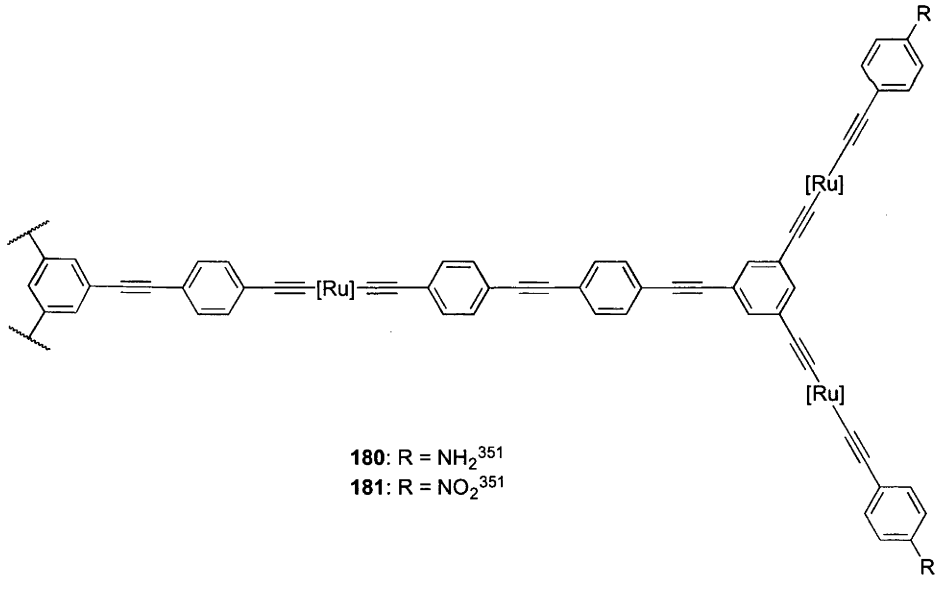

180: R = NH_2[351]
181: R = NO_2[351]

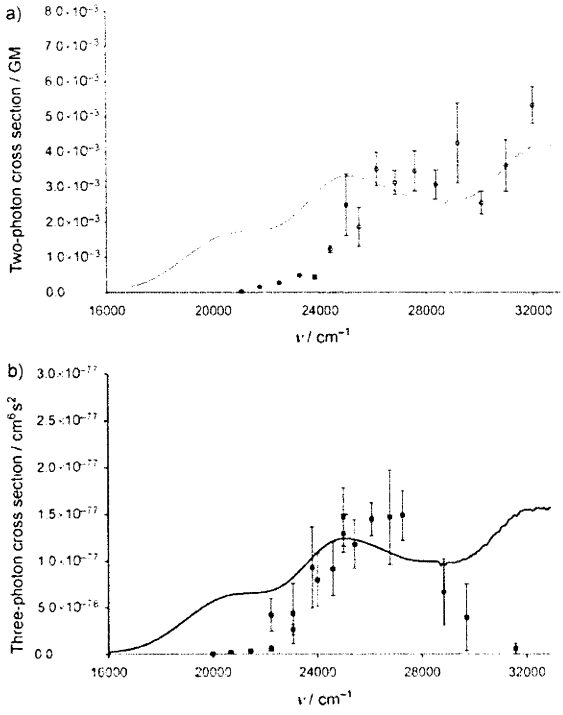

181: 2PA cross-section (a) and 3PA cross-section (b)[351]

N-cored analogues (**182** – **184**) have been examined because planarity at the sp^2-hybridized nitrogen and involvement in π-delocalization of the occupied p_z orbital may increase nonlinearity.[342] Spectral dependence studies of the cubic nonlinearity revealed 2PA behavior below 1000 nm, with maximal values suggestive of an NLO dendritic effect (a nonlinear increase in nonlinearity upon increasing dendrimer generation). Beyond 1000 nm, data are consistent with 3PA-induced photochemistry. The 2PA cross-sections of these dendrimers are larger than those of comparable N-cored organic dendrimers, an increase in performance that is maintained when the outcomes are scaled by "effective number of electrons", molecular weight, molecular volume, or even the cost of production.[366]

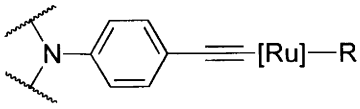

182: R = Cl[342]

183: R = C≡C-Ph[342]

184[342]

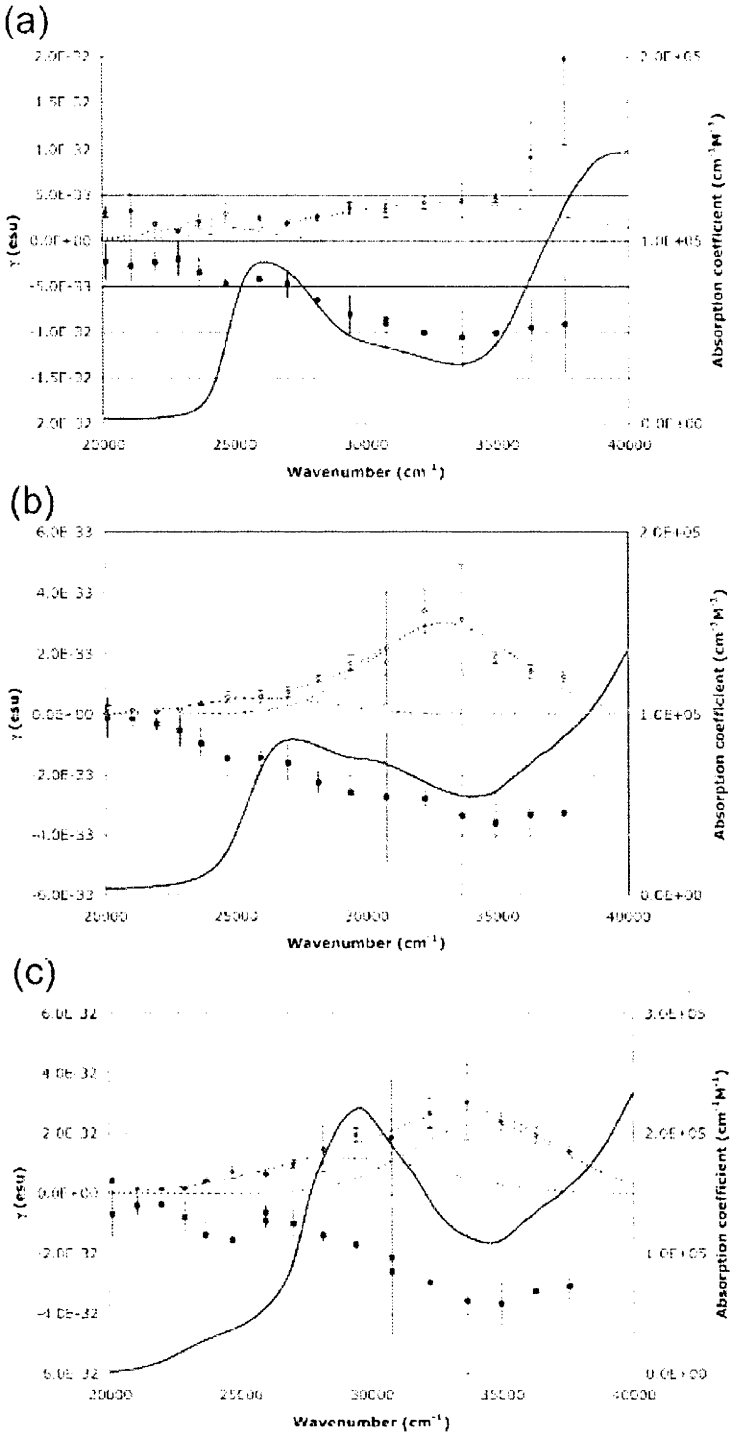

Wavelength dependence for **182** (a), **183** (b), and **184** (c)[342]

Cubic nonlinearities of ruthenium alkynyl complexes have been switched under electrochemical control.[367] In the resting state, the low-energy transition in these complexes is MLCT in nature. Oxidation, exploiting the $Ru^{II/III}$ couple, results in the appearance of a low-energy LMCT transition. The cubic nonlinearities are also modified following oxidation, the complexes being two-photon absorbers at 800 nm in the resting state and saturable absorbers at that wavelength following oxidation. This approach to switching nonlinearities has been extended to demonstrate multi-state NLO switching. Coupling the ruthenium alkynyl unit to a more easily oxidizable iron center permits sequential access to $Fe^{II}Ru^{II}$, $Fe^{III}Ru^{II}$, and $Fe^{III}Ru^{III}$ states on stepwise oxidation of **185**, with the oxidation processes resulting in strong changes to linear and NLO properties; in particular, the $Fe^{II}Ru^{II}$ form of **185** possesses negligible absorptive nonlinearity at 790 nm, but the $Fe^{III}Ru^{II}$ state is a two-photon absorber at this wavelength, and the $Fe^{III}Ru^{III}$ form is a saturable absorber (or in other words, the three oxidation states afford successively zero, positive, and negative values of the absorptive nonlinearity at this wavelength).[360]

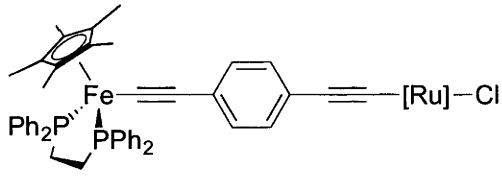

185: λ_{max} = 400 nm (CH_2Cl_2),
σ_2 (z-scan, fs, 790 nm) = 0 GM (CH_2Cl_2)[360]

185^{1+}: λ_{max} = 1124 nm (CH_2Cl_2),
σ_2 (z-scan, fs, 790 nm) = 420 GM (CH_2Cl_2)[360]

185^{2+}: λ_{max} = 706 nm (CH_2Cl_2),
σ_2 (z-scan, fs, 790 nm) = -250 GM (CH_2Cl_2)[360]

Three-state cubic NLO switching has also been demonstrated with **186**, but in this case using independent stimuli. Oxidation, as above, converts the $Ru^{II}{}_4$ state to the

Ru^{III}_4 form, whereas protonation affords a tetra(vinylidene) complex tetracation, in both cases resulting in strong changes to linear and NLO properties.[368] This idea has been extended to include photochemical switching – **187** contains a dithienylperfluorocyclopentene unit that can be reversibly photoisomerized between open and closed forms, alkynyl ligands that can be reversibly protonated to the corresponding vinylidene forms, and ruthenium centers that undergo reversible oxidation, the lack of reversible oxidation of the vinylidene forms restricting the number of switchable states to six. The six switchable states can be interconverted along seven pathways, each of which results in distinct changes to the nonlinear absorption; some of these outcomes have been used to demonstrate NOR and INHIBIT logic gates.[343]

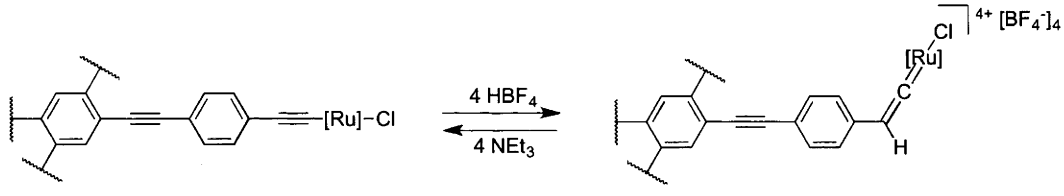

186: λ_{max} = 470 nm (CH_2Cl_2), $\sigma_{2,max}$ (z-scan, fs, 750 and 590 nm) = 1100 (750) and 3000 (590) GM (CH_2Cl_2)[368]
186^{4+}: λ_{max} = 925 nm (CH_2Cl_2), $\sigma_{2,max}$ (z-scan, fs, 750 nm) = -1800 GM (CH_2Cl_2)[368]
186-H_4^{4+}: λ_{max} = 410 nm (CH_2Cl_2), $\sigma_{2,max}$ (z-scan, fs, 750 and 590 nm) = 1000 (750) and 2000 (590) GM (CH_2Cl_2)[368]

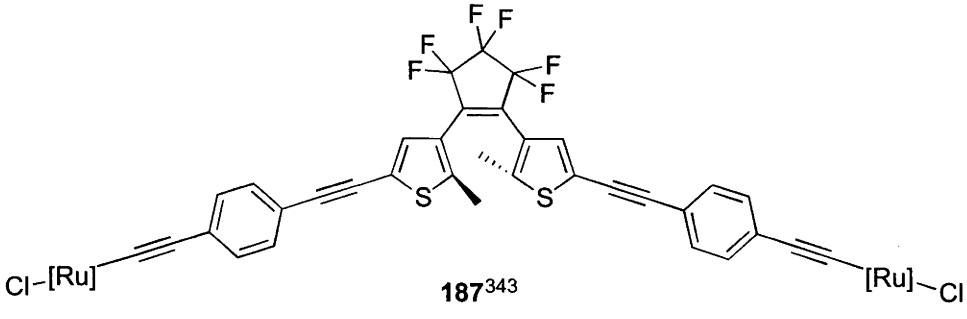

187[343]

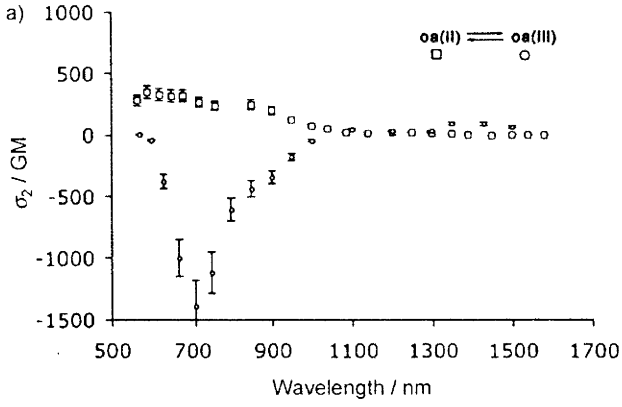

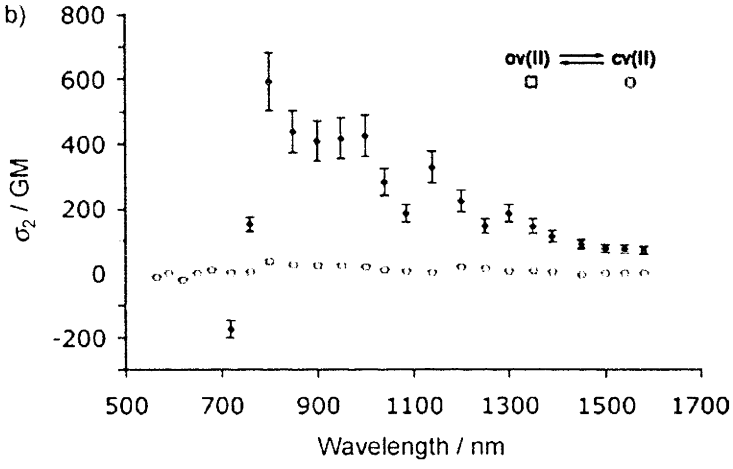

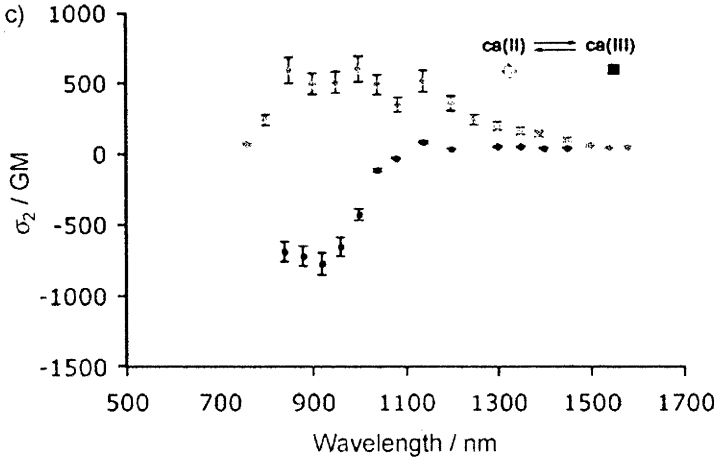

Switching wavelength dependence study of 2PA cross-sections of **187**[343]

The effect of *sp*-carbon chain lengthening on cubic NLO properties of the platinum-terminated polyynediyl complexes **188** - **194** has been examined by broad spectral range Z-scan studies.[349] 2PA merit increases markedly on lengthening the carbon chain, affording complexes with extremely high 2PA/MWt coefficients. The saturation length was not reached in these studies, despite examples up to C_{24} being assessed. Extrapolation to the C_∞ case suggested a 2PA maximum for carbyne at ca 1000 nm.

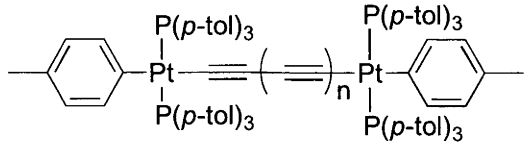

188: n = 2, λ_{max} = 329 nm (CH_2Cl_2), $\sigma_{2,max}$ (z-scan, fs) = 200 GM (CH_2Cl_2)[349]
189: n = 3, λ_{max} = 337 nm (CH_2Cl_2), $\sigma_{2,max}$ (z-scan, fs) = 305 GM (CH_2Cl_2)[349]
190: n = 4, λ_{max} = 350 nm (CH_2Cl_2), $\sigma_{2,max}$ (z-scan, fs) = 300 GM (CH_2Cl_2)[349]
191: n = 5, λ_{max} = 375 nm (CH_2Cl_2), $\sigma_{2,max}$ (z-scan, fs) = 862 GM (CH_2Cl_2)[349]
192: n = 7, λ_{max} = 411 nm (CH_2Cl_2), $\sigma_{2,max}$ (z-scan, fs) = 1450 GM (CH_2Cl_2)[349]
193: n = 9, λ_{max} = 443 nm (CH_2Cl_2), $\sigma_{2,max}$ (z-scan, fs) = 1400 GM (CH_2Cl_2)[349]
194: n = 11, λ_{max} = 467 nm (CH_2Cl_2), $\sigma_{2,max}$ (z-scan, fs) = 2200 GM (CH_2Cl_2)[349]

1.6 Conclusions

Inorganic materials continue to attract interest for their NLO properties. For quadratic properties, complexes incorporating pyridyl or polypyridyl ligands and complexes featuring porphyrins and related ligands have attracted the most interest. For cubic properties, metal alkynyl and porphyrin complexes have garnered considerable recent interest. For the measurement of cubic properties, recent work has focused on measurements over a number of wavelengths to provide more accurate determination of the maximal NLO response.

1.7 References

(1) Christodoulides, D. N.; Khoo, I. C.; Salamo, G. J.; Stegeman, G. I.; Van Stryland, E. W. *Adv. Opt. Photon.* **2010**, *2*, 60.
(2) Cheng, L. T.; Tam, W.; Stevenson, S. H.; Meredith, G. R.; Rikken, G.; Marder, S. R. *J. Phys. Chem.* **1991**, *95*, 10631.
(3) Zyss, J.; Ledoux, I. *Chem. Rev.* **1994**, *94*, 77.
(4) Clays, K.; Persoons, A. *Rev. Sci. Instrum.* **1992**, *63*, 3285.
(5) Olbrechts, G.; Strobbe, R.; Clays, K.; Persoons, A. *Rev. Sci. Instrum.* **1998**, *69*, 2233.
(6) Campo, J.; Desmet, F.; Wenseleers, W.; Goovaerts, E. *Opt. Express* **2009**, *17*, 4587.
(7) Jiang, Y.; Cao, Z. Q.; Shen, Q. S.; Dou, X. M.; Chen, Y. L.; Ozaki, Y. *J. Opt. Soc. Am. B-Opt. Phys.* **2000**, *17*, 805.
(8) Teng, C. C.; Man, H. T. *Appl. Phys. Lett.* **1990**, *56*, 1734.
(9) Boyd, R. W. *Nonlinear Optics*; Third Edition ed.; Academic Press: Amsterdam, 2008.
(10) Kajzar, F.; Messier, J. *Phys. Rev. A* **1985**, *32*, 2352.
(11) Sheik-Bahae, M.; Said, A. A.; Wei, T. H.; Hagan, D. J.; Van Stryland, E. W. *IEEE J. Quant. Electron.* **1990**, *26*, 760.
(12) Strohkendl, F. P.; Dalton, L. R.; Hellwarth, R. W.; Sarkas, H. W.; Kafafi, Z. H. *J. Opt. Soc. Am. B* **1997**, *14*, 92.
(13) Zhao, M.; Cui, Y.; Samoc, M.; Prasad, P. N.; Unroe, M. R.; Reinhardt, B. A. *J. Chem. Phys.* **1991**, *95*, 3991.
(14) Tseng, S. Y.; Cao, W. L.; Peng, W. H.; Hales, J. M.; Chi, S. H.; Perry, J. W. M., S.R.; Lee, C. H.; Herman, W. N.; Goldhar, J. *Opt. Express* **2006**, *14*, 8737.
(15) Xu, C.; Webb, W. W. *J. Opt. Soc. Am. B-Opt. Phys.* **1996**, *13*, 481.
(16) Sutherland, R. L.; McLean, D. G.; Sean, K. *Handbook of Nonlinear Optics*; Second Edition New York, 2003.
(17) Rau, I.; Kajzar, F.; Luc, J.; Sahraoui, B.; Boudebs, G. *J. Opt. Soc. Am. B-Opt. Phys.* **2008**, *25*, 1738.
(18) Cariati, E.; Pizzotti, M.; Roberto, D.; Tessore, F.; Ugo, R. *Coord. Chem. Rev.* **2006**, *250*, 1210.
(19) Deplano, P.; Pilia, L.; Espa, D.; Mercuri, M. L.; Serpe, A. *Coord. Chem. Rev.* **2010**, *254*, 1434.
(20) Frazier, C. C.; Harvey, M. A.; Cockerham, M. P.; Hand, H. M. *J. Phys. Chem.* **1986**, *90*, 5703.
(21) Coe, B. J. *Acc. Chem. Res.* **2006**, *39*, 383.
(22) Aubert, V.; Guerchais, V.; Ishow, E.; Hoang-Thi, K.; Ledoux, I.; Nakatani, K.; Le Bozec, H. *Angew. Chem. Int. Ed.* **2008**, *47*, 577.
(23) Tessore, F.; Roberto, D.; Ugo, R.; Mussini, P.; Quici, S.; Ledoux-Rak, I.; Zyss, J. *Angew. Chem. Int. Ed.* **2003**, *42*, 456.

(24) Dragonetti, C.; Righetto, S.; Roberto, D.; Ugo, R.; Valore, A.; Fantacci, S.; Sgamellotti, A.; De Angelis, F. *Chem. Commun.* **2007**, 4116.
(25) Fave, C.; Hissler, M.; Senechal, K.; Ledoux, I.; Zyss, J.; Reau, R. *Chem. Commun.* **2002**, 1674.
(26) Roberto, D.; Tessore, F.; Ugo, R.; Bruni, S.; Manfredi, A.; Quici, S. *Chem. Commun.* **2002**, 846.
(27) Valore, A.; Colombo, A.; Dragonetti, C.; Righetto, S.; Roberto, D.; Ugo, R.; De Angelis, F.; Fantacci, S. *Chem. Commun.* **2010**, *46*, 2414.
(28) Valore, A.; Cariati, E.; Dragonetti, C.; Righetto, S.; Roberto, D.; Ugo, R.; De Angelis, F.; Fantacci, S.; Sgamellotti, A.; Macchioni, A.; Zuccaccia, D. *Chem.-Eur. J.* **2010**, *16*, 4814.
(29) Coe, B. J.; Harries, J. L.; Harris, J. A.; Brunschwig, B. S.; Coles, S. J.; Light, M. E.; Hursthouse, M. B. *Dalton Trans.* **2004**, 2935.
(30) Coe, B. J.; Harris, J. A.; Brunschwig, B. S. *Dalton Trans.* **2003**, 2384.
(31) Coe, B. J.; Jones, L. A.; Harris, J. A.; Sanderson, E. E.; Brunschwig, B. S.; Asselberghs, I.; Clays, K.; Persoons, A. *Dalton Trans.* **2003**, 2335.
(32) Valore, A.; Balordi, M.; Colombo, A.; Dragonetti, C.; Righetto, S.; Roberto, D.; Ugo, R.; Benincori, T.; Rampinini, G.; Sannicolo, F.; Demartin, F. *Dalton Trans.* **2010**, *39*, 10314.
(33) Fonseca, A. M.; Belsley, M.; Gomes, E. M.; Castro, M. C. R.; Raposo, M. M. M. *Eur. J. Inorg. Chem.* **2010**, 2998.
(34) Labat, L.; Lamere, J. F.; Sasaki, I.; Lacroix, P. G.; Vendier, L.; Asselberghs, I.; Perez-Moreno, J.; Clays, K. *Eur. J. Inorg. Chem.* **2006**, 3105.
(35) Coe, B. J.; Fielden, J.; Foxon, S. P.; Asselberghs, I.; Clays, K.; Brunschwig, B. S. *Inorg. Chem.* **2010**, *49*, 10718.
(36) Coe, B. J.; Foxon, S. P.; Harper, E. C.; Raftery, J.; Shaw, R.; Swanson, C. A.; Asselberghs, I.; Clays, K.; Brunschwig, B. S.; Fitch, A. G. *Inorg. Chem.* **2009**, *48*, 1370.
(37) Coe, B. J.; Harries, J. L.; Harris, J. A.; Brunschwig, B. S.; Horton, P. N.; Hursthouse, M. B. *Inorg. Chem.* **2006**, *45*, 11019.
(38) Coe, B. J.; Harries, J. L.; Helliwell, M.; Brunschwig, B. S.; Harris, J. A.; Asselberghs, I.; Hung, S. T.; Clays, K.; Horton, P. N.; Hursthouse, M. B. *Inorg. Chem.* **2006**, *45*, 1215.
(39) Dumur, F.; Mayer, C. R.; Hoang-Thi, K.; Ledoux-Rak, I.; Miomandre, F.; Clavier, G.; Dumas, E.; Meallet-Renault, R.; Frigoli, M.; Zyss, J.; Secheresse, F. *Inorg. Chem.* **2009**, *48*, 8120.
(40) Tessore, F.; Roberto, D.; Ugo, R.; Pizzotti, M.; Quici, S.; Cavazzini, M.; Brun, S.; De Angelis, F. *Inorg. Chem.* **2005**, *44*, 8967.
(41) Dragonetti, C.; Righetto, S.; Roberto, D.; Ugo, R.; Valore, A.; Demartin, F.; De Angelis, F.; Sgamellotti, A.; Fantacci, S. *Inorg. Chim. Acta* **2008**, *361*, 4070.
(42) Boubekeur-Lecaque, L.; Coe, B. J.; Clays, K.; Foerier, S.; Verbiest, T.; Asselberghs, I. *J. Am. Chem. Soc.* **2008**, *130*, 3286.
(43) Coe, B. J.; Fielden, J.; Foxon, S. P.; Brunschwig, B. S.; Asselberghs, I.; Clays, K.; Samoc, A.; Samoc, M. *J. Am. Chem. Soc.* **2010**, *132*, 3496.

(44) Coe, B. J.; Foxon, S. P.; Harper, E. C.; Helliwell, M.; Raftery, J.; Swanson, C. A.; Brunschwig, B. S.; Clays, K.; Franz, E.; Garin, J.; Orduna, J.; Horton, P. N.; Hursthouse, M. B. *J. Am. Chem. Soc.* **2010**, *132*, 1706.
(45) Coe, B. J.; Harries, J. L.; Helliwell, M.; Jones, L. A.; Asselberghs, I.; Clays, K.; Brunschwig, B. S.; Harris, J. A.; Garin, J.; Orduna, J. *J. Am. Chem. Soc.* **2006**, *128*, 12192.
(46) Coe, B. J.; Harris, J. A.; Brunschwig, B. S.; Asselberghs, I.; Clays, K.; Garin, J.; Orduna, J. *J. Am. Chem. Soc.* **2005**, *127*, 13399.
(47) Coe, B. J.; Jones, L. A.; Harris, J. A.; Brunschwig, B. S.; Asselberghs, I.; Clays, K.; Persoons, A. *J. Am. Chem. Soc.* **2003**, *125*, 862.
(48) Coe, B. J.; Jones, L. A.; Harris, J. A.; Brunschwig, B. S.; Asselberghs, I.; Clays, K.; Persoons, A.; Garin, J.; Orduna, J. *J. Am. Chem. Soc.* **2004**, *126*, 3880.
(49) Le Bouder, T.; Maury, O.; Bondon, A.; Costuas, K.; Amouyal, E.; Ledoux, I.; Zyss, J.; Le Bozec, H. *J. Am. Chem. Soc.* **2003**, *125*, 12284.
(50) Senechal, K.; Maury, O.; Le Bozec, H.; Ledoux, I.; Zyss, J. *J. Am. Chem. Soc.* **2002**, *124*, 4560.
(51) Ledoux-Rak, I.; Zyss, J.; Le Bouder, T.; Maury, O.; Bondon, A.; Le Bozec, H. *J. Lumines.* **2005**, *111*, 307.
(52) Le Bozec, H.; Le Bouder, T.; Maury, O.; Ledoux, I.; Zyss, J. *J. Opt. A-Pure Appl. Opt.* **2002**, *4*, S189.
(53) Das, S.; Jana, A.; Ramanathan, V.; Chakraborty, T.; Ghosh, S.; Das, P. K.; Bharadwaj, P. K. *J. Organomet. Chem.* **2006**, *691*, 2512.
(54) Coe, B. J.; Harris, J. A.; Brunschwig, B. S. *J. Phys. Chem. A* **2002**, *106*, 897.
(55) Batema, G. D.; Lutz, M.; Spek, A. L.; van Walree, C. A.; Donega, C. D. M.; Meijerink, A.; Havenith, R. W. A.; Perez-Moreno, J.; Clays, K.; Buchel, M.; van Dijken, A.; Bryce, D. L.; van Klink, G. P. M.; van Koten, G. *Organometallics* **2008**, *27*, 1690.
(56) Coe, B. J.; Fitzgerald, E. C.; Helliwell, M.; Brunschwig, B. S.; Fitch, A. G.; Harris, J. A.; Coles, S. J.; Horton, P. N.; Hursthouse, M. B. *Organometallics* **2008**, *27*, 2730.
(57) Lucenti, E.; Cariati, E.; Dragonetti, C.; Manassero, L.; Tessore, F. *Organometallics* **2004**, *23*, 687.
(58) Pizzotti, M.; Ugo, R.; Dragonetti, C.; Annoni, E.; Demartin, F.; Mussini, P. *Organometallics* **2003**, *22*, 4001.
(59) Zhang, J.; Chu, B. W. K.; Zhu, N.; Yam, V. W. W. *Organometallics* **2007**, *26*, 5423.
(60) Coe, B. J.; McCleverty, J. A.; Meyer, T. J. (eds.) *Compr. Coord. Chem. II*, Elsevier Oxford (UK) 2004, *9*, 621.
(61) Coe, B. J. *Chem. Eur. J.* **1999**, *5*.
(62) Lee, K. S.; Kim, O.-K. *Photonics Sci. News* **1999**, *4*.
(63) Morales-Saavedra, O. G.; Sanchez-Vergara, M. E.; Rodriguez-Rosales, A. A.; Ortega-Martinez, R.; Ortiz-Rebollo, A.; Frontana-Uribe, B. A.; Garcia-Montalvo, V. *Mater. Chem. Phys.* **2010**, *123*, 776.
(64) De Souza, L. A.; Da Silva, A. M.; Junqueira, G. M. A.; Carvalho, A. C. M.; Dos Santos, H. F. *J. Mol. Struct.: THEOCHEM* **2010**, *959*, 92.

(65) Zawadzka, M.; Wang, J.; Blau, W. J.; Senge, M. O. *Chem. Phys. Lett.* **2009**, *477*, 330.
(66) Sheng, N.; Sun, J.; Bian, Y. Z.; Jiang, J. Z.; Xu, D. *J. Porphyr. Phthalocyanines* **2009**, *13*, 275.
(67) Reeve, J. E.; Collins, H. A.; De Mey, K.; Kohl, M. M.; Thorley, K. J.; Paulsen, O.; Clays, K.; Anderson, H. L. *J. Am. Chem. Soc.* **2009**, *131*, 2758.
(68) Odom, S. A.; Kelley, R. F.; Ohira, S.; Ensley, T. R.; Huang, C.; Padilha, L. A.; Webster, S.; Coropceanu, V.; Barlow, S.; Hagan, D. J.; Van Stryland, E. W.; Bredas, J. L.; Anderson, H. L.; Wasielewski, M. R.; Marder, S. R. *J. Phys. Chem. A* **2009**, *113*, 10826.
(69) Wahab, A.; Bhattacharya, M.; Ghosh, S.; Samuelson, A. G.; Das, P. K. *J. Phys. Chem. B* **2008**, *112*, 2842.
(70) Ray, P. C.; Bonifassi, P.; Leszczynski, J. *J. Phys. Chem. A* **2008**, *112*, 2870.
(71) Li, Y. J.; Pritchett, T. M.; Huang, J. D.; Ke, M. R.; Shao, P.; Sun, W. F. *J. Phys. Chem. A* **2008**, *112*, 7200.
(72) Larciprete, M. C.; Mangialardo, S.; Belardini, A.; Sibilia, C.; Bertolotti, M. *J. Appl. Phys.* **2008**, *104*, 4.
(73) Ishii, K.; Shiine, M.; Shimizu, Y.; Hoshino, S.; Abe, H.; Sogawa, K.; Kobayashi, N. *J. Phys. Chem. B* **2008**, *112*, 3138.
(74) Holtmann, J.; Walczuk, E.; Dede, M.; Wittenburg, C.; Heck, J.; Archetti, G.; Wortmann, R.; Kuball, H.-G.; Wang, Y.-H.; Liu, K.; Luo, Y. *J. Phys. Chem. B* **2008**, *112*, 14751.
(75) Chen, Z. H.; Zhong, C.; Zhang, Z.; Li, Z. Y.; Niu, L. H.; Bin, Y. J.; Zhang, F. S. *J. Phys. Chem. B* **2008**, *112*, 7387.
(76) Sankar, J.; Rath, H.; Prabhuraja, V.; Gokulnath, S.; Chandrashekar, T. K.; Purohit, C. S.; Verma, S. *Chem.-Eur. J.* **2007**, *13*, 105.
(77) Ostuni, R.; Larciprete, M. C.; Leahu, G.; Belardini, A.; Sibilia, C.; Bertolotti, M. *J. Appl. Phys.* **2007**, *101*, 5.
(78) Larciprete, M. C.; Ostuni, R.; Belardini, A.; Alonzo, M.; Leahu, G.; Fazio, E.; Sibilia, C.; Bertolotti, M. *Photonics Nanostruct.* **2007**, *5*, 73.
(79) Grishina, A. D.; Konnov, F. Y.; Gorbunova, Y. G.; Enakieva, Y. Y.; Pereshivko, L. Y.; Krivenko, T. V.; Savel'ev, V. V.; Vannikov, A. V.; Tsivadze, A. Y. *Russ. J. Phys. Chem. A* **2007**, *81*, 982.
(80) Zhang, T. G.; Zhao, Y. X.; Song, K.; Asselberghs, I.; Persoons, A.; Clays, K.; Therien, M. J. *Inorg. Chem.* **2006**, *45*, 9703.
(81) Dini, D.; Calvete, M. J. F.; Hanack, M.; Pong, R. G. S.; Flom, S. R.; Shirk, J. S. *J. Phys. Chem. B* **2006**, *110*, 12230.
(82) Bonifassi, P.; Ray, P. C.; Leszczynski, J. *Chem. Phys. Lett.* **2006**, *431*, 321.
(83) Zhang, T. G.; Zhao, Y. X.; Asselberghs, I.; Persoons, A.; Clays, K.; Therien, M. J. *J. Am. Chem. Soc.* **2005**, *127*, 9710.
(84) Liu, H. Y.; Tian, J. C.; Ying, X.; Xu, Z. G.; Liao, S. J.; Chang, C. K. *Chin. J. Struct. Chem.* **2005**, *24*, 263.
(85) Kumar, R.; Misra, R.; Prabhuraja, V.; Chandrashekar, T. K. *Chem.-Eur. J.* **2005**, *11*, 5695.
(86) Dini, D.; Hanack, M.; Meneghetti, M. *J. Phys. Chem. B* **2005**, *109*, 12691.

(87) Brown, R. J. C.; Kucernak, A. R.; Taylor, A. G. *Thin Solid Films* **2005**, *476*, 373.
(88) Annoni, E.; Pizzotti, M.; Ugo, R.; Quici, S.; Morotti, T.; Bruschi, M.; Mussini, P. *Eur. J. Inorg. Chem.* **2005**, 3857.
(89) Pizzotti, M.; Annoni, E.; Ugo, R.; Bruni, S.; Quici, S.; Fantucci, P.; Bruschi, M.; Zerbi, G.; Del Zoppo, M. *J. Porphyr. Phthalocyanines* **2004**, *8*, 1311.
(90) Manaka, T.; Li, C. Q.; Cheng, X. M.; Iwamoto, M. *J. Chem. Phys.* **2004**, *120*, 7725.
(91) Nagatani, H.; Samec, Z.; Brevet, P. F.; Fermin, D. J.; Girault, H. H. *J. Phys. Chem. B* **2003**, *107*, 786.
(92) Maya, E. M.; Garcia-Frutos, E. M.; Vasquez, P.; Torres, T.; Martin, G.; Rogo, G.; Agullo-Lopez, F.; Gonzalez-Jonte, R. H.; Ferro, R.; Garcia de la Vega, G.; Ledoux, I.; Zyss, J. *J. Phys. Chem. A* **2003**, *107*, 2110.
(93) Chen, Y.; Hanack, M.; O'Flaherty, S.; Bernd, G.; Zeug, A.; Roeder, B.; Blau, W. J. *Macromolecules* **2003**, *36*, 3786.
(94) Uyeda, H. T.; Zhao, Y. X.; Wostyn, K.; Asselberghs, I.; Clays, K.; Persoons, A.; Therien, M. J. *J. Am. Chem. Soc.* **2002**, *124*, 13806.
(95) Li, C. Q.; Manaka, T.; Cheng, X. M.; Iwamoto, M. *J. Appl. Phys.* **2002**, *92*, 6390.
(96) Di Bella, S.; Fragala, I. *New J. Chem.* **2002**, *26*, 285.
(97) de la Torre, G.; Vazquez, P.; Agullo-Lopez, F.; Torres, T. *Chem. Rev.* **2004**, *104*, 3723.
(98) Senge, M. O.; Fazekas, M.; Notaras, E. G. A.; Blau, W. J.; Zawadzka, M.; Locos, O. B.; Ni Mhuircheartaigh, E. M. *Adv. Mater.* **2007**, *19*, 2737.
(99) Trujillo, A.; Fuentealba, M.; Carrillo, D.; Manzur, C.; Ledoux-Rak, I.; Hamon, J. R.; Saillard, J. Y. *Inorg. Chem.* **2010**, *49*, 2750.
(100) Borbone, F.; Carella, A.; Caruso, U.; Roviello, G.; Tuzi, A.; Dardano, P.; Lettieri, S.; Maddalena, P.; Barsella, A. *Eur. J. Inorg. Chem.* **2008**, 1846.
(101) Gradinaru, J.; Forni, A.; Druta, V.; Tessore, F.; Zecchin, S.; Quici, S.; Garbalau, N. *Inorg. Chem.* **2007**, *46*, 884.
(102) Donmez, E.; Kara, H.; Karakas, A.; Unver, H.; Elmali, A. *Spectroc. Acta Pt. A-Molec. Biomolec. Spectr.* **2007**, *66*, 1141.
(103) Sheikhshoaie, I.; Mashhadizadeh, M. H.; Monadi, N. *Asian J. Chem.* **2006**, *18*, 25.
(104) Rivera, J. M.; Guzman, D.; Rodriguez, M.; Lamere, J. F.; Nakatani, K.; Santillan, R.; Lacroix, P. G.; Farfan, N. *J. Organomet. Chem.* **2006**, *691*, 1722.
(105) Rigamonti, L.; Demartin, F.; Forni, A.; Righetto, S.; Pasini, A. *Inorg. Chem.* **2006**, *45*, 10976.
(106) Liu, C. G.; Qiu, Y. Q.; Sun, S. L.; Chen, H.; Li, N.; Su, Z. M. *Chem. Phys. Lett.* **2006**, *429*, 570.
(107) Karakas, A.; Elmali, A.; Unver, H.; Kara, H.; Yahsi, Y. *Z.Naturforsch.(B)* **2006**, *61*, 968.
(108) Elmali, A.; Karakas, A.; Unver, H. *Chem. Phys.* **2005**, *309*, 251.
(109) Costes, J. P.; Lamere, J. F.; Lepetit, C.; Lacroix, P. G.; Dahan, F. *Inorg. Chem.* **2005**, *44*, 1973.

(110) Margeat, O.; Lacroix, P. G.; Costes, J. P.; Donnadieu, B.; Lepetit, C. *Inorg. Chem.* **2004**, *43*, 4743.
(111) Lacroix, P. G.; Averseng, F.; Malfant, I.; Nakatani, K. *Inorg. Chim. Acta* **2004**, *357*, 3825.
(112) Di Bella, S.; Fragala, I.; Guerri, A.; Dapporto, P.; Nakatani, K. *Inorg. Chim. Acta* **2004**, *357*, 1161.
(113) Borbone, F.; Caruso, U.; Centore, R.; De Maria, A.; Fort, A.; Fusco, M.; Panunzi, B.; Roviello, A.; Tuzi, A. *Eur. J. Inorg. Chem.* **2004**, 2467.
(114) Di Bella, S.; Fragala, I. *Eur. J. Inorg. Chem.* **2003**, 2606.
(115) Aiello, I.; Caruso, U.; Ghedini, A.; Panunzi, B.; Quatela, A.; Roviello, A.; Sarcinelli, F. *Polymer* **2003**, *44*, 7635.
(116) Ikeda, K.; Ohkoshi, S.; Hashimoto, K. *J. Electrochem. Soc.* **2002**, *149*, E445.
(117) Evans, C.; Luneau, D. *J. Chem. Soc.-Dalton Trans.* **2002**, 83.
(118) Cariati, F.; Caruso, U.; Centore, R.; Marcolli, W.; De Maria, A.; Panunzi, B.; Roviello, A.; Tuzi, A. *Inorg. Chem.* **2002**, *41*, 6597.
(119) Lacroix, P. G. *Eur. J. Inorg. Chem.* **2001**, 339.
(120) Powell, C. E.; Humphrey, M. G. *Coord. Chem. Rev.* **2004**, *248*, 725.
(121) Scarpaci, A.; Monnereau, C.; Hergue, N.; Blart, E.; Legoupy, S.; Odobel, F.; Gorfo, A.; Perez-Moreno, J.; Clays, K.; Asselberghs, I. *Dalton Trans.* **2009**, 4538.
(122) Rigamonti, L.; Babgi, B.; Cifuentes, M. P.; Roberts, R. L.; Petrie, S.; Stranger, R.; Righetto, S.; Teshome, A.; Asselberghs, I.; Clays, K.; Humphrey, M. G. *Inorg. Chem.* **2009**, *48*, 3562.
(123) Mendes, P. J.; Carvalho, A. J. P.; Ramalho, J. P. P. *J. Mol. Struct.: THEOCHEM* **2009**, *900*, 110.
(124) Babgi, B.; Rigamonti, L.; Cifuentes, M. P.; Corkery, T. C.; Randles, M. D.; Schwich, T.; Petrie, S.; Stranger, R.; Teshome, A.; Asselberghs, I.; Clays, K.; Samoc, M.; Humphrey, M. G. *J. Am. Chem. Soc.* **2009**, *131*, 10293.
(125) Tao, C. H.; Yang, H.; Zhu, N. Y.; Yam, V. W. W.; Xu, S. J. *Organometallics* **2008**, *27*, 5453.
(126) Sniechowski, M.; Niziol, J.; Luzny, W. *Fibres Text. East. Eur.* **2008**, *16*, 89.
(127) Luc, J.; Bouchouit, K.; Czaplicki, R.; Fillaut, J. L.; Sahraoui, B. *Opt. Express* **2008**, *16*, 15633.
(128) Fondum, T. N.; Green, K. A.; Randles, M. D.; Cifuentes, M. P.; Willis, A. C.; Teshome, A.; Asselberghs, I.; Clays, K.; Humphrey, M. G. *J. Organomet. Chem.* **2008**, *693*, 1605.
(129) Yuan, P.; Yin, J.; Yu, G. A.; Hu, Q. Y.; Liu, S. H. *Organometallics* **2007**, *26*, 196.
(130) Makowska-Janusik, M.; Kityk, I. V.; Gauthier, N.; Paul, F. *J. Phys. Chem. C* **2007**, *111*, 12094.
(131) Morrall, J. P. L.; Cifuentes, M. P.; Humphrey, M. G.; Kellens, R.; Robijns, E.; Asselberghs, I.; Clays, K.; Persoons, A.; Samoc, M.; Willis, A. C. *Inorg. Chim. Acta* **2006**, *359*, 998.
(132) Migalska-Zalas, A.; Luc, J.; Sahraoui, B.; Kityk, I. V. *Opt. Mater.* **2006**, *28*, 1147.

(133) Xia, H. P.; Wen, T. B.; Hu, Q. Y.; Wang, X.; Chen, X. G.; Shek, L. Y.; Williams, I. D.; Wong, K. S.; Wong, G. K. L.; Jia, G. C. *Organometallics* **2005**, *24*, 562.
(134) Humphrey, P. A.; Turner, P.; Masters, A. F.; Field, L. D.; Cifuentes, M. P.; Humphrey, M. G.; Asselberghs, I.; Persoons, A.; Samoc, M. *Inorg. Chim. Acta* **2005**, *358*, 1663.
(135) Green, M. L. H.; Marder, S. R.; Thompson, M. E.; Bandy, J. A.; Bloor, D.; Kolinsky, P. V.; Jones, R. J. *Nature* **1987**, *330*, 360.
(136) Steffens, S.; Prosenc, M. H.; Heck, J.; Asselberghs, I.; Clays, K. *Eur. J. Inorg. Chem.* **2008**, 1999.
(137) Qiu, Y. Q.; Liu, X. D.; Sun, S. L.; Fan, M.; Su, Z. M.; Wang, R. S. *J. Mol. Struct.: THEOCHEM* **2008**, *863*, 66.
(138) Krishnakumar, V.; Kalyanaraman, S.; Piasecki, M.; Kityk, I. V.; Bragiel, P. *J. Raman Spectrosc.* **2008**, *39*, 1450.
(139) Garcia, M. H.; Florindo, P.; Piedade, M. F. M.; Duarte, M. T.; Robalo, M. P.; Heck, J.; Wittenburg, C.; Holtmann, J.; Licandro, E. *J. Organomet. Chem.* **2008**, *693*, 2987.
(140) Reddy, A. R.; Ranjini, A.; Das, P. K.; Samuelson, A. G. *Inorg. Chim. Acta* **2007**, *360*, 2778.
(141) Mang, C. Y.; Huang, B. S.; Liu, C. P.; Wu, K. C. *J. Mol. Struct.: THEOCHEM* **2007**, *808*, 145.
(142) Fuentealba, M.; Toupet, L.; Manzur, C.; Carrillo, D.; Ledoux-Rak, I.; Hamon, J. R. *J. Organomet. Chem.* **2007**, *692*, 1099.
(143) Tian, X. H.; Ru, W.; Zhong, J. H.; Lin, J. P.; Li, C. Y.; Luo, X. L. *Chem. Phys.* **2006**, *324*, 667.
(144) Mang, C. Y.; Wu, K. C. *Int. J. Quantum Chem.* **2006**, *106*, 2529.
(145) Malessa, M.; Heck, J.; Kopf, J.; Garcia, M. H. *Eur. J. Inorg. Chem.* **2006**, 857.
(146) Liao, Y.; Eichinger, B. E.; Firestone, K. A.; Haller, M.; Luo, J. D.; Kaminsky, W.; Benedict, J. B.; Reid, P. J.; Jen, A. K. Y.; Dalton, L. R.; Robinson, B. H. *J. Am. Chem. Soc.* **2005**, *127*, 2758.
(147) Lee, I. S.; Choi, D. S.; Shin, D. M.; Chung, Y. K.; Choi, C. H. *Organometallics* **2004**, *23*, 1875.
(148) Wenseleers, W.; Goovaerts, E.; Hepp, P.; Garcia, M. H.; Robalo, M. P.; Dias, A. R.; Piedade, M. F. M.; Duarte, M. T. *Chem. Phys. Lett.* **2003**, *367*, 390.
(149) Shi, Y.; Zhang, C.; Zhang, H.; Bechtel, J. H.; Dalton, L. R.; Robinson, B. H.; Steier, W. H. *Science* **2000**, *288*.
(150) Lui, S.; Haller, M. A.; Ma, H.; Dalton, L. R.; Jang, S.-H.; Jen, A. K.-Y. *Adv. Mater.* **2003**, *127*, 2758.
(151) Shao, P.; Li, Y. J.; Yi, J.; Pritchett, T. M.; Sun, W. F. *Inorg. Chem.* **2010**, *49*, 4507.
(152) Natrajan, L. S.; Toulmin, A.; Chew, A.; Magennis, S. W. *Dalton Trans.* **2010**, *39*, 10837.
(153) Li, Y. J.; Pritchett, T. M.; Shao, P.; Haley, J. E.; Zhu, H. J.; Sun, W. F. *J. Organomet. Chem.* **2009**, *694*, 3688.

(154) Ge, Q.; Dalton, G. T.; Humphrey, M. G.; Samoc, M.; Hor, T. S. A. *Chem.-Asian J.* **2009**, *4*, 998.
(155) Ge, Q.; Corkery, T. C.; Humphrey, M. G.; Samoc, M.; Hor, T. S. A. *Dalton Trans.* **2009**, 6192.
(156) Dragonetti, C.; Balordi, M.; Colombo, A.; Roberto, D.; Ugo, R.; Fortunati, I.; Garbin, E.; Ferrante, C.; Bozio, R.; Abbotto, A.; Le Bozec, H. *Chem. Phys. Lett.* **2009**, *475*, 245.
(157) Boca, S. C.; Four, M.; Bonne, A.; van der Sanden, B.; Astilean, S.; Baldeck, P. L.; Lemercier, G. *Chem. Commun.* **2009**, 4590.
(158) Zhu, Q. Y.; Lu, W.; Zhang, Y.; Bian, G. Q.; Gu, J.; Lin, X. M.; Dai, M. *Eur. J. Inorg. Chem.* **2008**, 230.
(159) Xiang, H.; Tian, Z. Y.; Wang, S. F.; Wang, Z. W.; Li, Z.; Yang, H.; Yao, J. N.; Gong, Q. H. *Chin. Phys. B* **2008**, *17*, 2535.
(160) Girardot, C.; Cao, B.; Mulatier, J. C.; Baldeck, P. L.; Chauvin, J.; Riehl, D.; Delaire, J. A.; Andraud, C.; Lemercier, G. *Chemphyschem* **2008**, *9*, 1531.
(161) Sumalekshmy, S.; Henary, M. M.; Siegel, N.; Lawson, P. V.; Wu, Y.; Schmidt, K.; Bredas, J. L.; Perry, J. W.; Fahrni, C. J. *J. Am. Chem. Soc.* **2007**, *129*, 11888.
(162) Morales-Saavedra, O. G.; Vergara, M. E. S.; Rebollo, A. O.; Ortega-Martinez, R. *J. Phys. Chem. Solids* **2007**, *68*, 1571.
(163) Guo, S. L.; Li, T. P.; Wang, T. B.; Liu, Z. S.; Cao, T. D. *Opt. Mater.* **2007**, *29*, 494.
(164) Girardot, C.; Lemercier, G.; Mulatier, J. C.; Chauvin, J.; Baldeck, P. L.; Andraud, C. *Dalton Trans.* **2007**, 3421.
(165) Feuvrie, C.; Maury, O.; Le Bozec, H.; Ledoux, I.; Morrall, J. P.; Dalton, G. T.; Samoc, M.; Humphrey, M. G. *J. Phys. Chem. A* **2007**, *111*, 8980.
(166) Fabbrini, G.; Ricco, R.; Menna, E.; Maggini, M.; Amendola, V.; Garbin, M.; Villano, M.; Meneghetti, M. *Phys. Chem. Chem. Phys.* **2007**, *9*, 616.
(167) Coe, B. J.; Samoc, M.; Samoc, A.; Zhu, L. Y.; Yi, Y. P.; Shuai, Z. G. *J. Phys. Chem. A* **2007**, *111*, 472.
(168) Righetto, S.; Rondena, S.; Locatelli, D.; Roberto, D.; Tessore, F.; Ugo, R.; Quici, S.; Roma, S.; Korystov, D.; Srdanov, V. I. *J. Mater. Chem.* **2006**, *16*, 1439.
(169) Zheng, Q. D.; He, G. S.; Prasad, P. N. *J. Mater. Chem.* **2005**, *15*, 579.
(170) Yang, Z.; Wu, Z. K.; Ma, J. S.; Xia, A. D.; Li, Q. S.; Liu, C. L.; Gong, Q. H. *Appl. Phys. Lett.* **2005**, *86*, 3.
(171) Tian, Y. P.; Zhang, M. L.; Hu, Z. J.; Hu, H. M.; Wu, J. Y.; Zhang, X. J.; Zhang, S. Y.; Tao, X. T.; Jiang, M. H.; Chen, H. P.; Chantrapromma, S.; Fun, H. K. *Transit. Met. Chem.* **2005**, *30*, 778.
(172) Fan, Y. T.; Gang, L.; Li, Z. F.; Hou, H. W.; Mao, H. R. *J. Mol. Struct.* **2004**, *693*, 217.
(173) Fabbrini, G.; Menna, E.; Maggini, M.; Canazza, A.; Marcolongo, G.; Meneghetti, M. *J. Am. Chem. Soc.* **2004**, *126*, 6238.
(174) Sun, W. F.; Patton, T. H.; Stultz, L. K.; Claude, J. P. *Optics Commun.* **2003**, *218*, 189.

(175) Kar, S.; Miller, T. A.; Chakraborty, S.; Sarkar, B.; Pradhan, B.; Sinha, R. K.; Kundu, T.; Ward, M. D.; Lahiri, G. K. *Dalton Trans.* **2003**, 2591.
(176) Jiang, C. W.; Chao, H.; Li, R. H.; Li, H.; Jia, L. N. *J. Coord. Chem.* **2003**, *56*, 147.
(177) Mesnil, H.; Schanne-Klein, M. C.; Hache, F.; Alexandre, M.; Lemercier, G.; Andraud, C. *Phys. Rev. A* **2002**, *66*, 9.
(178) Jiang, C. W.; Chao, H.; Li, R. H.; Li, H.; Ji, L. N. *Transit. Met. Chem.* **2002**, *27*, 520.
(179) Fu, K. F.; Henbest, K.; Zhang, Y. F. J.; Valentin, S.; Sun, Y. P. *J. Photochem. Photobiol. A-Chem.* **2002**, *150*, 143.
(180) Chao, H.; Li, R. H.; Huang, Q. W.; Ji, L. N. *Chin. J. Chem.* **2002**, *20*, 1235.
(181) Andraud, C.; Fortrie, R.; Barsu, C.; Stéphan, O.; Chermette, H.; Baldeck, P. L. In *Photoresponsive Polymers II - Advances in Polymer Science*; Marder, S. R., Lee, K.-S., Eds.; Springer Verlag: Berlin, 2008; Vol. 214, p 149.
(182) Pawlicki, M.; Collins, H. A.; Denning, R. G.; Anderson, H. L. *Angew. Chem. Int. Ed.* **2009**, *48*, 3244.
(183) Yuksek, M.; Elmali, A.; Durmus, M.; Yaglioglu, H. G.; Unver, H.; Nyokong, T. *J. Opt.* **2010**, *12*, 9.
(184) Tekin, S.; Kurum, U.; Durmus, M.; Yaglioglu, H. G.; Nyokong, T.; Elmali, A. *Optics Commun.* **2010**, *283*, 4749.
(185) Poon, C. T.; Chan, P. S.; Man, C.; Jiang, F. L.; Wong, R. N. S.; Mak, N. K.; Kwong, D. W. J.; Tsao, S. W.; Wong, W. K. *J. Inorg. Biochem.* **2010**, *104*, 62.
(186) Ma, L.; Zhang, Y. D.; Yuan, P. *Opt. Express* **2010**, *18*, 17666.
(187) Dini, D.; Meneghetti, M.; Calvete, M. J. F.; Arndt, T.; Liddiard, C.; Hanack, M. *Chem.-Eur. J.* **2010**, *16*, 1212.
(188) D'Aleo, A.; Allali, M.; Picot, A.; Baldeck, P. L.; Toupet, L.; Andraud, C.; Maury, O. *Comptes Rend. Chim.* **2010**, *13*, 681.
(189) Carvalho, E. F. A.; Calvete, M. J. F.; Cavaleiro, J. A. S.; Dini, D.; Meneghetti, M.; Tome, A. C. *Inorg. Chim. Acta* **2010**, *363*, 3945.
(190) Yang, J. Y.; He, C. Y.; Song, Y. L.; Gu, J. H. *J. Opt. A: Pure Appl. Opt.* **2009**, *11*, 6.
(191) Saydam, S.; Yilmaz, E.; Bagci, F.; Yaglioglu, H. G.; Elmali, A.; Salih, B.; Bekaroglu, O. *Eur. J. Inorg. Chem.* **2009**, 2096.
(192) Odom, S. A.; Webster, S.; Padilha, L. A.; Peceli, D.; Hu, H.; Nootz, G.; Chung, S. J.; Ohira, S.; Matichak, J. D.; Przhonska, O. V.; Kachkovski, A. D.; Barlow, S.; Bredas, J. L.; Anderson, H. L.; Hagan, D. J.; Van Stryland, E. W.; Marder, S. R. *J. Am. Chem. Soc.* **2009**, *131*, 7510.
(193) Modibane, D. K.; Nyokong, T. *Polyhedron* **2009**, *28*, 1475.
(194) Kumar, R. S. S.; Rao, S. V.; Giribablu, L.; Rao, D. N. *Opt. Mater.* **2009**, *31*, 1042.
(195) Kueruem, U.; Ceyhan, T.; Elmali, A.; Bekaroglu, O. *Optics Commun.* **2009**, *282*, 2426.
(196) He, C. Y.; Duan, W. B.; Shi, G.; Wu, Y. Q.; Ouyang, Q. Y.; Song, Y. L. *Appl. Surf. Sci.* **2009**, *255*, 4696.

(197) Grishina, A. D.; Gorbunova, Y. G.; Pereshivko, L. Y.; Nekrasov, A. A.; Enakieva, Y. Y.; Krivenko, T. V.; Savel'ev, V. V.; Vannikov, A. V.; Tsivadze, A. Y. *Prot. Met. Phys. Chem. Surf.* **2009**, *45*, 535.
(198) Fisher, J. A. N.; Susumu, K.; Therien, M. J.; Yodh, A. G. *J. Chem. Phys.* **2009**, *130*, 8.
(199) Zhang, W.; Jiao, W. Y.; He, C. Y.; Yang, K.; Zhang, X. R.; Wang, Y. X.; Song, Y. L. *J. Phys B: At. Mol. Opt. Phys.* **2008**, *41*, 7.
(200) Yueksek, M.; Ceyhan, T.; Yaglioglu, H. G.; Elmali, A.; Bekaroglu, O. *Optics Commun.* **2008**, *281*, 2970.
(201) Yaglioglu, H. G.; Arslan, M.; Abdurrahmanoglu, S.; Unver, H.; Elmali, A.; Bekaroglu, O. *J. Phys. Chem. Solids* **2008**, *69*, 161.
(202) Wang, D.; Zhang, S. L.; Zhang, Y. H.; Wang, H.; Mu, H. X.; Wang, G. B.; Jiang, Z. H. *Dyes and Pigments* **2008**, *79*, 217.
(203) Venkatram, N.; Rao, D. N.; Giribabu, L.; Rao, S. V. *Appl. Phys. B: Lasers Opt.* **2008**, *91*, 149.
(204) Venkatram, N.; Rao, D. N.; Giribabu, L.; Rao, S. V. *Chem. Phys. Lett.* **2008**, *464*, 211.
(205) Thorley, K. J.; Hales, J. M.; Anderson, H. L.; Perry, J. W. *Angew. Chem. Int. Ed.* **2008**, *47*, 7095.
(206) Shi, G.; Wang, Y. X.; Liu, D. J.; Zhang, X. R.; Yang, J. Y.; Yang, K.; Song, Y. L. *J. Appl. Phys.* **2008**, *104*.
(207) Liu, Y. L.; Liu, Z. B.; Tian, J. G.; Zhu, Y.; Zheng, J. Y. *Optics Commun.* **2008**, *281*, 776.
(208) Li, F.; Zheng, Q. G.; Yang, G.; Dai, N. L.; Lu, P. X. *Mater. Lett.* **2008**, *62*, 3059.
(209) Li, F.; Lu, P. X.; Long, H.; Yang, G.; Li, Y. H.; Zheng, Q. Q. *Opt. Express* **2008**, *16*, 14571.
(210) Jha, P. C.; Minaev, B.; Agren, H. *J. Chem. Phys.* **2008**, *128*, 13.
(211) He, N.; Chen, Y.; Doyle, J.; Liu, Y.; Blau, W. J. *Dyes and Pigments* **2008**, *76*, 569.
(212) Grishina, A. D.; Gorbunova, Y. G.; Enakieva, Y. Y.; Krivenko, T. V.; Savel'ev, V. V.; Vannikov, A. V.; Tsivadze, A. Y. *High Energy Chem.* **2008**, *42*, 297.
(213) Farrer, N. J.; Sadler, P. J. *Aust. J. Chem.* **2008**, *61*, 669.
(214) Dy, J.; Ogawa, K.; Kamada, K.; Ohta, K.; Kobuke, Y. *Chem. Commun.* **2008**, 3411.
(215) Dini, D.; Calvete, M. J. F.; Hanack, M.; Meneghettit, M. *J. Phys. Chem. A* **2008**, *112*, 8515.
(216) Day, P. N.; Nguyen, K. A.; Pachter, R. *J. Chem. Theory Comput.* **2008**, *4*, 1094.
(217) Ceyhan, T.; Yuksek, M.; Yaglioglu, H. G.; Salih, B.; Erbil, M. K.; Elmali, A.; Bekaroglu, O. *Dalton Trans.* **2008**, 2407.
(218) Ceyhan, T.; Ozdag, M. A.; Salih, B.; Erbil, M. K.; Elmali, A.; Ozkaya, A. R.; Bekaroglu, O. *Eur. J. Inorg. Chem.* **2008**, 4943.
(219) Bin, Y. J.; Xu, S.; Li, Z. Y.; Huang, L.; Zhang, Z.; Zhang, F. S. *Chin. Phys. Lett.* **2008**, *25*, 3257.

(220) Yoon, M. C.; Noh, S. B.; Tsuda, A.; Nakamura, Y.; Osuka, A.; Kim, D. *J. Am. Chem. Soc.* **2007**, *129*, 10080.
(221) Yeh, H. C.; Chen, C. T.; Yu, J. W.; Tsai, P. C.; Wang, J. K. *J. Porphyr. Phthalocyanines* **2007**, *11*, 857.
(222) Vannikov, A. V.; Grishina, A. D. *High Energy Chem.* **2007**, *41*, 162.
(223) Sun, W. F.; Wang, G.; Li, Y. J.; Calvete, M. J. F.; Dini, D.; Hanack, M. *J. Phys. Chem. A* **2007**, *111*, 3263.
(224) Sathiyamoorthy, K.; Vijayan, C.; Kothiyal, M. P. *J. Phys. D-Appl. Phys.* **2007**, *40*, 6121.
(225) Mori, S.; Kim, K. S.; Yoon, Z. S.; Noh, S. B.; Kim, D.; Osuka, A. *J. Am. Chem. Soc.* **2007**, *129*, 11344.
(226) Mathews, S. J.; Kumar, S. C.; Giribabu, L.; Rao, S. V. *Mater. Lett.* **2007**, *61*, 4426.
(227) Liu, Y.; O'Flaherty, S. M.; Chen, Y.; Araki, Y.; Bai, J. R.; Doyle, J.; Blau, W. J.; Ito, O. *Dyes and Pigments* **2007**, *75*, 88.
(228) Li, Z.; Chen, Z.; Xu, S.; Niu, L.; Zhang, Z.; Zhang, F.; Kasatani, K. *Chem. Phys. Lett.* **2007**, *447*, 110.
(229) Kumar, R. S. S.; Rao, S. V.; Giribabu, L.; Rao, D. N. *Chem. Phys. Lett.* **2007**, *447*, 274.
(230) Kim, K. S.; Noh, S. B.; Katsuda, T.; Ito, S.; Osuka, A.; Kim, D. *Chem. Commun.* **2007**, 2479.
(231) Jiang, F. L.; Wong, W. K.; Zhu, X. J.; Zhou, G. J.; Wong, W. Y.; Wu, P. L.; Tam, H. L.; Cheah, K. W.; Ye, C.; Liu, Y. *Eur. J. Inorg. Chem.* **2007**, 3365.
(232) He, C. Y.; Wu, Y. Q.; Shi, G.; Jiang, L.; Duan, W.; Song, Y.; Chang, Q. *J. Porphyr. Phthalocyanines* **2007**, *11*, 496.
(233) Fu, S. T.; Zhu, X. J.; Zhou, G. J.; Wong, W. Y.; Ye, C.; Wong, W. K.; Li, Z. Y. *Eur. J. Inorg. Chem.* **2007**, 2004.
(234) Derkowska, B.; Wojdyla, M.; Czaplicki, R.; Bala, W.; Sahraoui, B. *Optics Commun.* **2007**, *274*, 206.
(235) Chen, Y.; He, N.; Doyle, J. J.; Liu, Y.; Zhuang, X. D.; Blau, W. J. *J. Photochem. Photobiol. A-Chem.* **2007**, *189*, 414.
(236) Chen, Y.; Doyle, J.; Liu, Y.; Strevens, A.; Lin, Y.; El-Khouly, M. E.; Araki, Y.; Blau, W. J.; Ito, O. *J. Photochem. Photobiol. A-Chem.* **2007**, *185*, 263.
(237) Arnbjerg, J.; Jimenez-Banzo, A.; Paterson, M. J.; Nonell, S.; Borrell, J. I.; Christiansen, O.; Ogilby, P. R. *J. Am. Chem. Soc.* **2007**, *129*, 5188.
(238) Zhu, R. Y.; Qiu, X. Q.; Chen, Y.; Qian, S. X. *Chin. Phys. Lett.* **2006**, *23*, 622.
(239) Zhang, X. B.; Feng, J. K.; Ren, A. M.; Sun, C. C. *J. Mol. Struct.: THEOCHEM* **2006**, *767*, 165.
(240) Wang, S. Q.; Gan, Q.; Zhang, Y. F.; Li, S. Y.; Xu, H. J.; Yang, G. Q. *ChemPhysChem* **2006**, *7*, 935.
(241) Tanihara, J.; Ogawa, K.; Kobuke, Y. *J. Photochem. Photobiol. A-Chem.* **2006**, *178*, 140.
(242) Santhi, A.; Namboodiri, V. V.; Radhakrishnan, P.; Nampoori, V. P. N. *J. Appl. Phys.* **2006**, *100*, 5.
(243) Rubio-Pons, O.; Luo, Y.; Agren, H. *J. Chem. Phys.* **2006**, *124*, 5.
(244) Ray, P. C.; Sainudeen, Z. *J. Phys. Chem. A* **2006**, *110*, 12342.

(245) Oar, M. A.; Dichtel, W. R.; Serin, J. M.; Frechet, J. M. J.; Rogers, J. E.; Slagle, J. E.; Fleitz, P. A.; Tan, L. S.; Ohulchanskyy, T. Y.; Prasad, P. N. *Chem. Mater.* **2006**, *18*, 3682.
(246) Morone, M.; Beverina, L.; Abbotto, A.; Silvestri, F.; Collini, E.; Ferrante, C.; Bozio, R.; Pagani, G. A. *Org. Lett.* **2006**, *8*, 2719.
(247) Liu, Z. B.; Zhu, Y. Z.; Zhu, Y.; Chen, S. Q.; Zheng, J. Y.; Tian, J. G. *J. Phys. Chem. B* **2006**, *110*, 15140.
(248) Humphrey, J. L.; Kuciauskas, D. *J. Am. Chem. Soc.* **2006**, *128*, 3902.
(249) Drobizhev, M.; Meng, F.; Rebane, A.; Stepanenko, Y.; Nickel, E.; Spangler, C. W. *J. Phys. Chem. A* **2006**, *110*, 9802.
(250) Drobizhev, M.; Makarov, N. S.; Stepanenko, Y.; Rebane, A. *J. Chem. Phys.* **2006**, *124*, 11.
(251) Doyle, J. J.; Ballesteros, B.; de la Torre, G.; McGovern, D. A.; Kelly, J. M.; Torres, T.; Blau, W. J. *Chem. Phys. Lett.* **2006**, *428*, 307.
(252) Dini, D.; Calvete, M. J. F.; Hanack, M.; Chen, W. Z.; Ji, W. *Arkivoc* **2006**, 77.
(253) Dini, D.; Calvete, M. J. F.; Hanack, M.; Amendolab, V.; Meneghetti, M. *Chem. Commun.* **2006**, *22*, 2394.
(254) Dini, D.; Calvete, M.; Vagin, S.; Hanack, M.; Eriksson, A.; Lopes, C. *J. Porphyr. Phthalocyanines* **2006**, *10*, 1165.
(255) Calvete, M. J. F.; Dini, D.; Hanack, M.; Sancho-Garcia, J. C.; Cheng, W.; Ji, W. *J. Mol. Model* **2006**, *12*, 543.
(256) Ahn, T. K.; Kim, K. S.; Kim, D. Y.; Noh, S. B.; Aratani, N.; Ikeda, C.; Osuka, A.; Kim, D. *J. Am. Chem. Soc.* **2006**, *128*, 1700.
(257) Ying, G.; Hanack, M.; Lee, Y. W.; Dini, D.; Pan, J. F. *Adv. Mater.* **2005**, *17*, 875.
(258) Sendhil, K.; Vijayan, C.; Kothiyal, M. P. *Opt. Mater.* **2005**, *27*, 1606.
(259) Ogawa, K.; Ohashi, A.; Kobuke, Y.; Kamada, K.; Ohta, K. *J. Phys. Chem. B* **2005**, *109*, 22003.
(260) Martin, R. B.; Li, H.; Gu, L.; Kuma, S.; Sanders, C. N. M.; Sun, Y.-P. *Opt. Mater.* **2005**, *27*, 1340.
(261) Kiran, P. P.; Reddy, D. R.; Maiya, B. G.; Dharmadhikari, A. K.; Kumar, G. R.; Rao, D. N. *Optics Commun.* **2005**, *252*, 150.
(262) Ikeda, C.; Yoon, Z. S.; Park, M.; Inoue, H.; Kim, D.; Osuka, A. *J. Am. Chem. Soc.* **2005**, *127*, 534.
(263) Fu, G.; Yoda, T.; Kasatani, K.; Okamoto, H.; Takenaka, S. *Jpn. J. Appl. Phys. Part 1 - Regul. Pap. Short Notes Rev. Pap.* **2005**, *44*, 3945.
(264) Drobizhev, M.; Stepanenko, Y.; Dzenis, Y.; Karotki, A.; Rebane, A.; Taylor, P. N.; Anderson, H. L. *J. Phys. Chem. B* **2005**, *109*, 7223.
(265) Calvete, M. J. F.; Dini, D.; Flom, S. R.; Hanack, M.; Pong, R. G. S.; Shirk, J. S. *Eur. J. Org. Chem.* **2005**, 3499.
(266) Zhou, X.; Ren, A. M.; Feng, J. K.; Liu, X. J. *THEOCHEM-J. Mol. Struct.* **2004**, *679*, 157.
(267) Zhan, H. B.; Chen, W. Z.; Wang, M. Q.; Zou, C. L.; *Chem. Phys. Lett.* **2004**, *389*, 119.

(268) Yin, Y. F.; Wang, X. R.; Ou, H. L.; Han, J. H. *Spectrosc. Spectr. Anal.* **2004**, *24*, 33.
(269) Wada, T.; Higo, T.; Irokawa, K.; Kimura, T.; Yamashita, M. *Jpn. J. Appl. Phys. Part 1 - Regul. Pap. Short Notes Rev. Pap.* **2004**, *43*, 4312.
(270) Liu, M. O.; Tai, C. H.; Wang, W. Y.; Chen, J. R.; Hu, A. T.; Wei, T. H. *J. Organomet. Chem.* **2004**, *689*, 1078.
(271) Karotki, A.; Drobizhev, M.; Dzenis, Y.; Taylor, P. N.; Anderson, H. L.; Rebane, A. *Phys. Chem. Chem. Phys.* **2004**, *6*, 7.
(272) Humphrey, J.; Kuciauskas, D. *J. Phys. Chem. B* **2004**, *108*, 12016.
(273) Hu, A. T.; Wang, W. Y.; Chen, J. R.; Liu, L. C.; Tai, C. H.; Wei, T. H. *Dyes and Pigments* **2004**, *62*, 11.
(274) Drobizhev, M.; Stepanenko, Y.; Dzenis, Y.; Karotki, A.; Rebane, A.; Taylor, P. N.; Anderson, H. L. *J. Am. Chem. Soc.* **2004**, *126*, 15352.
(275) Zhou, X.; Ren, A. M.; Feng, J. K.; Liu, X. J.; Zhang, Y. D. *ChemPhysChem* **2003**, *4*, 991.
(276) Zhong, X. H.; Feng, Y. Y.; Ong, S. L.; Hu, J. Y.; Ng, W. J.; Wang, Z. M. *Chem. Commun.* **2003**, 1882.
(277) Zhan, H.; Chen, W.; Chen, J.; Wang, M. *Mater. Lett.* **2003**, *57*, 1483.
(278) Zahn, H.; Chen, W.; Yu, H.; Weng, M. *Mater. Lett.* **2003**, *57*, 1361.
(279) Yang, G. Y.; Ang, S. G.; Chng, L. L.; Lee, Y. W.; Lau, E. W. P.; Lai, K. S.; Ang, H. G. *Chem.-Eur. J.* **2003**, *9*, 900.
(280) Wagin, S.; Yang, G. Y.; Lee, M. K. Y.; Hanack, M. *Opt. Commun.* **2003**, *228*, 119.
(281) Unnikrishnan, K. P.; Thomas, J.; Nampoori, V. P. N.; Vallabhan, C. P. G. *Optics Commun.* **2003**, *217*, 269.
(282) Unnikrishnan, K. P.; Thomas, J.; Nampoori, V. P. N.; Vallabhan, C. P. G. *Synth. Met.* **2003**, *139*, 371.
(283) Qu, S. L.; Gao, Y. C.; Zhao, C. J.; Wang, Y. X.; Fu, S. Y.; Song, Y. L.; Wang, D. Y.; Qiu, J. R.; Zhu, C. S. *Chem. Phys. Lett.* **2003**, *367*, 767.
(284) Ogawa, K.; Ohashi, A.; Kobuke, Y.; Kamada, K.; Ohta, K. *J. Am. Chem. Soc.* **2003**, *125*, 13356.
(285) O'Flaherty, S. M.; Hold, S. V.; Cook, M. J.; Torres, T.; Chen, Y.; Hanack, M.; Blau, W. J. *Adv. Mater.* **2003**, *15*, 19.
(286) McEwan, K.; Lewis, K.; Yang, G. Y.; Chng, L. L.; Lee, Y. W.; Lau, W. P.; Lai, K. S. *Adv. Funct. Mater.* **2003**, *13*, 863.
(287) Kobuke, Y.; Ogawa, K. *Bull. Chem. Soc. Jap.* **2003**, *76*, 689.
(288) Karotki, A.; Drobizhev, M.; Kruk, M.; Spangler, C. W.; Nickel, E.; Mamardashvili, N.; Rebane, A. *J. Opt. Soc. Am. B* **2003**, *20*, 321.
(289) Gonzalez-Cabello, A.; Claessens, C. G.; Martin-Fuch, G.; Ledoux-Rack, I.; Vazquez, P.; Zyss, J.; Agullo-Lopez, F.; Torres, T. *Synth. Met.* **2003**, *137*, 1487.
(290) Garcia-Frutos, E. M.; O'Flaherty, S. M.; Maya, E. M.; Torre, G. D. L.; Blau, W.; Vazquez, P.; Torres, T. *J. Mater. Chem.* **2003**, *13*, 749.
(291) Drobizhev, M.; Karotki, A.; Kruk, M.; Krivokapic, A.; Anderson, H. L.; Rebane, A. *Chem. Phys. Lett.* **2003**, *370*, 690.

(292) Chen, Y.; O'Flaherty, S. M.; Hanack, M.; Blau, W. J. *J. Mater. Chem.* **2003**, *13*, 2405.
(293) Chen, Y.; Fujitsuka, M.; O'Flaherty, S. M.; Hanack, M.; Blau, W. J. *Adv. Mater.* **2003**, *15*, 899.
(294) Auger, A.; Blau, W. J.; Burnham, P. M.; Chambrier, I.; Cook, M. J.; Isare, B.; Nekelson, F.; O'Flaherty, S. M. *J. Mater. Chem.* **2003**, *13*, 1042.
(295) Wei, T.-H.; Huang, T.-H.; Hu, J.-K. *J. Chem. Phys.* **2002**, *116*, 2536.
(296) Unnikrishnan, K. P.; Thomas, J.; Nampoori, V. P. N.; Vallabhan, C. P. G. *Optics Commun.* **2002**, *204*, 385.
(297) Unnikrishnan, K. P.; Thomas, J.; Nampoori, V. P. N.; Vallabhan, C. P. G. *Chem. Phys.* **2002**, *279*, 209.
(298) Unnikrishnan, K. P.; Thomas, J.; Nampoori, V. P. N.; Vallabhan, C. P. G. *Appl. Phys. B: Lasers Opt.* **2002**, *75*, 871.
(299) Screen, T. E. O.; Thorne, J. R. G.; Denning, R. G.; Bucknell, D. G.; Anderson, H. L. *J. Am. Chem. Soc.* **2002**, *124*, 9712.
(300) Sakai, Y.; Ueda, M.; Yahagi, A.; Tanno, N. *Polymer* **2002**, *43*, 3497.
(301) Kiran, P. P.; Reddy, D. R.; Maiya, B. G.; Dharmadhikari, A. K.; Kumar, G. R.; Desai, N. R. *Appl. Optics* **2002**, *41*, 7631.
(302) Drobizhev, M.; Karotki, A.; Kruk, M.; Rebane, A. *Chem. Phys. Lett.* **2002**, *355*, 175.
(303) Drobizhev, M.; Karotki, A.; Kruk, M.; Mamardashvili, N. Z.; Rebane, A. *Chem. Phys. Lett.* **2002**, *361*, 504.
(304) Chen, Y.; Subramaniam, L. R.; Subramaniam, G.; Fugitsuka, M.; Ito, O.; O'Flaherty, S.; Blau, W. J.; Schneider, T.; Dini, D.; Hanack, M. *Chem. Eur. J.* **2002**, *8*, 4248.
(305) Chen, Y.; O'Flaherty, S.; Fujitsuka, M.; Hanack, M.; Subramanian, L. R.; Ito, O.; Blau, W. J. *Chem. Mater.* **2002**, *14*, 5163.
(306) Barthel, M.; Dini, D.; Vagin, S.; Hanack, M. *Eur. J. Org. Chem.* **2002**, 3756.
(307) Zhu, P. W.; Wang, P.; Qiu, W. F.; Liu, Y. Q.; Ye, C.; Fang, G. Y.; Song, Y. L. *Appl. Phys. Lett.* **2001**, *78*, 1319.
(308) Screen, T. E. O.; Lawton, K. B.; Wilson, G. S.; Dolney, N.; Ispasoiu, R.; Goodson, T.; Martin, S. J.; Bradley, D. D. C.; Anderson, H. L. *J. Mater. Chem.* **2001**, *11*, 312.
(309) Sanghadasa, M.; Shin, I. S.; Clark, R. D.; Guo, H.; Penn, B. G. *J. Appl. Phys.* **2001**, *90*, 31.
(310) Qu, S. L.; Chen, Y.; Song, Y. L.; Wang, Y. X.; Zhao, X. L.; Liu, S. T.; Wang, D. Y. *Chin. Phys. Lett.* **2001**, *18*, 1476.
(311) Qu, S.; Chen, Y.; Weng, Y.; Song, Y.; Liu, S.; Zhao, X.; Weng, D. *Mater. Lett.* **2001**, *51*, 534.
(312) Ma, G. H.; Guo, L. J.; Mi, J.; Liu, Y.; Qian, S. X.; Pan, D. C.; Huang, Y. *Solid State Commun.* **2001**, *118*, 633.
(313) Henari, F. Z. *J. Opt. A-Pure Appl. Opt.* **2001**, *3*, 188.
(314) Guo, F. Q.; Sun, W. F.; Wang, D. Y.; Zhao, L. Z.; Lu, Z. Z.; Nie, Y. X. *Appl. Optics* **2001**, *40*, 1386.
(315) Gu, Y. Z.; Liang, Z. J.; Gan, F. X. *Opt. Mater.* **2001**, *17*, 471.

(316) Cheng, W. D.; Wu, D. S.; Zhang, H.; Chen, J. T. *J. Phys. Chem. B* **2001**, *105*, 11221.
(317) Cheng, W. D.; Wu, D. S.; Zhang, H.; Chen, J. T. *Phys. Rev. B* **2001**, *64*, 11.
(318) Chen, Y.; Song, Y. L.; Qu, S. L.; Wang, D. Y. *Opt. Mater.* **2001**, *18*, 219.
(319) Borissevitch, I. E.; Bezerra, A. G.; Gomes, A. S. L.; De Araujo, R. E.; De Araujo, C. B.; Oliveira, K. M. T.; Trsic, M. *J. Porphyr. Phthalocyanines* **2001**, *5*, 51.
(320) McEwan, K. J.; Bourhill, G.; Robertson, J. M.; Anderson, H. L. *J. Nonlinear Opt. Phys. Mater.* **2000**, *9*, 451.
(321) Zugazagoitia, J. S.; Maya, M.; Damian-Zea, C.; Navarro, P.; Beltran, H. I.; Peon, J. *J. Phys. Chem. A* **2010**, *114*, 704.
(322) Kumar, H. C. S.; Bhat, B. R.; Rudresha, B. J.; Ravindra, R.; Philip, R. *Chem. Phys. Lett.* **2010**, *494*, 95.
(323) Jayappa, R. B.; Bhat, B. R.; Ramakrishna, D.; Anthony, J. K.; Rotermund, F. *Synth. Met.* **2010**, *160*, 1584.
(324) Pietrangelo, A.; Sih, B. C.; Boden, B. N.; Wang, Z. W.; Li, Q. F.; Chou, K. C.; MacLachlan, M. J.; Wolf, M. O. *Adv. Mater.* **2008**, *20*, 2280.
(325) Huang, T.; Hao, Z. H.; Gong, H. M.; Liu, Z. J.; Mao, S.; Li, S. Y.; Zhai, Y. Y.; You, S. Z.; Wang, Q. Q.; Qin, J. G. *Chem. Phys. Lett.* **2008**, *451*, 213.
(326) Neves, U. M.; De Boni, L.; Ye, Z. H.; Bu, X. R.; Mendonca, C. R. *Chem. Phys. Lett.* **2007**, *441*, 221.
(327) Tedim, J.; Patricio, S.; Bessada, R.; Morais, R.; Sousa, C.; Marques, M. B.; Freire, C. *Eur. J. Inorg. Chem.* **2006**, 3425.
(328) Das, S.; Nag, A.; Goswami, D.; Bharadwaj, P. K. *J. Am. Chem. Soc.* **2006**, *128*, 402.
(329) Dakhel, A. A.; Ahmed, Y. A. M.; Henari, F. Z. *Opt. Mater.* **2006**, *28*, 925.
(330) Cardoso, M. R.; Neves, U. M.; Misoguti, L.; Ye, Z. H.; Bu, X. R.; Mendonca, C. R. *Opt. Mater.* **2006**, *28*, 1118.
(331) Yang, X. Q.; Qi, S. W.; Chen, K.; Zhang, C. P.; Tian, J. G.; Wu, Q. *Opt. Mater.* **2005**, *27*, 1358.
(332) Kong, L. Y.; Li, Z. W.; Okamura, T.; Ma, G. H.; Chu, Q.; Zhu, H. F.; Tang, S. H.; Sun, W. Y.; Ueyama, N. *Chem. Phys. Lett.* **2005**, *416*, 176.
(333) Floyd, J. M.; Gray, G. M.; VanEngen Spivey, A. G.; Lawson, C. M.; Pritchett, T. M.; Ferry, M. J.; Hoffman, R. C.; Mott, A. G. *Inorg. Chim. Acta* **2005**, *358*, 3773.
(334) Xue, Z. M.; Tang, Y. W.; Wu, J. Y.; Tian, Y. P.; Jiang, M. H.; Fun, H. K.; Usman, A. *Can. J. Chem.-Rev. Can. Chim.* **2004**, *82*, 1700.
(335) Qi, S. W.; Yang, X. Q.; Lu, R.; Chen, K.; Zhang, C. P.; Tian, J. G.; Xu, J. J.; Wu, Q. *J. Mod. Opt.* **2004**, *51*, 1671.
(336) Hou, H. W.; Li, G.; Song, Y. L.; Fan, Y. T.; Zhu, Y.; Zhu, L. *Eur. J. Inorg. Chem.* **2003**, 2325.
(337) Zhou, J. H.; Wang, Y. X.; Chen, X. T.; Song, Y. L.; Weng, L. H.; You, X. Z. *Chin. J. Struct. Chem.* **2002**, *18*, 533.
(338) Sun, W. F.; Zhang, B. G.; Li, Y. J.; Pritchett, T. M.; Li, Z. J.; Haley, J. E. *Chem. Mater.* **2010**, *22*, 6384.

(339) Kim, K. Y.; Shelton, A. H.; Drobizhev, M.; Makarov, N.; Rebane, A.; Schanze, K. S. *J. Phys. Chem. A* **2010**, *114*, 7003.
(340) Jeffery, C. J.; Cifuentes, M. P.; Dalton, G. T.; Corkery, T. C.; Randles, M. D.; Willis, A. C.; Samoc, M.; Humphrey, M. G. *Macromol. Rapid Commun.* **2010**, *31*, 846.
(341) Glimsdal, E.; Carlsson, M.; Kindahl, T.; Lindgren, M.; Lopes, C.; Eliasson, B. *J. Phys. Chem. A* **2010**, *114*, 3431.
(342) Roberts, R. L.; Schwich, T.; Corkery, T. C.; Cifuentes, M. P.; Green, K. A.; Farmer, J. D.; Low, P. J.; Marder, T. B.; Samoc, M.; Humphrey, M. G. *Adv.Mater.* **2009**, *21*, 2318.
(343) Green, K. A.; Cifuentes, M. P.; Corkery, T. C.; Samoc, M.; Humphrey, M. G. *Angew. Chem. Int. Ed.* **2009**, *48*, 7867.
(344) Dalton, G. T.; Cifuentes, M. P.; Watson, L. A.; Petrie, S.; Stranger, R.; Samoc, M.; Humphrey, M. G. *Inorg. Chem.* **2009**, *48*, 6534.
(345) Chan, C. K. M.; Tao, C. H.; Tam, H. L.; Zhu, N. Y.; Yam, V. W. W.; Cheah, K. W. *Inorg. Chem.* **2009**, *48*, 2855.
(346) Westlund, R.; Malmstrom, E.; Lopes, C.; Ohgren, J.; Rodgers, T.; Saito, Y.; Kawata, S.; Glimsdal, E.; Lindgren, M. *Adv. Funct. Mater.* **2008**, *18*, 1939.
(347) Westlund, R.; Glimsdal, E.; Lindgren, M.; Vestberg, R.; Hawker, C. J.; Lopes, C.; Malmstrom, E. *J. Mater. Chem.* **2008**, *18*, 166.
(348) Shao, P.; Li, Y. J.; Sun, W. F. *J. Phys. Chem. A* **2008**, *112*, 1172.
(349) Samoc, M.; Dalton, G. T.; Gladysz, J. A.; Zheng, Q.; Velkov, Y.; Aagren, H.; Norman, P.; Humphrey, M. G. *Inorg. Chem.* **2008**, *47*, 9946.
(350) Gauthier, N.; Argouarch, G.; Paul, F.; Humphrey, M. G.; Toupet, L.; Ababou-Girard, S.; Sabbah, H.; Hapiot, P.; Fabre, B. *Adv. Mater.* **2008**, *20*, 1952.
(351) Samoc, M.; Morrall, J. P.; Dalton, G. T.; Cifuentes, M. P.; Humphrey, M. G. *Angew. Chem. Int. Ed.* **2007**, *46*, 731.
(352) Rogers, J. E.; Slagle, J. E.; Krein, D. M.; Burke, A. R.; Hall, B. C.; Fratini, A.; McLean, D. G.; Fleitz, P. A.; Cooper, T. M.; Drobizhev, M.; Makarov, N. S.; Rebane, A.; Kim, K. Y.; Farley, R.; Schanze, K. S. *Inorg. Chem.* **2007**, *46*, 6483.
(353) Powell, C. E.; Hurst, S. K.; Morrall, J. P.; Cifuentes, M. P.; Roberts, R. L.; Samoc, M.; Humphrey, M. G. *Organometallics* **2007**, *26*, 4456.
(354) Powell, C. E.; Cifuentes, M. P.; Humphrey, M. G.; Willis, A. C.; Morrall, J. P.; Samoc, M. *Polyhedron* **2007**, *26*, 284.
(355) Luc, J.; Fillaut, J. L.; Niziol, J.; Sahraoui, B. *J. Optoelectron. Adv. Mater.* **2007**, *9*, 2826.
(356) Glimsdal, E.; Carlsson, M.; Eliasson, B.; Minaev, B.; Lindgren, M. *J. Phys. Chem. A* **2007**, *111*, 244.
(357) Dalton, G. T.; Cifuentes, M. P.; Petrie, S.; Stranger, R.; Humphrey, M. G.; Samoc, M. *J. Am. Chem. Soc.* **2007**, *129*, 11882.
(358) Vestberg, R.; Westlund, R.; Eriksson, A.; Lopes, C.; Carlsson, M.; Eliasson, B.; Glimsdal, E.; Lindgren, M.; Malmstrom, E. *Macromolecules* **2006**, *39*, 2238.
(359) Sun, W. F.; Zhu, H. J.; Barron, P. M. *Chem. Mater.* **2006**, *18*, 2602.

(360) Samoc, M.; Gauthier, N.; Cifuentes, M. P.; Paul, F.; Lapinte, C.; Dalton, G. T.; Humphrey, M. G. *Angew. Chem. Int. Ed.* **2006**, *45*, 7376.
(361) Guo, F. Q.; Sun, W. F. *J. Phys. Chem. B* **2006**, *110*, 15029.
(362) Xu, G. L.; Wang, C. Y.; Ni, Y. H.; Goodson, T. G.; Ren, T. *Organometallics* **2005**, *24*, 3247.
(363) Guo, F. Q.; Sun, W. F.; Liu, Y.; Schanze, K. *Inorg. Chem.* **2005**, *44*, 4055.
(364) Fillaut, J. L.; Perruchon, J.; Blanchard, P.; Roncali, J.; Golhen, S.; Allain, M.; Migalsaka-Zalas, A.; Kityk, I. V.; Sahraoui, B. *Organometallics* **2005**, *24*, 687.
(365) Cifuentes, M. P.; Humphrey, M. G.; Morrall, J. P.; Samoc, M.; Paul, F.; Lapinte, C.; Roisnel, T. *Organometallics* **2005**, *24*, 4280.
(366) Schwich, T.; Cifuentes, M. P.; Gugger, P. A.; Samoc, M.; Humphrey, M. G. *Adv. Mater.* **2010**, *23*, 1433.
(367) Powell, C. E.; Cifuentes, M. P.; Morrall, J. P.; Stranger, R.; Humphrey, M. G.; Samoc, M.; Luther-Davies, B.; Heath, G. A. *J. Am. Chem. Soc.* **2003**, *125*, 602.
(368) Dalton, G. T.; Cifuentes, M. P.; Petrie, S.; Stranger, R.; Humphrey, M. G.; Samoc, M. *J. Am. Chem. Soc.* **2007**, *129*, 11882.

Chapter 2

Osmium chloro-alkynyl heterobimetallic complexes

Chapter 2

Osmium chloro-alkynyl heterobimetallic complexes

Contents

2.1 Introduction

trans-[Os(C≡CR)Cl(diphosphine)$_2$] complexes have been reported by a number of groups in recent years. Lewis *et al.* describe the synthesis of a number of *trans*-[Os(C≡CR)Cl(dppm)$_2$] complexes prepared by stirring *cis*-[OsCl$_2$(dppm)$_2$], $NaPF_6$ and acetylene in CH_2Cl_2 at room temperature for 4 - 20 h, before deprotonating the resultant vinylidene complex with either basic alumina or DBU to form the corresponding alkynyl complex in up to 87% yield[1-4] (Scheme 2.1).

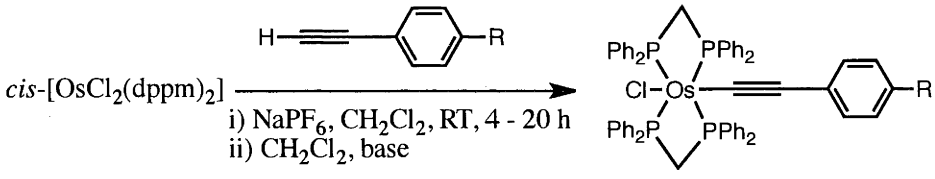

R = H, base = alumina (basic), yield not given
R = C≡CH, base = DBU, 71%
R = C_6H_4-4-C≡CH, base = DBU, 87%

Scheme 2.1. Three of the chloro-alkynyl complexes prepared by Lewis *et al.*[1,2]

Wong *et al.* synthesised two similar complexes using the same method in 65 and 51% yields[5] (Scheme 2.2).

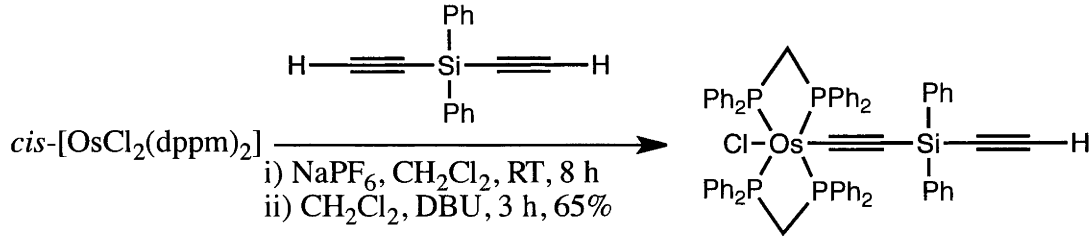

Scheme 2.2. One of the osmium chloro-alkynyl complexes formed by Wong *et al.*[5]

McDonagh *et al* synthesized an optically active osmium alkynyl complex (-)$_{365}$-*trans*-[Os(4-C≡C$C_6H_4NO_2$)Cl{(R,R)-diph}$_2$] in 59% yield by refluxing *cis*-[OsCl$_2${(R,R)-diph}$_2$], acetylene and $NaPF_6$ in toluene for 2 h, before deprotonating the resultant vinylidene complex with NaOMe[6] (Scheme 2.3).

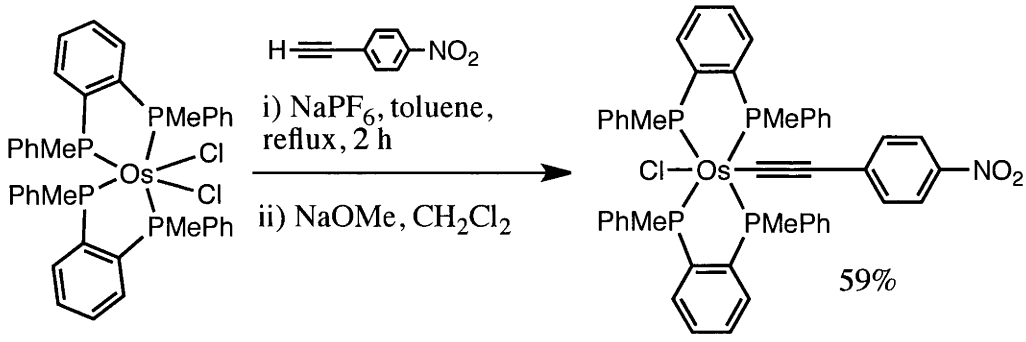

Scheme 2.3. The osmium chloro-alkynyl complex incorporating an optically active diphosphine ligand synthesised by McDonagh *et al.*[6]

Morrall *et al.* used a similar approach to form *trans*-[Os(C≡CR)Cl(dppe)$_2$] complexes, using NH_4PF_6 as the halide abstraction agent, NEt_3 as the base and a reaction time of 18 h, to afford three complexes with yields ranging from 36 - 44%[7] (Scheme 2.4).

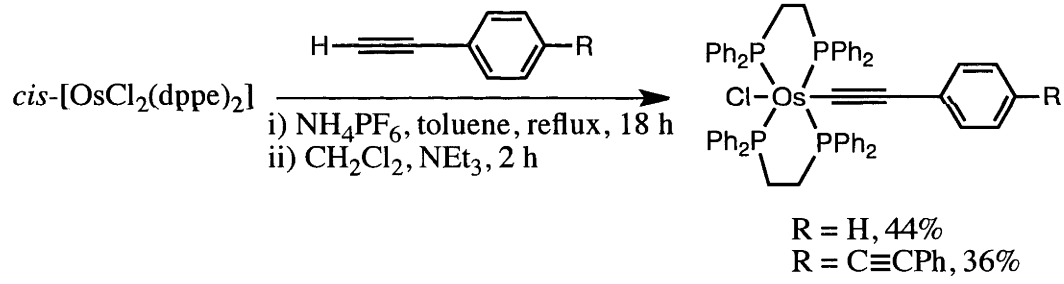

Scheme 2.4. Two of the osmium chloro-alkynyl complexes incorporating the *trans*-[Os(dppe)$_2$] metal centre formed by Morrall *et al.*[7]

There have been a number of recent reports on the formation of both homo-bimetallic[8-11] and hetero-bimetallic[1,12,13] group 8 metal complexes where the metal centres are separated by a 1,4-diethynylarene or oligo(*p*-phenyleneethynylene) moiety. The *trans, trans*-[(dppm)$_2$ClOs(C≡CC$_6$H$_4$-4-C≡C)RuCl(dppm)$_2$] complex synthesised by Younus et al[1] is of interest to this work due to its similarity to targets

of this project. It was formed in 45% yield from the reaction of *trans*-Os(C≡CC$_6$H$_4$-4-C≡CH)Cl(dppm)$_2$] with *cis*-[RuCl$_2$(dppm)$_2$], NaPF$_6$ and DBU in CH_2Cl_2 over two steps (Scheme 2.5). It was found to be air-sensitive, precluding satisfactory microanalysis data[1]. The electrochemical behaviour was investigated by cyclic voltammetry in CH_2Cl_2 and shown to have two processes at -0.02 and 0.34 V (ferrocene referenced to 0.46 V) assigned to oxidation at the osmium and ruthenium metal centres, respectively. The separation of the two processes (0.36 V) is 0.2 V greater than the gap between the potentials for the individual osmium and ruthenium mononuclear complexes.

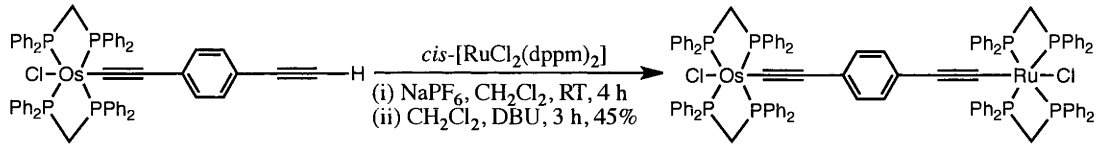

Scheme 2.5. Formation of heterobimetallic complex by Younus *et al.*[1]

2.2 Results and Discussion

2.2.1 Synthesis

Previously, chloro-alkynyl complexes incorporating the *trans*-[Os(dppe)$_2$] metal centre had been formed in modest yields (36 – 44%) under forcing conditions (refluxing toluene for 18 h)[7] (Scheme 2.4). Due to the disadvantages of this approach, an alternative route based on that taken with the analogous *trans*-[Os(dppm)$_2$][4] and *trans*-[Ru(dppe)$_2$][14] metal centres was used to access chloro-alkynyl complexes (Schemes 2.6 and 2.7). This approach involved stirring *cis*-[OsCl$_2$(dppe)$_2$], acetylene and halide abstraction agent (NH_4PF_6) in CH_2Cl_2 for 18 h, affording the vinylidene complex. Without isolation, the vinylidene complex was deprotonated to the corresponding alkynyl complex through the addition of a base (NEt_3). After purification, the chloro-alkynyl complexes

trans-[Os(C≡CC$_6$H$_4$-4-C≡CSiPr$^i_3$)Cl(dppe)$_2$] (**1**) and *trans*-[Os(C≡CC$_6$H$_4$-4-C≡CC$_6$H$_4$-4-C≡CSiPr$^i_3$)Cl(dppe)$_2$] (**5**) were isolated in excellent yield (85 and 91%, respectively) (Schemes 2.6 and 2.7). These complexes could be desilylated by stirring the CH_2Cl_2 solutions in the presence of NBu$^n_4$F. For complex **2,** where the silyl group is closer to the metal centre, the desilylation reaction proceeds at a much slower pace, but is complete after 48 h. Both *trans*-[Os(C≡CC$_6$H$_4$-4-C≡CH)Cl(dppe)$_2$] (**2**) and *trans*-[Os(C≡CC$_6$H$_4$-4-C≡CC$_6$H$_4$-4-C≡CH)Cl(dppe)$_2$] (**6**) were isolated in excellent yields (88 and 85%, respectively) (Schemes 2.6 and 2.7). The osmium-ruthenium complex **3** was synthesised through the reaction of *trans*-[Os(C≡CC$_6$H$_4$-4-C≡CH)Cl(dppe)$_2$] (**2**) with *cis*-[RuCl$_2$(dppe)$_2$] and $NaPF_6$, forming a vinylidene complex which was deprotonated in situ with NEt_3 to afford *trans, trans*-[(dppe)$_2$ClOs(C≡CC$_6$H$_4$-4-C≡C)RuCl(dppe)$_2$] (**3**) (Scheme 2.6). The bimetallic complex with a diethynyl bridge separating the metal centres was initially targeted, as it would allow much greater communication between the metals, which should result in a greater separation of redox potentials. Although **3** was synthesised successfully it was found to be air-sensitive; a similar problem was reported for the dppm analogue of **3**[15]. Due to the instability of **3**, it was reacted with a further aliquot of HC≡CC$_6$H$_4$-4-C≡CSiPr$^i_3$ to afford *trans, trans*-[(dppe)$_2$ClOs(C≡CC$_6$H$_4$-4-C≡C)Ru(C≡CC$_6$H$_4$-4-C≡CSiPr$^i_3$)(dppe)$_2$] (**4**) (Scheme 2.6).

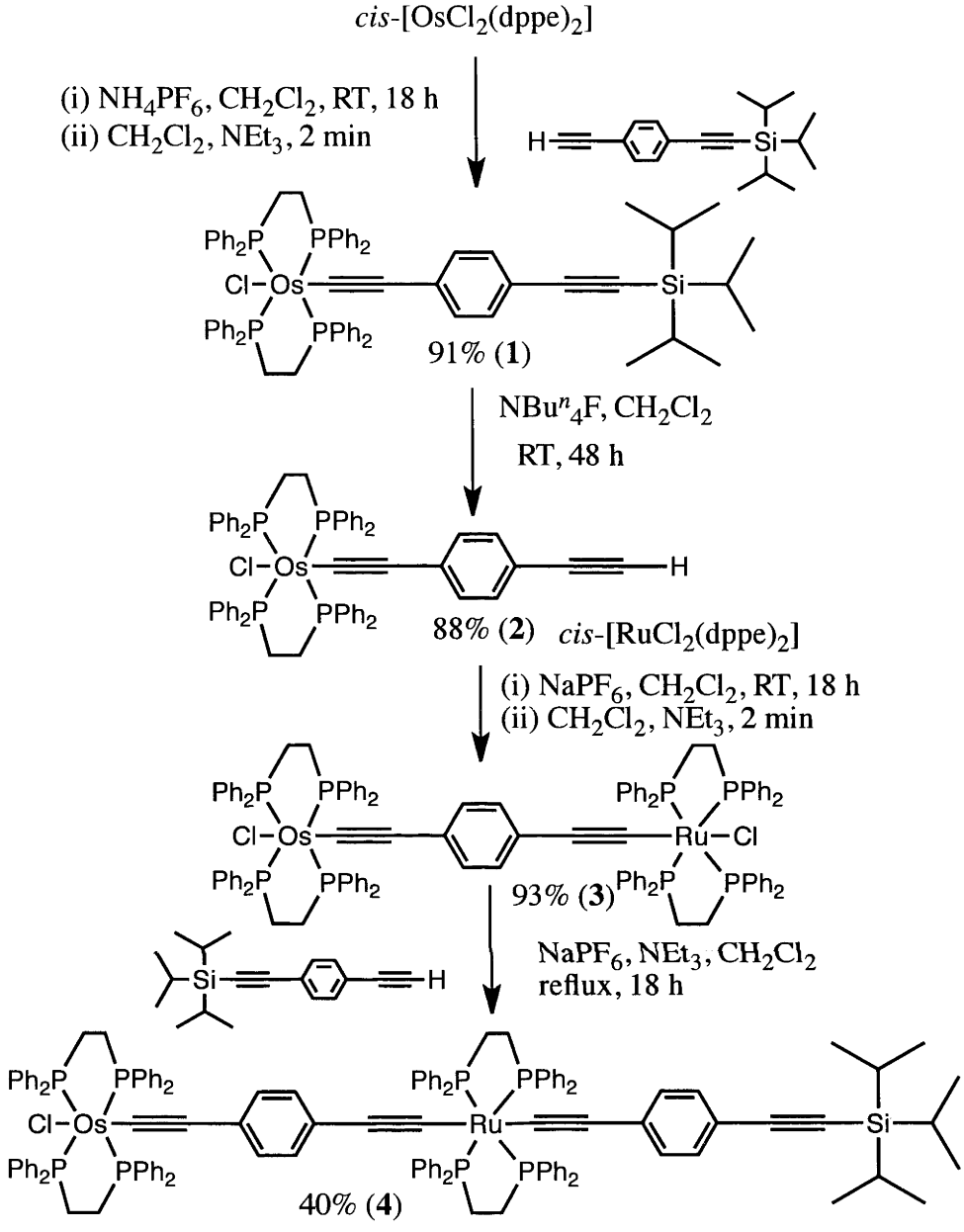

Scheme 2.6. Syntheses of **1** – **4**

It should be noted that the low yield for the formation of **4** is partly due to the use of chromatography in the purification step, with some product lost due to instability on alumina. Interestingly, it can be seen from the formation of **4** that reactivity towards bis-alkynyl formation under these conditions is favoured for the ruthenium metal

centre over the osmium metal centre. It was found that **4** was much more stable in air than **3**, although over time in the solid state there were significant levels of decomposition. It was reasoned that the longer bridge between the two metal centres results in greater complex stability so the triethynyl-linked complex *trans,trans*-[(dppe)$_2$ClOs(C≡CC$_6$H$_4$-4-C≡CC$_6$H$_4$-4-C≡C)RuCl(dppe)$_2$] (**7**) was synthesised under similar conditions as those used for the formation of **3** (Scheme 2.7). It was found that **7** was more stable in both solution and in air than **3** and **4**.

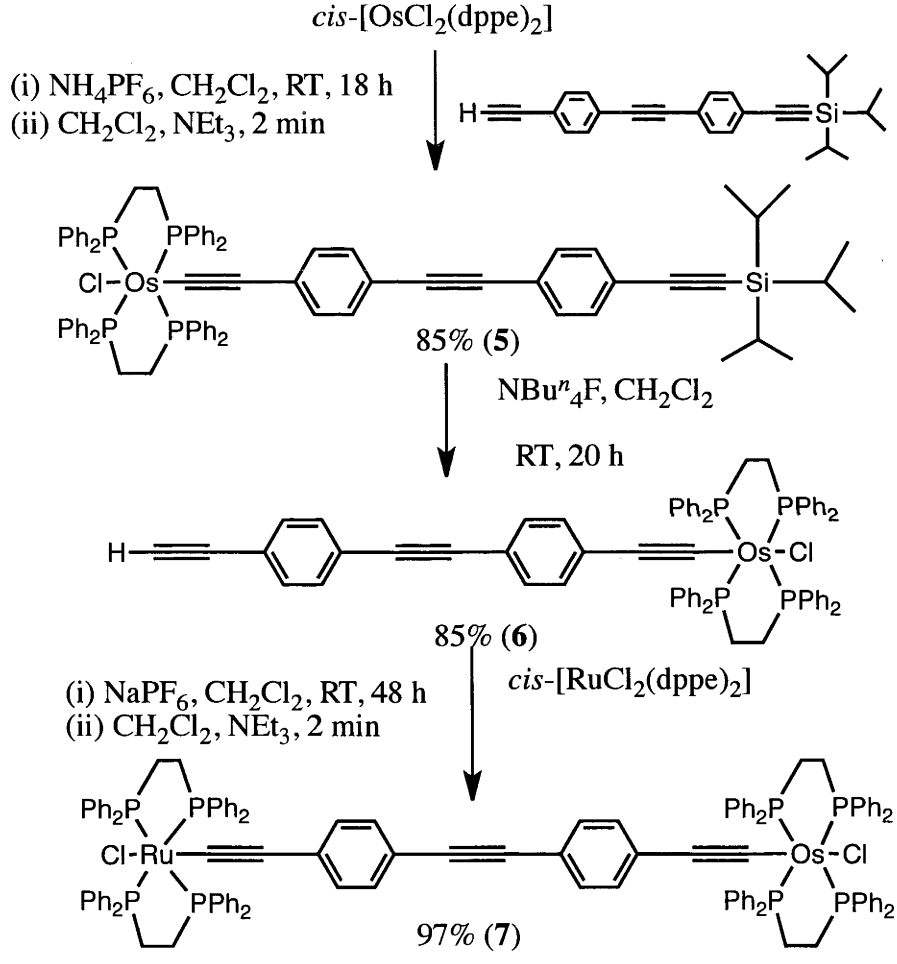

Scheme 2.7. Syntheses of **5** - **7**

In order to compare the properties of osmium chloro-alkynyl complexes to ruthenium chloro-alkynyl complexes, the ruthenium analogue of **5**,

trans-[Ru(C≡CC_6H_4-4-C≡CC_6H_4-4-C≡C$SiPr^i_3$)Cl(dppe)$_2$] (**8**) was also prepared (Scheme 2.8).

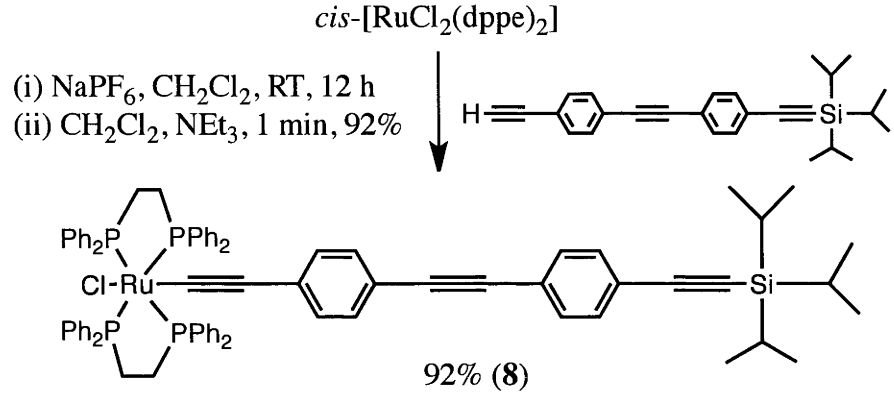

Scheme 2.8. Synthesis of **8**

2.2.2 Physical Properties

2.2.2.1 NMR spectroscopy

Complexes **1** – **8** were characterised by ^1H, ^{31}P and ^{13}C NMR spectroscopy in $CDCl_3$. The ^1H NMR spectra of complexes **1** – **8** are quite similar, with resonances in the range 6.5 – 7.5 ppm corresponding to aromatic protons. All of the complexes formed also have a multiplet in the region 2.5 – 2.8 ppm due to the bridgehead protons of the dppe ligands. For the isopropyl group on complexes **1**, **4**, **5**, and **8** there is a resonance at ca 1.1 ppm, appearing as a pseudo-singlet; the heptets corresponding to the methyne protons are not visible in the spectra. This isopropyl singlet is no longer present after desilylation to form complexes **2** and **6**, with the spectra now containing a signal corresponding to the acetylenic proton at ca 3.1 ppm. All complexes containing a *trans*-[Os(dppe)$_2$] metal centre (**1** – **7**) have a characteristic ^{31}P NMR signal in the range 16.0 – 16.6 ppm, which is consistent with previously reported resonances for this type of complex.[7] For complexes containing a *trans*-[RuCl(dppe)$_2$] metal centre (**3**, **7** and **8**), a characteristic ^{31}P resonance at ca 50

ppm is visible. On replacement of the chloro group with a second alkynyl group to form **4**, the signal for the phosphorus atoms attached to the ruthenium is found at 54.4 ppm, these resonances being consistent with previously reported findings for similar complexes[16]. For complexes **1** – **8**, ^{13}C NMR spectra have been recorded, where possible, to confirm the identity of the complexes; these are attached in Appendix A.

2.2.2.2 UV-Vis absorption spectroscopy

Complexes **1** – **8** were characterised by UV-Vis spectroscopy as CH_2Cl_2 solutions. The mononuclear complexes with C≡C-4-C_6H_4C≡C ligand (**1** and **2**) have one major absorption band centred at ca 372 nm. This is in contrast to the complexes with the triethynyl ligand C≡C-4-C_6H_4-C≡C-4-C_6H_4C≡C ligand, which all have two major absorption bands, located at ca 304 and 417 nm for the osmium complexes (**5** and **6**) and slightly blue-shifted to 297 and 409 nm for the ruthenium complex (**8**). Interestingly, the UV-Vis spectrum of the binuclear complex with the triethynyl C≡C-4-C_6H_4-C≡C-4-C_6H_4C≡C bridging ligand (**7**) shows only one band, located at 427 nm and red-shifted with respect to the component mononuclear complexes. Both of the binuclear complexes with the diethynyl C≡C-4-C_6H_4C≡C bridging ligand have a single absorption band, located at 373 nm for **3** and 389 nm for **4**. Although quantum mechanical calculations are required to definitively assign the absorption bands of these complexes, it is possible to tentatively assign transitions based on previous studies of similar osmium[7] and ruthenium[17] mononuclear complexes. It is likely that the dominant absorption bands for the mononuclear complexes **1**, **2**, **5**, **6** and **8** are metal-to-ligand charge transfer bands. In particular, these are likely to be either metal-to-ethynyl or metal-to-phosphorus transitions, with the former being lower in energy.

2.2.2.3 Infrared spectroscopy

Complexes **1** - **8** were investigated via solution infrared spectroscopy, the ν(C≡C) band being indicative of the presence of an alkynyl linkage. For the mononuclear $SiPr^{i}_{3}$-protected complexes (**1**, **5** and **8**) the band corresponding to ν(C≡CSi) is present at ca 2147 cm^{-1}, and an additional broad band is seen between 2053 – 2063 cm^{-1}. On desilylation, the band at ca 2147 cm^{-1} disappears and is replaced by a band at ca. 3300 cm^{-1} corresponding to ν(≡CH). On formation of the binuclear complexes (**3** and **7**), the ν(≡CH) band disappears.

2.2.2.4 Structural determinations

Single crystals suitable for X-ray crystallographic structure determinations were obtained for complexes **1**, **2** and **6** through the slow diffusion of n-hexane into CH_2Cl_2 solutions. The osmium metal centres all show distorted octahedral geometries, with the dppe ligands occupying the equatorial positions, and chloro and alkynyl ligands occupying the axial positions. The structures are given in Figures 2.1 - 2.3. Interestingly, a significant difference in the Os-Cl bond length can be seen on going from complexes **1** (2.532(2) Å) and **2** (2.5040(9) Å) to complex **6** (2.8479(8) Å). Both complexes **2** and **6** possess H-bonding between the Cl atom and the acetylene proton of the adjacent molecule (Figures 2.4 and 2.5). Additionally, the chlorine atom in complex **6** shows interactions with the protons of a CH_2Cl_2 solvent molecule (Figure 2.6), which may account for the elongated Os-Cl bond length.

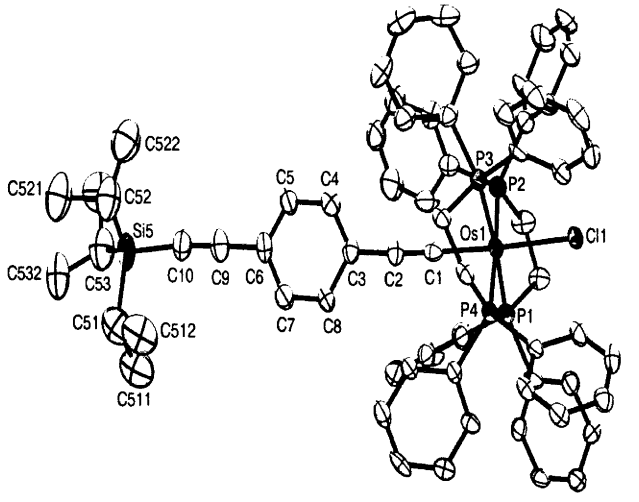

Figure 2.1. Molecular geometry and atomic labelling scheme for *trans*-[Os(C≡C-4-C_6H_4C≡C$SiPr^i_3$)Cl(dppe)$_2$] (**1**). Thermal ellipsoids at the 40% probability level are shown for non-hydrogen atoms. Hydrogen atoms have been omitted for clarity. Selected bond lengths (Å) and bond angles (°): Os(1)-Cl(1) 2.532(2), Os(1)-C(1) 1.995(9), C(1)-C(2) 1.215(12), Cl(1)-Os(1)-C(1) 171.9(2), Os(1)-C(1)-C(2) 178.4(8).

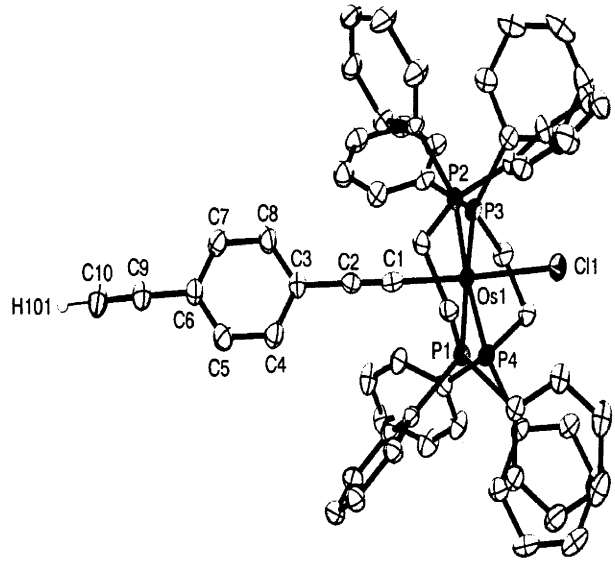

Figure 2.2. Molecular geometry and atomic labelling scheme for *trans*-[Os(C≡C-4-C_6H_4C≡CH)Cl(dppe)$_2$] (**2**). Thermal ellipsoids at the 40% probability level are shown for non-hydrogen atoms. Hydrogen atoms have been

omitted for clarity. Selected bond lengths (Å) and bond angles (°): Os(1)-Cl(1) 2.5040(9), Os(1)-C(1) 2.044(4), C(1)-C(2) 1.123(5), Cl(1)-Os(1)-C(1) 172.91(10), Os(1)-C(1)-C(2) 172.8(3).

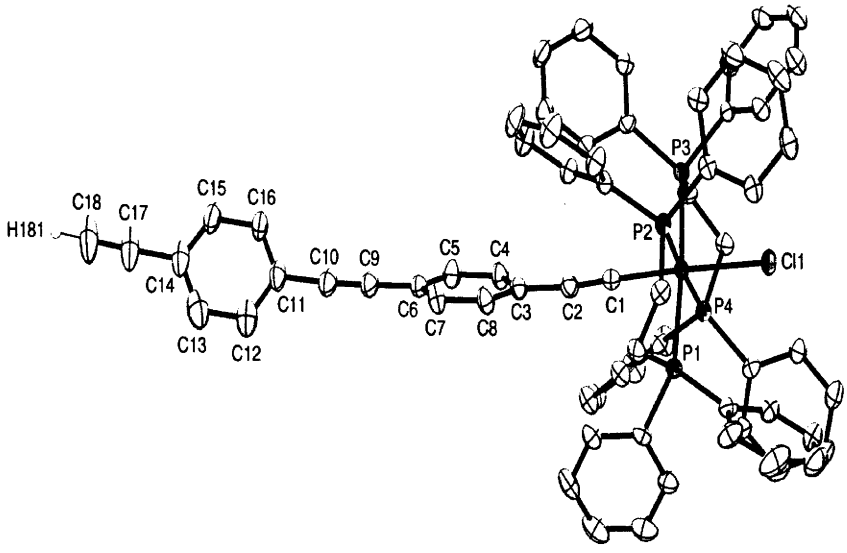

Figure 2.3. Molecular geometry and atomic labelling scheme for *trans*-[Os(C≡C-4-C_6H_4C≡C-4-C_6H_4C≡CH)Cl(dppe)$_2$] (**6**). Thermal ellipsoids at the 40% probability level are shown for non-hydrogen atoms. Hydrogen atoms have been omitted for clarity. Selected bond lengths (Å) and bond angles (°): Os(1)-Cl(1) 2.8479(8), Os(1)-C(1) 2.000(3), C(1)-C(2) 1.189(5), Cl(1)-Os(1)-C(1) 177.29(9), Os(1)-C(1)-C(2) 177.1(3).

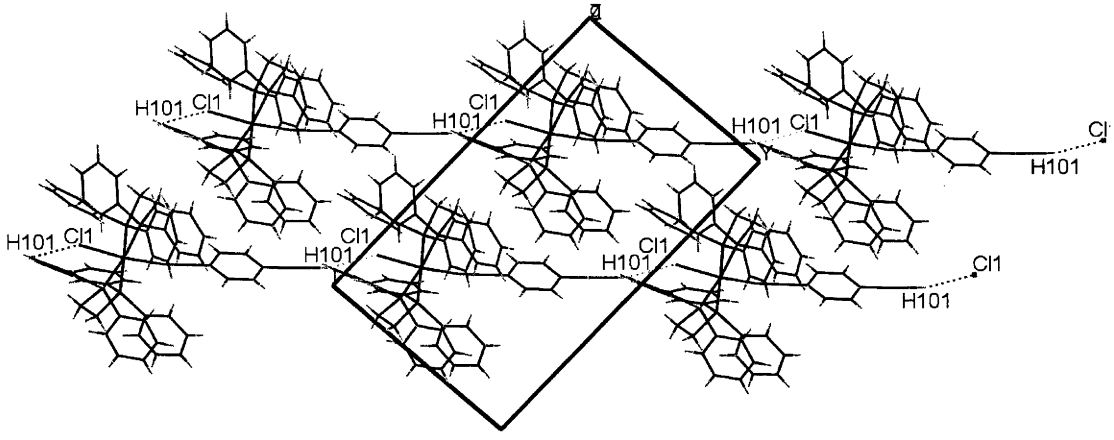

Figure 2.4. Cell-packing diagram of **2**, looking along the b axis of the unit cell. Hydrogen atoms have been omitted for clarity, with the exception of the acetylene protons. The Cl(1)•••H(101) contacts are ca 2.592 Å.

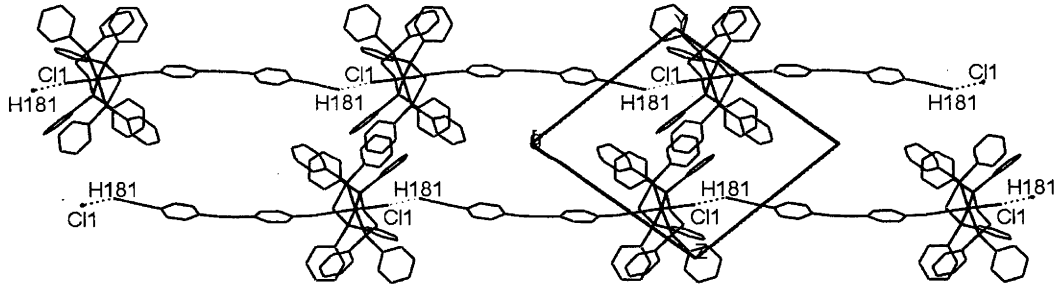

Figure 2.5. Cell-packing diagram of **6**, looking along the c axis of the unit cell. Hydrogen atoms and solvent molecules have been omitted for clarity, with the exception of the acetylene protons. The Cl(1)•••H(181) contacts are ca 2.780 Å.

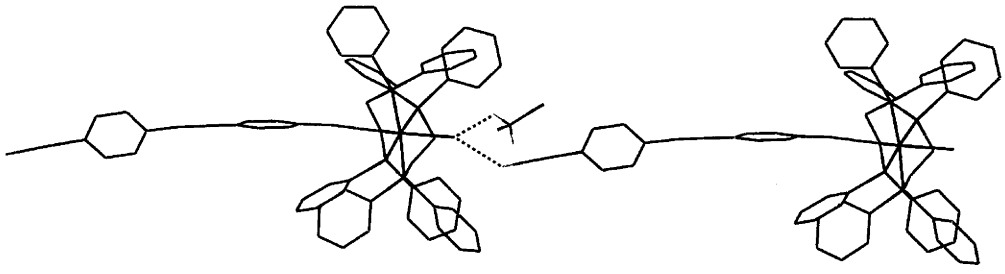

Figure 2.6. Fractional cell-packing diagram of **6**. Interactions of the terminal chlorine atom of one molecule with the terminal acetylene proton of an adjacent molecule and with a proton of the CH_2Cl_2 solvent molecule are indicated by dashed lines. The Cl•••H distances are 3.032 Å (solvent•••complex) and 2.780 Å (complex•••complex), respectively.

2.2.2.5 Electrochemistry

The redox potentials of complexes **1** – **8** in THF were investigated using cyclic voltammetry. The mononuclear osmium complexes (**1**, **2**, **5** and **6**) were all oxidised at potentials within the range of 0.45 – 0.49 V (Table 2.1). The oxidation potential of the ruthenium mononuclear complex (**8**) is 0.63 V, in the same range as other similar ruthenium complexes previously reported.[17] On forming the bimetallic complexes, the ease of oxidation for the osmium metal centre increases. This change in oxidation potential is affected by the length of the bridge separating the two metal centres, with the shorter bridge in complexes **3** and **4** resulting in a lower osmium oxidation potential than that in **7**. It should also be noted that the length of the bridge separating the metal centres affects the separation of the osmium and ruthenium potentials. A shorter bridge, as seen in complexes **3** and **4** has a larger separation of potentials compared to a longer bridge (**7**).

Complex	$E_{1/2}$ [i_{pc}/i_{pa}] $Os^{II/III}$ (V)	$E_{1/2}$ [i_{pc}/i_{pa}] $Ru^{II/III}$ (V)	$E_{1/2}$ $Ru^{II/III}$ - $E_{1/2}$ $Os^{II/III}$ (V)
1	0.49 [1]	—	—
2	0.45 [1]	—	—
3	0.22 [1]	0.51 [1]	0.29
4	0.31 [1]	0.59 [1]	0.28
5	0.45 [1]	—	—
6	0.45 [1]	—	—
7	0.41 [1]	0.62 [1]	0.21
8	0.63 [1]	—	—

Table 2.1. Cyclic voltammetric data for complexes **1** – **8**. THF solvent, Pt disk working-, Pt wire auxiliary-, and Ag/AgCl reference electrodes, ferrocene/ferrocenium couple at 0.56 V, ΔE_p of samples approximately matched that of the ferrocene/ferrocenium couple.

2.2.2.6 Spectroelectrochemistry

Electrolysis of complexes **1**, **4**, **5**, **7**, and **8** was carried out in an optically-transparent thin-layer electrochemical (OTTLE) cell in order to observe the changes in UV-Vis-NIR absorption spectra upon oxidation. Strong changes were observed for all the complexes examined (Figures 2.7 - 2.11). Previous reports for various examples of *trans*-[Os(C≡CR)Cl(dppe)$_2$][7] and *trans*-[Ru(C≡CR)Cl(dppe)$_2$][18,19] have shown the appearance of a low energy band on oxidation ascribed to a chloro-to-metal-ethynyl charge transfer. All three mononuclear complexes studied (Figures 2.7, 2.9 and 2.11) show this band, centred at ca 13400 cm^{-1} for osmium complexes **1** and **5**, and at 11200 cm^{-1} for the ruthenium complex **8**. The lower energy band for the ruthenium complex matches previously observed data[7,17]. The bimetallic complexes **4** (Figure 2.8) and **7** (Figure 2.10) display similar behaviour on oxidation. For the mono-oxidised species, a low energy band appears at 6508 cm^{-1}

for $\mathbf{4}^{+}$ and 8571 cm^{-1} for $\mathbf{7}^{+}$. On forming the doubly-oxidised species, this band is blue-shifted to 9600 cm^{-1} for $\mathbf{4}^{2+}$ and 11355 cm^{-1} for $\mathbf{7}^{2+}$, and becomes more intense. The low energy band appearing on the first oxidation for the binuclear complexes **4** and **7** may be ascribed to an inter-valence charge transfer (IVCT) process, particularly for complex **4** where the coupling between the metal centres evidenced by the large separation in redox potentials suggests an IVCT band should be present. However, the observation that the low energy band doesn't disappear but shifts to higher energy on the second oxidation discounts this assignment. An alternate assignment by Klein and co-workers[8] for similar homo-bimetallic ruthenium complexes proposes the low energy band appearing on oxidation is an intraligand transition from the former HOMO-1 to the newly formed SOMO, and the second lowest energy band at ca 20000 cm^{-1} is a transition from the SOMO to the LUMO. Quantum mechanical calculations are required for a more definitive assignment.

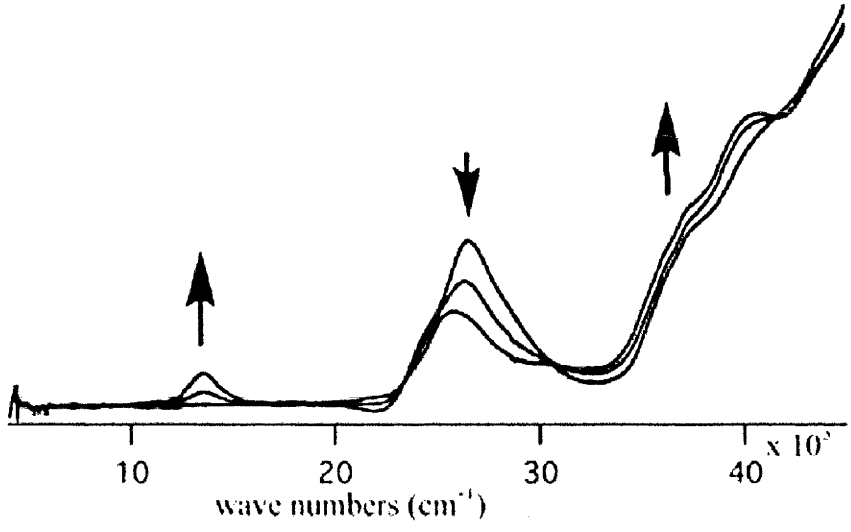

Figure 2.7. UV-vis-NIR spectral changes during electrochemical oxidation of *trans*-[Os(C≡CC_6H_4-4-C≡C$SiPr^i_3$)Cl(dppe)$_2$] (**1**).

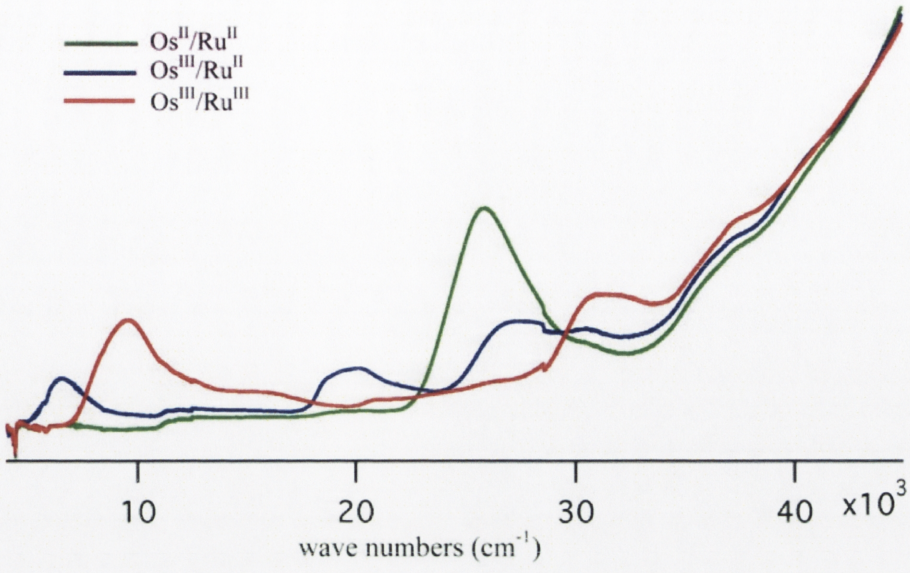

Figure 2.8. UV-vis-NIR spectral changes during electrochemical oxidation of *trans*-, *trans*-[(dppe)$_2$ClOs(C≡CC$_6$H$_4$-4-C≡C)Ru(C≡CC$_6$H$_4$-4-C≡CSiPr$^i_3$)(dppe)$_2$] (**4**).

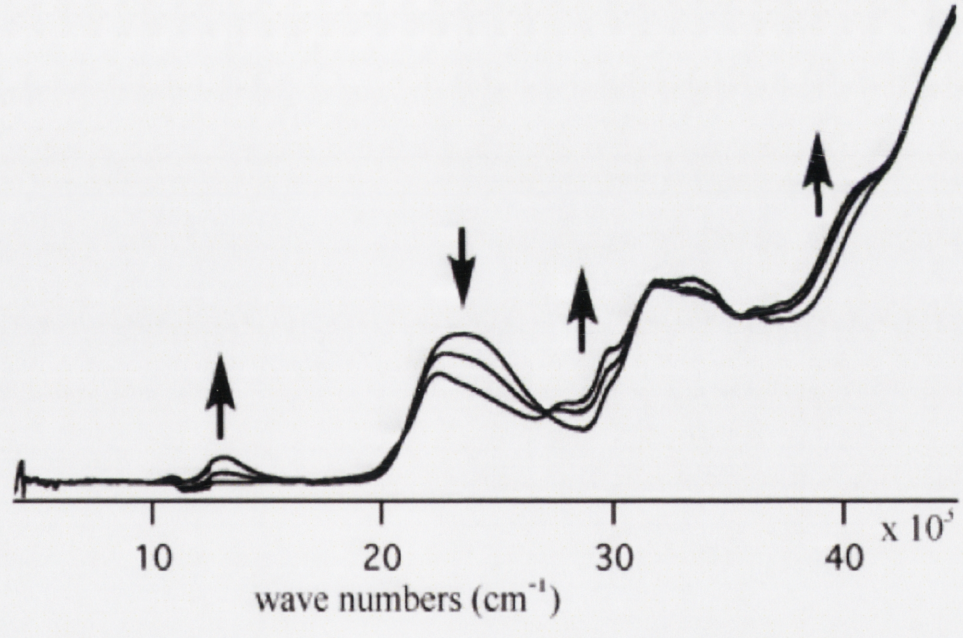

Figure 2.9. UV-vis-NIR spectral changes during electrochemical oxidation of *trans*-[Os(C≡CC$_6$H$_4$-4-C≡CC$_6$H$_4$-4-C≡CSiPr$^i_3$)Cl(dppe)$_2$] (**5**).

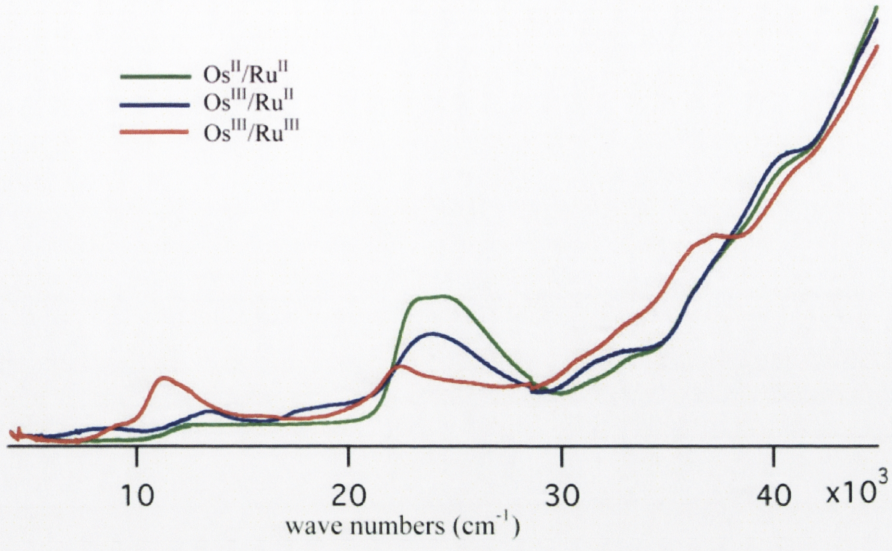

Figure 2.10. UV-vis-NIR spectral changes during electrochemical oxidation of *trans*,*trans*-[(dppe)$_2$ClOs(C≡CC$_6$H$_4$-4-C≡CC$_6$H$_4$-4-C≡C)RuCl(dppe)$_2$] (**7**).

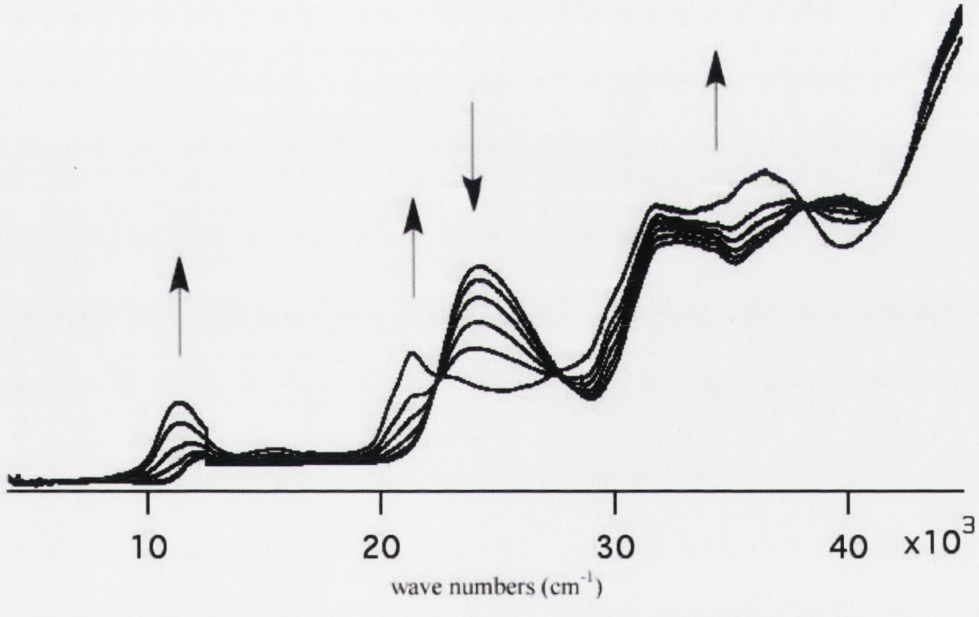

Figure 2.11. UV-vis-NIR spectral changes during electrochemical oxidation of *trans*-[Ru(C≡CC$_6$H$_4$-4-C≡CC$_6$H$_4$-4-C≡CSiPr$^i_3$)Cl(dppe)$_2$] (**8**).

Complex	λ_{max} (cm^{-1}) [ε] (10^4 M^{-1} cm^{-1}) [a]
1	26475 [1.4]
$\mathbf{1}^+$	13475 [0.3], 15885 [0.7]
4	25965 [3.5]
$\mathbf{4}^+$	6508 [1.3], 20205 [1.5], 27725 [2.2], 37492 sh [3.2]
$\mathbf{4}^{2+}$	9600 [2.1], 31175 [2.4], 37717 sh [3.4]
5	23685 [2.1], 33675 [3.0]
$\mathbf{5}^+$	13315 [0.4], 22575 [1.7], 29845 sh [2.4], 31905 [3.0]
7	24535 [4.8]
$\mathbf{7}^+$	8571 [0.9], 13555 [1.2], 23825 [3.6], 32812 [3.0], 40743 [9.5]
$\mathbf{7}^{2+}$	9305 sh [0.6], 11355 [2.1], 22605 [2.4], 37313 [6.5]
8	24450 [4.0], 33670 [3.8], 39840 [5.2]
$\mathbf{8}^+$	11265 [0.5], 21415 [1.8], 31856 [5.6], 36598 [6.5]

Table 2.2. Summary of optical data for complexes **1, 4, 5, 7** and **8**. [a] Electronic spectra were obtained at 298 K in THF using 0.3 M $(NBu^n_4)PF_6$ as supporting electrolyte and potentials ca 50-200 mV beyond $E_{1/2}$ for each couple.

2.2.2.7 Nonlinear optics

The third-order nonlinear optical properties of **7** have been measured using the Z-scan technique and are presented in chapter 4.

2.3 Conclusions

A series of mononuclear osmium complexes and binuclear osmium-ruthenium complexes have been formed with selected examples investigated structurally and electrochemically. All complexes possess a reversible redox process with the binuclear complexes having two. Spectroelectrochemical studies reveal large changes in the absorption properties on oxidation, which may be useful for optical or nonlinear optical switching.

2.4 Experimental Section

2.4.1 General

All reactions were performed under a nitrogen atmosphere using standard Schlenk techniques, with no precautions to exclude air during workup. CH_2Cl_2 was dried by distilling over calcium hydride, THF was distilled over sodium/benzophenone, and all other solvents were used as received. The term ''petrol'' refers to a fraction of petroleum ether of boiling range 60-80 °C. Column chromatography was performed using Sigma-Aldrich aluminium oxide (activated, basic, Brockmann 1, standard grade ca 150 mesh, 58 Å). Solvents and reagents were obtained from commercial sources and used as received, unless otherwise indicated. The following were prepared according to the literature: $HC{\equiv}CC_6H_4$-4-$C{\equiv}CSiPr^i_3$,[20] $HC{\equiv}CC_6H_4$-4-$C{\equiv}CC_6H_4$-4-$C{\equiv}CSiPr^i_3$,[21] *cis*-$[OsCl_2(DMSO)_4]$,[22] *cis*-$[RuCl_2(dppe)_4]$,[23] *cis*-$[OsCl_2(dppe)_4]$ was prepared via the following unpublished procedure by Morrall *et al.*: A mixture of 1,2-bis(diphenylphosphino)ethane (527 mg, 1.325 mmol) and *cis*-$[OsCl_2(DMSO)_4]$ (380 mg, 0.662 mmol) was heated in refluxing toluene (40 mL) for 18 h. The solution was allowed to cool to room temperature. The toluene-insoluble component was collected by filtration and washed with diethyl ether (690 mg, 98%).[24] ^{1}H NMR: δ 6.65-8.14 (m, 40H, Ar), 2.50 -2.92 (m, 8H, CH_2). ^{31}P NMR: δ 7.6 (t, $^2J_{pp}$ = 5.5 Hz), 5.3 (t, $^2J_{pp}$ = 5.5 Hz).

2.4.2 Instrumentation

Electrospray ionisation mass spectra (ESIMS) were obtained using a Waters-micromass LCT-ZMD single quadrupole liquid chromatograph instrument; peaks are reported as *m/z* (assignment, relative intensity). Microanalyses were carried out by the Microanalysis Service Unit, Australian National University. Infrared spectra were recorded as dichloromethane solutions using a Perkin-Elmer System 2000 FT-IR spectrometer. ^{1}H (300 MHz), $^{13}C\{^{1}H\}$ (75 MHz) and $^{31}P\{^{1}H\}$ (121 MHz) NMR spectra were recorded using a Varian Mercury-300 FT-NMR spectrometer and are referenced to residual chloroform (7.26 ppm (^{1}H), 77.0 ppm ($^{13}C\{^{1}H\}$)) or external 85% H_3PO_4 (0.0 ppm ($^{31}P\{^{1}H\}$). UV-Vis spectra were recorded as CH_2Cl_2 solutions in 1 cm quartz cells using a Cary 5 spectrophotometer.

Cyclic voltammetry measurements were recorded using an e-corder and EA161 potentiostat from eDaq Pty Ltd. Measurements were carried out at room temperature using Pt disc working-, Pt wire auxiliary-, and Ag/AgCl reference electrodes, such that the ferrocene/ferrocenium redox couple was located at 0.56 V. Scan rates were typically 100 mV s^{-1}. Electrochemical solutions contained 0.1 M $(NBu^{n}_{4})PF_6$ and ca 10^{-3} M complex in dried and distilled solvent; solutions were purged and maintained under a nitrogen atmosphere. Electronic spectra were recorded using a Cary 5 spectrophotometer. Solution spectra of the oxidized species were obtained at 298 K by electrogeneration in an optically-transparent thin-layer electrochemical (OTTLE) cell with potentials ca 50 - 200 mV beyond $E_{1/2}$ for each couple, to ensure complete electrolysis. Solutions were made up using 0.3 M $(NBu^{n}_{4})PF_6$ in THF.

2.4.3 ^{13}C NMR Numbering Scheme

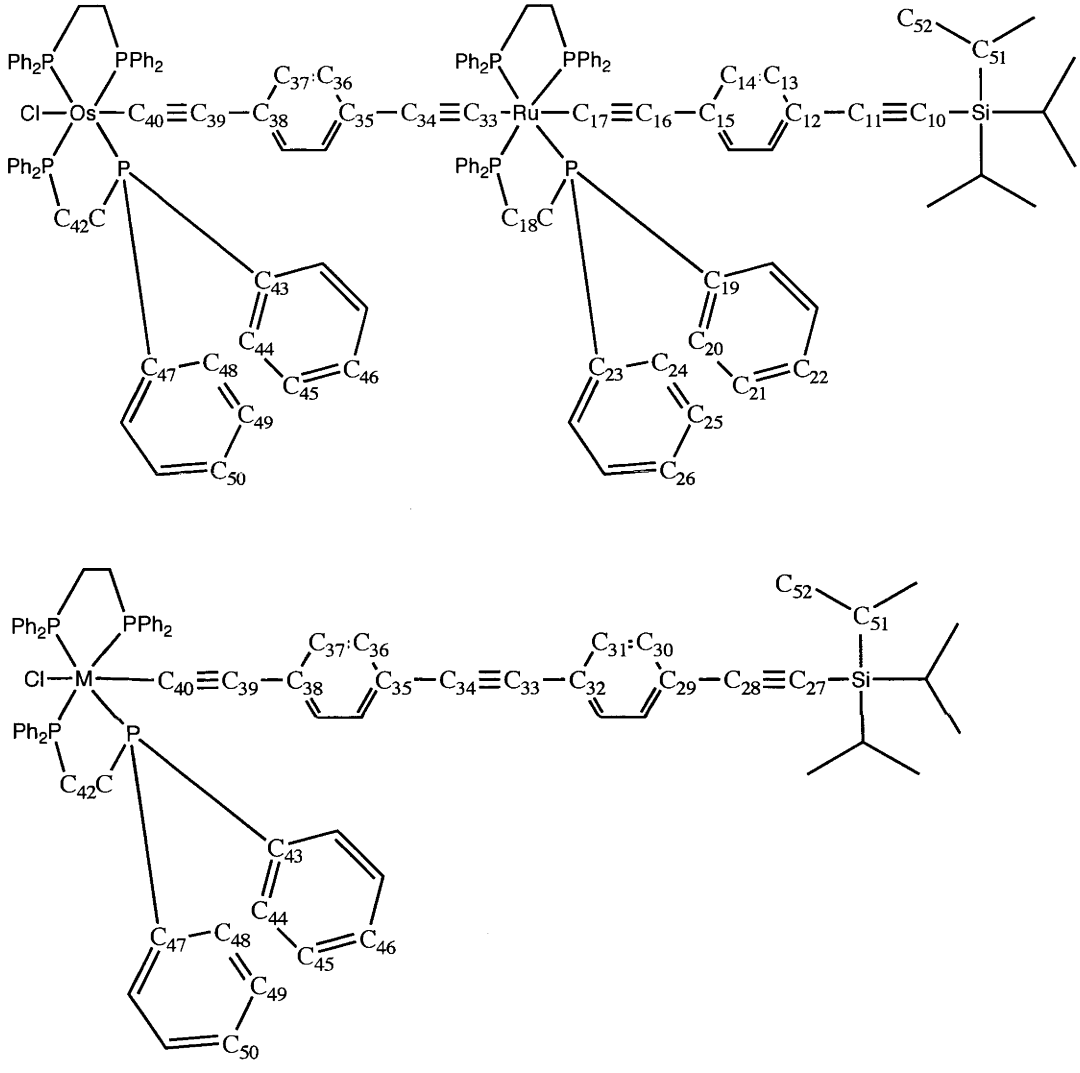

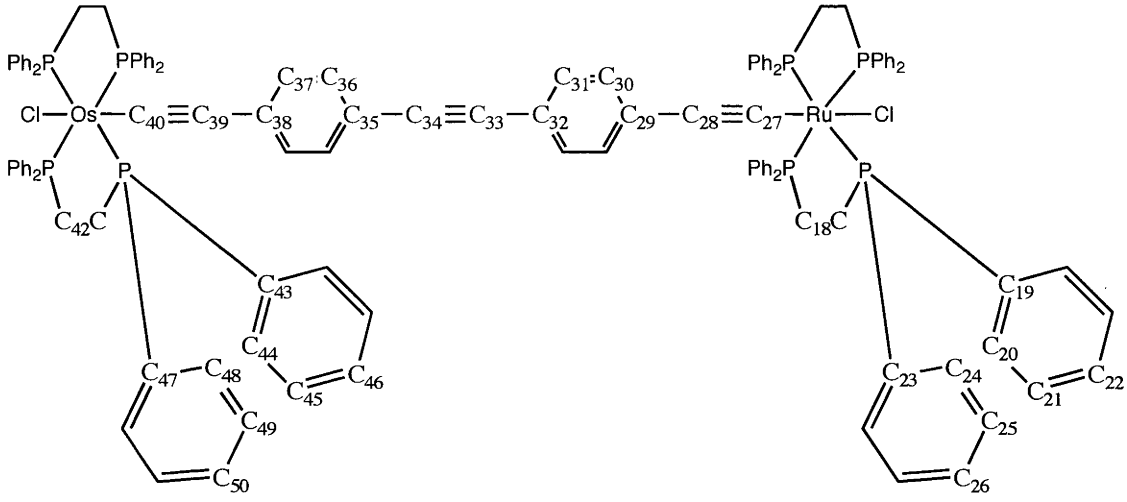

2.4.4 Synthesis and Characterization

trans-[Os(C≡CC$_6$H$_4$-4-C≡CSiPr$^i_3$)Cl(dppe)$_2$] (1)

A mixture of *cis*-[OsCl$_2$(dppe)$_2$] (**1**, 1.50 g, 1.42 mmol), HC≡CC$_6$H$_4$-4-C≡CSiPr$^i_3$ (2.00 g, 7.08 mmol), and NH_4PF_6 (289 mg, 1.77 mmol) was stirred in CH_2Cl_2 (150 mL) for 18 h. NEt_3 (15 mL) was then added, and the solution reduced to 60 mL in volume. The solution was added to methanol (200 mL), precipitating the solid product which was collected on a sintered glass filter funnel and washed with n-hexane (5 mL), affording **1** as a yellow powder (1.684 g, 91%). ESI MS: 1301 ([M - Cl + CH_3OH]$^+$, 100). Anal. Calcd for $C_{71}H_{73}ClOsP_4Si$: C 65.40, H 5.64%. Found: C 65.48, H 5.68%. UV-vis (CH_2Cl_2): λ 376 nm, ε 14900 M^{-1} cm^{-1}. IR (CH_2Cl_2) 2053 br cm^{-1} ν(OsC≡C), 2146 cm^{-1} ν(C≡CSi). ^{1}H NMR: δ 6.51-7.48 (m, 44H, Ar), 2.62 (m, 8H, CH_2), 1.14 (s, 21H, Pr$^i_3$). ^{31}P NMR: δ 16.1. ^{13}C NMR: δ 134.8, 134.6 (C_{47}, C_{43}, vtt, $|{}^1J_{PC} + {}^3J_{PC}| = 24$ Hz), 134.4, 134.2 (C_{48}, C_{44}), 132.6 (C_{38}), 131.2 & 130.2 (C_{37}, C_{36}), 128.9, 128.8 (C_{50}, C_{46}), 127.1, 126.9 (C_{49}, C_{45}), 116.4 (C_{35}), 110.3 (C_{39}), 108.4 (C_{40}, quint, $^2J_{PC}$ = 11 Hz), 89.6 (C_{33}), 31.4 (C_{42}, vtt, $|{}^1J_{PC} + {}^3J_{PC}|$ = 24 Hz), 18.7 (C_{52}), 11.4 (C_{51}).

***trans*-[Os(C≡CC$_6$H$_4$-4-C≡CH)Cl(dppe)$_2$] (2)**

A mixture of *trans*-[Os(C≡CC$_6$H$_4$-4-C≡CSiPr$^i_3$)Cl(dppe)$_2$] (**1**, 1.689 g, 1.29 mmol) and tetra-*n*-butylammonium fluoride (12.9 mL of a 1.0 M solution in THF, 12.9 mmol) was stirred in CH_2Cl_2 (200 mL) for 48 h. The solution volume was reduced to 40 mL, and then added to methanol (150 mL) to precipitate the product, which was collected on a sintered glass filter funnel. Complex **2** was obtained as an orange powder (1.305 g, 88%). ESI MS: 1145 ([M - Cl + CH_3OH]$^+$, 100). Anal. Calc. for $C_{62}H_{53}ClOsP_4$: C 64.89, H 4.65%. Found: C 64.95, H 4.74%. UV-vis (CH_2Cl_2): λ 371 nm, ε 15000 M^{-1} cm^{-1}. IR (CH_2Cl_2) 2064, 2039 (sh) cm^{-1} ν(C≡C), 3310 cm^{-1} ν(≡CH). ^{1}H NMR: δ 6.54-7.50 (m, 44H, Ar), 3.11 (s, 1H, C≡CH), 2.63 (m, 8H, CH_2). ^{31}P NMR: δ 16.1. ^{13}C NMR: δ 135.6, 134.6 (C_{47}, C_{43}, vtt, $|{}^1J_{PC} + {}^3J_{PC}|$ = 24 Hz), 134.3, 134.2 (C_{48}, C_{44}), 131.7 (C_{38}), 131.2, 130.3 (C_{37}, C_{36}), 128.9, 128.8 (C_{50}, C_{46}), 127.2, 126.8 (C_{49}, C_{45}), 114.8 (C_{35}), 110.2 (C_{39}), 109.1 (C_{40}, quint, $^2J_{PC}$ = 11 Hz), 85.0 (C_{34}), 76.7 (C_{33}), 31.4 (C_{42}, vtt, $|{}^1J_{PC} + {}^3J_{PC}|$ = 24 Hz).

***trans, trans*-[(dppe)$_2$ClOs(C≡CC$_6$H$_4$-4-C≡C)RuCl(dppe)$_2$] (3)**

A mixture of *trans*-[Os(C≡CC$_6$H$_4$-4-C≡CH)Cl(dppe)$_2$] (**2**, 1.00 g, 0.872 mmol), *cis*-[RuCl$_2$(dppe)$_2$] (2.10 g, 2.18 mmol) and $NaPF_6$ (295 mg, 1.74 mmol) was stirred in CH_2Cl_2 (200 mL) for 18 h. NEt_3 (20 mL) was added and the solvent volume reduced to 60 mL. The product was precipitated after the addition of methanol (150 mL), collected on a sintered glass filter funnel, and washed with *n*-hexane (10 mL), affording **2** as a yellow powder (1.695 g, 93%). ESI MS: 2085 ([M - Cl + CH_3CN]$^+$, 50). Anal. Calc. for $C_{114}H_{100}Cl_2OsP_8Ru$: C 65.83, H 4.85%. Found: C 65.04, H 4.57%. UV-vis (CH_2Cl_2): λ 373 nm, ε 45700 M^{-1} cm^{-1}. IR: (CH_2Cl_2) 2065, 2043 (sh) cm^{-1} ν(C≡C). ^{1}H NMR: δ 6.58-7.73 (m, 84H, Ar), 2.72 (m, 16H, CH_2). ^{31}P NMR: δ 16.2 (s, 4P, OsP), 50.2 (s, 4P, RuP). The complex was insufficiently soluble for ^{13}C NMR data to be obtained.

***trans, trans*-[(dppe)$_2$ClOs(C≡CC$_6$H$_4$-4-C≡C)Ru(C≡CC$_6$H$_4$-4-C≡CSiPr$^i_3$)(dppe)$_2$] (4)**

A mixture of *trans,trans*-[Cl(dppe)$_2$Os(C≡CC$_6$H$_4$-4-C≡C)RuCl(dppe)$_2$] (**3**, 400 mg, 0.192 mmol), HC≡CC$_6$H$_4$-4-C≡CSiPr$^i_3$ (217 mg, 0.769 mmol), $NaPF_6$ (65 mg, 0.385 mmol) and NEt_3 (0.1 mL) was stirred in refluxing CH_2Cl_2 (100 mL) for 18 h. The solvent mixture was absorbed onto basic alumina and the product eluted with 2:3 CH_2Cl_2/petrol, affording **4** as a yellow powder after reduction in volume of the solvent (177 mg, 40%). ESI MS: 2324 ([M - Cl + CH_3OH]$^+$, 5). Anal. Calc. for $C_{133}H_{125}ClOsP_8RuSi$: C 68.68, H 5.42%. Found: C 68.34, H 5.48%. UV-vis (CH_2Cl_2): λ 389 nm, ε 35000 M^{-1} cm^{-1}. IR: (CH_2Cl_2) 2058 (br) cm^{-1} ν(C≡C), 2147 cm^{-1} ν(C≡CSi). ^{1}H NMR: δ 6.90 - 7.82 (m, 88H, Ar), 2.65 (m, 16H, CH_2), 1.15 (s, 21H, ^{i}Pr). ^{31}P NMR: δ 16.6 (s, 4P, OsP), 54.3 (s, 4P, RuP). ^{13}C NMR: δ 137.4 (C_{23}, C_{19}), 136.5, 135.7 (C_{47}, C_{43}, tt, $|{}^1J_{PC} + {}^3J_{PC}|$ = 24 Hz), 134.4, 134.0 (C_{48}, C_{44}, C_{24}, C_{20}), 131.2, 131.2, 130.0, 129.7, 129.4, 129.1 (C_{37}, C_{36}, C_{14}, C_{13}, C_{35}, C_{15}), 128.6, 128.5 (C_{50}, C_{46}, C_{26}, C_{22}), 127.0 (C_{49}, C_{45} C_{25}, C_{21}), 116.7 (C_{12}), 110.0, 108.6, 108.5, 89.6, 89.5 (C_{10}, C_{11}, C_{16}, C_{34}, C_{39}), 32.4 (C_{18}, vtt, $|{}^1J_{PC} + {}^3J_{PC}|$ = 22 Hz), 31.5 (C_{42}, vtt, $|{}^1J_{PC} + {}^3J_{PC}|$ = 24 Hz), 18.7 (C_{52}), 11.4 (C_{51}), C_{40}, C_{38}, C_{33}, C_{17} (not detected).

***trans*-[Os(C≡CC$_6$H$_4$-4-C≡CC$_6$H$_4$-4-C≡CSiPr$^i_3$)Cl(dppe)$_2$] (5)**

A mixture of *cis*-[$OsCl_2$(dppe)$_2$] (600 mg, 0.567 mmol), HC≡CC$_6$H$_4$-4-C≡CC$_6$H$_4$-4-C≡CSiPr$^i_3$ (324 mg, 0.848 mmol), and NH_4PF_6 (153 mg, 0.938 mmol) was stirred in CH_2Cl_2 (115 mL) for 18 h. NEt_3 (10 mL) was added to the resulting dark brown solution, and the solution became orange. The volume of solvent was reduced by rotary evaporation to 50 mL, and the product was then precipitated from methanol (150 mL), collected on a sintered glass filter funnel and washed with *n*-hexane (5 mL), affording **5** as a yellow powder (680 mg, 85%). ESI MS: 1401 ([M - Cl + CH_3OH]$^+$, 30), 1369 ([M - Cl]$^+$, 30). Anal. Calcd for $C_{79}H_{77}ClOsP_4Si$: C 67.58, H 5.53%. Found: C 67.52, H 5.51%. UV-vis (CH_2Cl_2): λ

306 nm, ε 23200 M^{-1} cm^{-1}, λ 417 nm, ε 21200 M^{-1} cm^{-1}. IR (CH_2Cl_2) 2059 (br) cm^{-1} ν(C≡C), 2151 cm^{-1}, ν(C≡CSi). ^{1}H NMR: δ 6.56-7.51 (m, 48H, Ar), 2.64 (m, 8H, CH_2), 1.15 (s, 21H, Pr^i_3). ^{31}P NMR: δ 16.0. ^{13}C NMR: δ 135.8, 134.9 (C_{47}, C_{43}, vtt, $|{}^1J_{PC} + {}^3J_{PC}|$ = 24 Hz), 134.4, 134.2 (C_{48}, C_{44}), 131.5 (C_{38}), 131.9, 131.3, 130.8, 130.5 (C_{37}, C_{36}, C_{31}, C_{30}), 129.0, 128.8 (C_{50}, C_{46}), 127.2, 126.9 (C_{49}, C_{45}), 123.9, 122.6, 115.7 (C_{35}, C_{32}, C_{29}), 110.7, 106.9, 92.8, 92.4 (C_{39}, C_{34}, C_{33}, C_{28}), 109.9 (C_{40}, quint, $^2J_{PC}$ = 11 Hz), 87.3 (C_{27}), 31.4 (C_{42}, vtt, $|{}^1J_{PC} + {}^3J_{PC}|$ = 24 Hz), 18.7 (C_{52}), 11.3 (C_{51}), 18.7 (C_{52}), 11.4 (C_{51}).

***trans*-[Os(C≡CC$_6$H$_4$-4-C≡CC$_6$H$_4$-4-C≡CH)Cl(dppe)$_2$] (6)**

A mixture of *trans*-[Os(C≡CC$_6$H$_4$-4-C≡CC$_6$H$_4$-4-C≡CSiPr^i_3)Cl(dppe)$_2$] (**5**, 501 mg, 0.402 mmol) and tetra-*n*-butylammonium fluoride (4.84 mL of a 1.0 M solution in THF, 4.84 mmol) was stirred in CH_2Cl_2 (100 mL) for 20 h. The solution volume was reduced to 40 mL, and the product was precipitated on addition of methanol (150 mL). The product was collected on a sintered glass filter funnel and washed with methanol (20 mL), affording **6** as an orange powder (513 mg, 85%). ESI MS: 1245 ($[M - Cl + CH_3OH]^+$, 30), 1213 ($[M - Cl]^+$, 100). Anal. Calc. for $C_{70}H_{57}ClOsP_4$: C 67.38, H 4.60%. Found: C 67.44, H 4.91%. UV-vis (CH_2Cl_2): λ 304 nm, ε 27000 M^{-1} cm^{-1}, λ 416 nm, ε 30000 M^{-1} cm^{-1}. IR (CH_2Cl_2) 2058, 2027 (sh) cm^{-1} ν(C≡C), 3297 cm^{-1} ν(≡CH). ^{1}H NMR: δ 6.59-7.52 (m, 48H, Ar), 3.18 (s, 1H, C≡CH), 2.65 (m, 8H, CH_2). ^{31}P NMR: δ 16.0. ^{13}C NMR: δ 135.6, 134.8 (C_{47}, C_{43}, vtt, $|{}^1J_{PC} + {}^3J_{PC}|$ = 24 Hz), 134.6, 134.2 (C_{48}, C_{44}), 131.6 (C_{38}), 132.0, 131.1, 130.8, 130.5 (C_{37}, C_{36}, C_{31}, C_{30}), 129.0, 128.8 (C_{50}, C_{46}), 127.2, 126.9 (C_{49}, C_{45}), 124.5, 121.1, 115.6 (C_{35}, C_{32}, C_{29}), 110.0 (C_{40}, quint, $^2J_{PC}$ = 11 Hz), 110.7, 93.0, 89.0 (C_{39}, C_{34}, C_{33}), 83.5 (C_{28}), 78.6 (C_{27}), 31.4 (C_{42}, vtt, $|{}^1J_{PC} + {}^3J_{PC}|$ = 26 Hz).

***trans, trans*-[(dppe)$_2$ClOs(C≡CC$_6$H$_4$-4-C≡CC$_6$H$_4$-4-C≡C)RuCl(dppe)$_2$] (7)**

A mixture of *trans*-[Os(C≡CC$_6$H$_4$-4-C≡CC$_6$H$_4$-4-C≡CH)Cl(dppe)$_2$] (**6**, 501 mg, 0.402 mmol), *cis*-[RuCl$_2$(dppe)$_2$] (778 mg, 0.803 mmol) and $NaPF_6$ (353 mg, 2.09 mmol) was heated at reflux in CH_2Cl_2 (150 mL) for 48 h. NEt_3 (15 mL) was added and the solvent volume reduced to 30 mL. Methanol (150 mL) was added, precipitating the solid product, which was collected on a sintered glass filter funnel affording **7** as a yellow powder (841 mg, 97%). ESI MS: 2186 ([M - Cl + CH_3CN]$^+$, 1), 974 ([RuCl(NCMe)(dppe)$_2$]$^+$, 100). Anal. Calc. for $C_{122}H_{104}Cl_2OsP_8Ru$: C 67.21, H 4.81%. Found: C 67.20, H 5.08%. UV-vis (CH_2Cl_2): λ 427 nm, ε 47600 M^{-1} cm^{-1}. IR: (CH_2Cl_2) 2059 (br) cm^{-1} ν(C≡C). ^{1}H NMR: δ 6.57-7.55 (m, 88H, Ar), 2.66 (m, 16H, CH_2). ^{31}P NMR: δ 16.1 (s, 4P, OsP), 49.9 (s, 4P, RuP). ^{13}C NMR: δ 134.4, 134.3, 134.2 (C_{48}, C_{44}, C_{24}, C_{20}), 129.0, 128.8 (C_{50}, C_{46}, C_{26}, C_{22}), 127.2, 127.0, 126.9 (C_{49}, C_{45}, C_{25}, C_{21}), 30.6 (C_{42}, C_{18}); other signals were not observed due to poor solubility.

***trans*-[Ru(C≡CC$_6$H$_4$-4-C≡CC$_6$H$_4$-4-C≡CSiPr$^i_3$)Cl(dppe)$_2$] (8)**

A mixture of *cis*-[RuCl$_2$(dppe)$_2$] (1.5 g, 1.55 mmol), HC≡CC$_6$H$_4$-4-C≡CC$_6$H$_4$-4-C≡CSiPr$^i_3$ (770 mg, 2.01 mmol), and $NaPF_6$ (631 mg, 3.87 mmol) was stirred in CH_2Cl_2 (100 mL) for 12 h. NEt_3 (5 mL) was added to the red solution and the solution turned yellow. The volume of solvent was reduced by rotary evaporation to 40 mL, and the product was then precipitated from methanol (150 mL), collected on a sintered glass filter funnel and washed with petrol (20 mL), affording **8** as a yellow powder (1.86 g, 92%). ESI MS: 1320 ([M - Cl + $CNCH_3$]$^+$, 100). Anal. Calcd for $C_{79}H_{77}ClP_4RuSi$: C 72.16, H 5.90%. Found: C 72.03, H 6.12%. UV-vis (CH_2Cl_2): λ 251 nm, ε 51800 M^{-1} cm^{-1}, λ 297 nm, ε 38000 M^{-1} cm^{-1}, λ 409 nm, ε 40000 M^{-1} cm^{-1}. IR (CH_2Cl_2) 2063 (br) cm^{-1} ν(C≡C), 2152 cm^{-1}, ν(C≡CSi). ^{1}H NMR: δ 6.56 - 7.44 (m, 48H, Ar), 2.69 (m, 8H, CH_2), 1.14 (s, 21H, Pr$^i_3$). ^{31}P NMR: δ 49.8. ^{13}C NMR: δ 136.3, 135.5 (C_{47}, C_{43}, vtt, $|{}^1J_{PC} + {}^3J_{PC}|$ = 18 Hz), 134.4, 134.2

(C_{48}, C_{44}), 131.9 (2C), 131.2, 130.7, 130.2 (C_{38}, C_{37}, C_{36}, C_{31}, C_{30}), 128.9 (C_{50}, C_{46}), 127.2, 127.0 (C_{49}, C_{45}), 123.7, 122.8 (2C), 106.8 (2C), 92.5 (2C) (C_{39}, C_{35}, C_{34}, C_{33}, C_{32}, C_{29}, C_{28}), 89.5 (C_{27}), 30.6 (C_{42}, vtt, $|{}^{1}J_{PC} + {}^{3}J_{PC}|$ = 22 Hz), 18.7 (C_{52}), 11.3 (C_{27}), C_{40} (not detected).

2.5 References

(1) Younus, M.; Long, N. J.; Raithby, P. R.; Lewis, J. *J. Organomet. Chem.* **1998**, *570*, 55.

(2) Hodge, A. J.; Ingham, S. L.; Kakkar, A. K.; Khan, M. S.; Lewis, J.; Long, N. J.; Parker, D. G.; Raithby, P. R. *J. Organomet. Chem.* **1995**, *488*, 205.

(3) Long, N. J.; Martin, A. J.; Fabrizi de Biani, F.; Zanello, P. *J. Chem. Soc., Dalton Trans.* **1998**, 2017.

(4) Colbert, M. C. B.; Ingham, S. L.; Nicholas, J. L.; Long, N. J.; Raithby, P. R. *J. Chem. Soc., Dalton Trans.* **1994**, 2215.

(5) Wong, W.-Y.; Wong, C.-K.; Lu, G.-L. *J. Organomet. Chem.* **2003**, *671*, 27.

(6) McDonagh, A. M.; Cifuentes, M. P.; Humphrey, M. G.; Houbrechts, S.; Maes, J.; Persoons, A.; Samoc, M.; Luther-Davies, B. *J. Organomet. Chem.* **2000**, *610*, 71.

(7) Morrall, J. P.; Powell, C. E.; Stranger, R.; Cifuentes, M. P.; Humphrey, M. G.; Heath, G. A. *J. Organomet. Chem.* **2003**, *670*, 248.

(8) Klein, A.; Lavastre, O.; Fiedler, J. *Organometallics* **2006**, *25*, 635.

(9) Khairul, W. M.; Fox, M. A.; Schauer, P. A.; Yufit, D. S.; Albesa-Jove, D.; Howard, J. A. K.; Low, P. J. *Dalton Trans.* **2010**, *39*, 11605.

(10) Dalton, G. T.; Cifuentes, M. P.; Watson, L. A.; Petrie, S.; Stranger, R.; Samoc, M.; Humphrey, M. G. *Inorg. Chem.* **2009**, *48*, 6534.

(11) Colbert, M. C. B.; Lewis, J.; Long, N. J.; Raithby, P. R.; Younus, M.; White, A. J. P.; Williams, D. J.; Payne, N. N.; Yellowlees, L.; Beljonne, D.; Chawdhury, N.; Friend, R. H. *Organometallics* **1998**, *17*, 3034.

(12) Gauthier, N.; Olivier, C.; Rigaut, S.; Touchard, D.; Roisnel, T.; Humphrey, M. G.; Paul, F. *Organometallics* **2008**, *27*, 1063.

(13) Samoc, M.; Gauthier, N.; Cifuentes, M. P.; Paul, F.; Lapinte, C.; Dalton, G. T.; Humphrey, M. G. *Angew. Chem. Int. Ed.* **2006**, *45*, 7376.

(14) Touchard, D.; Morice, C.; Cadierno, V.; Haquette, P.; Toupet, L.; Dixneuf, P. H. *J. Chem. Soc., Chem. Commun.* **1994**, 859.

(15) Younus, M.; Long, N. J.; Raithby, P. R.; Lewis, J.; Page, N. A.; White, A. J. P.; Williams, D. J.; Colbert, M. C. B.; Hodge, A. J.; Khan, M. S.; Parker, D. G. *J. Organomet. Chem.* **1999**, *578*, 198.

(16) Touchard, D.; Haquette, P.; Guesmi, S.; Le Pichon, L.; Daridor, A.; Toupet, L.; Dixneuf, P. H. *Organometallics* **1997**, *16*, 3640.

(17) Powell, C. E.; Cifuentes, M. P.; Morrall, J. P.; Stranger, R.; Humphrey, M. G.; Samoc, M.; Luther-Davies, B.; Heath, G. A. *J. Am. Chem. Soc.* **2003**, *125*, 602.
(18) Cifuentes, M. P.; Powell, C. E.; Humphrey, M. G.; Heath, G. A.; Samoc, M.; Luther-Davies, B. *J. Phys. Chem. A* **2001**, *105*, 9625.
(19) Cifuentes, M. P.; Powell, C. E.; Morrall, J. P.; McDonagh, A. M.; Lucas, N. T.; Humphrey, M. G.; Samoc, M.; Houbrechts, S.; Asselberghs, I.; Clays, K.; Persoons, A.; Isoshima, T. *J. Am. Chem. Soc.* **2006**, *128*, 10819.
(20) Lavastre, O.; Ollivier, L.; Dixneuf, P.; Sibandhit, S. *Tetrahedron* **1996**, *52*, 5495.
(21) Lavastre, O.; Cabioch, S.; Dixneuf, P. H.; Vohlidal, J. *Tetrahedron* **1997**, *53*, 7595.
(22) Antonov, P. G.; Kukushkin, Y. N.; Konnov, V. I.; Kostikov, Y. P. *Koord. Khim.* **1980**, *6*, 1585.
(23) Green, K. A.; Cifuentes, M. P.; Corkery, T. C.; Samoc, M.; Humphrey, M. G. *Angew. Chem. Int. Ed.* **2009**, *48*, 7867.
(24) Morrall Joseph, P. *Unpublished results* **2006**.

Chapter 3

Osmium bis-alkynyl heterobimetallic complexes

Chapter 3

Osmium bis-alkynyl heterobimetallic complexes

Contents

3.1 Introduction

Whilst there have been numerous reports of ruthenium alkynyl complexes examined for nonlinear optical effects,[1-6] there have been far fewer reports of osmium complexes for the same applications. This is curious, as it has been shown previously that optical nonlinearities increase on proceeding down the group 8 metals.[7,8] One possible reason for the lack of development in this area is the ease with which unsymmetrical bis-alkynyl complexes of ruthenium are formed relative to the analogous osmium complexes, an important consideration if large, highly functionalised structures are to be prepared. Whilst there have been a few reports of symmetrical bis-alkynyl complexes of osmium,[9-16] the only report of unsymmetrically substituted osmium bis-alkynyl complexes involved the use of alkynyl-tin reagents and proceeded in approximately 30% yield[17] (Scheme 3.1).

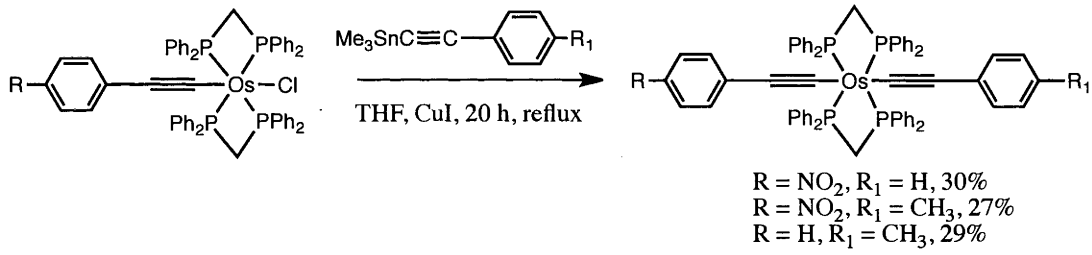

Scheme 3.1. Syntheses of unsymmetrical bis-alkynyl complexes by Younus *et al.*, utilising alkynyl-tin reagents[17]

A large number of hetero-multinuclear phenylethynyl complexes have been reported to date. These complexes include: iron-ruthenium,[18,19] rhenium-platinum,[20] iron-rhenium,[21] ruthenium-palladium,[22] iron-palladium,[22] ruthenium-platinum-iron-rhenium[23] and osmium-ruthenium[24] derivatives. One example of particular interest to this work is the iron-ruthenium hetero-bimetallic complex reported by Gauthier *et al.* (Figure 3.1).[3,19,25] This complex has been shown to be a good third-order nonlinear optical switch, with the complex possessing several desirable properties for this type of application:

- both the iron and ruthenium metal centres undergo reversible oxidation processes leading to three interchangeable states $Fe^{II}Ru^{II}$, $Fe^{III}Ru^{II}$, $Fe^{III}Ru^{III}$.
- the formation of each of the electrochemical species ($Fe^{II}Ru^{II}$, $Fe^{III}Ru^{II}$, $Fe^{III}Ru^{III}$) is accompanied by large changes in the optical absorption properties of the complex suggesting possible large changes in the nonlinear optical spectra.
- the ruthenium metal centre has two alkynyl ligands–one is attached to the iron metal centre, and the other remains free to potentially attach to either another metal centre, or to a surface for incorporation into molecular devices.
- the unsymmetrical nature of the two alkynyl ligands around the ruthenium metal centre allows greater design flexibility.

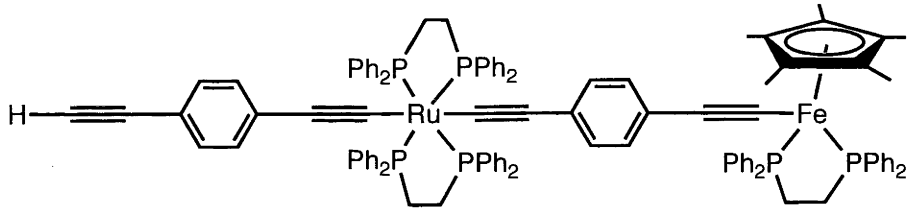

Figure 3.1 Hetero-bimetallic complex formed by Gauthier *et al.*[19]

3.2 Results and Discussion

3.2.1 Synthesis

The heterobimetallic complexes reported in Chapter 2 (**3**, **4** and **7**) have limited synthetic functionality as there is no convenient method of replacing the chloro ligand with a second alkynyl group. In order to extend the conjugated phenylethynyl chain, a route to unsymmetrically substituted bis-alkynyl osmium complexes was developed. The previously reported route using alkynyl-tin reagents was not attempted due to the low yields involved,[17] so the first attempt at preparing bis-alkynyl complexes involved refluxing *trans*-[Os(C≡CPh)Cl(dppe)$_2$] (**9**) with nitrophenylacetylene, NEt_3 and NH_4PF_6 in aromatic solvents with progressively

higher boiling points. It was found that for xylenes, mesitylene and 1,2-dichlorobenzene, no reaction was observed, and only starting material was recovered (Scheme 3.2).

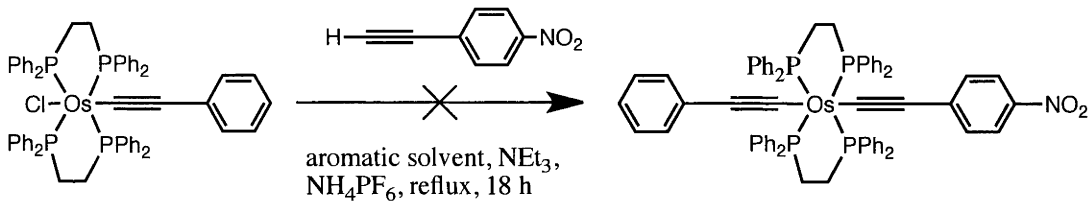

Scheme 3.2 Attempted formation of osmium bis-alkynyl complexes

When the synthesis of osmium bis-alkynyl complexes was attempted with the procedure used to prepare the analogous ruthenium complexes,[26] (complex **9** stirred at room temperature in the presence of NEt_3, NH_4PF_6 and phenylacetylene) the formation of the ammine complex, *trans*-$[Os(C{\equiv}CPh)(NH_3)(dppe)_2]PF_6$ (**13**), was observed (Scheme 3.3).

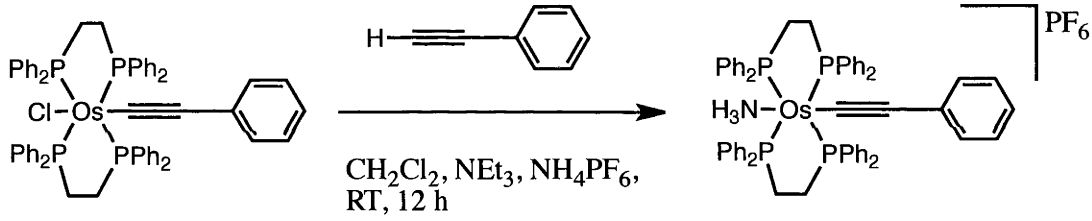

Scheme 3.3 Formation of osmium ammine-alkynyl complex

This cationic complex can be isolated through precipitation from petrol, with subsequent washing with methanol to remove any residual NH_4PF_6. It should be noted that phenylacetylene plays no part in the reaction, which proceeds in the same manner in the absence of acetylene. A number of different chloro-alkynyl complexes were formed and reacted in this manner, to demonstrate the general nature of this reaction, with the corresponding ammine-alkynyl complexes isolated in good yield (Scheme 3.4).

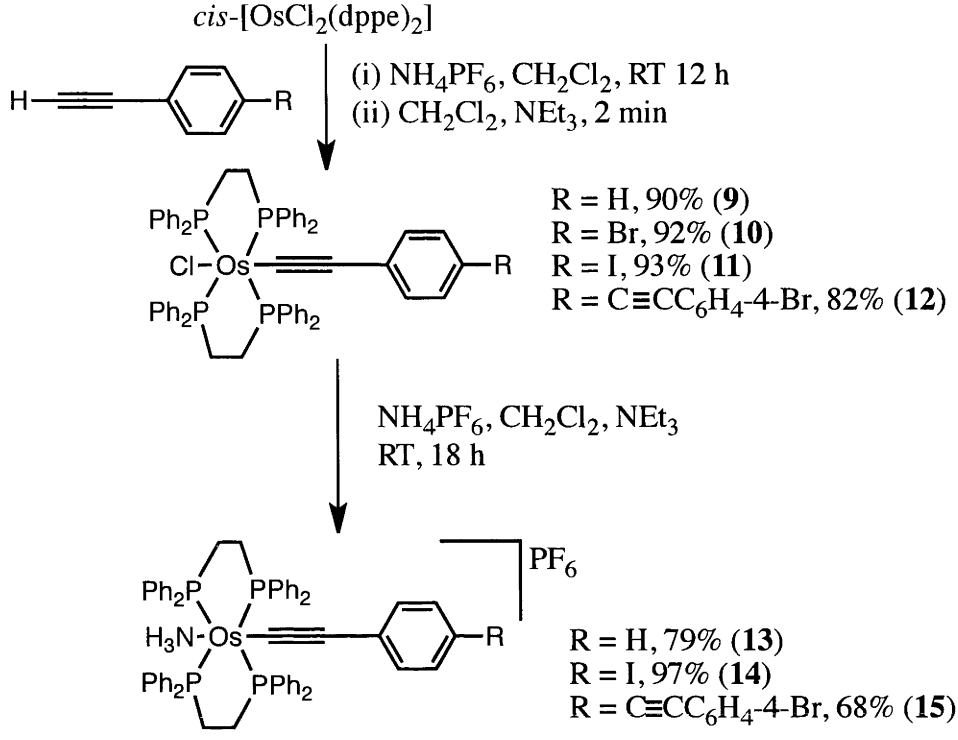

Scheme 3.4 Syntheses of chloro-alkynyl (**9** – **12**) and ammine-alkynyl (**13** – **15**) osmium complexes

Touchard *et al.* have shown that the ammine group in analogous ruthenium ammine-alkynyl complexes is labile, allowing substitution with carbonyl, hydride and isocyanide groups, as well as alkynyl groups[27] (Scheme 3.4).

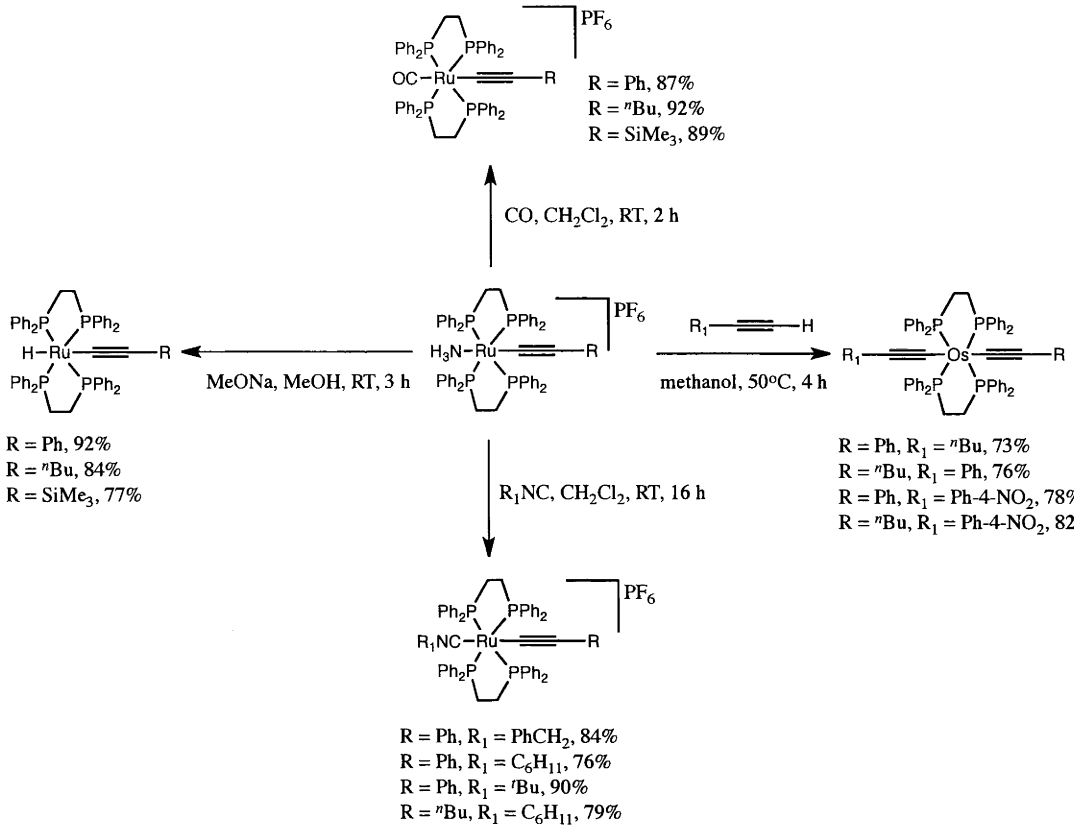

Scheme 3.5 Reactivity of ruthenium ammine-alkynyl complexes[27]

Ruthenium ammine-alkynyl complexes can be formed either from a chloro-alkynyl complex[28] or a bis-alkynyl complex.[26] Whilst the latter affords high yields with mild conditions, reaction with the former proceeded very slowly with no yields reported. It was of interest to determine whether a ruthenium ammine-alkynyl complex could be formed directly from a chloro-alkynyl complex quickly and in good yields. This was found to be the case, when using the modified conditions that were successful for the analogous osmium complex (addition of NEt_3), with the reaction of *trans*-$[Ru(C{\equiv}C_6H_4I)(Cl)(dppe)_2]$ yielding the corresponding ammine complex, *trans*-$[Ru(C{\equiv}C_6H_4I)(NH_3)(dppe)_2]PF_6$ (**16**), after 12 h at room temperature in 60% yield (Scheme 3.6).

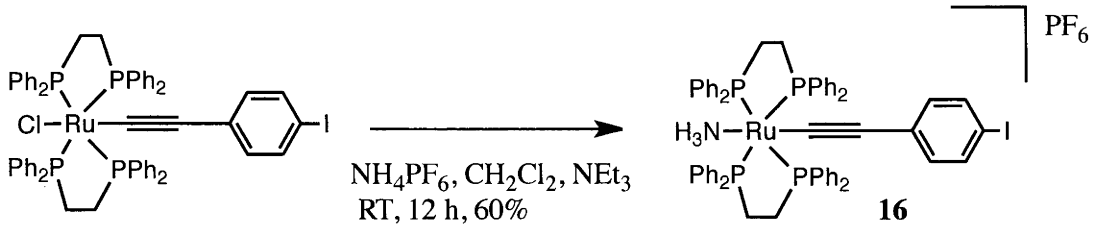

Scheme 3.6 Synthesis of *trans*-[Ru(C≡CC$_6$H$_4$I)(NH$_3$)(dppe)$_2$]PF$_6$ **(16)**

It has been shown previously that ruthenium ammine-alkynyl complexes can be used to form bis-alkynyl complexes, in good yields, by heating in methanol solutions containing acetylene for 4 hours (Scheme 3.5). Similar treatment of the osmium ammine-alkynyl complexes (**13** and **14**) afforded the corresponding bis-alkynyl complexes in good yields, although the reaction proceeded more slowly then with the ruthenium analogues (Scheme 3.7).

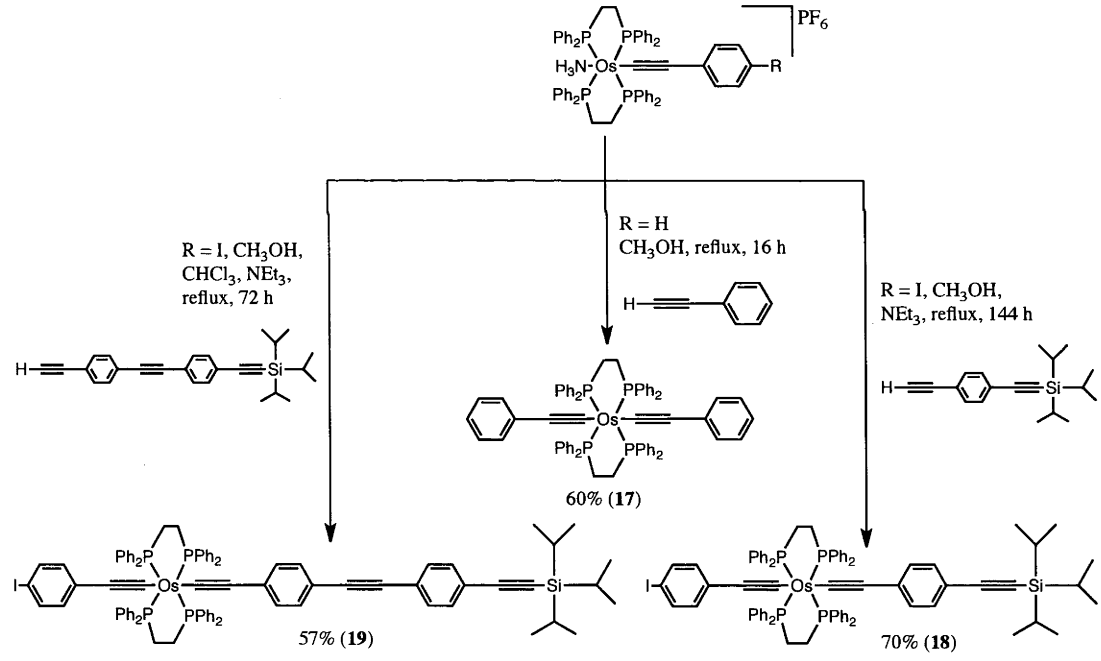

Scheme 3.7 Formation of osmium bis-alkynyl complexes (**17** – **19**)

The osmium chloro-alkynyl complexes (**9** – **12**) have some instability in solution, with decomposition observed by ^{31}P NMR (disappearance of product peaks and

appearance of new peaks over the course of several hours). The addition of NEt_3 to solutions containing these complexes appears to reduce this decomposition, so it was also added to the reaction mixtures for the formation of **18** and **19**. One of the decomposition products has been identified as *trans*-$[OsCl_2(dppe)_2]$, which has a singlet at 12.8 ppm in the ^{31}P NMR spectrum. This complex is formed in $CHCl_3$ (or $CDCl_3$) in the absence of NEt_3 presumably through reaction with the small amount of HCl present in the solent. This product was confirmed crystallographically, although the structure was not refined as it has been reported previously.[29] Chloroform was added to the reaction mixture for the formation of **19**, to aid solubility as the acetylene was insoluble in the CH_3OH/NEt_3 mixture.

Bis-alkynyl complexes with a triisopropysilyl-protected acetylene on one end and an aryl-iodo on the other (**18** and **19**), allow Sonogashira reaction with a trimethyl silyl-protected acetylene at the iodo site, yielding a complex that has two silyl protected alkynyl ligands that can be reacted independently, *trans*-$[Os(C{\equiv}C\text{-}4\text{-}C_6H_4\text{-}4\text{-}C{\equiv}CSiMe_3)(C{\equiv}CC_6H_4\text{-}4\text{-}C{\equiv}CSiPr^i_3)(dppe)_2]$ **(20)** (Scheme 3.7). Whilst both protecting groups can be removed using NBu^n_4F, use of KOH in a mixture of CH_2Cl_2 and CH_3OH (1:1) allows the trimethylsilyl group to be selectively cleaved, leaving the triisopropylsilyl group intact and allowing further unsymmetrical functionalization to be carried out. *trans*-$[Os(C{\equiv}C\text{-}4\text{-}C_6H_4\text{-}4\text{-}C{\equiv}CH)(C{\equiv}CC_6H_4\text{-}4\text{-}C{\equiv}CSiPr^i_3)(dppe)_2]$ **(21)** was isolated in 81% yield using these conditions (Scheme 3.7).

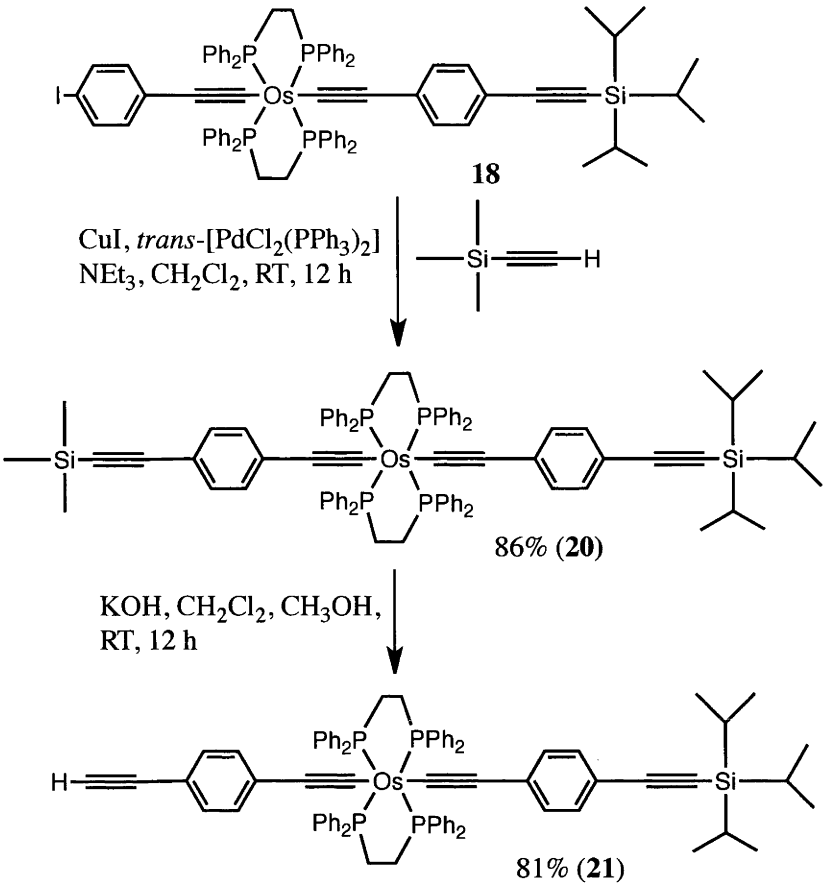

Scheme 3.7 Syntheses of complexes **20** and **21**

Complex **21** can be coupled to ruthenium chloro-alkynyl complexes via a ruthenium bis-alkynyl formation reaction to form the binuclear complexes **22** and **23** (Scheme 3.8).

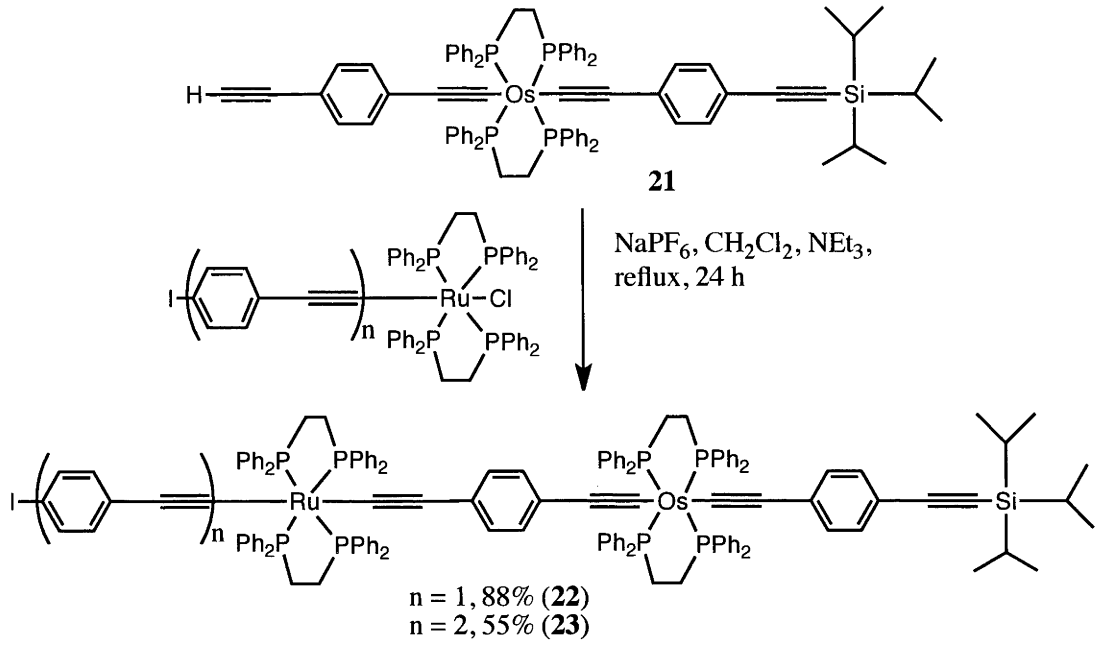

Scheme 3.8 Syntheses of complexes **22** and **23**

The binuclear complex **22** can be extended further through coupling at the iodo site via a Sonogashira reaction with trimethylsilylacetylene to form the binuclear complex with two different silyl groups (**24**), allowing selective deprotection and further unsymmetrical functionalisation (Scheme 3.9).

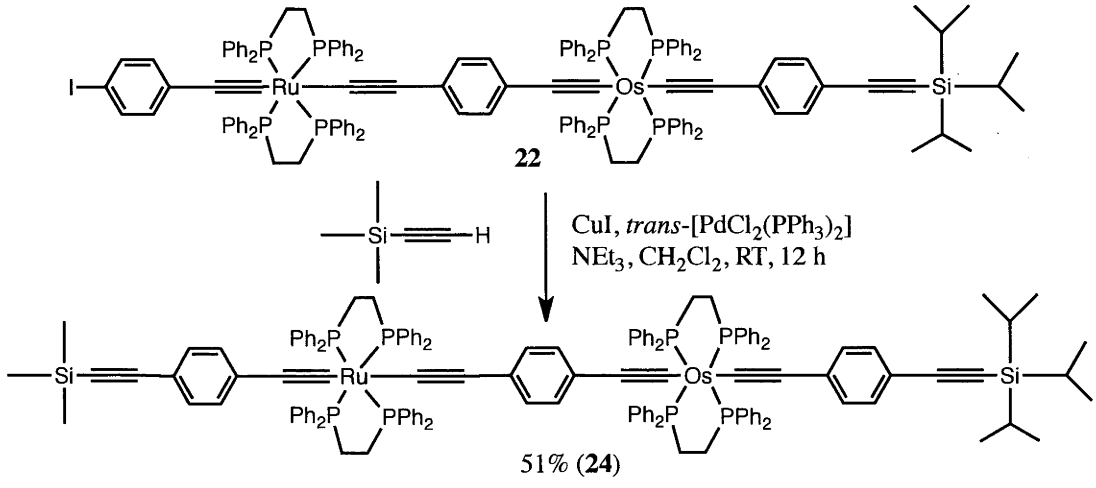

Scheme 3.9 Synthesis of complex **24**

In order to form difunctionalised bimetallic complexes incorporating the chain-lengthened C≡CC_6H_4-4-C≡CC_6H_4-4-C≡C bridge, complex **19** was desilylated by stirring a CH_2Cl_2 solution in the presence of NBu^n_4F at room temperature, yielding complex **25** in a 93% yield (Scheme 3.10).

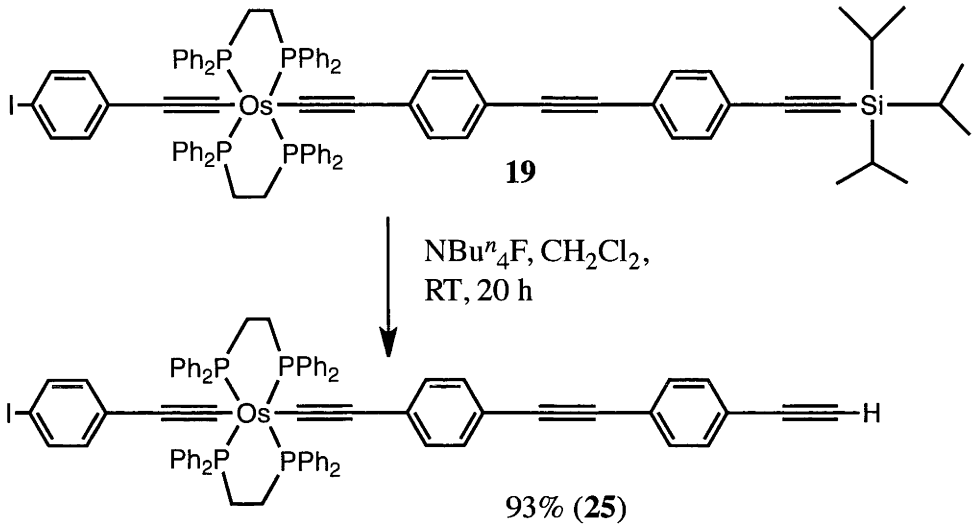

Scheme 3.10 Synthesis of complex **25**.

The free terminal alkynyl group on complex **25** can now be coupled to a ruthenium metal centre. Complex **25** was coupled to *cis*-[$RuCl_2$(dppe)$_2$] affording complex **26** in 87% yield (Scheme 3.11). This complex was then extended at the osmium centre through a Sonogashira reaction, replacing the iodo group with -C≡C$SiMe_3$ or -C≡CC_6H_4-4-C≡C$SiPr^i_3$ groups to yield complexes **27** and **28** (Scheme 3.11). Both of these complexes were purified by passing the solution through a small pad of alumina to remove residual catalyst.

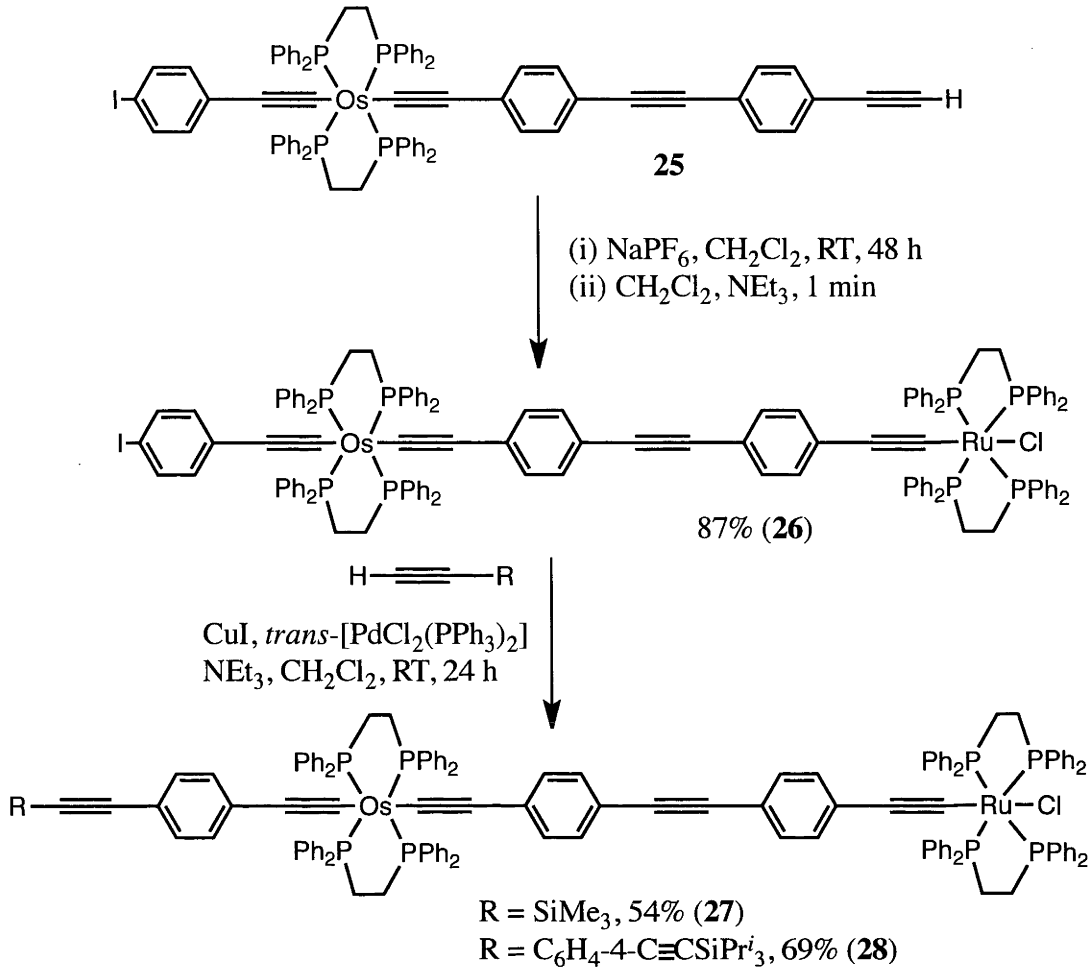

Scheme 3.11 Syntheses of complexes **26 - 28**

As shown in Chapter 2, when an osmium metal centre is separated from a ruthenium centre by a diethynylbenzene bridge (C≡CC_6H_4-4-C≡C), oxidation of the Os occurs at a lower potential compared to a mononuclear osmium complex, or a bimetallic complex where the osmium and ruthenium metal centres are separated by the triethynyl bridge (C≡CC_6H_4-4-C≡CC_6H_4-4-C≡C). As a result, a trimetallic complex containing one ruthenium and two osmium metal centres was targeted, with the osmium centres separated by both a diethynyl and triethynyl bridge from the central ruthenium metal centre. It was hoped that this complex would possess three individually-addressable redox states that might provide different optical absorption

properties. Complex **7** was coupled to complex **21** to afford the trinuclear complex (**29**) (Scheme 3.12).

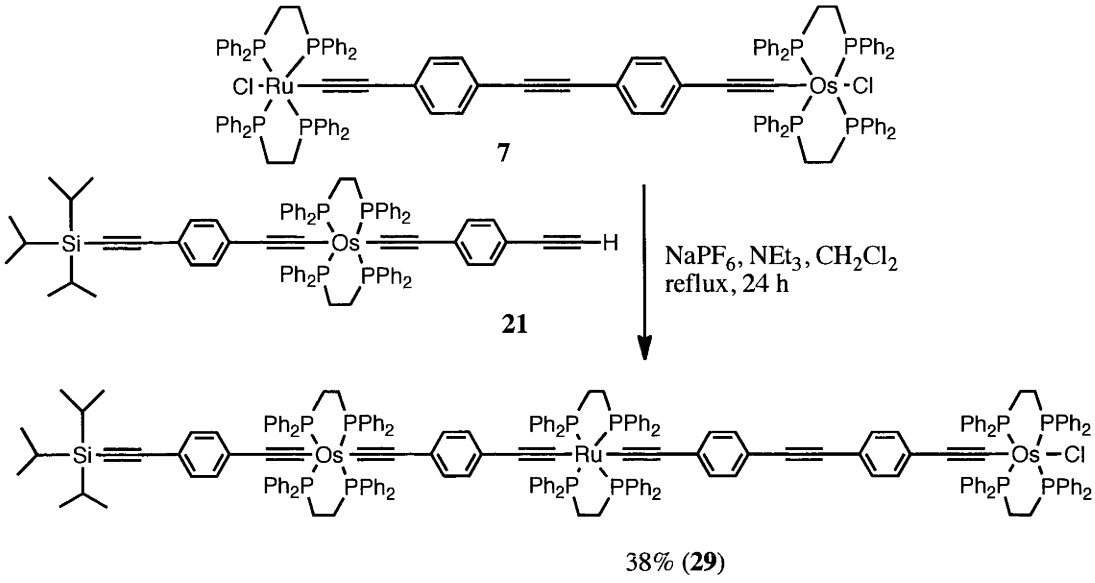

Scheme 3.12 Synthesis of complex **29**

3.2.2 Physical Properties

3.2.2.1 NMR spectroscopy

The mononuclear complexes (**10** – **21** and **25**) were characterised by ^{1}H, ^{31}P and ^{13}C NMR spectroscopy in $CDCl_3$; ^{13}C NMR data are assigned where possible and included (along with ^{1}H and ^{31}P NMR) in Appendix B. Complex **9** has previously been synthesised using a different route[30]. The multinuclear complexes (**22** – **24** and **26** – **29**) were characterised by ^{1}H and ^{31}P NMR spectroscopy, with low solubility precluding the use of ^{13}C NMR spectroscopy.

^{1}H NMR spectroscopy

The ^{1}H NMR spectra of chloro-alkynyl osmium complexes (**9** – **12**) show similar aromatic and dppe bridgehead resonances to that described earlier for the similar

chloro-alkynyl complexes **1**, **2**, **5**, and **6** in Chapter 1. Resonances due to the aromatic protons appear as multiplets within the range 6.34 – 7.51 ppm, and the dppe bridgehead protons show as multiplets within the range 2.61 – 2.64 ppm. For the ammine –alkynyl osmium complexes (**13 – 15**), the aromatic resonances extend over a wider range, 6.43 – 8.20 ppm. The bridgehead protons are largely unchanged on moving from the chloro to ammine complexes with a range of 2.61 – 2.63 ppm observed for **10 - 15**. The ammine-alkynyl complexes have an additional broad singlet corresponding to the three protons on the ammine ligand ranging from 1.00 – 1.05 ppm. The ammine-alkynyl ruthenium complex (**16**) has similar resonances as those seen for the osmium analogue, with aromatic proton resonances over a wide range, 6.42 – 8.13 ppm, and the dppe bridgehead resonances at 2.63 ppm. Signals attributed to the protons on the ammine ligand are significantly altered on moving from the osmium complexes (**13 – 15**) to the ruthenium complex (**16**) with an upfield shift to 0.28 ppm for the latter. For the bis-alkynyl mononuclear osmium complexes **17 – 19**, **20**, **21** and **25**, the aromatic proton resonances are spread over a smaller range (6.40 – 7.50 ppm) than the ammine alkynyl complexes. The bridgehead protons are within a similar range as the previous examples, and fall between 2.56 – 2.59 ppm. The mononuclear complexes with a $SiPr^{i}_{3}$ protecting group (**18**, **19**, **20** and **21**) have an additional resonance for the protons associated with the silyl group in the range of 1.14 – 1.15 ppm, as described previously in Chapter 2. On desilylation of **19** to form **25** this resonance is no longer present and is replaced by a resonance at 3.17 ppm corresponding to the acetylenic proton. In a similar manner, complex **20** has a resonance corresponding to the $SiMe_3$ group at 0.27 ppm which, upon removal to form **21**, is replaced with a resonance for the acetylenic proton at 3.10 ppm.

For the multinuclear complexes (**22 – 24** and **26 – 29**) proton resonances similar to the mononuclear complexes are seen. All of the bimetallic complexes have aromatic proton resonances within the range of 6.33 – 7.90 ppm, and dppe bridgehead signals within the range 2.56 – 2.70 ppm. For the multi-nuclear complexes that possess a $SiPr^{i}_{3}$ group (**22 – 24** and **28 - 29**) a resonance at ca. 1.28 ppm (C_6D_6) or 1.15 ppm

($CDCl_3$) is observed. Likewise, a resonance at 0.26 ppm ($CDCl_3$) is observed for complexes with a $SiMe_3$ group (**24** and **27**).

^{31}P NMR spectroscopy

The ^{31}P NMR spectra of the chloro-alkynyl osmium complexes (**9** – **12**) show a singlet resonance that falls within a narrow range 16.0 – 16.2 ppm that is very similar to the resonances observed for similar complexes in Chapter 2, as well as those reported in the literature[30]. For the ammine-alkynyl osmium complexes (**13** – **15**), the singlet resonance in the spectra for the four phosphine atoms are slightly downfield of the related chloro-alkynyl complexes, and within the range 19.8 – 19.9 ppm. The ammine-alkynyl complexes also have a characteristic septet spectral signal corresponding to the PF_6^- counter anion, with the central peak at -143.7 ppm and a J_{PF} coupling constant of 714 Hz. The spectrum for the ruthenium ammine complex (**16**) contains a resonance at 54 ppm, a 4 ppm downfield shift from its chloro-alkynyl precursor, as well as the signal due to the PF_6^- anion as mentioned above. For the osmium bis-alkynyl mononuclear complexes (**17** – **21** and **25**), a singlet resonance for the four phosphine atoms is found in the range of 16.5 – 16.7 ppm. A comparison of the above data with the ^{31}P NMR spectral data for similar ruthenium complexes highlights some differences. Spectra for ruthenium chloro-alkynyl complexes with a similar ligand environment to the above osmium complexes (**9** – **12**) have a singlet resonance in the region of 50 ppm,[26] whereas ruthenium bis-alkynyl complexes with similar ligands have a resonance at ca 54 ppm in the phosphorus spectrum.[31] It is interesting to note that while there is a similar downfield shift on moving from both a ruthenium and an osmium chloro-alkynyl complex to an ammine alkynyl-complex, moving from an ammine-alkynyl complex to a bis-alkynyl complex affords very little shift for ruthenium complexes but a ca 3 ppm upfield shift for the osmium complex. This results in very little difference (ca 0.3 ppm) between an osmium chloro-alkynyl and bis-alkynyl complex, whilst the 4 ppm difference for the ruthenium case provides a very valuable tool for distinguishing between the two types of complexes.

For the binuclear complexes (**22** – **24** and **26** – **28**) two resonances are visible in the ^{31}P NMR spectra that can be attributed to the phosphorus atoms attached to ruthenium and osmium. For the complexes with either a C≡CC_6H_4-4-C≡C bridge (**22** - **24**) or the longer C≡CC_6H_4-4-C≡CC_6H_4-4-C≡C bridge (**26** – **28**) no real difference in either the osmium or ruthenium phosphine resonances are observed, with the immediate ligand environment of the metal centre having the greatest influence on chemical shift. For the complexes with the diethynyl C≡CC_6H_4-4-C≡C bridge (**22** – **24**) the phosphorus atoms attached to osmium produce a resonance at 16.5 ppm corresponding to a bis-alkynyl environment. The phosphorus atoms attached to ruthenium in these complexes afford a resonance in the range of 54.2 – 54.3 ppm, corresponding to a ruthenium bis-alkynyl environment. Complexes with the longer triethynyl C≡CC_6H_4-4-C≡CC_6H_4-4-C≡C bridging unit (**26** – **28**) again have a phosphorus NMR resonance corresponding to a bis-alkynyl environment in the range of 16.4 – 16.6 ppm, attributed to the phosphorus atoms attached to the osmium, whereas those attached to ruthenium produce a resonance at 49.9 ppm, which matches previously observed signals for the chloro-alkynyl ruthenium environment.[31]

The trinuclear complex **29** contains a ruthenium bis-alkynyl centre as well as two distinct osmium environments, bis-alkynyl and chloro-alkynyl. The phosphorus atoms in each of these three metal atoms possess distinct chemical shifts; signals at 15.8, 16.5 and 54.3 ppm are assigned to osmium chloro-alkynyl, osmium bis-alkynyl and ruthenium bis-alkynyl environments, respectively.

^{13}C NMR spectroscopy

One area of confusion in the literature is the assignment of the carbon NMR resonances corresponding to the dppe ligands attached to a metal. Although this has primarily concerned the $Ru(dppe)_2$ metal centre, it has been found that the osmium complexes synthesised in this work have very similar ^{13}C resonances to their

ruthenium analogues, with the major difference being the alkynyl carbon adjacent to the osmium centre being shifted between 12 – 22 ppm upfield compared to the ruthenium analogues. In the past, the phenyl carbons of the dppe ligand have either been grouped together, labelled as $C_{43} \equiv C_{47}$, $C_{44} \equiv C_{48}$, $C_{45} \equiv C_{49}$ and $C_{46} \equiv C_{50}$, with a multiplet assigned for $C_{43} \equiv C_{47}$ (numbering shown in Figure 3.2) and doublets with $^2J_{PC}$, $^3J_{PC}$ and $^4J_{PC}$ for each of the other carbons respectively. These carbon resonances have also been reported as having distinct chemical shifts for the related aryl carbon atoms C_{43} C_{47}, C_{44} C_{48}, C_{45} C_{49}, C_{46} C_{50}. In this work, the latter approach has been taken for a number of reasons.

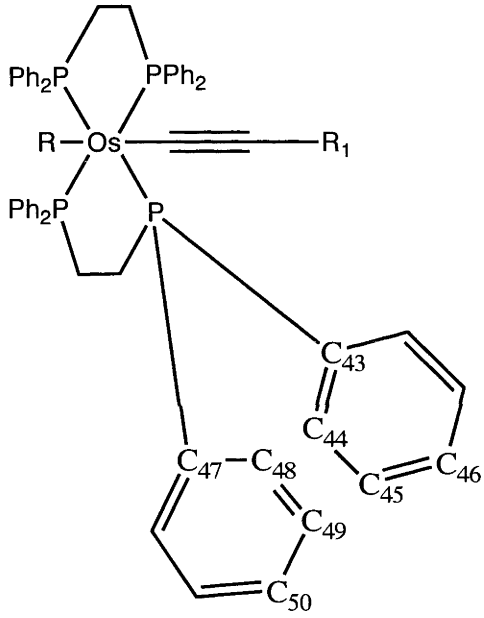

Figure 3.2 Labelling for dppe phenyl carbons where R = Cl, $NH_3\{PF_6\}$ or an alkynyl group, and R_1 is an aromatic group.

One of the most compelling pieces of data supporting this assignment is the large separation of these pairs of carbon atoms upon formation of the ammine complex from the chloro precursor. While the separation of these carbons is between 6 and 23 Hz for the chloro complex (Figure 3.3), upon substitution with an ammine ligand the separation between C_{44} and C_{48} increases to 486 Hz (Figure 3.4).

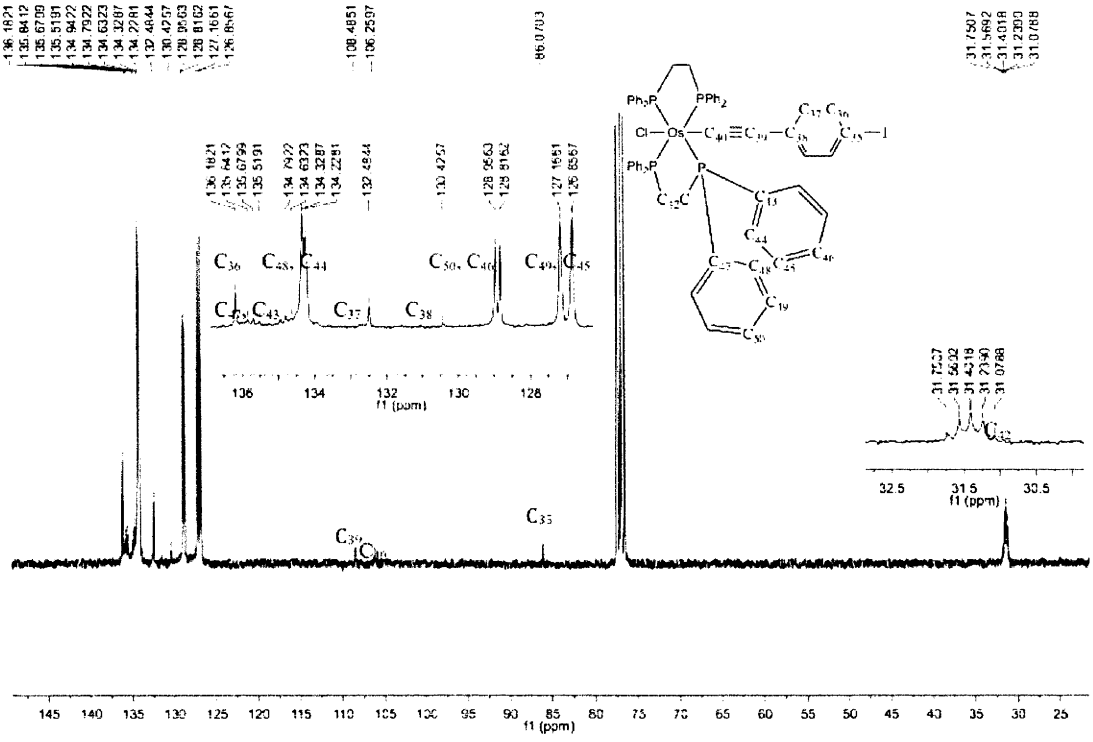

Figure 3.3 Carbon NMR spectrum of **11** with dppe phenyl carbons in inset

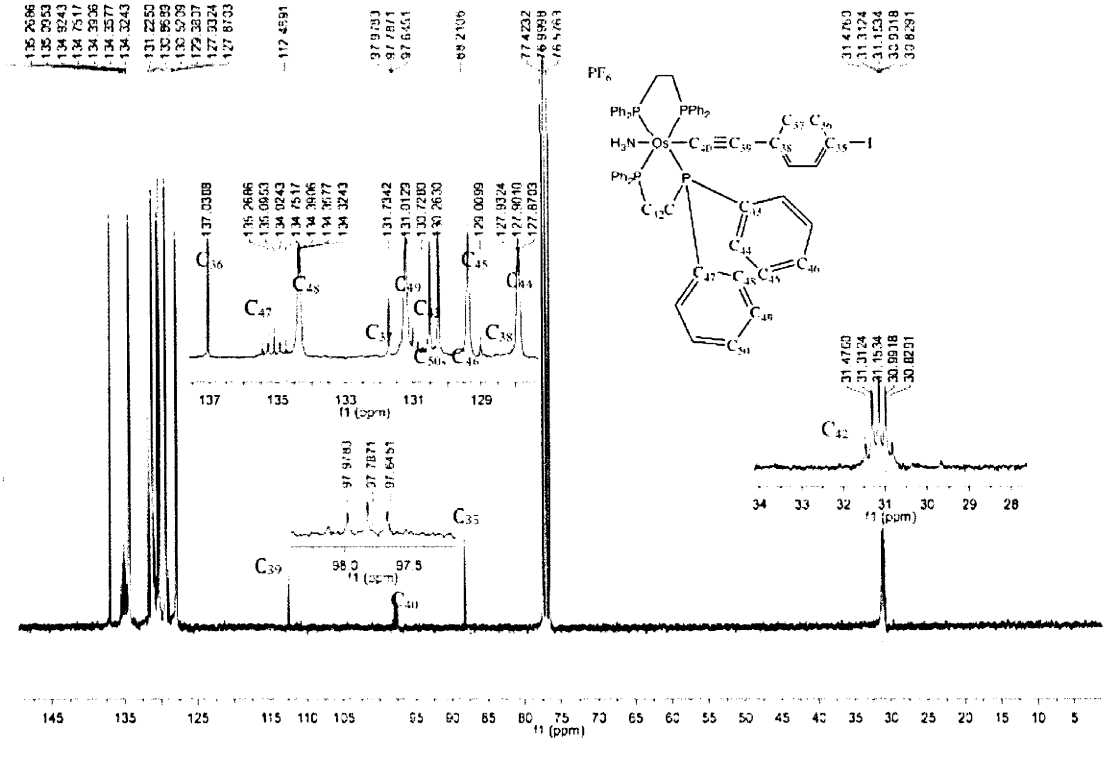

Figure 3.4 Carbon NMR spectrum of **14** with dppe phenyl carbons in inset

If these signals constituted a doublet, the $^{2}J_{PC}$ would be equal to 486 Hz. As this is larger than one would expect for carbon-phosphorus coupling, it is unlikely the observed signals are the result of coupling and are rather two unique signals. Furthermore, on forming the bis-alkynyl complex, the signals corresponding to each pair of carbon atoms coalesce (Figure 3.5). If these signals corresponded to doublets it is unlikely that the coupling would decrease to zero under these circumstances.

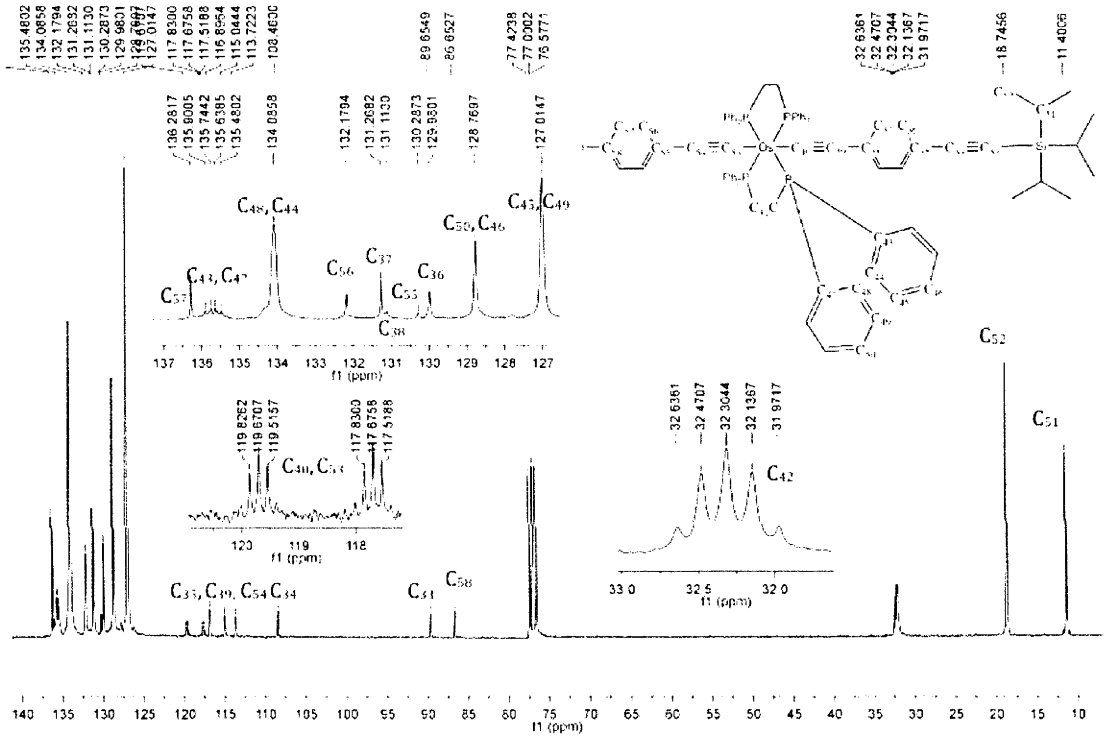

Figure 3.5 Carbon NMR spectrum of **18** with dppe phenyl carbons in inset

Another interesting aspect to the carbon spectra obtained is the coupling of carbons C_{42}, C_{43} and C_{47}. As these carbons are one bond from a phosphorus atom, it might initially be thought that a doublet due to $^{1}J_{PC}$ would be observed. The signal that is observed, however, appears to have five signals similar to that seen for C_{40} where $^{2}J_{PC}$ coupling to all four phosphorus atoms is observed. What is actually being observed in this case is a higher order effect where, rather then coupling just to the

adjacent phosphorus atom, the strong coupling of the phosphorus atoms through the metal to the corresponding *trans*-phosphorus atom causes a virtual triplet-of-triplet to be observed (Figures 3.3, 3.4 and 3.5). For these peaks, the *J*-coupling observed is measured between the two second most intense signals and corresponds to $|{}^{1}J_{PC} + {}^{3}J_{PC}|$.

The formation of both *trans*-[Os(C≡C-4-C_6H_4Br)Cl(dppe)$_2$] **(10)** and *trans*-[Os(C≡C-4-C_6H_4I)Cl(dppe)$_2$] **(11)** allows the effect of increasing the size and electronegativity of the substituent *para* to the ethynyl group on the neighbouring carbon resonances to be explored. If we look at the resonances of C_{35} and C_{36}, i.e. the carbons closest to the halogen, we can see a resonance of 115.5 ppm for C_{35} and 130.3 ppm for C_{36} for **10** (Figure 3.6). On moving to **11,** where the bromine has been replaced by the larger less electronegative iodine, we can see the carbon directly adjacent to the change (C_{35}) is much more shielded and undergoes a large upfield shift to 108.5 ppm, and C_{36} is deshielded and undergoes a downfield shift to 136.2 ppm (Figure 3.3).

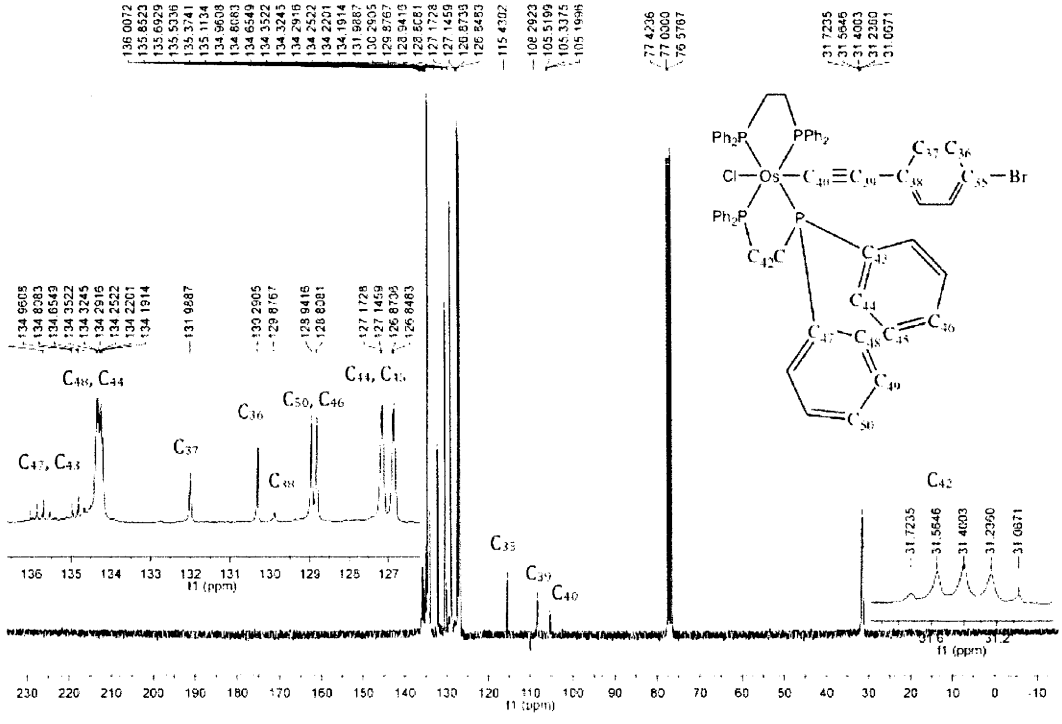

Figure 3.6 Carbon NMR spectrum of **10**

3.2.2.2 UV-Vis absorption spectroscopy

Complexes **10** – **29** were characterised by UV-Vis spectroscopy as CH_2Cl_2 solutions (Table 3.1). For the chloro-alkynyl complexes (**9** – **12**), replacing the hydrogen *para* to the ethynyl group in **9** with a bromo in **10** and an iodo in **11,** results in a red-shift in the λ_{max} by 15 - 25 nm, with λ_{max} = 324 nm for **9**,[30] 340 nm for **10** and 364 nm for **11**. On moving to complex **12** with the diphenylethynyl ligand, two absorption bands are present at 284 nm and 400 nm, matching the data seen for complexes with the longer ethynyl ligands in Chapter 2. As mentioned therein, it is possible to assign these transitions based on studies reported for **9**,[30] with the dominant absorption band assigned to a metal-to-ethynyl ligand charge transfer.

The ammine-alkynyl complexes (**13** – **16**) are all blue-shifted with respect to the corresponding chloro-alkynyl complexes. For the phenylethynyl complex **13** and the iodophenylethynyl complex **14**, a blue-shift of ca 46 nm to 275 nm and 319 nm, respectively, is observed. For the bromodiphenylethynyl complex **15** a blue shift of 38 nm and only one absorption band (362 nm) is observed. For the ruthenium complex **16** a smaller blue shift of 22 nm is observed to 318 nm[6]. It is not possible to assign these transitions without quantum mechanical calculations.

For the mononuclear bisalkynyl complexes (**17** – **21** and **25**), increasing the length of the phenylethynyl ligands results in a red-shift in the lowest energy band, with λ_{max} equal to 336 nm (**17**), 378 nm (**18**), 387 nm (**20**) and 414 nm (**19**). For the mononuclear complexes with a longer triethynyl C≡CC_6H_4-4-C≡CC_6H_4-4-C≡C ligand (**19** and **25**) the absorption spectra is more complex then those with the shorter diethynyl C≡CC_6H_4-4-C≡C groups with multiple bands observed.

The binuclear complexes with a diethynyl C≡CC_6H_4-4-C≡C bridge between the metal centres (**22** - **24**) show a large increase in the extinction coefficient compared to the corresponding mononuclear complexes. For complexes **22** and **24,** a single

absorption band at 387 nm and 391 nm, respectively, is observed. For complex **23,** where the ruthenium terminal peripheral ligand is the longer diethynyl C≡CC_6H_4-4-C≡CC_6H_4-4-I, a slight red-shift to 400 nm is observed. For the binuclear complexes with the longer triethynyl C≡CC_6H_4-4-C≡CC_6H_4-4-C≡C bridging ligand (**26** – **28**), a red-shift of the lowest energy band is observed relative to the complexes with the C≡CC_6H_4-4-C≡C bridge with λ_{max} at 423 nm (**26**), 425 nm (**27**) and 434 nm (**28**) for the dominant absorption band. For the trinuclear complex (**29**), a very broad absorption band with a λ_{max} at 402 nm is observed, as well as an increase in the extinction coefficient compared to the binuclear complexes.

Complex	UV-Vis: λ_{max} (nm) [ε] (10^4 M^{-1} cm^{-1})	IR (cm^{-1})
10	340 [2.1]	2067 ν(C≡C)
11	364 [2.2]	2064 ν(C≡C)
12	400 [3.3], 284 [2.7]	2056 ν(C≡C), 2070 ν(C≡C)
13	301 [1.9], 275 [1.8]	2076 ν(C≡C)
14	319 [2.9]	2076 ν(C≡C)
15	362 [4.5]	2062 ν(C≡C), 2074 ν(C≡C)
16	318 [1.8]	2076 ν(C≡C)
17	336 [2.9]	2060 ν(C≡C)
18	378 [4.6]	2055 ν(C≡C), 2150 ν(C≡CSi)
19	414 [3.7], 322 [3.8], 291 sh [3.1], 274 sh [3.3]	2054 ν(C≡C), 2152 ν(C≡CSi)
20	387 [6.1]	2048 ν(C≡C), 2147 ν(C≡CSi)
21	384 [4.4]	2053 ν(C≡C), 2146 ν(C≡CSi), 3302 ν(≡CH),
22	387 [7.8]	2057 ν(C≡C), 2145 ν(C≡C)
23	400 [11.0], 314 [4.4]	2053 ν(C≡C), 2146 ν(C≡CSi)
24	391 [9.8]	2055 ν(C≡C), 2147 ν(C≡CSi)
25	411 [3.8], 324 [3.6], 276 sh [3.4], 265 sh [3.9]	2053 ν(C≡C), 3296 ν(≡CH)
26	423 [5.7], 308 [2.7]	2056 ν(C≡C)
27	425 [8.0]	2054 ν(C≡C), 2148 ν(C≡CSi)
28	434 [7.9], 304 [4.3]	2053 ν(C≡C), 2153 ν(C≡CSi)
29	402 [11.0]	2054 ν(C≡C), 2145 ν(C≡CSi)

Table 3.1 UV-Vis and infrared absorptions for complexes **10 - 29**

3.2.2.3 Infrared spectroscopy

Infrared absorption spectroscopy was carried out on complexes **10** – **29** as CH_2Cl_2 solutions, with the presence of an absorption corresponding to ν(C≡C) providing confirmation on the formation of a metal-alkynyl complex (Table 3.1). For the chloro-alkynyl complexes (**10** – **12**), broad bands in the region of 2056 – 2070 cm^{-1} corresponding to ν(C≡C) are present. For the osmium ammine-alkynyl complexes (**13** – **15**), bands corresponding to ν(C≡C) are slightly blue-shifted in comparison to their parent chloro-alkynyl complexes, with resonances in the range of 2062 – 2076 cm^{-1}. For the ruthenium ammine-alkynyl complex **16,** a band at 2076 cm^{-1} is present, blue-shifted by 8 cm^{-1} compared to its parent chloro-alkynyl complex.[6] For the bis-alkynyl complexes **17** – **29**, a broad band for the *ν*(C≡C) is observed in the range of 2048 - 2060 cm^{-1}. In addition to these bands complexes possessing a silyl group (**18** – **20**, **22** – **24**, **27** – **29**) also have a band for *ν*(C≡C-Si) in the region of 2045 – 2053 cm^{-1}. For those complexes where the silyl group has been cleaved to afford a terminal acetylene, there is a broad band for *ν*(≡CH) at: 3302 cm^{-1} (**21**) and 3296 cm^{-1} (**25**).

3.2.2.4 Structural determinations

To confirm the identity of many of the osmium mononuclear complexes, single crystals were grown by slow diffusion of CH_2Cl_2 solutions into *n*-hexane, and the complex structures were determined using single crystal X-ray diffraction. The structures of several chloro-alkynyl (**9** - **11**), ammine-alkynyl (**13** - **15**) and bis-alkynyl (**17** and **19**) complexes were determined in this manner. For all of these complexes, the bond lengths and angles fall into the range reported for similar osmium or ruthenium complexes.[16,17,26,32,33]

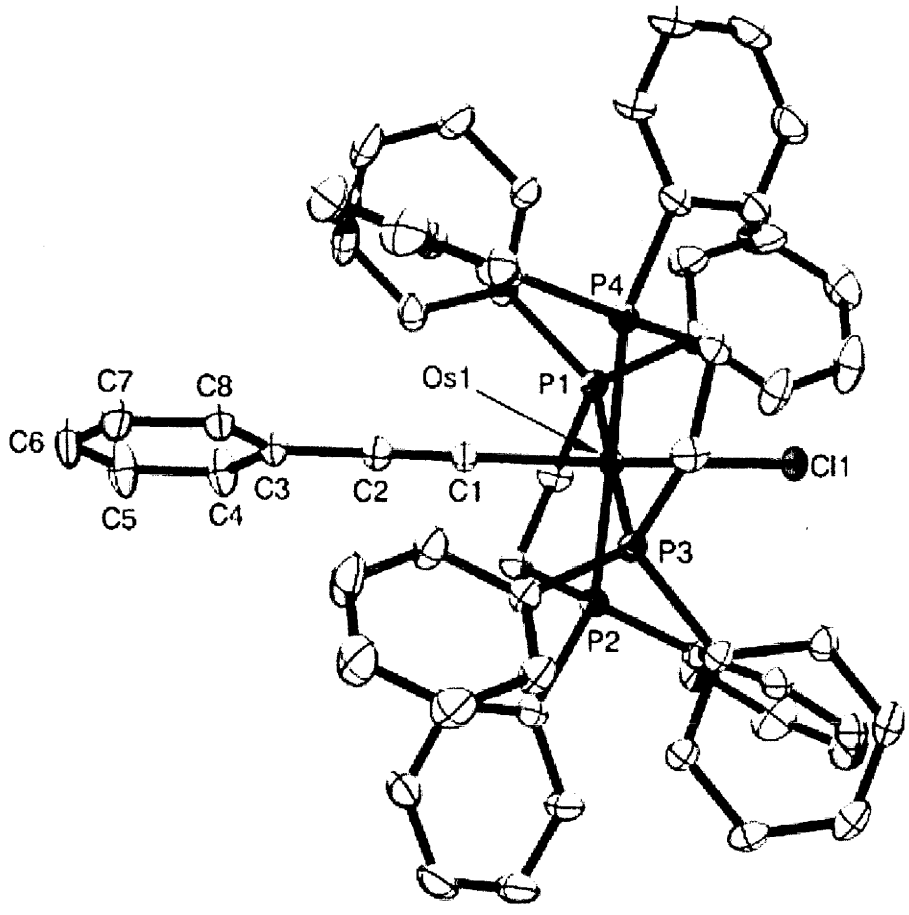

Figure 3.7 Molecular structure and atomic numbering scheme for *trans*-[Os(C≡CPh)Cl(dppe)$_2$] (**9**). Thermal ellipsoids are displayed on a 40 % probability level. Hydrogen atoms are omitted for clarity. Selected bond lengths: Os-P(1) 2.3704(8), Os-P(2) 2.3501(8), Os-P(3) 2.3806(8), Os-P(4) 2.3513(8), Os-Cl 2.5017(7), Os-C(1) 2.006(3), C(1)-C(2) 1.219(5) Å.

Selected bond lengths for Ru analogue: Ru-P(1) 2.3680(14), Ru-P(2) 2.3524(14), Ru-P(3) 2.3917(14), Ru-P(4) 2.3734(14), Ru-Cl 2.4786(13), Ru-C(1) 2.007(5), C(1)-C(2) 1.198(7) Å.[33]

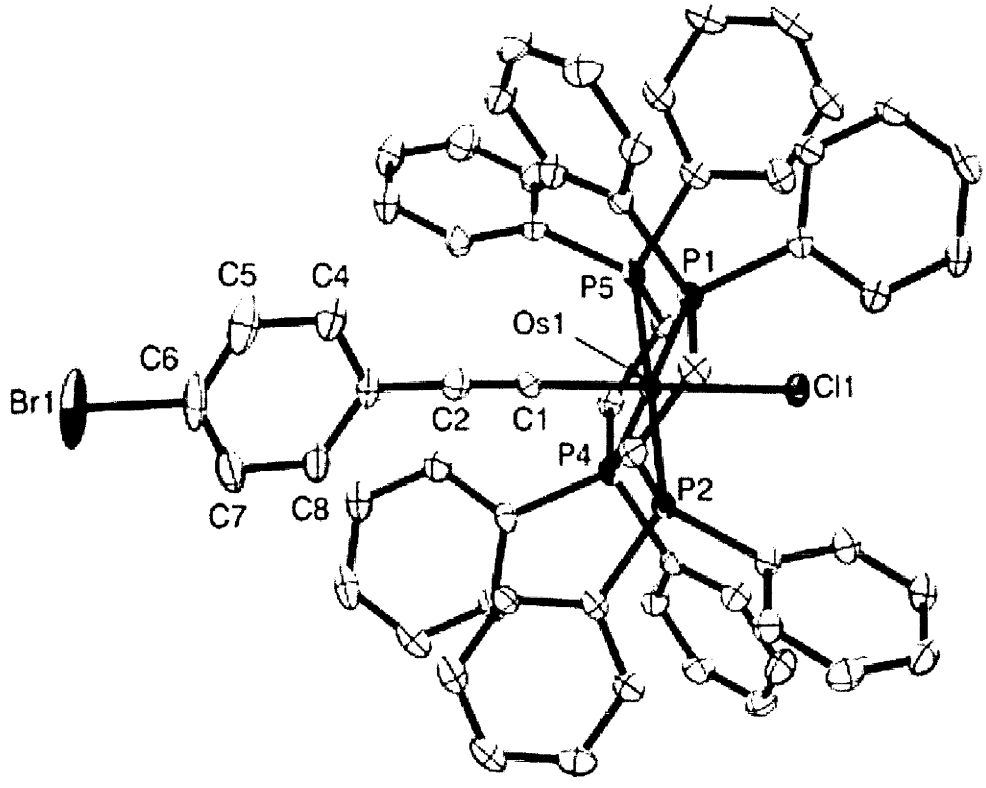

Figure 3.8 Molecular structure and atomic numbering scheme for *trans*-[Os(C≡C-4-C_6H_4Br)Cl(dppe)$_2$] (**10**). Thermal ellipsoids are displayed on a 40 % probability level. Hydrogen atoms are omitted for clarity. Selected bond lengths: Os-P(1) 2.3571(12), Os-P(2) 2.3811(12), Os-P(3) 2.3810(12), Os-P(4) 2.3637(12), Os-Cl 2.5191(11), Os-C(1) 2.018(4), C(1)-C(2) 1.195(6) Å.

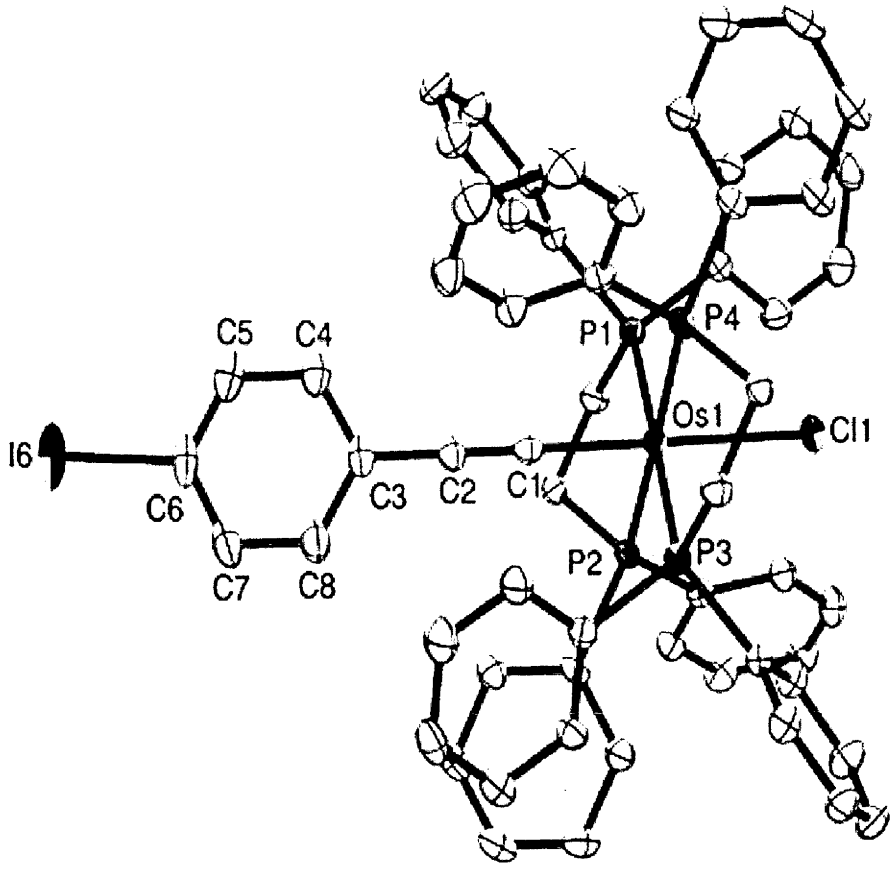

Figure 3.9 Molecular structure and atomic numbering scheme for *trans*-[Os(C≡C-4-C_6H_4I)Cl(dppe)$_2$] (**11**). Thermal ellipsoids are displayed on a 40 % probability level. Hydrogen atoms are omitted for clarity. Selected bond lengths: Os-P(1) 2.3561(8), Os-P(2) 2.3808(8), Os-P(3) 2.3669(8), Os-P(4) 2.3839(8), Os-Cl , Os-C(1) 2.5202(8), C(1)-C(2) 1.215(5) Å.

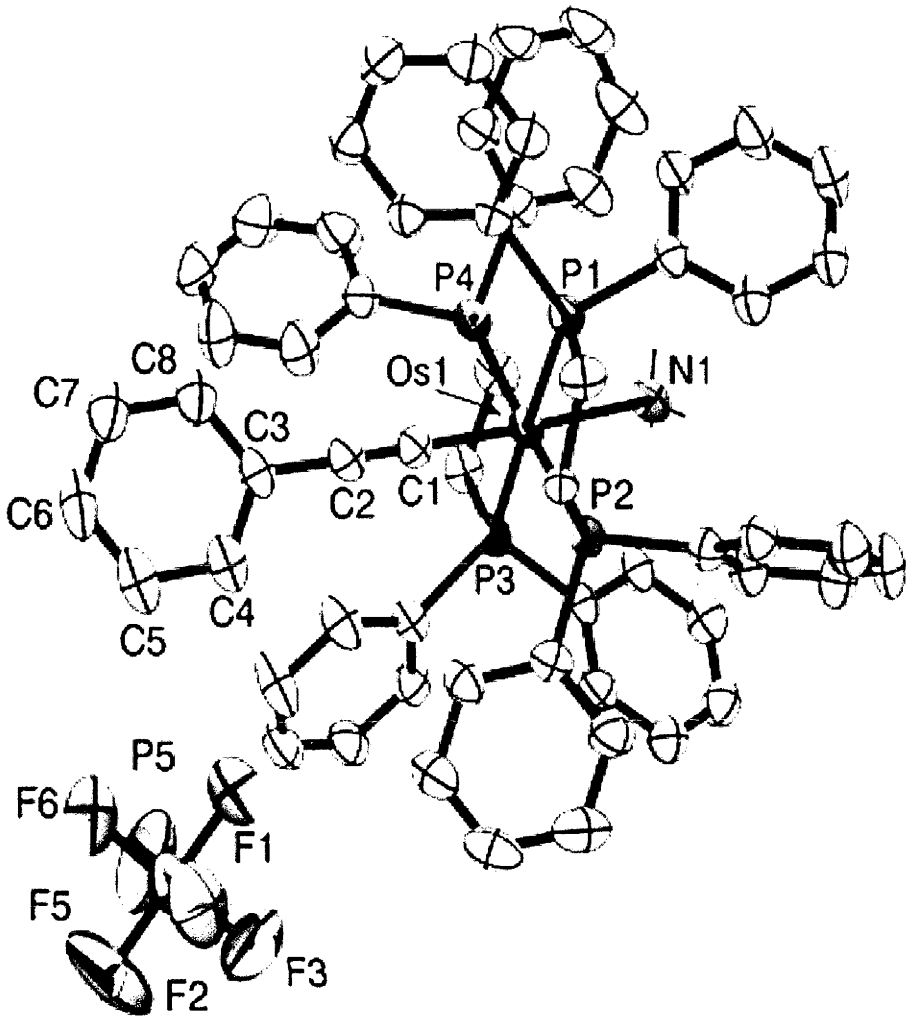

Figure 3.10 Molecular structure and atomic numbering scheme for *trans*-[Os(C≡CPh)(NH_3)(dppe)$_2$]PF_6 (**13**). Thermal ellipsoids are displayed on a 40 % probability level. Hydrogen atoms are omitted for clarity with the exception of the NH_3 ligand. Selected bond lengths: Os-P(1) 2.357(2), Os-P(2) 2.3655(19), Os-P(3) 2.382(2), Os-P(4) 2.394(2), Os-N 2.216(7), Os-C(1) 2.043(7), C(1)-C(2) 1.192(11) Å.

Selected bond lengths of Ru analogue: Ru-P(1) 2.401(1), Ru-P(2) 2.347(1), Ru-P(3) 2.385(1), Ru-P(4) 2.347(1), Ru-N 2.215(5), Ru-C(1) 2.014(5), C(1)-C(2) 1.187(7) Å.[26]

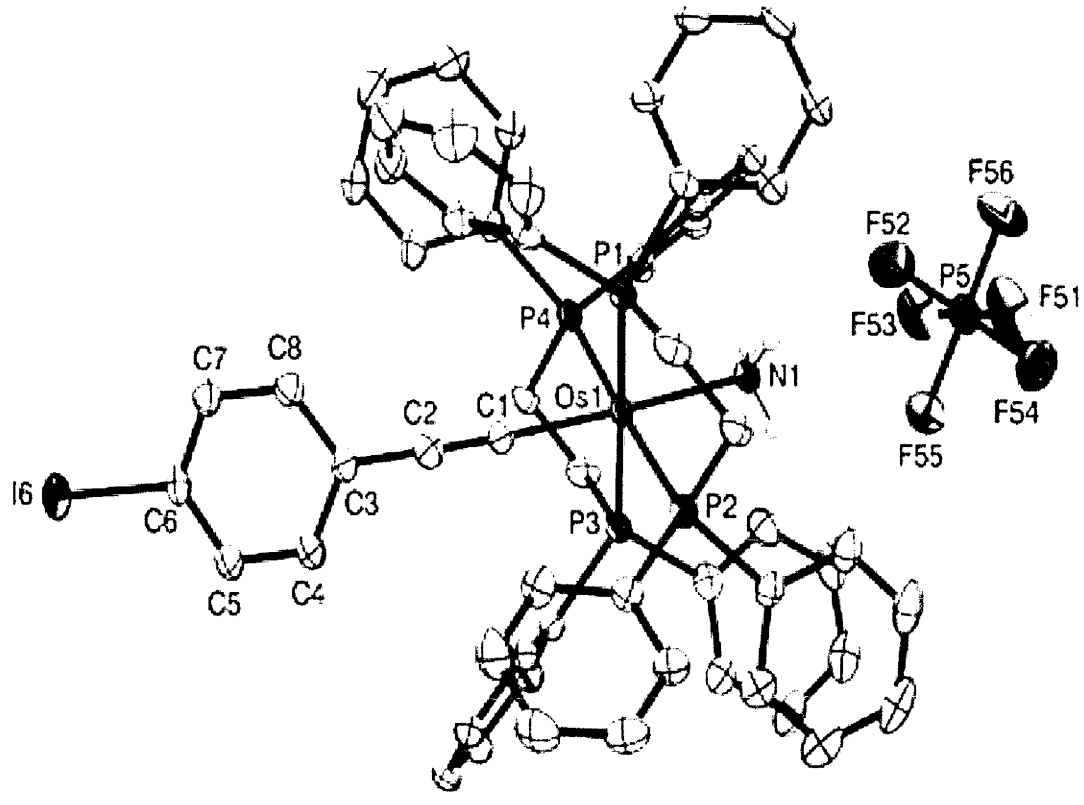

Figure 3.11 Molecular structure and atomic numbering scheme for *trans*-[Os(C≡C-4-C_6H_4I)(NH_3)(dppe)$_2$]PF_6 (**14**). Thermal ellipsoids are displayed on a 40 % probability level. Hydrogen atoms are omitted for clarity with the exception of the NH_3 ligand. Selected bond lengths: Os-P(1) 2.3741(9), Os-P(2) 2.3735(9), Os-P(3) 2.3961(9), Os-P(4) 2.3859(9), Os-N 2.244(3), Os-C(1) 2.042(4), C(1)-C(2) 1.199(5) Å.

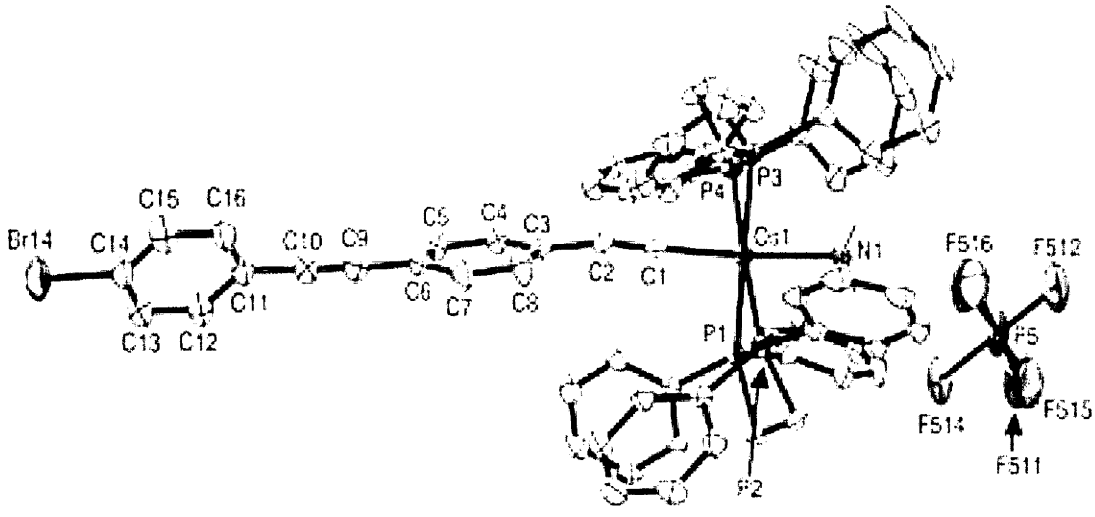

Figure 3.12 Molecular structure and atomic numbering scheme for *trans*-[Os(C≡CC_6H_4-4-C≡CC_6H_4-4-Br)(NH_3)(dppe)$_2$]PF_6 (**15**). Thermal ellipsoids are displayed on a 40 % probability level. Hydrogen atoms are omitted for clarity with the exception of the NH_3 ligand.

Selected bond lengths: Os-P(1) 2.3865(9), Os-P(2) 2.3839(9), Os-P(3) 2.3640(9), Os-P(4) 2.3580(9), Os-N 2.248(3), Os-C(1) 2.019(4), C(1)-C(2) 1.204(5), C(9)-C(10) 1.175(6) Å.

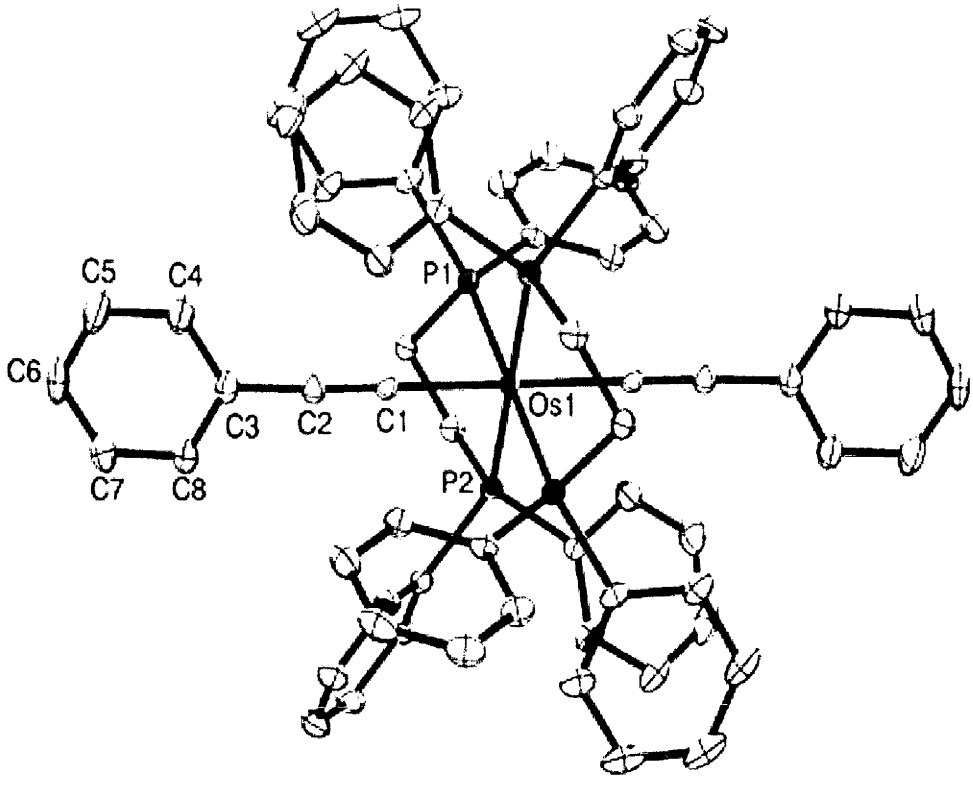

Figure 3.13 Molecular structure and atomic numbering scheme for *trans*-$[Os(C{\equiv}CPh)_2(dppe)_2]$ (**17**). Thermal ellipsoids are displayed on a 40 % probability level. Hydrogen atoms are omitted for clarity. Selected bond lengths: Os-P(1) 2.3598(4), Os-P(2) 2.3535(4), Os-C(1) 2.0721(17), C(1)-C(2) 1.212(2) Å.

Selected bond lengths for Ru analogue: Ru-P(1) 2.363(2), Ru-P(2) 2.356(2), Ru-P(3) 2.360(2), Ru-P(4) 2.362(2), Ru-C(1) 2.061(5), Ru-C(1') 2.061(5), C(1)-C(2) 1.194(7), C(1')-C(2') 1.207(7) Å.[16]

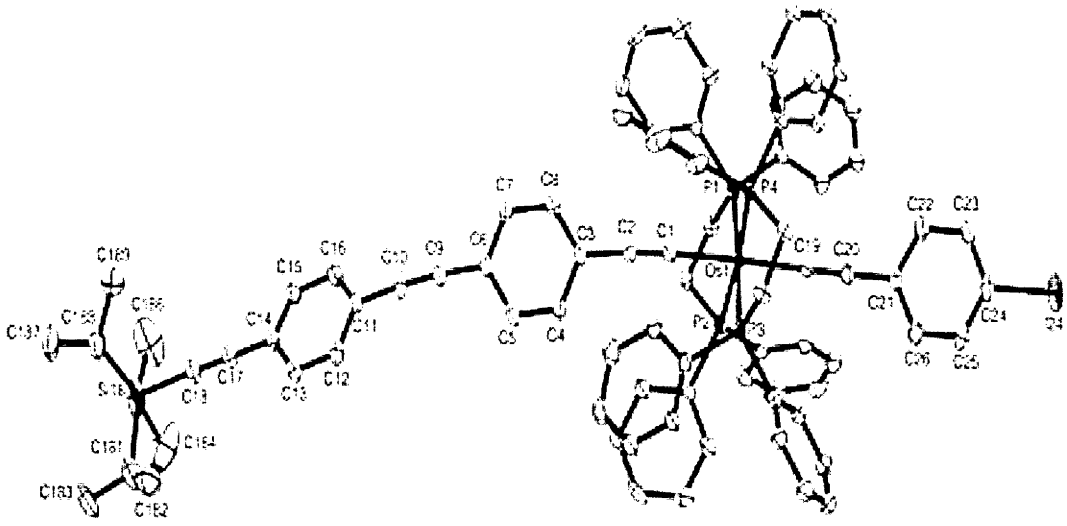

Figure 3.14 Molecular structure and atomic numbering scheme for *trans*-[Os(C≡C-4-C_6H_4I)(C≡CC_6H_4-4-C≡CC_6H_4-4-C≡C$SiPr^i_3$)(dppe)$_2$] (**19**). Thermal ellipsoids are displayed on a 40 % probability level. Hydrogen atoms are omitted for clarity. Selected bond lengths: Os-P(1) 2.3705(14), Os-P(2) 2.3671(14), Os-P(3) 2.3523(14), Os-P(4) 2.3569, Os-C(1) 2.067(5), Os-C(19) 2.061(5), C(1)-C(2) 1.201(8), C(19)-C(20) 1.218(8).

3.2.2.5 Electrochemistry

Cyclic voltammetry was used to determine the redox potentials of the $Os^{II/III}$ couple for mononuclear complexes **10** – **21** and **25**, either as CH_2Cl_2 or as THF solutions using Pt disk working-, Pt wire auxiliary-, and Ag/AgCl reference electrodes. It is not possible to directly compare the potentials of complexes that were obtained in different solvents due to the shift in redox potentials (e.g. *trans*, *trans*-[(dppe)$_2$ClOs(C≡C-4-C_6H_4-4-C≡C)RuCl(dppe)$_2$] (**4**), $Os^{II/III}$ = 0.10 and $Ru^{II/III}$ = 0.44 V (CH_2Cl_2); $Os^{II/III}$ = 0.31 and $Ru^{II/III}$ = 0.59 V (THF)). If we compare the oxidation potentials of the chloro-alkynyl complexes (**10** - **12**), we can see that for **10** and **11**, the potential is ca 0.27 V (CH_2Cl_2) and for **12** 0.45 V (THF), This is probably primarily due to the change of solvent as it has been shown previously that minimal change occurs in the redox potential on chain lengthening

(*trans*-[Os(C≡CPh)Cl(dppe)$_2$] (**9**) $Os^{II/III}$ = 0.26, *trans*-[Os(C≡CC_6H_4-4-C≡CPh)Cl(dppe)$_2$] $Os^{II/III}$ = 0.29)[30]. On forming the cationic ammine complexes, oxidation of the metal centre to give the corresponding dications is significantly more difficult than oxidation of the neutral complexes, as would be expected. The redox potentials for the osmium ammine complexes are ca 0.75 V in CH_2Cl_2 and 0.87 V in THF. The ruthenium ammine complex is significantly more difficult to oxidise than the analogous osmium complex with a redox potential of 0.95 V (CH_2Cl_2). For the mononuclear osmium bis-alkynyl complexes (**17** - **21** and **25**) redox potentials fall within the range of 0.22 – 0.29 V for measurements in CH_2Cl_2 and 0.48 – 0.52 V for measurements in THF (Table 3.2). On going from **17** to **18** there is an increase in the oxidation potential from 0.22 V to 0.29 V. Whilst it is not immediately apparent why this is the case it is interesting to note that for a similar ruthenium example no increase was apparent on increasing the length of the phenylethynyl ligand (*trans*-[Ru(C≡CPh)Cl(dppe)$_2$] $Ru^{II/III}$ = 0.45, *trans*-[Ru(C≡CC_6H_4-4-C≡CPh)Cl(dppe)$_2$] $Ru^{II/III}$ = 0.45).[31] It is interesting to note that for the symmetrical osmium bis-alkynyl complex (**17**) a second irreversible process is observed at 0.61 V. It is not clear why this is the case for this complex while the other osmium bis-alkynyl complexes have only one reversible process. All other $Os^{II/III}$ couples were reversible with an i_{pc}/i_{pa} ratio of 1, and peak separations similar to that observed for the internal ferrocene/ferrocenium standard.

Complex	$E_{1/2}$ [i_{pc}/i_{pa}] [a] (V)	Solvent
trans-[Os(C≡CPh)Cl(dppe)$_2$] (**9**)	0.26 [1][30]	CH_2Cl_2
trans-[Os(C≡C-4-C_6H_4Br)Cl(dppe)$_2$] (**10**)	0.27 [1]	CH_2Cl_2
trans-[Os(C≡C-4-C_6H_4I)Cl(dppe)$_2$] (**11**)	0.27 [1]	CH_2Cl_2
trans-[Os(C≡CC_6H_4-4-C≡CC_6H_4-4-Br)Cl(dppe)$_2$] (**12**)	0.45 [1]	THF
trans-[Os(C≡CPh)(NH_3)(dppe)$_2$]PF_6 (**13**)	0.74 [1]	CH_2Cl_2
trans-[Os(C≡C-4-C_6H_4I)(NH_3)(dppe)$_2$]PF_6 (**14**)	0.77 [1]	CH_2Cl_2
trans-[Os(C≡CC_6H_4-4-C≡CC_6H_4-4-Br)(NH_3)(dppe)$_2$]PF_6 (**15**)	0.87 [1]	THF
trans-[Ru(C≡C-4-C_6H_4I)(NH_3)(dppe)$_2$]PF_6 (**16**)	0.95 [1]	CH_2Cl_2
trans-[Os(C≡CPh)$_2$(dppe)$_2$] (**17**)	0.22 [1] 0.61 [0.8]	CH_2Cl_2
trans-[Os(C≡C-4-C_6H_4I)(C≡CC_6H_4-4-C≡CSiPr^i_3)(dppe)$_2$] (**18**)	0.29 [1]	CH_2Cl_2
trans-[Os(C≡C-4-C_6H_4I)(C≡CC_6H_4-4-C≡CC_6H_4-4-C≡CSiPr^i_3)(dppe)$_2$] (**19**)	0.48 [1]	THF
trans-[Os(C≡C-4-C_6H_4C≡CSiMe_3)(C≡CC_6H_4-4-C≡CSiPr^i_3)(dppe)$_2$] (**20**)	0.51 [1]	THF
trans-[Os(C≡C-4-C_6H_4C≡CH)(C≡CC_6H_4-4-C≡CSiPr^i_3)(dppe)$_2$] (**21**)	0.52 [1]	THF
trans-[Os(C≡C-4-C_6H_4I)(C≡CC_6H_4-4-C≡CC_6H_4-4-C≡CH)(dppe)$_2$] (**25**)	0.48 [1]	THF

Table 3.2 Cyclic voltammetric data for complexes **9** – **21** and **25**. Pt disk working-, Pt wire auxiliary-, and Ag/AgCl reference electrodes, ferrocene/ferrocenium couple at 0.46 V [1] (CH_2Cl_2) and 0.56 V [1] THF.

Cyclic voltammetry measurements were carried out on the binuclear complexes **22** – **24** and **26** – **28**, and the trinuclear complex **29**, as THF solutions using Pt disk

working-, Pt wire auxiliary-, and Ag/AgCl reference electrodes (Table 3.3). As shown in the previous Chapter, moving from complexes with the shorter diethynyl C≡CC$_6$H$_4$-4-C≡C bridge (**22** - **24**) to those with the longer triethynyl C≡CC$_6$H$_4$-4-C≡CC$_6$H$_4$-4-C≡C bridge (**26** - **28**) results in an increase in oxidation potentials for both the osmium and ruthenium metal centres, and a decrease in the separation of the two oxidation processes. Apart from these differences between the two bridging units, functionalising the peripheral acetylide ligands by chain lengthening has little effect on the overall redox properties. The complexes with the shorter bridge possess an osmium redox couple that falls within the narrow range of 0.28 – 0.32 V, a ruthenium redox couple within the range of 0.56 – 0.60 V, and a separation between the two processes that ranges from 0.26 – 0.28 V. For the complexes possessing a longer bridge, osmium redox potentials fall within the range of 0.45 – 0.47 V. The ruthenium potentials range from 0.63 – 0.64 V, and the separation between the two redox processes ranges from 0.17 – 0.18 V.

The trinuclear complex **29**, incorporating two osmium and one ruthenium metal centre had been designed to possess three individually addressable redox properties. By having the osmium separated from the ruthenium metal centre by both the short C≡CC$_6$H$_4$-4-C≡C phenylethynyl bridge and a longer C≡CC$_6$H$_4$-4-C≡CC$_6$H$_4$-4-C≡C bridge, it had been hoped that the better coupling with the shorter bridge would reduce the corresponding osmium redox potential more than for the osmium attached through the longer bridging unit. This was found to be the case with three separate redox processes observed for the trinuclear complex. The first process is located at 0.31 V and can be attributed to the osmium atom separated from the ruthenium metal centre by a diethynyl C≡CC$_6$H$_4$-4-C≡C bridge. This potential falls within the range observed for the above examples with this type of bridge. The second process is found at 0.42 V and is assigned to the osmium atom separated from the ruthenium metal centre by the longer bridge. This is slightly lower than the range given from the above examples but is about the same as the potential for **7** (0.41 V) (Chapter 2) where the peripheral ligand was also a chloro ligand. The third process assigned to

ruthenium is found at 0.58 V, and falls in-between the potentials given above for the smaller and larger bridging groups (Table 3.3).

Complex	$E_{1/2}$ (V) $[i_{pc}/i_{pa}]^a$ $Os^{II/III}$	$E_{1/2}$ (V) $[i_{pc}/i_{pa}]^a$ $Ru^{II/III}$	$E_{1/2}$ $Ru^{II/III}$ - $E_{1/2}$ $Os^{II/III}$ (V)
22	0.30 [1]	0.56 [1]	0.26
23	0.28 [1]	0.56 [1]	0.28
24	0.32 [1]	0.60 [1]	0.28
26	0.46 [1]	0.63 [1]	0.17
27	0.45 [1]	0.63 [1]	0.18
28	0.47 [1]	0.64 [1]	0.17
29	0.31 [1], 0.42 [1]	0.58 [1]	0.27, 0.16

Table 3.3 Cyclic voltammetric data for complexes **22** - **24** and **26** - **29**. [a] THF solvent, Pt disk working-, Pt wire auxiliary-, and Ag/AgCl reference electrodes, ferrocene/ferrocenium couple at 0.56 V [1].

3.2.2.6 Spectroelectrochemistry

Spectroelectrochemical studies were carried out on representative examples of mononuclear, binuclear and trinuclear complexes. Complex **13** was investigated as a representative example of an ammine alkynyl complex. Upon oxidation of **13,** a decrease in the intensity of the absorption band centred at 32930 cm^{-1} was observed, accompanied by an increase in the band centred around 40000 cm^{-1} and the appearance of two broad absorption bands at lower energy, centred at 14775 cm^{-1} and 25222 cm^{-1} (Figure 3.15).

Complexes **17** and **20** were measured as representative examples of bis-alkynyl complexes (Figures 3.16 and 3.17). Oxidation of both complexes results in a decrease in the intensity of the main absorption band for the neutral species, located

at 29900 cm^{-1} for **17** and 25800 cm^{-1} **20**. For similar ruthenium bis-alkynyl complexes this band has been assigned to metal-to-ethynyl charge-transfer processes[31]. In addition, oxidation of each complex affords a low energy band centred at 10400 cm^{-1} for **17** and 9800 cm^{-1} for **20**. Assuming the same transitions as for the analogous ruthenium complexes, this band can be assigned to a ethynyl-to-metal charge-transfer. The energy of these transitions is ca. 1000 cm^{-1} higher in energy for the osmium complexes than for the analogous ruthenium complex. A feature of the low energy absorption band for both Os^{III} and Ru^{III} species is the associated fine structure, suggesting vibrational interactions related to the ethynyl bond stretch[31,34]. All three of these complexes showed reversible processes at room temperature, indicated by clean isobestic points on oxidation and recovery of the starting spectrum on application of a reducing potential (Figures 3.15 – 3.17).

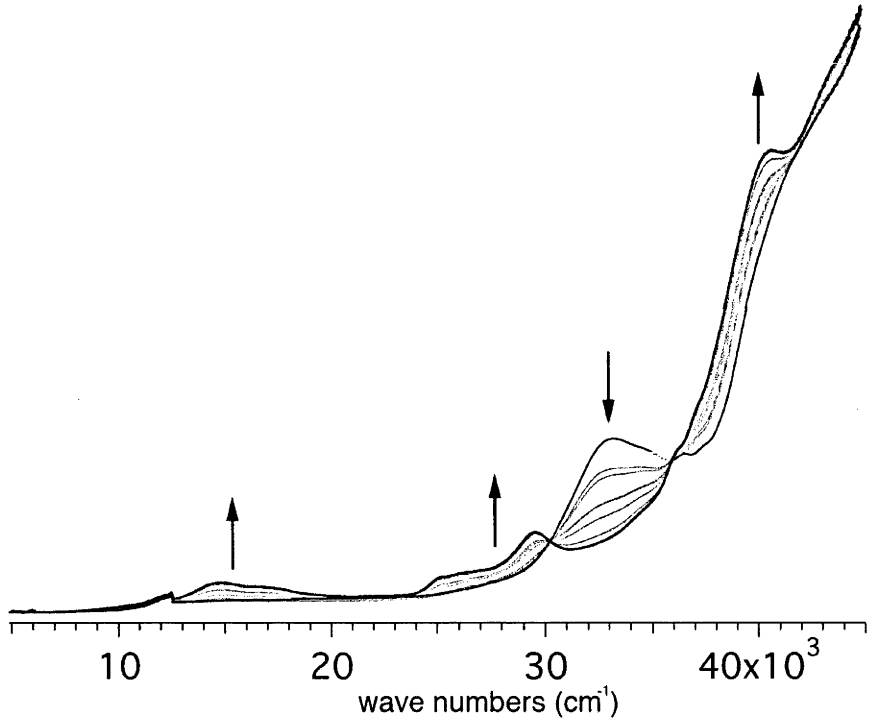

Figure 3.15 UV-Vis-NIR spectral changes during electrochemical oxidation of *trans*-$[Os(C{\equiv}CPh)(NH_3)(dppe)_2]PF_6$ (**13**).

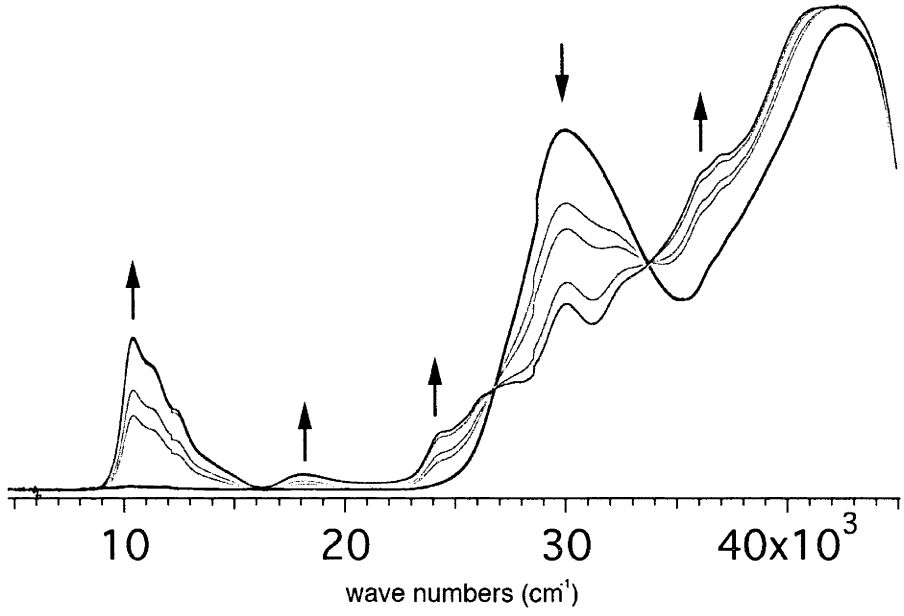

Figure 3.16 UV-Vis-NIR spectral changes during the first electrochemical oxidation step of *trans*-[Os(C≡CPh)$_2$(dppe)$_2$] (**17**).

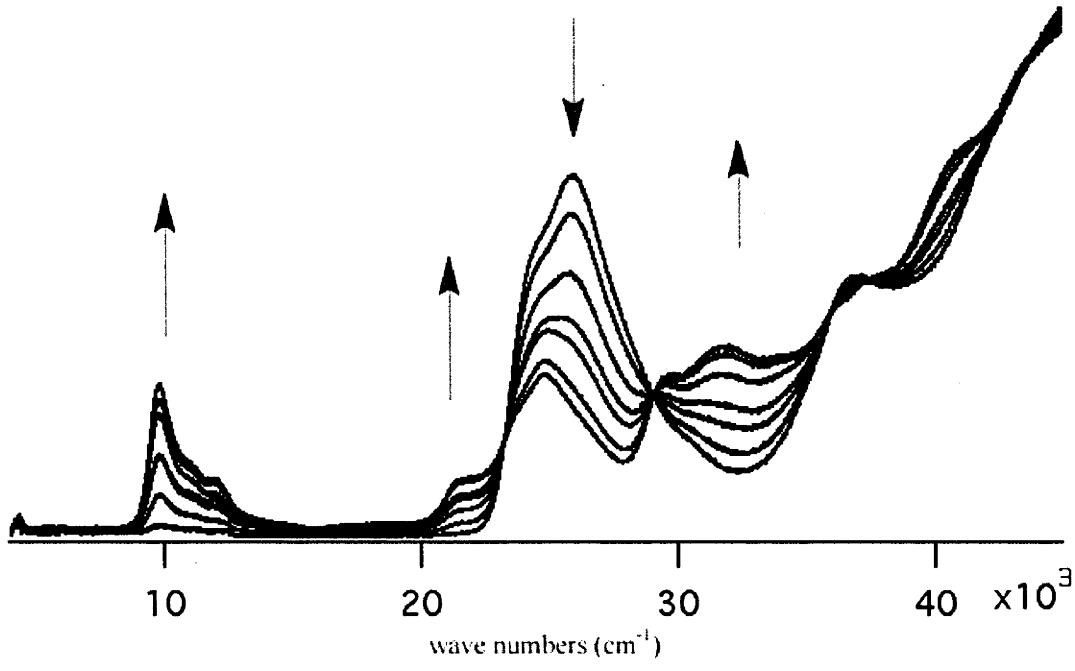

Figure 3.17 UV-Vis-NIR spectral changes during the oxidation of *trans*-[Os(C≡C-4-C$_6$H$_4$-4-C≡CSiMe$_3$)(C≡CC$_6$H$_4$-4-C≡CSiPr$^i_3$)(dppe)$_2$] (**20**)

Complex	ν_{max} (cm^{-1}) [e] ($10^4 M^{-1} cm^{-1}$)[a]
13	32930 [2.4]
$\mathbf{13}^{2+}$	14775 [0.4] 16490 br, sh [0.4] 25222 [0.5] 26680 sh [0.6] 29545 [1.2]
17	29910 [2.8] 42590 [3.8]
$\mathbf{17}^{+}$	10435 [1.2] 11330 sh [1.0] 12385 sh [0.7] 18070 [0.2] 24420 [0.5] 26370 [0.8] 30100 [1.5] 41220 [3.8]
20	25840 [6.1]
$\mathbf{20}^{+}$	9817 [2.3], 10903 sh [0.8], 11775 sh [0.5], 21920 [0.6], 24855 [2.5], 29765 [2.4], 31891 [2.9], 37260 [4.2], 41444 [6.7]

Table 3.3 Summary of optical data for mononuclear complexes **13**, **17**, **20**.
[a] Electronic spectra were obtained at 298 K in CH_2Cl_2 using 0.3 M $(Bu^n_4N)PF_6$ as supporting electrolyte and with potentials ca 200 mV beyond $E_{1/2}$ for each couple.

Spectroelectrochemical studies were carried out on complex **24** (Figure 3.18) as a representative example of the complexes that possess a diethynyl C≡CC_6H_4-4-C≡C bridge between metal centres, where the external ligands attached to both the osmium and ruthenium sites are ethynyl groups. This complex is very similar to *trans*-,*trans*-[$(dppe)_2ClOs(C{\equiv}C\text{-}4\text{-}C_6H_4\text{-}4\text{-}C{\equiv}C)Ru(dppe)_2(C{\equiv}CC_6H_4\text{-}4\text{-}C{\equiv}CSiPr^i_3)$] (**4**, Chapter 2) with the chloro ligand attached to the osmium metal centre in **4** being replaced by a C≡CC_6H_4-4-C≡$CSiPr^i_3$ unit in complex **24**. Oxidation of **24** at 0.4 V affords the cationic Os^{III}/Ru^{II} complex and a steady decrease in the intensity of the main absorption band centred at 25600 cm^{-1}, with concomitant appearance of intense low energy absorption bands centred at 6420 cm^{-1} and 20165 cm^{-1}. As mentioned earlier for **4** although a broad, low-energy IVCT band is expected for these complexes in view of the electrochemical evidence for some electronic communication between the metal centres, it is unlikely to be the band centred at

6420 cm^{-1}. Rather, the alternate assignment offered by Klein and co-workers for the similar ruthenium homo-bimetallic complex is more likely to apply for the hetero-bimetallic **24**. They assign the band at 6420 cm^{-1} to a former HOMO-1 to newly formed SOMO transition, and the band at 20165 cm^{-1} to a SOMO-to-LUMO transition[34]. Further oxidation to the Os^{III}/Ru^{III} dicationic species at 0.7 V results in a blue-shift to 9575 cm^{-1}, and increases in intensity of the lowest energy band, adding further support to it not being an IVCT band. The close similarities between the spectroelectrochemical behaviour of **4** and **24** indicates that the behaviour is dominated by the metal and bridge composition, with the peripheral ligands having less effect. The clean isobestic points for each of the processes described above and ability to recover the starting spectrum on applying a reducing voltage illustrate the reversibility of the processes.

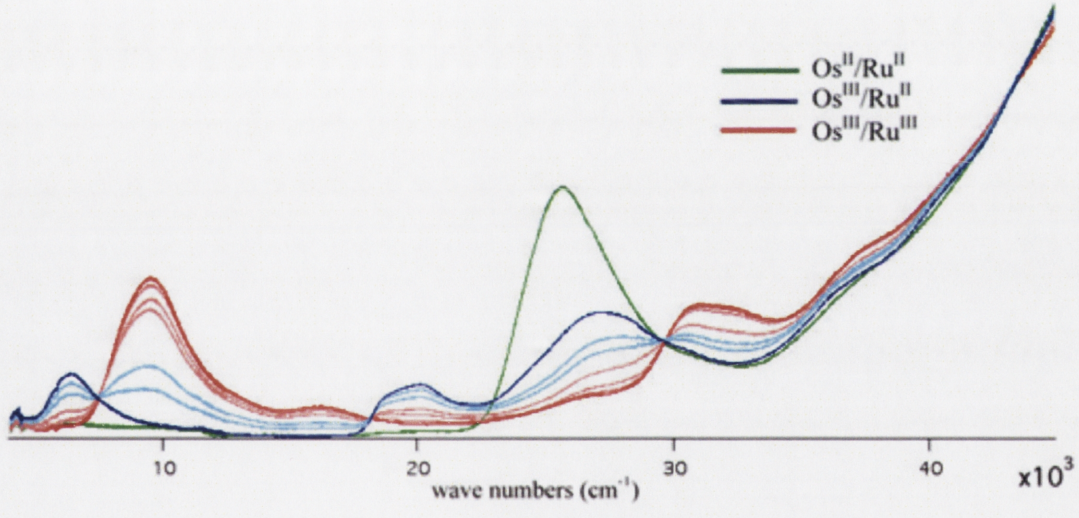

Figure 3.18 UV-Vis-NIR spectral changes during electrochemical oxidation of *trans*-,*trans*-[($Pr^i_3SiC{\equiv}CC_6H_4$-4-C≡C)(dppe)$_2$Os(C≡CC_6H_4-4-C≡C)Ru(dppe)$_2$(C≡CC_6H_4-4-C≡$CSiMe_3$)] (**24**)

Complexes **26**, **27** and **28** show similar electrochemical behaviour, so the spectroelectrochemical behaviour of **28** was investigated as a representative example to determine the effect of replacing the chloro ligand in complex *trans*-,*trans*-

[(dppe)$_2$ClOs(C≡CC$_6$H$_4$-4-C≡CC$_6$H$_4$-4-C≡C)RuCl(dppe)$_2$] (**7** Chapter 2) with an extended phenylethynyl ligand (Figure 3.19). Oxidation of **28** at 0.57 V affords the cationic Os^{III}/Ru^{II} complex and results in a decrease in intensity of the main absorption band for the neutral species centred at 23041 cm^{-1}, and the subsequent appearance of a very broad absorption band with a maximum at 9612 cm^{-1}. A second low energy absorption band at 19958 cm^{-1} also appears for the Os^{III}/Ru^{II} species. Oxidation to the Os^{III}/Ru^{III} species on applying 0.8 V results in the disappearance of the band at 9612 cm^{-1} and appearance of a less broad absorption band with a maximum at 9436 cm^{-1}. The absorption bands are similar to those seen for complex **7**, however, for the Os^{III}/Ru^{II} species **7**, the low energy bands are more distinct rather than one broad band, and for the Os^{III}/Ru^{III} species, the low energy band is more intense for **7** than for **28**. Although it can be speculated that the transitions assigned to these bands are the same as for the short-bridge complex **24**, quantum mechanical calculations are required to confirm this assignment.

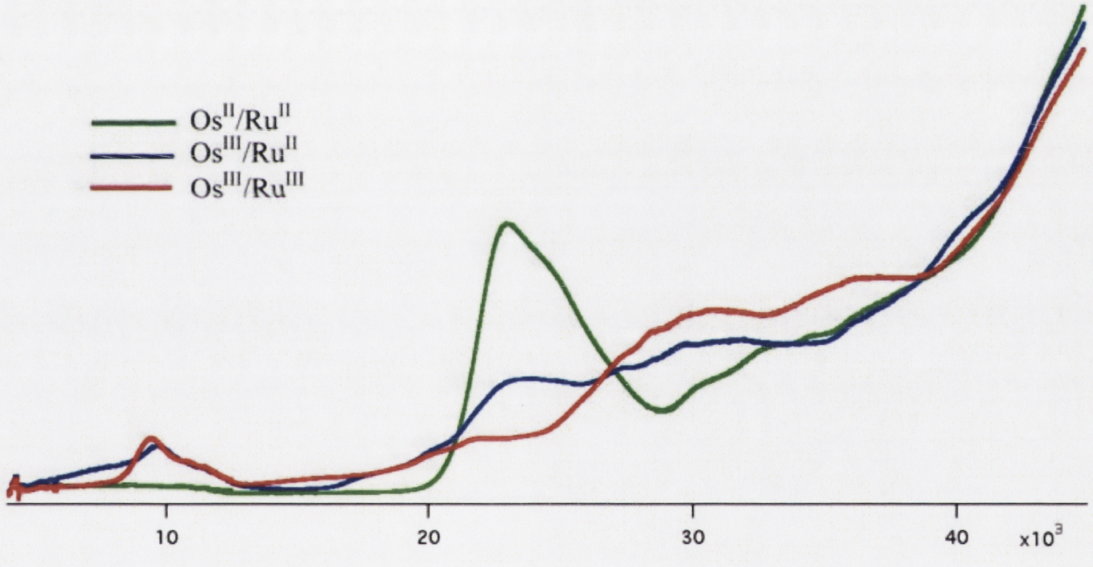

Figure 3.19 UV-Vis-NIR spectral changes during electrochemical oxidation of *trans*-,*trans*-[(dppe)$_2$(Pr$^i_3$SiC≡CC$_6$H$_4$-4-C≡CC$_6$H$_4$-4-C≡C)Os(C≡CC$_6$H$_4$-4-C≡CC$_6$H$_4$-4-C≡C)Ru(Cl)(dppe)$_2$] (**28**)

It was hoped that the trinuclear complex **29**, possessing three distinct redox potentials, would have distinctive optical absorption spectra for each of the resultant complexes. However, when the spectroelectrochemical study of **29** was carried out in THF it was found that only two distinct absorption traces were obtained (Figure 3.20). The first trace was obtained on applying 0.4 V and resembles the absorption spectra obtained for the Os^{III}/Ru^{II} species of **24**, with low energy bands with at 6360 and 18685 cm^{-1} (compared with 6420 and 20165 cm^{-1} for **24**). On increasing the applied voltage to 0.55 V, the formation of a species with a low energy band blue-shifted to 9555 cm^{-1} and disappearance of the band at 18685 cm^{-1} is observed. These spectral characteristics are similar to those observed for the Os^{III}/Ru^{III} species of **24**, which has a lowest energy band at 9575 cm^{-1}. On increasing the voltage to 0.75 V, no further spectral changes are observed. On applying a reducing voltage (-0.5 V) the neutral species is recovered with some loss of peak height due to decomposition. It is difficult to assign the two spectra obtained, since there are three redox processes contributing to the observed spectral changes, but due to similarities to the spectral progressions of **24**, the two processes can be tentatively assigned to $Os^{III}/Ru^{II}/Os^{II}$ + $Os^{III}/Ru^{II}/Os^{III}$ and $Os^{III}/Ru^{III}/Os^{III}$.

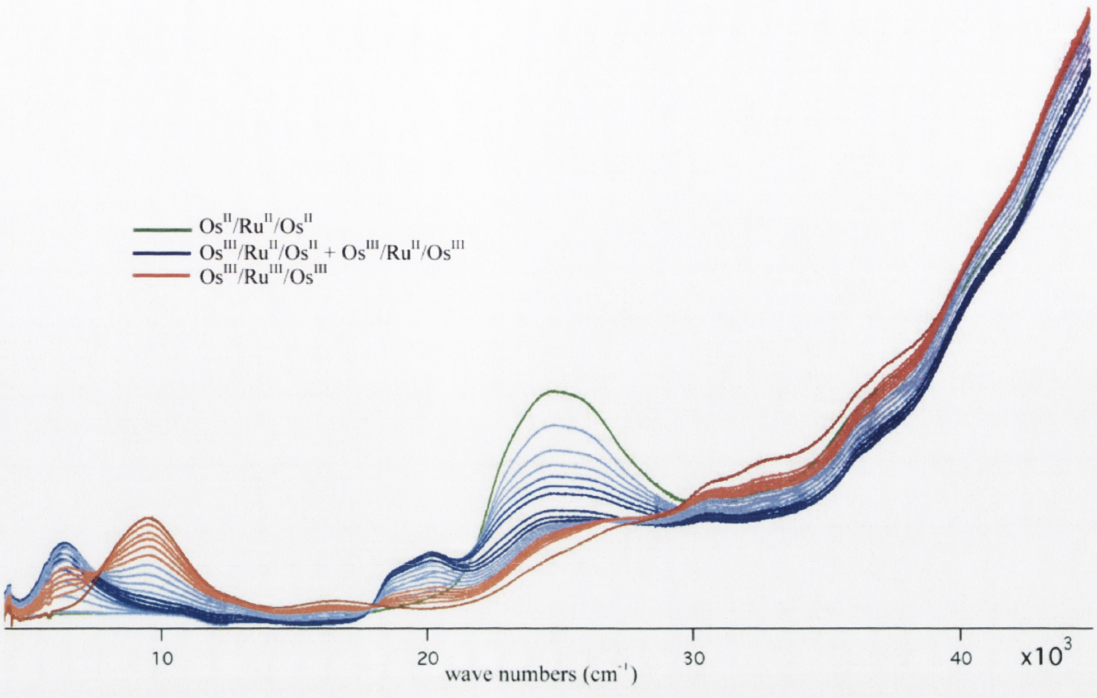

Figure 3.20 UV-Vis-NIR spectral changes during electrochemical oxidation of *trans*-,*trans*-,*trans*-[(Pr^i_3SiC≡CC_6H_4-4-C≡C)(dppe)$_2$Os(C≡CC_6H_4-4-C≡C)Ru(dppe)$_2$(C≡CC_6H_4-4-C≡CC_6H_4-4-C≡C)Os(dppe)$_2$Cl] (**29**)

Complex	ν_{max} (cm^{-1}) [ε] (10^4 M^{-1} cm^{-1}) [a]
24	25575 [9.8]
$\mathbf{24}^{+}$	6420 [2.4], 20165 [1.9], 26465 [6.0]
$\mathbf{24}^{2+}$	9575 [6.3], 16293 [1.4], 26649 [1.8], 31035 [5.3]
28	23041 [7.9], 32895 [4.3]
$\mathbf{28}^{+}$	9612 [0.8], 19958 [0.5], 23290 [2.5], 30620 [4.2], 40370 [7.9]
$\mathbf{28}^{2+}$	9436 [0.9], 21536 [0.8], 29989 [5.0], 36162 [6.1]
29	24622 [11.3]
$\mathbf{29}^{2+}$	6360 [3.2], 18685 [2.0], 20282 [2.9], 24691 [5.2]
$\mathbf{29}^{3+}$	9555 [4.8], 16533 [0.4], 30770 [6.6]

Table 3.4 Summary of optical data for complexes **24**, **29** and **30**. [a] Electronic spectra were obtained at 298 K in THF using 0.3 M $(NBu^n_4)PF_6$ as supporting electrolyte with potentials ca 50-200 mV beyond $E_{1/2}$ for each couple.

3.2.2.7 Quantum mechanical calculations

DFT calculations at the SOAP/TZP//PBE/TZP level of theory were carried out on **17** and $\mathbf{17}^{+}$ in order to assign the UV-Vis absorption bands for the osmium bis-alkynyl complexes. Orbital diagrams are shown in Figure 3.21 and results tabulated and compared to experimental data in Table 3.5.

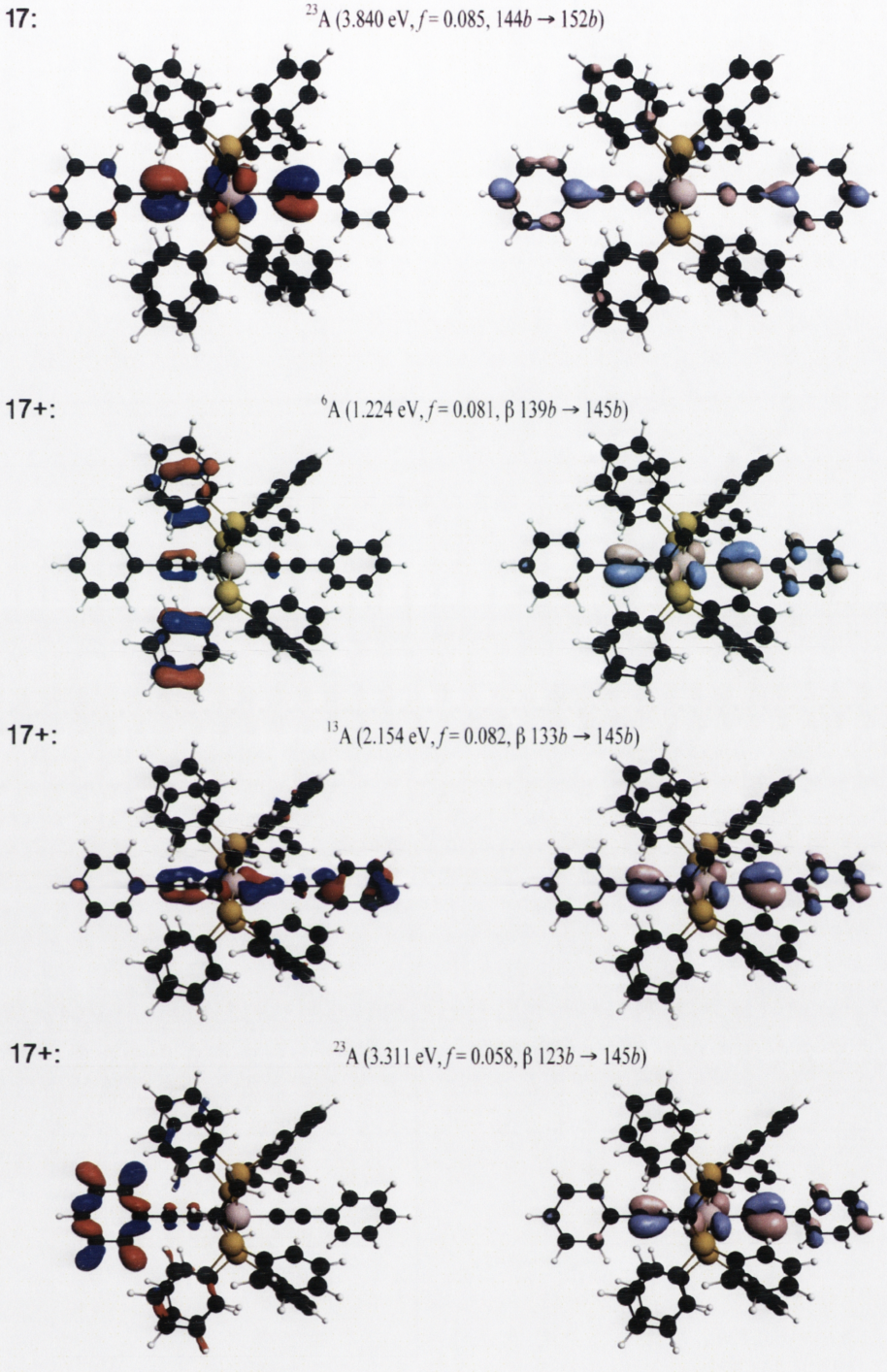

Figure 3.21 Orbital diagrams showing transitions for **17** and **17**$^{+}$

For the neutral complex **17**, the calculations show transparency below 25000 cm^{-1} and are in good agreement with the observed experimental data. The experimentally observed absorption band at 29900 cm^{-1} matches well with the calculated bands at 27111 and 30975 cm^{-1} arising from Os d_{xz} + C_2Ph $\pi \rightarrow C_2Ph$ π^* and Os d_{yz} + C_2 $\pi \rightarrow$ Ph π^* transitions (Figure 3.21 and Table 3.5). For the oxidised complex $\mathbf{17}^+$, absorption bands below 25000 cm^{-1} are observed experimentally at 10400, 18000 and 24400 cm^{-1}. These match well with the calculated bands at 9872, 17361 and 26738 cm^{-1} (Figure 3.21) and can be assigned to C_2 $\pi \rightarrow$ Os d_{xz} + C_2 π^*, Os d_{xz} + C_2 $\pi \rightarrow$ Os d_{xz} + C_2 π^* and dppe $\rightarrow$ Os d_{xz} + C_2 π^*, respectively.

Complex	Expt ν_{max} (cm^{-1}) [ε] (10^4 M^{-1} cm^{-1})	Calcd ν_{max} (cm^{-1}) [*f*]
17	29900 [2.8]	27111 [0.084] 30795 [0.085]
$\mathbf{17}^+$	10400 [1.2] 18000 [0.2]	9872 [0.081] 17361[0.082]
	24400 [0.5]	26738 [0.059]

Table 3.5 Experimental and calculated absorption bands for **17** and $\mathbf{17}^+$

3.2.2.8 Nonlinear optics

The third-order nonlinear optical properties of **24** and **29** were measured using the Z-scan technique. The results of this investigation and associated discussion can be found in Chapter 4

3.3 Conclusions

A new route into osmium bis-alkynyl complexes has been developed proceeding via an ammine adduct. This route has been shown to be high yielding and facile with a variety of ammine-alkynyl and bis-alkynyl complexes isolated. From these bis-alkynyl complexes, bimetallic derivatives incorporating ruthenium have been formed and shown to be more stable in solution than the analogous complexes with an osmium chloro-alkynyl metal centre. Electrochemically, all of these complexes have

reversible oxidation processes with the oxidised species giving rise to new, low-energy absorption bands that may be useful for on-resonant nonlinear optical switching.

3.4 Experimental Section

3.4.1 General

All reactions were performed under a nitrogen atmosphere using standard Schlenk techniques, with no precautions to exclude air during workup. CH_2Cl_2 was dried by distilling over calcium hydride, THF was distilled over sodium/benzophenone, methanol was dried according to the method of Pangborn and co-workers,[35] and all other solvents were used as received. The term ''petrol'' refers to a fraction of petroleum ether of boiling range 60-80 °C. Column chromatography was performed using Sigma-Aldrich aluminium oxide (activated, basic, Brockmann 1, standard grade ca 150 mesh, 58 Å). Solvents and reagents were obtained from commercial sources and used as received, unless otherwise indicated. The following were prepared according to the literature: $HC{\equiv}CC_6H_4$-4-$C{\equiv}CSiPr^i_3$[36], $HC{\equiv}CC_6H_4$-4-$C{\equiv}CC_6H_4$-4-$C{\equiv}CSiPr^i_3$[37], *cis*-$[OsCl_2(DMSO)_4]$[38], *cis*-$[RuCl_2(dppe)_2]$[2], $HC{\equiv}CC_6H_4$-4-Br[39], $HC{\equiv}CC_6H_4$-4-I[37], $HC{\equiv}CC_6H_4$-4-$C{\equiv}CC_6H_4$-4-Br[40], *trans*-$[Ru(C{\equiv}C\text{-}4\text{-}C_6H_4I)Cl(dppe)_2]$[6]. *trans*-$[Ru(C{\equiv}CC_6H_4\text{-}4\text{-}C{\equiv}CC_6H_4\text{-}4\text{-}I)Cl(dppe)_2]$ was provided by Mr Torsten Schwich. *cis*-$[OsCl_2(dppe)_2]$ was prepared via the following unpublished procedure by Morrall and *et al.*[41]: A mixture of 1,2-bis(diphenylphosphino)ethane (527 mg, 1.325 mmol) and *cis*-$[OsCl_2(DMSO)_4]$ (380 mg, 0.662 mmol) was heated in refluxing toluene (40 mL) for 18 h. The solution was allowed to cool to room temperature. The toluene-insoluble component was collected by filtration and washed with diethyl ether (690 mg, 98%). ^{1}H NMR: δ 6.65-8.14 (m, 40H, Ar), 2.50-2.92 (m, 8H, CH_2). ^{31}P NMR: δ 7.6 (t, $^2J_{pp}$ = 5.5 Hz), 5.3 (t, $^2J_{pp}$ = 5.5 Hz).

3.4.2 Instrumentation

Electrospray ionisation mass spectra (ESIMS) were obtained using a Waters-micromass LCT-ZMD single quadrupole liquid chromatograph instrument; peaks are reported as *m/z* (assignment, relative intensity). Microanalyses were carried out by the Microanalysis Service Unit, Australian National University. Infrared spectra were recorded as dichloromethane solutions using a Perkin-Elmer System 2000 FT-IR spectrometer. ^{1}H (300 MHz), $^{13}C\{^{1}H\}$ (75 MHz) and $^{31}P\{^{1}H\}$ (121 MHz) NMR spectra were recorded using a Varian Mercury-300 FT-NMR spectrometer and are referenced to residual chloroform (7.26 ppm (^{1}H), 77.0 ppm ($^{13}C\{^{1}H\}$)) or external 85% H_3PO_4 (0.0 ppm ($^{31}P\{^{1}H\}$)). UV-Vis spectra were recorded as CH_2Cl_2 solutions in 1 cm quartz cells using a Cary 5 spectrophotometer.

Cyclic voltammetry measurements were recorded using an e-corder and EA161 potentiostat from eDaq Pty Ltd. Measurements were carried out at room temperature using Pt disk working-, Pt wire auxiliary-, and Ag/AgCl reference electrodes, such that the ferrocene/ferrocenium redox couple was located at 0.56 V. Scan rates were typically 100 mV s^{-1}. Electrochemical solutions contained 0.1 M $(NBu^{n}_{4})PF_6$ and ca 10^{-3} M complex in dried and distilled solvent; solutions were purged and maintained under a nitrogen atmosphere. Electronic spectra were recorded using a Cary 5 spectrophotometer. Solution spectra of the oxidized species were obtained at 298 K by electrogeneration in an optically-transparent thin-layer electrochemical (OTTLE) cell with potentials ca 50 - 200 mV beyond $E_{1/2}$ for each couple, to ensure complete electrolysis. Solutions were made up using 0.3 M $(NBu^{n}_{4})PF_6$ in THF or CH_2Cl_2.

3.4.3 ^{13}C NMR numbering Scheme

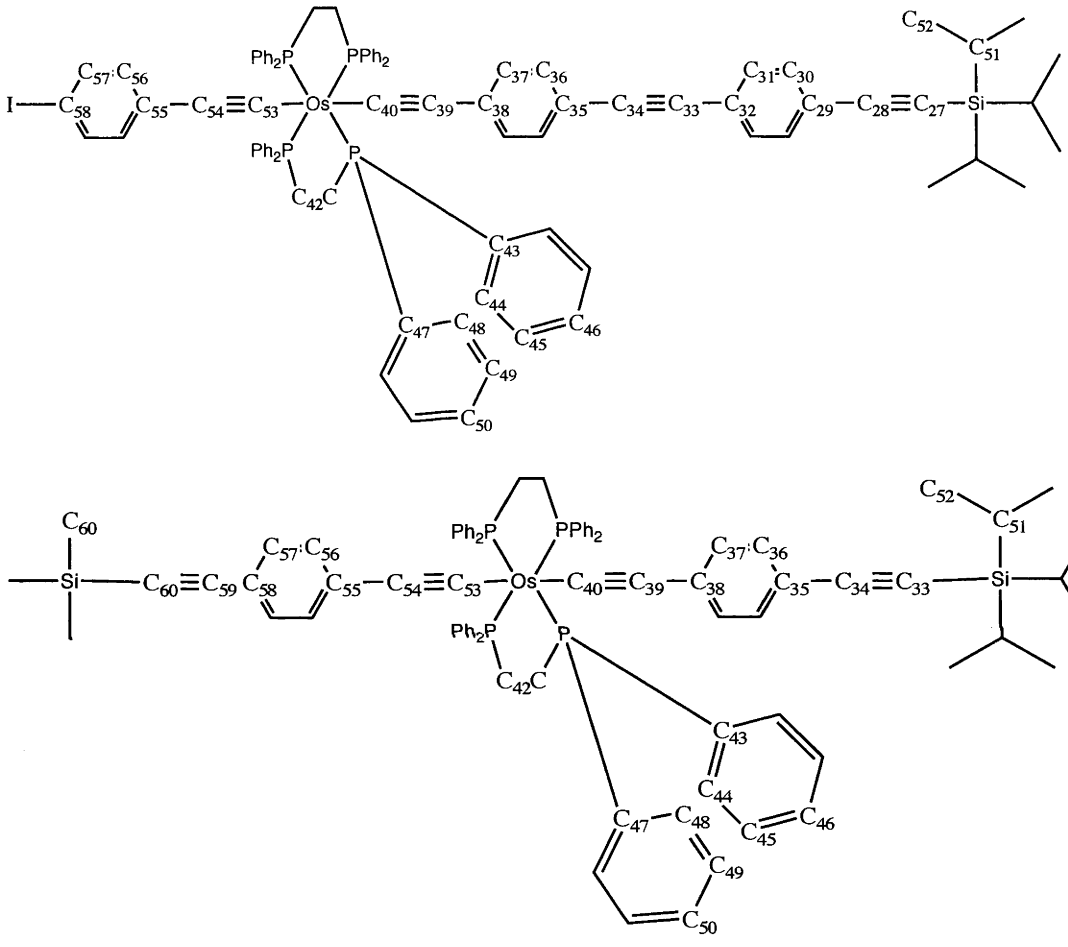

3.4.4 Synthesis and Characterization

trans-[Os(C≡CPh)Cl(dppe)$_2$] (9)

A mixture of *cis*-[$OsCl_2(\eta^2$-dppe)$_2$] (600 mg, 0.567 mmol), NH_4PF_6 (115 mg, 0.709 mmol) and phenylacetylene (0.579 mg, 5.67 mmol) was stirred at room temperature in CH_2Cl_2 (100 mL) for 18 h. NEt_3 (5 mL) was added, and the solution was reduced

in volume to 50 mL. Methanol was added, and the resulting precipitate collected and washed with petrol (50 mL) to give **9** as a yellow powder (573 mg, 90%), identified by comparison with spectroscopic data in the literature[30] (^{31}P NMR: δ 16.4).

***trans*-[Os(C≡C-4-C_6H_4Br)Cl(dppe)$_2$] (10)**

A mixture of *cis*-[$OsCl_2(dppe)_2$] (800 mg, 0.756 mmol), NH_4PF_6 (154 mg, 0.945 mmol) and 1-bromo-4-ethynylbenzene (206 mg, 1.13 mmol) was stirred in CH_2Cl_2 (100 mL) for 12 h. NEt_3 (5 mL) was added and the solution was reduced to 50 mL. The solution was added to methanol (150 mL), precipitating a solid that was collected and washed with petrol (50 mL), affording **10** as a yellow powder (836 mg, 92%). ESI MS: 1199 ([M - Cl + CH_3OH]$^+$, 100). Anal. Calcd for $C_{60}H_{52}BrClOsP_4$: C 59.93, H 4.36%. Found: C 60.22, H 4.28%. UV-vis: λ 340 nm, ε 21000 M^{-1} cm^{-1}. IR: 2067 cm^{-1} ν(OsC≡C). ^{1}H NMR: δ 6.45-7.51 (m, 44H, Ar), 2.62 (m, 8H, CH_2). ^{31}P NMR: δ 16.2. ^{13}C NMR: δ 135.7, 134.8 (C_{47}, C_{43}, vtt, $|{}^1J_{PC} + {}^3J_{PC}|$ = 22 Hz), 134.3, 134.2 (C_{48}, C_{44}), 132.0 (C_{37}), 130.3 (C_{36}), 129.9 (C_{38}), 129.0, 128.8 (C_{50}, C_{46}), 127.2 & 126.9 (C_{49}, C_{45}), 115.5 (C_{35}), 108.3 (C_{39}), 105.5 (C_{40}, quint, $^2J_{PC}$ = 12 Hz), 31.4 (C_{42}, vtt, $|{}^1J_{PC} + {}^3J_{PC}|$ = 26 Hz).

***trans*-[Os(C≡C-4-C_6H_4I)Cl(dppe)$_2$] (11)**

A mixture of *cis*-[$OsCl_2(dppe)_2$] (3.65 g, 3.45 mmol), NH_4PF_6 (703 mg, 4.31 mmol) and 1-iodo-4-ethynylbenzene (1.18 g, 5.17 mmol) was stirred in CH_2Cl_2 (150 mL) for 12 h. NEt_3 (10 mL) was added and the solution was reduced in volume to 80 mL and added to methanol, precipitating a product that was collected and washed with petrol (50 mL) to give **11** as a yellow powder (4.02 g, 93%). ESI MS: 1247 ([M - Cl + CH_3OH]$^+$, 100). Anal. Calcd for $C_{60}H_{52}ClIOsP_4$: C 57.67, H 4.19%. Found: C 57.59, H 4.04%. UV-vis: λ 364 nm, ε 22000 M^{-1} cm^{-1}. IR: 2064 cm^{-1} ν(OsC≡C). ^{1}H NMR: δ 6.34-7.51 (m, 44H, Ar), 2.61 (m, 8H, CH_2). ^{31}P NMR: δ 16.2. ^{13}C NMR: δ 136.2 (C_{36}) 135.7, 134.8 (C_{47}, C_{43}, vtt, $|{}^1J_{PC} + {}^3J_{PC}|$ = 22 Hz), 134.3, 134.2 (C_{48}, C_{44}),

132.5 (C_{37}), 130.4 (C_{38}), 129.0, 128.8 (C_{50}, C_{46}), 127.1, 126.9 (C_{49}, C_{45}), 108.5 (C_{35}), 106.3 (C_{40}, coupling not visible), 86.1 (C_{39}), 31.4 (C_{42}, vtt, $|{}^1J_{PC} + {}^3J_{PC}| = 24$ Hz).

***trans*-[Os(C≡CC$_6$H$_4$-4-C≡CC$_6$H$_4$-4-Br)Cl(dppe)$_2$] (12)**

A mixture of *cis*-[$OsCl_2(dppe)_2$] (500 mg, 0.473 mmol), HC≡CC$_6$H$_4$-4-C≡CC$_6$H$_4$-4-Br (266 mg, 0.945 mmol) and NH_4PF_6 (96 mg, 0.591 mmol) were stirred in CH_2Cl_2 (100 ml) for 16 h. NEt_3 (5 ml) was added and the mixture stirred for 1 min. The solvent was reduced in volume to 40 mL and a solid precipitated on addition of methanol (150 mL). The solid was collected on a sintered glass filter funnel and washed with petrol (40 mL) to remove excess acetylene, affording **12** as an orange powder (504 mg, 82%). ESI MS: 1299 ([M - Cl + CH_3OH]$^+$, 90), 1308 ([M - Cl + CH_3CN]$^+$, 80). Anal. Calcd for $C_{68}H_{56}BrClOsP_4$: C 62.70, H 4.33%. Found: C 62.28, H 4.55%. UV-vis: λ 400 nm, ε 33000 M^{-1} cm^{-1}, λ 284 nm, ε 27000 M^{-1} cm^{-1}. IR: 2056 cm^{-1} ν(C≡C), 2070 cm^{-1} ν(C≡C). ^{1}H NMR: δ 6.56-7.50 (m, 48H, Ar), 2.64 (m, 8H, CH_2). ^{31}P NMR: δ 16.0. ^{13}C NMR: δ 135.6, 134.7 (C_{47}, C_{43}, vtt, $|{}^1J_{PC} + {}^3J_{PC}| = 22$ Hz), 134.3, 134.2 (C_{48}, C_{44}), 132.7, 131.5, 130.7, 130.6, 121.7 (C_{37}, C_{36}, C_{31}, C_{30}, C_{29}), 128.9, 128.8 (C_{50}, C_{46}), 127.2 & 126.9 (C_{49}, C_{45}), 31.3 (C_{42}, vtt, $|{}^1J_{PC} + {}^3J_{PC}| = 22$ Hz); other signals were not observed due to poor solubility.

***trans*-[Os(C≡CPh)(NH_3)(dppe)$_2$]PF_6 (13)**

A mixture of *trans*-[Os(C≡CPh)Cl(dppe)$_2$] (**9**, 270 mg, 0.240 mmol), NH_4PF_6 (58 mg, 0.360 mmol) and NEt_3 (6 mL) was stirred in CH_2Cl_2 (100 mL) for 18 h. The solution was reduced to 50 mL, and a solid precipitated from petrol (200 mL), collected and washed with methanol, affording **13** as a pale yellow powder (238 mg, 79%). The sample can be further purified through crystallization from toluene. ESI MS: 1089 ([Os(C≡CPh)(dppe)$_2$]$^+$, 100), 988 ([Os(dppe)$_2$]$^+$, 30). Anal. Calc. for $C_{60}H_{56}F_6NOsP_5$: C 57.65, H 4.51, N 1.12%. Found: C 57.54, H 4.74, N 1.12%. IR: ν(OsC≡C) 2076 cm^{-1}. UV-Vis: λ 275 nm, ε 17700 M^{-1} cm^{-1}; 301 nm, ε 18600 M^{-1}

cm^{-1}. ^1H NMR: δ 6.42-8.20 (m, 45H, Ph), 2.61 (m, 8H, CH_2), 1.00 (s, 3H, NH_3). ^{31}P NMR: δ 19.9, -143.7 (sept, PF_6, J_{PF} = 714 Hz). ^{13}C NMR: δ 135.4 (C_{47}, vtt, $|{}^1J_{PC} + {}^3J_{PC}|$ = 24 Hz), 134.4 (C_{48}), 131.7 (C_{49}), 130.4, 130.2 (C_{50}, C_{46}), 129.9 (C_{37}), 129.7 (C_{43}, coupling not observed), 129.3 (C_{45}), 128.1 (C_{35}), 127.8 (C_{44}), 124.0 (C_{36}), 31.2 (C_{42}, vtt, $|{}^1J_{PC} + {}^3J_{PC}|$ = 24 Hz); C_{40}, C_{39}, C_{38} not detected.

***trans*-[Os(C≡C-4-C_6H_4I)(NH_3)(dppe)$_2$]PF_6 (14)**

A mixture of *trans*-[Os(C≡C-4-C_6H_4I)Cl(dppe)$_2$] (**11**, 4.00 g, 3.20 mmol), NH_4PF_6 (1.04 g, 6.4 mmol) and NEt_3 (4 mL) was stirred in CH_2Cl_2 (200 mL) for 18 h. The solution was reduced to 100 mL, and a solid precipitated by addition of the solution to petrol. The solid was collected and washed with methanol, affording **14** as a pale yellow powder (4.269 g, 97%). ESI MS: 1232 ([M - PF_6]$^+$, 100). Anal. Calcd for $C_{60}H_{55}F_6INOsP_5$: C 52.37, H 4.03, N 1.02%. Found: C 52.36, H 3.92, N 1.04%. UV-vis: λ 319 nm, ε 29000 M^{-1} cm^{-1}. IR: 2076 cm^{-1} ν(OsC≡C). ^1H NMR: δ 6.42-8.13 (m, 44H, Ar), 2.61 (m, 8H, CH_2), 1.02 (s, 3H, NH_3). ^{31}P NMR: δ 19.9, -143.7 (sept, PF_6, J_{PF} = 714 Hz). ^{13}C NMR: δ 137.0 (C_{36}), 135.1 (C_{47}, vtt, $|{}^1J_{PC} + {}^3J_{PC}|$ = 26 Hz), 134.4 (C_{48}), 131.7 (C_{37}), 131.2 (C_{49}), 131.0 (C_{43}, tt, $|{}^1J_{PC} + {}^3J_{PC}|$ = 22 Hz), 130.5, 130.3 (C_{50}, C_{46}), 129.4 (C_{45}), 129.0 (C_{38}), 127.9 (C_{44}), 112.5 (C_{35}), 97.8 (C_{40}, quint, $^2J_{PC}$ = 11 Hz), 88.2 (C_{39}), 31.2 (C_{42}, vtt, $|{}^1J_{PC} + {}^3J_{PC}|$ = 24 Hz).

***trans*-[Os(C≡CC_6H_4-4-C≡CC_6H_4-4-Br)(NH_3)(dppe)$_2$]PF_6 (15)**

A mixture of *trans*-[Os(C≡CC_6H_4-4-C≡CC_6H_4-4-Br)Cl(dppe)$_2$] (**12**, 400 mg, 0.307 mmol), NH_4PF_6 (200 mg, 1.23 mmol) and NEt_3 (1 mL) were stirred in CH_2Cl_2 (100 mL) for 24 h. The solvent volume was reduced to 60 mL and salts were precipitated on addition of petrol (150 mL). The solution was filtered to remove the salts and product was crystallized through evaporation of CH_2Cl_2/petrol mix at room temperature over a period of 8 h. The orange crystals were collected on a sintered glass filter funnel and were washed with methanol to afford **15** as a dark orange

crystalline product (300 mg, 68%). ESI MS: 1267 ([M - NH3-PF6]$^+$, 100). Anal. Calcd for $C_{68}H_{59}BrF_6NOsP_5$: C 57.15, H 4.16, N 0.98%. Found: C 57.01, H 4.34, N 0.94%. UV-vis: λ 362 nm, ε 45000 M^{-1} cm^{-1}. IR: 2074 (br) cm^{-1} ν(OsC≡C), 2062 cm^{-1} ν(C≡C). ^{1}H NMR: δ 6.43 - 8.15 (m, 48H, Ar), 2.63 (m, 8H, CH_2), 1.05 (s, 3H, NH_3). ^{31}P NMR: δ 19.8, -143.7 (sept, PF_6, J_{PF} = 714 Hz). ^{13}C NMR: δ 135.1 (C_{47}, vtt, $|{}^1J_{PC} + {}^3J_{PC}|$ = 24 Hz), 134.4 (C_{48}), 131.3 (C_{49}), 131.0 (C_{43}, vtt, $|{}^1J_{PC} + {}^3J_{PC}|$ = 20 Hz), 132.8, 131.6, 131.4, 129.9 (C_{37}, C_{36}, C_{31}, C_{30}, C_{29}), 130.5, 130.2 (C_{50}, C_{46}), 129.4 (C_{45}), 128.9 (C_{38}), 127.9 (C_{44}), 122.1, 117. 8, 114.1, 91.2, 89.0 (C_{39}, C_{35}, C_{34}, C_{33}, C_{32}), 31.2 (C_{42}, tt, $|{}^1J_{PC} + {}^3J_{PC}|$ = 22 Hz); C_{40} not visible.

***trans*-[Ru(C≡C-4-C_6H_4I)(NH_3)(η^2-dppe)$_2$]PF_6 (16)**

A mixture of *trans*-[Ru(C≡C-4-C_6H_4I)Cl(η^2-dppe)$_2$] (250 mg, 0.215 mmol), NH_4PF_6 (105 mg, 0.646 mmol) and Et_3N (1 mL) was stirred in CH_2Cl_2 (60 mL) for 12 h. The solution was reduced to 10 mL and added to petrol (100 mL), precipitating a solid that was collected on a sintered glass filter funnel and washed with methanol to give **16** as a pale yellow powder (167 mg, 60 %). ESI MS: 1126 ([Ru(C≡C-4-C_6H_4I)(dppe)$_2$]$^+$, 100), 898 ([Ru(dppe)$_2$]$^+$, 50). Anal. Calcd for $C_{60}H_{55}F_6INP_5Ru$: C 56.00, H 4.31, N 1.09%. Found: C 55.69, H 4.54, N 1.03%. UV-vis (CH_2Cl_2): λ 318 nm, ε 18000 M^{-1} cm^{-1}. IR (CH_2Cl_2) 2076 cm^{-1} ν(Ru-C≡C). ^{1}H NMR: δ 6.42-8.13 (m, 44H, Ar), 2.63 (m, 8H, CH_2), 0.28 (s, 3H, NH_3). ^{31}P NMR: δ 54.0 (s, PPh_2), -143.7 (sept, PF_6, J_{PF} = 714 Hz). ^{13}C NMR: δ 137.2 (C_{36}), 135.8 (C_{47}, vtt, $|{}^1J_{PC} + {}^3J_{PC}|$ = 22 Hz), 134.4 (C_{48}), 131.6 (C_{43}, vtt, $|{}^1J_{PC} + {}^3J_{PC}|$ = 20 Hz), 131.5 (C_{37}), 131.3 (C_{49}), 130.2, 130.5 (C_{50}, C_{46}), 129.4 (C_{45}), 128.4 (C_{38}), 128.0 (C_{44}), 119.9 (C_{40}, quint, $^2J_{PC}$ = 16 Hz), 116.4 (C_{39}), 88.7 (C_{35}), 30.3 (C_{42}, vtt, $|{}^1J_{PC} + {}^3J_{PC}|$ = 24 Hz).

***trans*-[Os(C≡CPh)$_2$(dppe)$_2$] (17).**

A mixture of *trans*-[Os(C≡CPh)(NH$_3$)(dppe)$_2$]PF$_6$ (**13**, 200 mg, 0.160 mmol) and phenylacetylene (0.5 mL, 5 mmol) was heated in refluxing methanol (100 mL) for 16 h. The solution was allowed to cool to room temperature and the pale yellow powder was collected by filtration and identified as **17** (114 mg, 60%). The sample can be further purified through crystallization from toluene. ESI MS: 1191 ([Os(C≡CPh)$_2$(dppe)$_2$]$^+$, 100), 1089 ([Os(C≡CPh)(dppe)$_2$]$^+$, 60), 988 ([Os(dppe)$_2$]$^+$, 20). Anal. Calc. for $C_{68}H_{58}OsP_4$: C 68.67, H 4.92%. Found: C 68.57, H 5.08%. IR: 2060 (br) cm^{-1} ν(OsC≡C). UV-Vis: λ 336 nm, ε 28600 M^{-1} cm^{-1}. ^{1}H NMR: δ 6.50-7.50 (m, 50H, Ph), 2.58 (m, 8H, CH_2). ^{31}P NMR: δ 16.7. ^{13}C NMR: δ 136.2 (C_{47}, C_{43}), 134.3 (C_{48}, C_{44}, coupling not observed), 130.5, 127.4 (C_{37}, C_{36}), 128.7 (C_{50}, C_{46}), 127.0 (C_{49}, C_{45}), 122.7 (C_{35}), 32.6 (C_{42}, coupling not observed); C_{38}, C_{39}, C_{40} not detected.

***trans*-[Os(C≡C-4-C$_6$H$_4$I)(C≡CC$_6$H$_4$-4-C≡CSiPr$^i_3$)(dppe)$_2$] (18)**

trans-[Os(C≡C-4-C$_6$H$_4$I)(NH$_3$)(dppe)$_2$]PF$_6$ (**14**, 2.30 g, 1.67 mmol), [(4-ethynylphenyl)ethynyl](triisopropyl)silane (1.88 g, 6.68 mmol) and NEt$_3$ (1 mL) were heated in refluxing methanol (200 mL) for 144 h. The resulting solid was collected and washed with methanol (50 mL) and petrol (50 mL), affording **18** as a yellow powder (1.76 g, 70%). HRMS (ESI): Calc.: 1497.348 [M + H]$^+$, Found: 1497.352. Anal. Calc. for $C_{79}H_{77}IOsP_4Si$: C 63.45, H 5.19%. Found: C 63.44, H 5.35%. IR: 2055 (br) cm^{-1} ν(OsC≡C), 2150 cm^{-1} ν(C≡CSi). UV-Vis: λ 378 nm, ε 46000 M^{-1} cm^{-1}. ^{1}H NMR: δ 6.40-7.43 (m, 52H, Ph), 2.57 (m, 8H, CH_2), 1.14 (s, 21H, Pr^i). ^{31}P NMR: δ 16.7. ^{13}C NMR: δ 136.3 (C_{57}), 135.6 (C_{47}, C_{43}, vtt, $|{}^1J_{PC} + {}^3J_{PC}| = 24$ Hz), 134.1 (C_{48}, C_{44}), 132.2 (C_{56}), 131.3 (C_{37}), 131.1 (C_{38}), 130.3 (C_{55}), 130.0 (C_{36}), 128.8 (C_{50}, C_{46}), 127.0 (C_{49}, C_{45}), 119.7, 117.7 (C_{40}, C_{53}, quint, $^2J_{PC} = 12$ Hz), 116.9, 115.0, 113.7 (C_{35}, C_{39}, C_{54}), 108.5 (C_{34}), 89.7 (C_{33}), 86.7 (C_{58}), 31.4 (C_{42}, vtt, $|{}^1J_{PC} + {}^3J_{PC}| = 26$ Hz), 18.7 (C_{52}), 11.4 (C_{51}).

trans-[Os(C≡C-4-C_6H_4I)(C≡CC_6H_4-4-C≡CC_6H_4-4-C≡C$SiPr^i_3$)(dppe)$_2$] (19)

trans-[Os(C≡C-4-C_6H_4I)(NH_3)(dppe)$_2$]PF_6 (**15**, 450 mg, 0.327 mmol), HC≡CC_6H_4-4-C≡CC_6H_4-4-C≡C$SiPr^i_3$ (375 mg, 0.981 mmol), Et_3N (1 mL) were heated in a refluxing mixture of methanol (50 mL) and $CHCl_3$ (50 mL) for 72 h. The solution was taken to dryness and the residue dissolved in a minimum amount of CH_2Cl_2 (10 ml) and precipitated out of methanol (200 mL). The solid was collected on a sintered glass filter funnel and washed with pentane (40 mL), affording **19** as a yellow powder (296 mg, 57%). ESI MS: 1619 ($[(M + Na)]^+$, 5), 1635 ($[(M + K)]^+$, 5). HRMS (ESI): Calc.: 1619.3625 $[M + Na]^+$, Found: 1619.3615. Anal. Calc. for $C_{87}H_{81}IOsP_4Si$: C 65.49, H 5.12%. Found: C 65.26, H 5.22%. IR: 2054 (br) cm^{-1} ν(OsC≡C), 2152 cm^{-1} ν(C≡CSi). UV-Vis: λ 414 nm, ε 37000 M^{-1} cm^{-1}, λ 322 nm, ε 38000 M^{-1} cm^{-1}, λ 291 nm (sh), ε 31000 M^{-1} cm^{-1}, λ 274 nm (sh), ε 33000 M^{-1} cm^{-1}. ^{1}H NMR: δ 6.41-7.45 (m, 52H, Ph), 2.59 (m, 8H, CH_2), 1.14 (s, 21H, ^{i}Pr). ^{31}P NMR: δ 16.5 ppm. ^{13}C NMR: δ 136.3 (C_{57}), 135.5 (C_{47}, C_{43}, vtt, $|{}^1J_{PC} + {}^3J_{PC}| = 24$ Hz), 134.1 (C_{48}, C_{44}), 132.2 (C_{56}), 131.9 (C_{37}), 131.4, 131.3 (C_{55}, C_{38}), 131.1, 131.0, 130.2 (C_{36}, C_{31}, C_{30}), 128.8 (C_{50}, C_{46}), 127.0 (C_{49}, C_{45}), 123.8, 122.6, 116.2, 115.4, 113.8, 106.8, 92.7, 92.4 (C_{54}, C_{39}, C_{35}, C_{34}, C_{32}, C_{29}, C_{28}, C_{27}), 89.3 (C_{33}), 86.7 (C_{58}), 33.3 (C_{42}, vtt, $|{}^1J_{PC} + {}^3J_{PC}| = 24$ Hz), 18.7 (C_{52}), 11.3 (C_{51}); C_{53}, C_{40} not observed.

trans-[Os(C≡C-4-C_6H_4-4-C≡C$SiMe_3$)(C≡CC_6H_4-4-C≡C$SiPr^i_3$)(dppe)$_2$] (20)

A mixture of _trans_-[Os(C≡C-4-C_6H_4I)(C≡CC_6H_4-4-C≡C$SiPr^i_3$)(dppe)$_2$] (**18**, 1.80 g, 1.21 mmol), trimethylsilylacetylene (591 mg, 6.02 mmol), CuI (20 mg) and _trans_-[$PdCl_2(PPh_3)_2$] (50 mg) was stirred in a mixture of CH_2Cl_2 (100 mL) and NEt_3 (100 mL) for 12 h. The mixture was absorbed onto basic alumina and eluted with a mixture of petrol and CH_2Cl_2 (2:1). The solution was taken to dryness. The resultant residue was dissolved in minimum of dichloromethane (20 mL), precipitated out of methanol (120 mL) and collected on a sinter glass filter funnel, affording **21** as a

yellow powder (1.50 g, 86%). ESI MS: 1466 ($[M]^+$, 30). HRMS (ESI): Calc.: 1466.4840 $[M]^+$, Found: 1466.4834. Anal. Calc. for $C_{84}H_{86}OsP_4Si_2$: C 68.83, H 5.91%. Found: C 68.47, H 5.95%. UV-vis (CH_2Cl_2): λ 387 nm, ε 61000 M^{-1} cm^{-1}. IR (CH_2Cl_2) 2048 (br) cm^{-1} ν(C≡C), 2147 (br) cm^{-1} ν(C≡CSi). ^1H NMR: δ 7.44 – 6.88 (m, 48H, Ar), 2.56 (m, 8H, CH), 1.15 (s, 21H, $SiPr^i_3$), 0.27 (s, 9H, $SiMe_3$). ^{31}P NMR: δ 16.5. ^{13}C NMR: δ 135.7 (C_{47}, C_{43}, vtt, $|{}^1J_{PC} + {}^3J_{PC}|$ = 24 Hz), 134.1 (C_{48}, C_{44}), 132.2 (C_{56}), 131.4, 131.1 (C_{55}, C_{38}), 131.3, 131.2 (C_{56}, C_{37}), 130.0 (C_{57}, C_{36}), 128.8 (C_{50}, C_{46}), 127.0 (C_{49}, C_{45}), 120.4, 119.6 (C_{53}, C_{40}, quint, $^2J_{PC}$ = 12 Hz), 116.9, 116.3, 115.4, 108.5, 106.5 (C_{59}, C_{58}, C_{54}, C_{39}, C_{35}, C_{34}), 93.6, 89.7 (C_{60}, C_{33}), 32.3 (C_{42}, vtt, $|{}^1J_{PC} + {}^3J_{PC}|$ = 26 Hz), 18.7 (C_{52}), 11.4 (C_{51}), 0.15 (C_{61}).

trans-[Os(C≡C-4-C_6H_4C≡CH)(C≡CC_6H_4-4-C≡C$SiPr^i_3$)(dppe)$_2$] (21)

A mixture of *trans*-[Os(C≡C-4-C_6H_4C≡C$SiMe_3$)(C≡CC_6H_4-4-C≡C$SiPr^i_3$)(dppe)$_2$] (**20**, 1.00 g, 0.695 mmol) and KOH (266 mg, 4.17 mmol) was stirred in a mixture of CH_2Cl_2 (50 mL) and methanol (50 mL) for 12 h. The reaction mixture was then taken to dryness. The resultant residue was dissolved in minimum of CH_2Cl_2 (20 mL), precipitated in methanol (150 mL) and collected on a sintered glass filter funnel, affording **21** as a orange powder (788 mg, 81 %). ESI MS: 1394 ($[M]^+$, 100). HRMS (ESI): Calc.: 1394.4435 $[M]^+$, Found: 1394.4438. Anal. Calc. for $C_{81}H_{78}OsP_4Si$: C 69.81, H 5.64%. Found: C 69.88, H 5.39%. UV-vis (CH_2Cl_2): λ 384 nm, ε 44000 M^{-1} cm^{-1}. IR (CH_2Cl_2) 2053 (br) cm^{-1} ν(C≡C), 2146 cm^{-1} ν(C≡CSi), 3302 (br) cm^{-1} ν(≡CH). ^1H NMR: δ 7.43 – 6.60 (m, 48H, Ar), 3.14 (s, 1H, C≡CH), 2.59 (m, 8H, CH), 1.15 (s, 21H, $SiPr^i_3$). ^{31}P NMR: δ 16.6. ^{13}C NMR: δ 135.6 (C_{47}, C_{43}, vtt, $|{}^1J_{PC} + {}^3J_{PC}|$ = 24 Hz), 134.1 (C_{48}, C_{44}), 131.6, 131.1 (C_{55}, C_{38}), 131.3, 131.2 (C_{56}, C_{37}), 130.02, 130.00 (C_{57}, C_{36}), 128.8 (C_{50}, C_{46}), 127.0 (C_{49}, C_{45}), 120.3, 119.6 (C_{53}, C_{40}, quint, $^2J_{PC}$ = 12 Hz), 116.9, 115.3, 115.2, 108.4 (C_{58}, C_{54}, C_{39}, C_{35}, C_{34}), 89.6 (C_{33}), 84.9 (C_{59}), 76.7 (C_{60}), 32.3 (C_{42}, vtt, $|{}^1J_{PC} + {}^3J_{PC}|$ = 26 Hz), 18.7 (C_{52}), 11.4 (C_{51}).

***trans*-,*trans*-[(Pr^i_3SiC≡CC_6H_4-4-C≡C)(dppe)$_2$Os(C≡C-4-C_6H_4C≡C)Ru(dppe)$_2$(C≡CC_6H_4-4-I)] (22)**

A mixture of *trans*-[Os(C≡C-4-C_6H_4C≡CH)(C≡CC_6H_4-4-C≡CSiPr^i_3)(dppe)$_2$] (**21**, 300 mg, 0.215 mmol), *trans*-[Ru(C≡C-4-C_6H_4I)Cl(dppe)$_2$] (250 mg, 0.215 mmol), $NaPF_6$ (72 mg, 0.43 mmol) and NEt_3 (12 drops) were refluxed in CH_2Cl_2 (100 mL) for 24 h. The reaction volume was reduced to 40 mL and a solid precipitated on addition of methanol (150 mL). The solid was collected and washed with pentane (40 mL) to give **23** as an orange powder (479 mg, 88%). ESI MS: 2518 ($[M]^+$, 2). HRMS (ESI): Calc.: 2518.5468 $[M]^+$, Found: 2518.5520. Anal. Calc. for $C_{141}H_{129}IOsP_8RuSi$: C 67.27, H 5.16%. Found: C 67.44, H 5.42%. UV-vis (CH_2Cl_2): λ 387 nm, ε 78000 M^{-1} cm^{-1}. IR (CH_2Cl_2): 2057 (br) cm^{-1} ν(C≡C), 2145 cm^{-1} ν(C≡CSi). ^{1}H NMR (C_6D_6): δ 7.88 – 6.60 (m, 92H, Ar), 2.56 (m, 16H, CH), 1.27 (s, 21H, SiPr^i_3). ^{31}P NMR (C_6D_6): δ 54.3 (4P, RuP), 16.5 (4P, OsP).

***trans*-,*trans*-[(Pr^i_3SiC≡CC_6H_4-4-C≡C)(dppe)$_2$Os(C≡C-4-C_6H_4C≡C)Ru(dppe)$_2$(C≡CC_6H_4-4-C≡CC_6H_4-4-I)] (23)**

A mixture of *trans*-[Os(C≡C-4-C_6H_4C≡CH)(C≡CC_6H_4-4-C≡CSiPr^i_3)(dppe)$_2$] (**21**, 100 mg, 0.0718 mmol), *trans*-[Ru(C≡CC_6H_4-4-C≡CC_6H_4-4-I)(Cl)(dppe)$_2$] (90 mg, 0.0718 mmol), $NaPF_6$ (24 mg, 0.144 mmol) and NEt_3 (5 drops) were heated in refluxing CH_2Cl_2 (60 mL) for 24 h. The reaction volume was reduced to 30 mL and a solid precipitated by addition of the solution to methanol (150 mL). The solid was collected and washed with pentane (40 mL) affording **23** as an orange powder (104 mg, 55%). ESI MS: 2618 ($[M]^+$, 2). HRMS (ESI): Calc.: 2618.5781 $[M]^+$, Found: 2618.5789. Anal. Calc. for $C_{149}H_{133}IOsP_8RuSi$: C 68.37, H 5.12%. Found: C 68.83, H 5.23%. UV-vis (CH_2Cl_2): λ 400 nm, ε 110000 M^{-1} cm^{-1}, λ 315 nm sh, ε 44000 M^{-1} cm^{-1}. IR (CH_2Cl_2): (br) 2053 cm^{-1} ν(C≡C), 2146 cm^{-1} ν(C≡CSi). ^{1}H NMR (C_6D_6): δ 7.90 – 6.84 (m, 96H, Ar), 2.58 (m, 16H, CH), 1.27 (s, 21H, SiPr^i_3). ^{31}P NMR (C_6D_6): δ 54.2 (4P, RuP), 16.5 (4P, OsP).

***trans*-,*trans*-[(Pr^i_3SiC≡CC_6H_4-4-C≡C)(dppe)$_2$Os(C≡C-4-C_6H_4C≡C)Ru(dppe)$_2$(C≡CC_6H_4-4-C≡CSiMe_3)] (24)**

A mixture of *trans*-,*trans*-[(Pr^i_3SiC≡CC_6H_4-4-C≡C)(dppe)$_2$Os(C≡C-4-C_6H_4C≡C)Ru(dppe)$_2$(C≡C-4-C_6H_4I)] (**22**, 300 mg, 0.119 mmol), HC≡CSiMe_3 (70 mg, 0.715 mmol), *trans*-[$PdCl_2(PPh_3)_2$] (50 mg, 0.07 mmol), CuI (20 mg, 0.11 mmol) were stirred in a mixture of CH_2Cl_2 (50 mL) and NEt_3 (50 mL) for 12 h. The reaction mixture was absorbed onto alumina, eluting with a mixture of CH_2Cl_2/petrol (1:1). The solvent was removed and the residue taken up in a minimum of CH_2Cl_2 (10 mL), precipitated from petrol (150 mL) and collected on a sintered glass filter funnel to give **24** as an orange powder (151 mg, 51%). ESI MS: 2489 ($[M]^+$, 5). Anal. Calc. for $C_{146}H_{138}OsP_8RuSi_2$: C 70.48, H 5.59%. Found: C 70.12, H 5.85%. UV-vis (CH_2Cl_2): λ 391 nm, ε 98000 M^{-1} cm^{-1}. IR (CH_2Cl_2): 2055 (br) cm^{-1} ν(C≡C), 2147 (br) cm^{-1} ν(C≡CSi). ^{1}H NMR: δ 7.70 - 6.53 (m, 92H, Ar), 2.64 (m, 16H, CH), 1.15 (s, 21H, $SiPr^i_3$), 0.26 (s, 9H, $SiMe_3$). ^{31}P NMR: δ 54.2 (4P, RuP), 16.5 (4P, OsP).

***trans*-[Os(C≡CC_6H_4I)(C≡CC_6H_4-4-C≡CC_6H_4-4-C≡CH)(dppe)$_2$] (25)**

A mixture of *trans*-[Os(C≡C-4-C_6H_4I)(C≡CC_6H_4-4-C≡CC_6H_4-4-C≡CSiPr^i_3)(dppe)$_2$] (**19**, 965 mg, 0.605 mmol) and NBu^n_4 (6.05 ml of a 1.0M solution in THF, 6.05 mmol) was stirred in CH_2Cl_2 (150 mL) for 20 h. The solution volume was reduced to 40 mL with a solid precipitated from methanol (150 mL) and collected on a sintered glass filter funnel, affording **25** as a orange powder (811 mg, 93 %). ESI MS: 1440 ($[M]^+$, 40), ($[(M-C≡CC_6H_4$-4-C≡CH)$]^+$, 70). HRMS (ESI): Calc.: 1440.2386 $[M]^+$, Found: 1440.2383. Anal. Calc. for $C_{78}H_{61}IOsP_4$: C 65.09, H 4.27%. Found: C 65.30, H 4.22%. UV-Vis: λ 411 nm, ε 38000 M^{-1} cm^{-1}, λ 324 nm , ε 36000 M^{-1} cm^{-1}, λ 276

nm (sh), ε 34000 M^{-1} cm^{-1}, λ 265 nm (sh), ε 39000 M^{-1} cm^{-1}. IR (CH_2Cl_2): 2053 (br) cm^{-1} ν(C≡C), 3296 cm^{-1} ν(≡CH). ^{1}H NMR: δ 6.91 - 7.47 (m, 52H, Ar), 3.17 (s, 1H, C≡CH), 2.57 (m, 8H, CH). ^{31}P NMR: δ 16.6. ^{13}C NMR: δ 136.3 (C_{57}) 135.5 (C_{47}, C_{43}, vtt, $|{}^1J_{PC} + {}^3J_{PC}| = 24$ Hz), 134.1 (C_{48}, C_{44}), 132.2 (C_{56}), 132.0 (C_{37}), 131.2, 131.0, 130.2 (C_{36}, C_{31}, C_{30}), 128.8 (C_{50}, C_{46}), 127.0 (C_{49}, C_{45}), 86.7 (C_{58}), 83.4 (C_{28}), 76.6 (C_{27}) 33.3 (C_{42}, vtt, $|{}^1J_{PC} + {}^3J_{PC}| = 24$ Hz); C_{55}, C_{53}, C_{54}, C_{40}, C_{39}, C_{38}, C_{35}, C_{34}, C_{32}, C_{29}, C_{28}, C_{27} not observed.

trans-,trans-[(dppe)$_2$(IC$_6$H$_4$-4-C≡C)Os(C≡CC$_6$H$_4$-4-C≡CC$_6$H$_4$-4-C≡C)RuCl(dppe)$_2$] (26)

A mixture of _trans-_[Os(C≡C-4-C$_6$H$_4$I)(C≡CC$_6$H$_4$-4-C≡CC$_6$H$_4$-4-C≡CH)(dppe)$_2$] (**25**, 800 mg, 0.556 mmol), _cis-_[RuCl(dppe)$_2$] (1.08 g, 1.11 mmol) and $NaPF_6$ (470 mg, 2.78 mmol) were stirred in CH_2Cl_2 (150 mL) for 48 h. NEt_3 (10 mL) was added and the reaction stirred for 1 min. The reaction volume was reduced to 60 mL and a solid precipitated on addition to methanol (200 mL). The solid was collected and washed with petrol (30 mL), affording **21** as a yellow powder (1.16 g, 87%). ESI MS: 2253 ([M - I - Cl + MeCN + H]$^+$, 5). Anal. Calc. for $C_{130}H_{108}ClIOsP_8Ru$: C 65.84, H 4.59%. Found: C 65.30, H 4.84%. UV-vis (CH_2Cl_2): λ 423 nm, ε 57000 M^{-1} cm^{-1}, λ 308 nm, ε 27000 M^{-1} cm^{-1}. IR (CH_2Cl_2): 2056 (br) cm^{-1} ν(C≡C). ^{1}H NMR: δ 6.33 - 7.46 (m, 92H, Ar), 2.7 (m, 8H, RuPCH) 2.6 (m, 8H, OsPCH) ^{31}P NMR: δ 49.9 (4P, RuP), 16.6 (4P, OsP).

trans-,trans-[(dppe)$_2$(Me$_3$SiC≡CC$_6$H$_4$-4-C≡C)Os(C≡CC$_6$H$_4$-4-C≡CC$_6$H$_4$-4-C≡C)RuCl(dppe)$_2$] (27)

A mixture of _trans-,trans-_[(dppe)$_2$(IC$_6$H$_4$-4-C≡C)Os(C≡CC$_6$H$_4$-4-C≡CC$_6$H$_4$-4-C≡C)RuCl(dppe)$_2$] (**26**, 1.20 g, 0.505 mmol), HC≡CSiMe$_3$ (497 mg, 5.05 mmol), _trans-_[PdCl$_2$(PPh$_3$)$_2$] (50 mg, 0.07 mmol), and CuI (20 mg, 0.11 mmol) were stirred in a mixture of CH_2Cl_2 (100 mL) and NEt_3 (100 mL) for 24 h. The reaction mixture

was absorbed onto alumina and the column eluted with a mixture of CH_2Cl_2/petrol (2:1) (300 mL). The product was then eluted with CH_2Cl_2/petrol (3:1) (200 mL). The solvent was removed affording **27** as a yellow powder (640 mg, 54%). ESI MS: 2349 ([M - Cl + MeCN]$^+$, 10), HRMS (ESI): Calc.: 2348.5749 [M - Cl + MeCN]$^+$, Found: 2348.5745. Anal. Calc. for $C_{135}H_{117}ClOsP_8RuSi$: C 69.23, H 5.04%. Found: C 68.71, H 5.04%. UV-vis (CH_2Cl_2): λ 425 nm, ε 80000 M^{-1} cm^{-1}. IR (CH_2Cl_2): 2054 (br) cm^{-1} ν(C≡C), 2148 cm^{-1} ν(C≡CSi). ^{1}H NMR: δ 6.56 - 7.48 (m, 96H, Ar), 2.7 (m, 8H, RuPCH) 2.6 (m, 8H, OsPCH), 0.26 (s, 9H, $SiMe_3$). ^{31}P NMR: δ 49.9 (4P, RuP), 16.4 (4P, OsP).

***trans*-,*trans*-[(dppe)$_2$(Pr$^i_3$SiC■CC$_6$H$_4$-4-C■CC$_6$H$_4$-4-C■C)Os(C■CC$_6$H$_4$-4-C■CC$_6$H$_4$-4-C■C)RuCl(dppe)$_2$] (28)**

A mixture of *trans*-,*trans*-[(dppe)$_2$(IC$_6$H$_4$-4-C≡C)Os(C≡CC$_6$H$_4$-4-C≡CC$_6$H$_4$-4-C≡C)RuCl(dppe)$_2$] (**26**, 600 mg, 0.253 mmol), HC≡CC$_6$H$_4$-4-C≡CSiPr$^i_3$ (143 mg, 0.506 mmol), *trans*-[$PdCl_2(PPh_3)_2$] (50 mg, 0.070 mmol), and CuI (20 mg, 0.11 mmol) were stirred in a mixture of CH_2Cl_2 (100 mL) and NEt_3 (100 mL) for 24 h. The crude product was absorbed onto alumina and the column eluted with a mixture of CH_2Cl_2/petrol (2:1) (350 mL). The solvent was removed and the resulting residue dissolved in CH_2Cl_2 (20 mL). The product was precipitated from petrol and collected on a sintered glass filter funnel, affording **28** as a yellow powder (444 mg, 69%). ESI MS: 2533 ([M - Cl + MeCN]$^+$, 5), HRMS (ESI): Calc.: 2532.7001 [M - Cl + MeCN]$^+$, Found: 2532.7000. Anal. Calc. for $C_{149}H_{133}ClOsP_8RuSi$: C 70.84, H 5.31%. Found: C 70.41, H 5.16%. UV-vis (CH_2Cl_2): λ 434 nm, ε 79000 M^{-1} cm^{-1}, λ 304 nm, ε 43000 M^{-1} cm^{-1}. IR (CH_2Cl_2): 2053 (br) cm^{-1} ν(C≡C), 2153 cm^{-1} ν(C≡CSi). ^{1}H NMR: δ 6.57 - 7.45 (m, 96H, Ar), 2.70 (m, 8H, RuPCH), 2.60 (m, 8H, OsPCH), 1.15 (s, 21H, SiPr$^i_3$). ^{31}P NMR: δ 49.9 (4P, RuP), 16.4 (4P, OsP).

***trans*-,*trans*-,*trans*-[(Pr^i_3SiC≡CC_6H_4-4-C≡C)(dppe)$_2$Os(C≡CC_6H_4-4-C≡C)Ru(dppe)$_2$(C≡CC_6H_4-4-C≡CC_6H_4-4-C≡C)OsCl(dppe)$_2$] (29)**

A mixture of *trans,trans*-[(dppe)$_2$ClOs(C≡CC_6H_4-4-C≡CC_6H_4-4-C≡C)RuCl(dppe)$_2$] (**7**, 100 mg, 0.045 mmol), *trans*-[Os(C≡C-4-C_6H_4-4-C≡CH)(C≡CC_6H_4-4-C≡C$Si Pr^i_3$)(dppe)$_2$] (**23**, 63 mg, 0.045 mmol), $NaPF_6$ (15 mg, 0.92 mmol) and Et_3N (10 drops) were refluxed in CH_2Cl_2 (50 mL) for 24 h. The solvent volume was reduced to 10 mL and the crude product precipitated upon addition of methanol (100 mL). The solid was collected on a sintered glass filter funnel, and then washed through the sinter with a mixture of CH_2Cl_2/Et_3N (40:1) (60 mL). The solvent was removed and the residue taken up in a minimum of CH_2Cl_2 (15 mL), precipitated from pentane (100 mL) and collected on a sintered glass filter funnel, affording **29** as a yellow powder (60 mg, 38%). ESI MS: 3539 ($[M]^+$, 1), HRMS (ESI): Calc.: 3538.8746 $[M]^+$, Found: 3538.8748. UV-vis (CH_2Cl_2): λ 402 nm, ε 110000 M^{-1} cm^{-1}. IR (CH_2Cl_2): 2054 (br) cm^{-1} ν(C≡C), 2145 cm^{-1} ν(C≡CSi). ^{1}H NMR (C_6D_6): δ 7.90 – 6.33 (m, 132H, Ar), 2.59 (m, 24H, CH), 1.28 (s, 21H, $SiPr^i_3$). ^{31}P NMR (C_6D_6): δ 54.3 (4P, RuP), 16.5 (4P, OsP), 15.8 (4P, ClOsP). Accurate microanalysis was not obtained.

3.5 References

(1) Roberts, R. L.; Schwich, T.; Corkery, T. C.; Cifuentes, M. P.; Green, K. A.; Farmer, J. D.; Low, P. J.; Marder, T. B.; Samoc, M.; Humphrey, M. G. *Adv. Mater.* **2009**, *21*, 2318.

(2) Green, K. A.; Cifuentes, M. P.; Corkery, T. C.; Samoc, M.; Humphrey, M. G. *Angew. Chem. Int. Ed.* **2009**, *48*, 7867.

(3) Samoc, M.; Gauthier, N.; Cifuentes, M. P.; Paul, F.; Lapinte, C.; Dalton, G. T.; Humphrey, M. G. *Angew. Chem. Int. Ed.* **2006**, *45*, 7376.

(4) Samoc, M.; Morrall, J. P.; Dalton, G. T.; Cifuentes, M. P.; Humphrey, M. G. *Angew. Chem. Int. Ed.* **2007**, *46*, 731.

(5) Babgi, B.; Rigamonti, L.; Cifuentes, M. P.; Corkery, T. C.; Randles, M. D.; Schwich, T.; Petrie, S.; Stranger, R.; Teshome, A.; Asselberghs, I.; Clays, K.; Samoc, M.; Humphrey, M. G. *J. Am. Chem. Soc.* **2009**, *131*, 10293.

(6) Hurst, S. K.; Cifuentes, M. P.; McDonagh, A. M.; Humphrey, M. G.; Samoc, M.; Luther-Davies, B.; Asselberghs, I.; Persoons, A. *J. Organomet. Chem.* **2002**, *642*, 259.
(7) Powell, C. E.; Cifuentes, M. P.; McDonagh, A. M.; Hurst, S. K.; Lucas, N. T.; Delfs, C. D.; Stranger, R.; Humphrey, M. G.; Houbrechts, S.; Asselberghs, I.; Persoons, A.; Hockless, D. C. R. *Inorg. Chim. Acta* **2003**, *352*, 9.
(8) Delfs, C. D.; Stranger, R.; Humphrey, M. G.; McDonagh, A. M. *J. Organomet. Chem.* **2000**, *607*, 208.
(9) Werner, H.; Gotzig, J. *Organometallics* **1983**, *2*, 547.
(10) Werner, H.; Meyer, U.; Esteruelas, M. A.; Sola, E.; Oro, L. A. *J. Organomet. Chem.* **1989**, *366*, 187.
(11) Gotzig, J.; Werner, R.; Werner, H. *J. Organomet. Chem.* **1985**, *290*, 99.
(12) Espuelas, J.; Esteruelas, M. A.; Lahoz, F. J.; Oro, L. A.; Valero, C. *Organometallics* **1993**, *12*, 663.
(13) Esteruelas, M. A.; Lahoz, F. J.; Lopez, A. M.; Onate, E.; Oro, L. A. *Organometallics* **1995**, *14*, 2496.
(14) Buil, M. L.; Esteruelas, M. A.; Lopez, A. M.; Onate, E. *Organometallics* **1997**, *16*, 3169.
(15) Lai, S.-W.; Lau, T.-C.; Fung, W. K. M.; Zhu, N.; Che, C.-M. *Organometallics* **2003**, *22*, 315.
(16) Atherton, Z.; Faulkner, C. W.; Ingham, S. L.; Kakkar, A. K.; Khan, M. S.; Lewis, J.; Long, N. J.; Raithby, P. R. *J. Organomet. Chem.* **1993**, *462*, 265.
(17) Younus, M.; Long, N. J.; Raithby, P. R.; Lewis, J.; Page, N. A.; White, A. J. P.; Williams, D. J.; Colbert, M. C. B.; Hodge, A. J.; Khan, M. S.; Parker, D. G. *J. Organomet. Chem.* **1999**, *578*, 198.
(18) Gauthier, N.; Argouarch, G.; Paul, F.; Toupet, L.; Ladjarafi, A.; Costuas, K.; Halet, J.-F.; Samoc, M.; Cifuentes, M. P.; Corkery, T. C.; Humphrey, M. G. *Chem.-Eur. J.* **2011**, *17*, 5561.
(19) Gauthier, N.; Olivier, C.; Rigaut, S.; Touchard, D.; Roisnel, T.; Humphrey, M. G.; Paul, F. *Organometallics* **2008**, *27*, 1063.
(20) Lam, S. C.-F.; Yam, V. W.-W.; Wong, K. M.-C.; Cheng, E. C.-C.; Zhu, N. *Organometallics* **2005**, *24*, 4298.
(21) Wong, K. M.-C.; Lam, S. C.-F.; Ko, C.-C.; Zhu, N.; Yam, V. W.-W.; Roue, S.; Lapinte, C.; Fathallah, S.; Costuas, K.; Kahlal, S.; Halet, J.-F. *Inorg. Chem.* **2003**, *42*, 7086.
(22) Lavastre, O.; Plass, J.; Bachmann, P.; Guesmi, S.; Moinet, C.; Dixneuf, P. H. *Organometallics* **1997**, *16*, 184.
(23) Packheiser, R.; Ecorchard, P.; Rueffer, T.; Lang, H. *Organometallics* **2008**, *27*, 3534.
(24) Younus, M.; Long, N. J.; Raithby, P. R.; Lewis, J. *J. Organomet. Chem.* **1998**, *570*, 55.
(25) Gauthier, N.; Argouarch, G.; Paul, F.; Humphrey, M. G.; Toupet, L.; Ababou-Girard, S.; Sabbah, H.; Hapiot, P.; Fabre, B. *Adv. Mater.* **2008**, *20*, 1952.

(26) Touchard, D.; Haquette, P.; Guesmi, S.; Le Pichon, L.; Daridor, A.; Toupet, L.; Dixneuf, P. H. *Organometallics* **1997**, *16*, 3640.
(27) Touchard, D.; Guesmi, S.; Le Pichon, L.; Daridor, A.; Dixneuf, P. H. *Inorg. Chim. Acta* **1998**, *280*, 118.
(28) Touchard, D.; Morice, C.; Cadierno, V.; Haquette, P.; Toupet, L.; Dixneuf, P. H. *J. Chem. Soc., Chem. Commun.* **1994**, 859.
(29) Levason, W.; Champness, N. R.; Webster, M. *Acta Cryst.* **1993**, *C49*, 1884.
(30) Morrall, J. P.; Powell, C. E.; Stranger, R.; Cifuentes, M. P.; Humphrey, M. G.; Heath, G. A. *J. Organomet. Chem.* **2003**, *670*, 248.
(31) Powell, C. E.; Cifuentes, M. P.; Morrall, J. P.; Stranger, R.; Humphrey, M. G.; Samoc, M.; Luther-Davies, B.; Heath, G. A. *J. Am. Chem. Soc.* **2003**, *125*, 602.
(32) Hodge, A. J.; Ingham, S. L.; Kakkar, A. K.; Khan, M. S.; Lewis, J.; Long, N. J.; Parker, D. G.; Raithby, P. R. *J. Organomet. Chem.* **1995**, *488*, 205.
(33) Faulkner, C. W.; Ingham, S. L.; Khan, M. S.; Lewis, J.; Long, N. J.; Raithby, P. R. *J. Organomet. Chem.* **1994**, *482*, 139.
(34) Klein, A.; Lavastre, O.; Fiedler, J. *Organometallics* **2006**, *25*, 635.
(35) Pangborn, A. B.; Giardello, M. A.; Grubbs, R. H.; Rosen, R. K.; Timmers, F. J. *Organometallics* **1996**, *15*, 1518.
(36) Lavastre, O.; Ollivier, L.; Dixneuf, P.; Sibandhit, S. *Tetrahedron* **1996**, *52*, 5495.
(37) Lavastre, O.; Cabioch, S.; Dixneuf, P. H.; Vohlidal, J. *Tetrahedron* **1997**, *53*, 7595.
(38) Antonov, P. G.; Kukushkin, Y. N.; Konnov, V. I.; Kostikov, Y. P. *Koord. Khim.* **1980**, *6*, 1585.
(39) Hsung, R. P.; Chidsey, C. E. D.; Sita, L. R. *Organometallics* **1995**, *14*, 4808.
(40) Lin, J.-C.; Kim, J.-H.; Kellar, J. A.; Hersam, M. C.; Nguyen, S. T.; Bedzyk, M. J. *Langmuir* **2010**, *26*, 3771.
(41) Morrall, J. P. *Unpublished procedure* **2011**

Chapter 4

Branched heterobimetallic complexes

Contents

4.1 Introduction

It has been shown that large electron delocalised structures have much greater two-photon absorption cross-sections (σ_2) compared to linear structures, with some of the largest σ_2 found for highly branched dendrimeric structures.[1,2] This has been shown to be the case even when the σ_2 is scaled for molecular weight or molecular volume.[3] For this reason, larger branched structures incorporating the osmium and ruthenium metal centres explored in Chapters 2 and 3 were targeted as part of this work.

Previously, a heterobimetallic 1,3,5-substituted benzene complex incorporating ruthenium and iron metal centres was synthesised by Gauthier and *et al.*[4] The complex was investigated electrochemically and spectroelectrochemically and was shown to possess three redox states ($Fe^{II}Ru^{II}$, $Fe^{III}Ru^{II}$, $Fe^{III}Ru^{III}$) with distinct optical absorption properties. These changes in the optical absorption behaviour were used to conduct on-resonant switching of the third-order nonlinear optical effects at 750 nm and 1250 nm.

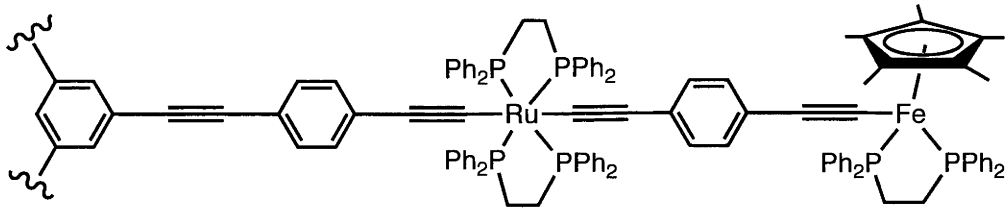

Figure 4.1. Hexanuclear bimetallic complex synthesised by Gauthier *et al.*,[4] where the arm shown is repeated at the wavy lines.

The heterobimetallic dendrimers explored in this work are large, branched structures consisting of a core unit incorporating three metal centres and three wedges containing a differing metal centre (Figure 4.2). The organic molecules linking the metal centres together are conjugated phenyl-ethynyl chains.

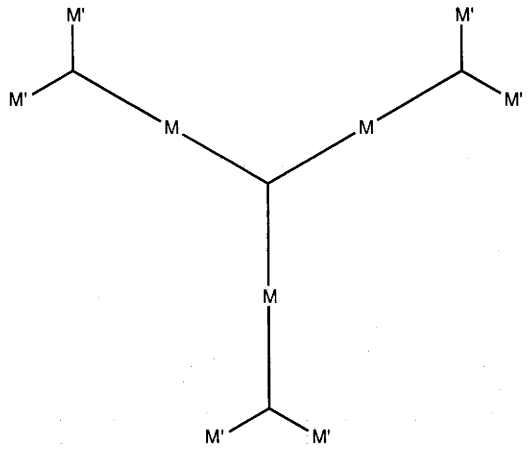

Figure 4.2. Schematic of a heterobimetallic dendrimer with the core and associated metal centres shown in red, and the "wedges" and associated metal centres shown in blue.

Due to the difficulty in representing these large macromolecular structures, dendritic complexes containing equivalent "arms" will be shown with a single arm from the core and a wavy line depicting the repeating unit (Figure 4.3).

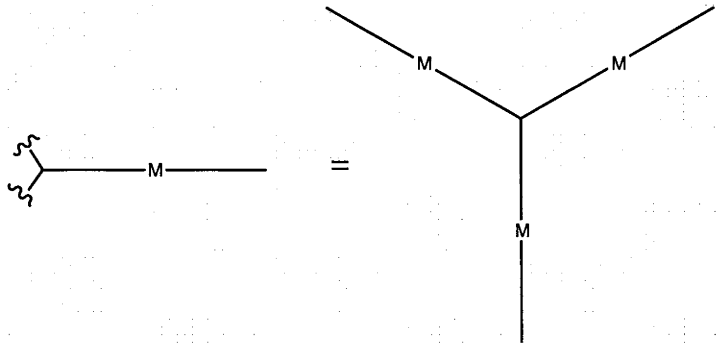

Figure 4.3. Schematic of macromolecular structure and the wavy line contraction used.

Powell and *et al.* have synthesised a heterobimetallic dendrimer incorporating platinum metal centres within the core, and ruthenium metal centres in the wedge

(Figure 4.4).[5] This complex is not suitable for use as a multistate nonlinear optical switch, as the platinum metal centres are not reversibly oxidised. Z-scan measurements at 800 nm have shown a significantly lower absorptive component of γ compared to the analogous complex with ruthenium in place of the platinum metal centres. This was rationalised by the increased electron density obtained by the replacement of the 16 valence-electron platinum by the 18 valence-electron ruthenium.

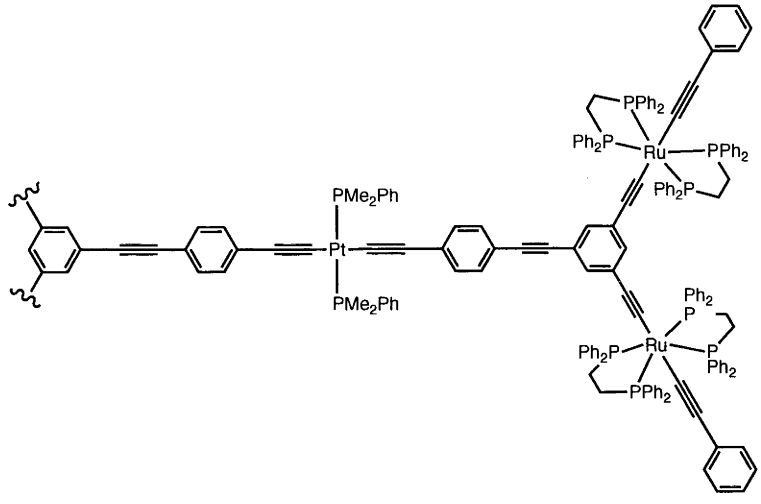

Figure 4.4. The heterobimetallic dendrimer formed by Powell and co-workers[5]

Another branched metal alkynyl complex that was utilised as a nonlinear optical switch was the cruciform ruthenium alkynyl complex formed by Dalton *et al.*(Figure 4.5).[6] This complex can be switched between three different states using the reversible Ru^{II}/Ru^{III} couple and the reversible protonation to the vinylidene complex. These three states all possessed different optical and nonlinear optical absorption properties.

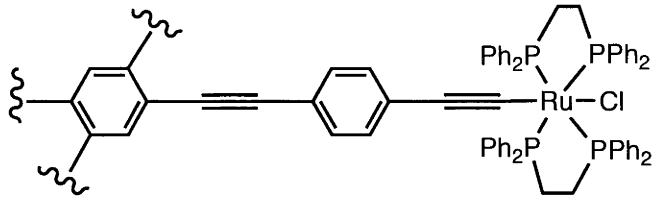

Figure 4.5. The cruciform ruthenium alkynyl complex synthesised by Dalton *et al.*[6]

4.2 Results and Discussion

4.2.1 Synthesis

To form 1,3,5-substituted benzene bimetallic complexes, complex **18** formed in Chapter 3 was desilylated using NBu^n_4F to afford *trans*-[Os(C≡C-4-C_6H_4I)(C≡CC_6H_4-4-C≡CH)(dppe)$_2$] (**30**) in 53% yield (Scheme 4.1). This complex has a pendent ethynyl group which can be coupled to a ruthenium centre, as well as an aryl-iodo which could be further functionalised via a Sonogashira reaction with an ethynyl moiety.

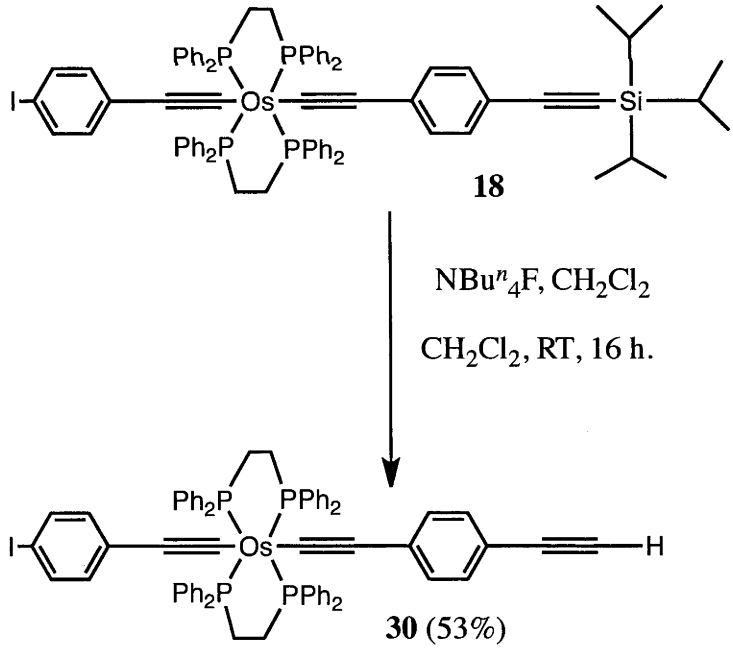

Scheme 4.1. Synthesis of *trans*-[Os(C≡C-4-C_6H_4I)(C≡CC_6H_4-4-C≡CH)(dppe)$_2$] (**30**).

Making use of the pendent ethynyl group, complex **30** can be coupled to 1,3,5-C_6H_3(C≡CC_6H_4-4-C≡CC_6H_4-4-C≡C-*trans*-[RuCl(dppe)$_2$])$_3$ to afford 1,3,5-C_6H_3(C≡CC_6H_4-4-C≡CC_6H_4-4-C≡C-*trans*-[Ru(dppe)$_2$]C≡CC_6H_4-4-C≡C-*trans*-[Os(dppe)$_2$]C≡C-4-C_6H_4I)$_3$ (**31**) in a 51% yield (Scheme 4.2).

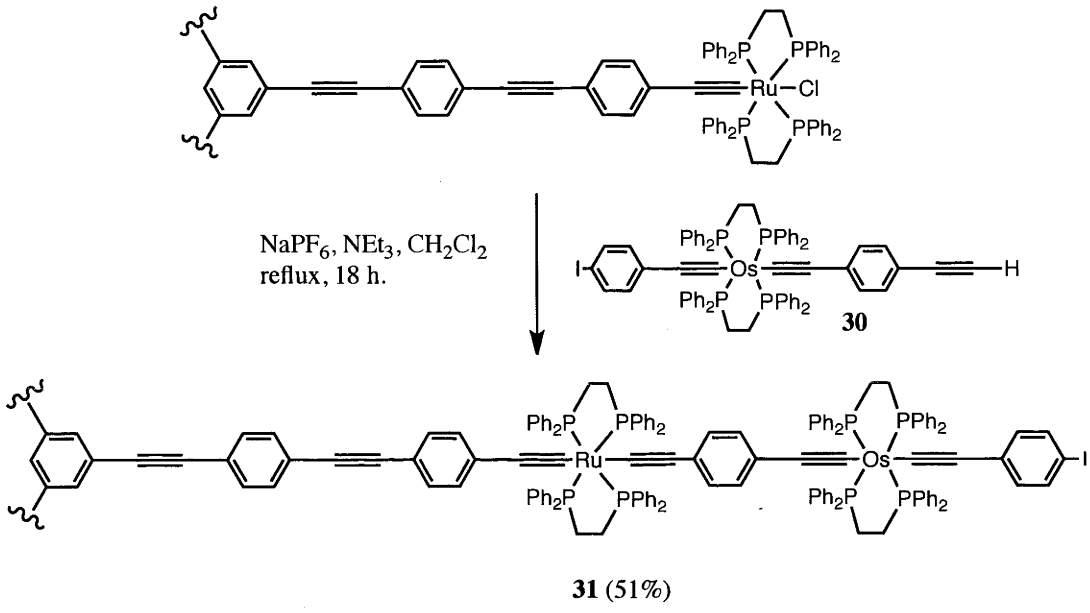

Scheme 4.2. Synthesis of **31**.

In a similar manner, **25** was coupled to the same 1,3,5-substituted ruthenium chloro-alkynyl complex to afford 1,3,5-C_6H_3(C≡CC_6H_4-4-C≡CC_6H_4-4-C≡C-*trans*-[Ru(dppe)$_2$]C≡CC_6H_4-4-C≡CC_6H_4-4-C≡C-*trans*-[Os(dppe)$_2$]C≡C-4-C_6H_4I)$_3$ (**32**) in 53% yield (Scheme 4.3). This complex is analogous to **31** except the longer triethynyl C≡CC_6H_4-4-C≡CC_6H_4-4-C≡C bridge separates the osmium and ruthenium metal centres in **32** rather than the shorter diethynyl C≡CC_6H_4-4-C≡C bridge in complex **31**. The formation of these two complexes should allow a greater understanding of the influence of the length of the bridge on the nonlinear optical properties.

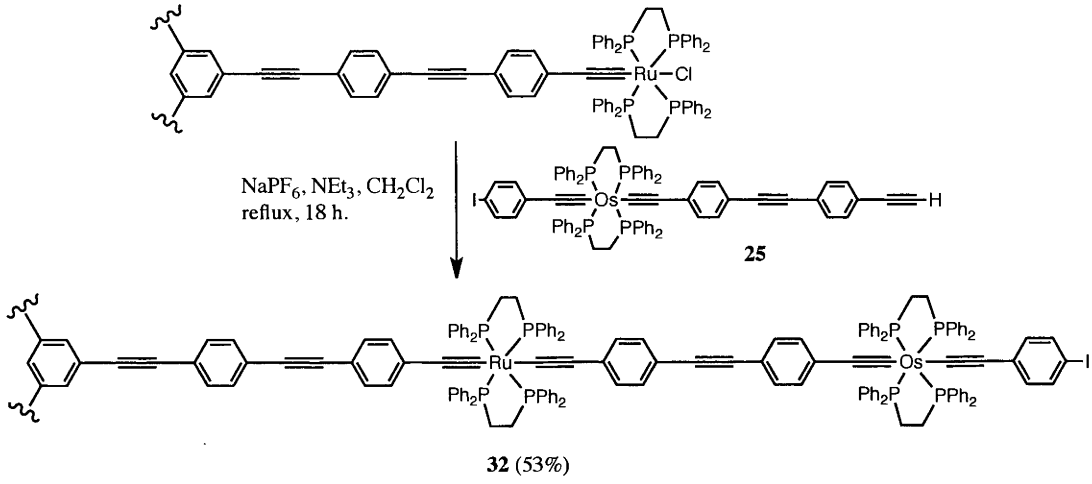

Scheme 4.3. Synthesis of **32**

Previously, it has been shown that increasing the branching points within 1,3,5 substituted benzene complexes to form dendrimers can lead to an increase in magnitude of the third-order nonlinear optical effects.[7,8] Although metal alkynyl dendrimers have been formed previously, they have either been monometallic[2,9,10] or multimetallic examples using metals without a reversible redox process[5], making them poor candidates for multistate nonlinear optical switches. It has been shown that metal centres with an 18 valence-electron configuration possess greater nonlinear optical effects than metal centres with less valence electrons, further limiting the choice of metals available for maximising the nonlinear optical effects.[8]

A phenylethynyl dendrimer incorporating both the *trans*-[Os(dppe)$_2$] and *trans*-[Ru(dppe)$_2$] metal centres was targeted in order to determine whether it could act as a multistate nonlinear optical switch. The formation of a branching point is possible by reacting a bulky metal centre such as *cis*-[RuCl$_2$(dppe)$_2$] with 1,3,5-(HC≡C)$_3$C$_6$H$_3$, where the steric bulk of the metal centre limits addition to only two of the three ethynyl sites;[11,12] this then allows further functionalization at the remaining ethynyl site to form a complex that can act as a branching point in dendrimers. With the analogous osmium metal centre possessing similar steric bulk, it was envisaged that a similar branching point could be formed under the same conditions. An excess of *cis*-[OsCl$_2$(dppe)$_2$] was reacted with 1,3,5-(HC≡C)$_3$C$_6$H$_3$ with the same conditions

used previously to form osmium chloro-alkynyl complexes, to afford 1-(HC≡C)C_6H_3-3,5-{C≡C-*trans*-[OsCl(dppe)$_2$]}$_2$ (**33**) in 74% yield (Scheme 4.4). Another target was the formation of a dendrimer incorporating osmium ammine-alkynyl metal centres. By having the cationic wedge incorporated in the dendrimer it was envisaged that the osmium metal centres would be more difficult to oxidise than the internal ruthenium metal centres affording two independent redox switches. To form the osmium ammine-alkynyl wedge, 1-(HC≡C)C_6H_3-3,5-{C≡C-*trans*-[OsCl(dppe)$_2$]}$_2$ (**33**) was stirred in the presence of NH_4PF_6 and NEt_3 in CH_2Cl_2 at room temperature for 24 h to afford [1-(HC≡C)C_6H_3-3,5-{C≡C-*trans*-[Os(NH_3)(dppe)$_2$]}$_2$](PF_6)$_2$ (**34**) in 51% yield (Scheme 4.4). Unfortunately oxidation of the metal centres in **34** (described fully elsewhere) was found to be irreversible, making formation of the dendrimer incorporating this wedge undesirable.

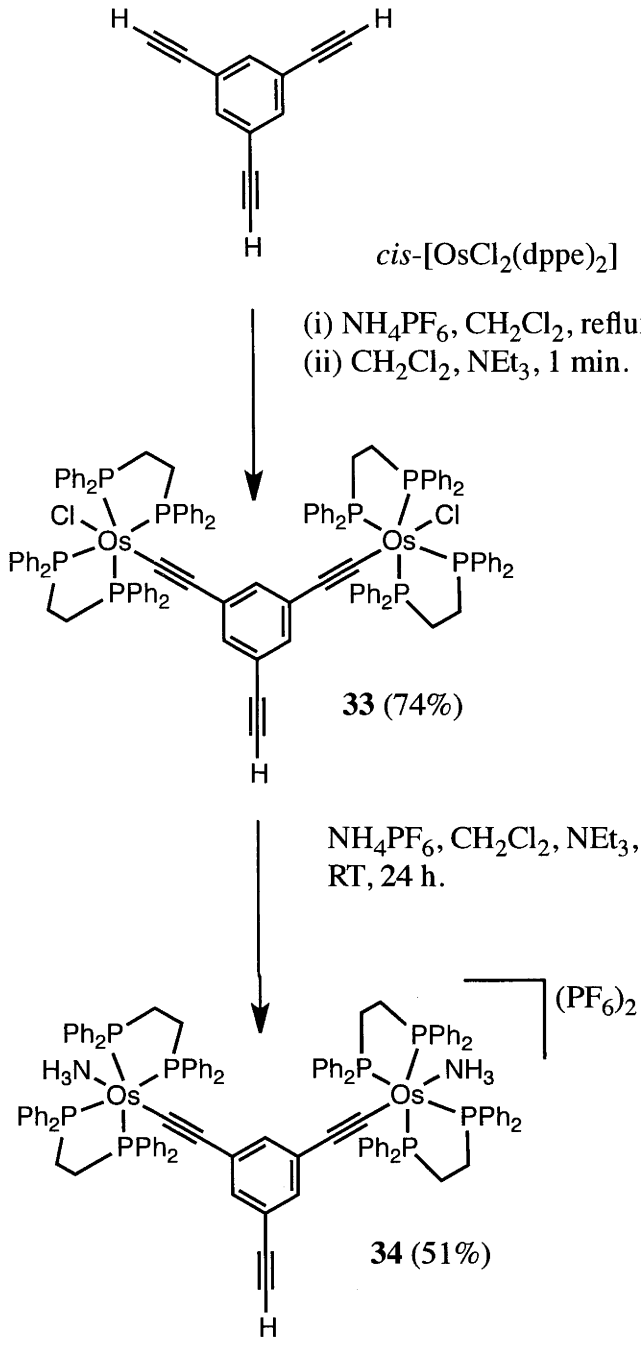

Scheme 4.4. Syntheses of complexes **33** and **34**

It has been shown that if a metal centre is resistant to the formation of bis-alkynyl complexes directly from a chloro-alkynyl complex such as *trans*-[MCl(C≡CR)(dppm)$_2$] (M = Ru or Os), then careful stoichiometric addition of

the metal centre to 1,3,5-$(HC{\equiv}C)_3C_6H_3$, will result in coupling of the metal centre to only one of the three ethynyl sites.[11] *Trans*-$[OsCl(C{\equiv}CR)(dppe)_2]$ complexes, unlike their ruthenium analogous, are resistant to bis-alkynyl formation, and addition of a stoichiometric amount to 1,3,5-$(HC{\equiv}C)_3C_6H_3$ gave 1,3-$(HC{\equiv}C)_2C_6H_3$-5-{C≡C-*trans*-$[OsCl(dppe)_2]$} (**35**) in 33% yield after 50 min (Scheme 4.5). The low yield for this reaction is more a reflection on the difficulty of purifying this very soluble product without the use of chromatography, where complexes of this type have exhibited instability, rather then the formation of a significant amount of di-substituted product (less then 20% by ^{31}P NMR).

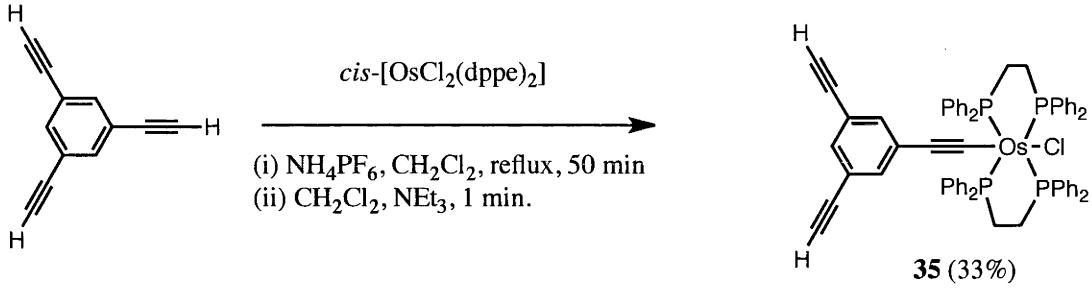

35 (33%)

Scheme 4.5 Synthesis of 1,3-$(HC{\equiv}C)_2C_6H_3$-5-{C≡C-*trans*-$[OsCl(dppe)_2]$} (**35**)

The bimetallic dendrimer was formed by coupling the ruthenium core 1,3,5-$C_6H_3(C{\equiv}CC_6H_4$-4-$C{\equiv}CC_6H_4$-4-C≡C-*trans*-$[Ru(dppe)_2]C{\equiv}CC_6H_4$-4-$C{\equiv}CC_6H_4$-4-$I)_3$ with the osmium wedge **33** via a Sonogashira reaction using a Pd(0)/CuI catalyst. The bimetallic dendrimer, **36**, was isolated in 34% yield, after refluxing in a NEt_3/CH_2Cl_2 mix (1:1) for 48 h (Scheme 4.6). The mixture of homo-coupled and unreacted wedge can be removed from the product by trituration with a petrol/CH_2Cl_2 (7:3) mixture.

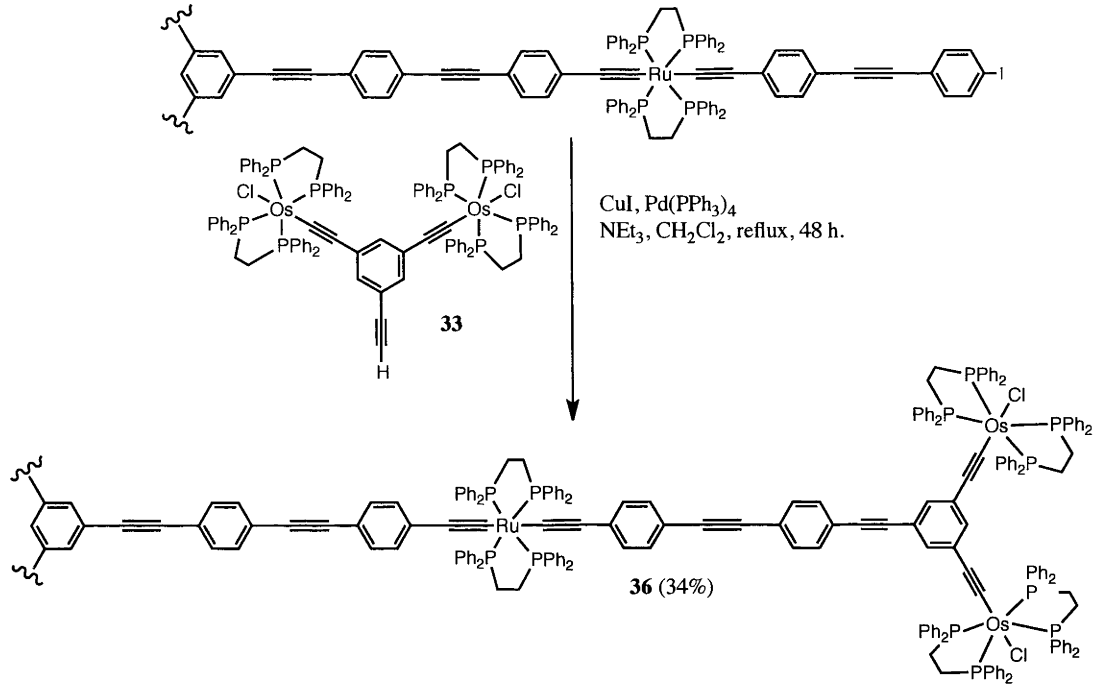

Scheme 4.6. Synthesis of **36**

The mononuclear wedge complex **35** can be coupled to 1,3,5-C_6H_3(C≡CC_6H_4-4-C≡CC_6H_4-4-C≡C-*trans*-[RuCl(dppe)$_2$])$_3$ using the conditions reported previously for the formation of ruthenium bis-alkynyl complexes; the steric bulk of the *trans*-[Ru(dppe)$_2$] and *trans*-[Os(dppe)$_2$] metal centres ensures coupling at only one of the two ethynyl sites on **35,** affording 1,3,5-{C≡CC_6H_4-4-C≡CC_6H_4-4-C≡C-*trans*-[Ru(dppe)$_2$]-1-C≡CC_6H_3-3-(C≡CH)-5-(C≡C-*trans*-[Os(dppe)$_2$]Cl)}$_3C_6H_3$ (**37**) in 71% yield (Scheme 4.7). Coupling in this manner leaves a pendent ethynyl group that can potentially be coupled to an organic molecule or a less bulky metal centre.

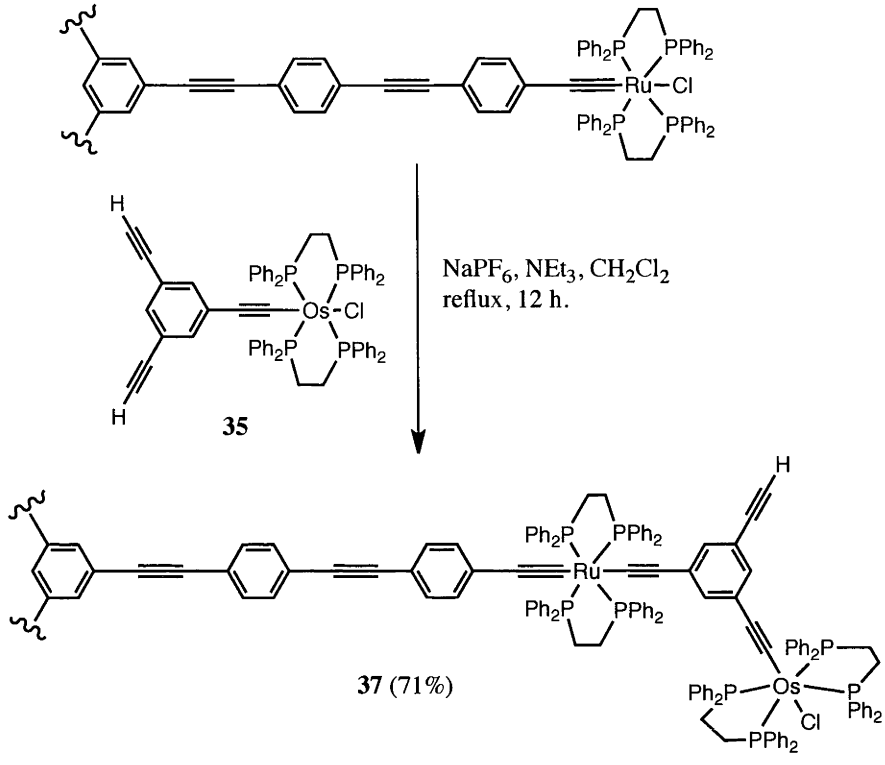

Scheme 4.7. Synthesis of **37**

Recently it has been shown that triarylamine-based dendrimers have very high two-photon absorption cross-sections, as well as instantaneous three-photon absorption.[2] A bimetallic triarylamine complex was targeted to determine whether these desirable properties could be switched between three states upon stepwise oxidation of the osmium and ruthenium metal centres. Complexes with the diethynyl (C≡CC$_6$H$_4$-4-C≡C) bridge have more intense changes in the optical spectra on oxidation of the metal centres compared to similar complexes containing the longer triethynyl (C≡CC$_6$H$_4$-4-C≡CC$_6$H$_4$-4-C≡C) bridge. For this reason, *trans*-[Os(C≡C-4-C$_6$H$_4$C≡CH)(C≡CC$_6$H$_4$-4-C≡CSiPr$^i_3$)(dppe)$_2$] (**21**) was coupled to N(C$_6$H$_4$-4-C≡C-*trans*-[RuCl(dppe)$_2$])$_3$, using the conditions used previously for the formation of ruthenium bis-alkynyl complexes, to afford N(C$_6$H$_4$-4-C≡C-*trans*-[Ru(dppe)$_2$]C≡CC$_6$H$_4$-4-C≡C-*trans*-[Os(dppe)$_2$]C≡CC$_6$H$_4$-4-C≡CSiPr$^i_3$)$_3$ (**38**) in 28% yield (Scheme 4.8).

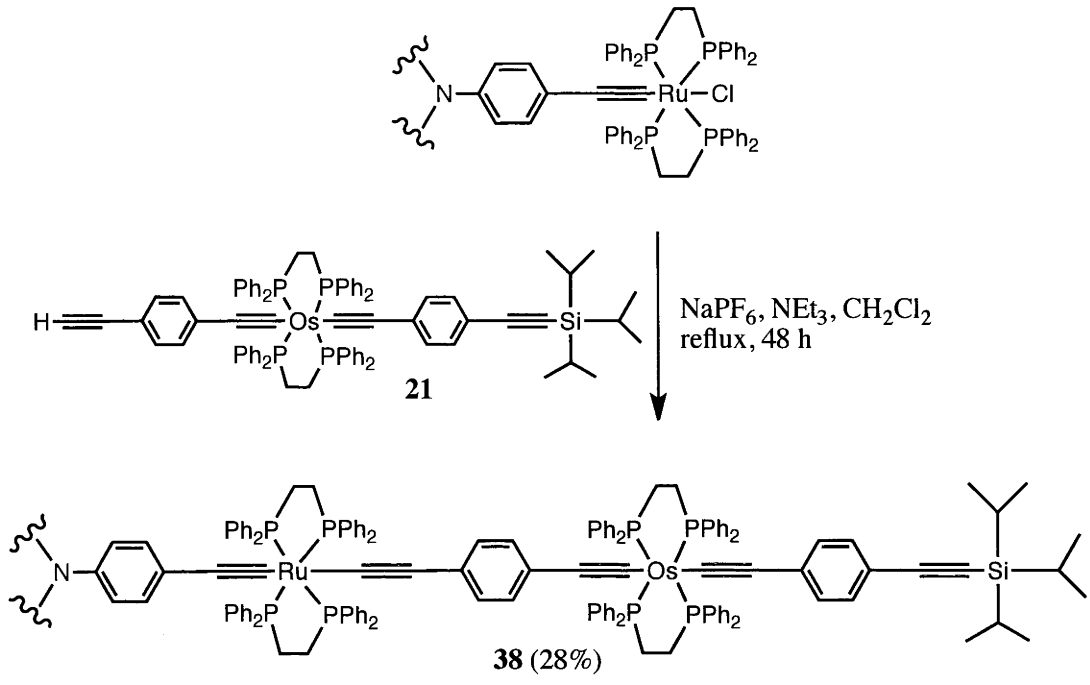

Scheme 4.8. Synthesis of 1,3,5-N(C_6H_4-4-C≡C-*trans*-[Ru(dppe)$_2$]C≡CC_6H_4-4-C≡C-*trans*-[Os(dppe)$_2$]C≡CC_6H_4-4-C≡CSiPr^i_3)$_3$ (**38**)

4.2.2 Physical Properties

4.2.2.1 NMR Spectroscopy

Complexes **30** – **38** were characterised by ^{1}H and ^{31}P NMR spectroscopy (Table 4.1). In addition, ^{13}C NMR spectroscopy has been used to characterise the homometallic complexes **30**, **33** and **35**, with peaks assigned where possible and displayed in Appendix C. The bimetallic complexes **31**, **32**, **36** - **38** and homometallic ammine complex (**34**), proved insufficiently soluble for useful ^{13}C NMR spectra to be obtained.

^{1}H NMR

The neutral complexes (**31** – **33** and **35** – **38**) have multiplets in the range of 7.90 – 6.41 ppm corresponding to aromatic protons and multiplets in the range of 2.83 – 2.49 ppm corresponding to the dppe bridgehead protons. For **35,** the range for the aromatic protons is larger as shown previously for ammine-alkynyl complexes, with multiplets in the range of 8.14 – 6.38 ppm. Complex **35** also has a multiplet at 2.62 ppm for dppe bridgehead protons, and a broad resonance at 0.99 ppm for the ammine protons. For complexes with acetylenic protons (**30**, **33**, **34**, **35** and **37**) a resonance in the range 3.16 – 3.12 ppm ($CDCl_3$) or 2.91 - 2.82 ppm (C_6D_6) is visible. Complex **38** also has a pseudo-singlet at 1.23 ppm (C_6D_6) corresponding to the methyl protons of the $SiPr^{i}_3$ group with the heptet corresponding to the methyne proton not visible, as discussed previously in Chapter 2.

^{31}P NMR

Resonances from the ^{31}P NMR spectra of complexes **30** – **38** are shown in Table 4.1. All complexes show similar peaks to those described in Chapters 2 and 3 for osmium- and ruthenium- bound phosphorus atoms. An interesting observation is that, for the osmium chloro-alkynyl wedge **33** and dendrimers **36** and **37**, the resonance for the osmium bound phosphorus atoms (16.5 – 16.6 ppm) is the same as for the phosphorus atoms in the complexes incorporating an osmium bis-alkynyl environment (**30** – **32** and **38**). However, for the mononuclear chloro-alkynyl complex **35** the resonance is at 16.0 ppm, matching the previously observed data for these complexes in Chapters 2 and 3.

Complex	Solvent	OsP (ppm)	RuP (ppm)
30	$CDCl_3$	16.6	—
31	C_6D_6	16.6	54.2
32	C_6D_6	16.6	54.1
33	C_6D_6	16.6	—
34	$CDCl_3$	19.6	—
35	C_6D_6	16.0	—
36	C_6D_6	16.5	54.0
37	C_6D_6	16.5	54.5
38	C_6D_6	16.4	54.4

Table 4.1. ^{31}P NMR spectral resonances for complexes **30** – **38**, measured in $CDCl_3$ or C_6D_6

4.2.2.2 UV-Vis absorption spectroscopy

The extinction coefficients of the absorption bands are greatly enhanced on moving from the linear complexes described in Chapters 2 and 3 to branched structures incorporating more metals. The mononuclear **30** has λ_{max} at 373 nm, with ε = 58000, whereas the hexanuclear complex **31**, has absorption bands at λ_{max} = 344 and 386 nm, and a shoulder at λ_{max} = 417 nm, with ε = 220000, 221000 and 145000, respectively (Figure 4.6). On moving to the hexanuclear complex with the longer triethynyl ($C{\equiv}CC_6H_4$-4-$C{\equiv}CC_6H_4$-4-$C{\equiv}C$) bridge between the osmium and ruthenium metal centres (**32**), the lowest energy band is red shifted, with two main absorption bands at λ_{max} = 334 and 428 nm and an increase in the intensity of the lowest energy band with ε = 269000 (Figure 4.6).

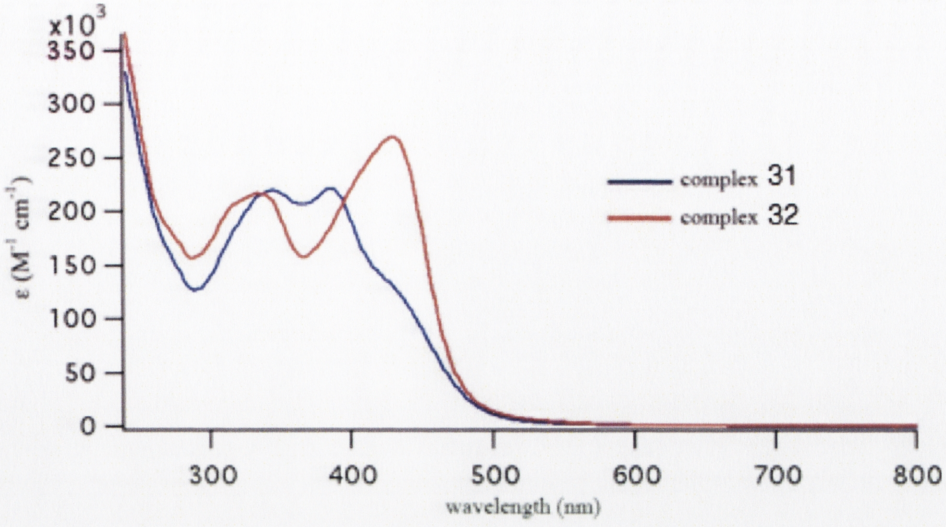

Figure 4.6. UV-Vis absorption spectrums of complexes **31** and **32**

The UV-Vis absorption spectra of wedge complexes **33**, **34** and **35** were measured in CH_2Cl_2, with absorption bands within the range of 352 – 321 nm (Figure 4.7). On going from the mononuclear complex **35** to the binuclear complexes **33** and **34,** a doubling of intensity is observed. On forming the ammine-alkynyl complex **34** from the chloro-alkynyl complex **33**, a blue shift is observed from 340 nm to 321 nm (Figure 4.7). This matches the earlier observations made in Chapter 3 for other chloro-alkynyl and ammine-alkynyl complexes.

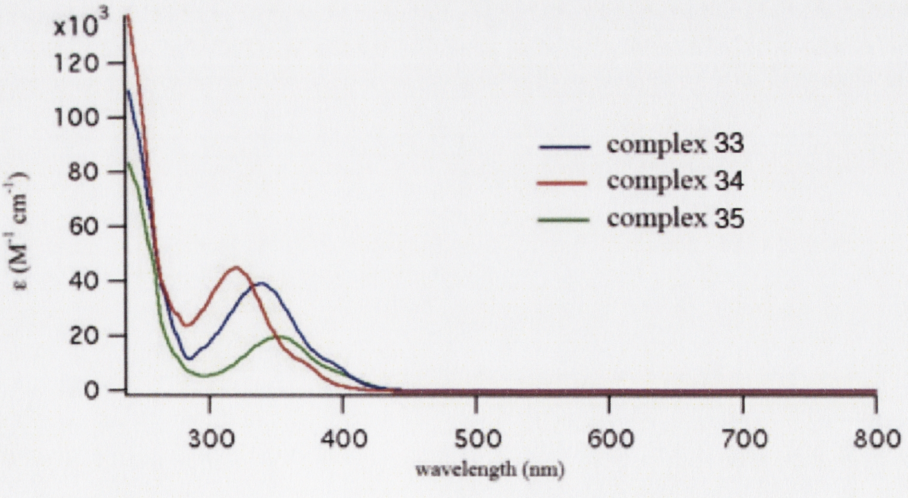

Figure 4.7. UV-Vis absorption spectra of complexes **33**, **34** and **35**

The two dendrimers **36** and **37** have similar absorption bands, with those for the larger and more metallated **36** being more intense. Both complexes have two dominant absorption bands at 334 and 423 nm for **36**, and 336 and 420 nm for **37**, with the higher-energy band being much more intense in both cases. Complex **38** has an interesting absorption spectrum compared to the other branched systems as it has only one relatively narrow absorption band compared to the two for **31**, **32**, **36** and **37**. This band has a λ_{max} = 391 nm, and is very intense, with ε = 340000.

4.2.2.3 Infrared spectroscopy

The IR spectra for complexes **30** – **38** as CH_2Cl_2 solutions showed a broad band in the range of 2064 – 2051 cm^{-1} for ν(C≡C). In addition to this band, complexes **30**, **33**, **34**, **35** and **37** had a band within the range of 3294 – 3303 cm^{-1} for ν(≡CH). For complex **38**, a band at 2146 cm^{-1} was assigned to ν(C≡C-Si). As shown previously, on moving from a chloro-alkynyl complex (**33**) to an ammine-alkynyl complex (**34**), a slight blue shift in ν(C≡C) is seen from 2054 to 2064 cm^{-1}.

4.2.2.4 Electrochemistry

The electrochemical properties of complexes **30** – **38** were measured as THF solutions, using cyclic voltammetry. For the mononuclear complexes **30** and **35**, a reversible process (due to the $Os^{II/III}$ redox couple) at 0.51 V and 0.54 V, respectively is observed (Table 4.2). On coupling **30** to a triruthenium core complex to form the heterometallic dendritic complex (**31**), electron donation from the ruthenium metal centres across the short diethynyl (C≡CC_6H_4-4-C≡C) bridge results in a decrease of the $Os^{II/III}$ redox potential to 0.24 V. On forming the hexanuclear heterometallic complex with the triethynyl unit separating the osmium and ruthenium metal centres (**32**), we can see once again a reduction in the $Os^{II/III}$ redox couple (0.39 V) compared to the mononuclear osmium precursor (0.51 V), however it is significantly higher than the same oxidation in the diethynyl bridged dendrimer (**31**). The reduced ease of

the osmium oxidation is accounted for by the reduced donating ability of the ruthenium metal centre across the longer triethynyl ($C{\equiv}CC_6H_4$-4-$C{\equiv}CC_6H_4$-4-$C{\equiv}C$) bridge.

For the binuclear wedge complexes **33** and **34**, two-redox potentials are observed indicating that some electronic communication is possible across the $C{\equiv}CC_6H_4$-3-$C{\equiv}C$ bridging unit; as expected, the dicationic **34** is harder to oxidise. The redox potentials for **34** are irreversible, thus making it unsuitable for nonlinear optical switching. The heterometallic dendrimer **36** has three well-separated redox potentials; the first two at 0.37 and 0.52 V can be assigned to osmium metal centre oxidation and match potentials determined for the precursor wedge **33**. The third potential at 0.62 V can be assigned to the three ruthenium metal centre oxidations.

For the smaller hexanuclear heterometallic dendrimer **37**, two processes were observed; the first process at 0.43 V can be assigned to the osmium metal oxidations, and the second process at 0.71 V to the ruthenium metal oxidations. The osmium centres are easier to oxidise compared to the precursor (**35**), suggesting that the ruthenium metal centre is able to donate electron-density across the $C{\equiv}CC_6H_4$-3-$C{\equiv}C$ bridge, although the increased ease of oxidation is much less than in the complexes with the *para* substituted $C{\equiv}CC_6H_4$-4-$C{\equiv}C$ bridge.

For the N-cored heterometallic dendrimer **38**, two processes are observed; the first assigned to oxidation of the osmium centres is found at 0.30 V, and the second assigned to the ruthenium oxidation is at 0.57 V. Although a process assigned to the amine oxidation at higher potential is expected this was not observed for **38**. Comparing **38** to the aryl cored complex **31**, which has the same diethynyl ($C{\equiv}CC_6H_4$-4-$C{\equiv}C$) bridge between osmium and ruthenium metal centres, shows some interesting results. Whilst the ruthenium process occurs at the same potential for both of these complexes, oxidation of the osmium centres occurs at a slightly higher potential in **38** than in **31**. Although there are a number of structural differences between the two complexes, it does suggest that the peripheral ligands

can have an observable impact on the electronic properties of these bridged systems. Another interesting observation for **38** is that, although the precursor ruthenium complex possesses four distinct redox processes, one for each ruthenium centre, as well as one at higher potential for the ammine[13], in **38** this is not the case, with all three osmium centres and all three ruthenium centres being oxidised simultaneously (Table 4.2).

Complex	$E_{1/2}$ (V) [i_{pc}/i_{pa}] $Os^{II/III}$	$E_{1/2}$ (V) [i_{pc}/i_{pa}]$Ru^{II/III}$	$E_{1/2}$ $Ru^{II/III}$ - $E_{1/2}$ $Os^{II/III}$ (V)
30	0.51 [1]	—	—
31	0.24[1]	0.57[1]	0.33
32	0.39[1]	0.59[1]	0.20
33	0.36 [1], 0.51 [1]	—	—
34	0.89 irr., 1.04 irr.	—	—
35	0.54 [1]	—	—
36	0.37 [1], 0.52 [1]	0.62 [1]	0.26, 0.11
37	0.43 [1]	0.71 [1]	0.28
38	0.30 [1]	0.57 [1]	0.27

Table 4.2. Cyclic voltammetric data for complexes **30** – **38**. THF solvent, Pt disk working-, Pt wire auxiliary-, and Ag/AgCl reference electrodes, ferrocene/ferrocenium couple at 0.56 V [1]. ΔE_p of samples approximately matched that of the ferrocene/ferrocenium couple.

4.2.2.5 Spectroelectrochemistry

Spectroelectochemical studies were carried out on the heterometallic dendrimer complexes **31**, **32** and **38** as THF solutions in an OTTLE cell at room temperature.

The hexanuclear complexes with a diethynyl ($C{\equiv}CC_6H_4$-4-$C{\equiv}C$) bridge between the osmium and ruthenium centres (**31** and **38**) show similar behaviour (Figures 4.8 and 4.10). On oxidation of the osmium metal centre for both complexes the absorption band for the neutral species decreases in intensity and low energy bands appear at 6353 and 20315 cm^{-1} for **31** and 6253 and 20035 cm^{-1} for **38**. The second oxidation process at the ruthenium metal centre results in the lowest energy band undergoing a blue shift to 9823 cm^{-1} for **31** and 9878 cm^{-1} for **38** and the band at ca 20000 cm^{-1} for both complexes disappearing. One major difference between **31** and **38** is that oxidation of ruthenium, in **31**, results in the intensity of the lowest energy band increasing from ε = 85000 to 150000 M^{-1} cm^{-1}, whereas for **38** very little change in intensity is observed (ε = 160000 to 162000 M^{-1} cm^{-1}). For complex **32,** where the longer triethynyl ($C{\equiv}CC_6H_4$-4-$C{\equiv}CC_6H_4$-4-$C{\equiv}C$) bridge separates the osmium and ruthenium metal centres, oxidation of the osmium metal centre results in a very broad low energy band with λ_{max} = 9945 cm^{-1}, while oxidation of the ruthenium metal centre results in the formation of two bands at low energy (ν_{max} = 8000 and 9565 cm^{-1}). Spectroelectrochemical studies were also carried out on the dendrimers **36** and **37**, however these processes proved irreversible at room temperature.

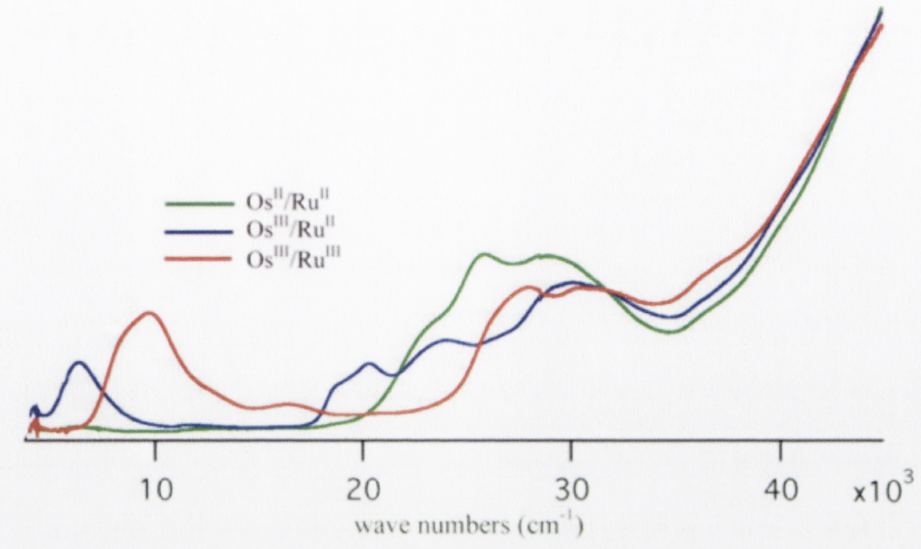

Figure 4.8. UV-Vis-NIR spectral changes during electrochemical oxidation of **31**.

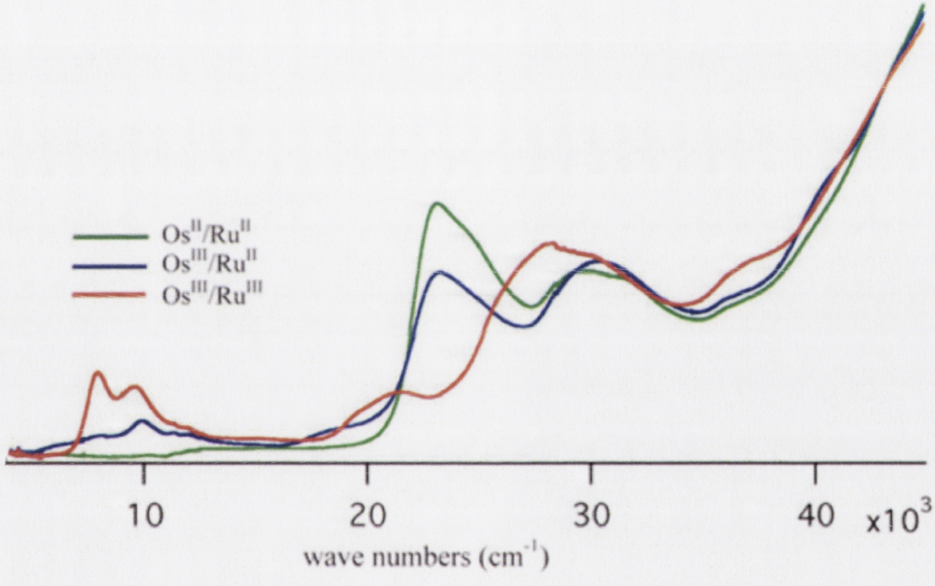

Figure 4.9. UV-Vis-NIR spectral changes during electrochemical oxidation **32**.

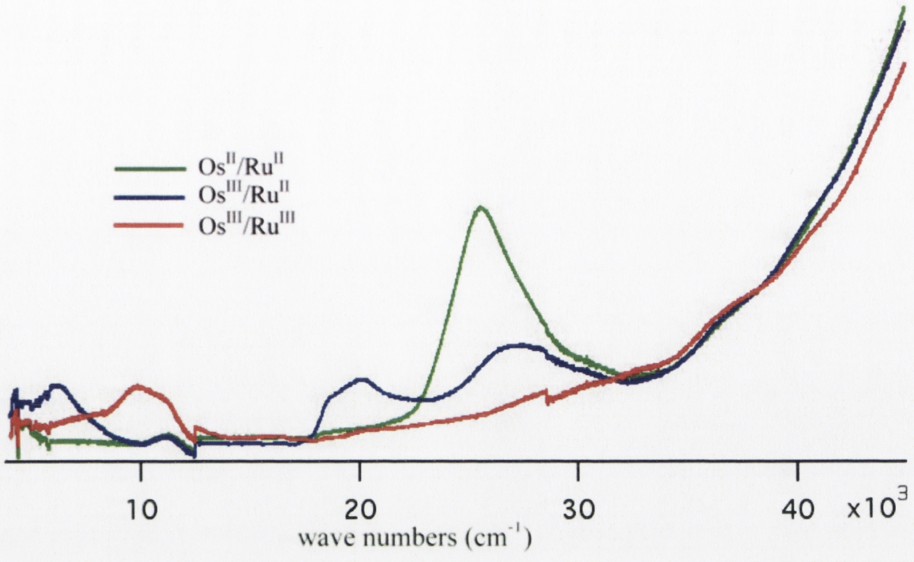

Figure 4.10. UV-Vis-NIR spectral changes during electrochemical oxidation of **39**.

Complex	ν_{max} (cm^{-1}) [ε] (10^4 M^{-1} cm^{-1})
31	25906 [22.1], 29940 [22.0]
31$^+$	6353 [8.5], 20315 [9.2], 23991 [12.9], 30395 [18.9]
31^{2+}	9823 [15.0], 16511 [4.1], 28105 [18.1], 30548 [18.1]
32	23364 [26.9], 29994 [21.9]
32$^+$	9945 [3.9], 23415 [19.4], 30495 [20.3]
32^{2+}	8000 [8.8], 9565 [7.4], 21641 [6.9], 28505 [21.8],
38	25625 [34.0]
38$^+$	6253 [16.0], 18628 [14.6], 20035 [16.6], 27515 [20.0]
38^{2+}	9878 [16.2], 16300 [11.4], 36592 [24.4]

Table 4.3. Summary of optical data for complexes **31**, **32** and **38**. Electronic spectra were obtained at 298 K in THF using 0.3 M (NBu^n_4)PF_6 as supporting electrolyte with potentials ca 50-200 mV beyond $E_{1/2}$ for each couple.

4.2.2.6 Nonlinear optical study

The third-order nonlinear optical (NLO) properties of a selection of the heterometallic complexes formed in this work were measured using the Z-scan technique (cf. Chapter 1) in order to determine the real and imaginary components of the third-order molecular susceptibilities (γ_{real}, $\gamma_{imaginary}$), as well as the two-photon absorption cross-section (σ_2). A small amount (1 drop) of NEt_3 was added to CH_2Cl_2 solutions of each complex to prevent the decomposition that has been observed previously (cf. discussion in Chapter 3). The complexes that were investigated include linear and star-shaped heterometallic complexes with the diethynyl ($C{\equiv}CC_6H_4$-4-$C{\equiv}C$) and triethynyl ($C{\equiv}CC_6H_4$-4-$C{\equiv}CC_6H_4$-4-$C{\equiv}C$) bridges separating the osmium and ruthenium centres (**7**, **24**, **31**, **32**), as well as the trinuclear complex (**29**), N-cored heterometallic complex (**38**) and nonanuclear heterometallic dendrimer (**36**) (Figure 4.11).

Off-resonant measurements were carried out at 530, 555, 800, 1200 and 1500 nm using 130 fs pulses with repetition rate 1kHz in order to limit observations to the instantaneous two-photon-absorption processes (no excited-state contributions). In contrast to reports on similar ruthenium complexes,[2,8,14] all of the complexes measured here showed photochemical instability when exposed to the beam, as evidenced by a coloured spot observed under the focussed beam from the laser. This decomposition was observed at all of the wavelengths except 530 nm, where only complex **36** was unstable. The photochemical decomposition was such that accurate values were not able to be obtained, so discussion will be limited to the 530 nm values.

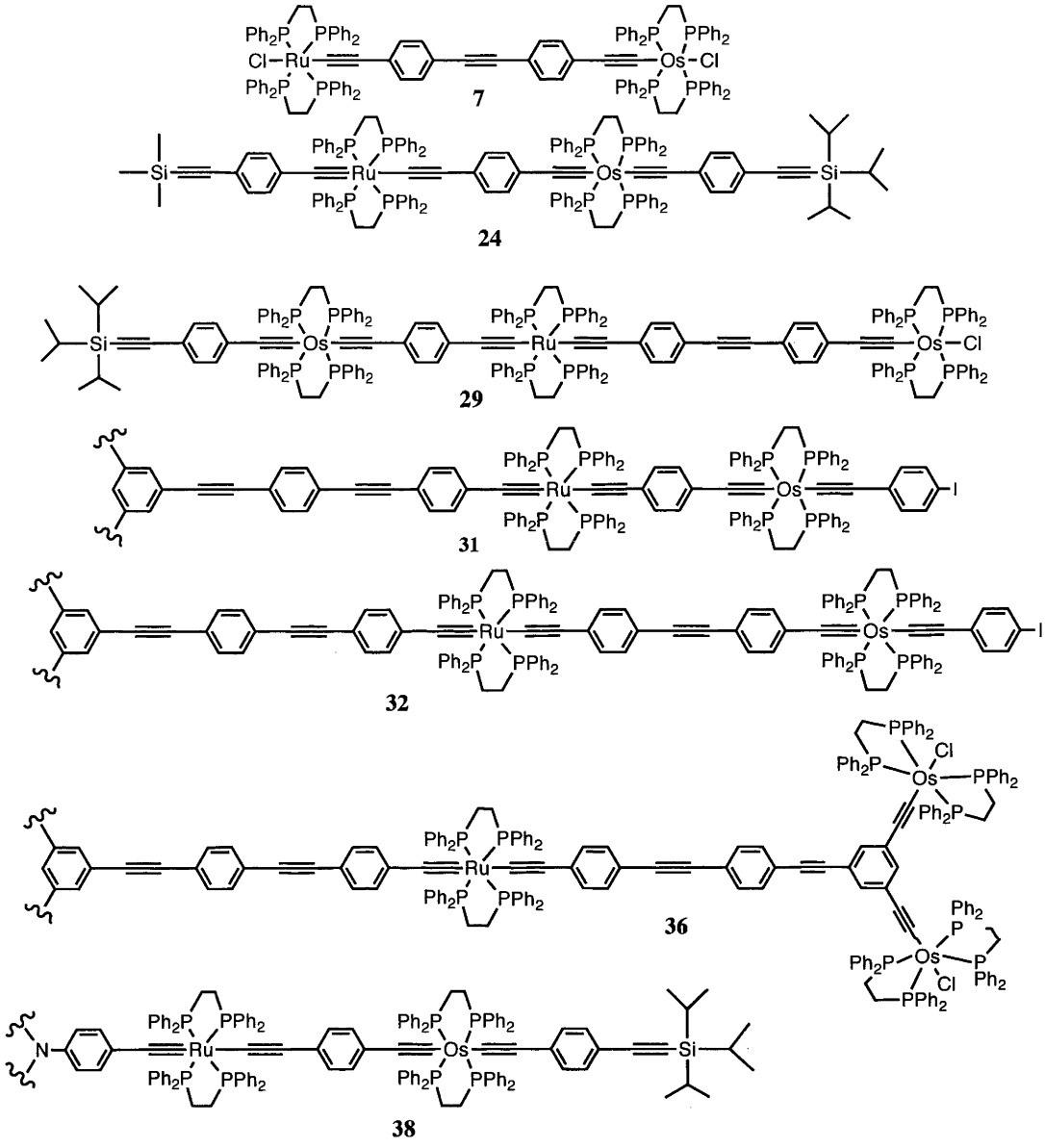

Figure 4.11 Complexes investigated using the Z-scan technique.

Although no photochemical instability was observed at 530 nm for all the complexes except **36**, the data still needs to be carefully examined to determine whether a good theoretical fit is able to be obtained, and whether any deviation from the theoretical fit is observed (evidence of instability). For complexes **24** and **31** good correlation was obtained with very little deviation from the open aperture theoretical fit, allowing the data to be considered accurate (within the error margin) (Figures 4.12 – 4.15). For complexes **7**, **29**, **32** and **38** a small deviation from the theoretical fit

occurred past the focal point and suggests the presence of a small amount of photochemical instability, allowing accurate values to be obtained, however, with the caveat that the complexes are partially unstable at 530 nm.

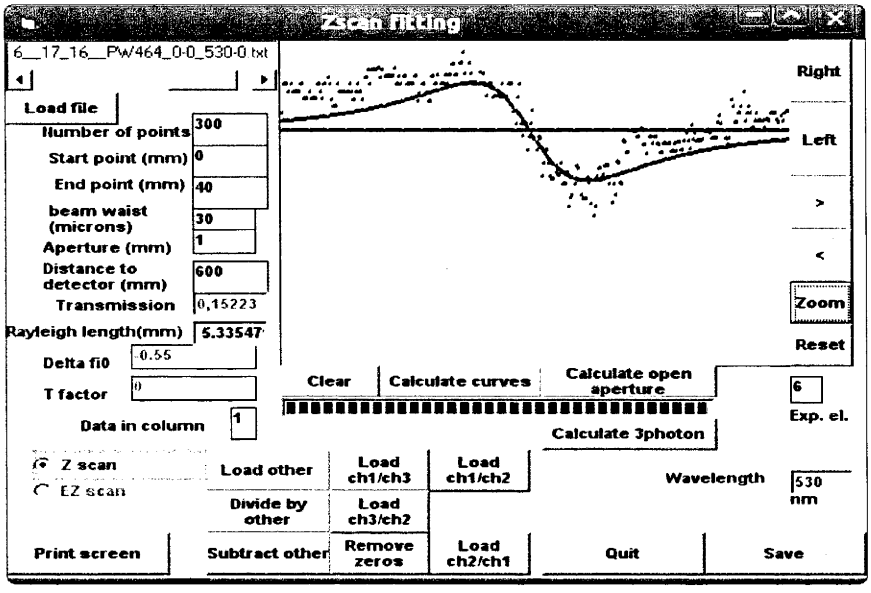

Figure 4.12 Z-scan closed aperture trace and theoretical fit for **24** at 530 nm.

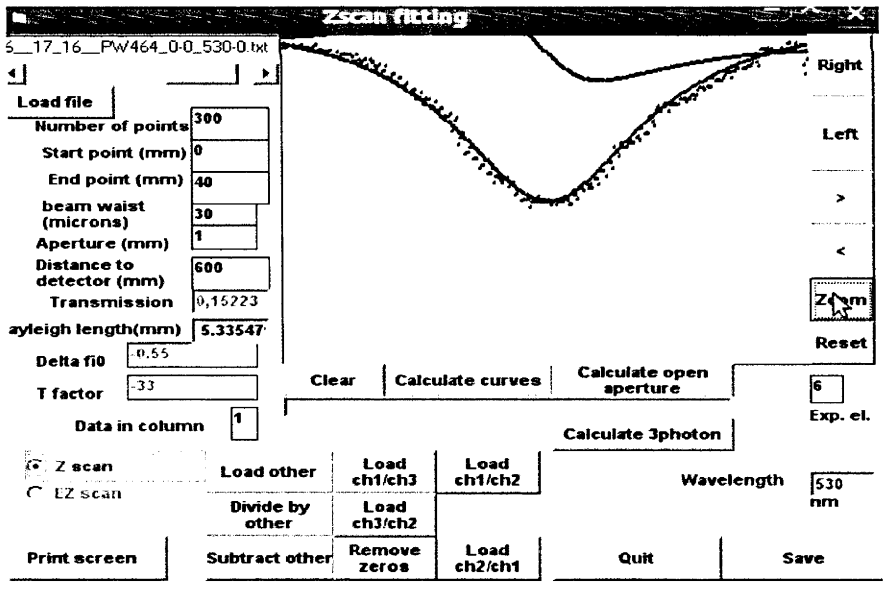

Figure 4.13 Z-scan open aperture trace and theoretical fit for **24** at 530 nm.

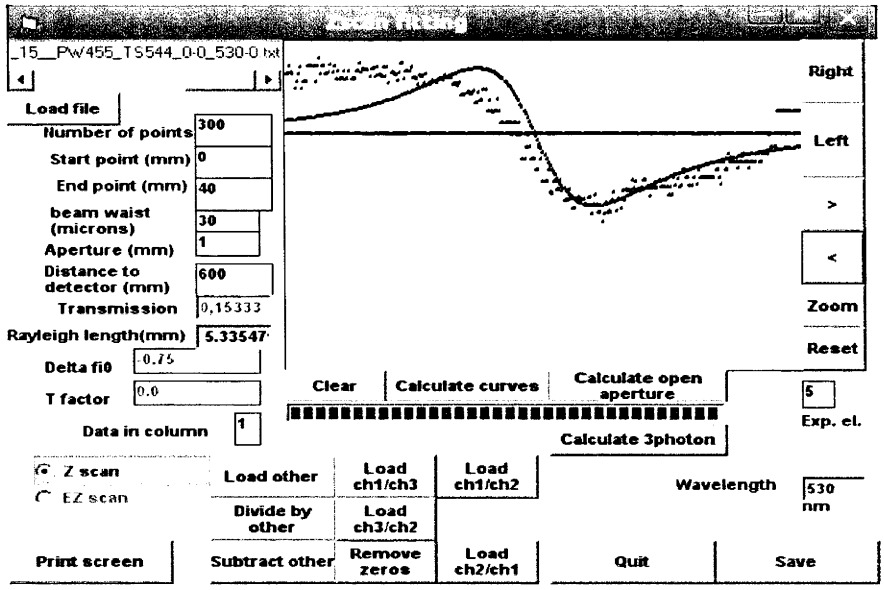

Figure 4.14 Z-scan closed aperture trace and theoretical fit for **31** at 530 nm.

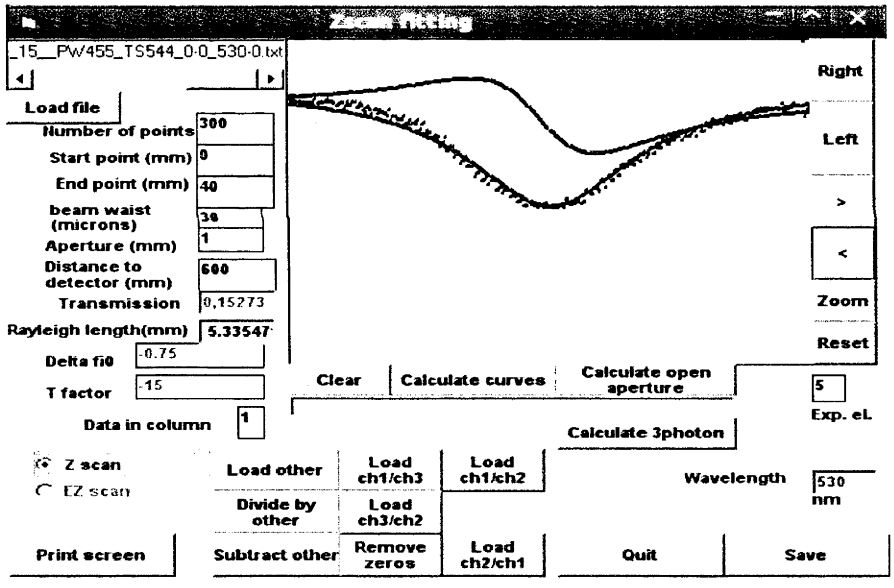

Figure 4.15 Z-scan open aperture trace and theoretical fit for **31** at 530 nm.

For complex **36,** where photochemical instability was observed experimentally, the open aperture scan shows significant deviation from the theoretical fit past the focal point precluding the determination of accurate values (Figure 4.16).

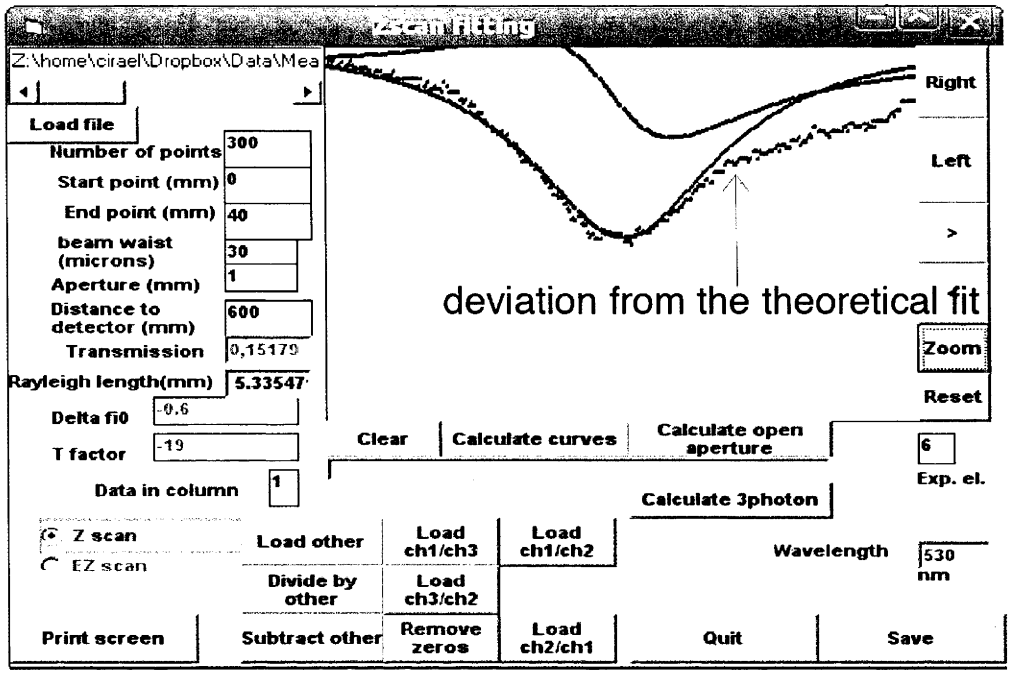

Figure 4.16 Z-scan open aperture trace and theoretical fit for **36** at 530 nm.

Third-order NLO parameters (γ_{real}, $\gamma_{imaginary}$ and σ_2) were calculated along with the associated errors and collected in Table 4.4.

Complex	γ_{real} (esu) x 10^{-32}	$\gamma_{imaginary}$ (esu) x 10^{-32}	σ_2 (GM) x 10^4	Comments
7	-5.40 ± 0.179	2.93 ± 0.253	1.62 ± 0.140	minor instability
24	-6.29 ± 0.216	7.22 ± 0.527	3.99 ± 0.292	good data
29	-9.79 ± 0.334	6.86 ± 0.629	3.80 ± 0.348	minor instability
31	-22.3 ± 1.94	13.5 ± 1.92	7.45 ± 1.07	good data
32	-27.4 ± 0.865	21.3 ± 1.94	11.79 ± 1.08	minor instability
38	-23.8 ± 4.01	16.7 ± 4.08	9.23 ± 2.25	minor instability

Table 4.4 Third-order NLO data for complexes **7**, **24**, **29**, **31**, **32** and **38** at 530 nm.

As discussed in Chapter 1, it is not possible to compare the magnitude of the NLO response between complexes only measured at a single wavelength, as it is not known whether this corresponds to ≤ the maximum NLO response. It is possible to compare the values obtained here with other data obtained at multiple wavelengths provided it is recognised that the complexes measured at a single wavelength may have a higher maximum NLO response at a wavelength other than 530 nm. A variety of linear and branched ruthenium alkynyl complexes measured over a spectrum of wavelengths were chosen as comparison complexes (Figure 4.17 and Table 4.5).

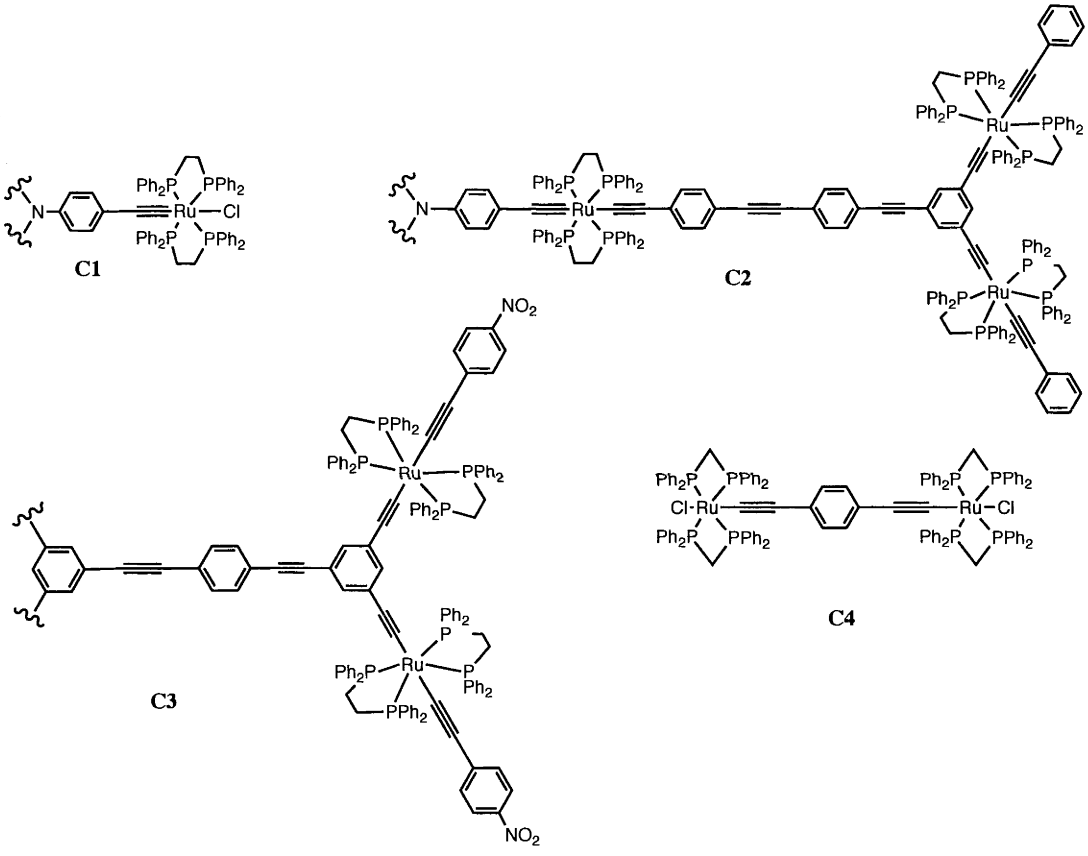

Figure 4.17 Ruthenium alkynyl complexes chosen from the literature[2,8,14] for comparison.

Complex	γ_{real} (esu) x 10^{-32} (λ_{max} [nm])	$\gamma_{imaginary}$ (esu) x 10^{-32} (λ_{max} [nm])	σ_2 (GM) x 10^4 (λ_{max} [nm])	reference
C1	-1.0 (600)	2.0 (530, not used for σ_2 calculation)	0.1720 (606)	2
C2	-3.7 (600)	3.0 (580)	1.06 (582)	2
C3	-2.8 (700)	λ_{max} not given -0.62 at 800 nm	-0.5 (760)	8
C4	0.1 (690)	0.21 (630)	0.06 (630)	14

Table 4.5 Third-order NLO parameters for ruthenium alkynyl complexes from the literature

A comparison between the linear complexes **C4** and **7**, **24** and **29** show over an order of magnitude increase in all three third-order parameters (γ_{real}, $\gamma_{imaginary}$ and σ_2). For **24**, which has the same bridge between metal centres as **C4**, the σ_2 increases by almost two orders of magnitude. It should be noted again that the values obtained for the osmium-containing complexes here are not necessarily the maxima but are ≤ to the maxima. It is also interesting to note that the osmium-containing linear complexes have higher values for all third-order parameters when compared to all of the ruthenium-containing comparison complexes (**C1** – **C4**), with the largest reported σ_2 (**C2**) approximately 25% of the σ_2 for the linear complex **24**. Unsurprisingly, the branched osmium-containing complexes have even higher NLO parameters than the linear structures, although no trends can be drawn as only one wavelength gave valid values. It is clear from the limited amount of data that has been collected that a significant increase in the third-order NLO response is produced on replacing ruthenium with osmium in these types of metal alkynyl complexes. Further studies, perhaps using a solvent system that can stabilize the complexes under examination is required before further trends can be drawn or switching studies carried out.

4.3 Conclusions

A series of branched metal alkynyl complexes containing ruthenium and osmium metal atoms have been synthesised and demonstrated to be suitable three-state optical switches with significant difference in the optical absorption properties of each of the states. The third-order NLO properties of several of these branched complexes, as well as some linear complexes formed in Chapters 2 and 3, have been measured using the Z-scan technique. All of the complexes showed photochemical instability at 580, 800, 1200 and 1500 nm under the conditions used. At 530 nm all of the complexes measured, except the osmium-ruthenium dendrimer **36**, produced valid results with no observed photochemical instability and very little deviation from the theoretical fit used to obtain values. In particular, complexes **24** and **31** showed no evidence of any photochemical instability in the data or measurement at 530 nm. The magnitude of the values for the NLO parameters at this wavelength suggest that incorporation of osmium into metal alkynyl complexes results in significant increase in the third-order NLO properties. Measurements where the complexes are stable over broad-spectrum wavelength studies are required before trends can be drawn from the data and switching carried out.

4.4 Experimental section

4.4.1 General

All reactions were performed under a nitrogen atmosphere using standard Schlenk techniques, with no precautions to exclude air during workup. CH_2Cl_2 was dried by distilling over calcium hydride, THF was distilled over sodium/benzophenone, and all other solvents were used as received. The term ''petrol'' refers to a fraction of petroleum ether of boiling range 60-80 °C. Column chromatography was performed using Sigma-Aldrich aluminium oxide (activated, basic, Brockmann 1, standard grade ca 150 mesh, 58 Å). Solvents and reagents were obtained from commercial sources and used as received, unless otherwise indicated. The following additional

materials were prepared according to literature procedures and were provided by Mr Torsten Schwich: $N(C_6H_4\text{-}4\text{-}C{\equiv}C\text{-}\textit{trans}\text{-}[RuCl(dppe)_2])_3$[2] and $1,3,5\text{-}(HC{\equiv}C)_3C_6H_3$.[15] The following new materials were provided by Mr Torsten Schwich: $1,3,5\text{-}C_6H_3(C{\equiv}CC_6H_4\text{-}4\text{-}C{\equiv}CC_6H_4\text{-}4\text{-}C{\equiv}C\text{-}\textit{trans}\text{-}[RuCl(dppe)_2])_3$, $1,3,5\text{-}C_6H_3(C{\equiv}CC_6H_4\text{-}4\text{-}C{\equiv}CC_6H_4\text{-}4\text{-}C{\equiv}C\text{-}\textit{trans}\text{-}[Ru(dppe)_2]C{\equiv}CC_6H_4\text{-}4\text{-}C{\equiv}CC_6H_4\text{-}4\text{-}I)_3$. All other materials were used as received.

4.4.2 Instrumentation

Electrospray ionisation mass spectra (ESIMS) were obtained using a Waters-micromass LCT-ZMD single quadrupole liquid chromatograph; peaks are reported as *m/z* (assignment, relative intensity). Microanalyses were carried out by the Microanalysis Service Unit, Australian National University. Infrared spectra were recorded as dichloromethane solutions using a Perkin-Elmer System 2000 FT-IR spectrometer. ^1H (300 MHz), $^{13}C\{^1H\}$ (75 MHz) and $^{31}P\{^1H\}$ (121 MHz) NMR spectra were recorded using a Varian Mercury-300 FT-NMR spectrometer and are referenced to residual chloroform (7.26 ppm (^1H), 77.0 ppm ($^{13}C\{^1H\}$)) or external 85% H_3PO_4 (0.0 ppm ($^{31}P\{^1H\}$). UV-Vis spectra were recorded as CH_2Cl_2 solutions in 1 cm quartz cells using a Cary 5 spectrophotometer.

Cyclic voltammetry measurements were recorded using an e-corder and EA161 potentiostat from eDaq Pty Ltd. Measurements were carried out at room temperature using Pt disc working-, Pt wire auxiliary-, and Ag/AgCl reference electrodes, such that the ferrocene/ferrocenium redox couple was located at 0.56 V. Scan rates were typically 100 mV s^{-1}. Electrochemical solutions contained 0.1 M $(NBu^n_4)PF_6$ and ca 10^{-3} M complex in dried and distilled solvent; solutions were purged and maintained under a nitrogen atmosphere. Electronic spectra were recorded using a Cary 5 spectrophotometer. Solution spectra of the oxidized species were obtained at 298 K by electrogeneration in an optically-transparent thin-layer electrochemical (OTTLE)

cell with potentials ca 50 - 200 mV beyond $E_{1/2}$ for each couple, to ensure complete electrolysis. Solutions were made up using 0.3 M $(NBu^n_4)PF_6$ in THF.

Third-order NLO measurements were carried out using the standard Z-scan technique with simultaneous recording of the open aperture and closed aperture signals. An amplified femtosecond laser system consisting of a Quantronix Integra-C regenerative amplifier operating as an 800 nm pump and a Quantronix-Palitra-FS BIBO crystal-based optical parametric amplifier was used. Measurements were carried out for the following wavelengths: 530, 555, 800, 1200 and 1500 nm. The pulse duration was approximately 130 fs and the repetition rate was 1 kHz. The pulse energy was adjusted to keep the nonlinear phase shifts obtainable from the samples in the range of 0.5 - 1.5 rad, which typically corresponded to light intensities on the order of 100 GW/cm^2. This was achieved by attenuating the beam power with the help of neutral density filters. Additionally, some colour glass filters were used to remove unwanted spectral components of the Palitra output. The source beam was focused to provide a focal spot in the range $w_0 \approx 25$ - 50 μm. This led to the Rayleigh range being kept well in excess of the total light path in the sample (about 3 mm, including the solution and the walls of the glass cell). The solutions of the measured compounds and the reference solvent were placed in Starna glass cuvettes with 1 mm path length (in order to fulfill the thin sample condition). The cuvettes were moved along the source beam (z-axis) through its focus covering a travel distance of 40 mm (-20 mm to +20 mm). The data were collected by three InGaAs photodiodes that were measuring signals proportional to the intensities of reference, closed aperture and open aperture beams. Signals from the photodiodes were fed into a digital oscilloscope, transferred to a personal computer and collected by custom software, written in LabVIEW[17]. All measurements were calibrated using signals obtained from a 4.66 mm thick fused silica plate.

Analysis of the obtained measured data was performed using custom software[18] implementing computation of theoretical Z-scans according to equations introduced by Sheik-Bahae *et. al.*[16] Fitting the theoretical curves to the measured traces gave

the parameters (nonlinear phase shift, T parameter and beam radius at the focal spot) that were then used in the calculation of the real and imaginary parts of the second hyperpolarizability γ, and the effective two-photon absorption cross section which is related to the imaginary part of γ. The above mentioned calculations were made assuming additivity of solvent and solution nonlinearities, and using the Lorentz local field approximation.

4.4.3 ^{13}C NMR Numbering Scheme

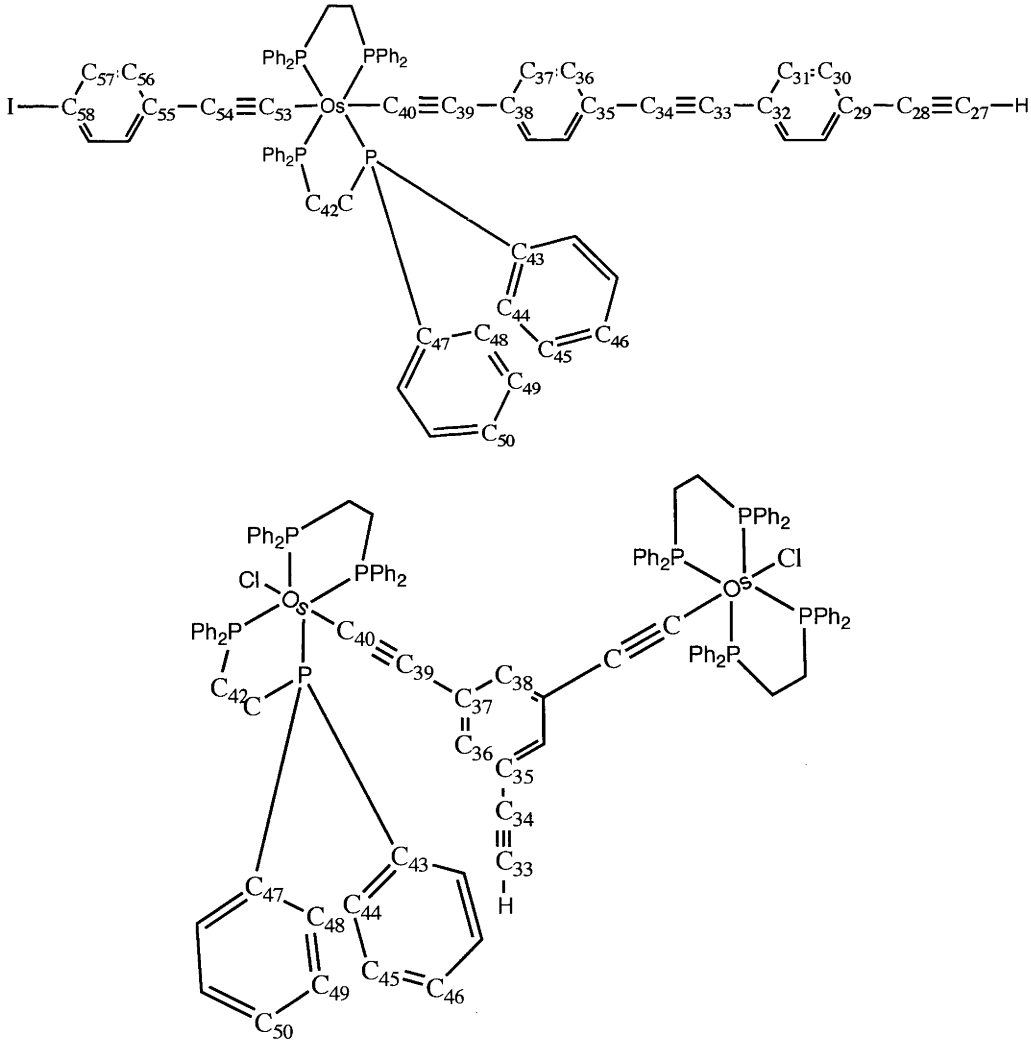

4.4.4 Synthesis and Characterization

trans-[Os(C≡C-4-C_6H_4I)(C≡CC_6H_4-4-C≡CH)(dppe)$_2$] (30)

A mixture of *trans*-[Os(C≡C-4-C_6H_4I)(C≡CC_6H_4-4-C≡C$SiPr^i_3$)(η^2-dppe)$_2$] (**18**, 350 mg, 0.234 mmol) and NBu^n_4F (0.7 mL of a 1.0 M solution in THF, 0.7 mmol) was stirred in dichloromethane (100 mL) for 16 h. The solution volume was reduced to 40 mL, and added to methanol (130 mL), precipitating the product, which was collected on a sintered glass filter funnel affording **30** as a yellow powder (166 mg, 53 %). ESI MS: 1340 ($[M]^+$, 100). HRMS (ESI): Calc.: 1340.2072 $[M]^+$, Found: 1340.2070. Anal. Calc. for $C_{70}H_{57}IOsP_4$: C 62.78, H 4.29%. Found: C 62.89, H 4.07%. UV-vis (CH_2Cl_2): λ 373 nm, ε 58000 M^{-1} cm^{-1}. IR (CH_2Cl_2): 2056 (br) cm^{-1} ν(C≡C), 3294 cm^{-1} ν(≡CH). ^{1}H NMR: δ 7.43 – 6.41 (m, 48H, Ar), 3.12 (s, 1H, C≡CH), 2.58 (m, 8H, CH_2). ^{31}P NMR: δ 16.6. ^{13}C NMR: δ 136.3 (C_{57}), 135.6 (C_{47}, C_{43}, vtt, $|{}^1J_{PC} + {}^3J_{PC}|$ = 24 Hz), 134.1 (C_{48}, C_{44}), 132.2 (C_{56}), 131.6 (C_{38}), 131.3 (C_{37}), 130.3 (C_{55}), 130.1 (C_{36}), 128.8 (C_{50}, C_{46}), 127.0 (C_{49}, C_{45}), 120.2, 117.4 (C_{40}, C_{53}, quint, $^2J_{cp}$ = 12 Hz), 115.3, 115.0, 113.7 (C_{35}, C_{39}, C_{54}), 86.7 (C_{58}), 84.9 (C_{34}), 76.7 (C_{33}), 32.3 (C_{42}, vtt, $|{}^1J_{PC} + {}^3J_{PC}|$ = 26 Hz).

1,3,5-C_6H_3(C≡CC_6H_4-4-C≡CC_6H_4-4-C≡C-*trans*-[Ru(dppe)$_2$]C≡CC_6H_4-4-C≡C-*trans*-[Os(dppe)$_2$]C≡C-4-C_6H_4I)$_3$ (31)

A mixture of 1,3,5-C_6H_3(C≡CC_6H_4-4-C≡CC_6H_4-4-C≡C-*trans*-[RuCl(dppe)$_2$])$_3$ (42 mg, 0.0118 mmol), *trans*-[Os(C≡C-4-C_6H_4I)(C≡CC_6H_4-4-C≡CH)(dppe)$_2$] (**30**, 52 mg, 0.039 mmol), $NaPF_6$ (23 mg, 0.135 mmol) and Et_3N (10 drops) were stirred in refluxing CH_2Cl_2 (90 mL) for 24 h. The solvent volume was reduced to 3 mL and the crude reaction mixture filtered through a pipette containing cotton wool. The product was precipitated from methanol (100 mL) and collected on a sintered glass filter funnel. The product was redissolved in a minimum of dichloromethane (2 mL) and

precipitated from *n*-pentane (100 mL) and collected once more on a sintered glass filter funnel to afford **31** as an orange powder (45 mg, 51%). ESI MS: 2178 ([*trans*-[Ru(NCMe)(dppe)$_2$]C≡CC_6H_4-4-C≡C-*trans*-[Os(dppe)$_2$]C≡CC_6H_4I]$^+$, 1) Anal. Calc. for $C_{426}H_{339}I_3Ru_3Os_3P_{24}$: C 68.62, H 4.58%. Found: C 68.11, H 4.30%. UV-vis (THF): λ 344 nm, ε 220000 M^{-1} cm^{-1}; λ 386 nm, ε 221000 M^{-1} cm^{-1}, λ 417 nm (sh), ε 145000 M^{-1} cm^{-1}. IR (CH_2Cl_2): 2056 (br) cm^{-1} *ν*(C≡C). ^{1}H NMR (C_6D_6): δ 7.90 – 6.59 (m, 291H, Ar), 2.58 (m, 48H, CH_2). ^{31}P NMR (C_6D_6): δ 54.2 (RuP), 16.6 (OsP).

1,3,5-C_6H_3(C■CC_6H_4-4-C■CC_6H_4-4-C■C-*trans*-[Ru(dppe)$_2$]C■CC_6H_4-4-C■CC_6H_4-4-C■C-*trans*-[Os(dppe)$_2$]C■C-4-C_6H_4I)$_3$ (32)

A mixture of 1,3,5-C_6H_3(C≡CC_6H_4-4-C≡CC_6H_4-4-C≡C-*trans*-[RuCl(dppe)$_2$])$_3$ (43 mg, 0.012 mmol), *trans*-[Os(C≡C-4-C_6H_4I)(C≡CC_6H_4-4-C≡CC_6H_4-4-C≡CH)(dppe)$_2$] (**21**, 70 mg, 0.048 mmol), $NaPF_6$ (24 mg, 0.146 mmol) and Et_3N (10 drops) were stirred in refluxing CH_2Cl_2 (60 mL) for 24 h. The solution was reduced to 3 mL and filtered through cotton wool in a pipette into stirring methanol (100 mL), forming an orange precipitate. The precipitate was collected, dissolved in CH_2Cl_2 (2 mL), precipitated from *n*-pentane (80 mL) and collected on a sintered glass filter funnel, affording **32** as a orange-brown powder (50 mg, 50%). ESI MS: 2378 ([*trans*-[Ru(NCMe)(dppe)$_2$]C≡CC_6H_4-4-C≡CC_6H_4-4-C≡C-*trans*-[Os(dppe)$_2$]C≡CC_6H_4I]$^+$, 1). Anal. Calc. for $C_{450}H_{351}I_3Ru_3Os_3P_{24}$: C 69.68, H 4.56%. Found: C 69.15, H 5.00%. UV-vis (THF): λ 334 nm, ε 219000 M^{-1} cm^{-1}, λ 428 nm, ε 269000 M^{-1} cm^{-1}. IR (CH_2Cl_2): 2052 (br) cm^{-1} *ν*(C≡C). ^{1}H NMR ($CDCl_3$): δ 7.55 – 6.69 (m, 295H, Ar), 2.57 (m, 48H, CH_2). ^{31}P NMR (C_6D_6): δ 54.1 (RuP), 16.6 (OsP).

1-(HC■C)C_6H_3-3,5-{C■C-*trans*-[OsCl(dppe)$_2$]}$_2$ (33)

A mixture of 1,3,5-(HC≡C)$_3C_6H_3$ (50 mg, 0.333 mmol), *cis*-[$OsCl_2$(dppe)$_2$] (1.23 g, 1.17 mmol) and NH_4PF_6 (237 mg, 1.46 mmol) were stirred in refluxing CH_2Cl_2 (100

mL) for 12 h. The mixture was allowed to cool to room temperature, Et_3N (2 mL) added and the mixture reduced in volume to 40 mL. The product was precipitated from methanol (150 mL) and collected on a sintered glass filter funnel, washing with *n*-pentane (40 mL) to give a pale yellow powder **33** (540 mg, 74%). ESI MS: 2194 ($[M]^+$, 100), HRMS (ESI): Calc.: 2195.4411 $[M + H]^+$, Found: 2195.4458. Anal. Calc. for $C_{116}H_{100}Cl_2Os_2P_8$: C 63.53, H 4.60%. Found: C 63.19, H 4.34%. UV-vis (CH_2Cl_2): λ 397 nm (sh), ε 7000, λ 340 nm, ε 27000 M^{-1} cm^{-1}. IR (CH_2Cl_2): 2054 cm^{-1} (br) ν(C≡C), 3302 cm^{-1} ν(≡CH). ^1H NMR (C_6D_6): δ 7.70 – 6.88 (m, 83H, Ar), 2.91 (s, 1H, C≡CH), 2.65 (m, 16H, CH_2). ^{31}P NMR: δ 16.6. ^{13}C NMR: δ 136.0, 134.8 (C_{47}, C_{43}, vtt, $|{}^1J_{PC} + {}^3J_{PC}|$ = 24 Hz), 134.4, 134.2 (C_{48}, C_{44}), 131.0 (C_{37}), 130.2 (C_{36}), 130.0 (C_{38}), 129.0, 128.6 (C_{50}, C_{46}), 127.2, 126.7 (C_{49}, C_{45}), 120.0 (C_{35}), 109.6 (C_{39}), 100.9 (C_{40}, quint $^2J_{CP}$ = 11 Hz), 85.3 (C_{34}), 74.6 (C_{33}), 31.6 (C_{42}, vtt, $|{}^1J_{PC} + {}^3J_{PC}|$ = 26 Hz).

[1-(HC■C)C_6H_3-3,5-{C■C-*trans*-[$Os(NH_3)(dppe)_2$]}$_2$]$(PF_6)_2$ (34)

A mixture of 1-(HC≡C)C_6H_3-3,5-{C≡C-*trans*-[$OsCl(dppe)_2$]}$_2$ (**33**, 200 mg, 0.091 mmol), NH_4PF_6 (89 mg, 0.55 mmol) and Et_3N (2 mL) were stirred in CH_2Cl_2 (100 mL) for 24 h. The solution was reduced in volume to 60 mL and the product precipitated by addition to stirring *n*-pentane (150 mL). The solid was collected and washed with methanol (50 mL), affording **34** as a white powder (114 mg, 51%). ESI MS: 2302 ($[M - PF_6]^+$, 50), Anal. Calc. for $C_{116}H_{106}P_{10}F_{12}Os_2N_2$: C 56.96, H 4.37, N 1.15%. Found: C 56.68, H 4.53, N 0.91%. UV-vis (CH_2Cl_2): λ 321 nm, ε 45000 M^{-1} cm^{-1}, λ 372 nm (sh), ε 11000 M^{-1} cm^{-1}. IR (CH_2Cl_2): 2064 cm^{-1} ν(C≡C), 3301 cm^{-1} ν(≡CH). ^1H NMR ($CDCl_3$): δ 8.14 – 6.38 (m, 83H, Ar), 3.16 (s, 1H, C≡CH), 2.62 (m, 16H, CH_2), 0.99 (s, br, 3H, NH_3). ^{31}P NMR: δ 19.6 (OsP), -143.7 (sept, PF_6, J_{PF} = 714 Hz).

1,3-(HC≡C)$_2$C$_6$H$_3$-5-{C≡C-*trans*-[OsCl(dppe)$_2$]} (35)

A mixture of 1,3,5-(HC≡C)$_3$C$_6$H$_3$ (47 mg, 0.312 mmol), *cis*-[OsCl$_2$(dppe)$_2$] (297 mg, 0.281 mmol) and NH_4PF_6 (51 mg, 312 mmol) were stirred in CH_2Cl_2 (50 mL) for 50 min. NEt_3 (1 mL) was added and the reaction mixture stirred for a further 1 min. The solvent was removed and the crude product suspended in methanol (50 mL) and filtered through a sintered glass filter funnel washing with *n*-pentane (30 mL) to afford **35** as a pale yellow powder (120 mg, 33%). ESI MS: 1172 ([M]$^+$, 100), HRMS (ESI): Calc.: 1173.2479 [M + H]$^+$, Found: 1173.2469. Anal. Calc. for $C_{64}H_{53}ClOsP_4$: C 65.61, H 4.60%. Found: C 66.01, H 4.67%. UV-vis (CH_2Cl_2): λ 352 nm, ε 20000 M^{-1} cm^{-1}. IR (CH_2Cl_2): 2057 cm^{-1} *ν*(C≡C), 3301 cm^{-1} *ν*(≡CH). ^{1}H NMR (C_6D_6): δ 7.81 – 6.98 (m, 43H, Ar), 2.82 (s, 2H, C≡CH), 2.56 (m, 8H, CH_2). ^{31}P NMR (C_6D_6): δ 16.0. ^{13}C NMR ($CDCl_3$): δ 135.5 – 135.0 (m, C_{47}, C_{43}), 134.9 (C_{36}), 134.5, 134.0 (C_{48}, C_{44}), 129.0 (C_{50}, C_{46}), 127.2, 126.9 (C_{49}, C_{45}), 121.2 (C_{35}), 83.5 (C_{34}), 76.3 (C_{33}), 31.4 (C_{42}, vtt, $|{}^1J_{CP} + {}^3J_{CP}|$ = 24 Hz); C_{40}, C_{39}, C_{37}, C_{38} not observed.

1,3,5-C$_6$H$_3${C≡CC$_6$H$_4$-4-C≡CC$_6$H$_4$-4-C≡C-*trans*-[Ru(dppe)$_2$]C≡CC$_6$H$_4$-4-C≡CC$_6$H$_4$-4-C≡C-3,5-C$_6$H$_3$(C≡C-*trans*-[Os(dppe)$_2$]Cl)$_2$}$_3$ (36)

A mixture of 1,3,5-C$_6$H$_3$(C≡CC$_6$H$_4$-4-C≡CC$_6$H$_4$-4-C≡C-*trans*-[Ru(dppe)$_2$]C≡CC$_6$H$_4$-4-C≡CC$_6$H$_4$-4-I)$_3$ (40 mg, 0.009 mmol), 1-(HC≡C)C$_6$H$_3$-3,5-{C≡C-*trans*-[OsCl(dppe)$_2$]}$_2$ (**33**, 80 mg, 0.036 mmol), Pd(PPh$_3$)$_4$ (3 mg), CuI (1 mg) and Et_3N (30 mL) were refluxed in CH_2Cl_2 (30 mL) for 48 h. The solvent was removed, the reaction mixture dissolved in a minimum of CH_2Cl_2 (5 mL) and the product precipitated from a CH_2Cl_2/pentane mixture (3/7). The product was collected on a sintered glass filter funnel, redissolved in CH_2Cl_2 (5 mL) and reprecipitated from the CH_2Cl_2/pentane mixture to afford **36** as an orange powder (33 mg, 34%). Anal. Calc. for $C_{612}H_{492}Cl_6Os_6P_{36}Ru_3$: C 69.22, H 4.67%. Found: C 68.78, H 4.93%. UV-vis

(THF): λ 278 nm, ε 250000 M^{-1} cm^{-1}, λ 334 nm, ε 350000 M^{-1} cm^{-1}, λ 423 nm, ε 240000 M^{-1} cm^{-1}. IR (CH_2Cl_2): 2052 cm^{-1} ν(C≡C). ^{1}H NMR (C_6D_6): δ 7.70 – 6.87 (m, 420 H, Ar), 2.65 (m, 48H, Os-P-CH_2), 2.49 (m, 24H, Ru-P-CH_2). ^{31}P NMR: δ 54.0 (RuP), 16.5 (OsP).

1,3,5-C_6H_3{C≡CC_6H_4-4-C≡CC_6H_4-4-C≡C-*trans*-[Ru(dppe)$_2$]-1-C_6H_3-3-(C≡CH)-5-(C≡C-*trans*-[OsCl(dppe)$_2$])}$_3$ (37)

A mixture of 1,3,5-C_6H_3(C≡CC_6H_4-4-C≡CC_6H_4-4-C≡C-*trans*-[RuCl(dppe)$_2$])$_3$ (48 mg, 0.014 mmol), 1,3-(HC≡C)$_2C_6H_3$-5-{C≡C-*trans*-[OsCl(dppe)$_2$]} (**35**, 50 mg, 0.043 mmol), $NaPF_6$ (14 mg, 0.083 mmol) and Et_3N (5 drops) were heated in refluxing CH_2Cl_2 (50 mL) for 12 h. The reaction mixture was reduced in volume to 20 mL and the crude product precipitated by addition of methanol (100 mL). The product was further purified by dissolving in a minimum of CH_2Cl_2, filtering through a small cotton wool plug and precipitating from CH_2Cl_2/pentane (4:1) twice, to yield **37** as a yellow powder (68 mg, 71%). Anal. Calc. for $C_{408}H_{327}Cl_3Os_3P_{24}Ru_3$: C 70.47, H 4.74%. Found: C 70.51, H 4.79%. UV-vis (THF): λ 336 nm, ε 220000 M^{-1} cm^{-1}, λ 420 nm, ε 120000 M^{-1} cm^{-1}. IR (CH_2Cl_2): 2051 cm^{-1} ν(C≡C), 3303 cm^{-1} ν(≡CH). ^{1}H NMR (C_6D_6): δ 6.9 – 7.9 (m, 276H, Ar), 2.90 (s, 3H, C≡CH), 2.70 (m, 48H, CH_2). ^{31}P NMR (C_6D_6): δ 54.5 (RuP), 16.5 (OsP).

N(C_6H_4-4-C≡C-*trans*-[Ru(dppe)$_2$]C≡CC_6H_4-4-C≡C-*trans*-[Os(dppe)$_2$]C≡CC_6H_4-4-C≡C$SiPr^i_3$)$_3$ (38)

A mixture of N(C_6H_4-4-C≡C-*trans*-[RuCl(dppe)$_2$])$_3$ (40.6 mg, 0.013 mmol), *trans*-[Os(C≡C-4-C_6H_4C≡CH)(C≡CC_6H_4-4-C≡C$SiPr^i_3$)(dppe)$_2$] (**23**, 80 mg, 0.057 mmol), $NaPF_6$ (46 mg, 0.27 mmol) and NEt_3 (10 drops) were heated in refluxing CH_2Cl_2 (50 mL) for 48 h. The solvent volume was reduced to 10 mL and the product precipitated upon addition of methanol (100 mL). The product was redissolved in a minimum of

CH_2Cl_2 (5 mL), precipitated from a CH_2Cl_2/pentane (1:5) mixture and collected on a sintered glass filter funnel to yield **38** as a yellow powder (24 mg, 26%). Anal. Calc. for $C_{423}H_{387}NOs_3P_{24}Ru_3Si_3$: C 70.70, H 5.43, N 0.19%. Found: C 70.38, H 5.16, N 0.25%. UV-vis (THF): λ 391 nm, ε 340000 M^{-1} cm^{-1}. IR (CH_2Cl_2) 2055 cm^{-1} ν(C≡C), 2146 cm^{-1} ν(C≡C-Si). ^{1}H NMR (C_6D_6): δ 7.86 – 6.83 (m, 276H, Ar), 2.83 (m, 48H, CH_2), 1.23 (s, 63H $SiPr^i_3$). ^{31}P NMR (C_6D_6): δ 54.4 (RuP), 16.4 (OsP).

4.5 References

(1) Cifuentes, M. P.; Powell, C. E.; Morrall, J. P.; McDonagh, A. M.; Lucas, N. T.; Humphrey, M. G.; Samoc, M.; Houbrechts, S.; Asselberghs, I.; Clays, K.; Persoons, A.; Isoshima, T. *J. Am. Chem. Soc.* **2006**, *128*, 10819.

(2) Roberts, R. L.; Schwich, T.; Corkery, T. C.; Cifuentes, M. P.; Green, K. A.; Farmer, J. D.; Low, P. J.; Marder, T. B.; Samoc, M.; Humphrey, M. G. *Adv. Mater.* **2009**, *21*, 2318.

(3) Schwich, T.; Cifuentes, M. P.; Gugger, P. A.; Samoc, M.; Humphrey, M. G. *Adv. Mater.* **2011**, *23*, 1433.

(4) Gauthier, N.; Argouarch, G.; Paul, F.; Toupet, L.; Ladjarafi, A.; Costuas, K.; Halet, J.-F.; Samoc, M.; Cifuentes, M. P.; Corkery, T. C.; Humphrey, M. G. *Chem. Eur. J.* **2011**, *17*, 5561.

(5) Powell, C. E.; Cifuentes, M. P.; Humphrey, M. G.; Willis, A. C.; Morrall, J. P.; Samoc, M. *Polyhedron* **2007**, *26*, 284.

(6) Dalton, G. T.; Cifuentes, M. P.; Petrie, S.; Stranger, R.; Humphrey, M. G.; Samoc, M. *J. Am. Chem. Soc.* **2007**, *129*, 11882.

(7) Samoc, M.; Powell, C. E.; Morrall, J. P.; Ward, S. A.; Cifuentes, M. P.; Notaras, E. G. A.; Humphrey, M. G. *Nonlin. Opt. Transmission Multiphoton Proc. Org. - Proc. SPIE* **2004**, *5516*, 86.

(8) Powell, C. E.; Hurst, S. K.; Morrall, J. P.; Cifuentes, M. P.; Roberts, R. L.; Samoc, M.; Humphrey, M. G. *Organometallics* **2007**, *26*, 4456.

(9) Onitsuka, K.; Ohara, N.; Takei, F.; Takahashi, S. *Organometallics* **2008**, *27*, 25.

(10) Onitsuka, K.; Fujimoto, M.; Kitajima, H.; Ohshiro, N.; Takei, F.; Takahashi, S. *Chem. Eur. J.* **2004**, *10*, 6433.

(11) Long, N. J.; Martin, A. J.; Fabrizi de Biani, F.; Zanello, P. *J. Chem. Soc., Dalton Trans.* **1998**, 2017.

(12) Hurst, S. K.; Cifuentes, M. P.; Humphrey, M. G. *Organometallics* **2002**, *21*, 2353.

(13) Onitsuka, K.; Ohara, N.; Takei, F.; Takahashi, S. *Dalton Trans.* **2006**, 3693.

(14) Dalton, G. T.; Cifuentes, M. P.; Watson, L. A.; Petrie, S.; Stranger, R.; Samoc, M.; Humphrey, M. G. *Inorg. Chem.* **2009**, *48*, 6534.

(15) MacBride, J. A. H.; Wade, K. *Synth. Commun.* **1996**, *26*, 2309.

(16) Sheik-Bahae, M.; Said, A. A.; Wei, T. H.; Hagan, D. J.; Van Stryland, E. W. *IEEE J. Quant. Electron.* **1990**, *26*, 760.
(17) Samoc, M. *Unpublished procedure* **2011**.
(18) Parjaszewski, K. *Unpublished procedure* **2011**.

Chapter 5

Iron alkynyl complexes

Chapter 5

Iron alkynyl complexes

Contents

5.1 Introduction

Iron alkynyl complexes have been studied extensively for nonlinear optical[1-3] and switching applications[4,5]. Whereas redox processes involving the ruthenium and osmium complexes described in Chapters 2, 3 and 4 possess significant alkynyl character, redox processes at iron alkynyl complexes are predominantly metal centred due to the lower energy of the d orbital of iron compared to the heavier group VIII metals.[6]

The metal centre Fe(dppe)Cp* is commonly used to form iron alkynyl complexes due to favourable electrochemical properties and well explored chemistry. However, the use of this metal centre also has several disadvantages. The formation of alkynyl complexes requires the use of a polar solvent (MeOH) in which some acetylene precursors are insoluble and the alkynyl complexes are prone to oxidation; the latter requires the use of stringent anaerobic conditions. It has been shown that the use of the $Fe(CO)_2Cp^*$ metal centre can allow the formation of iron alkynyl complexes without either of these prohibitive conditions. Although the $Fe(CO)_2Cp^*$ metal centre doesn't exhibit reversible redox activity, it is possible to substitute either one or both of the carbonyl groups for phosphines to afford a complex with a reversible redox process.[7-9]

Previously, Lapinte and co-workers synthesised a butadiynyl complex incorporating the $Fe(CO)_2Cp^*$ metal centre in good yield from $FeI(CO)_2Cp^*$ and lithium alkynyl precursors (Scheme 5.1). After deprotection this complex could be coupled to a Fe(dppe)Cp* metal centre forming a binuclear donor-acceptor complex. Complexes of this type have potential use as second-order NLO-active materials (where a permanent dipole is required) as well as switchable rectifying components in molecular electronics.[7]

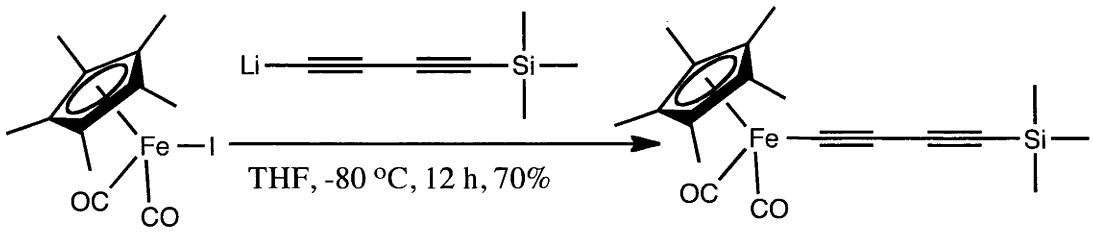

Scheme 5.1. Formation of $Fe(C{\equiv}CC{\equiv}CSiMe_3)(CO)_2Cp^*$ by Coat *et al.* [7]

Diiron complexes with a diethynylbenzene bridge have been extensively investigated, with the bridge shown to be largely innocent in the electrochemical behaviour.[10-12] This allows these complexes to form mixed-valent species following the first iron oxidation. Most of the diiron complexes with this type of bridging ligand have been symmetrical and involved two metal centres with similar electronic behaviour. Donor-accepter unsymmetrical binuclear iron complexes with a diethynylbenzene bridge have, by comparison, been less explored, but remain an interesting area of investigation due to their potential rectifying nature.

5.2 Results and Discussion

5.2.1 Synthesis

Formation of mononuclear alkynyl complexes incorporating the $Fe(CO)_2Cp^*$ metal centre was achieved by using an alkynyl cuprate reagent formed in situ through the reaction of CuI and acetylene in NEt_3. This cuprate was then reacted with the $Fe(CO)_2Cp^*$ metal centre to form the iron alkynyl complex. It should be noted that these complexes are light sensitive, with all reactions performed with the exclusion of light to limit decomposition.

Reaction of $FeCl(CO)_2Cp^*$ in this manner with either $HC{\equiv}CC_6H_4$-4-$C{\equiv}CSiPr^i_3$ or $HC{\equiv}CC_6H_4$-4-$C{\equiv}CSiMe_3$ afforded the mononuclear iron alkynyl complex with a silyl protected ethynyl group that on desilyation can be further functionalised (Scheme 5.2). Both the triisopropylsilyl (**39**) and trimethylsilyl (**40**) protected complexes were formed in good yields (78% and 73%).

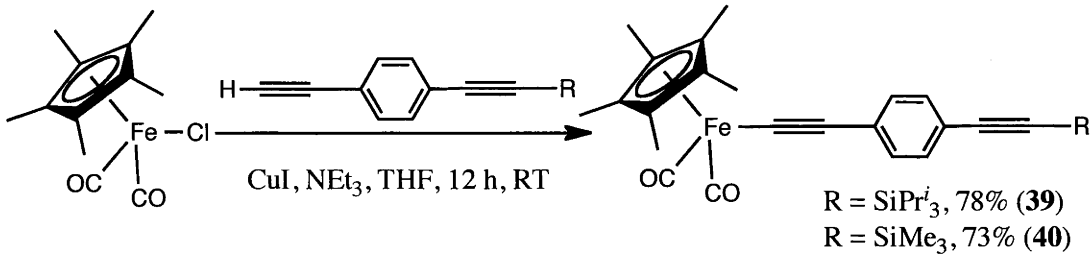

Scheme 5.2. Formation of iron alkynyl complexes with a protected 4-ethynylphenylethynyl ligand from alkynyl cuprate reagents

Utilising the same procedure used to form **39** and **40,** the analogous complexes where the ethynyl groups are *meta* to one another were formed (Scheme 5.3). While the complex with a triisopropylsilyl (**41**) protecting group was isolated in good yield (74%) the yield for the complex with the trimethylsilyl (**42**) protecting group was lower (36%). This is primarily due to the high solubility of the iron alkynyl complex and the synthetic difficulty in purifying the complexes. Although the complexes are filtered through a small pad of alumina to remove most contaminants, washing with pentane is needed to remove impurities such as grease. Unlike the ruthenium and osmium complexes formed in earlier chapters these iron complexes are very soluble in most solvents including pentane. Even when washing with a small amount (10 mL) of cold pentane, significant sample is lost, accounting for the low yield for **42**. An unidentified by-product of these reactions is a Cp*-containing compound (by ^{1}H NMR). This compound has very similar solubility to the desired product and is difficult to remove, with several washings required which lowers the yield. This by-product is easier to remove on cleavage of the silyl group or substitution of one of the carbonyls for a PPh_3 group.

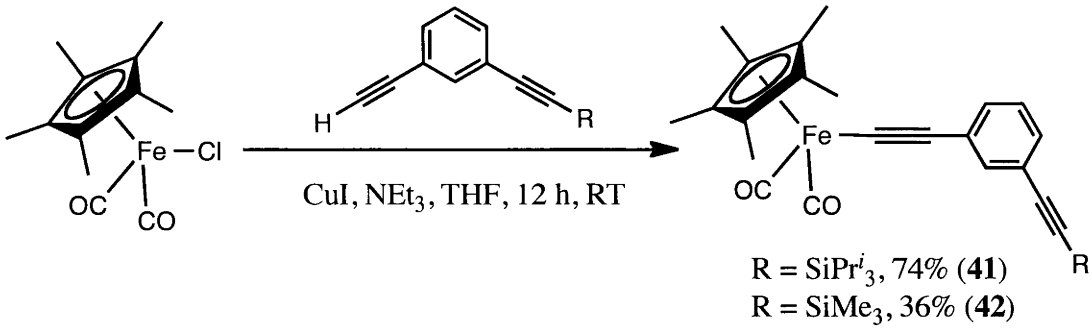

Scheme 5.3. Formation of iron alkynyl complexes with a protected 3-ethynylphenylethynyl ligand

Both the triisopropyl- and trimethyl- silyl groups can be removed under the same conditions by stirring the complexes in the presence of NBu^n_4F for 15 h. In this manner the complexes with ethynyl groups *para* to one another **39** and **40** (Scheme 5.4) and those *meta* to one another **41** and **42** (Scheme 5.5) can be desilylated to afford complexes **43** and **44,** respectively. Once again the low isolated yields for some of these reactions is due to the high solubility of the products and the difficulties in removing impurities.

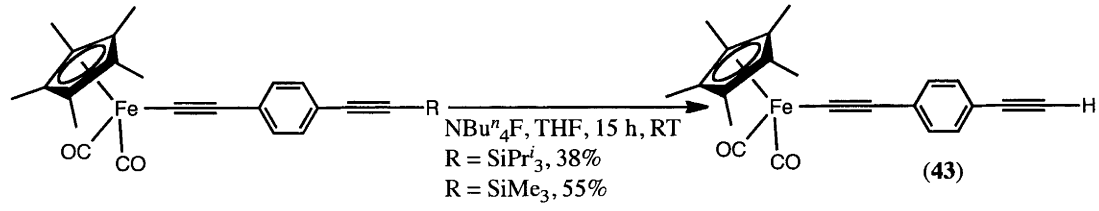

Scheme 5.4. Desilylation of complexes **39** and **40** to form complexes with an acetylene *para* to the acetylide bond (**43**)

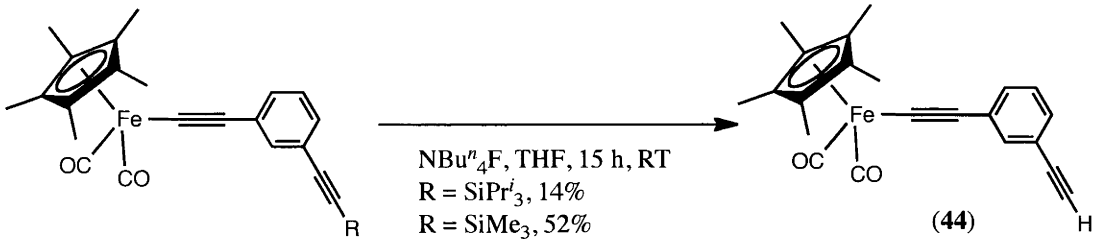

Scheme 5.5. Desilylation of complexes **41** and **42** to form complexes with an acetylene *meta* to the acetylide bond (**44**)

As mentioned in the introduction, the ability to substitute either one or both of the carbonyls with phosphines is an important property of the $FeCl(CO)_2Cp^*$ metal centre. On replacement of the two carbonyls with a dppe ligand or one of the carbonyls with a PPh_3 ligand, the resultant complexes exhibit reversible redox processes, making them useful for electrochemical switching. Complex **39** can have one carbonyl substituted for a PPh_3 molecule under UV irradiation (Scheme 5.6). Although an excess of PPh_3 is used, only one carbonyl is substituted due to the steric bulk of the PPh_3. The complex $Fe(C{\equiv}CC_6H_4\text{-}4\text{-}C{\equiv}CSiPr^i_3)(CO)(PPh_3)Cp^*$ (**45**) is formed in moderate yields (42%), with the solubility of the product and some decomposition under the reaction conditions accounting for the low yield.

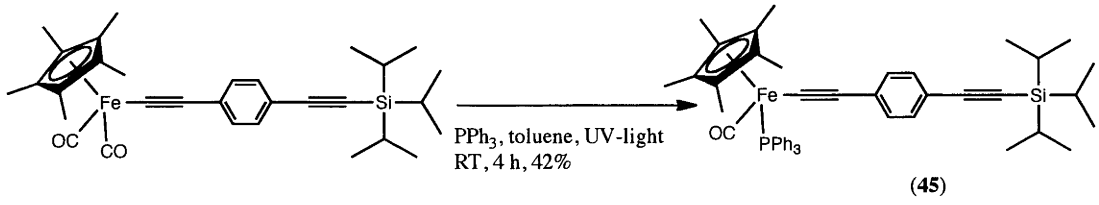

Scheme 5.6. Formation of **45** by ligand substitution under irradiation with UV light

Using the same conditions, one of the carbonyl groups in complex **41** can be substituted for a PPh_3 group to afford $Fe(C{\equiv}CC_6H_4\text{-}3\text{-}C{\equiv}CSiPr^i_3)(CO)(PPh_3)Cp^*$ (**46**) (Scheme 5.7) in a 30% yield. Once again some decomposition occurs under UV conditions with a darkening of the reaction mixture observed.

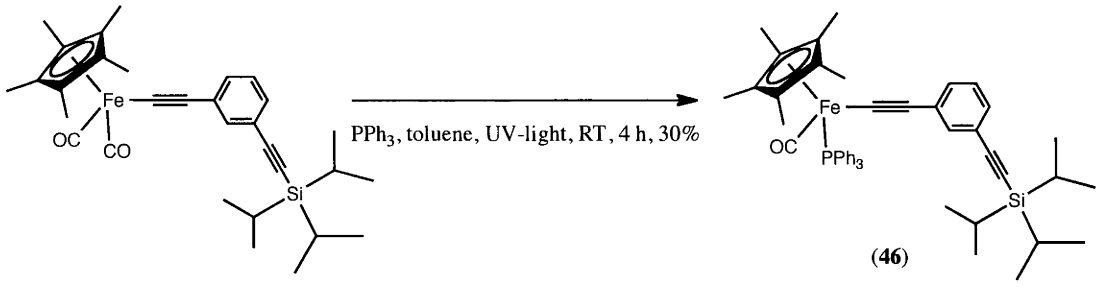

Scheme 5.7. Formation of **46** by ligand substitution under irradiation with UV light

Attachment of an electron rich metal centre Fe(dppe)Cp* to the acetylene site in complexes **43** and **44** creates a binuclear complex where the electron deficient $Fe(CO)_2Cp^*$ metal centre can act as an electron acceptor and Fe(dppe)Cp* as a donor. Complexes of this type have potential applications as a rectifying unit in molecular electronics or as a 2nd order nonlinear optical material. The Fe(dppe)Cp* metal centre, possessing a reversible redox process, also allows these complexes to be electrochemically switchable, increasing the potential uses. As mentioned earlier Lapinte and co-workers have previously explored complexes of this type with a butadiynyl bridge between the metal centres.[7]

The binuclear complex, $\{Fe(dppe)Cp^*\}(\mu\text{-}C{\equiv}CC_6H_4\text{-}4\text{-}C{\equiv}C)\{Fe(CO)_2Cp^*\}$ (**47**) was formed by stirring $Fe(C{\equiv}CC_6H_4\text{-}4\text{-}C{\equiv}CH)(CO)_2Cp^*$ (**44**) with a halide abstraction agent (KPF_6) and the FeCl(dppe)Cp* metal centre in a CH_3OH/THF mixture (1:1) for 16 h. The resultant vinylidene complex could then be deprotonated to the acetylide by stirring a THF solution with KO^{t}Bu to afford **47** in 31% yield (Scheme 5.8).

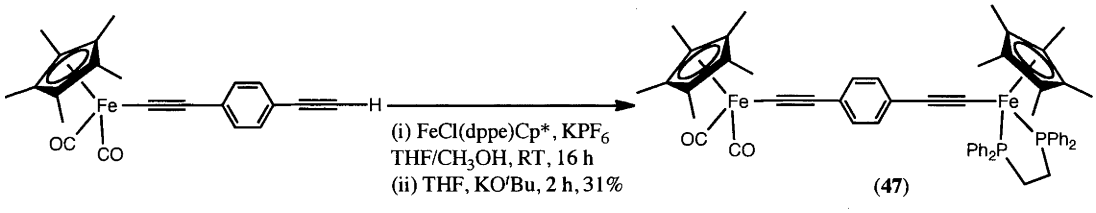

Scheme 5.8. Formation of the binuclear complex **47**

The binuclear complex where the ethynyl bonds are *meta* to one another can be formed in 68% yield using the same conditions to those used for the formation of the analogous *para* example (Scheme 5.9).

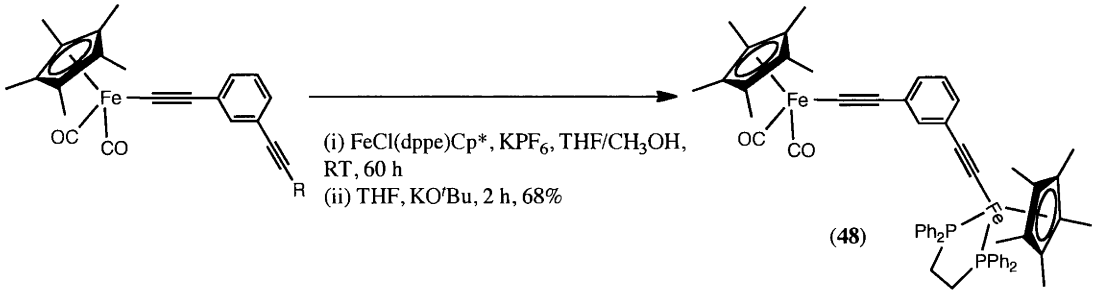

Scheme 5.9. Formation of the binuclear complex **48**

5.2.2 Physical properties

5.2.2.1 NMR spectroscopy

Complexes **39** – **48** were characterised using ^{1}H NMR. In addition the phosphorus containing complexes **45** – **48** were characterised using ^{31}P NMR and complexes **39** – **46** were characterised using ^{13}C NMR, with signals assigned where possible, and otherwise grouped. Useful ^{13}C NMR data were unable to be obtained for the binuclear complexes (**47** and **48**) due to the ease of oxidation of the Fe(dppe)Cp* metal centre and the associated broadening of the NMR signals.

^{1}H NMR

The proton NMR spectra of complexes **39** – **48** were measured in C_6D_6 and showed characteristic signals. For all of the complexes a singlet between 1.39 - 1.53 ppm for the methyl protons of the Cp* group is visible. The binuclear complexes have two methyl resonances within this range. The complexes with a silyl group **39** – **42**, **45** and **46** either have a resonance at ca 0.4 ppm for a $SiMe_3$ or at ca 1.19 ppm for a $SiPr^{i}_3$ group. As discussed in Chapter 2, the resonance at 1.19 ppm is a pseudo

singlet with the heptet corresponding to the methyne proton not observed. All of the complexes have resonances within the range 8.06 – 6.76 ppm corresponding to aromatic protons in the phenylethynyl ligand (**39** – **48**), PPh_3 ligand (**45** and **46**) and dppe ligand (**47** and **48**).

^{31}P NMR

The ^{31}P NMR spectra of the two complexes with a PPh_3 ligand (**45** and **46**) and the two binuclear complexes with a dppe ligand (**47** and **48**) were measured as C_6D_6 solutions. For complexes **45** and **46** a singlet at ca 76 ppm corresponds to the metal-bound PPh_3 ligand. For the binuclear complexes a singlet at 101.6 ppm corresponding to the two phosphorus atoms in the dppe ligand was observed.

5.2.2.2 UV-Vis spectroscopy

The UV-Vis absorption spectra of complexes **40** and **42** – **48** were measured in CH_2Cl_2 (Table 5.1). Complexes **39** and **41** were not measured due to similarities to **40** and **42**. The di-carbonyl complexes with ethynyl groups *para* to one another (**40** and **43**) have an absorption band at 325 nm (**40**) and 316 nm (**43**). For the analogous complexes with the ethynyl groups *meta* to one another (**42** and **44**) the absorption band is blue-shifted to ca 289 nm. The PPh_3 containing complexes (**45** and **46**) have absorption bands at 339 and 369 nm (**45**) and 298 nm (**46**). The bimetallic complexes (**47** and **48**) have absorption bands at 372, 292 and 263 nm (**47**) and 367 and 281 nm (**48**).

Complex	λ_{max}/nm [$\varepsilon/10^4$ $M^{-1}cm^{-1}$]
$Fe(C{\equiv}CC_6H_4\text{-}4\text{-}C{\equiv}CSiMe_3)(CO)_2Cp^*$ (**40**)	325 [3.3]
$Fe(C{\equiv}CC_6H_4\text{-}3\text{-}C{\equiv}CSiMe_3)(CO)_2Cp^*$ (**42**)	288 [1.4]
$Fe(C{\equiv}CC_6H_4\text{-}4\text{-}C{\equiv}CH)(CO)_2Cp^*$ (**43**)	316 [2.8]
$Fe(C{\equiv}CC_6H_4\text{-}3\text{-}C{\equiv}CH)(CO)_2Cp^*$ (**44**)	289 [1.8]
$Fe(C{\equiv}CC_6H_4\text{-}4\text{-}C{\equiv}CSiPr^i_3)(CO)(PPh_3)Cp^*$ (**45**)	339 [1.7], 369 [1.3]
$Fe(C{\equiv}CC_6H_4\text{-}3\text{-}C{\equiv}CSiPr^i_3)(CO)(PPh_3)Cp^*$ (**46**)	298 [1.7]
{Fe(dppe)Cp*}(μ-$C{\equiv}CC_6H_4$-4-$C{\equiv}C$){$Fe(CO)_2Cp^*$} (**47**)	372 [1.5], 292 [1.9], 263 [2.2]
{Fe(dppe)Cp*}(μ-$C{\equiv}CC_6H_4$-3-$C{\equiv}C$){$Fe(CO)_2Cp^*$} (**48**)	367 [9.0], 281 [1.8]

Table 5.1 UV-Vis absorption data for complexes **41** and **43** – **47**.

5.2.2.3 Infrared spectroscopy

The carbonyl groups attached to the Fe metal centre can act as a probe into the electronics of the metal centre. The shifting of the carbonyl bands to a lower energy would be indicative of a more electron rich metal centre, as one might expect to see if the electron density is increased by the presence of an electron donor.[7] The IR carbonyl and ethynyl stretches of complexes **39** – **48** were measured in CH_2Cl_2 (Table 5.2). On substituting one of the carbonyls for a PPh_3 the metal centre becomes much more electron rich and the band for the remaining carbonyl is shifted ca 40 cm^{-1} to lower energy (Table 5.2). However, on forming the bimetallic complexes (**47** and **48**) very little change is observed for the carbonyl bands. This is in contrast to the changes reported for analogous complexes with a butadiynyl bridge between the metal centres, where a red-shift of ca 10 cm^{-1} was observed.[7]

Complex	ν(CO)	ν(C≡C)
$Fe(C{\equiv}CC_6H_4\text{-}4\text{-}C{\equiv}CSiPr^i_3)(CO)_2Cp^*$ (**39**)	2018, 1969	2150, 2096
$Fe(C{\equiv}CC_6H_4\text{-}4\text{-}C{\equiv}CSiMe_3)(CO)_2Cp^*$ (**40**)	2018, 1969	2152, 2096
$Fe(C{\equiv}CC_6H_4\text{-}3\text{-}C{\equiv}CSiPr^i_3)(CO)_2Cp^*$ (**41**)	2018, 1968	2150, 2100
$Fe(C{\equiv}CC_6H_4\text{-}3\text{-}C{\equiv}CSiMe_3)(CO)_2Cp^*$ (**42**)	2018, 1969	2152, 2100
$Fe(C{\equiv}CC_6H_4\text{-}4\text{-}C{\equiv}CH)(CO)_2Cp^*$ (**43**)	2018, 1969	2095
$Fe(C{\equiv}CC_6H_4\text{-}3\text{-}C{\equiv}CH)(CO)_2Cp^*$ (**44**)	2018, 1969	2096
$Fe(C{\equiv}CC_6H_4\text{-}4\text{-}C{\equiv}C\text{-}SiPr^i_3)(CO)(PPh_3)Cp^*$ (**45**)	1924	2148, 2076
$Fe(C{\equiv}CC_6H_4\text{-}3\text{-}C{\equiv}C\text{-}SiPr^i_3)(CO)(PPh_3)Cp^*$ (**46**)	1927	2152, 2077
$\{Fe(dppe)Cp^*\}(\mu\text{-}C{\equiv}CC_6H_4\text{-}4\text{-}C{\equiv}C)\{Fe(CO)_2Cp^*\}$ (**47**)	2017, 1966	2095, 2053
$\{Fe(dppe)Cp^*\}(\mu\text{-}C{\equiv}CC_6H_4\text{-}3\text{-}C{\equiv}C)\{Fe(CO)_2Cp^*\}$ (**48**)	2018, 1969	2098, 2049

Table 5.2 Infra-red absorption data for complexes **39** - **48**

5.2.2.4 Electrochemistry

The electrochemical behaviour of complexes **39** – **48** was measured using cyclic voltammetry (Table 5.3). For the mononuclear $Fe(CO)_2Cp^*$ complexes **39** – **44** no reversible processes were seen with only an irreversible process at ca 1 V observed. For the mononuclear complexes in which one of the carbonyl groups had been substituted for a PPh_3 (**45** and **46**) a reversible process at 0.45 V, corresponding to the Fe^{II}/Fe^{III} redox couple, was observed. For the binuclear complexes **47** and **48** only one reversible process at ca - 0.2 V, corresponding to the Fe^{II}/Fe^{III} redox couple of the Fe(dppe)Cp* metal centre, was observed, along with an irreversible process at ca 1 V for the the $Fe(CO)_2Cp^*$ metal centre.

Complex	$E_{1/2}$ [i_{pc}/i_{pa}] [a] (V)
$Fe(C{\equiv}CC_6H_4\text{-}4\text{-}C{\equiv}CSiPr^i_3)(CO)(PPh_3)Cp^*$ (**45**)	0.45 [1]
$Fe(C{\equiv}CC_6H_4\text{-}3\text{-}C{\equiv}CSiPr^i_3)(CO)(PPh_3)Cp^*$ (**46**)	0.45 [1]
$\{Fe(dppe)Cp^*\}(\mu\text{-}C{\equiv}CC_6H_4\text{-}4\text{-}C{\equiv}C)\{Fe(CO)_2Cp^*\}$ (**47**)	- 0.18 [1]
$\{Fe(dppe)Cp^*\}(\mu\text{-}C{\equiv}CC_6H_4\text{-}3\text{-}C{\equiv}C)\{Fe(CO)_2Cp^*\}$ (**48**)	- 0.20 [1]

Table 5.3 Cyclic voltammetric data for complexes **45** – **48**. [a]In CH_2Cl_2, SCE reference electrode, ferrocene/ferrocenium couple at 0.46 V [1]. Peak separation of processes is approximately the same as for the ferrocene/ferrocenium couple.

5.2.2.5 Spectroelectrochemistry

Electrolysis of complexes **45** - **48** was carried out in an optically-transparent thin-layer electrochemical (OTTLE) cell in order to observe the changes in UV-Vis-NIR absorption spectra upon oxidation. For **45** and **46** (Figures 5.1 and 5.2) the oxidised complex was found to be unstable, with the loss of ca. 30% peak height for each scan and unclean isobestic points. For **45** oxidation to the Fe^{III} species results in a low-energy band at 12600 cm^{-1} and decrease in the intensity of the bands between 25000 and 30000 cm^{-1}. For **46** the changes observed upon oxidation are similar but less dramatic, with the appearance of a low intensity, broad absorption band between 12000 cm^{-1} and 23000 cm^{-1} and a decrease in the intensity of the absorption band around 30000 cm^{-1}.

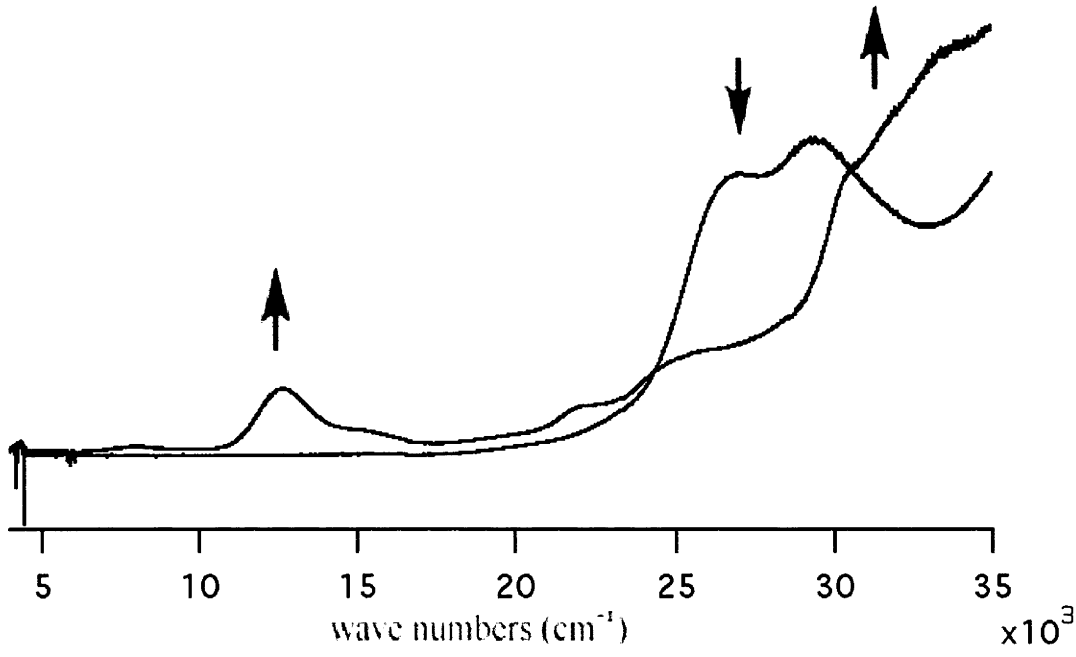

Figure 5.1 UV-Vis-NIR spectral changes during electrochemical oxidation of **45**

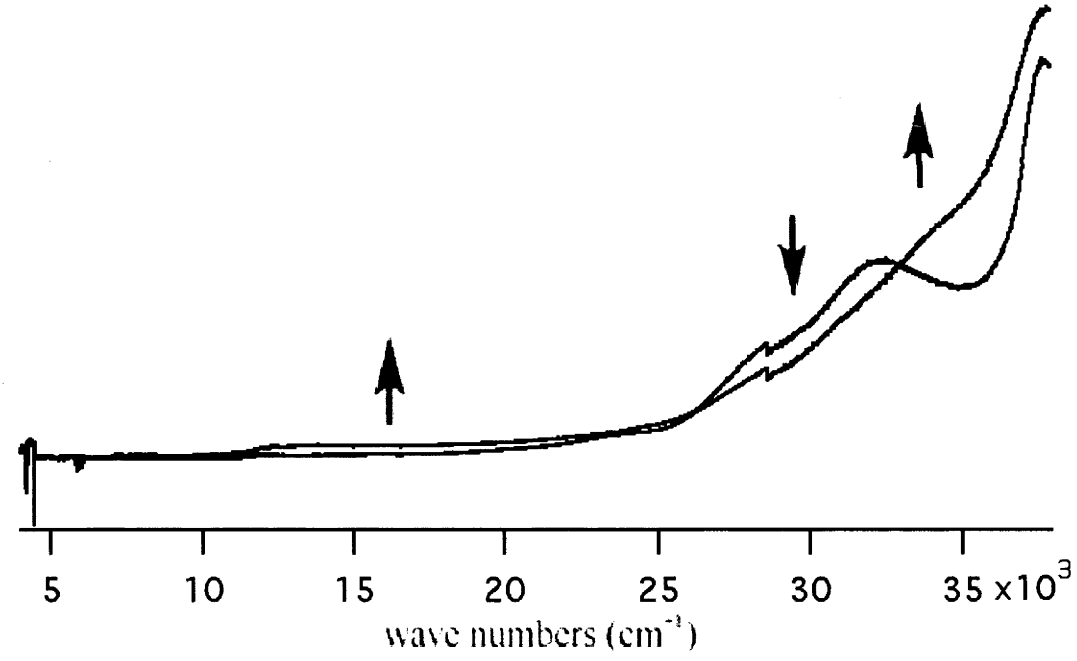

Figure 5.2 UV-Vis-NIR spectral changes during electrochemical oxidation of **46**

For the binuclear complexes **47** and **48** the process associated with the Fe(dppe)Cp* metal centre was shown to be reversible, cycling between the neutral and oxidised

species a number of times being accomplished without loss of peak height and with clean isobestic points. For **47** it was found that the starting material was already significantly oxidised (ca 50%) despite the precautions to exclude air and operating under an argon atmosphere. To obtain the neutral species a reducing voltage was initially applied before the material was oxidised. The changes on oxidation are very similar to those observed for **45**, which has the same $C{\equiv}CC_6H_4$-4-$C{\equiv}C$ ligand. The formation of a low energy band at ca 12000 cm^{-1} is accompanied by a decrease in intensity of the absorption bands between 22000 cm^{-1} and 27000 cm^{-1} (Figure 5.3). For **48** it was found that the starting material had no oxidised material present, as on applying a reducing voltage no changes were observed. On oxidation similar absorption bands to **46,** with the same $C{\equiv}CC_6H_4$-3-$C{\equiv}C$ ligand, are observed with a low intensity broad band between 13000 cm^{-1} and 20000 cm^{-1} and a slight decrease in the intensity of the absorption bands between 25000 cm^{-1} and 30000 cm^{-1} (Figure 5.4).

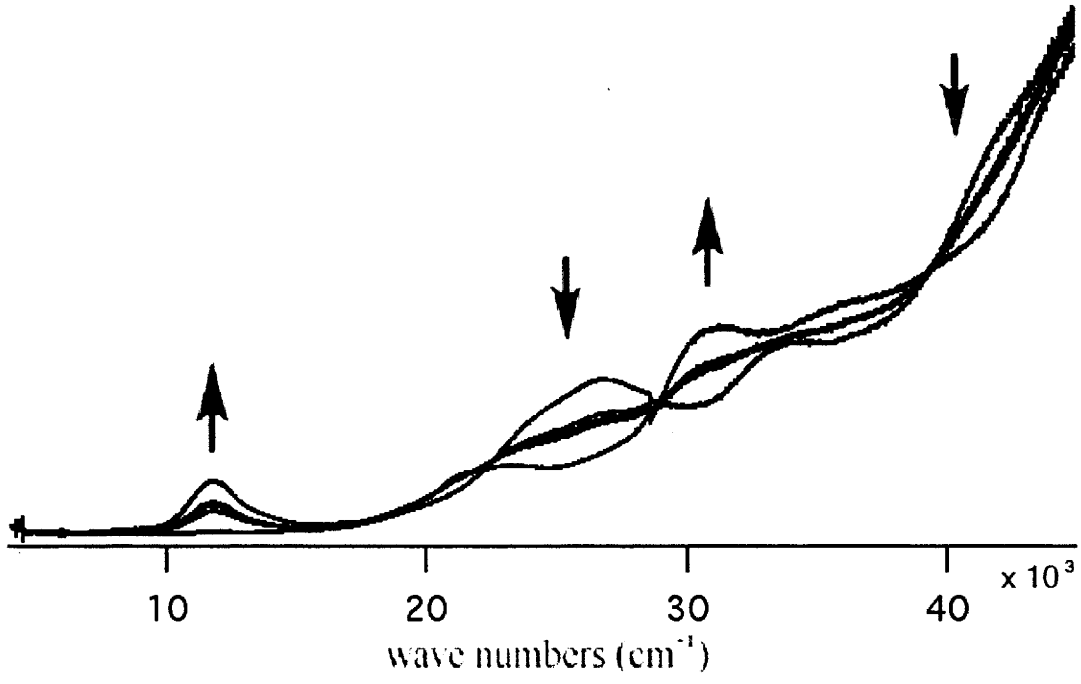

Figure 5.3 UV-Vis-NIR spectral changes during electrochemical oxidation of **47**

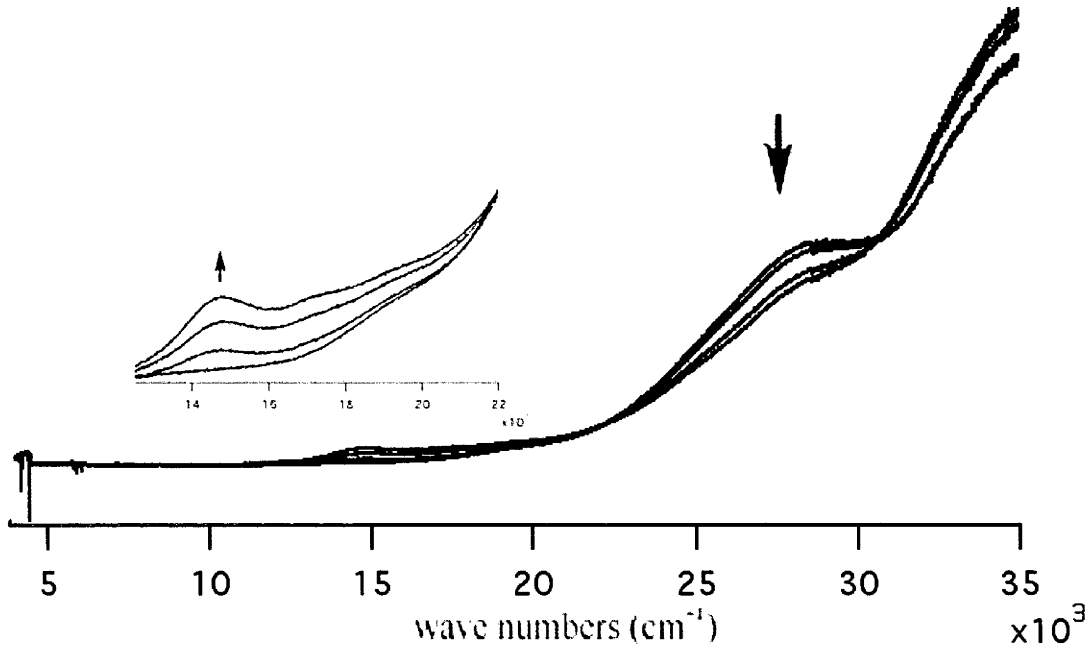

Figure 5.4 UV-Vis-NIR spectral changes during electrochemical oxidation of **48**

Complex	ν_{max} (cm^{-1}) [ε] (10^4 M^{-1} cm^{-1}) [a]
45	27000 [1.3], 29500 [1.7], 38000 [2.0]
45$^+$	12600 [0.4], 22200 [0.3], 25900 [0.6], 36800 [2.4]
46	32500 [1.7], 37700 [3.3]
46$^+$	13800 [0.1], 34500 [1.9], 37700 [3.6]
47	26800 [1.5], 34200 [1.9], 38000 [2.2]
47$^+$	11800 [0.4], 21600 [0.5], 31000 [2.1]
48	28300 [0.9], 35000 [1.8]
48$^+$	14800 [0.02], 29200 [0.8]

Table 4.3. Summary of optical data for complexes **45**, **46**, **47** and **48** [a] Electronic spectra were obtained at 298 K in CH_2Cl_2 using 0.3 M $(NBu^n_4)PF_6$ as supporting electrolyte with potentials ca 50-200 mV beyond $E_{1/2}$ for each couple.

5.3 Conclusions

A series of iron phenylethynyl complexes have been synthesised. The $Fe(CO)_2Cp^*$ centre has been used due to its lower sensitivity to oxidation than the more commonly used Fe(dppe)Cp* centre. It has been shown that one of the carbonyl ligands can be substituted for a PPh_3 group, to form a complex that has a reversible redox process as shown by cyclic voltammetry, but spectroelectrochemistry shows that the oxidised material is unstable at room temperature with significant loss of peak height on cycling. The formation of two binuclear complexes with a $C{\equiv}CC_6H_4$-4-$C{\equiv}C$ and a $C{\equiv}CC_6H_4$-3-$C{\equiv}C$ bridge separating a $Fe(CO)_2Cp^*$ from a Fe(dppe)Cp* centre has been achieved. The Fe(dppe)Cp* centre exhibits a reversible redox process as shown by cyclic voltammetry and spectroelectrochemistry.

5.4 Experimental section

5.4.1 General

All manipulations were carried out under inert atmospheres. Solvents or reagents were used as follows: Et_2O and *n*-pentane, distilled from Na/benzophenone; CH_2Cl_2, distilled from CaH_2 and purged with argon; NEt_3 distilled from KOH. Photolyses were performed with a Heraeus UV lamp (TQ150, 150 W, medium pressure) equipped with a quartz jacket. Solvents and reagents were obtained from commercial sources and used as received, unless otherwise indicated. Materials were prepared as stated previously. In addition the following additional materials were prepared according to literature procedures and were kindly provided by Dr Katy Green and Dr Gilles Argouarch: $FeCl(CO)_2Cp^*$[13], FeCl(dppe)Cp*[14], $HC{\equiv}CC_6H_4$-4-$C{\equiv}CSiPr^i_3$[15], $HC{\equiv}CC_6H_4$-3-$C{\equiv}CSiPr^i_3$[16], $HC{\equiv}CC_6H_4$-3-$C{\equiv}CSiMe_3$[17], $HC{\equiv}CC_6H_4$-4-$C{\equiv}CSiMe_3$[17]. Complexes **39** and **41** were initially prepared by Dr Katy Green.

5.4.2 Instrumentation

NIR spectra were recorded on a Cary 5000 spectrometer. UV-Visible spectra were recorded on an UVIKON XL spectrometer (250-12500 cm^{-1}). NMR spectra were obtained on a Bruker 200 DPX. Chemical shifts are given in parts per million relative to tetramethylsilane (TMS) for ^{1}H and ^{13}C spectra, and relative to H_3PO_4 for ^{31}P spectra. Cyclic voltammograms were recorded using a EG&G potentiostat (M.263) on platinum electrodes referenced to a SCE electrode and were calibrated with the ferrocene/ferrocenium couple taken at 0.46 V in CH_2Cl_2. LSIMS analyses were effected at the "Centre Regional de Mesures Physiques de l'Ouest" (C.R.M.P.O.) on a high resolution MS/MS ZabSpec TOF Micromass spectrometer (8 kV). Electronic spectra were recorded using a Cary 5 spectrophotometer. Solution spectra of the oxidized species were obtained at 298 K by electrogeneration in an optically-transparent thin-layer electrochemical (OTTLE) cell with potentials ca 50 - 200 mV beyond $E_{1/2}$ for each couple, to ensure complete electrolysis; solutions were made up in 0.3 M $(NBu^{n}_{4})PF_6$ in CH_2Cl_2.

5.4.3 Synthesis and Characterization

$Fe(C{\equiv}CC_6H_4\text{-}4\text{-}C{\equiv}CSiPr^{i}_{3})(CO)_2Cp^*$ (39)

CuI (91 mg, 0.478 mmol) was dissolved in NEt_3 (20 mL) and stirred for 10 min. This solution was then added to a solution of $HC{\equiv}CC_6H_4\text{-}4\text{-}C{\equiv}CSiPr^{i}_{3}$ (497 mg, 1.76 mmol) in THF (20 mL) and stirred for 30 min. $FeCl(CO)_2Cp^*$ (542 mg, 1.92 mmol) was dissolved in THF (20 mL), stirred for 10 min and then added to the CuI/acetylene solution. The reaction mixture was stirred for 12 h. The solvent was removed and the crude reaction mixture was passed through a short pad of alumina eluting with CH_2Cl_2. After evaporation of the solvent the product was dissolved in diethyl ether (10 mL) and precipitated with pentane (100 mL) at -70 °C, affording **39** as a yellow powder (723 mg, 78 %). ESI HRMS: *m/z* 551.2040 $[M + Na]^+$, *m/z* calcd

for $[C_{31}H_{40}O_2NaSi^{56}Fe]$ 551.2039. Anal. Calcd for $C_{25}H_{28}O_2SiFe$: C, 70.44; H, 7.63 Found: C, 69.41 H, 7.80. IR (CH_2Cl_2): 2150 cm^{-1} ν(C≡C-Si), 2096 cm^{-1} ν(Fe-C≡C), 2018 cm^{-1} ν(C≡O), 1969 cm^{-1} ν(C≡O). ^1H NMR (C_6D_6, 200 MHz): δ 7.42 (m, 4H, Ar), 1.42 (s, 15H, Cp*), 1.19 (s, 21H, $SiPr^i_3$). ^{13}C NMR (C_6D_6, 50 MHz): δ 215.3 (C≡O), 132.3(C_{ArH}), 131.6 (C_{ArH}), 130.2 (C_{Ar}), 120.0 (C_{Ar}), 113.8 (C≡C), 110.0 (C≡C), 109.0 (C≡C), 97.1 ($\underline{C}_5Me_5$), 90.5 (C≡CSi), 19.0 ($Si(CH\underline{Me}_2)_3$), 11.8 ($Si(\underline{C}HMe_2)_3$), 9.6 ($C_5\underline{Me}_5$).

$Fe(C{\equiv}CC_6H_4\text{-}4\text{-}C{\equiv}CSiMe_3)(CO)_2Cp^*$ (40)

CuI (91 mg, 0.48 mmol) was dissolved in 20 mL of NEt_3 and stirred for 10 min. This solution was then added to a solution of $HC{\equiv}CC_6H_4\text{-}4\text{-}C{\equiv}CSiMe_3$ (322 mg, 1.63 mmol) in THF (20 mL) and stirred for 30 min. $FeCl(CO)_2Cp^*$ (500 mg, 1.77 mmol) was dissolved in THF (20 mL), stirred for 10 min and then added to the CuI/acetylene solution. The reaction mixture was stirred for 12 h. The solvent was removed and the crude reaction mixture was passed through a short pad of alumina, eluting with CH_2Cl_2. The solvent was removed and the product was washed with cold pentane (10 mL), affording **40** as a yellow powder (530 mg, 73 %). HRMS: *m/z* 467.1098 $[M + Na]^+$, *m/z* calcd for $[C_{25}H_{28}O_2NaSi^{56}Fe]$ 467.1100. IR (CH_2Cl_2) 2152 cm^{-1} ν(C≡C-Si), 2096 cm^{-1} ν(Fe-C≡C), 2018 cm^{-1} ν(C≡O), 1969 cm^{-1} ν(C≡O). UV-vis (CH_2Cl_2, λ_{max}/nm [$\varepsilon/10^3$ $M^{-1}cm^{-1}$]): 325 [33.3]. ^1H NMR (C_6D_6): δ 7.43 (m, 4H, Ar), 1.40 (s, 15H, Cp*), 0.24 (s, 9H, $SiMe_3$). $^{13}C\{^1H\}$ NMR (C_6D_6): δ 215.3 (C≡O), 132.1 (C_{ArH}), 131.6 (C_{ArH}), 130.2 (C_{Ar}), 119.6 (C_{Ar}), 113.7 (C≡C), 110.4 (C≡C), 106.9 (C≡C), 97.1 ($\underline{C}_5Me_5$), 94.3 (C≡C), 9.6 ($C_5\underline{Me}_5$) 0.2 ($SiMe_3$).

$Fe(C{\equiv}CC_6H_4\text{-}3\text{-}C{\equiv}CSiPr^i_3)(CO)_2Cp^*$ (41)

CuI (107 mg, 0.56 mmol) was dissolved in 20 mL of NEt_3 and stirred for 10 min. This solution was then added to a solution of $HC{\equiv}CC_6H_4\text{-}3\text{-}C{\equiv}CSiPr^i_3$ (604 mg, 2.14

mmol) in THF (20 mL) and stirred for 30 min. $FeCl(CO)_2Cp^*$ (626 mg, 2.21 mmol) was dissolved in THF (20 mL), stirred for 10 min and added to the CuI/acetylene solution. The reaction mixture was stirred for 12 h. The solvent was removed and the crude reaction mixture passed through a short pad of alumina, eluting with CH_2Cl_2. The solvent was removed, the product dissolved in diethyl ether (10 mL) and precipitated with pentane (100 mL) at -70 °C, affording **41** as a yellow powder (823 mg, 74 %). Anal. Calcd for $C_{25}H_{28}O_2SiFe$: C, 70.44; H, 7.63. Found: C, 69.68 H, 7.72. HRMS: *m/z* 551.2040 $[M + Na]^+$, *m/z* calcd for $[C_{22}H_{20}O_2Na^{56}Fe]$ 551.20392. IR (CH_2Cl_2): 2150 cm^{-1} ν(C≡C-Si), 2100 cm^{-1} ν(Fe-C≡C), 2018 cm^{-1} ν(C≡O), 1968 cm^{-1} ν(C≡O). ^1H NMR (C_6D_6): δ 7.94 (s, 1H, Ar), 7.46 (d, 1H, ^3J = 7.4 Hz, Ar), 7.24 (d, 1H, ^3J = 7.5 Hz, Ar), 6.86 (dd, 1H, ^3J = 7.4 Hz, Ar), 1.41 (s, 15H, Cp*), 1.17 (m, 21H, $SiPr^i_3$). $^{13}C\{^1H\}$ NMR (C_6D_6): δ 215.3 (C≡O), 135.2 (C_{ArH}) 132.0 (C_{ArH}), 130.0 (C_{Ar}), 128.8 (C_{ArH}), 128.4(C_{ArH}), 123.6 (C_{Ar}), 112.6 (C≡C), 108.6 (C≡C), 107.4 (C≡C), 97.1 ($\underline{C}_5Me_5$), 89.8 (C≡*C*-Si), 19.0 ($Si(CH\underline{Me}_2)_3$), 11.8 ($Si(\underline{C}HMe_2)_3$), 9.6 ($C_5\underline{Me}_5$).

$Fe(C{\equiv}CC_6H_4$-3-$C{\equiv}CSiMe_3)(CO)_2Cp^*$ (42)

CuI (91 mg, 0.48 mmol) was dissolved in 20 mL of NEt_3 and stirred for 10 min. This solution was then added to a solution of $HC{\equiv}CC_6H_4$-3-$C{\equiv}CSiMe_3$ (322 mg, 1.63 mmol) in THF (20 mL) and stirred for 30 min. $FeCl(CO)_2Cp^*$ (500 mg, 1.77 mmol) was dissolved in THF (20 mL), stirred for 10 min and added to the CuI/acetylene solution. The reaction mixture was stirred for 12 h. The solvent was removed and the crude reaction mixture passed through a short pad of alumina, eluting with CH_2Cl_2. The solvent was removed and the product was washed with cold pentane (10 mL), affording **42** as a yellow powder (260 mg, 36 %). HRMS: *m/z* 467.1099 $[M + Na]^+$, *m/z* calcd for $[C_{25}H_{28}O_2NaSi^{56}Fe]$ 467.1100. IR (CH_2Cl_2): 2152 cm^{-1} ν(C≡C-Si), 2100 cm^{-1} ν(Fe-C≡C), 2018 cm^{-1} ν(C≡O), 1969 cm^{-1} ν(C≡O). UV-vis (CH_2Cl_2, λ_{max}/nm [$\varepsilon/10^3$ $M^{-1}cm^{-1}$]): 288 [13.8]. ^1H NMR (C_6D_6): δ 8.00 (s, 1H, Ar), 7.47 (d, 1H, ^3J = 7.5 Hz, Ar), 7.29 (d, 1H, ^3J = 7.7 Hz, Ar), 6.85 (dd, 1H, ^3J = 7.8 Hz, Ar),

1.39 (s, 15H, Cp*), 0.22 (s, 9H, $SiMe_3$). ^{13}C NMR (C_6D_6): δ 215.4 (C≡O), 135.3 (C_{ArH}), 132.0 (C_{ArH}), 128.5 (C_{ArH}), 128.4 (C_{ArH}), 130.1 (C_{Ar}), 123.5 (C_{Ar}), 112.6 (C≡C), 107.4 (C≡C), 106.5 (C≡C), 97.1 ($\underline{C}_5Me_3$), 93.6 (C≡*C*-Si), 9.6 ($C_5\underline{Me}_3$), 0.13 ($SiMe_3$).

Fe(C≡CC$_6$H$_4$-4-C≡CH)(CO)$_2$Cp* (43)

From Fe(C≡CC$_6$H$_4$-4-C≡CSiPr$^i_3$)(CO)$_2$Cp*:

NBu$^n_4$F (0.04 mL of a 1.0 M solution in THF, 0.04 mmol) and Fe(C≡CC$_6$H$_4$-4-C≡CSiPr$^i_3$)(CO)$_2$Cp* (67 mg, 0.127 mmol) were stirred in THF (50 mL) for 15 h. The solvent was removed and the residue dissolved in CH_2Cl_2 and passed through a short pad of alumina, eluting with CH_2Cl_2. The solvent was removed and the product dissolved in a minimum of diethyl ether (15 mL) and precipitated with pentane (100 mL) at -70 °C, affording **43** as an orange powder (18 mg, 38 %).

From Fe(C≡CC$_6$H$_4$-4-C≡CSiMe$_3$)(CO)$_2$Cp*:

NBu$^n_4$F (0.32 mL of a 1.0 M solution in THF, 0.32 mmol) and Fe(C≡CC$_6$H$_4$-4-C≡CSiMe$_3$)(CO)$_2$Cp* (480 mg, 1.08 mmol) were stirred in THF (30 mL) for 15 h. The solvent was removed and the residue dissolved in CH_2Cl_2 and passed through a short pad of alumina. The solvent was removed and the product washed with cold pentane (20 mL), affording **43** as an orange powder (220 mg, 55 %). HRMS: *m/z* 395.0707 $[M + Na]^+$, *m/z* calcd for $[C_{22}H_{20}O_2Na^{56}Fe]$ 395.0705. IR (CH_2Cl_2): 3297 cm^{-1} ν(≡CH), 2095 cm^{-1} ν(C≡C), 2018 cm^{-1} ν(C≡O), 1969 cm^{-1} ν(C≡O). UV-vis (CH_2Cl_2, λ_{max}/nm [ε/10^3 $M^{-1}cm^{-1}$]): 316 [27.5]. ^1H NMR (C_6D_6): δ 7.41 (m, 4H, Ar), 2.77 (s, 1H, C≡CH), 1.41 (s, 15H, Cp*). ^{13}C-NMR{^1H} (C_6D_6): δ 215.4 (C≡O), 132.2 (C_{ArH}), 131.7 (C_{ArH}), 130.2 (C_{Ar}), 118.6 (C_{Ar}), 113.6 (C≡C), 110.2 (C≡C), 97.1 ($\underline{C}_5Me_5$), 84.6 ($\underline{C}$≡CH), 78.1 (C≡$\underline{C}$H), 9.7 ($C_5\underline{Me}_5$).

Fe(C≡CC$_6$H$_4$-3-C≡CH)(CO)$_2$Cp* (44)

From Fe(C≡CC$_6$H$_4$-3-C≡CSiPr$^i_3$)(CO)$_2$Cp*:
NBu$^n_4$F (0.06 mL of a 1.0M solution in THF, 0.06 mmol) and Fe(C≡CC$_6$H$_4$-3-C≡CSiPr$^i_3$)(CO)$_2$Cp* (99 mg, 0.187 mmol) were stirred in THF (50 mL) for 15 h. The solvent was removed and the residue dissolved in CH_2Cl_2 and passed through a short pad of alumina, eluting with CH_2Cl_2. The solvent was removed and the product washed with pentane (10 mL), affording **44** as an orange powder (10 mg, 14 %).

From Fe(C≡CC$_6$H$_4$-3-C≡CSiMe$_3$)(CO)$_2$Cp*:
NBu$^n_4$F (0.20 mL of a 1.0M solution in THF, 0.20 mmol) and Fe(C≡CC$_6$H$_4$-3-C≡CSiMe$_3$)(CO)$_2$Cp* (300 mg, 0.675 mmol) were stirred in THF (30 mL) for 15 h. The solvent was removed and the residue dissolved in CH_2Cl_2 and passed through a short pad of alumina, eluting with CH_2Cl_2. The solvent was removed and the product washed with cold pentane (20 mL), affording **44** as an orange powder (130 mg, 52 %). HRMS: *m/z* 395.0706 $[M + Na]^+$, *m/z* calcd for $[C_{22}H_{20}O_2Na^{56}Fe]$ 395.0705. IR (CH_2Cl_2): 3300 cm^{-1} ν(≡CH), 2096 cm^{-1} ν(C≡C), 2018 cm^{-1} ν(C≡O), 1969 cm^{-1} ν(C≡O). UV-vis (CH_2Cl_2, λ_{max}/nm [ε/10^3 M^{-1}cm^{-1}]): 289 [18.4]. ^{1}H NMR (C_6D_6): δ 7.98 (s, 1H, Ar), 7.49 (d, 1H, ^3J = 7.5, Ar), 7.24 (d, 1H, ^3J = 7.6, Ar), 6.85 (dd, 1H, ^3J = 7.7, Ar), 2.68 (s, 1H, C≡CH), 1.40 (s, 15H, Cp*). ^{13}C NMR (C_6D_6): δ 215.3 (C≡O), 135.4 (C_{ArH}), 132.1 (C_{ArH}), 130.1 (C_{Ar}), 128.5 (obscured, C_{ArH}), 122.5 (C_{Ar}), 112.6 (C≡C), 107.5 (C≡C), 97.0 ($\underline{C}_5Me_5$), 84.3 ($\underline{C}$≡CH), 77.3 (C≡$\underline{C}$H), 9.6 ($C_5\underline{Me}_5$).

Fe(C≡CC$_6$H$_4$-4-C≡CSiPr$^i_3$)(CO)(PPh$_3$)Cp* (45)

Fe(C≡CC$_6$H$_4$-4-C≡CSiPr$^i_3$)(CO)$_2$Cp* (250 mg, 0.473 mmol) and PPh_3 (124 mg, 0.473 mmol) were dissolved in toluene (20 mL) and irradiated with UV light for 4 h. The solvent was removed and the crude product dissolved in a minimum of diethyl

ether (5 mL) and precipitated with pentane (20 mL) at -70 °C, affording **45** as a dark orange powder (150 mg, 42 %). HRMS: *m/z* 762.3100 $[M]^+$, *m/z* calcd for $[C_{48}H_{55}OSiP^{56}Fe]$ 762.3104. IR (CH_2Cl_2): 2148 cm^{-1} ν(C≡C-Si), 2076 cm^{-1} ν(Fe-C≡C), 1924 cm^{-1} ν(C≡O). UV-vis (CH_2Cl_2, λ_{max}/nm [ε/10^3 $M^{-1}cm^{-1}$]): 339 [17.3], 369 [13.2]. ^1H NMR (C_6D_6): δ 7.89 – 7.02 (m, 19H, Ar), 1.43 (s, 15H, Cp*), 1.21 (m, 21H, $SiPr^i_3$). ^{31}P NMR (C_6D_6): δ 75.6 (s, PPh_3). ^{13}C NMR (C_6D_6): δ 222.4 (d, J_{CP} = 29 Hz, C≡O), 136.3 (m, J_{CP} = 41 Hz, C_{Ar}), 134.4 (m, C_{ArH}), 132.2 (C_{ArH}), 130.8 (C_{ArH}), 131.1 (C_{Ar}), 129.7 (C_{ArH}), 127.9 (m, C_{ArH}), 119.3 (C≡C/C_{Ar}), 118.6 (C≡C/C_{Ar}), 109.4 (C≡C), 93.6 ($\underline{C}_5Me_5$), 89.9 (C≡CSi), 19.0 (Si(CH$\underline{Me}_2$)$_3$), 11.8 (Si($\underline{C}$HMe$_2$)$_3$), 9.8 ($C_5\underline{Me}_5$)

Fe(C≡CC_6H_4-3-C≡C$SiPr^i_3$)(CO)(PPh_3)Cp* (46)

Fe(C≡CC_6H_4-3-C≡C$SiPr^i_3$)$(CO)_2$Cp* (115 mg, 0.218 mmol) and PPh_3 (57 mg, 0.218 mmol) were dissolved in toluene (20 mL) and irradiated with UV light for 4 h. The solvent was removed, and the residue extracted with a minimum of diethyl ether (5 mL) and the product precipitated with pentane (20 mL) at -70 °C, affording **46** as a dark orange powder (50 mg, 30 %). HRMS: *m/z* 762.3090 $[M]^+$, *m/z* calcd for $[C_{48}H_{55}OSiP^{56}Fe]$ 762.3104. IR (CH_2Cl_2): 2152 cm^{-1} ν(C≡C-Si), 2077 cm^{-1} ν(Fe-C≡C), 1927 cm^{-1} ν(C≡O). UV-vis (CH_2Cl_2, λ_{max}/nm [ε/10^3 $M^{-1}cm^{-1}$]): 298 [16.8]. ^1H NMR (C_6D_6): δ 7.89 – 6.87 (m, 19H, Ar), 1.41 (s, 15H, Cp*), 1.19 (m, 21H, $SiPr^i_3$). ^{31}P NMR (C_6D_6): δ 75.8 (s, PPh_3). ^{13}C NMR (C_6D_6): δ 222.4 (d, J_{CP} = 29 Hz, C≡O), 136.3 (m, J_{CP} = 41 Hz, C_{Ar}), 134.5 (C_{ArH}), 134.3 (m, C_{ArH}), 131.3 (C_{ArH}), 130.9 (C_{Ar}), 129.7 (m, C_{ArH}), 128.2 (C_{ArH}), 128.0 (m, C_{Ar}), 127.8 (C_{ArH}), 123.5 (C_{Ar}), 117.9 (C≡C), 117.8 (C≡C), 109.1 (C≡C), 93.6 ($\underline{C}_5Me_5$), 89.2 (C≡*C*Si), 19.0 (Si(CH$\underline{Me}_2$)$_3$), 11.8 (Si($\underline{C}$HMe$_2$)$_3$), 9.8 ($C_5\underline{Me}_5$).

{Fe(dppe)Cp*}(μ-C≡CC$_6$H$_4$-4-C≡C){Fe(CO)$_2$Cp*} (47)

Fe(C≡CC$_6$H$_4$-4-C≡CH)(CO)$_2$Cp* (150 mg, 0.403 mmol), FeCl(dppe)Cp* (277 mg, 0.443) and KPF_6 (110 mg, 0.604 mmol) were suspended in 80 mL of a methanol/THF solvent mixture (1:1) and stirred at room temperature for 16 h. The solvent was removed and the vinylidene complex was extracted with CH_2Cl_2 (20 mL). The CH_2Cl_2 solution was reduced to 10 mL and the vinylidene complex was precipitated with pentane (40 mL). The vinylidene complex was dissolved in THF (40 mL) and KO^{t}Bu (67 mg, 0.604 mmol) added. The solution was stirred at room temperature for 2 h. The solvent was removed and the product extracted with toluene (80 mL). The solvent was removed and the product washed with pentane (30 mL) at -70 °C, to afford **47** as a dark orange powder (264 mg, 68 %). HRMS: *m/z* 960.2603 $[M]^+$, *m/z* calcd for $[C_{58}H_{58}O_2P_2{}^{56}Fe_2]$ 960.2605. IR (CH_2Cl_2): 2095 cm^{-1} ν(C≡C-Fe(CO)$_2$(Cp*)), 2053 cm^{-1} ν(C≡C-Fe(dppe)(Cp*)), 2017 cm^{-1} ν(C≡O), 1966 cm^{-1} ν(C≡O). UV-vis (CH_2Cl_2, λ_{max}/nm [ε/10^3 M^{-1}cm^{-1}]): 439 [5.5], 333 [11.6], 263 [22.1]. ^{1}H NMR (C_6D_6): δ 8.15 – 7.45 (m, 24H, Ar), 2.61 (m, 4H, CH_2), 1.56 (s, 15H, Cp*), 1.46 (s, 15H, Cp*). ^{31}P NMR: δ (ppm) 101.6 (s, 2P, dppe).

{Fe(dppe)Cp*}(μ-C≡CC$_6$H$_4$-3-C≡C){Fe(CO)$_2$Cp*} (48)

Fe(C≡CC$_6$H$_4$-3-C≡CH)(CO)$_2$Cp* (150 mg, 0.403 mmol), FeCl(dppe)Cp* (277 mg, 0.443) and KPF_6 (110 mg, 0.604 mmol) were suspended in 80 mL of a methanol/THF solvent mixture (1:1) and stirred at room temperature for 60 h. The solvent was removed and the vinylidene complex was extracted with CH_2Cl_2 (20 mL). The solution volume was reduced to 10 mL and the vinylidene intermediate was precipitated upon addition of pentane (60 mL). The vinylidene complex was dissolved in THF (40 mL) and KO^{t}Bu (67 mg, 0.604 mmol) added. The solution was stirred at room temperature for 2 h. The solvent was removed and the product extracted with toluene (80 mL). The solvent was removed and the product washed with pentane (30 mL) at -70 °C, affording **48** as a dark orange powder (120 mg, 31

%). HRMS: *m/z* 960.2607 $[M]^+$, *m/z* calcd for $[C_{58}H_{58}O_2P_2{}^{56}Fe_2]$ 960.2605. IR(CH_2Cl_2): 2098 cm^{-1} ν(C≡C-Fe(CO)$_2$Cp*), 2049 cm^{-1} ν(C≡C-Fe(dppe)Cp*), 2018 cm^{-1} ν(C≡O), 1969 cm^{-1} ν(C≡O). UV-vis (CH_2Cl_2, λ_{max}/nm [ε/10^3 $M^{-1}cm^{-1}$]): 367 [6.2], 281 [18.3]. ^{1}H NMR (C_6D_6): δ 8.06 - 6.76 (m, 24H, Ar), 2.61 (m, 4H, CH_2), 1.53 (s, 15H, Cp*), 1.48 (s, 15H, Cp*). ^{31}P NMR: δ 101.6 (s, 2P, dppe).

5.5 References

(1) Weyland, T.; Ledoux, I.; Brasselet, S.; Zyss, J.; Lapinte, C. *Organometallics* **2000**, *19*, 5235.
(2) Samoc, M.; Gauthier, N.; Cifuentes, M. P.; Paul, F.; Lapinte, C.; Dalton, G. T.; Humphrey, M. G. *Angew. Chem. Int. Ed.* **2006**, *45*, 7376.
(3) Cifuentes, M. P.; Humphrey, M. G.; Morrall, J. P.; Samoc, M.; Paul, F.; Lapinte, C.; Roisnel, T. *Organometallics* **2005**, *24*, 4280.
(4) Gauthier, N.; Argouarch, G.; Paul, F.; Humphrey, M. G.; Toupet, L.; Ababou-Girard, S.; Sabbah, H.; Hapiot, P.; Fabre, B. *Adv. Mater.* **2008**, *20*, 1952.
(5) Gauthier, N.; Olivier, C.; Rigaut, S.; Touchard, D.; Roisnel, T.; Humphrey, M. G.; Paul, F. *Organometallics* **2008**, *27*, 1063.
(6) Pevny, F.; Di Piazza, E.; Norel, L.; Drescher, M.; Winter, R. F.; Rigaut, S. *Organometallics* **2010**, *29*, 5912.
(7) Coat, F.; Guillevic, M.-A.; Toupet, L.; Paul, F.; Lapinte, C. *Organometallics* **1997**, *16*, 5988.
(8) Argouarch, G.; Grelaud, G.; Paul, F. *Organometallics* **2010**, *29*, 4414.
(9) Wong, A.; Kang, P. C. W.; Tagge, C. D.; Leon, D. R. *Organometallics* **1990**, *9*, 1992.
(10) Le Narvor, N.; Lapinte, C. *Organometallics* **1995**, *14*, 634.
(11) Medei, L.; Orian, L.; Semeikin, O. V.; Peterleitner, M. G.; Ustynyuk, N. A.; Santi, S.; Durante, C.; Ricci, A.; Lo Sterzo, C. *Eur. J. Inorg. Chem.* **2006**, 2582.
(12) Field, L. D.; George, A. V.; Laschi, F.; Malouf, E. Y.; Zanello, P. *J. Organomet. Chem.* **1992**, *435*, 347.
(13) Akita, M.; Terada, M.; Tanaka, M.; Morooka, Y. *J. Organomet. Chem.* **1996**, *510*, 255.
(14) Roger, C.; Hamon, P.; Toupet, L.; Rabaa, H.; Saillard, J. Y.; Hamon, J. R.; Lapinte, C. *Organometallics* **1991**, *10*, 1045.
(15) Lavastre, O.; Ollivier, L.; Dixneuf, P.; Sibandhit, S. *Tetrahedron* **1996**, *52*, 5495.
(16) Henze, O.; Lentz, D.; Schluter, A. D. *Chem.-Eur. J.* **2000**, *6*, 2362.
(17) Argouarch, G.; Paul, F. *Unpublished results* **2011**

Appendix A

Chapter 2 NMR spectra

cis-$[OsCl_2(dppe)_2]$ ^1H NMR

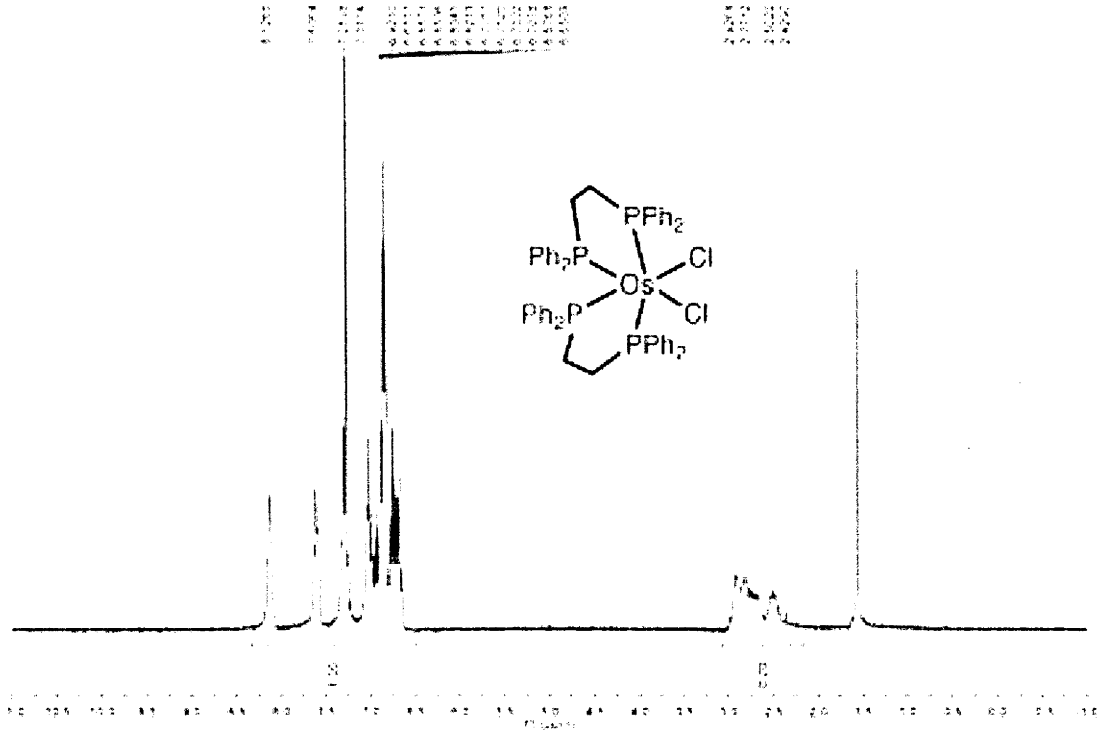

cis-$[OsCl_2(dppe)_2]$ ^{31}P NMR

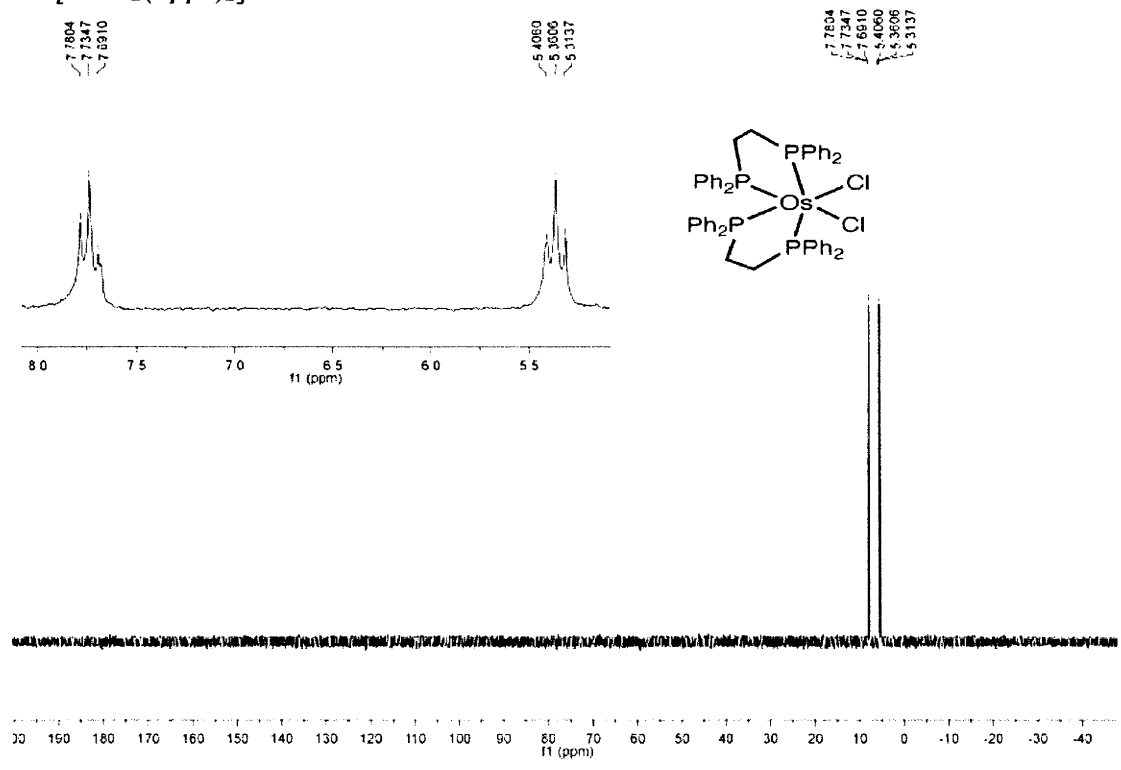

1 ^{1}H NMR

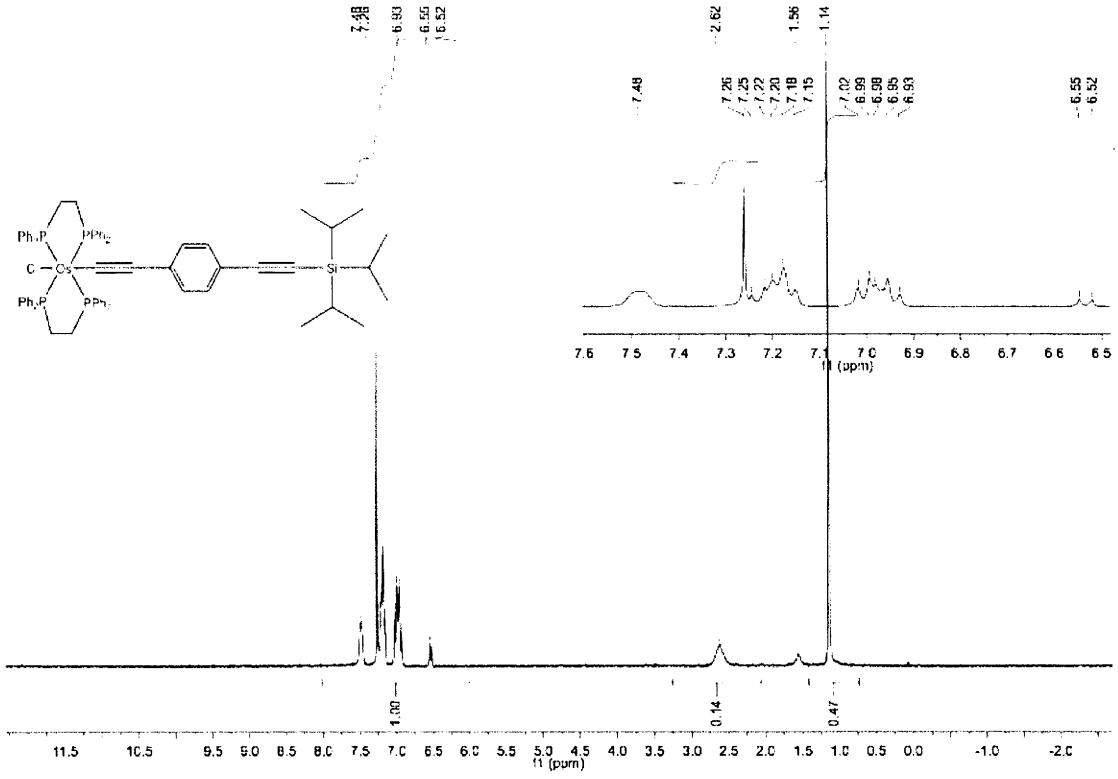

1 ^{31}P NMR

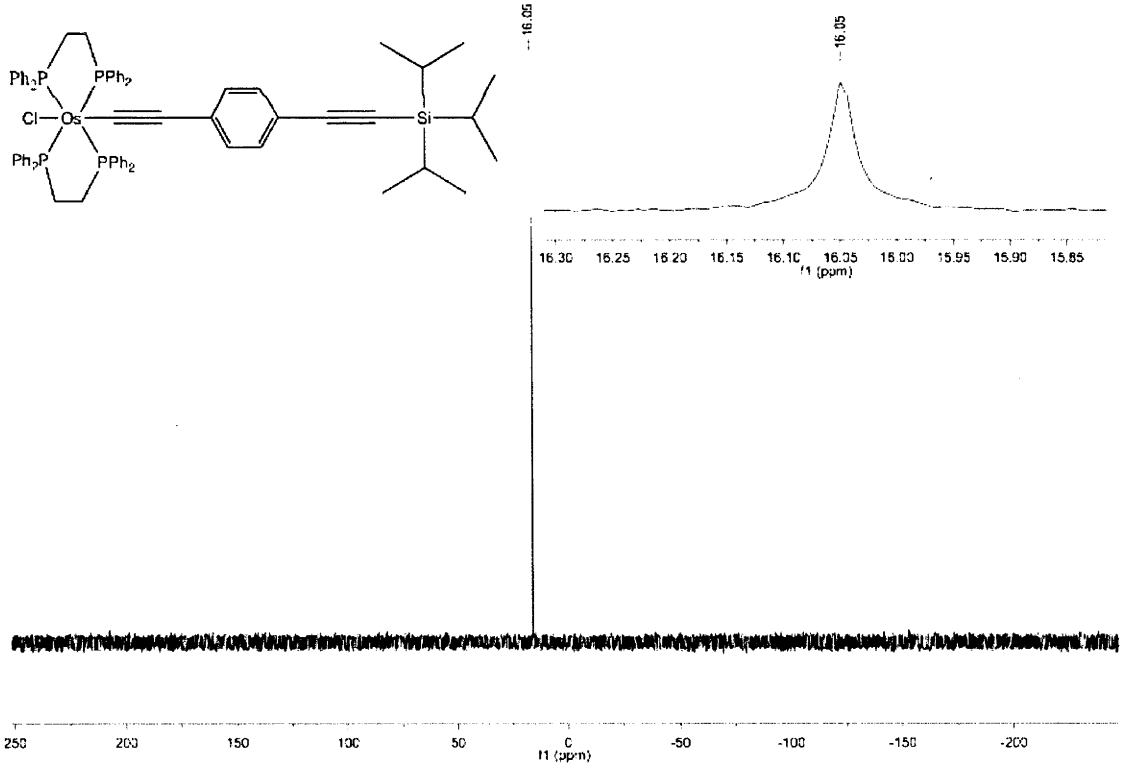

1 ^{13}C NMR

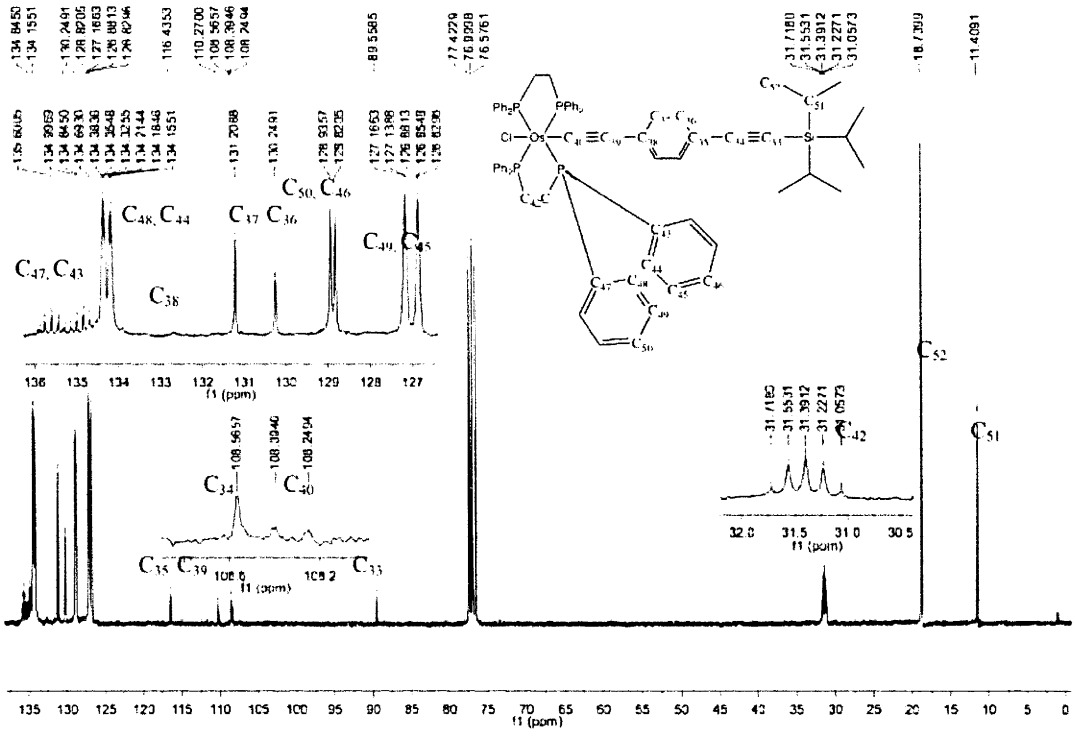

2 ^{1}H NMR

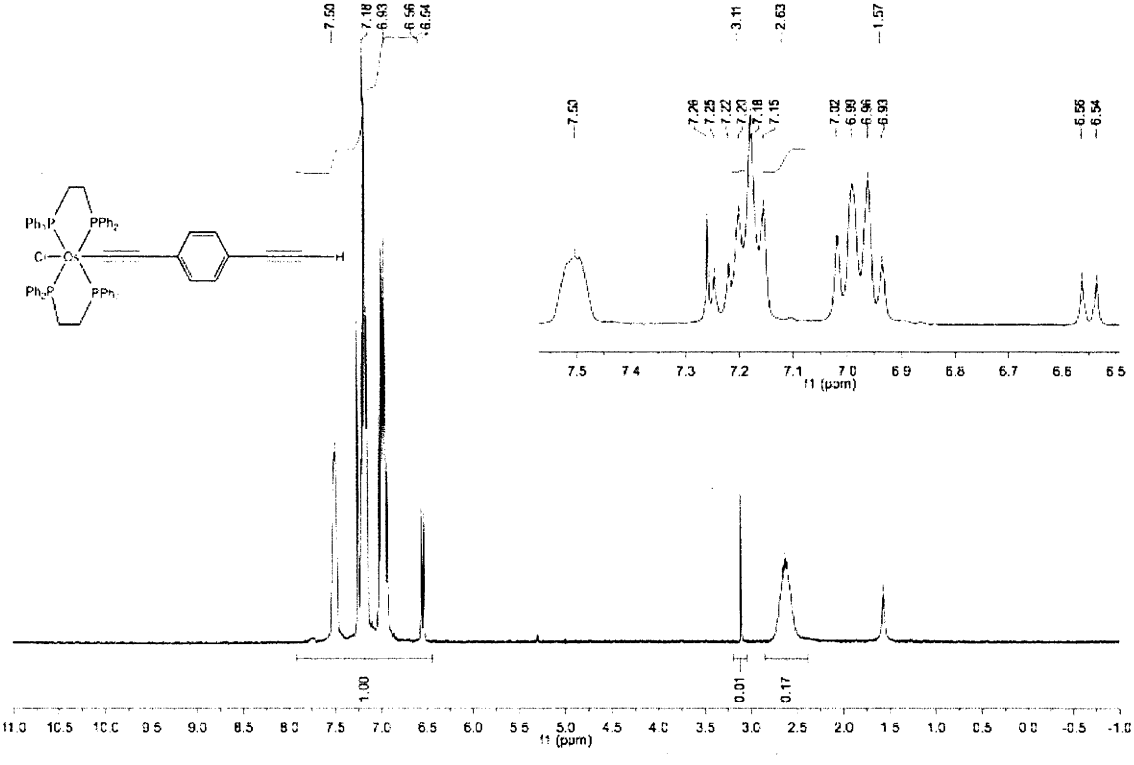

2 ^{31}P NMR

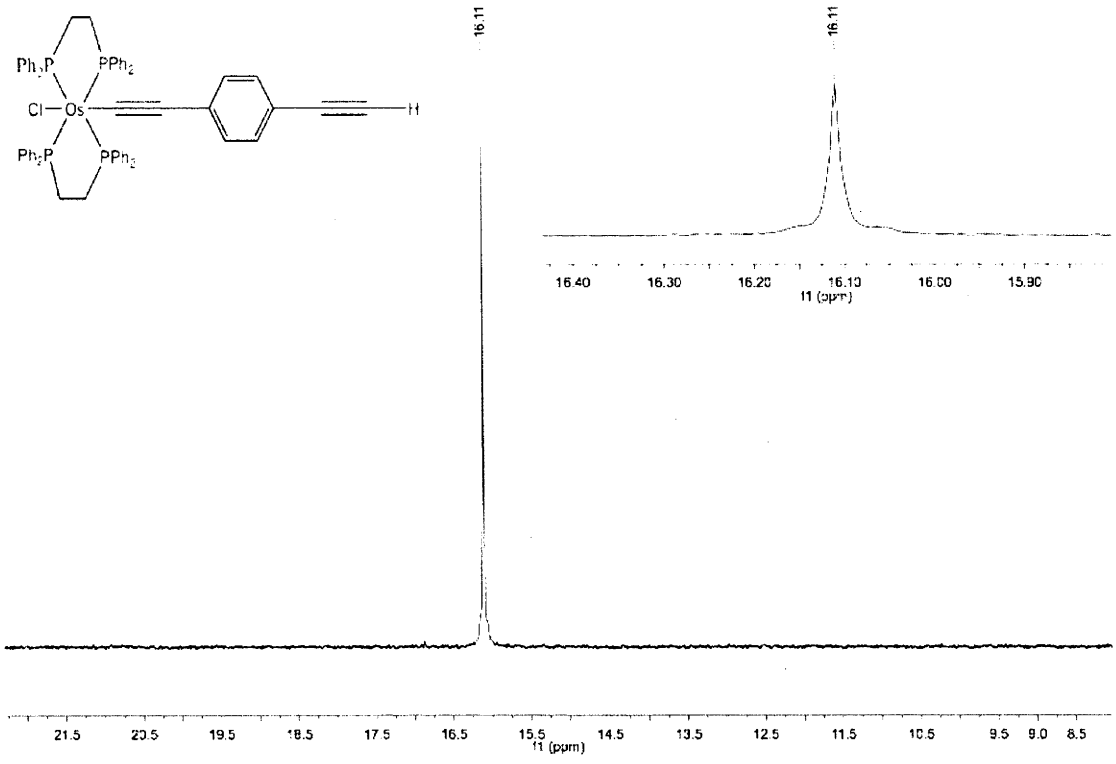

2 ^{13}C NMR

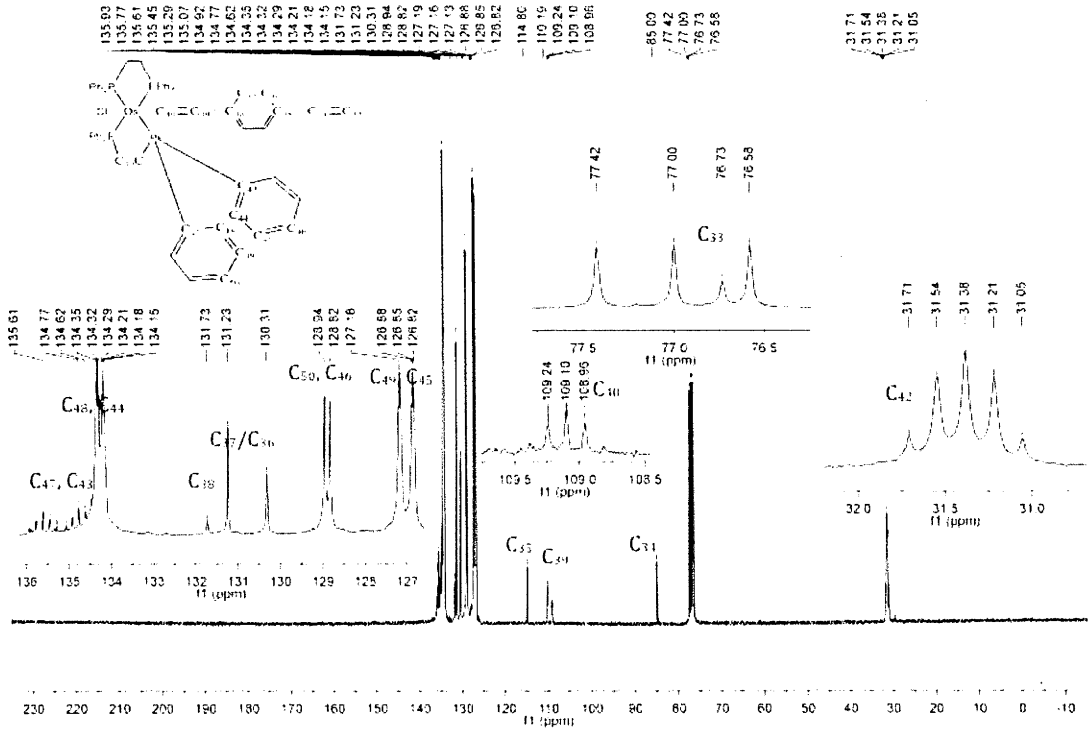

3 ^{1}H NMR

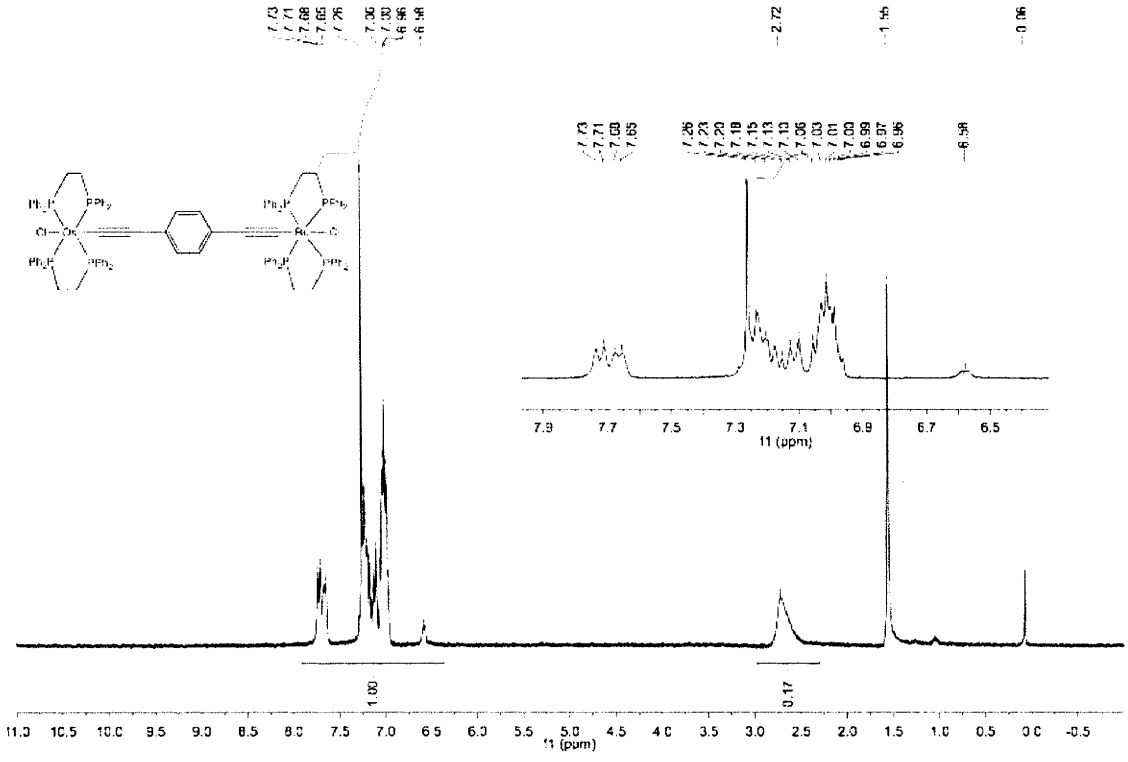

3 ^{31}P NMR

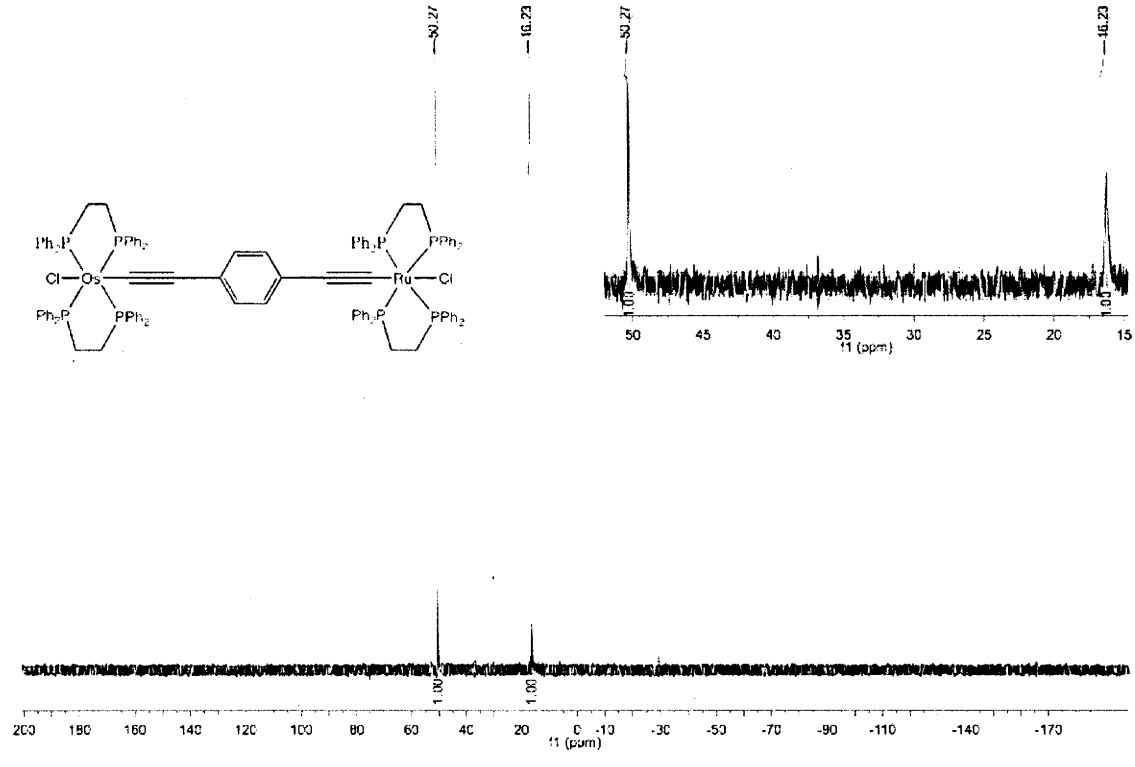

4 ^{1}H NMR

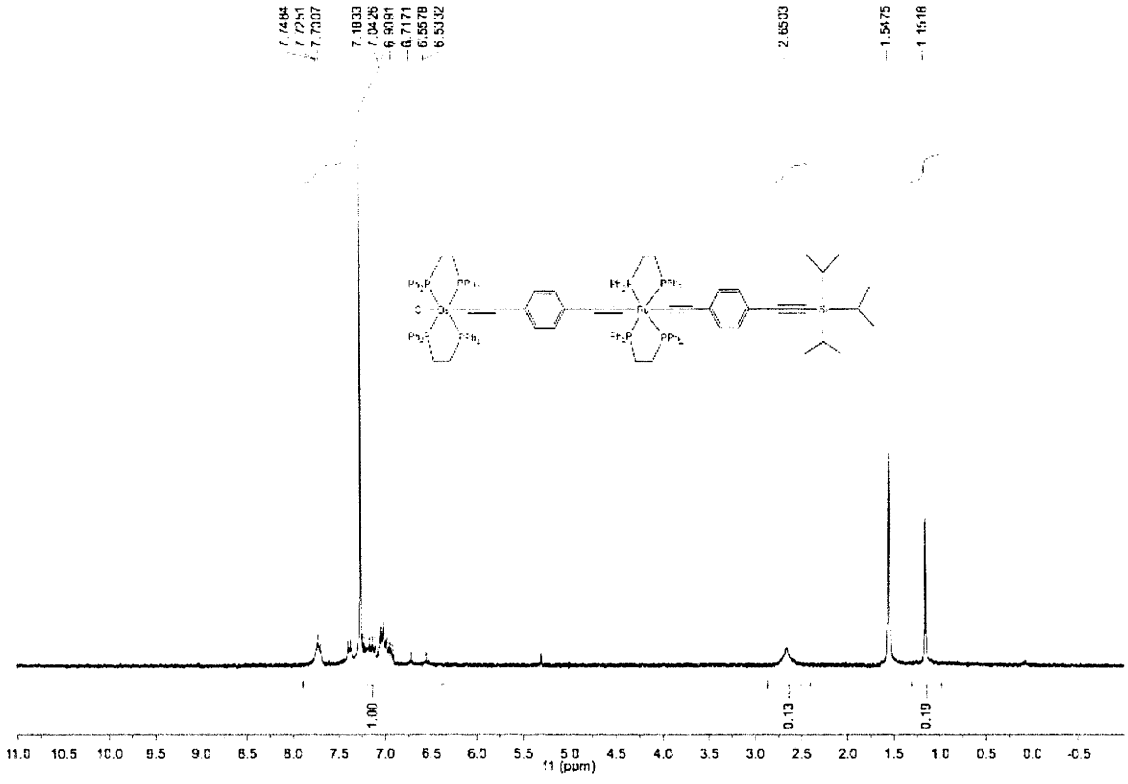

4 ^{31}P NMR

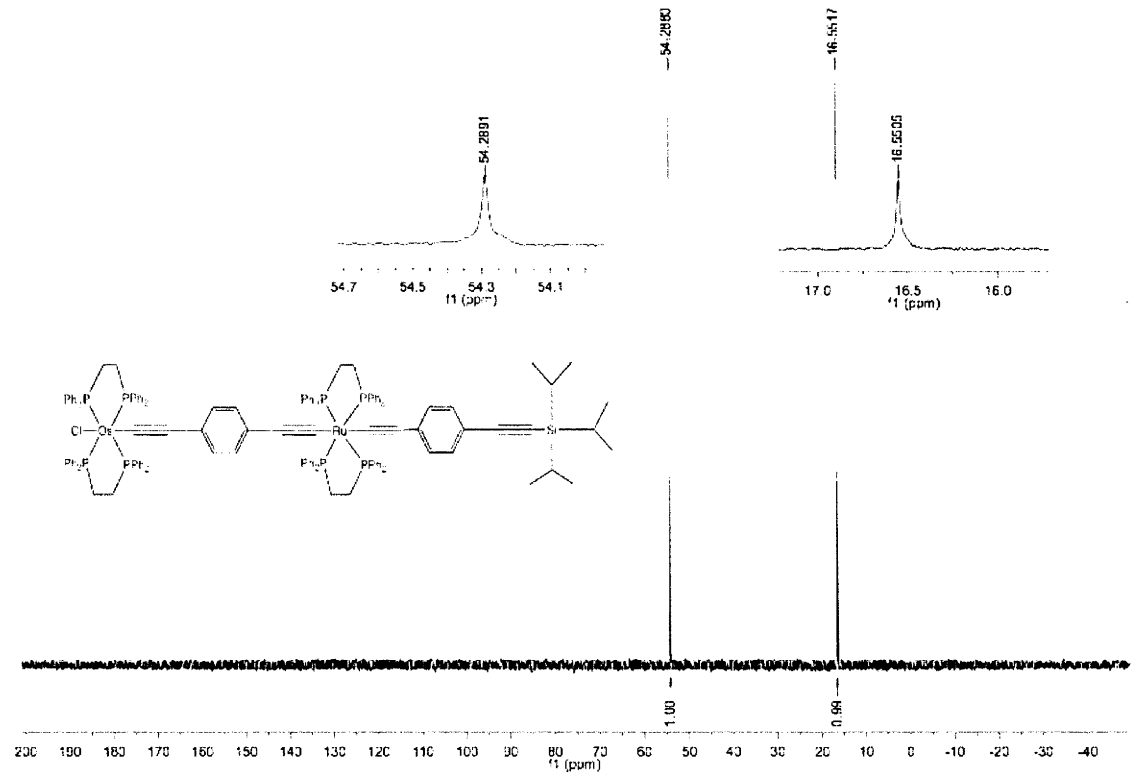

4 ^{13}C NMR

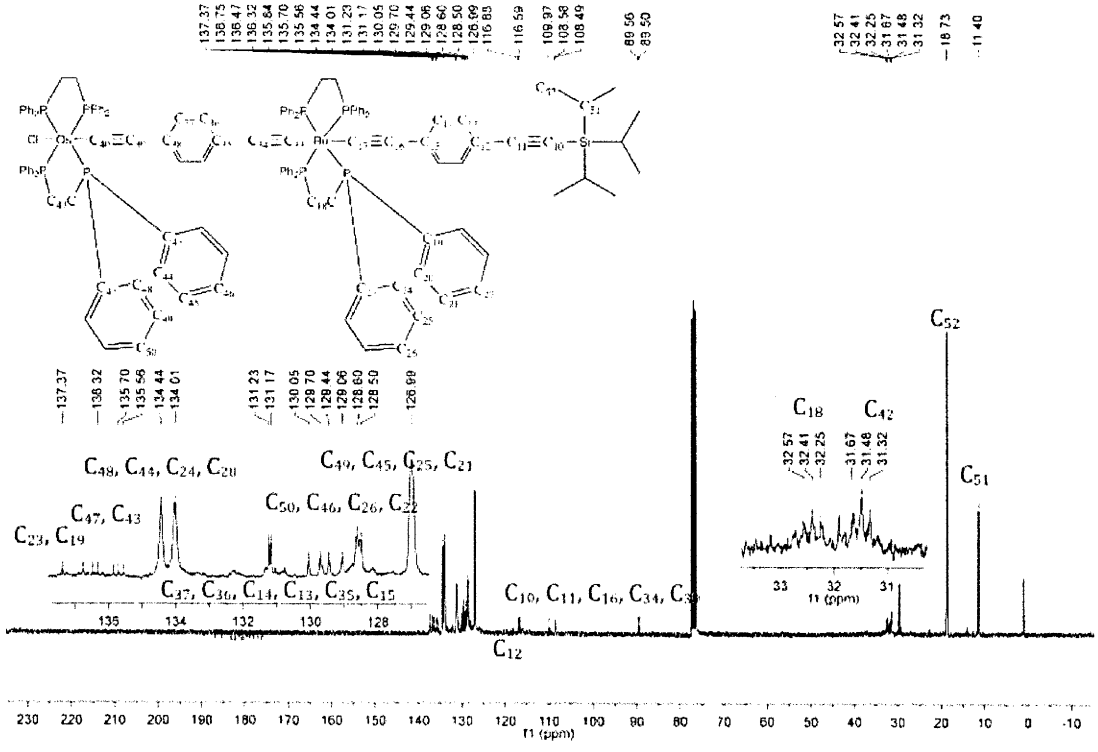

5 ^{1}H NMR

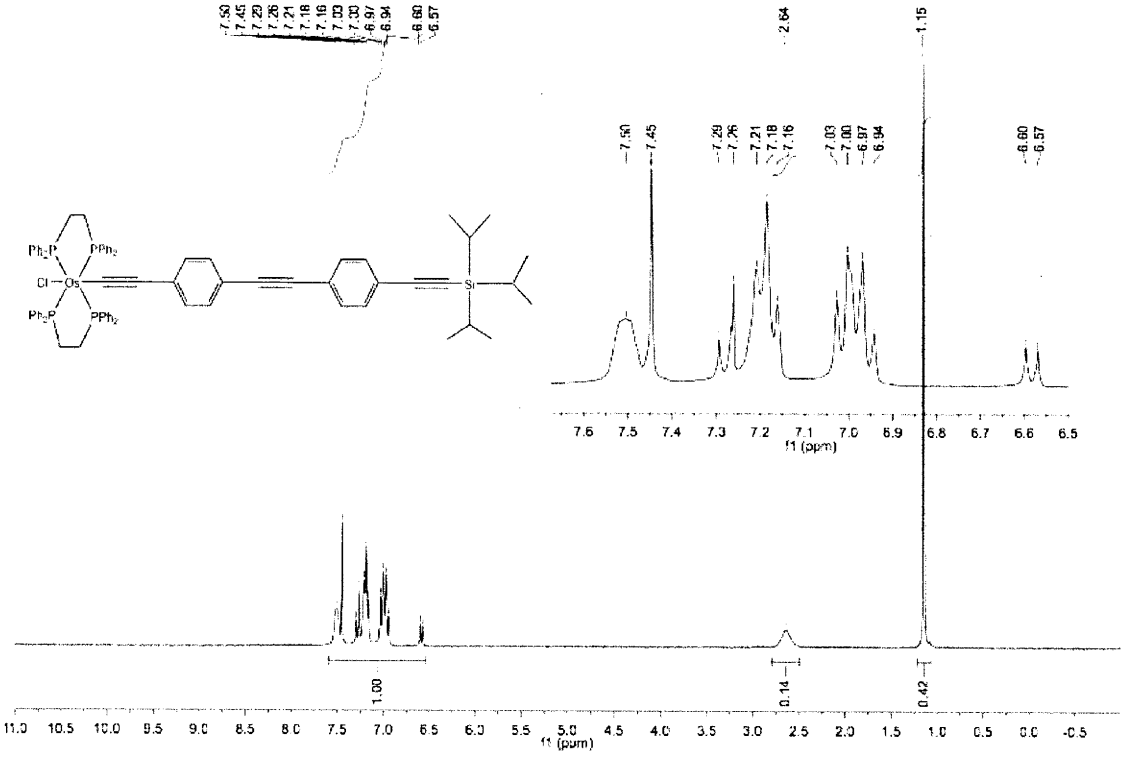

5 ^{13}P NMR

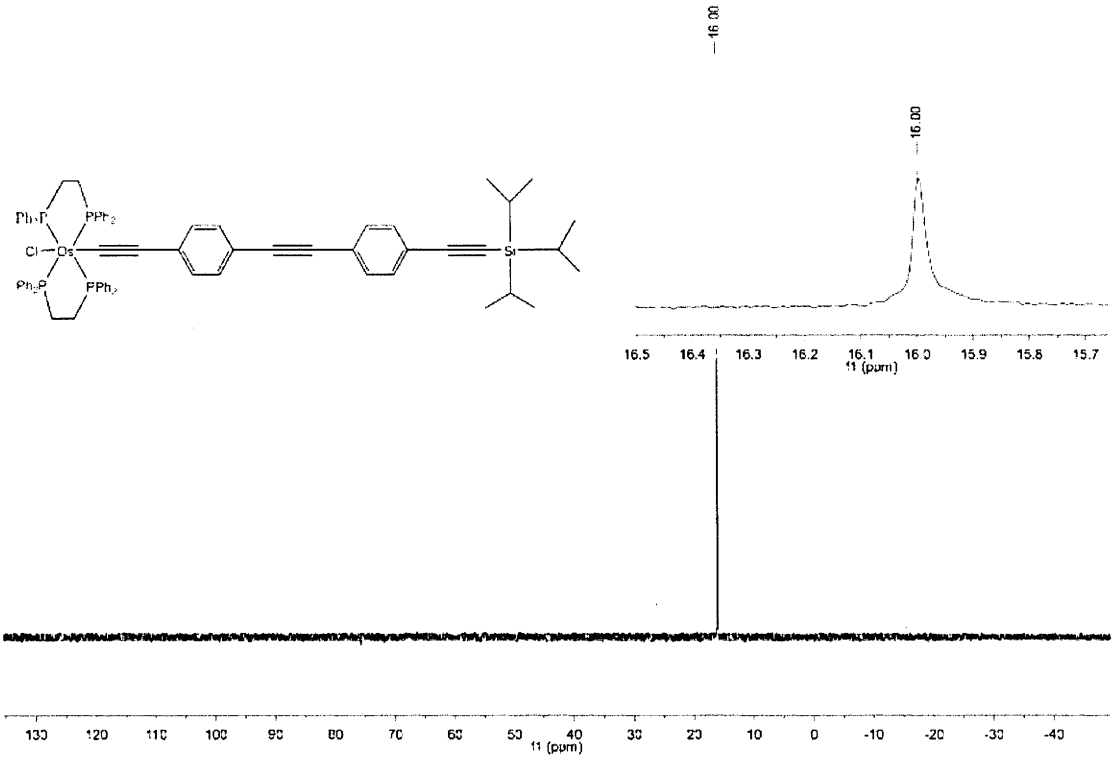

5 ^{13}C NMR

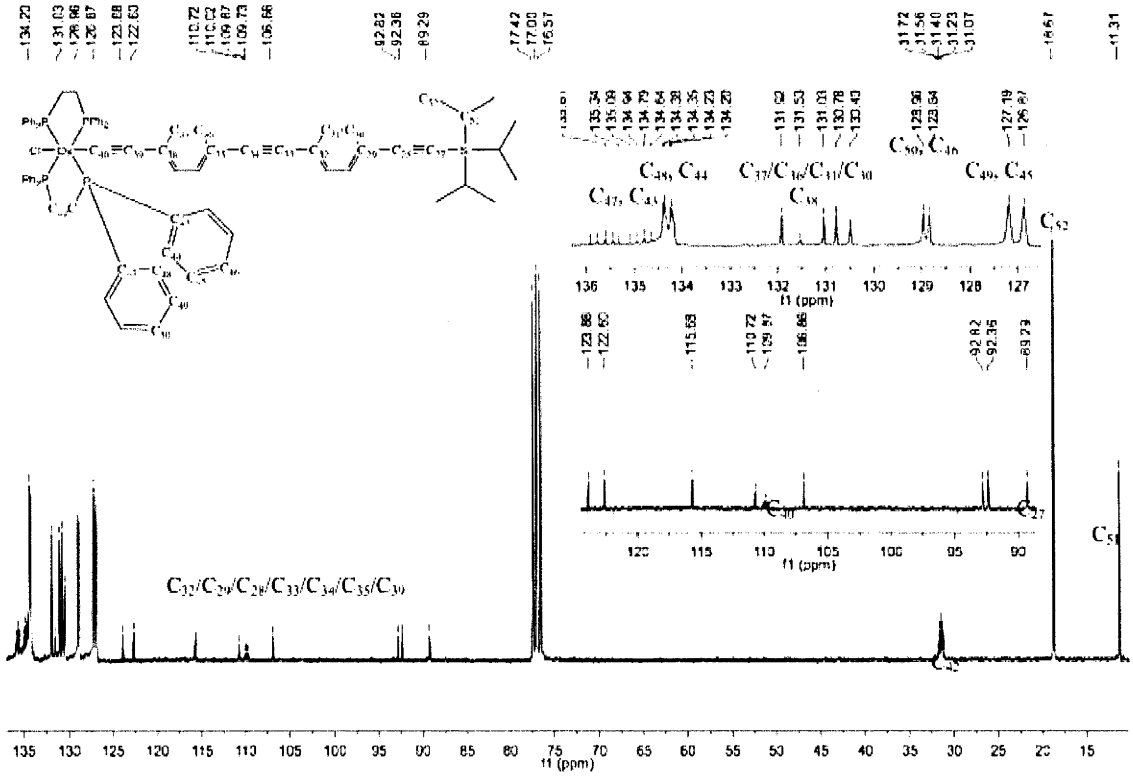

6 ^{1}H NMR

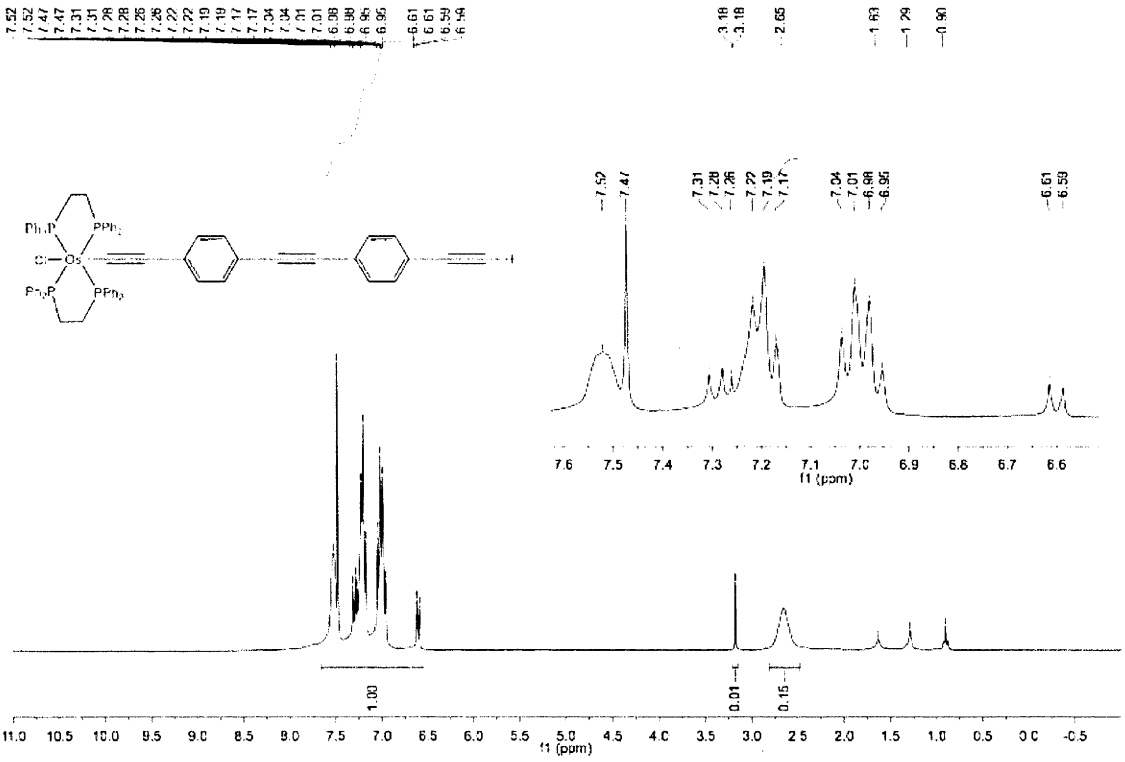

6 ^{31}P NMR

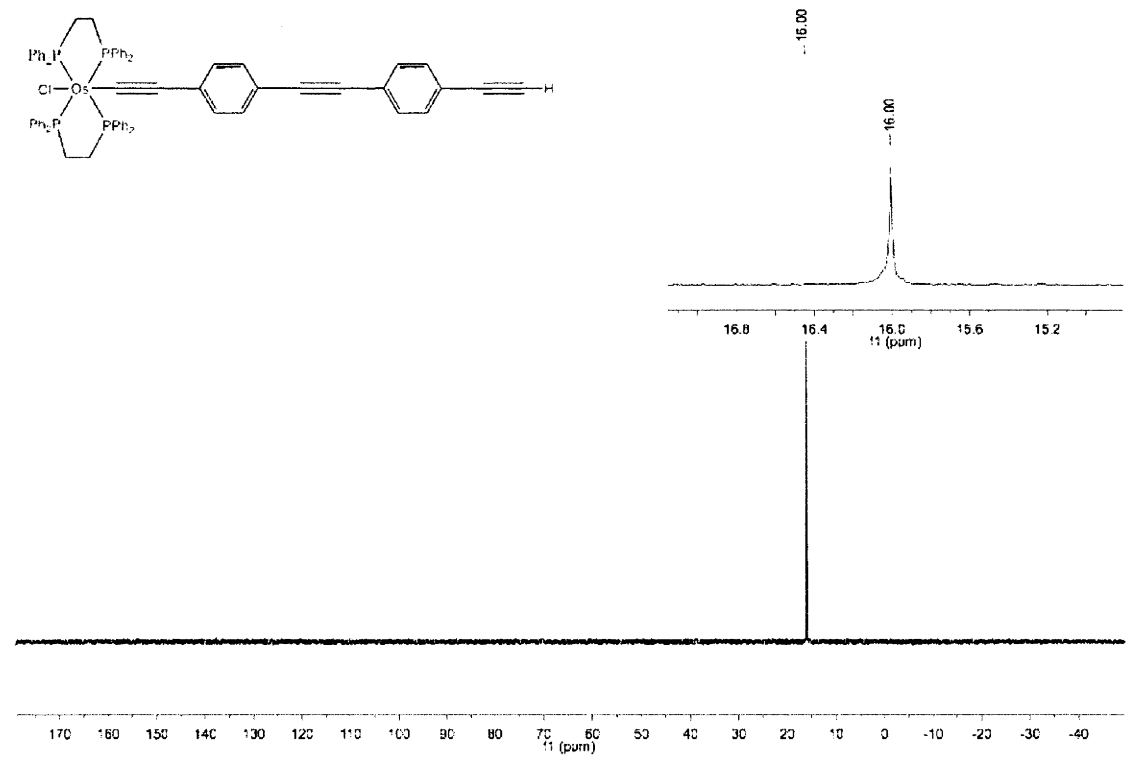

6 ^{13}C NMR

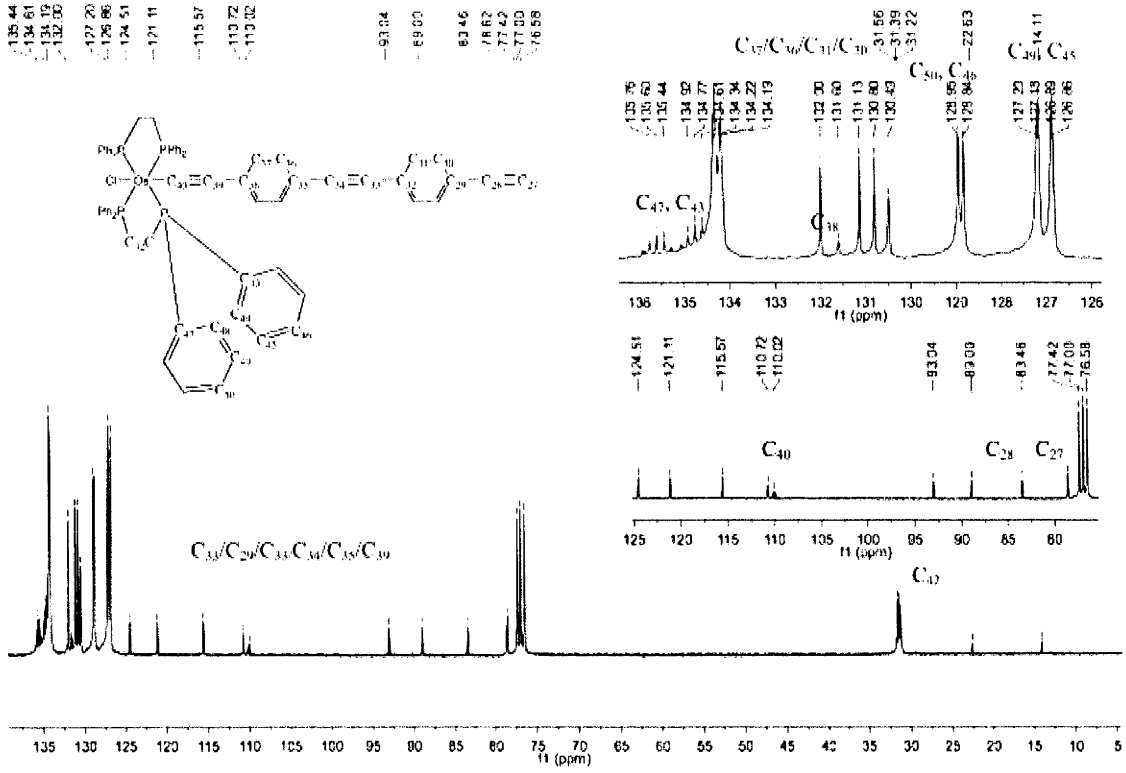

7 ^{1}H NMR

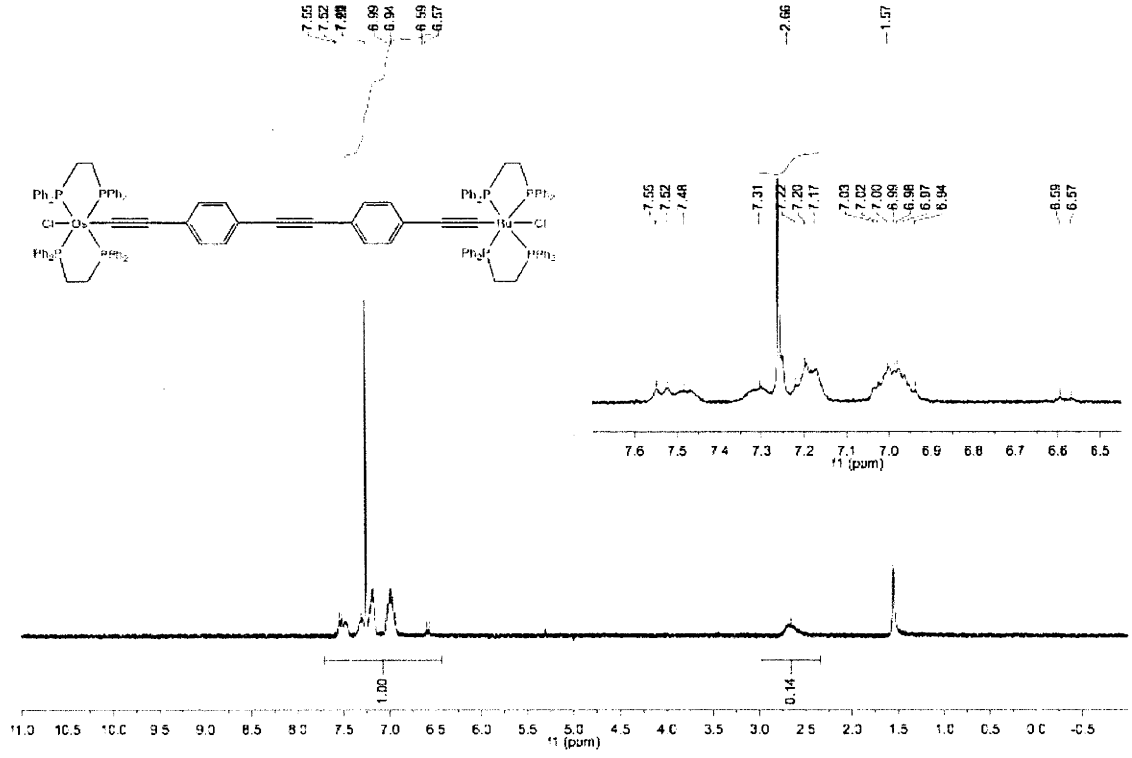

7 ^{31}P NMR

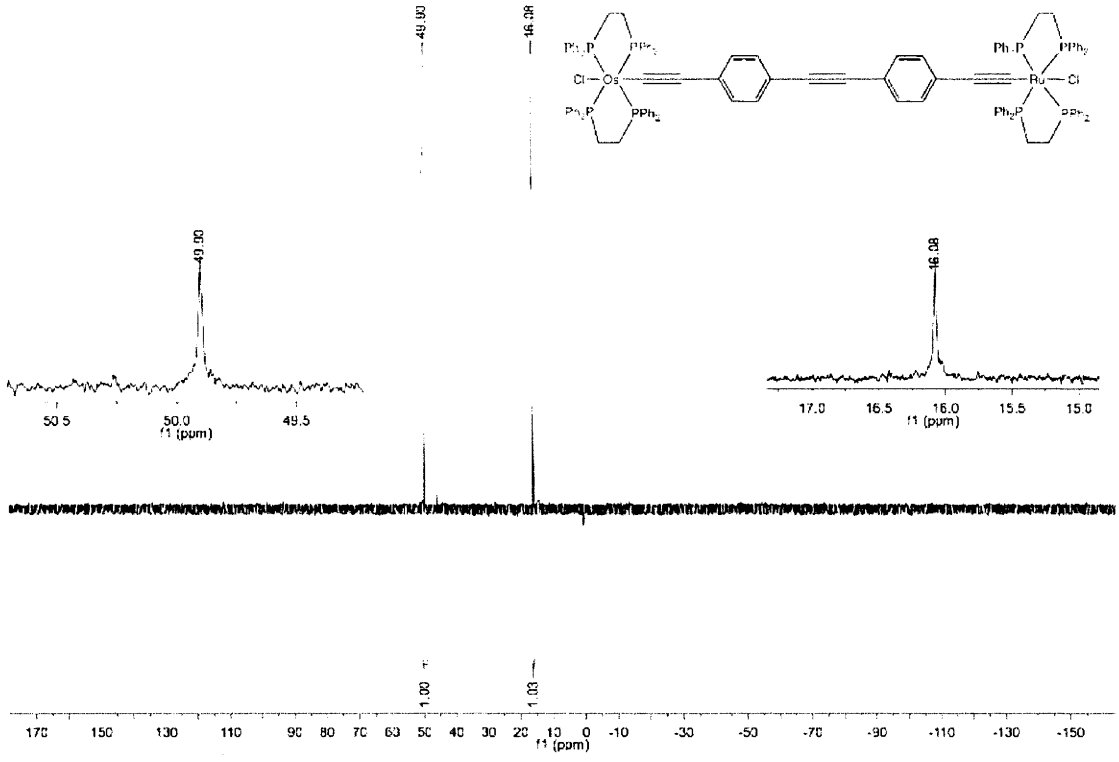

7 ^{13}C NMR

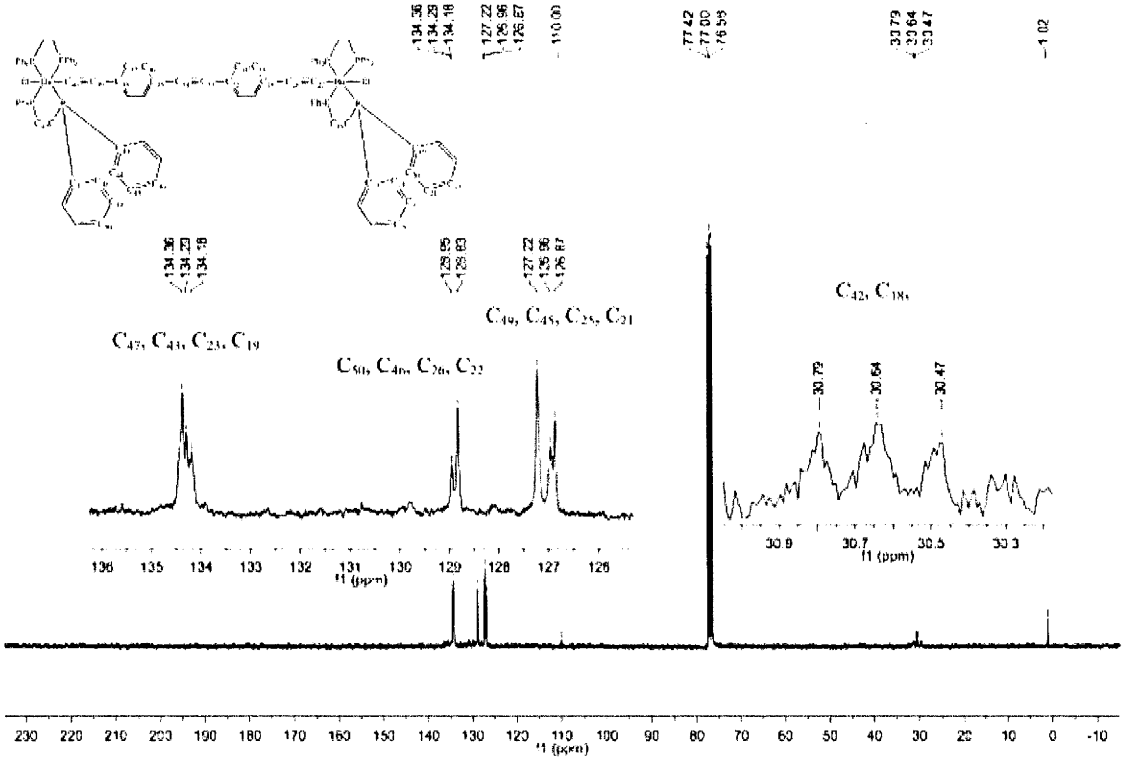

8 ^{1}H NMR

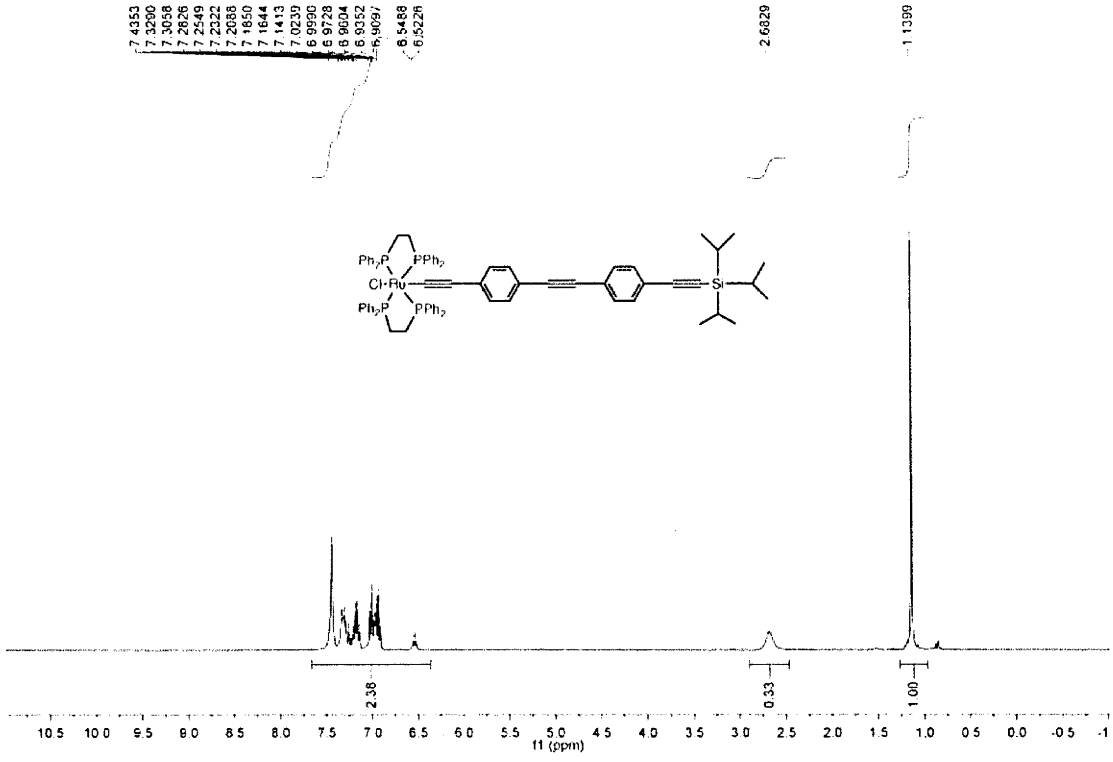

8 ^{31}P NMR

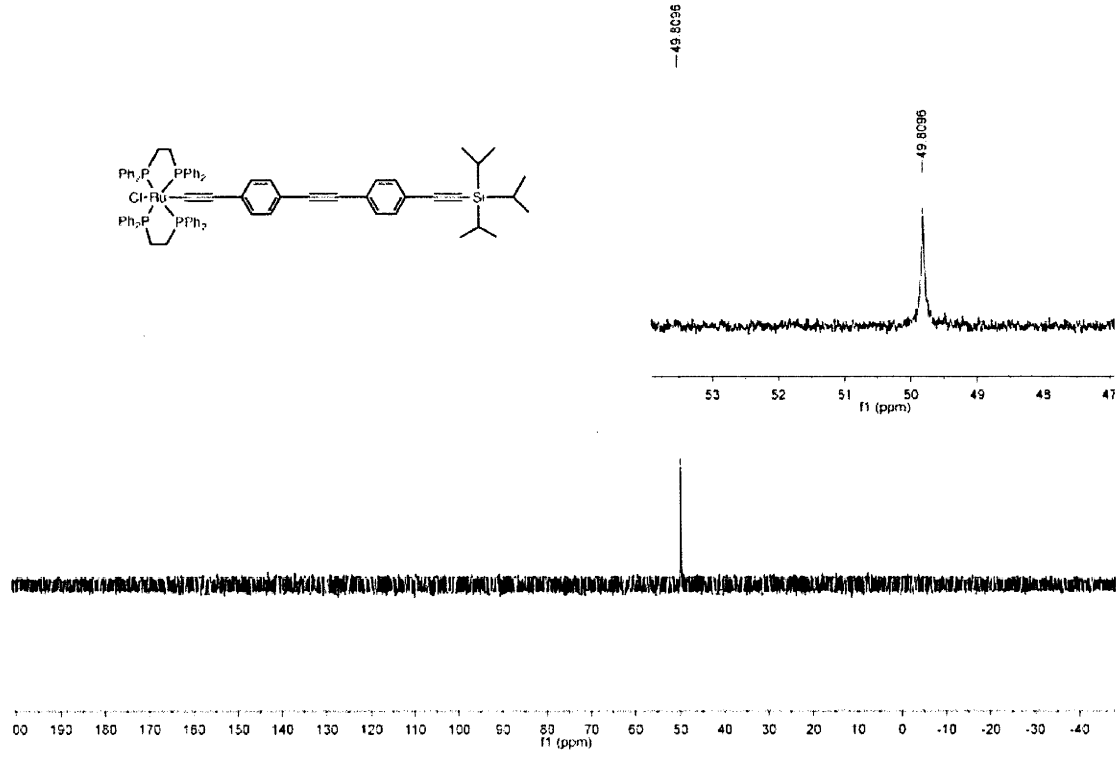

8 ^{13}C NMR

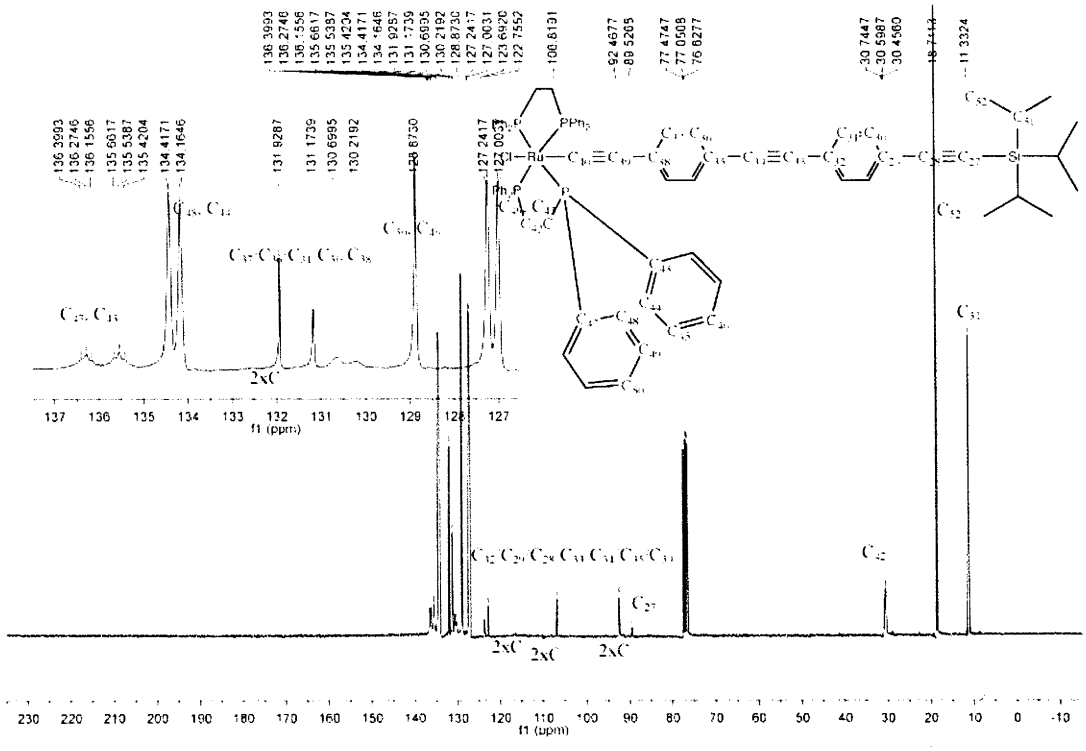

Appendix B

Chapter 3 NMR spectra

10 ^{1}H NMR

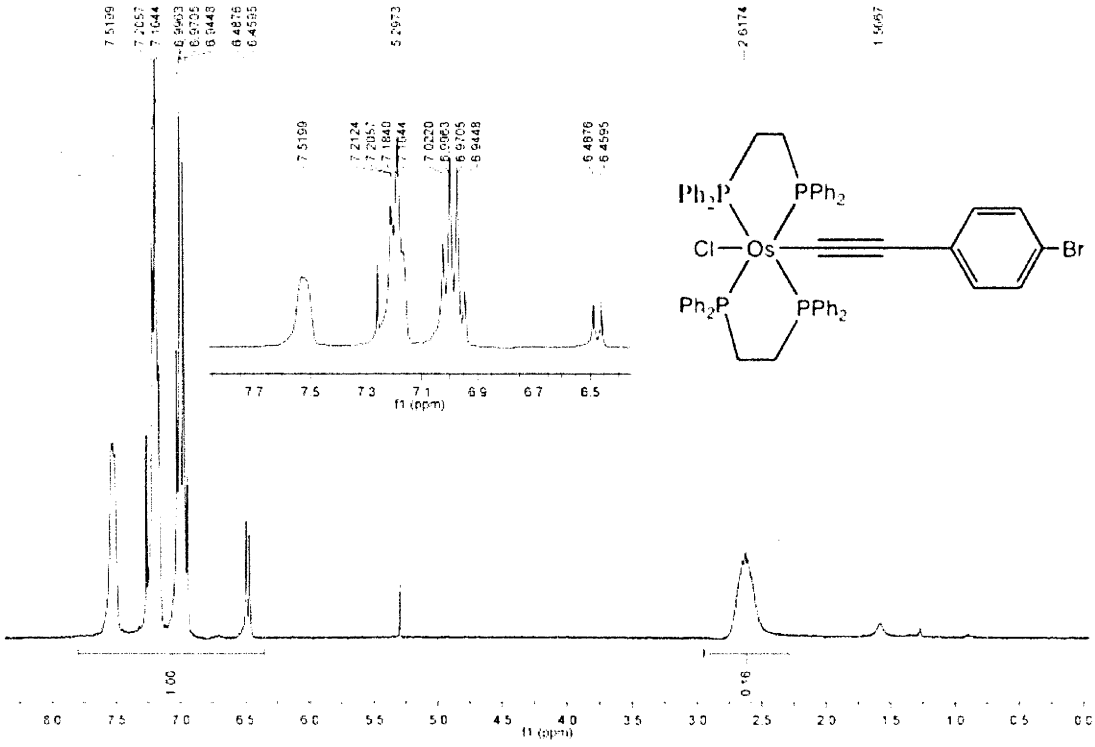

10 ^{31}P NMR

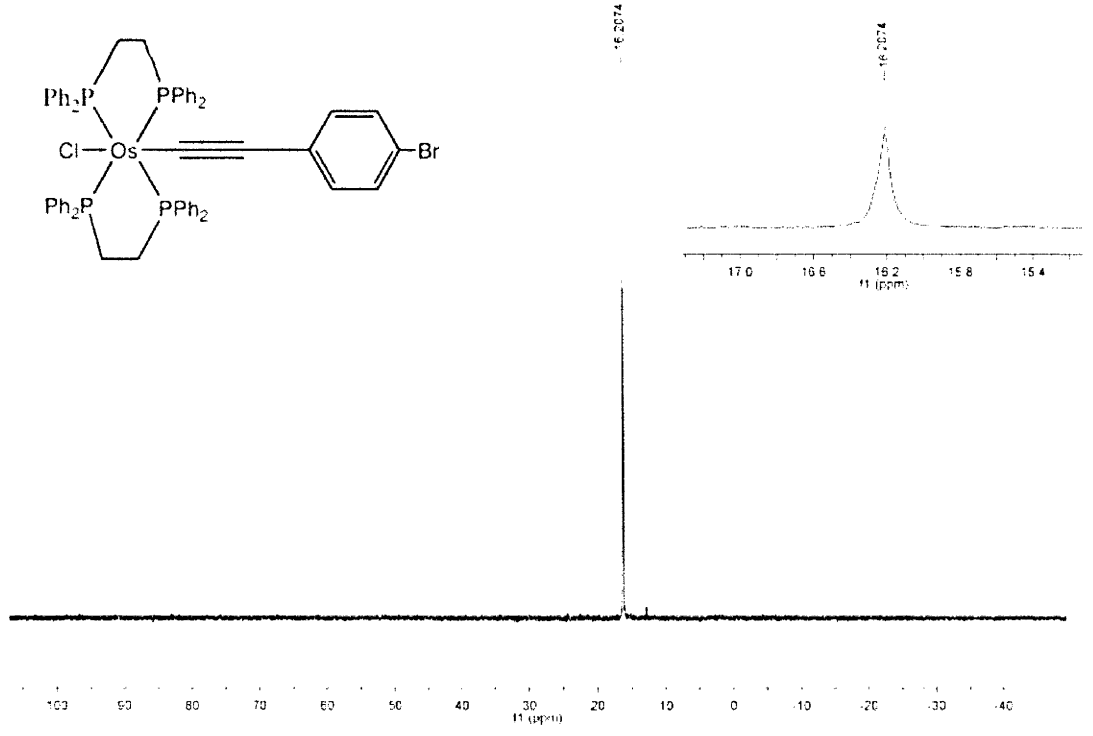

10 ^{13}C NMR

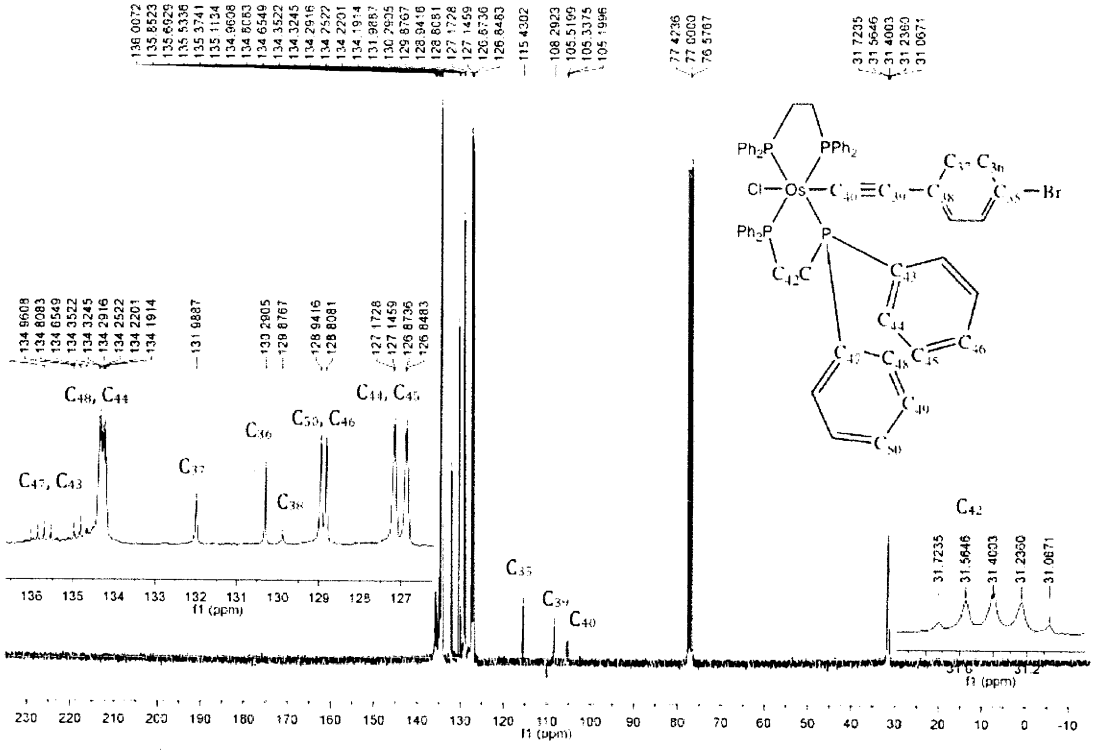

11 ^{1}H NMR

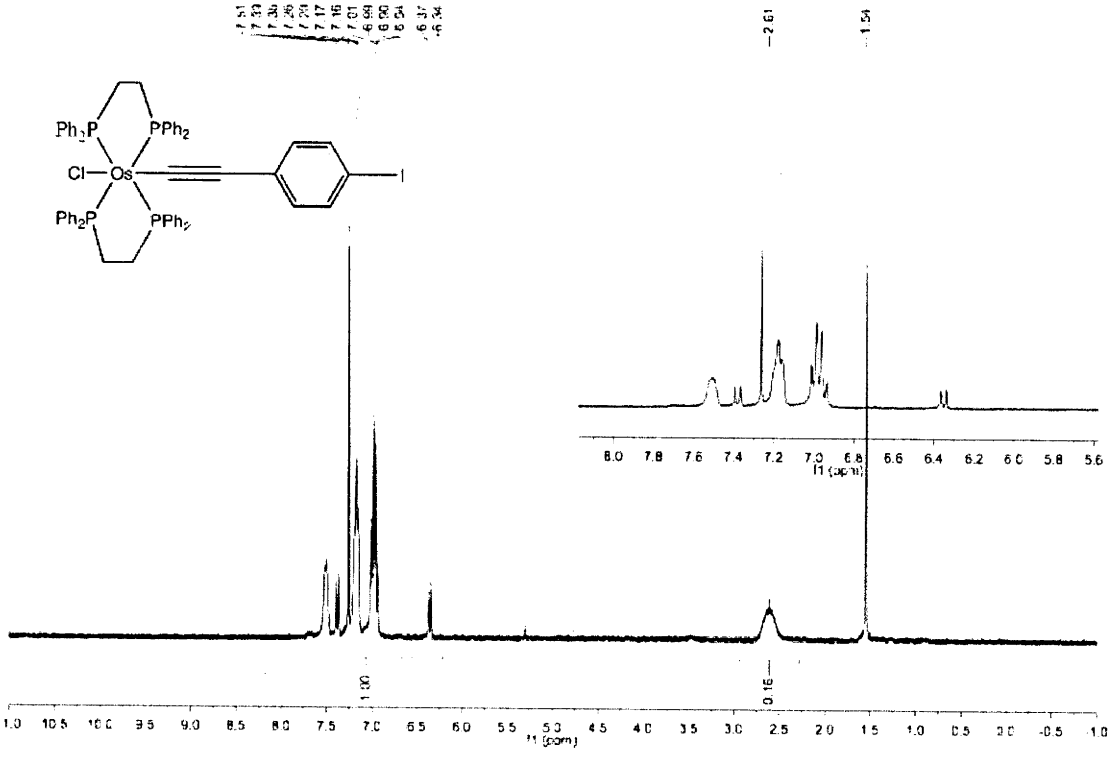

11 ^{31}P NMR

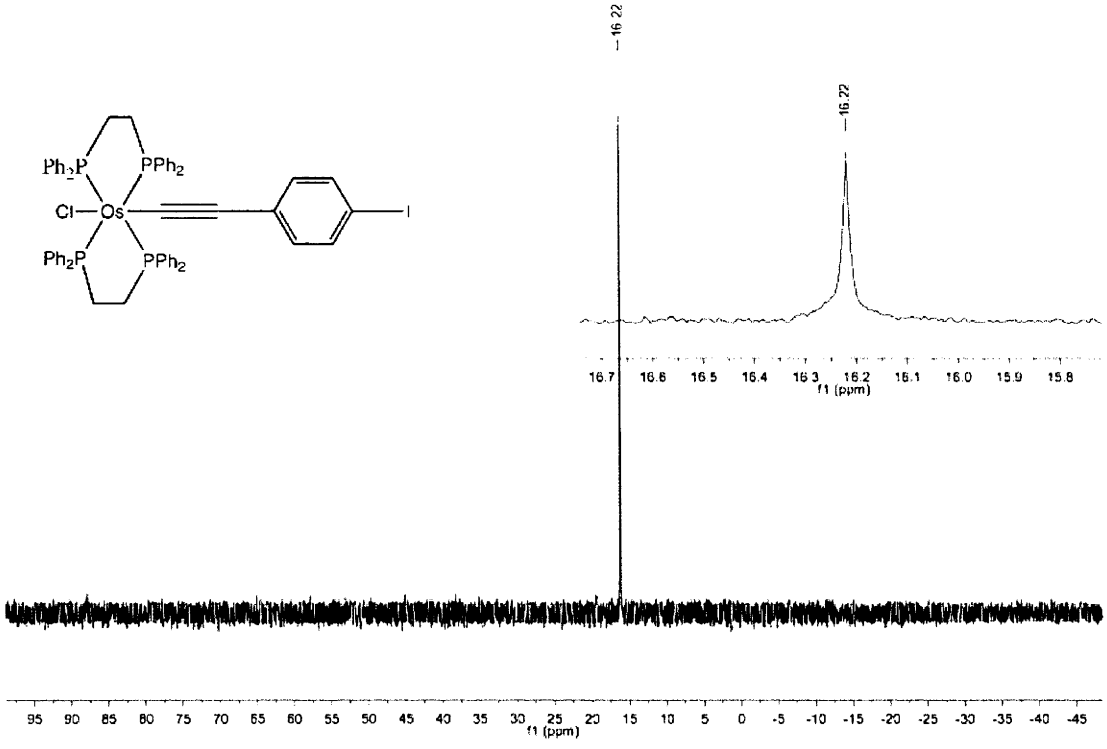

11 ^{13}C NMR

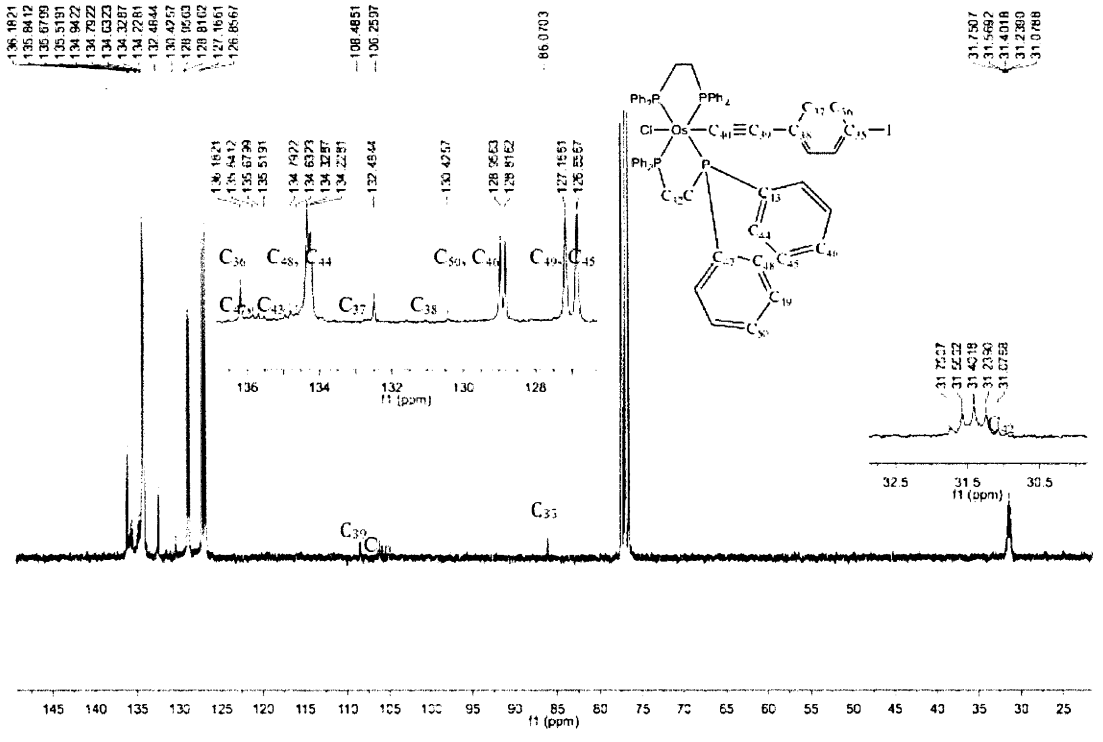

12 ^{1}H NMR

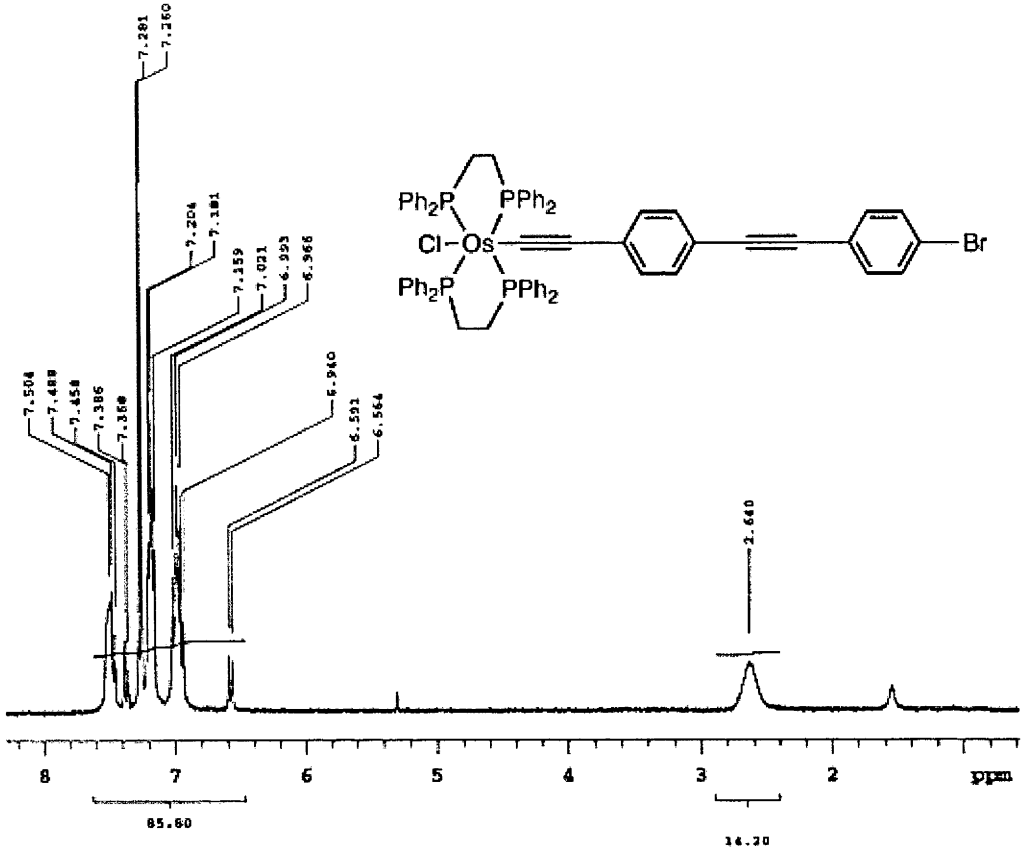

12 ^{31}P NMR

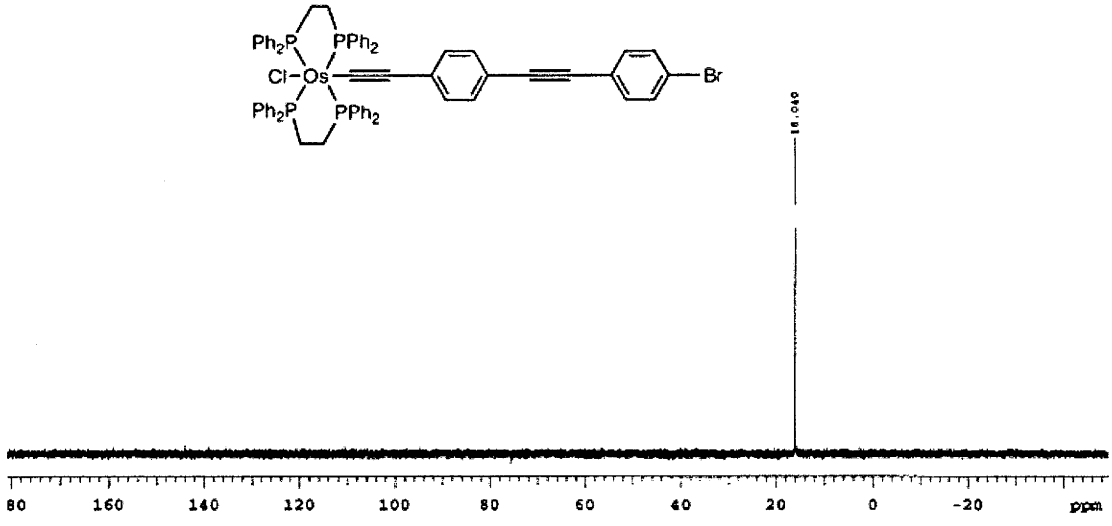

12 ^{13}C NMR

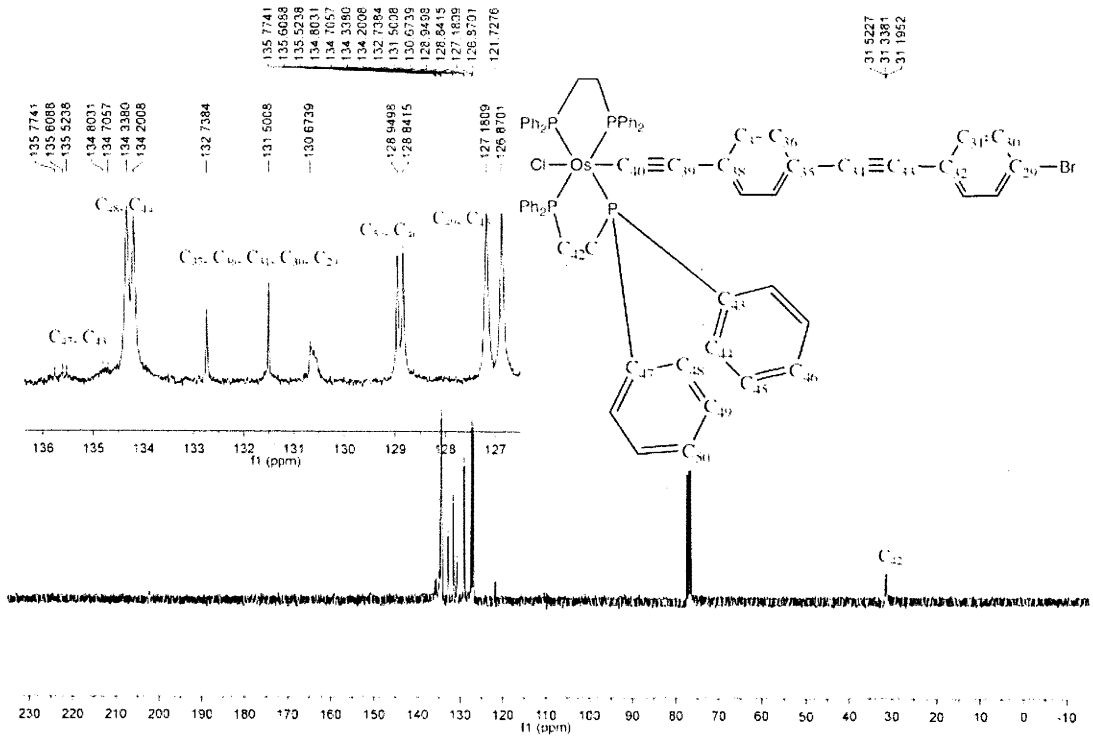

13 ^{1}H NMR

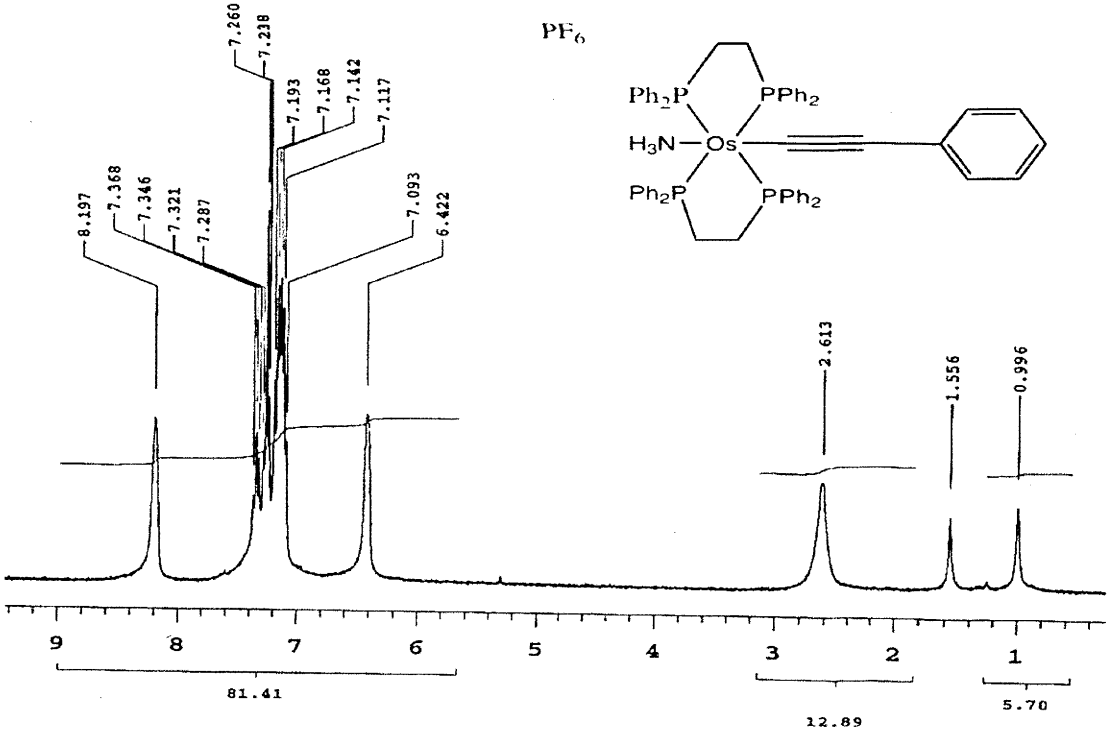

13 ^{31}P NMR

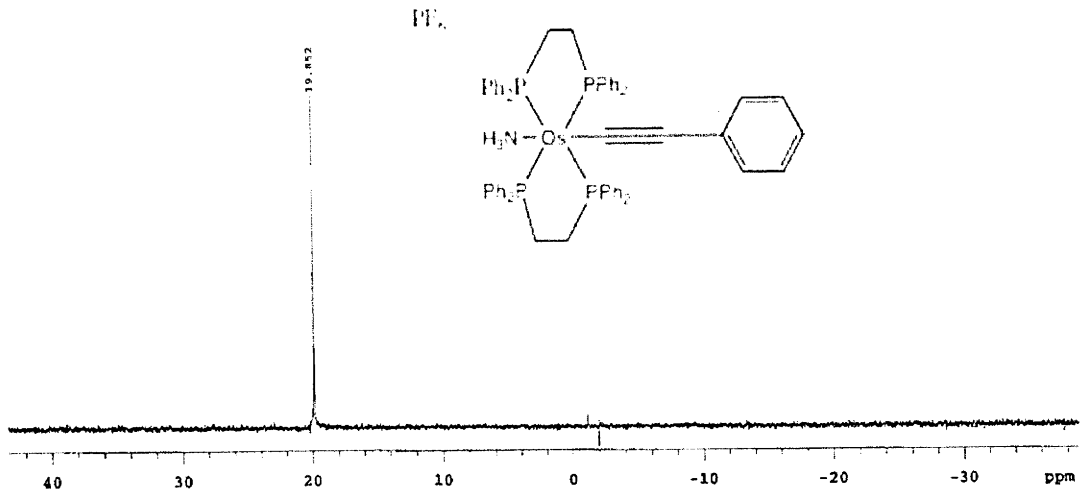

13 ^{13}C NMR

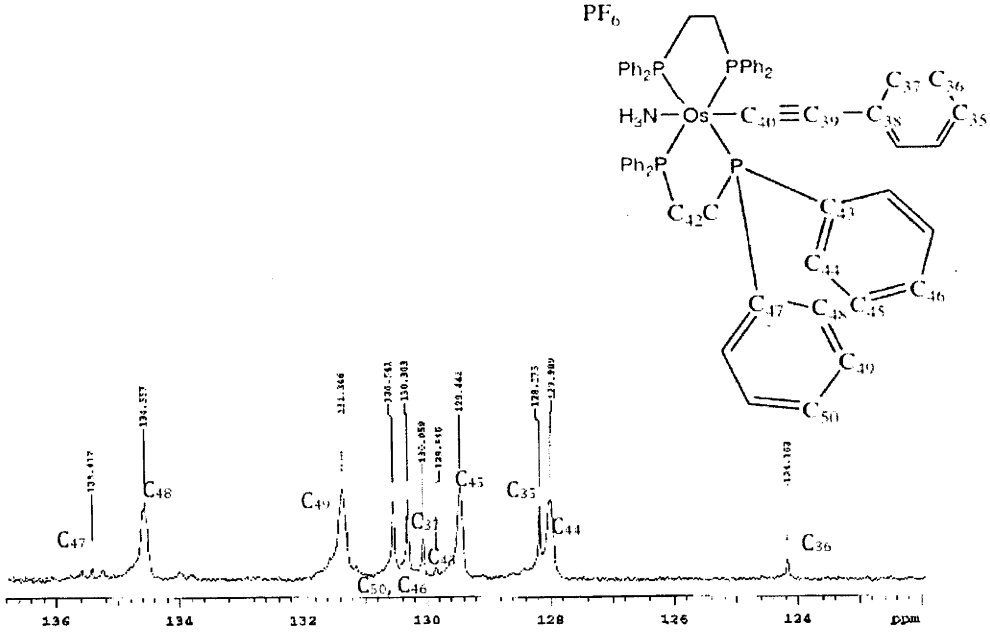

14 ^{1}H NMR

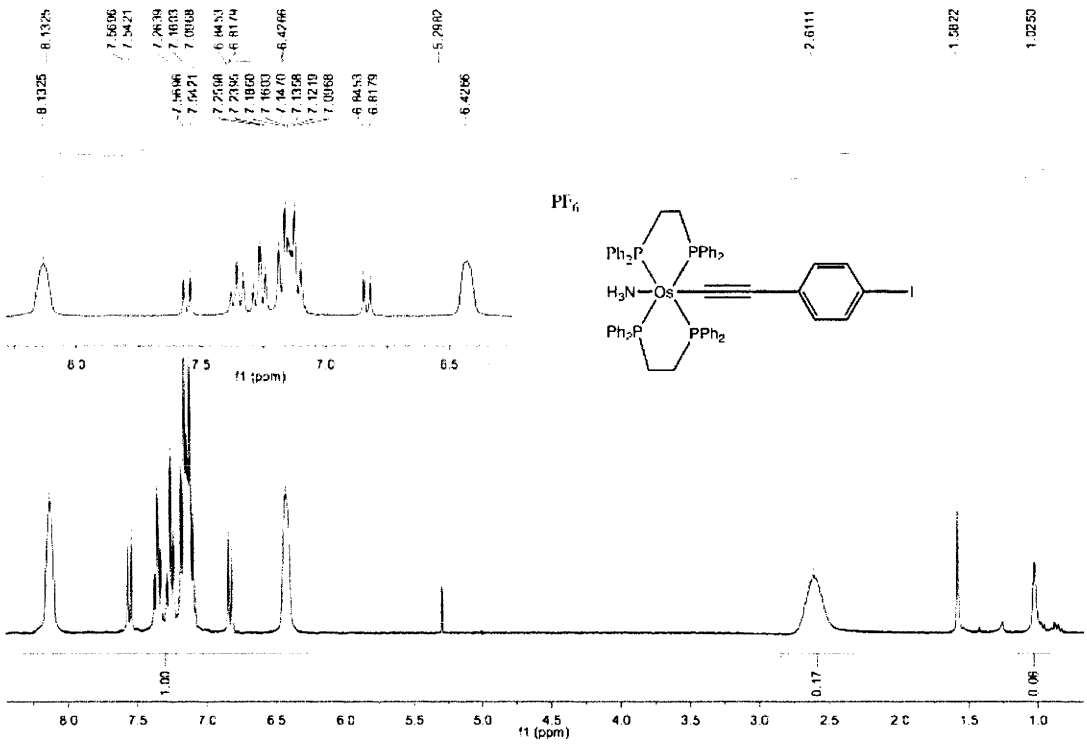

14 ^{31}P NMR

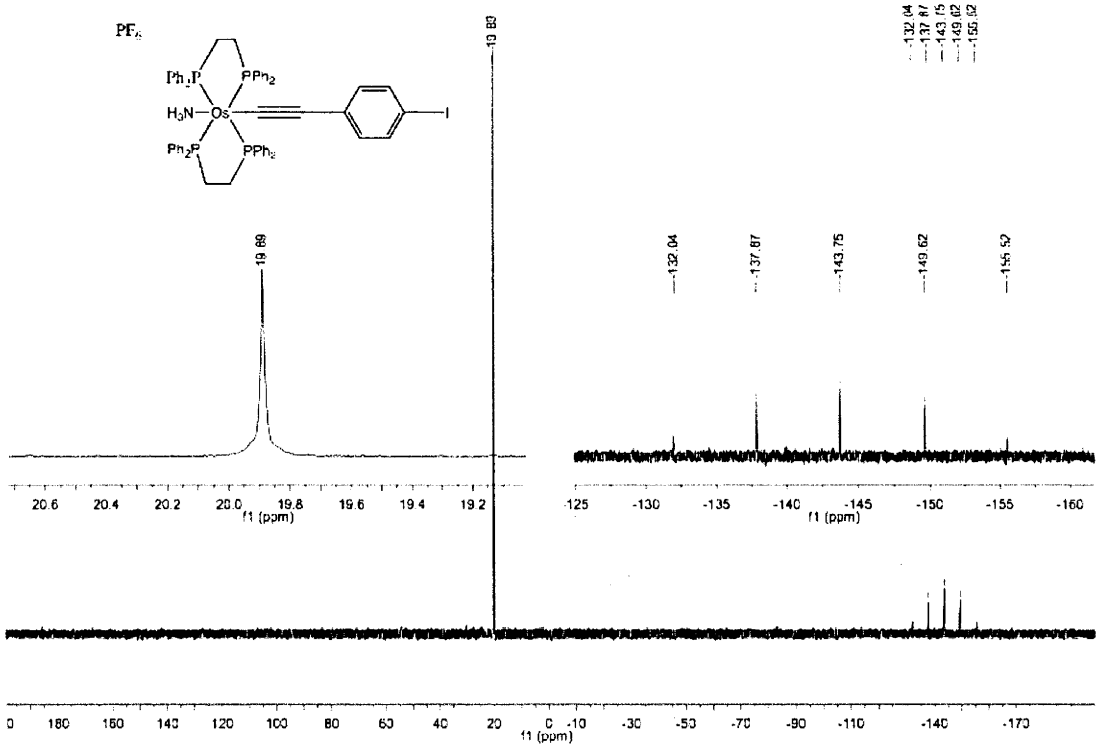

14 ^{13}C NMR

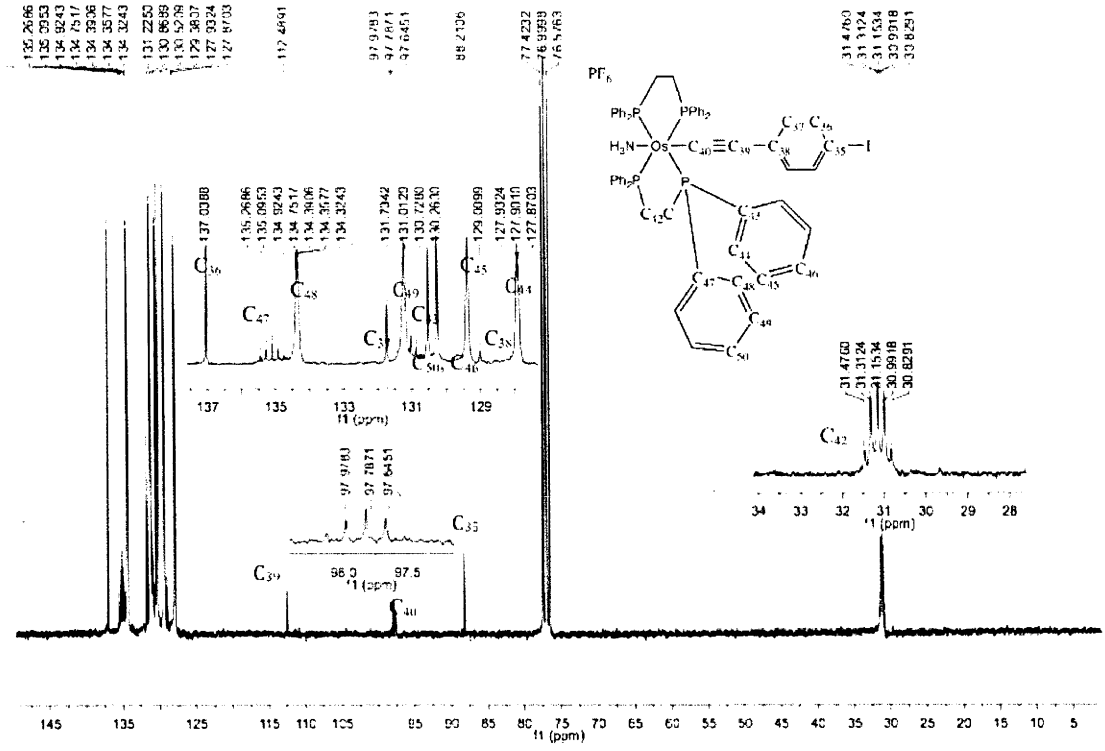

15 ^{1}H NMR

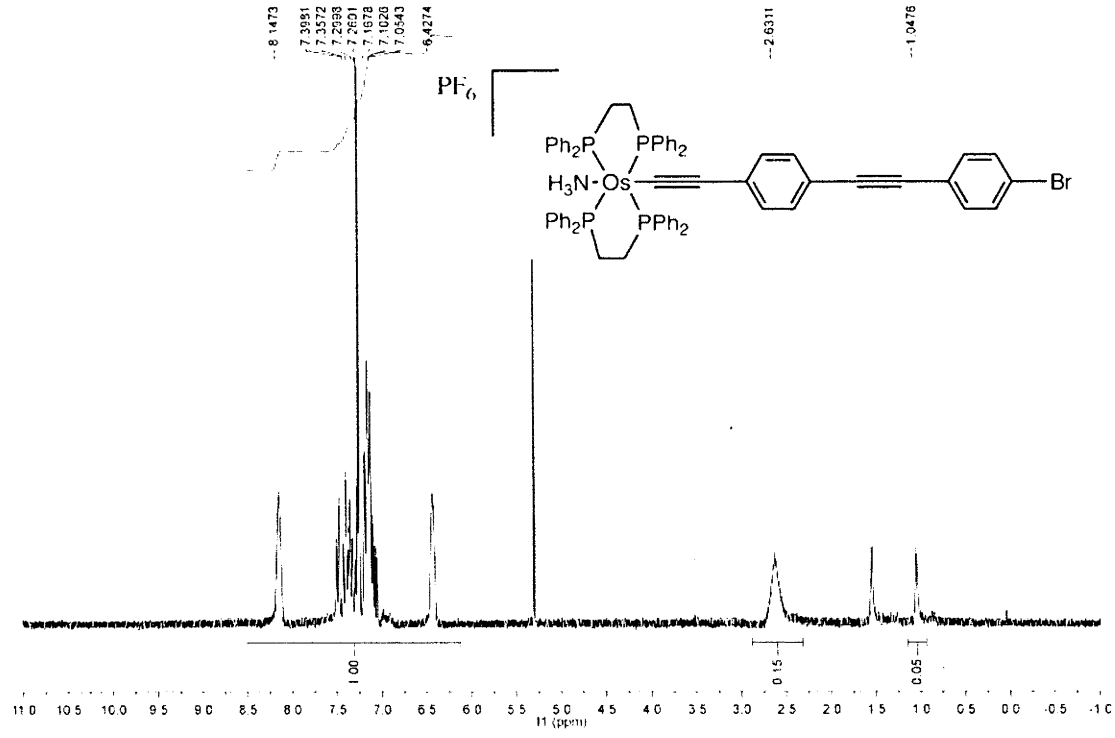

15 ^{31}P NMR

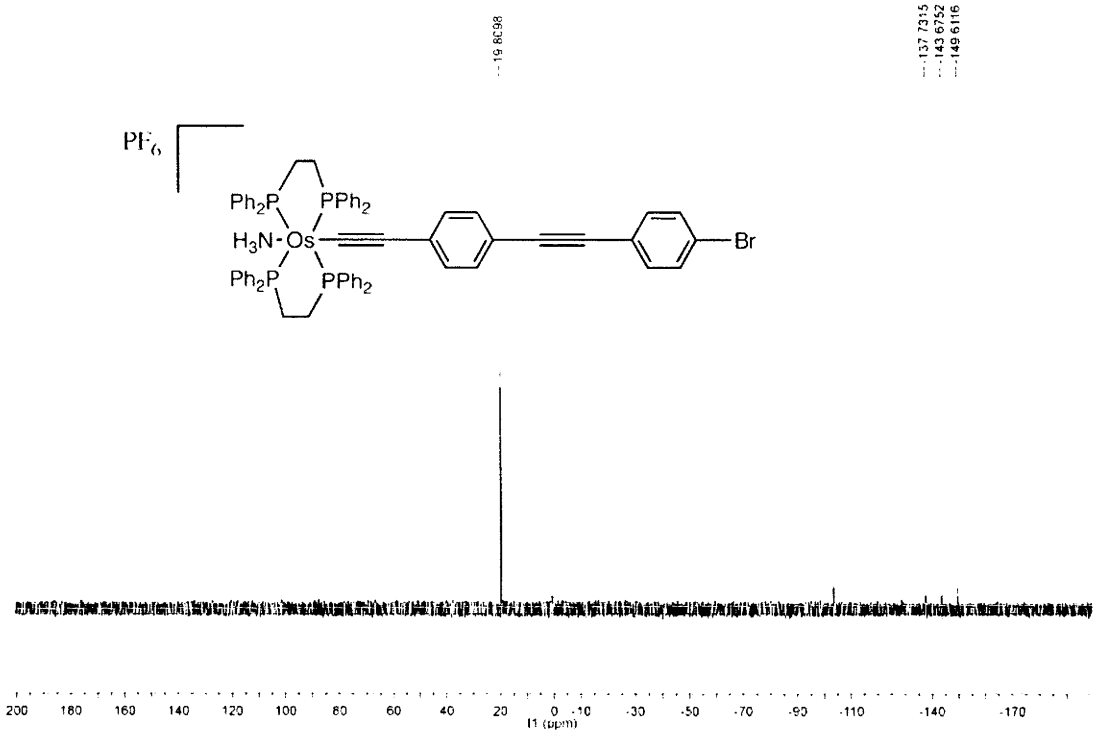

15 ^{13}C NMR

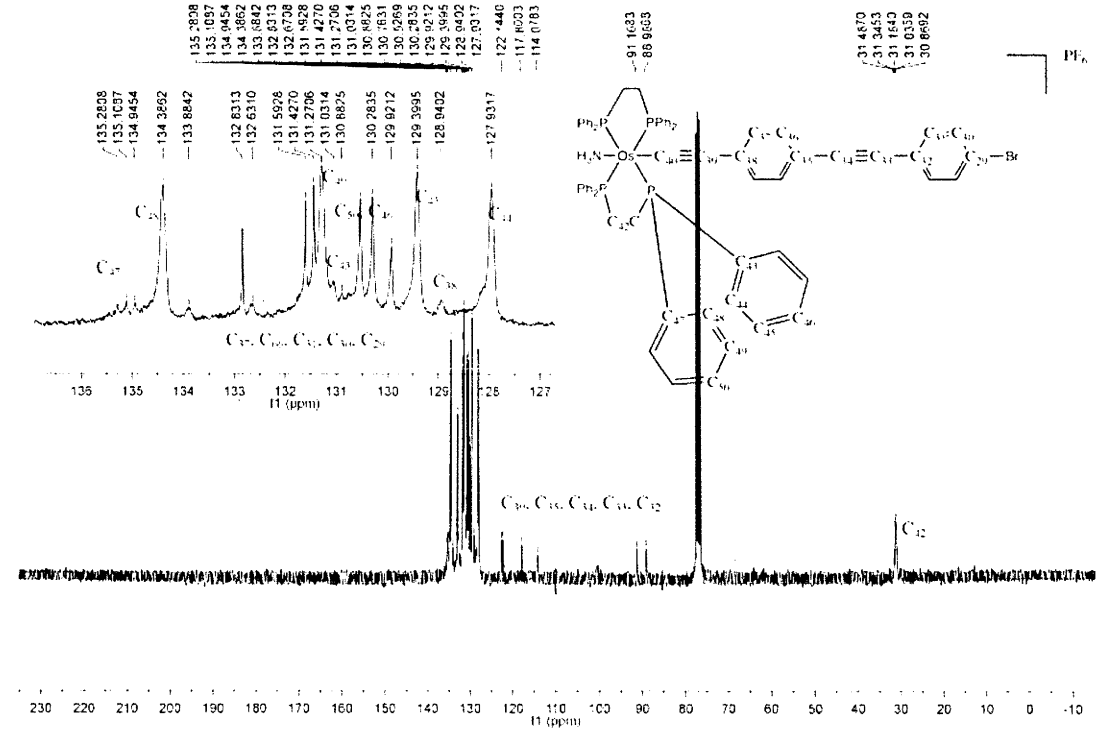

16 ^{1}H NMR

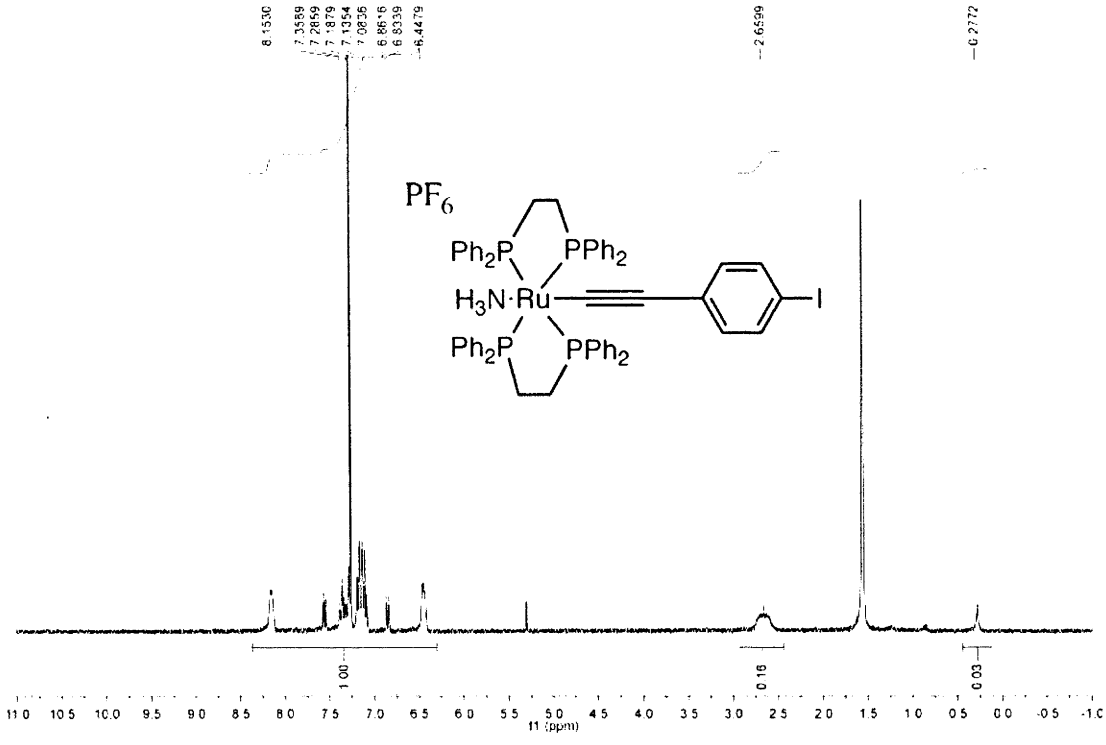

16 ^{31}P NMR

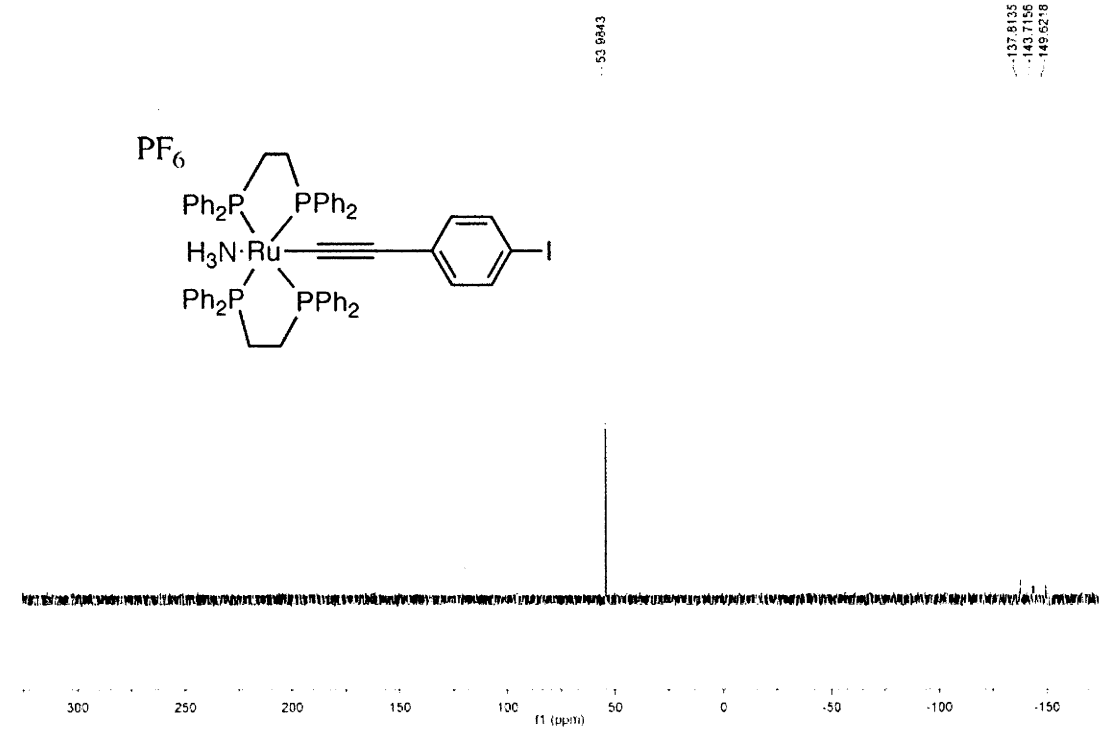

16 ^{13}C NMR

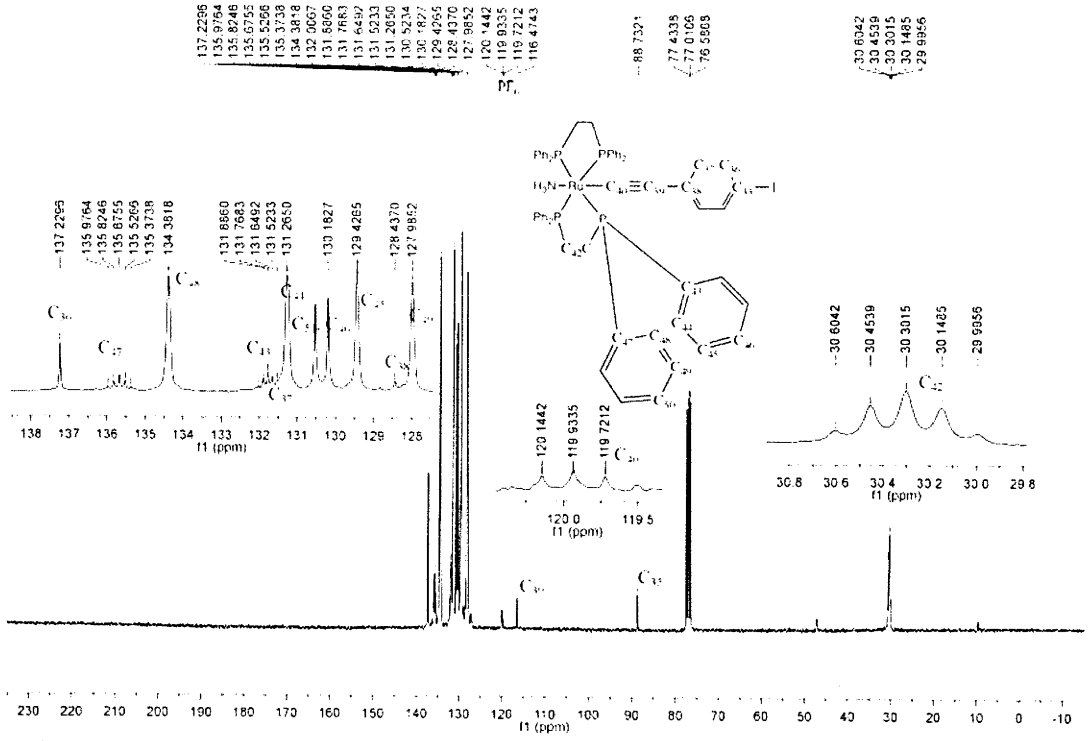

17 ^{1}H NMR

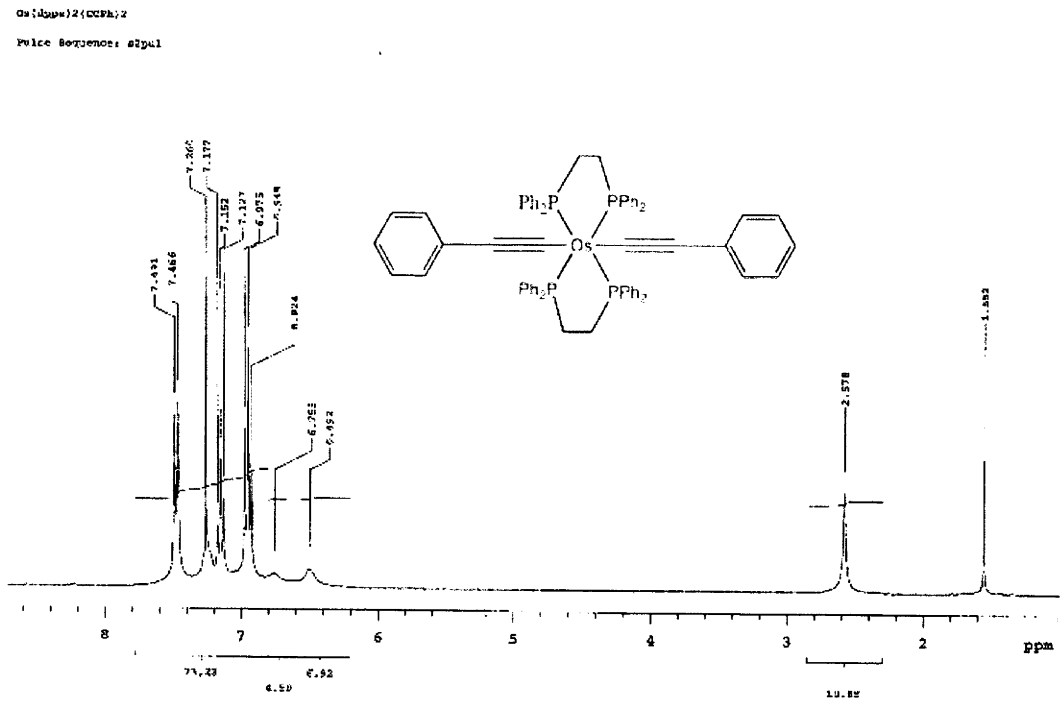

17 ^{31}P NMR

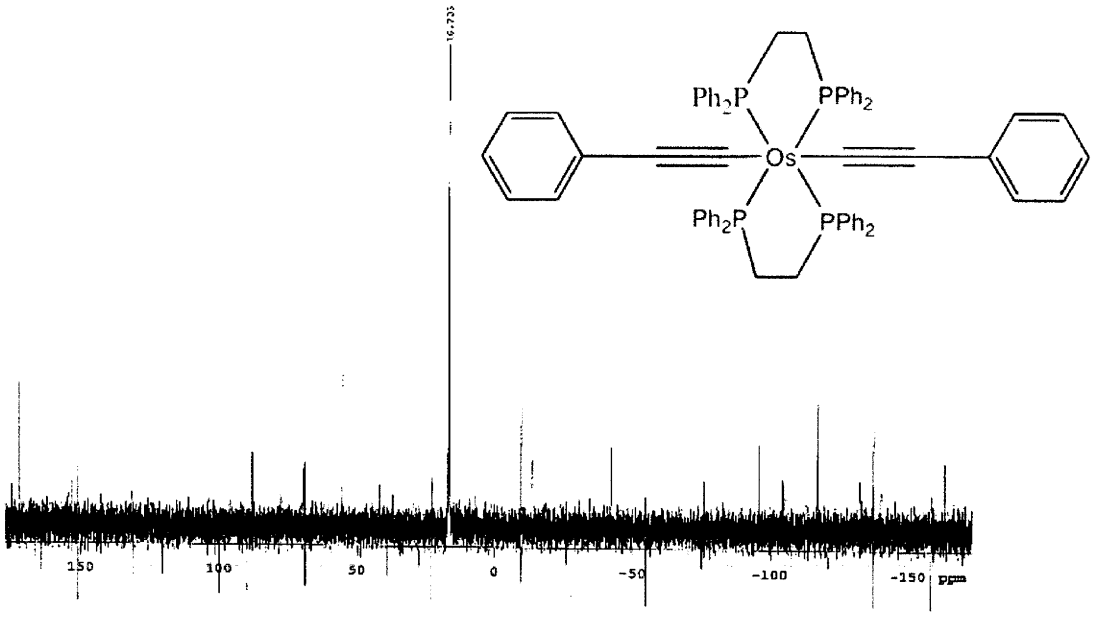

17 ^{13}C NMR

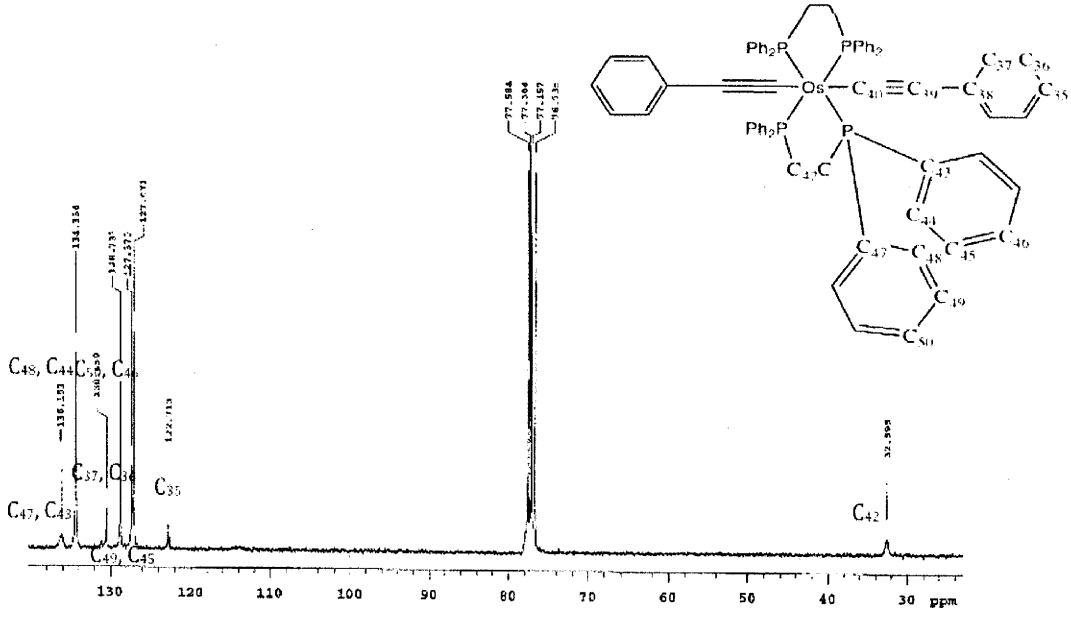

18 ^{1}H NMR

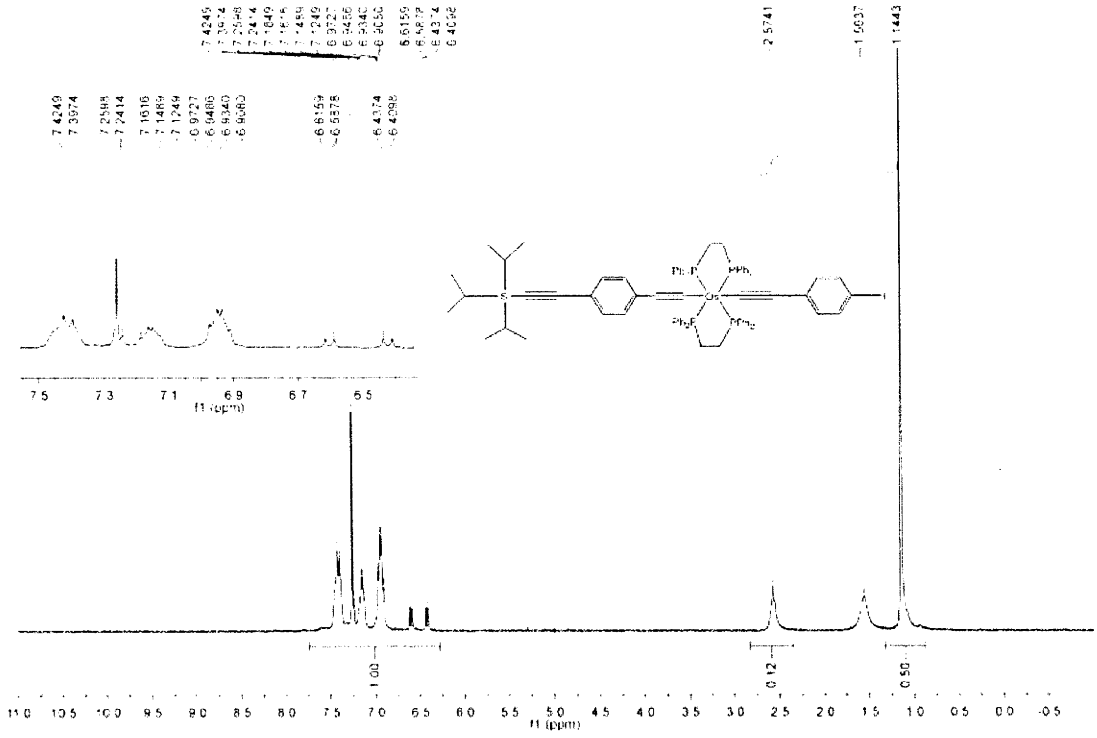

18 ^{31}P NMR

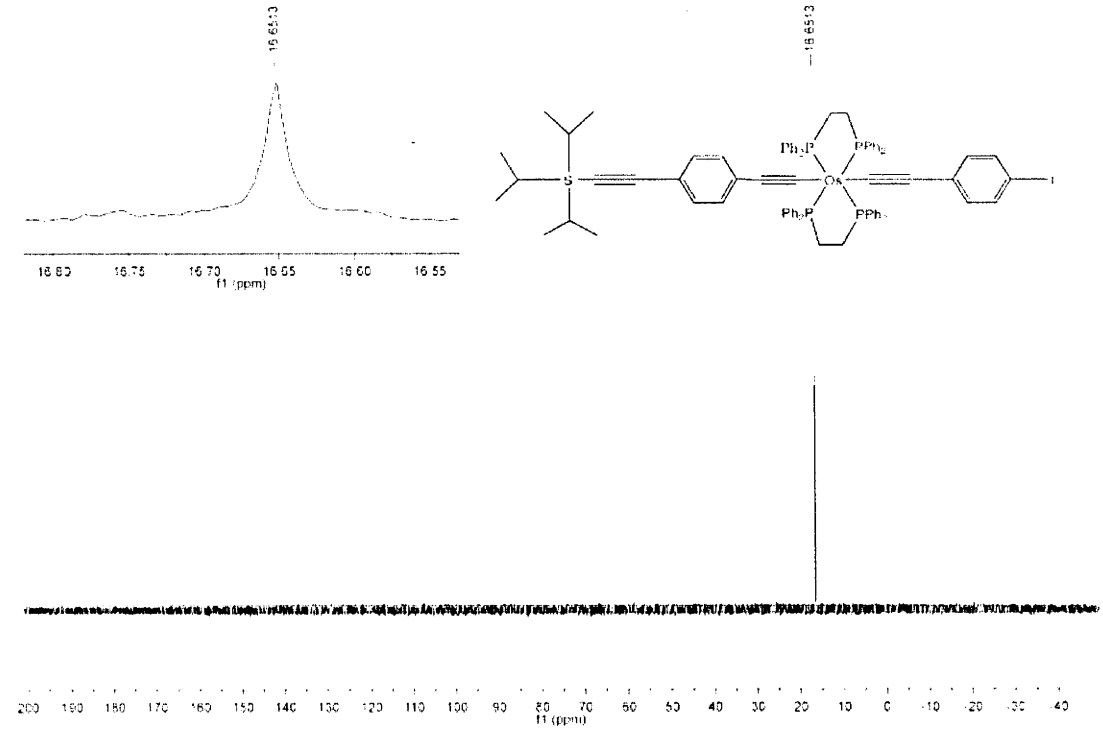

18 ^{13}C NMR

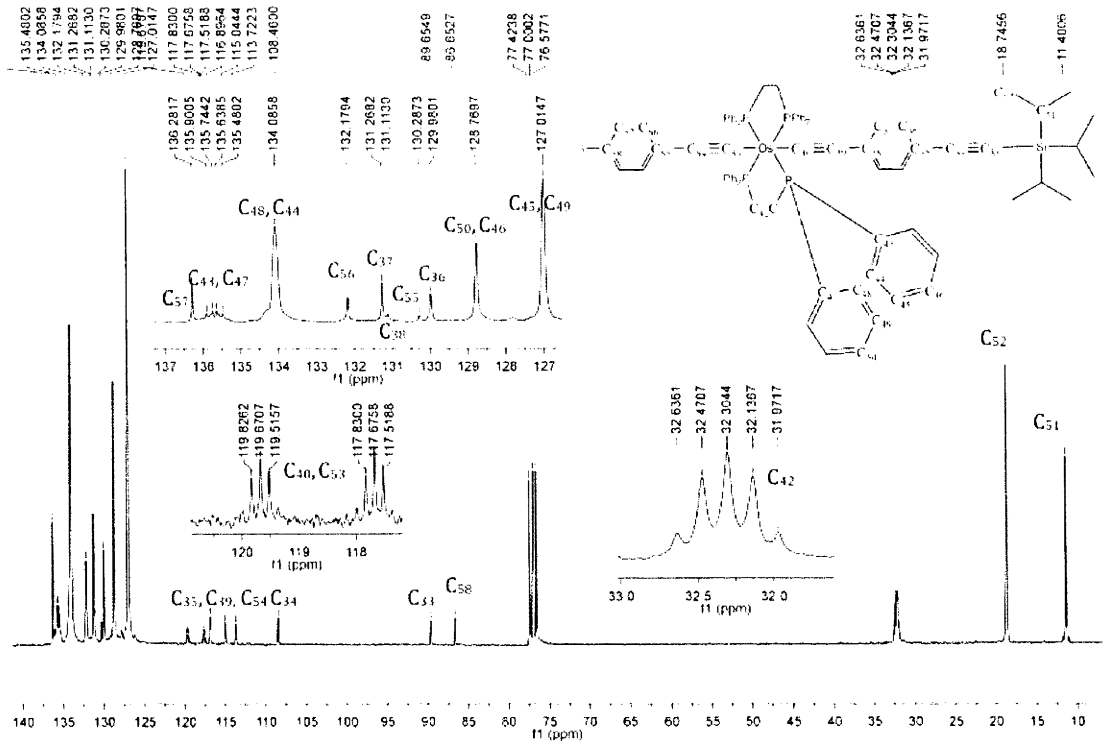

19 ^{1}H NMR

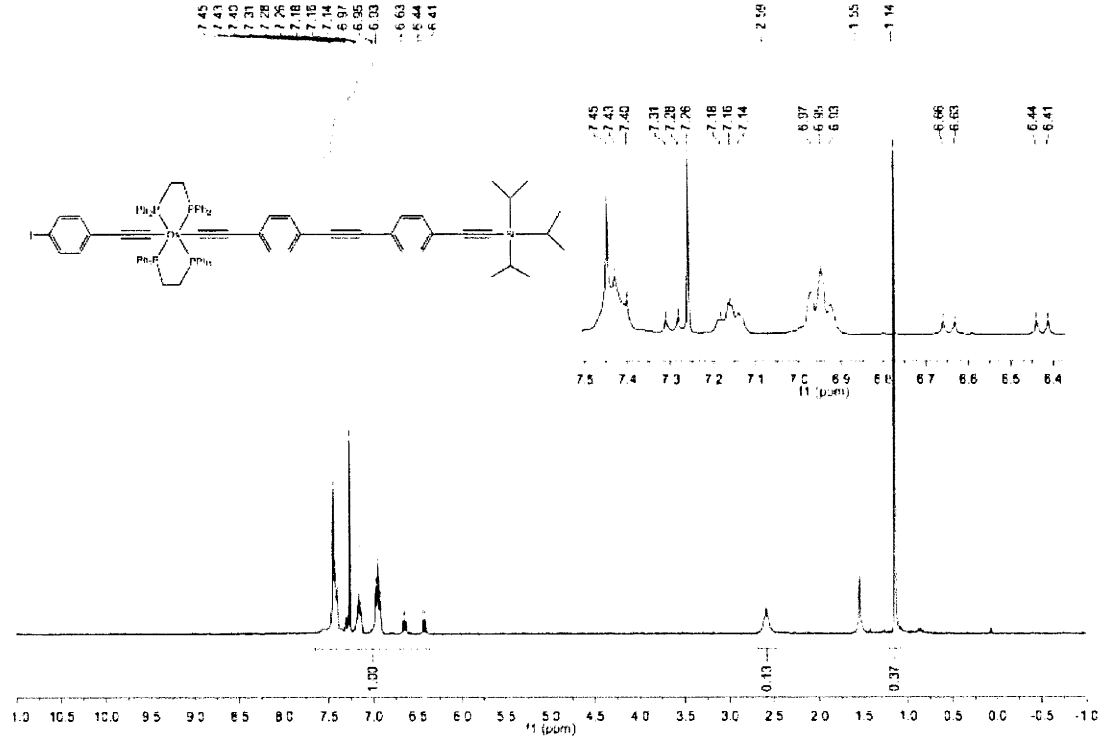

19 ^{31}P NMR

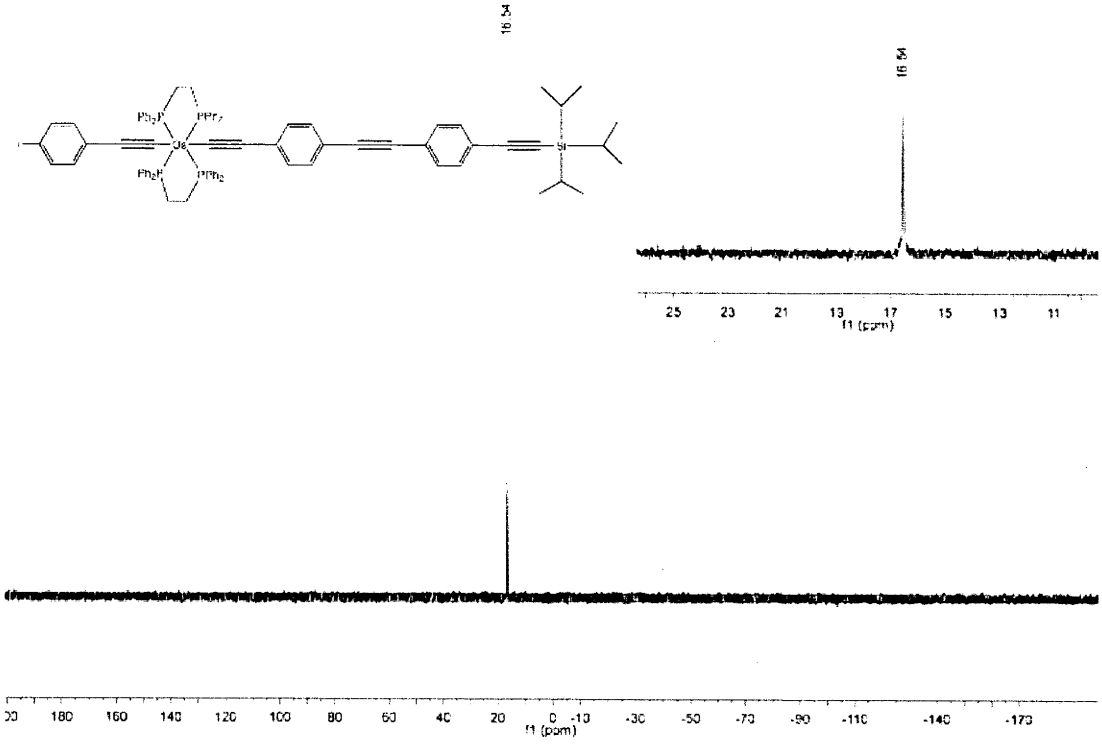

19 ^{13}C NMR

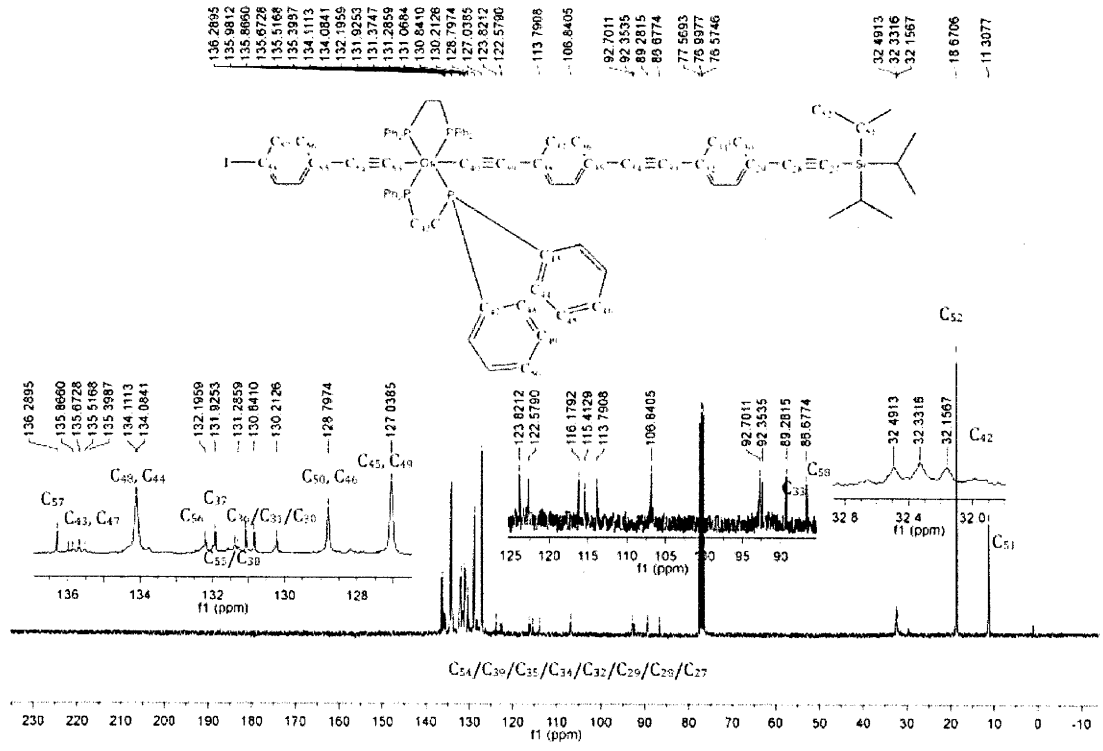

20 ^{1}H NMR

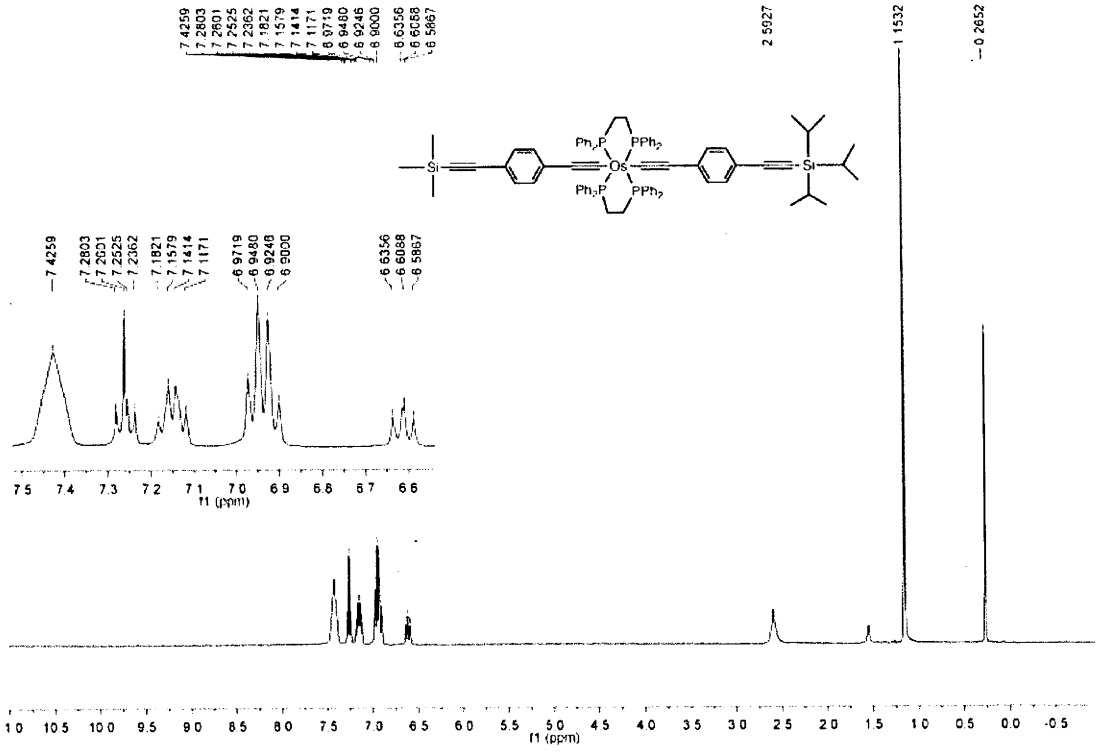

20 ^{31}P NMR

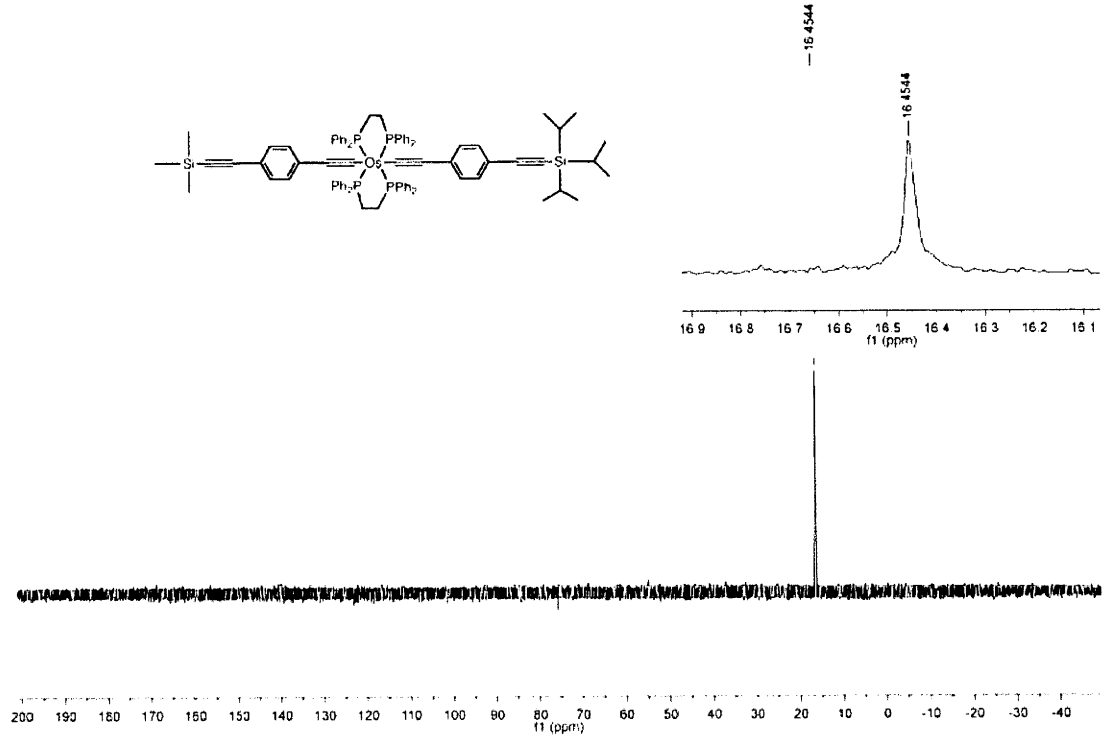

20 ^{13}C NMR

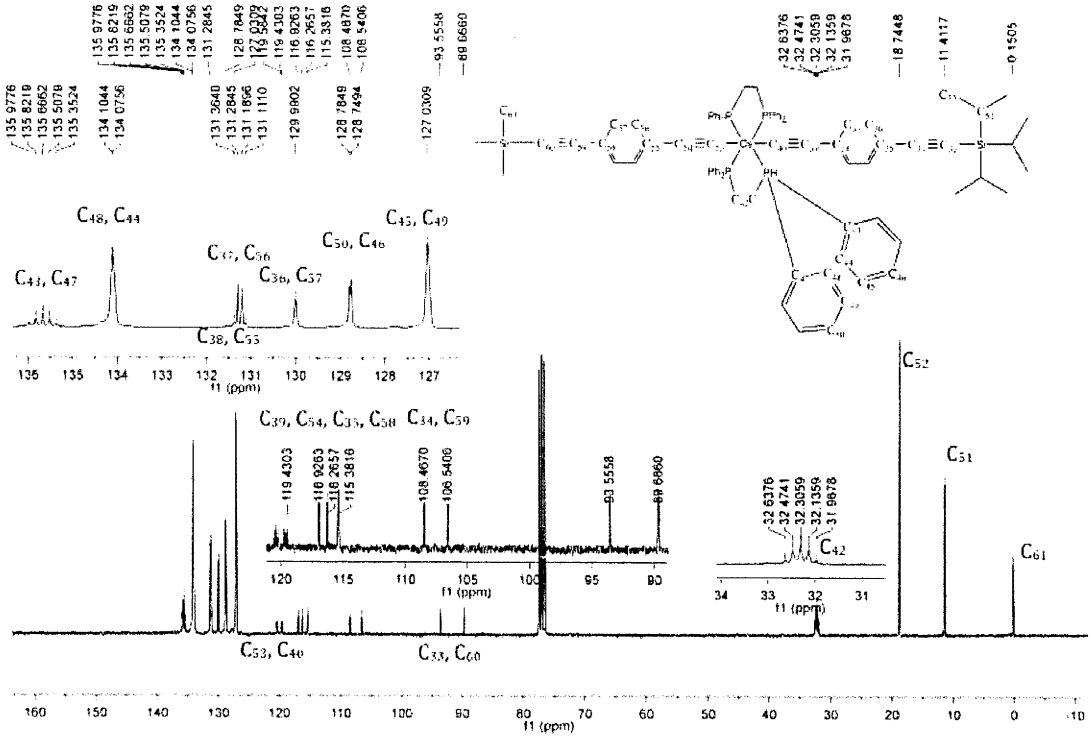

21 ^{1}H NMR

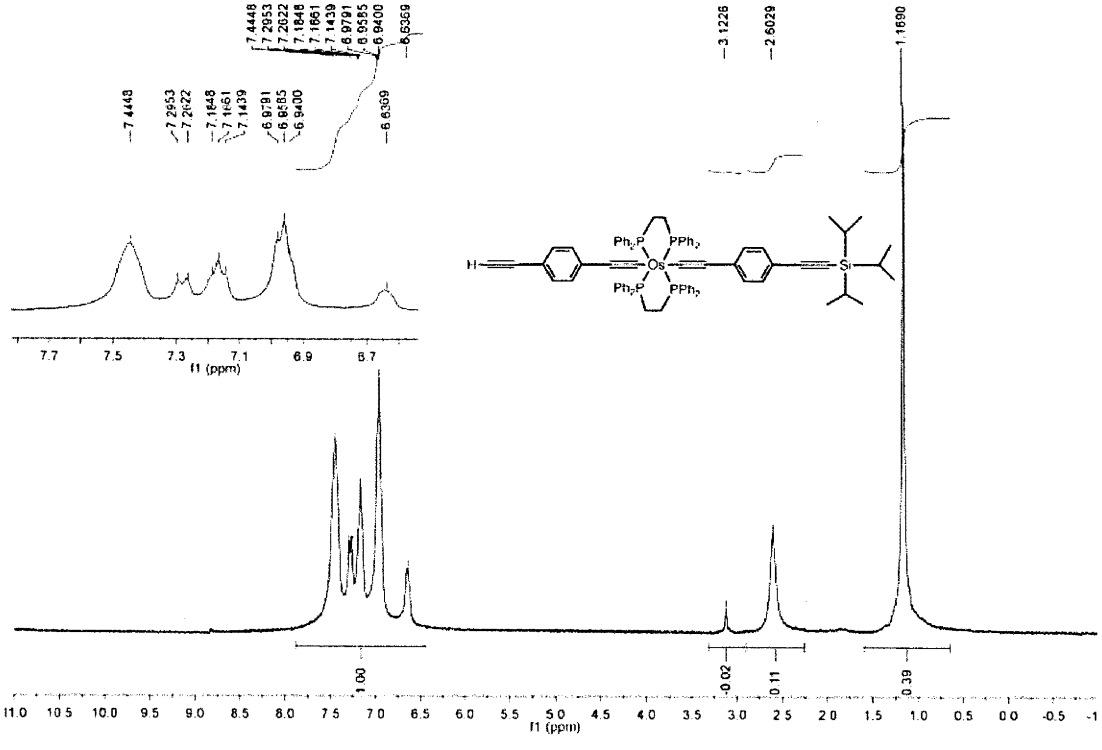

21 ^{31}P NMR

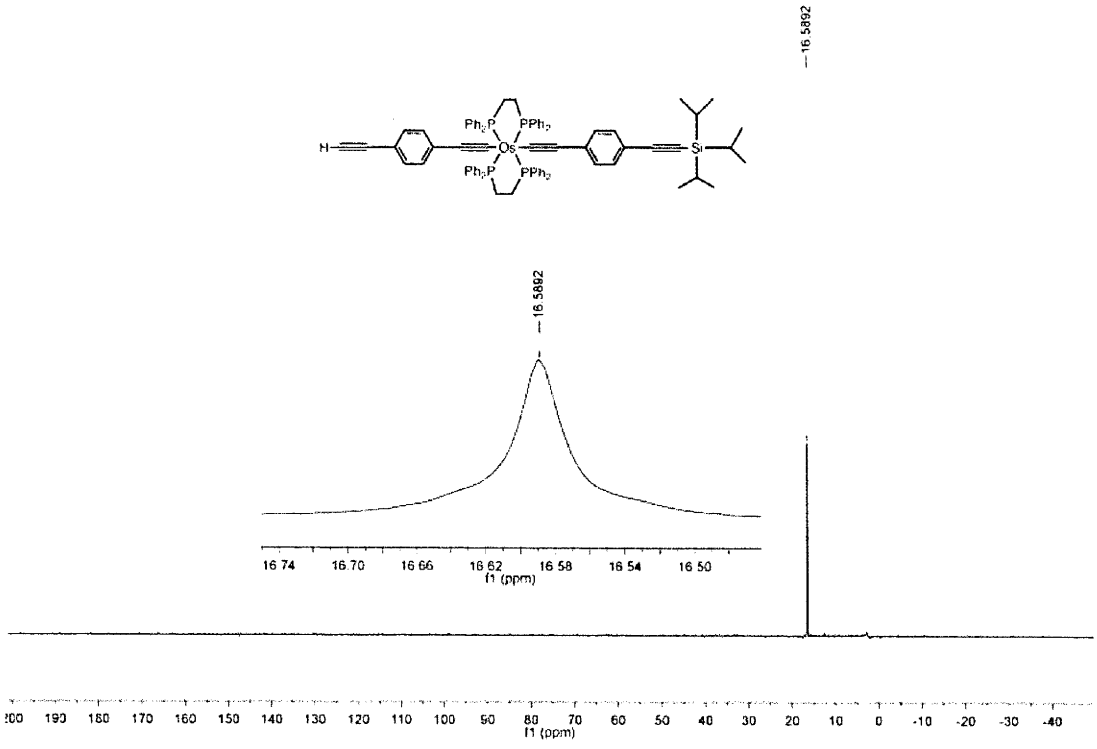

21 ^{13}C NMR

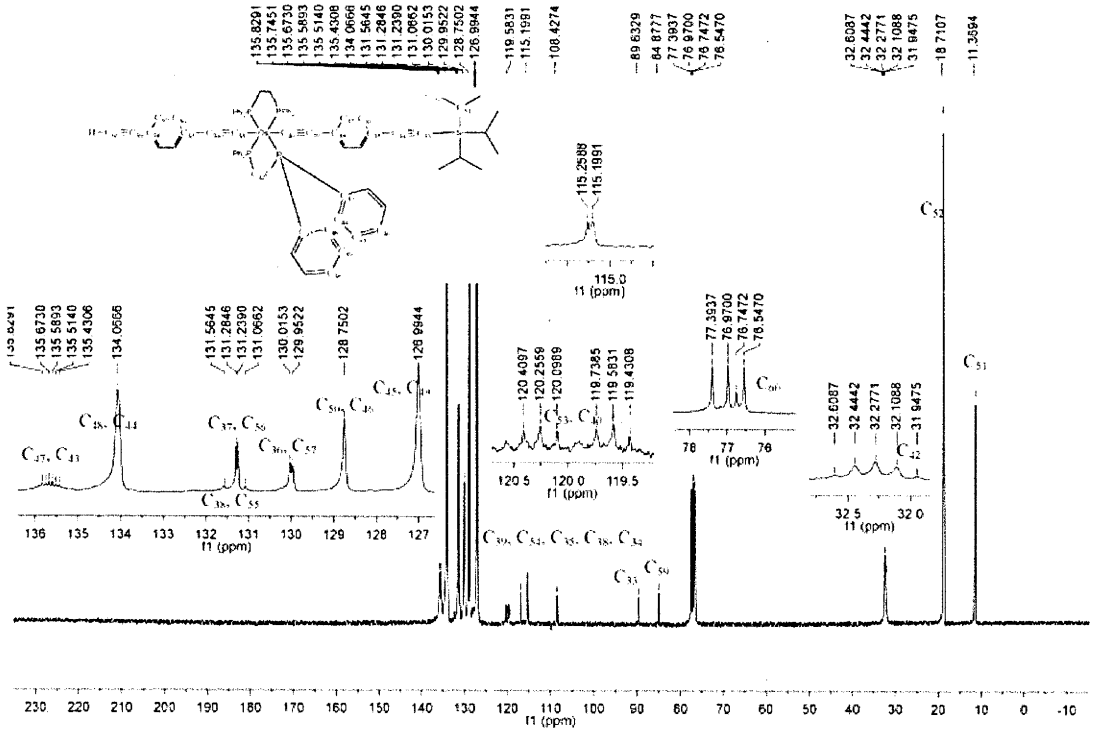

22 ^{1}H NMR

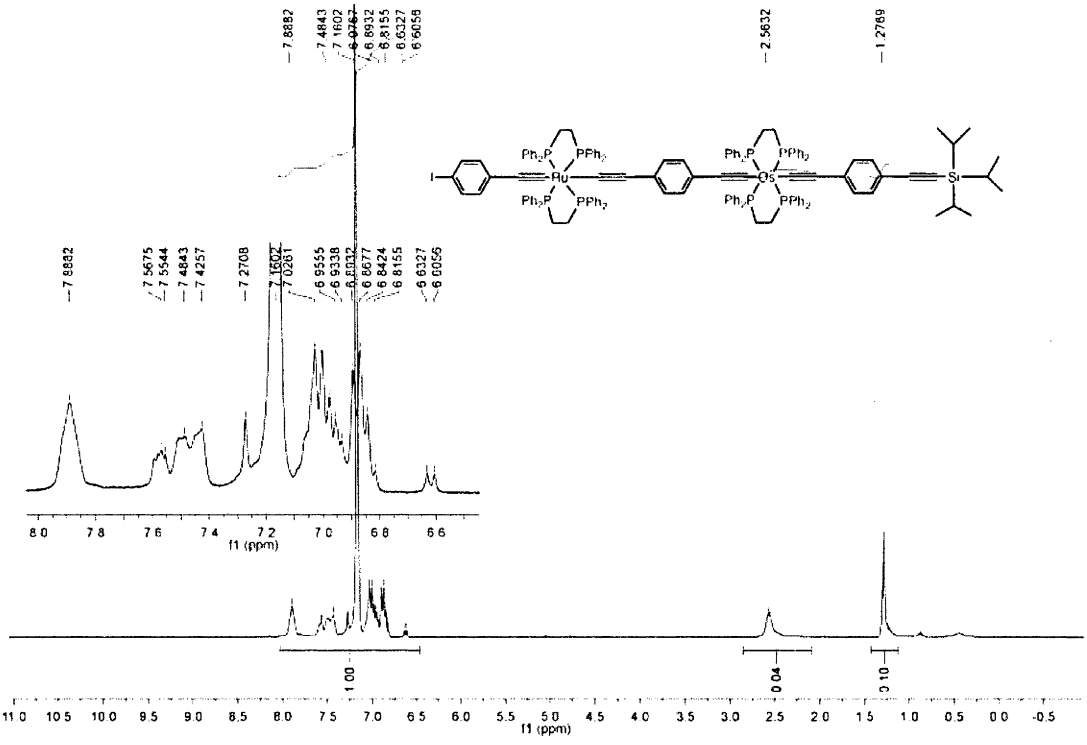

22 ^{13}P NMR

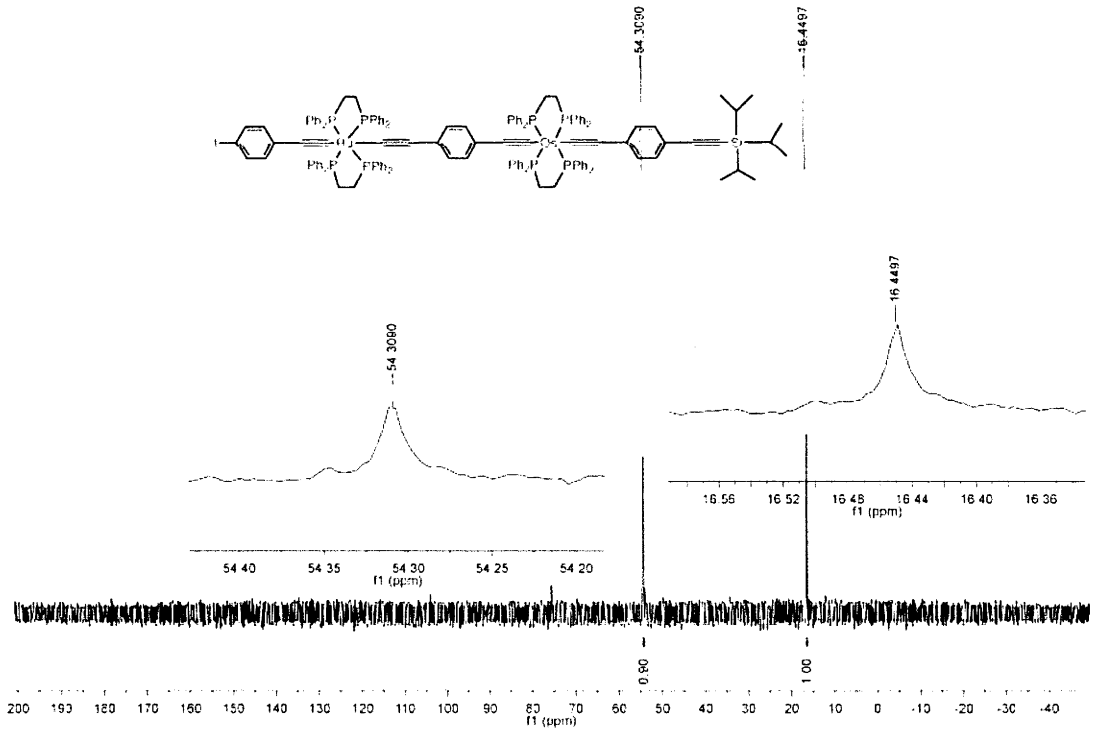

23 ^{1}H NMR

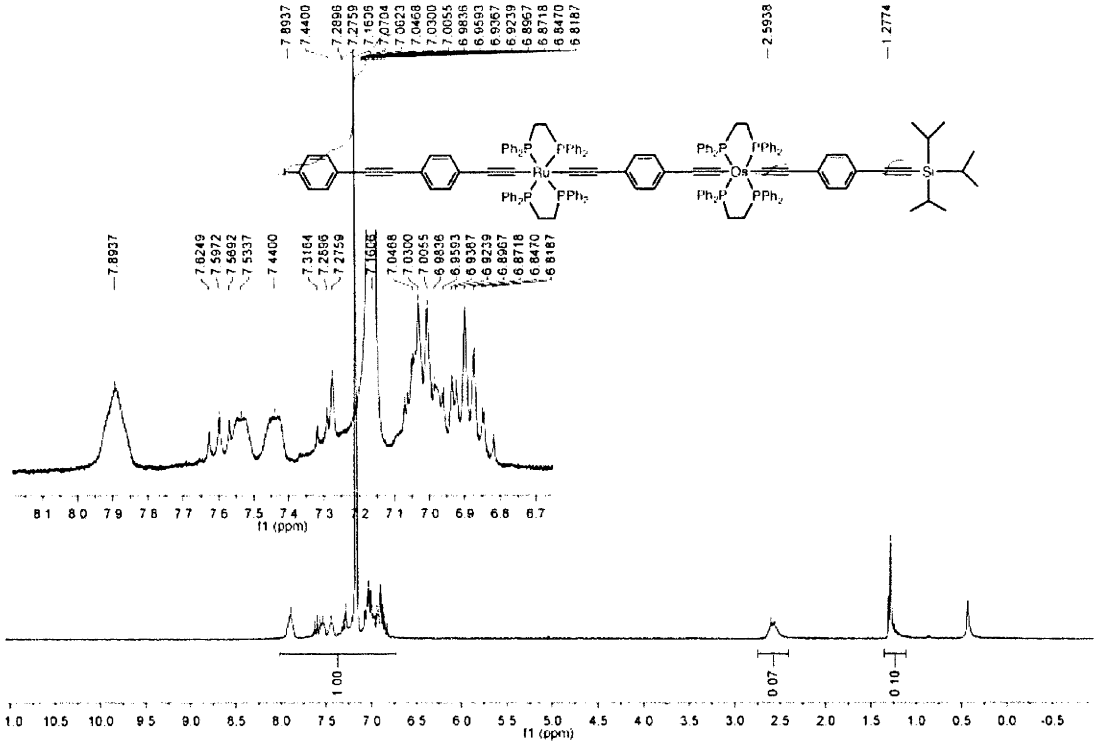

23 ^{13}P NMR

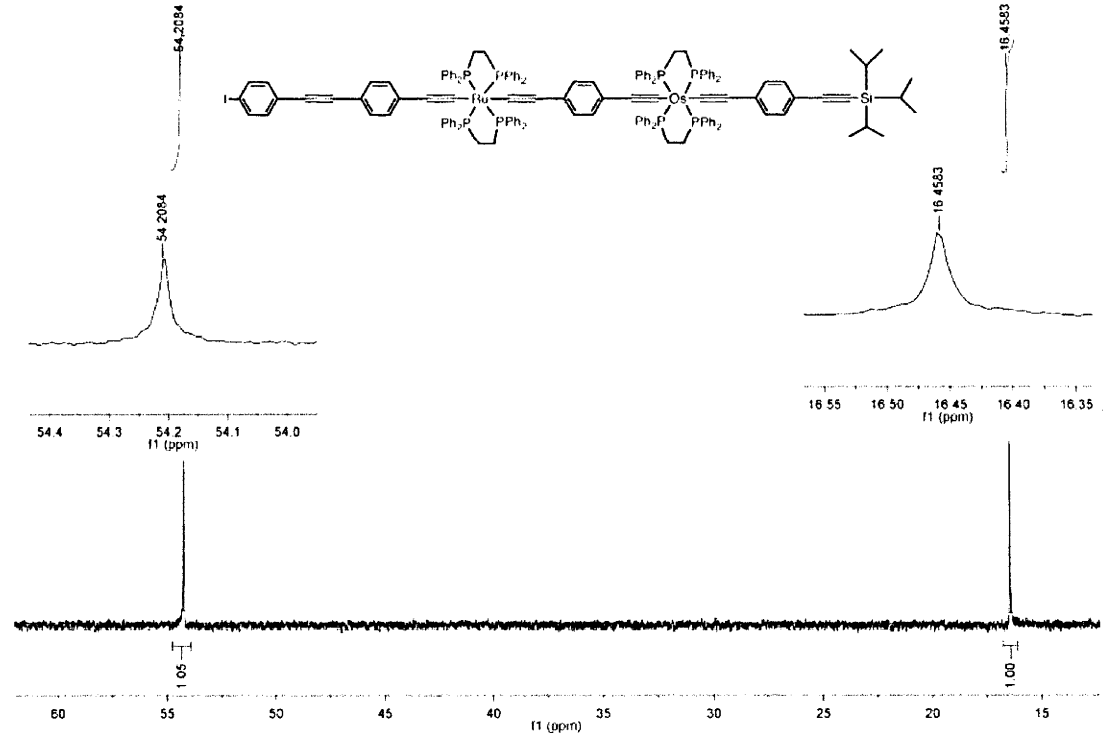

24 ^{1}H NMR

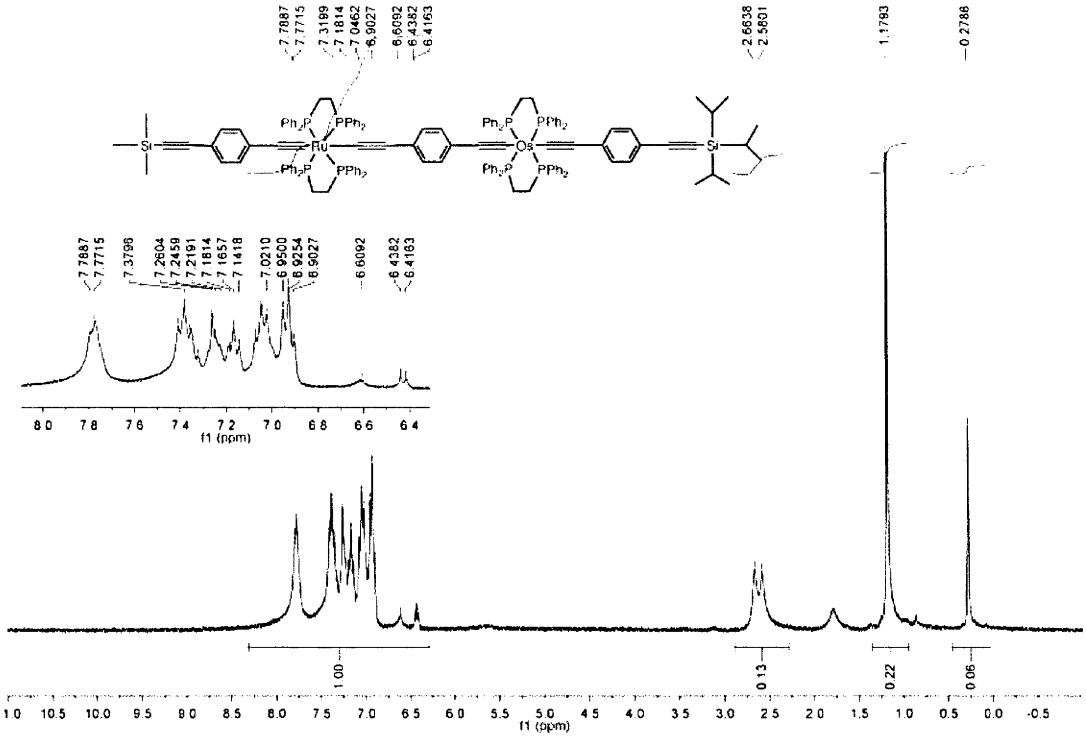

24 ^{13}P NMR

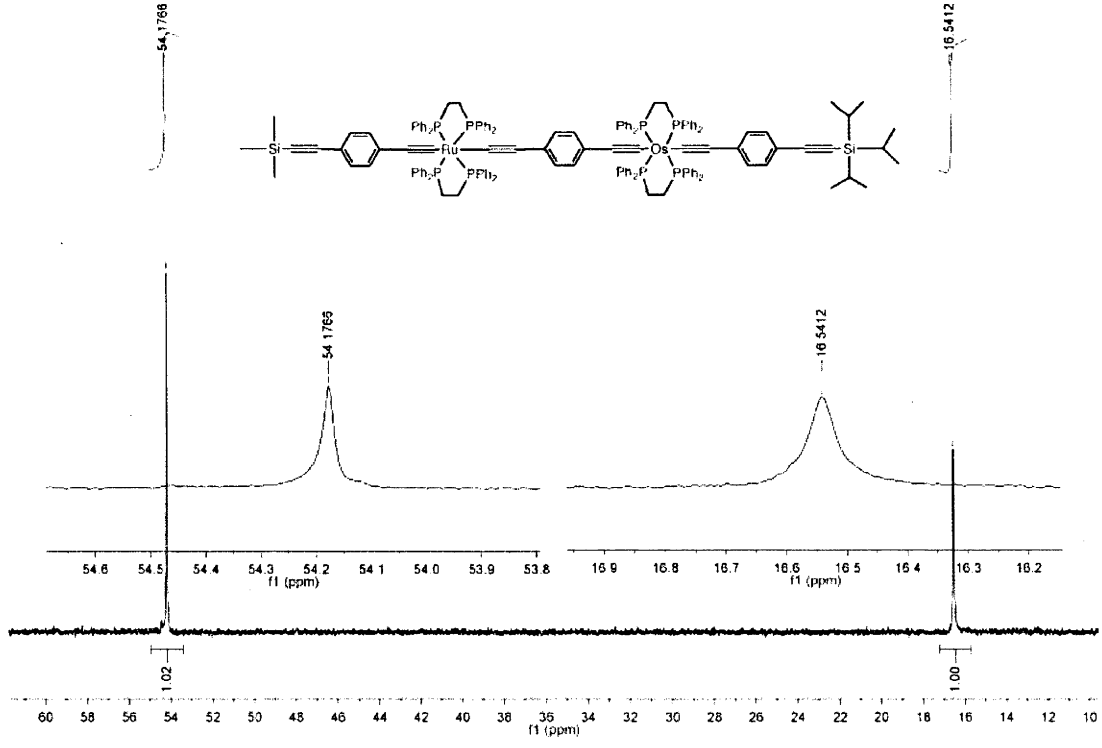

25 ^{1}H NMR

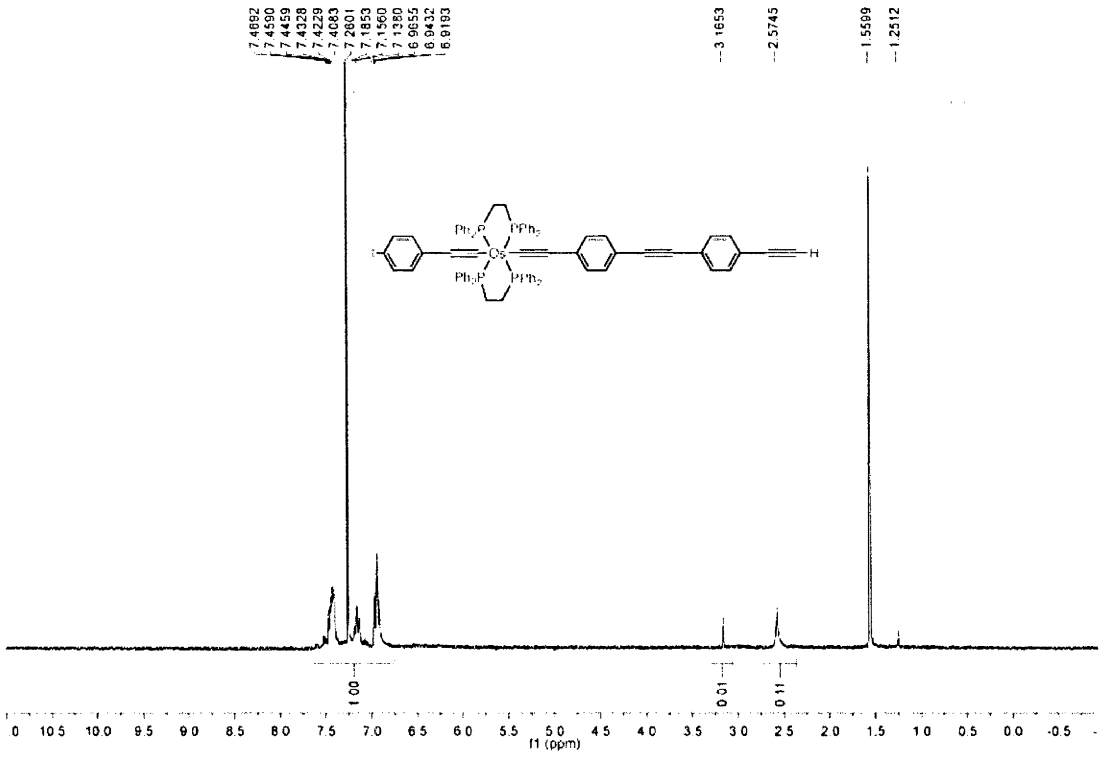

25 ^{13}P NMR

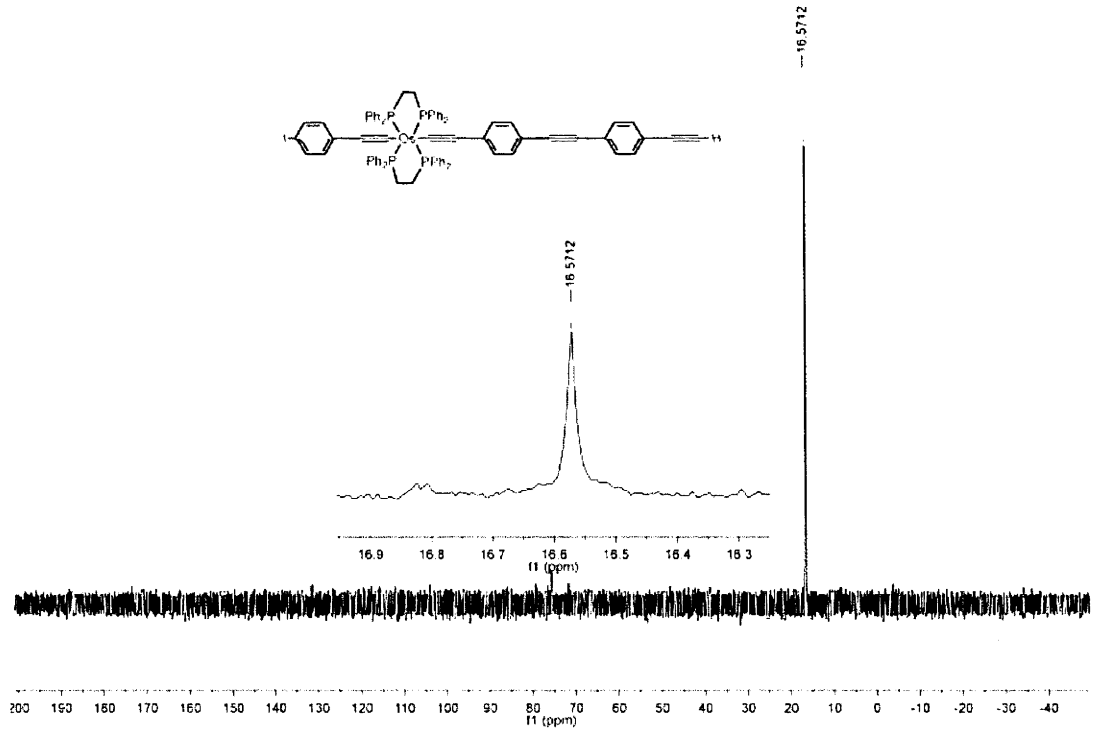

25 ^{13}C NMR

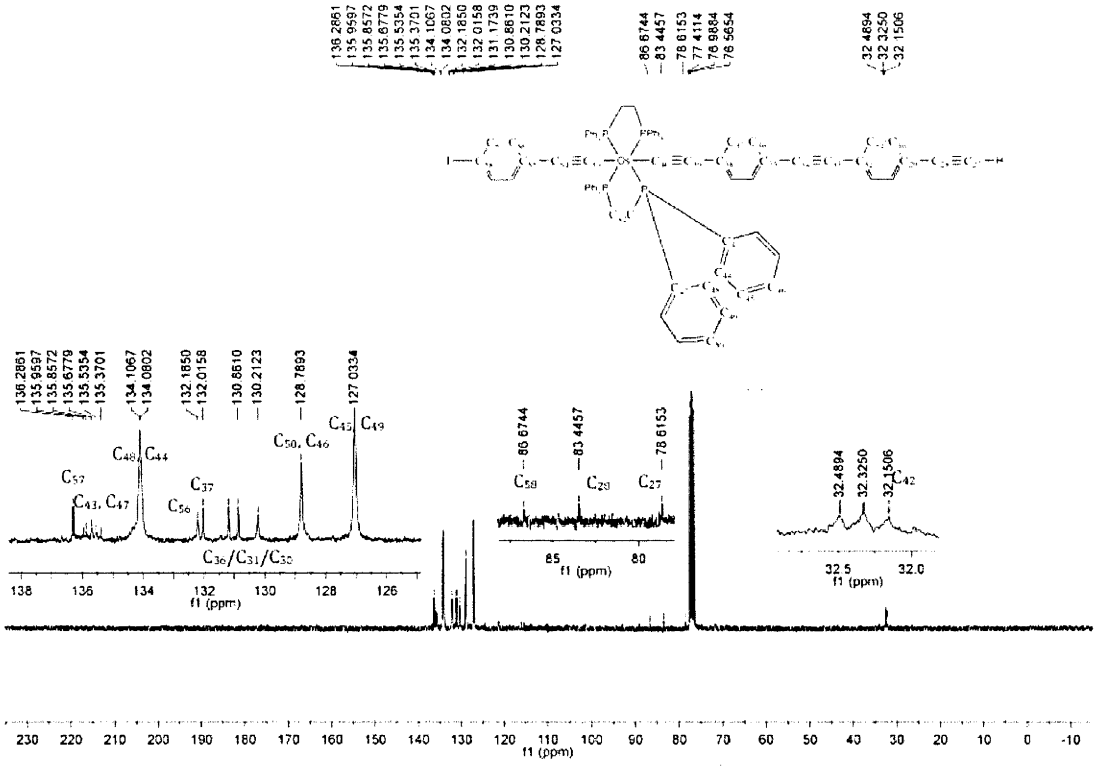

26 ^{1}H NMR

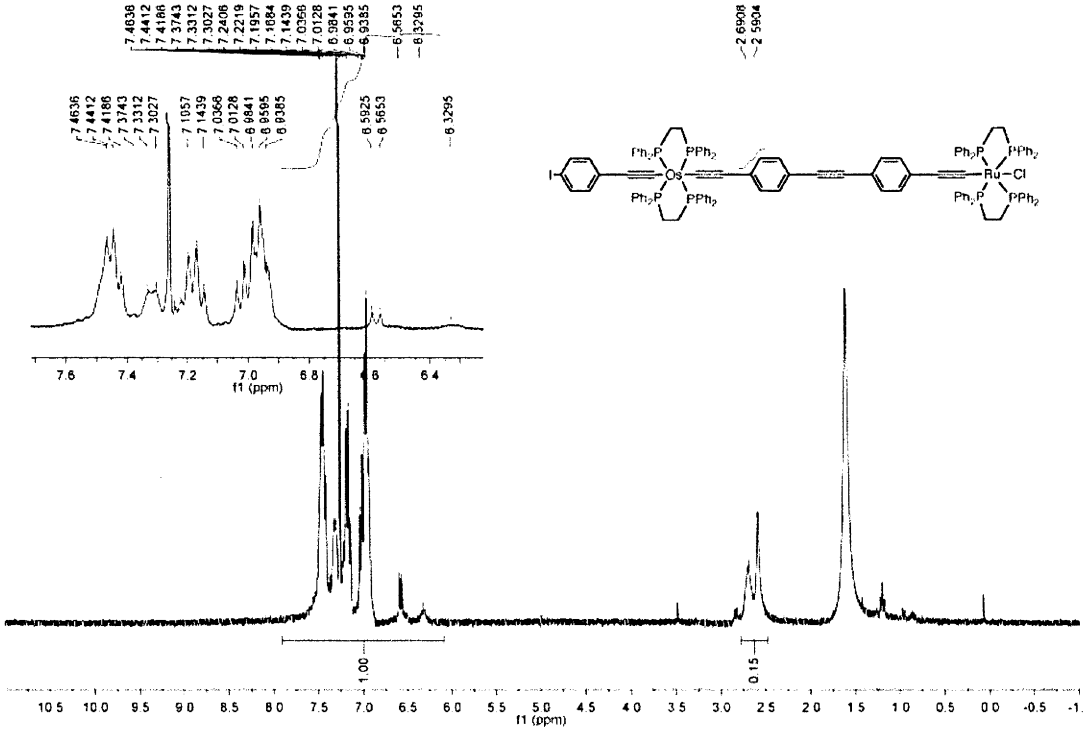

26 ^{13}P NMR

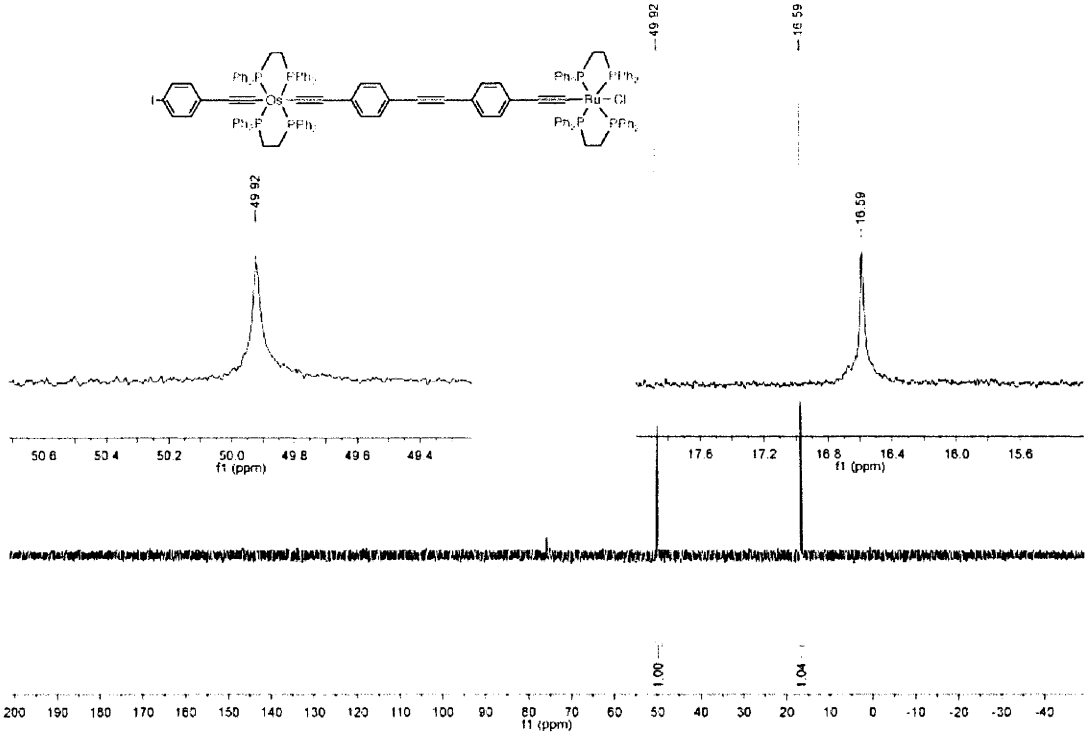

27 ^{1}H NMR

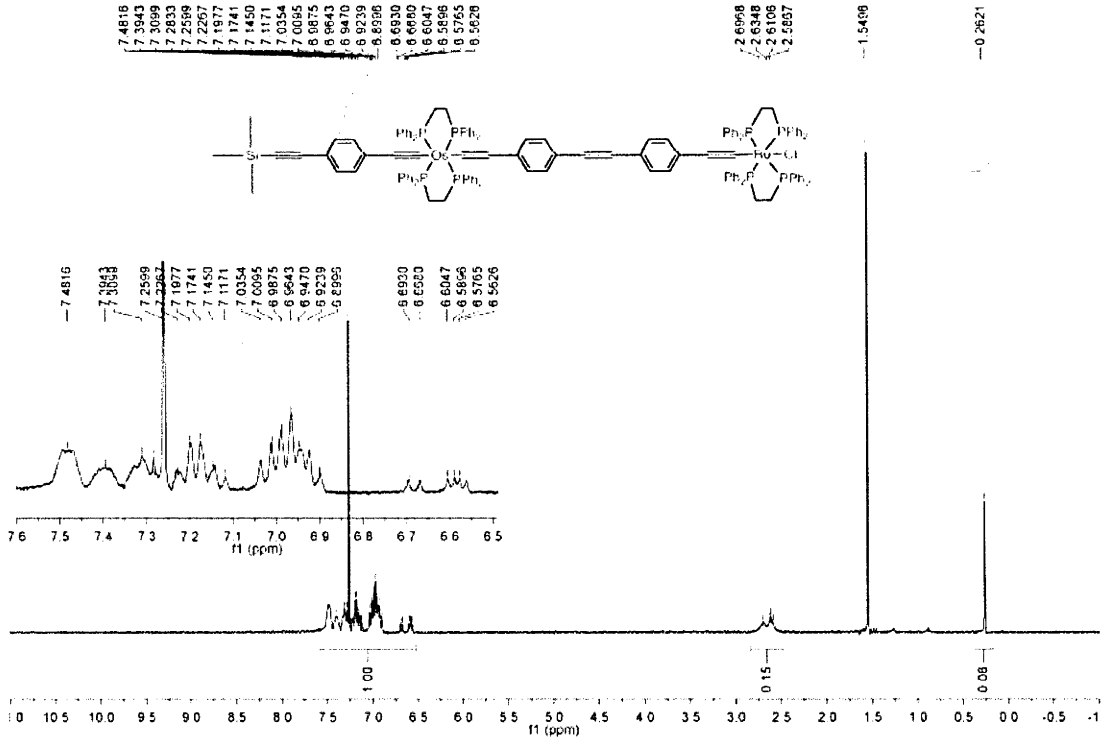

27 ^{13}P NMR

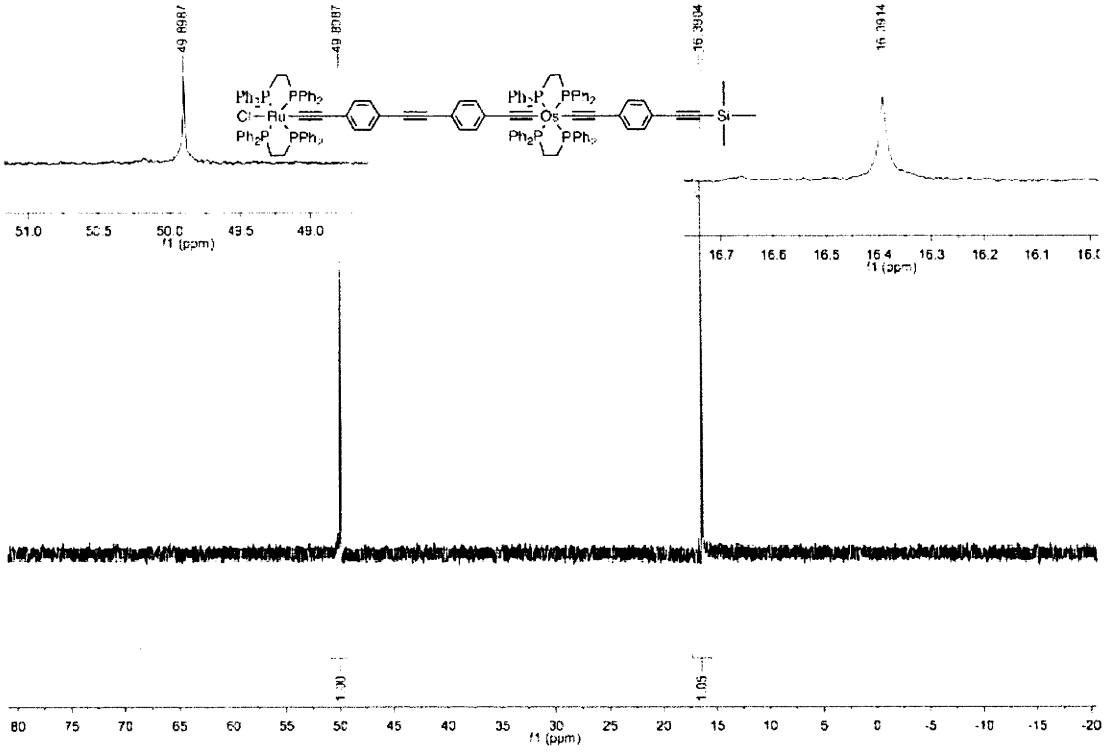

28 ^{1}H NMR

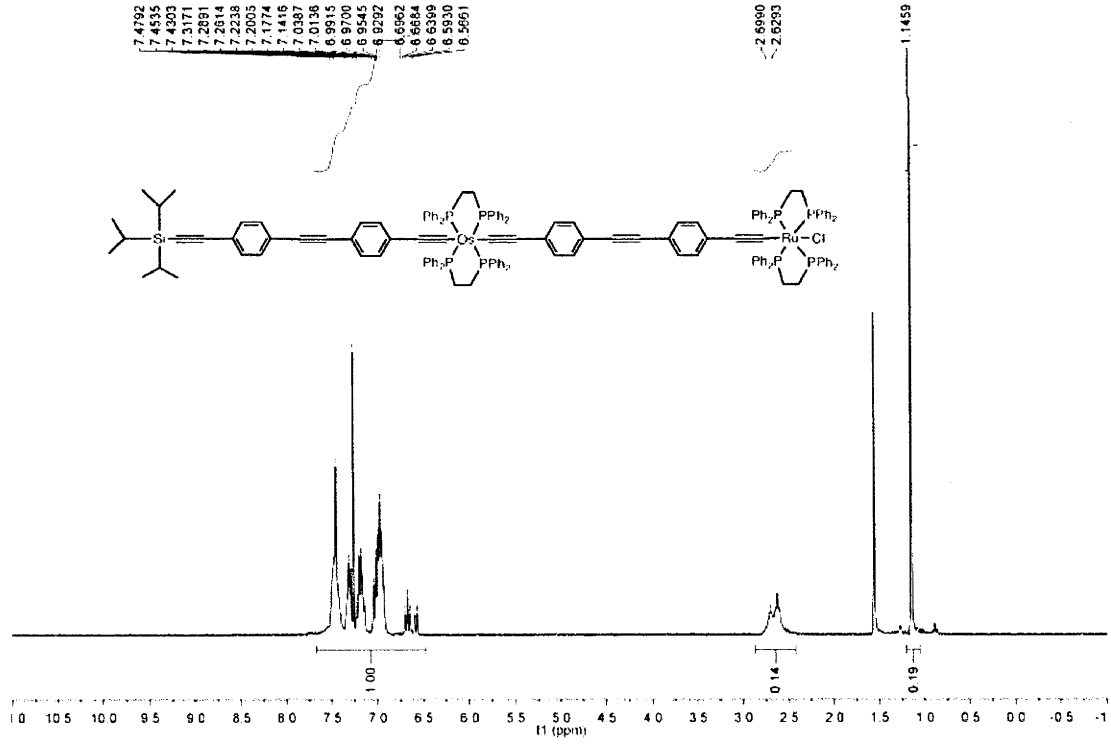

28 ^{13}P NMR

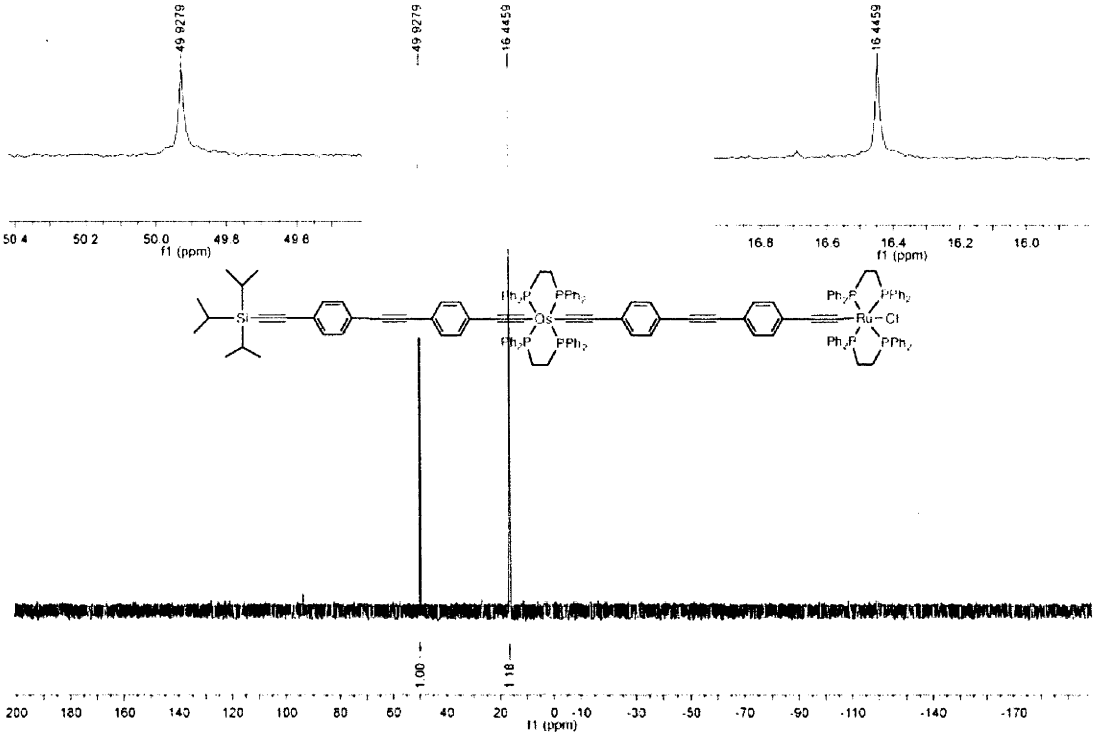

29 ^{1}H NMR

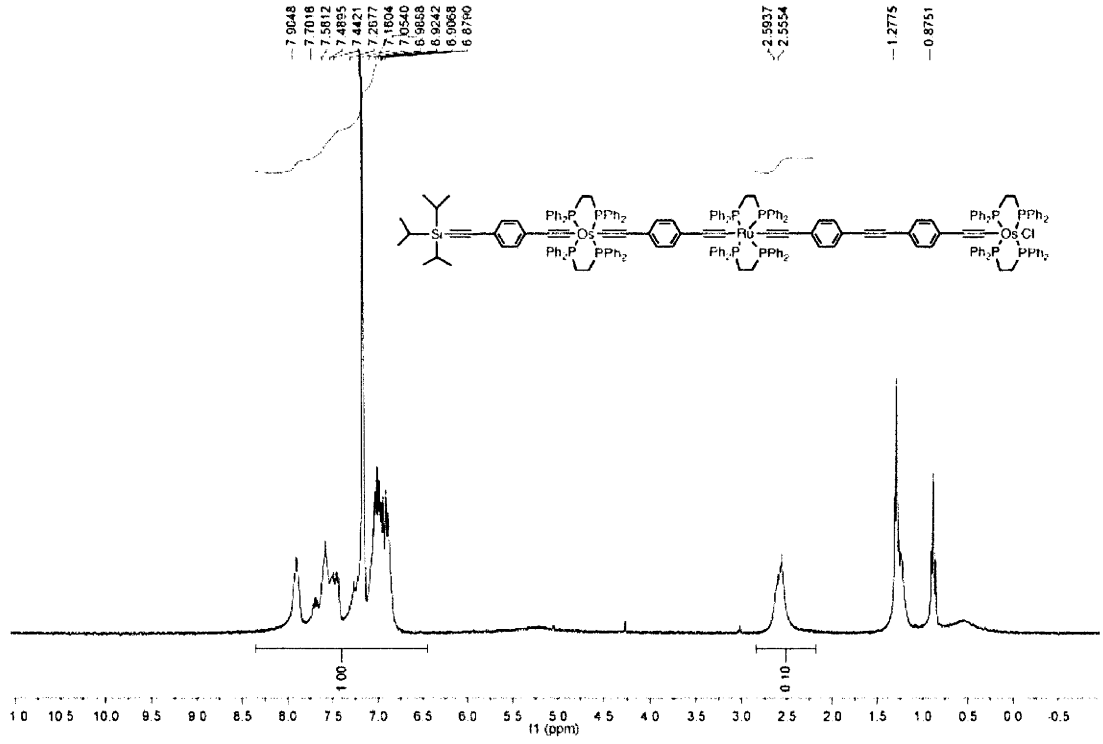

29 ^{13}P NMR

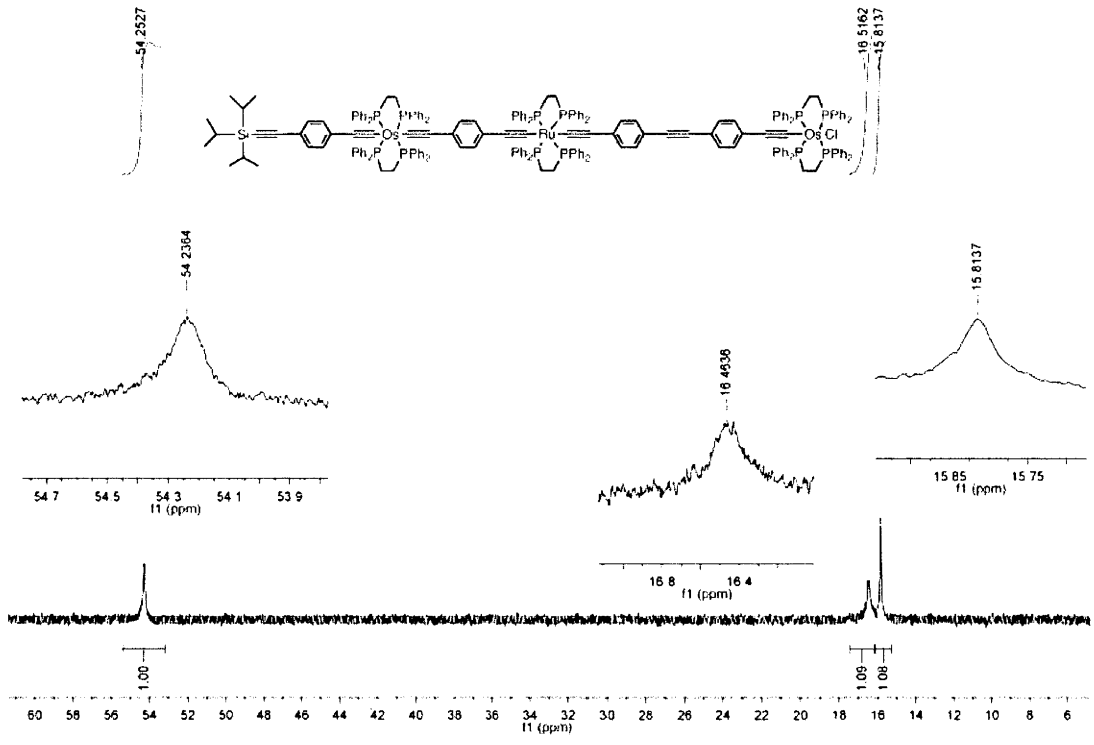
54.2527
16.5162
15.8137
54.2364
16.4636
15.8137
f1 (ppm)
1.00
1.00
1.08

Appendix C

Chapter 4 NMR spectra

30 ^{1}H NMR

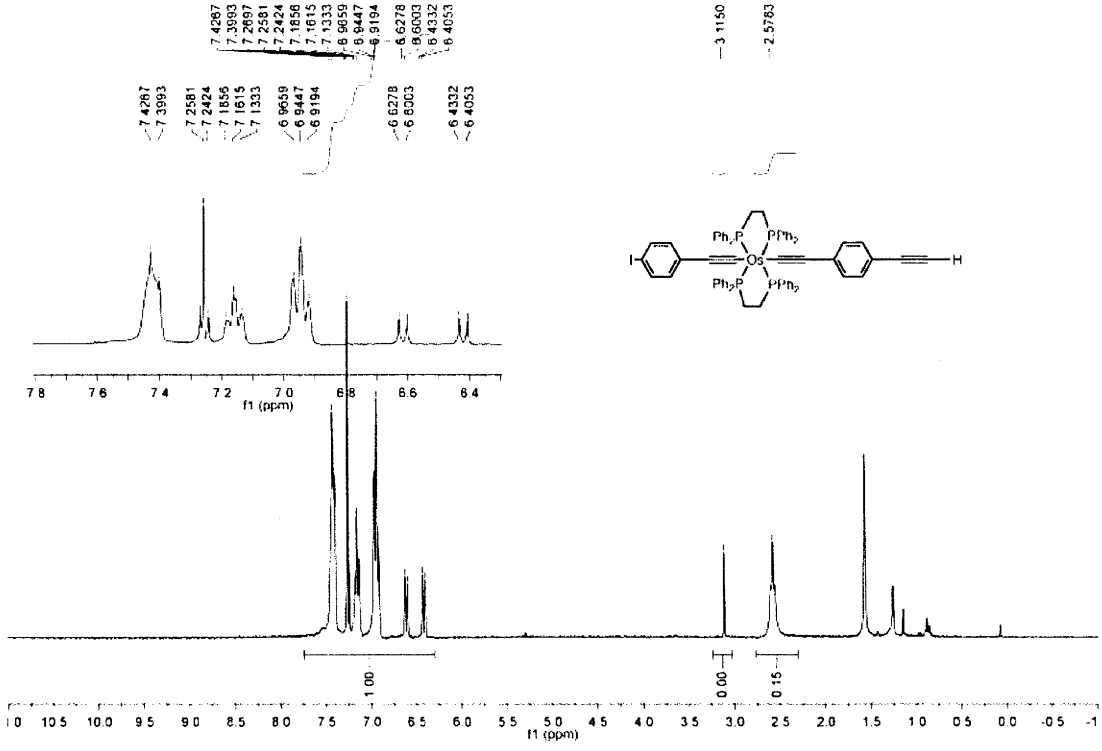

30 ^{31}P NMR

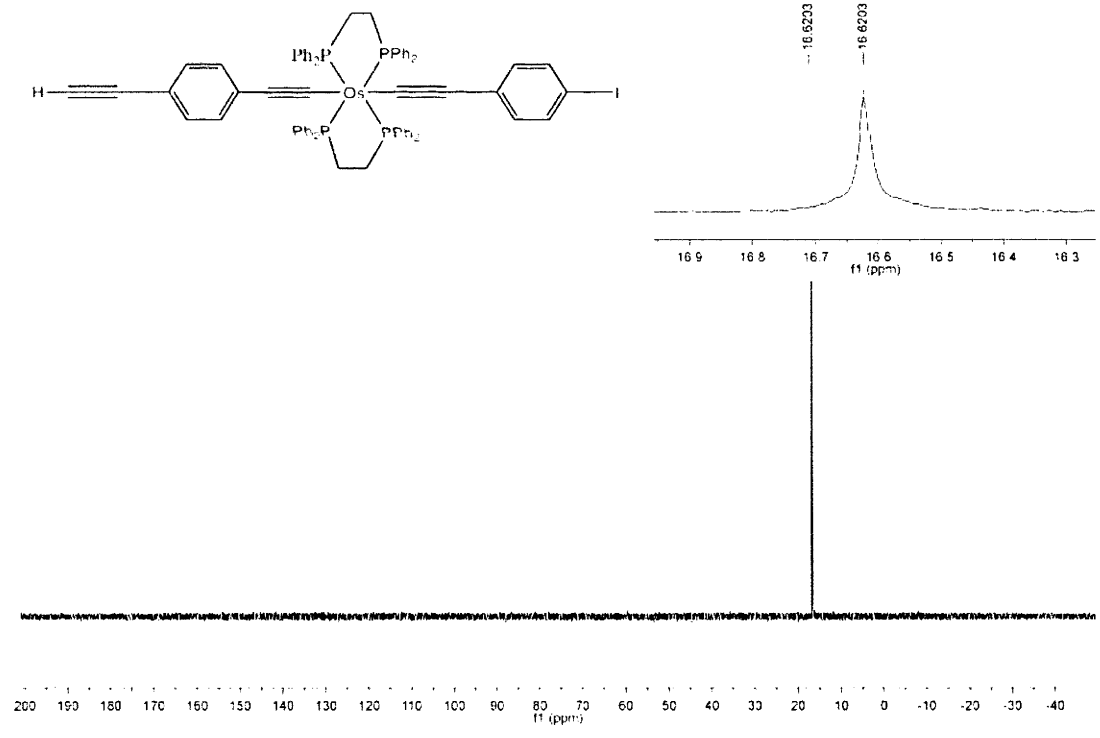

30 ^{13}C NMR

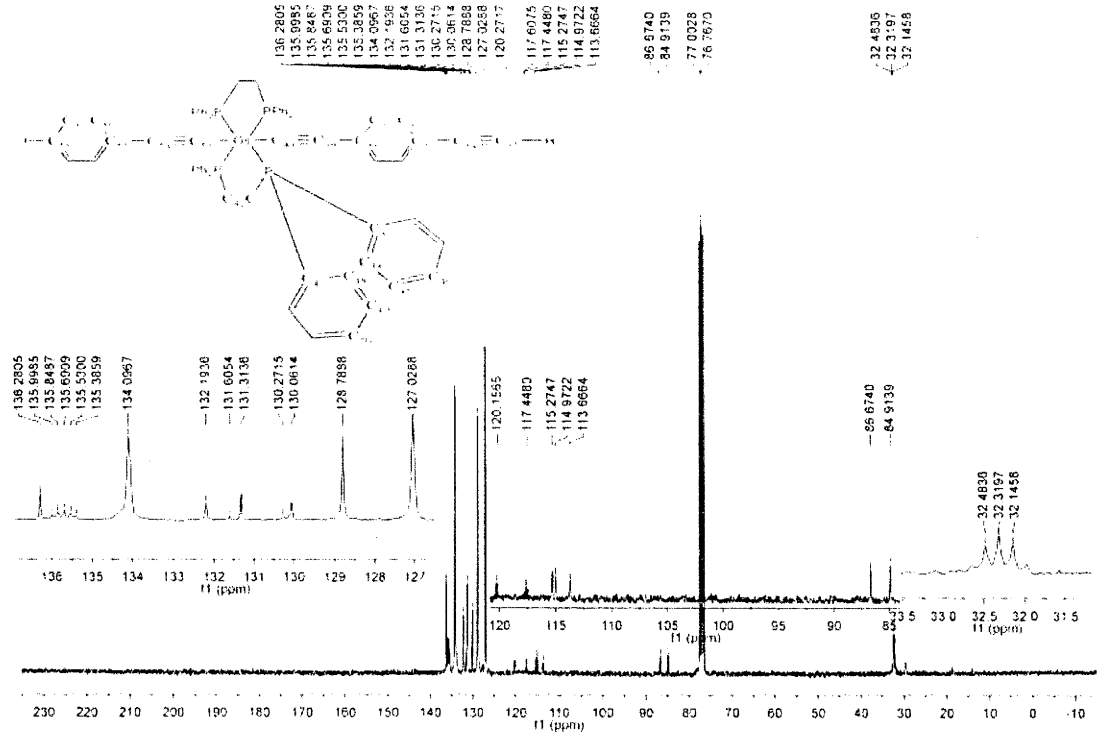

31 ^{1}H NMR

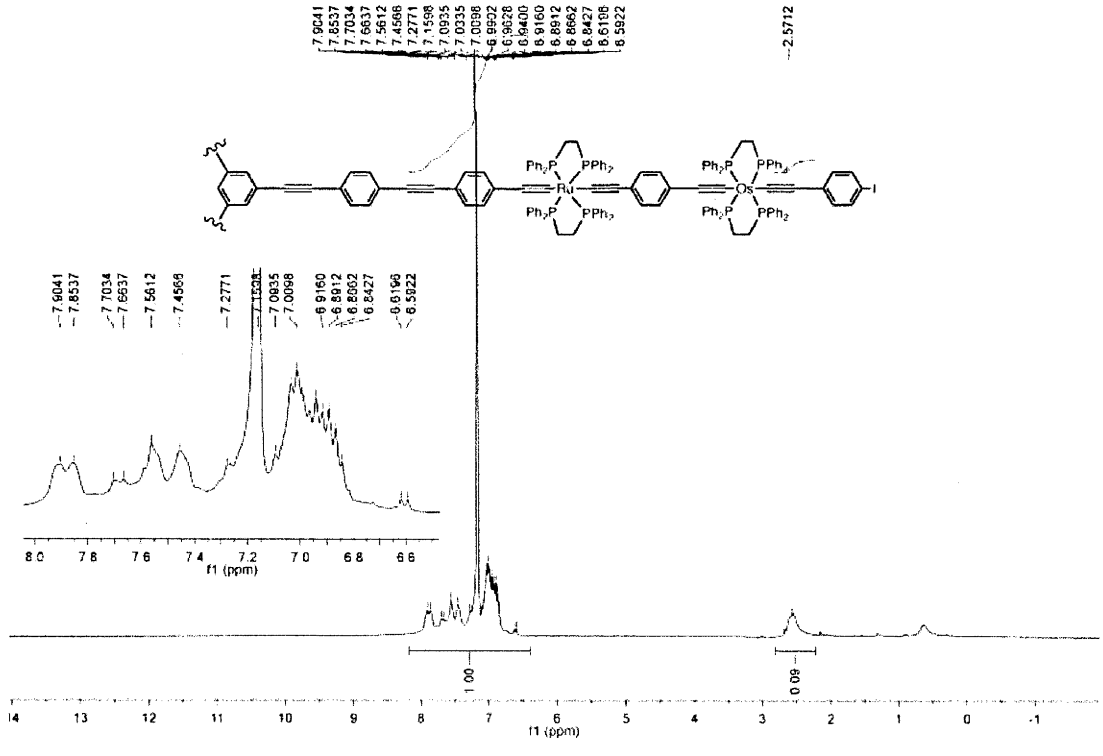

31 ^{31}P NMR

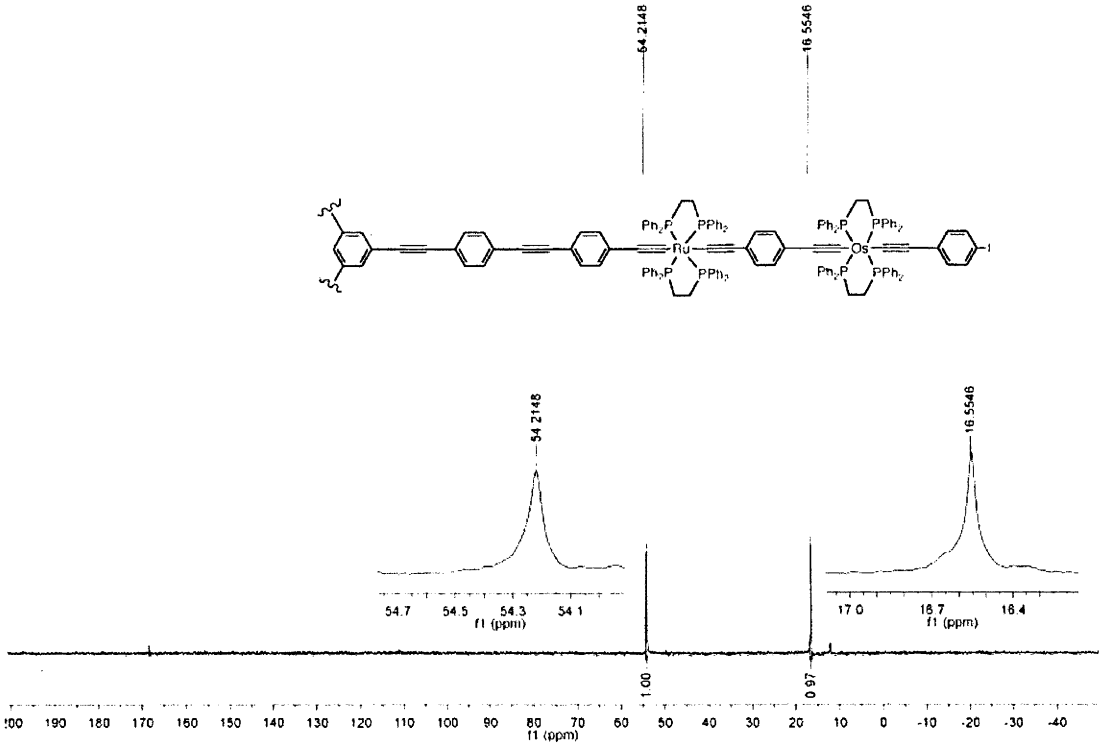

32 ^{1}H NMR

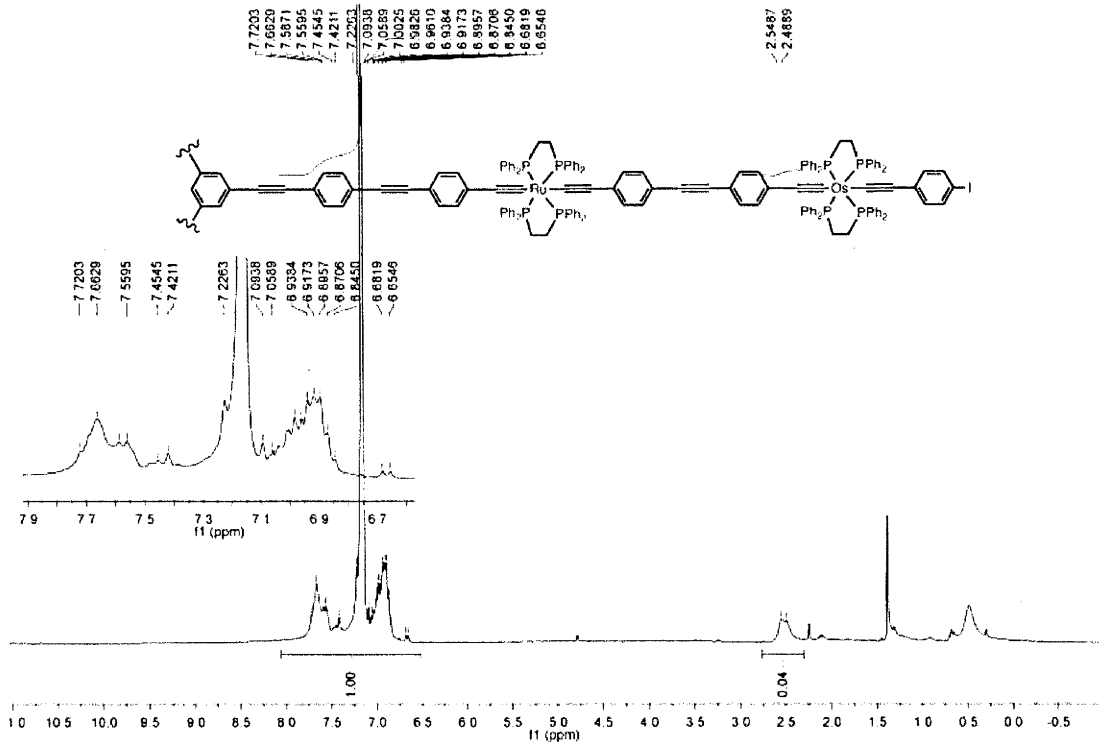

32 ^{31}P NMR

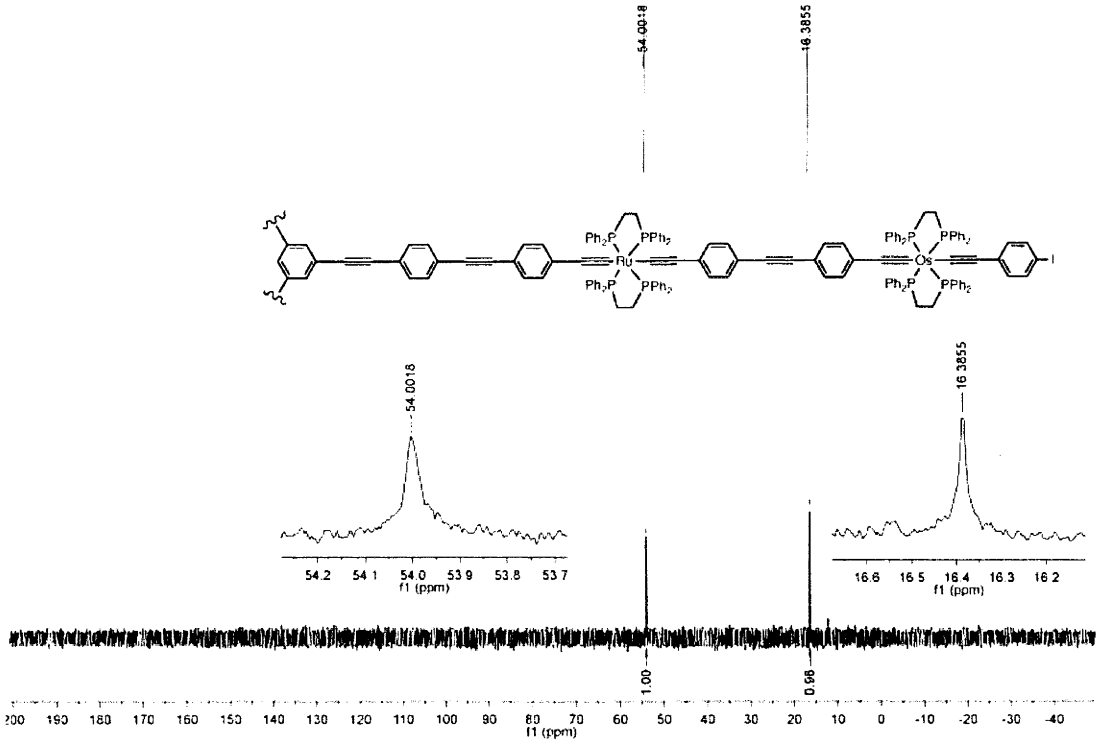

33 ^{1}H NMR

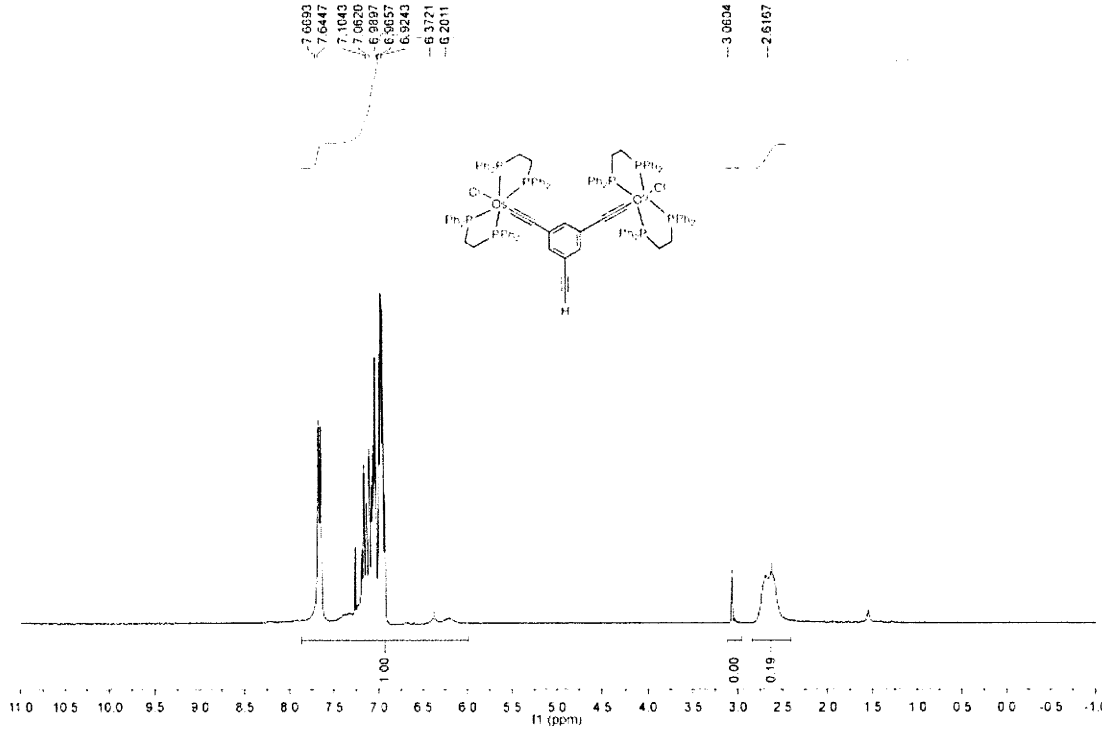

33 ^{31}P NMR

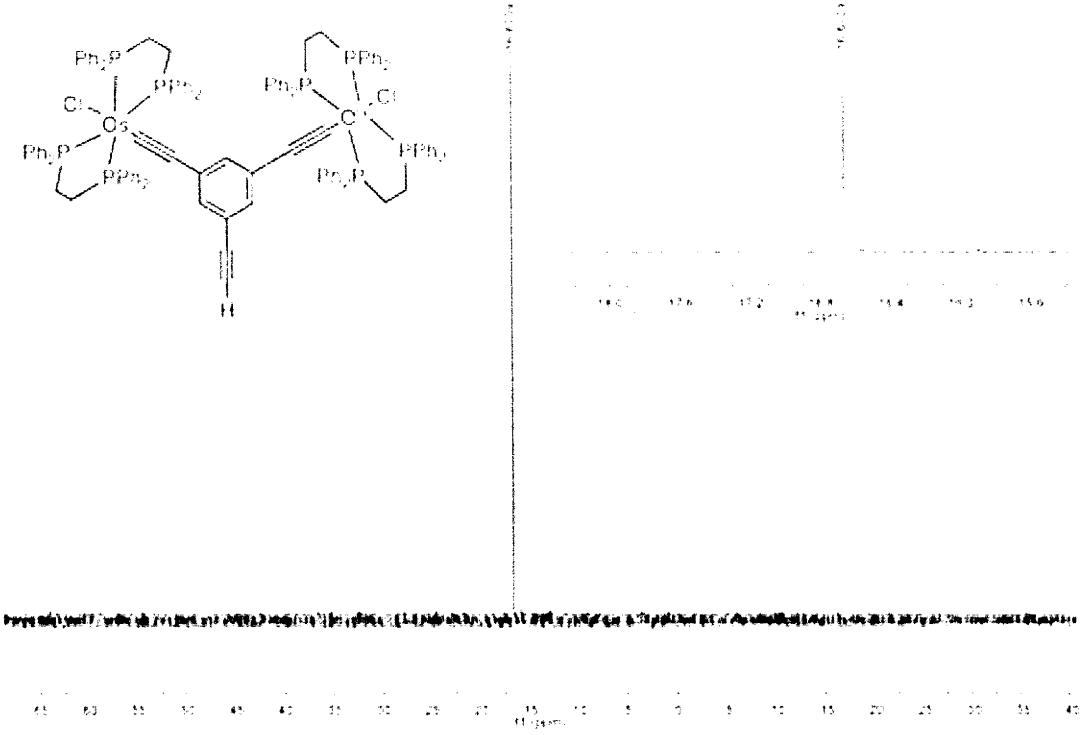

33 ^{13}C NMR

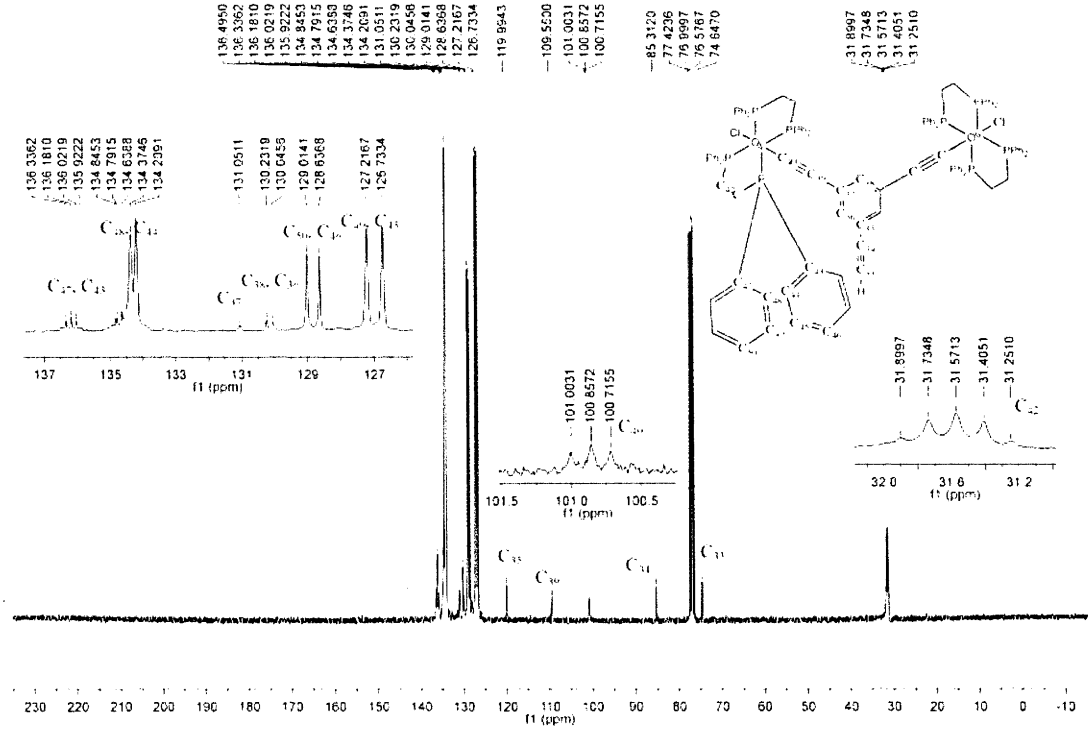

34 ^{1}H NMR

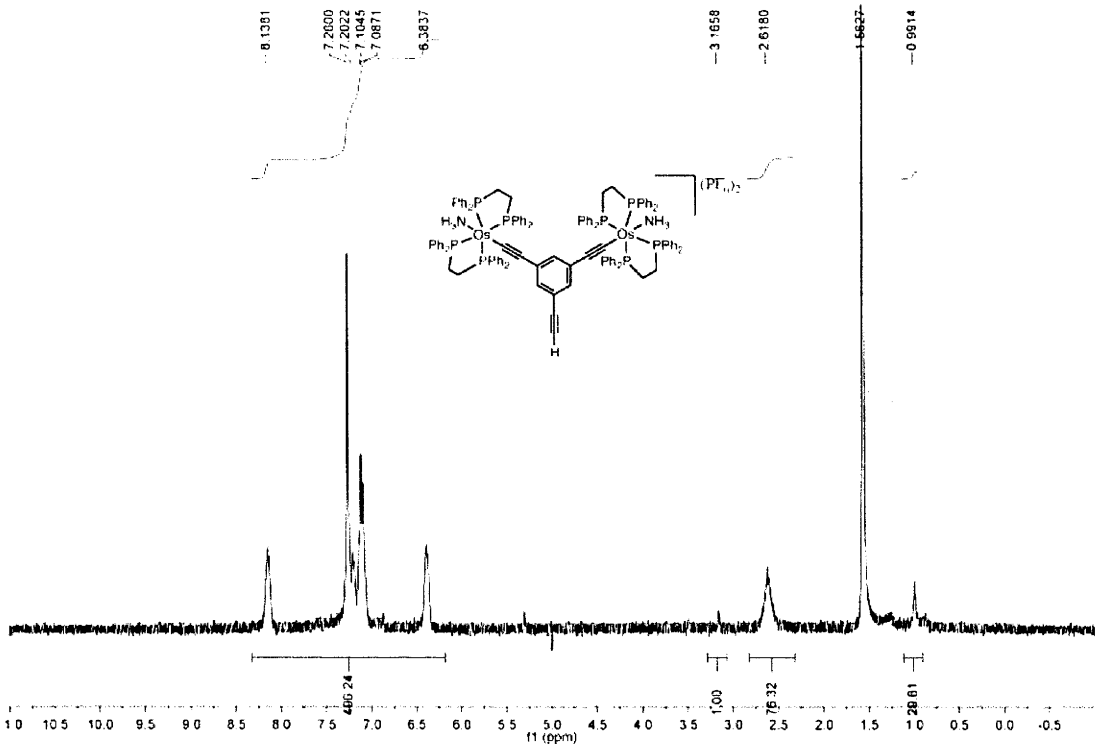

34 ^{31}P NMR

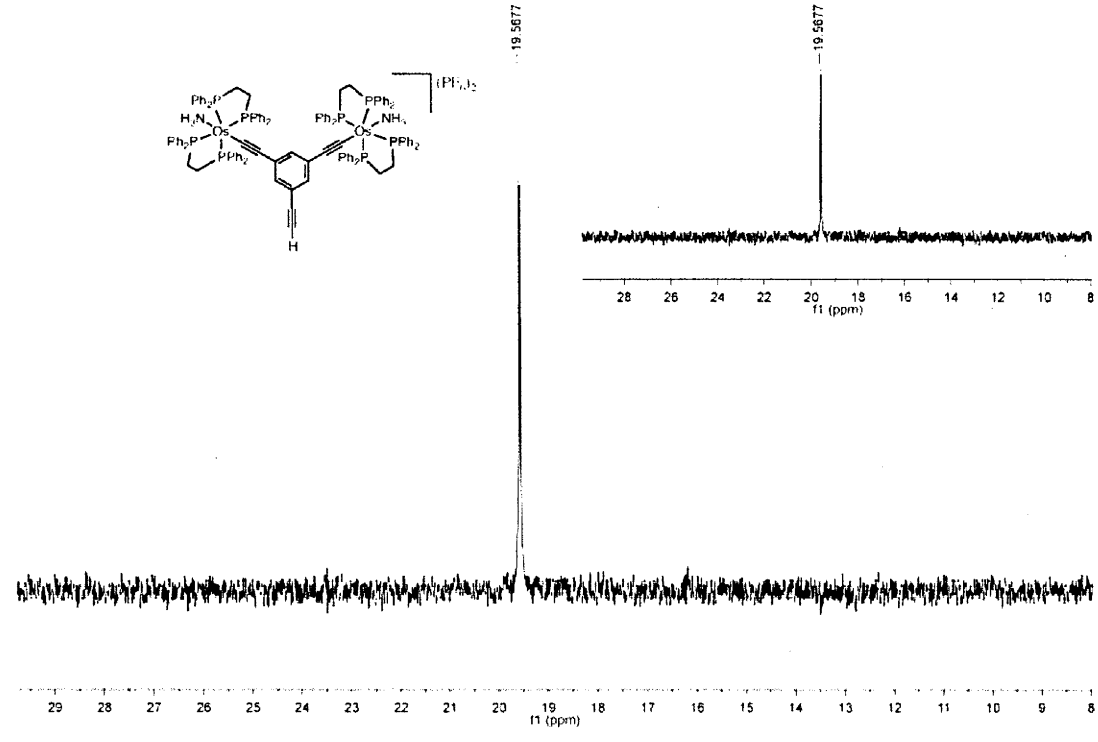

35 ^{1}H NMR

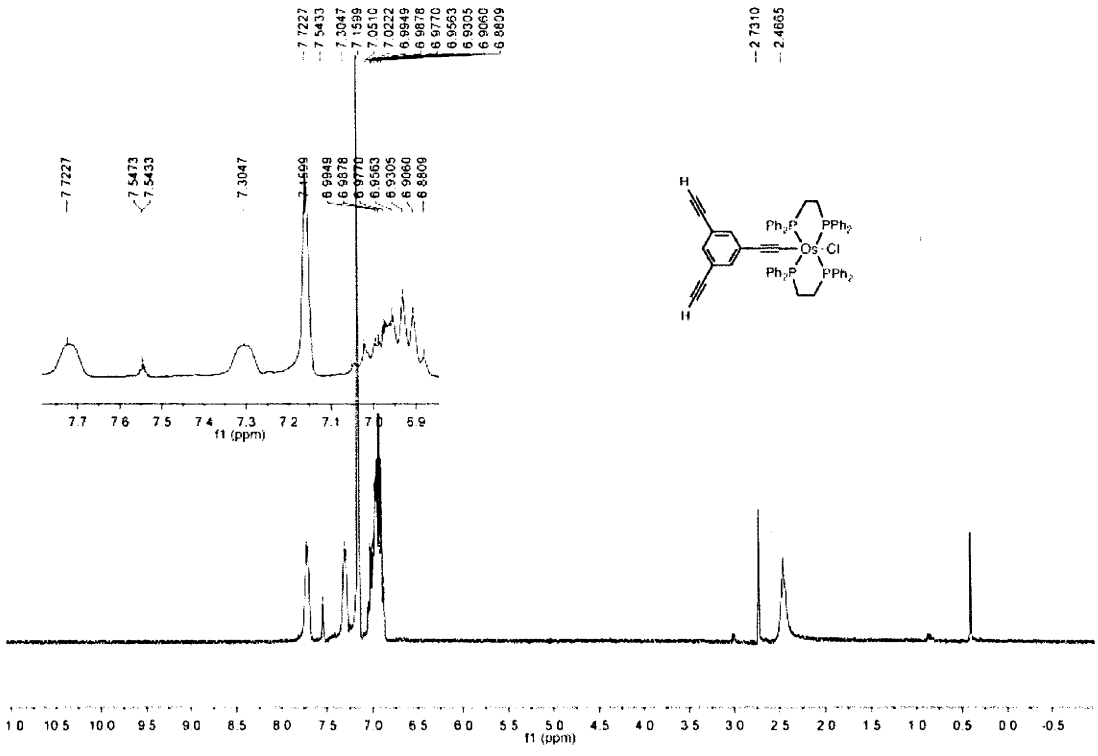

35 ^{31}P NMR

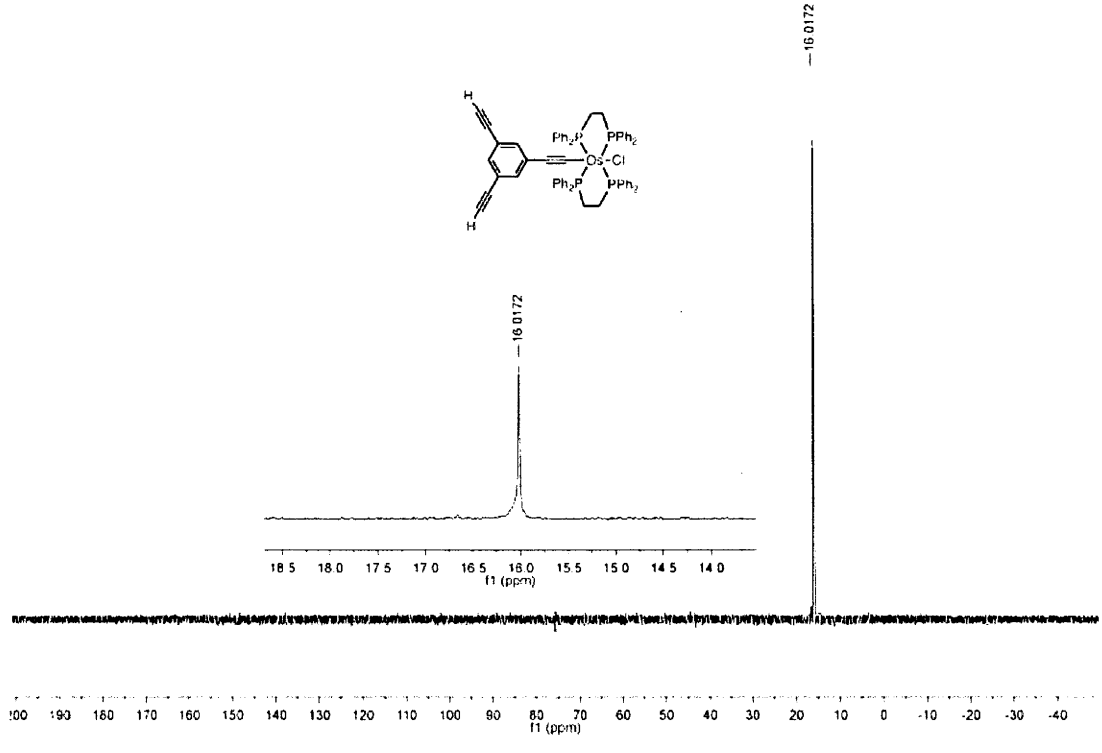

35 ^{13}C NMR

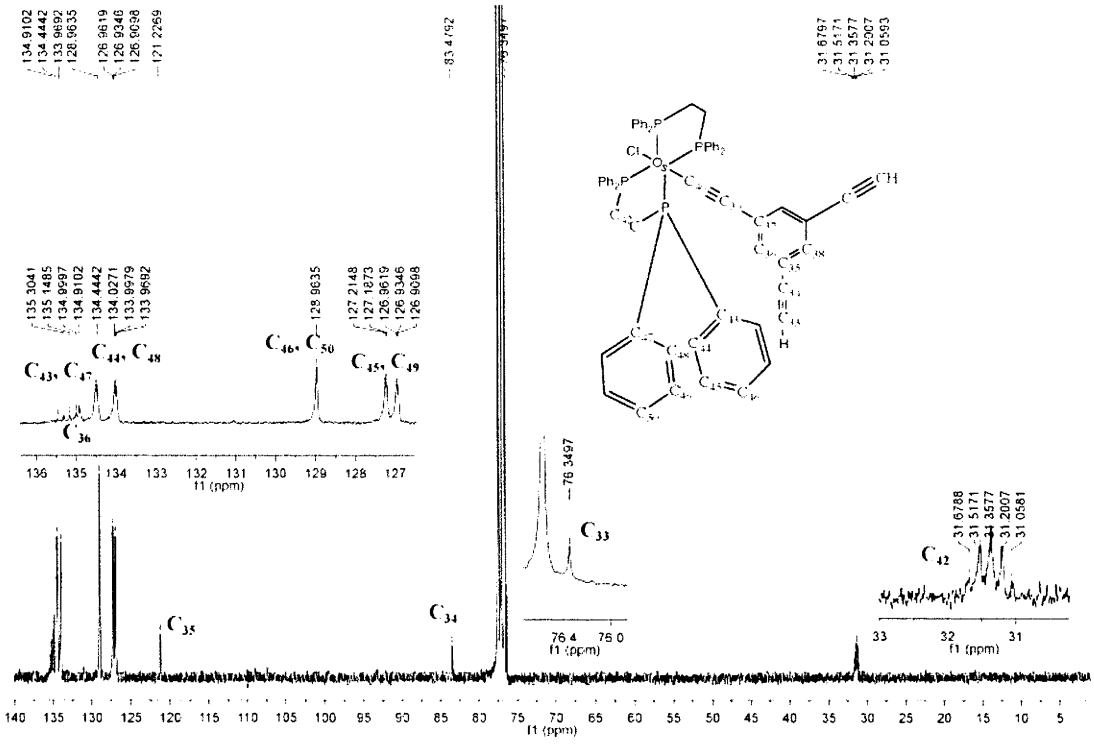

36 ^{1}H NMR

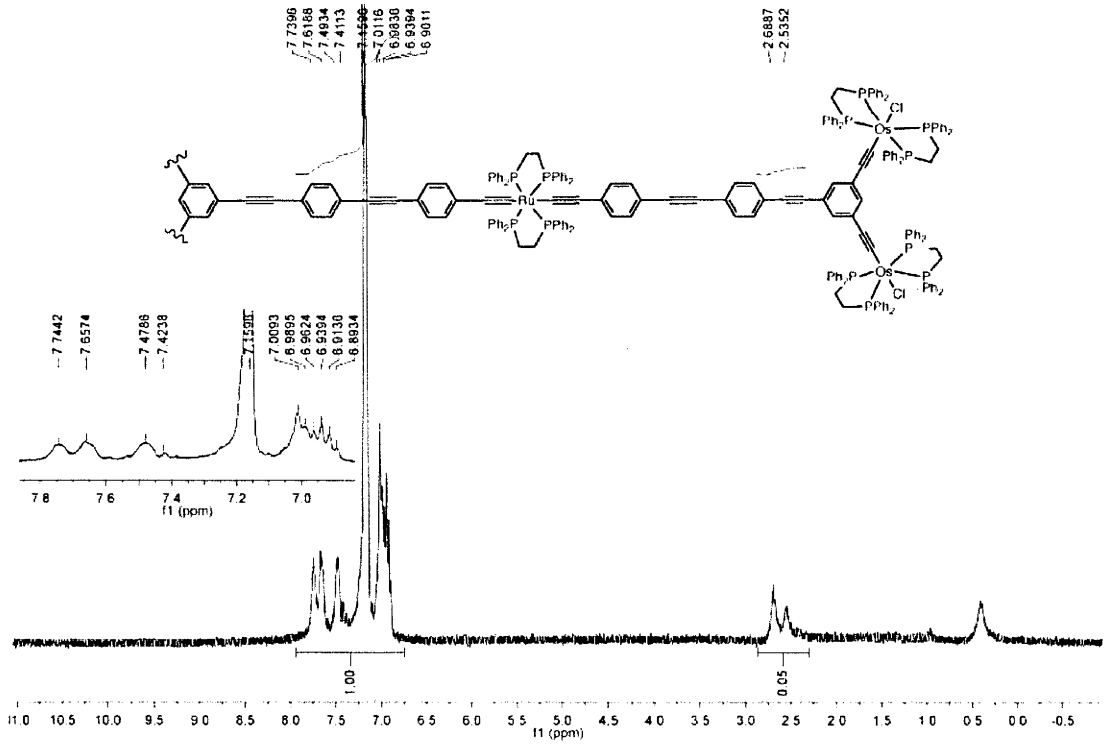

36 ^{31}P NMR

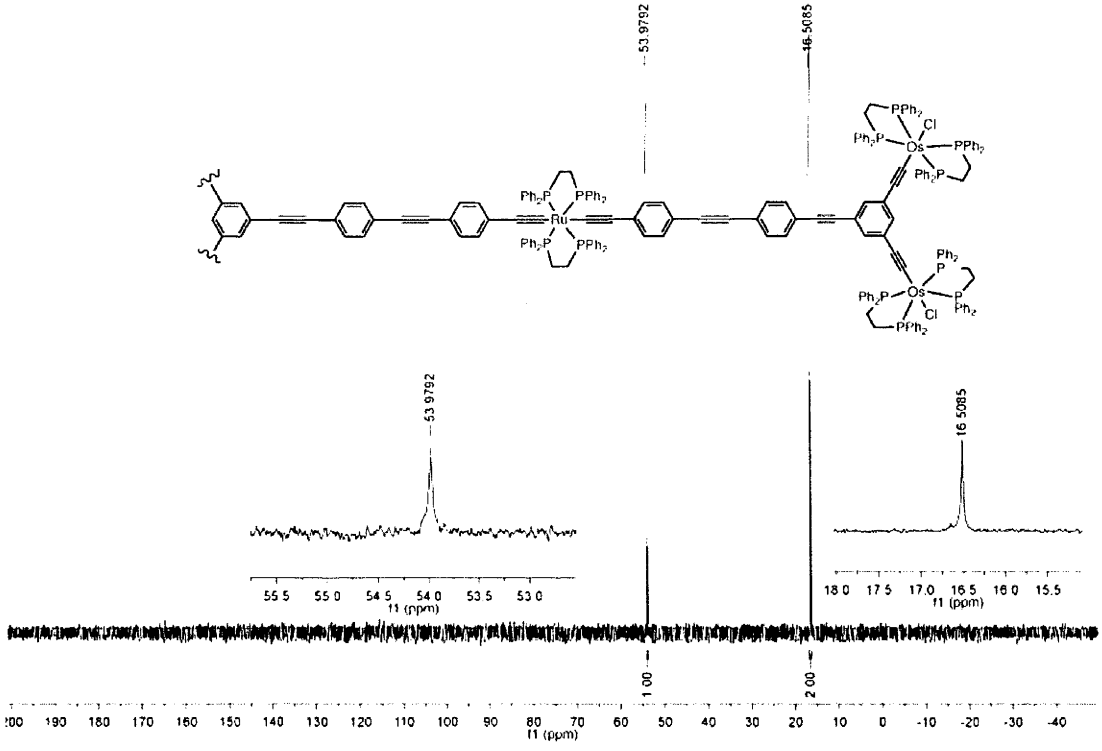

37 ^{1}H NMR

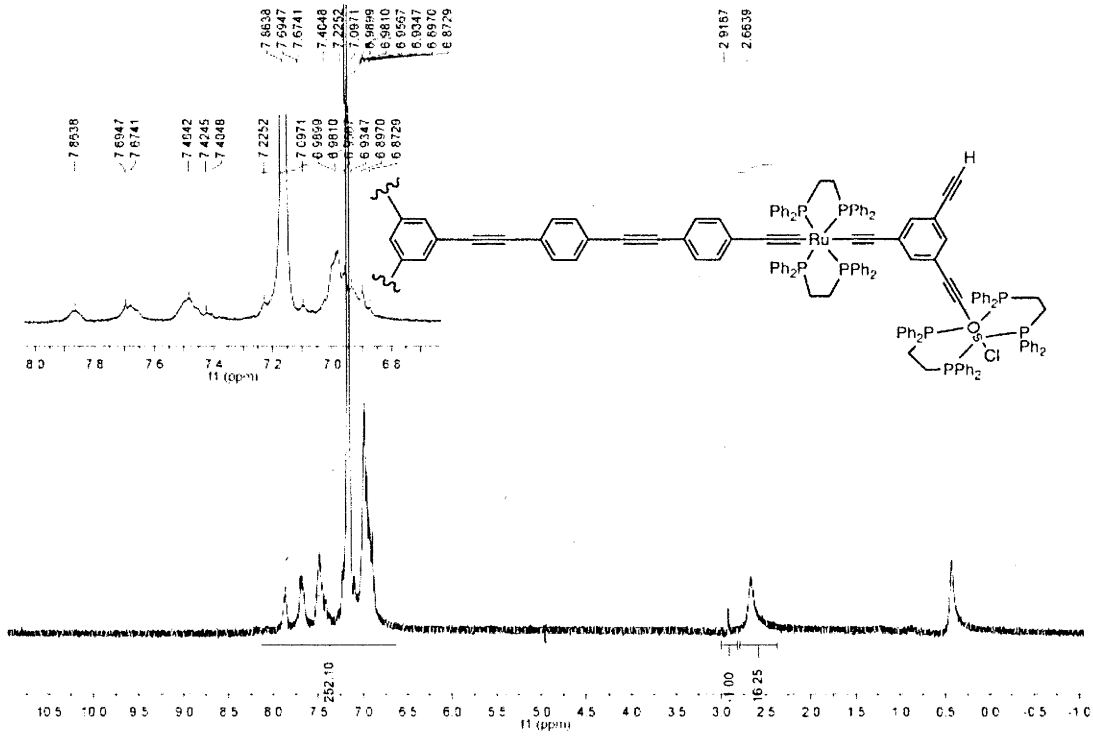

37 ^{31}P NMR

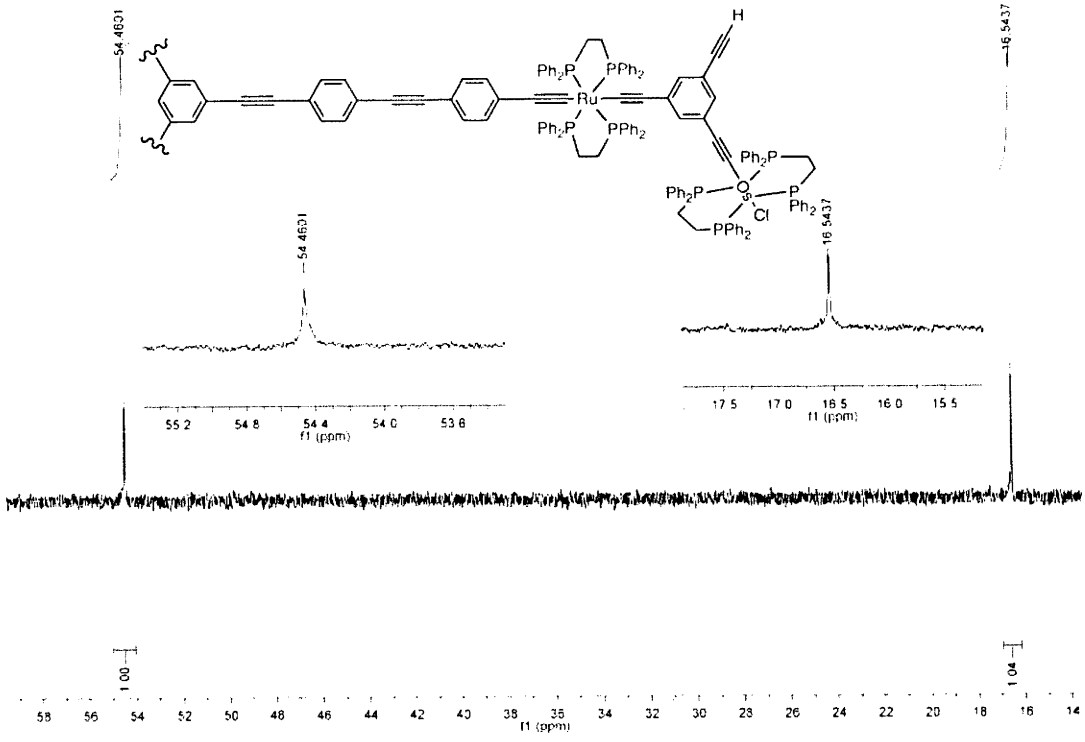

38 ^{1}H NMR

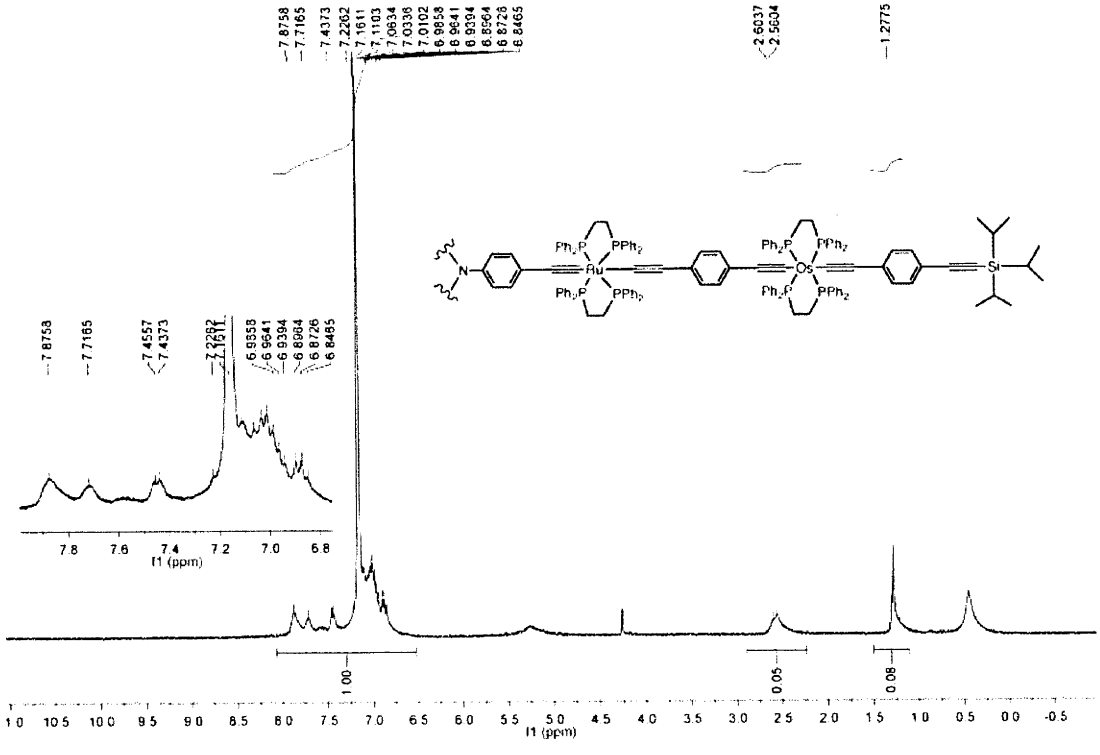

38 ^{31}P NMR

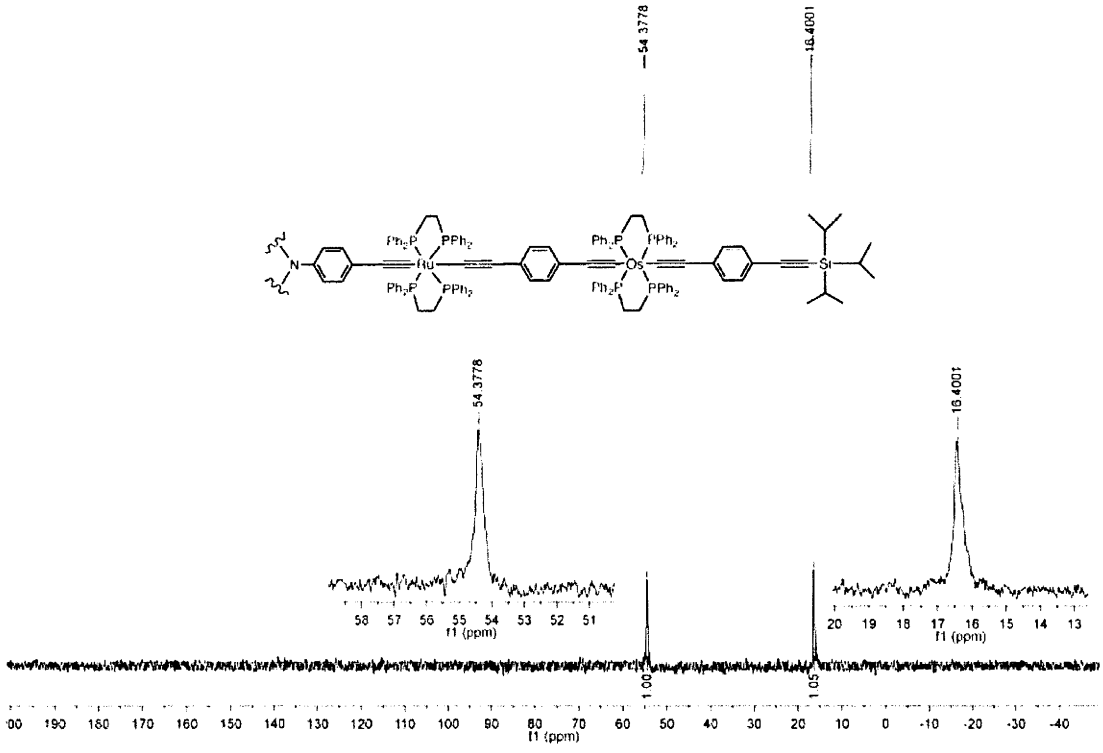

Appendix D

Crystallographic data

	1	**2**	**6 • CH_2Cl_2**
Chem. Formula	$C_{71}H_{73}ClOsP_4Si$	$C_{62}H_{53}ClOsP_4$	$C_{71}H_{59}Cl_3OsP_4$
M (g/mol)	1303.99	1147.65	1332.70
Cryst. color / habit	Yellow / plate	Yellow / block	Orange / block
Cryst. dim. (mm^3)	0.05 x 0.09 x 0.15	0.08 x 0.11 x 0.20	0.07 x 0.10 x 0.10
Temp. (K)	200	200	200
λ (Å)	0.71073	0.71073	0.71073
Cryst. Syst.	Monoclinic	Monoclinic	Triclinic
Space group (N^o)	P 2_1/a (14)	P 2_1/c (14)	P -1 (2)
a (Å)	13.9487(3)	11.4941(2)	13.2687(2)
b (Å)	17.1350(3)	22.4668(3)	14.5124(2)
c (Å)	26.3883(5)	19.3328(3)	16.3888(2)
α (deg)			79.035(10)
β (deg)	96.9911(10)	93.9699(7)	89.6495(9)
γ (deg)			74.8444(7)
V ($Å^3$)	6260.2(2)	4980.44(13)	2987.30(7)
Z	4	4	2
D_{calcd} (g/cm^{-3})	1.38	1.53	1.48
Transm. Factors	0.76-0.90	0.67-0.82	0.79-0.86
μ (mm^{-1})	2.24	2.78	2.42
Theta (deg)	2.6-25.0	2.7-27.9	2.6-27.5
h_{min}/h_{max}	-16/16	-15/15	-17/17
k_{min}/k_{max}	-20/20	-29/29	-18/18
l_{min}/l_{max}	-31/31	-25/25	-20/21
F(000)	2664	2312	1344
Compl. (%)	100	99.7	99.9
R_{int} (%)	22.0	7.8	7.0
Total reflections	123175	116730	67979
Unique refl. (N_0)	11102	12195	13678
N_0 [I > 2.0 σ(I)]	4170	9118	11596
N^o of param.	703	613	712
GoF	1.02	0.95	0.97
Flack-Parameter	-	-	-
R[F^2 > 2 σ(F^2)](%)	3.2	3.5	3.3
wR(F^2) (%)	12.7	7.2	7.0

$R = \sum||F_o|-|F_c||/\sum|F_o|$,

$wR = [\sum w(|F_0|-|F_c|)^2/\sum wF_0^2]^{1/2}$ where $w = [\sigma_c^2(F_o) + (p^2/4)F_o^2]^{-1}$

	9 · 0.5C_7H_8	**10 · CH_2Cl_2**	**11 · CH_2Cl_2**
Chem. Formula	$C_{63.5}H_{56.5}ClOsP_4$	$C_{61}H_{54}BrCl_3OsP_4$	$C_{61}H_{54}Cl_3IOsP_4$
M (g/mol)	1169.2	1287.47	1334.46
Cryst. color / habit	Yellow/ rod	Yellow/block	Yellow/ plate
Cryst. dim. (mm^3)	0.44 x 0.11 x 0.10	0.11 x 0.18 x 0.27	0.09 x 0.13 x 0.16
Temp. (K)	200	200	200
λ (Å)	0.71073	0.71073	0.71073
Cryst. Syst.	Monoclinic	Triclinic	Monoclinic
Space group (N°)	P 1 2_1/n 1	P -1(1)	P 1 2_1/a 1(14)
a (Å)	13.7138(1)	9.2626(1)	9.3045(1)
b (Å)	22.7102(3)	12.9132(2)	48.1334(5)
c (Å)	17.3934(2)	23.9301(4)	12.9892(2)
α (deg)		93.264(1)	
β (deg)	103.8598(6)	93.976(1)	99.5615(3)
γ (deg)		99.222(1)	
V ($Å^3$)	5259.34(10)	2811.74(7)	5736.49(12)
Z	4	2	4
D_{calcd} (g/cm^{-3})	1.48	1.52	1.55
Transm. Factors	0.75-0.77	0.48-0.71	0.66-0.78
μ (mm^{-1})	2.64	3.27	3.05
Theta (deg)	2.6-30.0	2.57-27.49	2.56-27.47
h_{min}/h_{max}	-19/19	-12/11	-12/12
k_{min}/k_{max}	-31/31	-16/16	-62/62
l_{min}/l_{max}	-24/24	-31/31	-12/12
F(000)	2362	1284	2640
Compl. (%)		100	93
R_{int} (%)	5.0	7.3	4.3
Total reflections	124257	61755	64677
Unique refl. (N_0)	15388	12843	12387
N_0 [I > 2.0 σ(I)]	11292	10259	11163
N° of param.	631	631	631
GoF	0.92	0.95	0.98
Flack-Parameter	-	-	-
R[$F^2 > 2\ \sigma(F^2)$](%)	2.1	3.7	3.1
w$R(F^2)$ (%)	5.6	7.1	7.5

$R = \sum||F_o|-|F_c||/\sum|F_o|$,

$wR = [\sum w(|F_0|-|F_c|)^2/\sum wF_0^2]^{1/2}$ where $w = [\sigma_c^2(F_o) + (p^2/4)F_o^2]^{-1}$

	13 · $2C_7H_8$	**14**	**15 · CH_2Cl_2**
Chem. Formula	$C_{74}H_{72}F_6NOsP_5$	$C_{60}H_{55}F_6INOsP_5$	$C_{69}H_{61}BrCl_2F_6NOsP_5$
M (g/mol)	1434.45	1376.06	1514.12
Cryst. color / habit	Yellow/plate	Yellow/plate	Yellow/block
Cryst. dim. (mm^3)	0.09 x 0.14 x 0.15	0.07 x 0.21 x 0.24	0.06 x 0.07 x 0.11
Temp. (K)	200	200	200
λ (Å)	0.71073	0.71073	0.71073
Cryst. Syst.	Orthorhombic	Orthorhombic	Orthorhombic
Space group (N°)	P c a 2_1(29)	P c a 2_1	P bca(61)
a (Å)	17.8849(2)	24.2797(3)	17.6946(1)
b (Å)	15.6530(2)	9.764(1)	23.1349(2)
c (Å)	23.5329(3)	22.6269	32.7147(2)
α (deg)			90.0
β (deg)			90.0
γ (deg)			90.0
V ($Å^3$)	6588.09(14)	5364.15(11)	13392.18(16)
Z	4	4	8
D_{calcd} (g/cm^{-3})	1.45	1.70	1.50
Transm. Factors	0.75-0.84	0.53-0.82	0.75-0.85
μ (mm^{-1})	2.12	3.16	2.76
Theta (deg)	1.93-27.47	2.68-27.86	Collected: 2.6-28.0 Refined: 2.6-25.0
h_{min}/h_{max}	-22/23	-31/31	-20/21
k_{min}/k_{max}	-20/19	-12/12	-27/27
l_{min}/l_{max}	-30/30	-29/29	-38/38
F(000)	2912	2720	6048
Compl. (%)	100	100	100
R_{int} (%)	6.2	9.6	7.1
Total reflections	98993	75500	189505
Unique refl. (N_0)	15029	12764	12785
N_0 [I > 2.0 σ(I)]	11475	11445	8988
N° of param.	720	668	766
GoF	0.97	0.95	0.95
Flack-Parameter	-0.022(5)	-0.015(3)	-
R[$F^2 > 2\ \sigma(F^2)$](%)	3.8	2.5	3.1
wR(F^2) (%)	9.8	5.6	7.2

$R = \sum||F_o|-|F_c||/\sum|F_o|$,

$wR = [\sum w(|F_0|-|F_c|)^2/\sum wF_0^2]^{1/2}$ where $w = [\sigma_c^2(F_o) + (p^2/4)F_o^2]^{-1}$

	17 · 2C$_7$H$_8$	**19**
Chem. Formula	$C_{82}H_{74}OsP_4$	$C_{87}H_{81}I_{1.07}OsP_4Si$
M (g/mol)	1373.59	1604.69
Cryst. color / habit	Yellow/plate	yellow/plate
Cryst. dim. (mm^3)	0.17 x 0.22 x 0.32	0.23 x 0.09 x 0.04
Temp. (K)	200	200
λ (Å)	0.71073	0.71073
Cryst. Syst.	Triclinic	Triclinic
Space group (N°)	P -1(1)	P-1(1)
a (Å)	9.5310(1)	13.5087(2)
b (Å)	12.9852(2)	14.3396(2)
c (Å)	14.3474(2)	21.9504(3)
α (deg)	81.8841(7)	99.0901(8)
β (deg)	75.5031(9)	102.5757(6)
γ (deg)	74.2740(8)	101.3641(9)
V (Å^3)	1649.65(4)	3977.95(10)
Z	1	2
D_{calcd} (g/cm^{-3})	1.38	1.34
Transm. Factors	0.57-0.72	0.82-0.92
μ (mm^{-1})	2.08	2.16
Theta (deg)	2.94-27.91	2.62-27.49
h_{min}/h_{max}	-12/12	-17/17
k_{min}/k_{max}	-17/17	-18/18
l_{min}/l_{max}	-18/18	-28/28
F(000)	702	1620
Compl. (%)	100	100
R_{int} (%)	3.2	7.2
Total reflections	37667	84298
Unique refl. (N_0)	7880	18225
N_0 [I > 2.0 σ(I)]	7833	14664
N° of param.	394	855
GoF	0.98	0.98
Flack-Parameter	-	-
R[F^2 > 2 σ(F^2)](%)	1.9	5.4
wR(F^2) (%)	3.8	14.6

$R = \sum||F_o|-|F_c||/\sum|F_o|$,

$wR = [\sum w(|F_0|-|F_c|)^2/\sum wF_0^2]^{1/2}$ where $w = [\sigma_c^2(F_o) + (p^2/4)F_o^2]^{-1}$